

*Final*

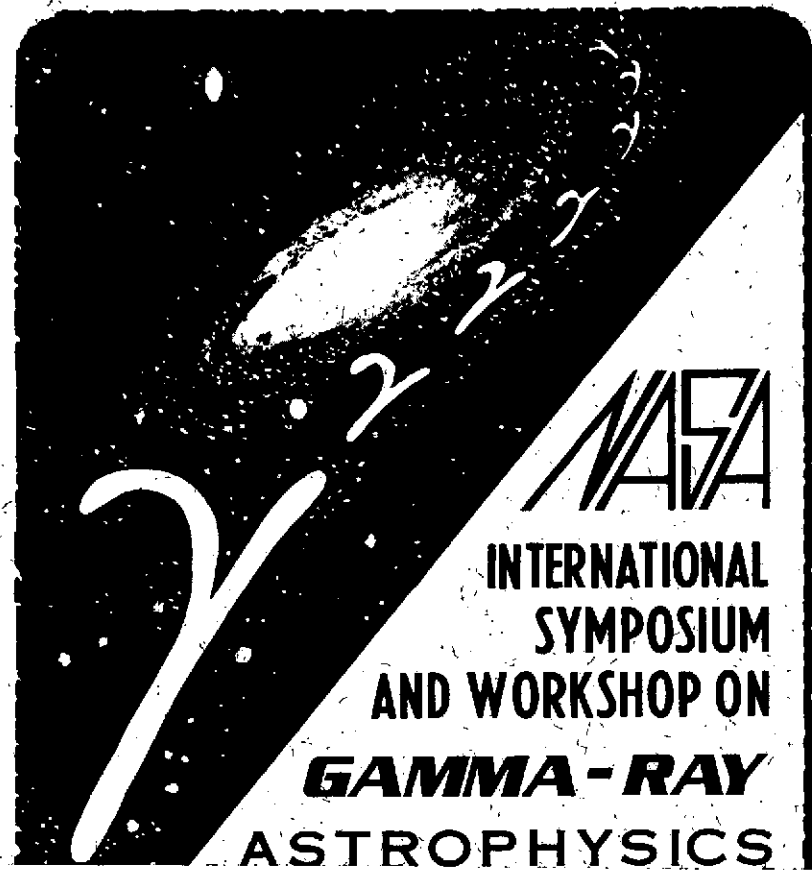
(19)

X-641-73-180

PREPRINT

NASA TM X 66279

# INVITED PAPERS



## ASTROPHYSICS

(NASA-TM-X-66279) INTERNATIONAL SYMPOSIUM AND WORKSHOP ON GAMMA-RAY ASTROPHYSICS

Invited Papers (NASA) ~~447~~ p HC \$24.50  
448

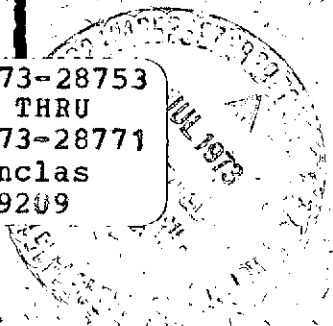
CSSL 03B

N73-28753  
THRU

N73-28771

Unclas

G3/29 09209



F. W. STECKER

J. I. TROMBKA

JUNE 1973

GODDARD SPACE FLIGHT CENTER

GREENBELT, MARYLAND

PROCEEDINGS OF THE INTERNATIONAL SYMPOSIUM AND WORKSHOP ON  
GAMMA-RAY ASTROPHYSICS

EDITORS' PREFACE:

This preprint contains photocopies of manuscripts of the invited papers presented in the morning sessions of the symposium only. It represents the editors' conviction that these manuscripts should be available to the astrophysics community in preprint form as quickly as possible.

This preprint, of course, is not meant to represent the final form of the entire proceedings of the symposium and workshop. A written version of the afternoon workshop-discussion sessions is now in preparation. The final published version of the symposium proceedings will contain this additional material based on transcripts of the afternoon workshop-discussion sessions as well as manuscripts of some short contributions made during these sessions.

F. W. STECKER

J. I. TROMBKA

NASA Goddard Space Flight Center

Greenbelt, Maryland

June, 1973

INTERNATIONAL SYMPOSIUM AND WORKSHOP  
ON GAMMA-RAY ASTROPHYSICS

NASA/GODDARD SPACE FLIGHT CENTER  
April 1973

C O N T E N T S

- W. L. KRAUSHAAR ✓ 1  
... Diffuse Cosmic X-rays Below 1 keV
- D. SCHWARTZ ✓ 2  
H. GURSKY  
... The X-ray Emissivity of the Universe between 2 and 200 keV
- L. E. PETERSON ✓ 3  
J. I. TROMKA  
... The Measurement and Interpretation of the Cosmic Gamma-Ray  
Spectrum Between 0.3 and 27 MeV as Obtained During the  
Apollo Mission
- G. H. SHARE ✓ 4  
... Recent Observations of Cosmic Gamma-Rays from 10 MeV to  
1 GeV
- K. PINKAU ✓ 5  
... Report on European Gamma-Ray Astronomy Results
- D. A. KNIFFEN ✓ 6  
C. E. FICHEL  
R. C. HARTMAN  
... Preliminary Results on SAS-2 Observations of > 3 MeV  
Gamma-Radiation
- G. G. FAZIO ✓ 7  
... Observations of High Energy Gamma-Rays
- D. J. FORREST ✓ 8  
E. L. CHUPP  
A. N. SURI  
C. REPPIN  
... Observations of Gamma-Rays in Solar Flares
- R. COWSIK ✓ 9  
... The Astrophysics of the Diffuse Background of X-rays and  
Gamma-Rays

- F. W. STECKER  
 . . . Mechanisms for the Production of the Diffuse Gamma-Ray Continuum Radiation ✓ 10
- V. L. GINZBURG  
 . . . Gamma-Ray Astronomy and Cosmic-Ray Origin Theory ✓ 11
- D. D. CLAYTON  
 . . . Prospects for Nuclear Gamma-Ray Line Astronomy ✓ 12
- A. W. STRONG  
 J. W DOWCZYK  
 A. W. WOLFENDALE  
 . . . Ultra-High Energy Gamma-Rays ✓ 13
- R. OMNES  
 . . . Matter-Antimatter Cosmology ✓ 14
- B. LEROY  
 J. P. NICOLLE  
 E. SCHATZMAN  
 . . . The Deuterium Puzzle in the Symmetric Universe ✓ 15
- J. L. PUGET  
 . . . The Gamma-Ray Background Spectrum and Annihilation Rate in the Baryon Symmetric Big-Bang Cosmology ✓ 16
- F. W. STECKER  
 J. L. PUGET  
 . . . Distortion of the Microwave Blackbody Background Radiation Implied by the Baryon Symmetric Cosmology of Omnes and the Galaxy Formation Theory of Stecker and Puget ✓ 17
- G. STEIGMAN  
 . . . Antimatter in the Universe? ✓ 18

173-28754

DIFFUSE COSMIC X-RAYS BELOW 1 KeV

William L. Kraushaar  
Department of Physics  
University of Wisconsin  
Madison, Wisconsin

Prepared for "International Symposium on Cosmic Gamma Rays", Goddard  
Space Flight Center, Greenbelt, Maryland, April 30 - May 2, 1973

Supported in part by NASA grant NGL 50-002-044

The study of diffuse X-rays in the energy region below 1 KeV has had a somewhat rocky past and has suffered from having attracted cosmological interest early in its young life. Much of the available data and interpretation can be found in recent review articles by Silk (1973), Felten (1972), Field (1972) and Kato (1972). In this short review I cannot discuss all the measurements or all the ideas that have been put forward. I will, therefore, restrict my discussion to a description of those features of the low energy diffuse flux on which there is general observational agreement and to some interpretive matters which I believe have been overlooked or at least underemphasized. Also, most of the discussion will be restricted to the energy region below 280 eV, the Carbon K edge.

### I. Intensity

The soft X-ray diffuse intensity is everywhere convincingly larger than would be expected from an extrapolation of the high energy isotropic, unabsorbed and almost certainly extragalactic power law spectrum. Data in support of this conclusion are shown in Figures 1 and 2, taken from papers by the Wisconsin (Bunner et al., 1971) and NRL (Davidsen et al., 1972) groups. The solid curves in both figures are the predicted proportional counter response given only the high energy power law spectrum, with no interstellar absorption, as an input spectrum. The prominent bumps in these curves result from the X-ray transmission edges of the counter windows. The intensity ratio, pole to plane, is about 3 to 1 and while there can be some argument about a possible extragalactic contribution to the high latitude intensity, the plane intensity must be of relatively local origin because the column density for unit optical depth is only  $2.5 \times 10^{20}$  atoms/cm<sup>2</sup> or about 200 pc (with  $n = 0.4$  atoms/cm<sup>3</sup>) in these directions.

## II. Spatial Structure

The soft X-ray intensity shows three broad classes of spatial structure.

First, there is the gross tendency for the intensity to be small in the galactic plane and enhanced by perhaps a factor 3 at high northern galactic latitudes. This is shown in Figures 3 and 4, surveys of the NRL (Davidsen et al., 1972) and Wisconsin (Bunner et al., 1972), (Williamson, F. W., 1973), (Sanders, W., 1973) groups. The polar enhancement is more obvious in the north than in the south, although there are some isolated line scans that make the case for apparent enhancement in the south more convincing (Bunner et al., 1969, 1971), (Garmire and Riegler, 1972).

Next, the soft X-ray intensity is by no means just a simple function of galactic latitude, nor is it correlated, except the grossest sense, with the column density of interstellar hydrogen gas. There are large high intensity spatial features. None of these features except the North Polar Spur appear to correlate well with other astrophysical phenomena. Figure 5, taken from part of the Wisconsin survey (Bunner et al., 1972) shows soft X-ray counting rate versus time along the scan path, plotted together with estimated expected transmission. The bands on the time axes coincide with the North Polar Radio Spur and approximately, it is seen, with regions of enhanced X-ray intensity. Notice that there is little if any detailed correlation of X-ray intensity with gas transmission. This, together with the observed large intensity in the galactic plane, is strong evidence that much of the soft X-ray emission originates within the bounds of the galaxy's interstellar gas.

Third, there are at least three soft X-ray emitting regions of small angular extent, Puppis-A and Vela X (Palmieri et al., 1971) (Grader et al., 1970) and the Cygnus Loop (Seward et al., 1971). Three others have been

reported, but to date have not been confirmed. The three confirmed sources are all supernova remnants, are at small galactic latitudes and are of a class not numerous enough to account for the entire diffuse background. Of course, one or a few nearby remnants would be of large angular extent and confuse our whole picture. But galactic loop structures, aside from the North Polar Spur, do not appear to be strong soft X-ray emitters. Incidentally, the observation of soft X-ray emission from near the North Polar Spur has not been confirmed by others. Only one other observation near the Spur has been reported, but the sensitivity level is not clear (Hayakawa et al., 1972).

III. Nature of the Local Emission

The nature of the local emission remains a mystery. Particularly puzzling is the relative constancy of the intensity in the galactic plane. Near  $l^{II} = 240^\circ$ , for example, OAO-Lyman- $\alpha$  observations (Savage and Jenkins, 1972) show there to be very small gas column densities out to several hundred parsecs. Similarly the 21 cm emission profiles in this region show little or no low-velocity gas. Yet the soft X-ray intensity near  $l^{II} = 240^\circ$  appears featureless. If the emission in the plane were from a more-or-less uniformly-distributed population of stars, the soft X-ray intensity, one would think, would be large where the local absorbing gas density is small. Early type stars, it is true, are relatively rare in this region.

Also puzzling is the relation between the soft X-ray intensities measured in the  $E < 180$  eV (Boron K edge filter) and  $E < 280$  eV (Carbon K edge filter) regions (Bunner et al., 1973). X-rays of  $E < 180$  eV are more strongly attenuated by absorbing material. Thus in Figure 6 I show the rates in the two types of detectors measured while the detectors were holding on a fixed high latitude point as the rocket emerged from the Earth's atmosphere. As expected the rates are not proportional to each other, but

the Boron filter rate changes more rapidly than the Carbon K filter rate. Yet when these two detectors scanned about the sky while free of atmospheric absorption, the two rates show no systematic tendency that would suggest that intensity variations are due to simple variation in amount of absorbing material between source and detector. Apparently emission irregularities dominate spatial absorption features. Sometimes variations in the Carbon K filter rates are accompanied by proportional variations in the Boron K filter rates. This behavior is to be expected if diffuse X-ray emission and absorption are in equilibrium along the line of sight, or if the emission is so local that there is little (or at least constant) absorption in different directions.

Lack of confirmed discrete point sources of soft X-rays (Bunner et al., 1969) and the apparent granularity of the spatial structure of the diffuse flux (Gorenstein and Tucker, 1972) suggest that if the source is stars of a special type, their local space density must be large,  $\geq 10^{-2} \text{ (pc)}^{-3}$  or more than 1 in 10 of all known stars.

In our first publication on this subject (Bunner et al., 1969), we suggested a population of stars with a scale height larger than that of the gas as a possible source of the soft diffuse X-rays. The model provides the enhanced intensity at high galactic latitudes, a source of the galactic plane emission and requires no extragalactic component. At energies between 0.5 and 1 KeV, however, the model predicts an enhanced intensity at intermediate galactic latitudes where absorption by the interstellar gas has not yet dominated the effect of increased path length through the emitting region. This enhanced intensity is not observed. The model has been discussed in more detail by several other authors (Gorenstein and Tucker, 1972), (Garmire and Riegler, 1972), (Davidsen et al., 1972), (Kato, 1972), (Hayakawa, 1972).

Emission by the interstellar gas itself would appear to provide a reasonable model for the origin of the diffuse X-rays in the galactic plane, for the absorption optical depth in the plane is large at whatever longitude. X-ray emission is a very inefficient process when compared with ionization, however, and the resulting heating of the cool interstellar medium, if the X-rays are produced in the gas, cannot be accommodated even if a suitable charged particle source is postulated ad hoc (Bunner et al., 1971). A multi-component interstellar medium requires further study as far as X-ray-emitting possibilities are concerned. Emission by the interstellar gas or by objects with the same spatial distribution as the gas, results in an intensity proportional to  $(1-e^{-\tau})$ , where  $\tau$  is the absorption optical depth. To match the observations, therefore, an extragalactic component is required and there results a net intensity proportional to  $A + Be^{-\tau}$ . This same form of the intensity dependence on  $\tau$  results from the assumption of extragalactic plus isotropic unabsorbed components, as discussed by Davidsen et al. (1972).

IV. Extragalactic Component?

Because of possible cosmological significance, there has been a persistent desire to have at least a large portion of the high latitude diffuse soft X-ray flux be interpreted as extragalactic in origin. The point is simply that the lack of red-shifted Lyman- $\alpha$  absorption in the spectra of quasars puts severe limits on the density of a possible intergalactic un-ionized gas. Hence, if the universe is closed, it is argued, the required mass must be in hot ionized gas since the observed average density of mass in the form of galaxies is small by a factor of about 60. Extragalactic soft X-rays would provide a possible indicator of this hot gas. Or, turning the argument around, a demonstrated lack of extragalactic soft

X-rays would put limits on the possible density and temperature of a postulated hot intergalactic medium (Field, 1972), (Field and Henry, 1964).

The observed X-ray intensity enhancement toward the galactic poles, where the gas density is small and expected X-ray transmission is large, suggests but by no means demonstrates an extragalactic origin. In the first place, the sources could be mingled with or just outside the galactic gas. In the second place, the correlation of intensity with expected gas transmission is poor. Of course, there are several possible causes for this poor correlation. Transmissions are deduced from 21 cm hydrogen emission measurements and helium, not hydrogen, is responsible for most of the soft X-ray absorption (Brown and Gould, 1970). There could be an unsuspected number of small unresolved cool clouds of gas and these would confuse both the column density measurement and X-ray transmission estimates. These rationalizations would be comforting if we had prior knowledge of extragalactic soft X-rays, and knew there to be no high latitude galactic emission. But the reverse logic provides a decidedly weak case (if any) for a hot intergalactic medium.

We hoped our search for absorption by the gas of the Small Magellanic Cloud would clarify these matters. Before making the observation we decided among ourselves that the most unsatisfactory result possible would be an X-ray intensity that was constant as we scanned across the SMC, for then neither emission nor absorption by the SMC would be clearly demonstrated. That, of course, is exactly what happened (McCammon et al., 1971) as shown in Figure 7.

Given this apparent lack of absorption the the SMC, we cannot exclude an extragalactic soft X-ray intensity,  $J_0$ , that is just compensated by emission from the cloud itself. The consequences of this assumption, however, are rather interesting. Let  $S$  be the X-ray emission rate per nucleon

of stellar matter in the SMC and  $n_s$  and  $n_g$  be the smoothed out or average nucleon density of stars and gas, respectively. Then if emission and absorption just compensate

$$J_0 \sigma n_g = S n_s$$

where  $\sigma$  is the X-ray absorption cross-section per hydrogen atom (Brown and Gould, 1970). The contribution to the extragalactic intensity from all galaxies out to a distance  $\sim \frac{c}{2H}$  is then

$$J_G \approx \frac{c}{2H} n_0 S$$

where  $n_0$  is the average density of galactic matter. According to Noonan (1971),  $\rho_0$  for  $H = 50 \text{ km s}^{-1} \text{ Mpc}^{-1}$  is  $7.5 \times 10^{-32} \text{ g cm}^{-3}$  so  $n_0$  is  $\sim 4.2 \times 10^{-8} \text{ cm}^{-3}$ . We then have

$$\frac{J_G}{J_0} \approx \frac{c}{2H} n_0 \sigma \left( \frac{n_g}{n_s} \right)_{\text{SMC}}$$

In the SMC ( $n_g/n_s$ ) is about 0.5, so  $J_G/J_0$  is about 0.8. In short, if we attempt to save the hot intergalactic medium by supposing that the lack of absorption by the SMC results from self-emission, the entire or at least a large part of the supposed extragalactic soft X-ray intensity arise from the superposed emission from other galaxies. There is then little or no intensity left to be accounted for by the hot gas.

If instead we suppose the emission to be somehow proportional to the gas of the SMC and proportional to the gas in other galaxies too, with the same emissivity, the value of  $J_G/J_0$  is reduced by a factor of perhaps 10. This is because we estimate the ratio of gas mass to star mass in the SMC to be about 10 times that of other galaxies.

~~1173-2876~~

Figure 8 shows how the SMC measurement and measurements of the diffuse background radiation at higher X-ray energies restrict the temperature of a hot intergalactic gas. This is essentially Figure 1 of Field and Henry (1964), but a Hubble constant  $H_0 = 50 \text{ km sec}^{-1} \text{ Mpc}^{-1}$  has been assumed rather than 100. The density assumed is sufficient to just close the universe ( $\Omega=1$ ), the clumping factor ( $C = \overline{n^2}/\bar{n}^2$ ) is taken as 1, the integration is carried out only to  $Z=1$ , and the expansion is assumed to proceed with  $\gamma=5/3$ .

As pointed out by Field (1972) the measured intensities in a real universe with a given  $T_0$  must exceed those plotted. Because the SMC measurement falls so near the "Big Bang Envelope" line, it in fact (with  $H_0 = 50$ ) excludes very little -- only a band of temperatures near  $(2 \times 10^6)^\circ\text{K}$ . On the other hand, and this is the point I wish to emphasize, the diffuse soft X-ray measurements cannot, taken alone, be said to provide positive evidence for a hot dense intergalactic medium.

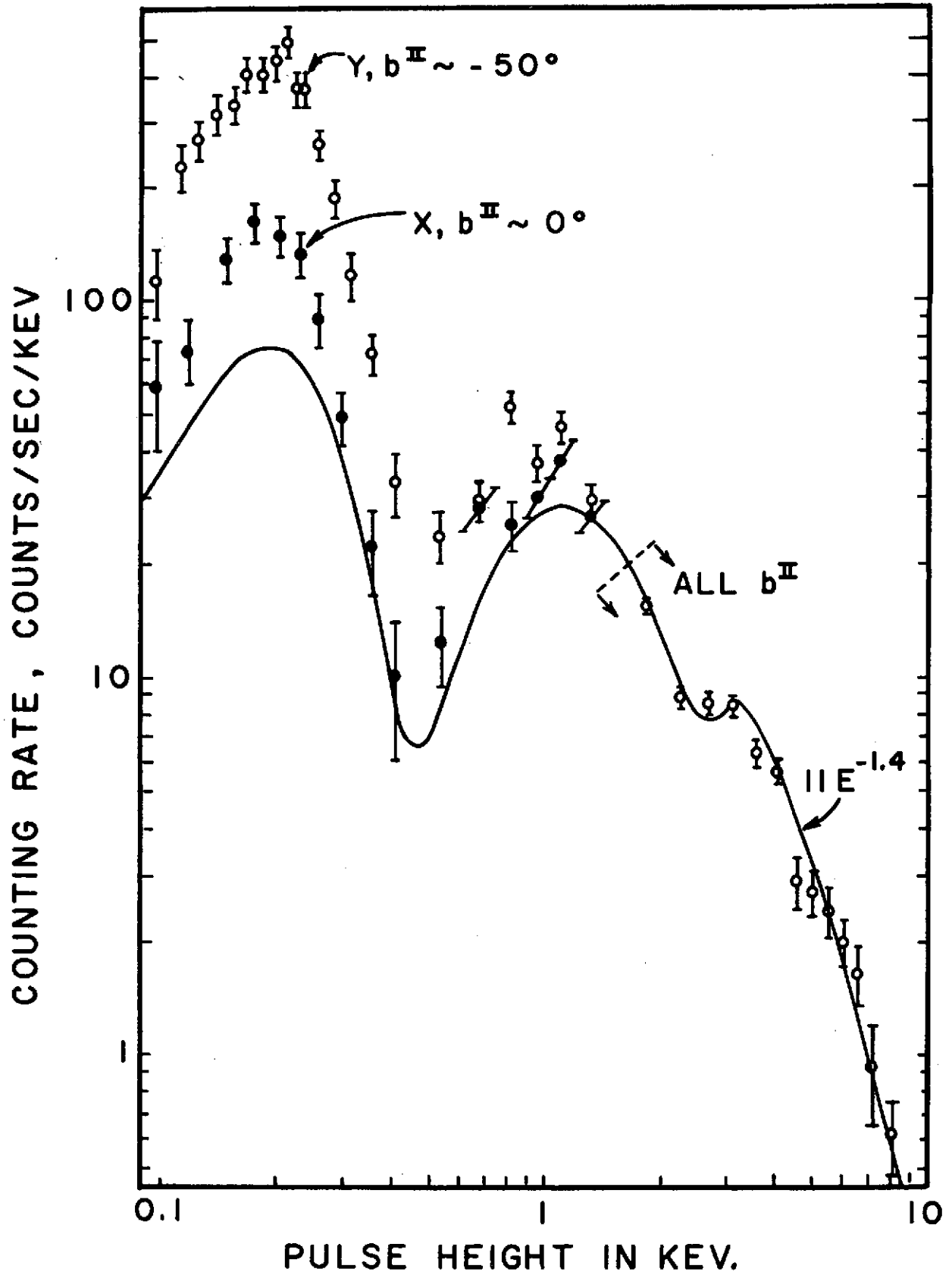
Figure Captions

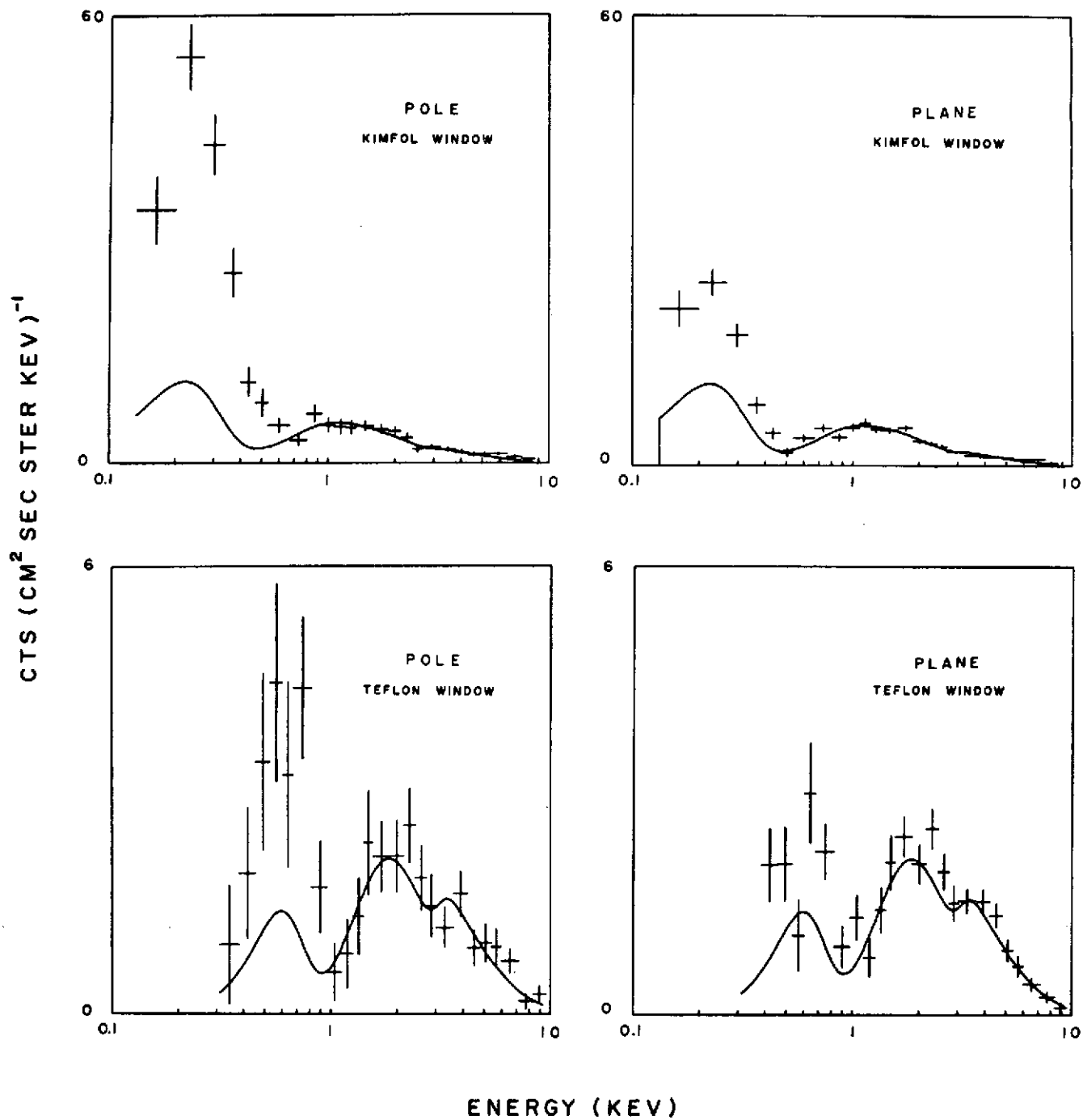
- Figure 1 Proportional counter pulse height spectra near the galactic plane and at a high galactic latitude. From Bunner et al. (1971).
- Figure 2 Pulse height data taken with Kimfol and Teflon counter windows. From Davidsen et al. (1972).
- Figure 3 Spatial distribution of X-rays of  $E < 280$  eV. The coordinate system is centered at the galactic anti-center. From Davidsen et al. (1972).
- Figure 4 Spatial distribution of X-rays of  $E < 280$  eV. The upper coordinate system is centered at the galactic center, while the lower coordinate system is centered at the galactic anti-center. From Bunner et al. (1972), Williamson (1973) and Sanders (1973).
- Figure 5 Counting rate of soft X-rays and X-ray transmission vs. time along the scan path. Data from Bunner et al. (1972).
- Figure 6 Counting rate of  $E < 180$  eV X-rays vs. rate of  $E < 280$  eV X-rays. Data from Bunner et al. (1973).
- Figure 7 X-ray counting rate of X-rays ( $E < 280$  eV) in directions near the Small Magellanic Cloud. Solid calculated curves assume in A: absorption by galactic and SMC gas; B: absorption by SMC gas only; C: absorption by galactic gas only; and D: extrapolated power law spectrum extragalactic; rest of local origin. From McCammon et al. (1971).
- Figure 8 Predicted X-ray intensities from a hot intergalactic medium with density sufficient to close the universe. From Field and Henry (1964).

References

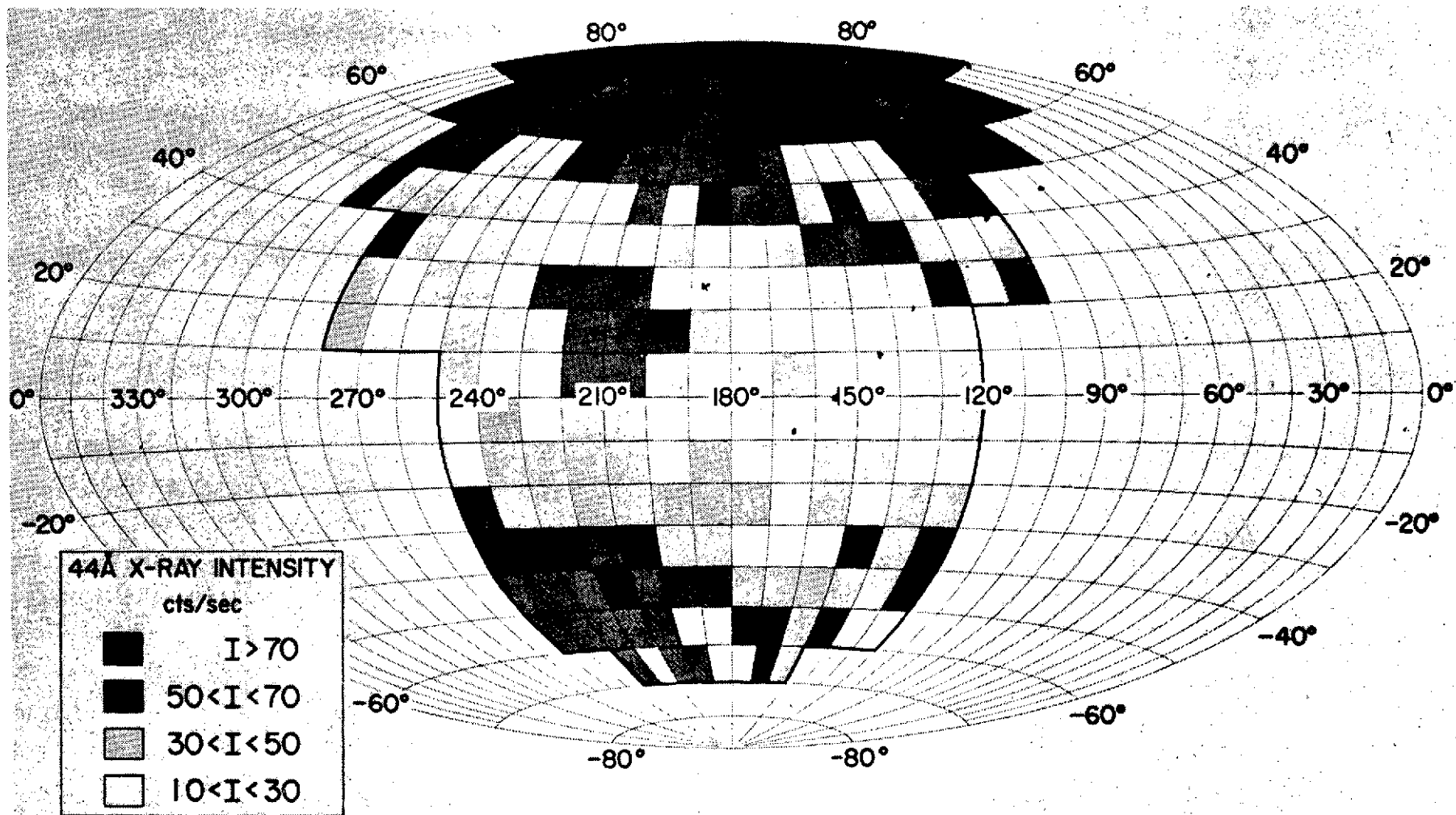
1. Brown, R. and Gould, R. 1970, Phys. Rev. D. 1, 2252.
2. Bunner, A., Coleman, P., Kraushaar, W., McCammon, D., Palmieri, T., Shilepsky, A. and Ulmer, M. 1969, Nature 223, 1222.
3. Bunner, A., Coleman, P., Kraushaar, W. and McCammon, D. 1971, Ap. J. Letters 167, L3.
4. Bunner, A., Coleman, P., Kraushaar, W., and McCammon, D. 1972, Ap. J. Letters 172, L67.
5. Bunner, A., Coleman, P., Kraushaar, W., McCammon, D. and Williamson, F. 1973, Ap. J. 179, 781.
6. Davidsen, A., Shulman, S., Fritz, G., Meekins, R., Henry, R. and Friedman, H. 1972, Ap. J. 177, 629.
7. Felten, J. E. 1972, I.A.U. Symposium #55, Madrid.
8. Field, G. B. and Henry R. C. 1964, Ap. J. 140, 1002.
9. Field, G. 1972, Annual Review of Astronomy and Astrophysics 10, 227.
10. Garmire, G. and Riegler, G. 1972, Astronomy and Astrophysics 21, 131.
11. Gorenstein, P. and Tucker, W. 1972, Ap. J. 176, 333.
12. Hayakawa, S. 1972, preprint.
13. Grader, R., Hill, R. and Stoering, J. 1970, Ap. J. Letters 161, L45.
14. Hayakawa, S., Kato, T., Kohno, T., Nishimura, K., Tanaka, Y. and Yamashita, K. 1972, Astrophysics and Space Science 17,
15. Kato, T. 1972, Astrophysics and Space Science 16, 478.
16. McCammon, D., Bunner, A., Coleman, P. and Kraushaar, W. 1971, Ap. J. Letters 168, L33.
17. Noonan, T. W. 1971, Proc. Astron. Soc. Pacific 83, 31.
18. Palmieri, T., Burginyon, G., Grader, R., Hill, R., Seward, F. and Stoering, J. 1971, Ap. J. 169, 33.

- 19. Sanders, W. 1973, Unpublished Ph.D. thesis, University of Wisconsin, Madison.
- 20. Savage, B. D. and Jenkins, E. B. 1972, Ap. J. 172, 491.
- 21. Seward, F., Burginyon, G., Grader, R., Hill, R., Palmieri, T. and Stoering, J. 1971, Ap. J. 169, 515.
- 22. Silk, J. 1973, preprint.
- 23. Williamson, F. W. 1973, Unpublished Ph.D. thesis, University of Wisconsin, Madison.

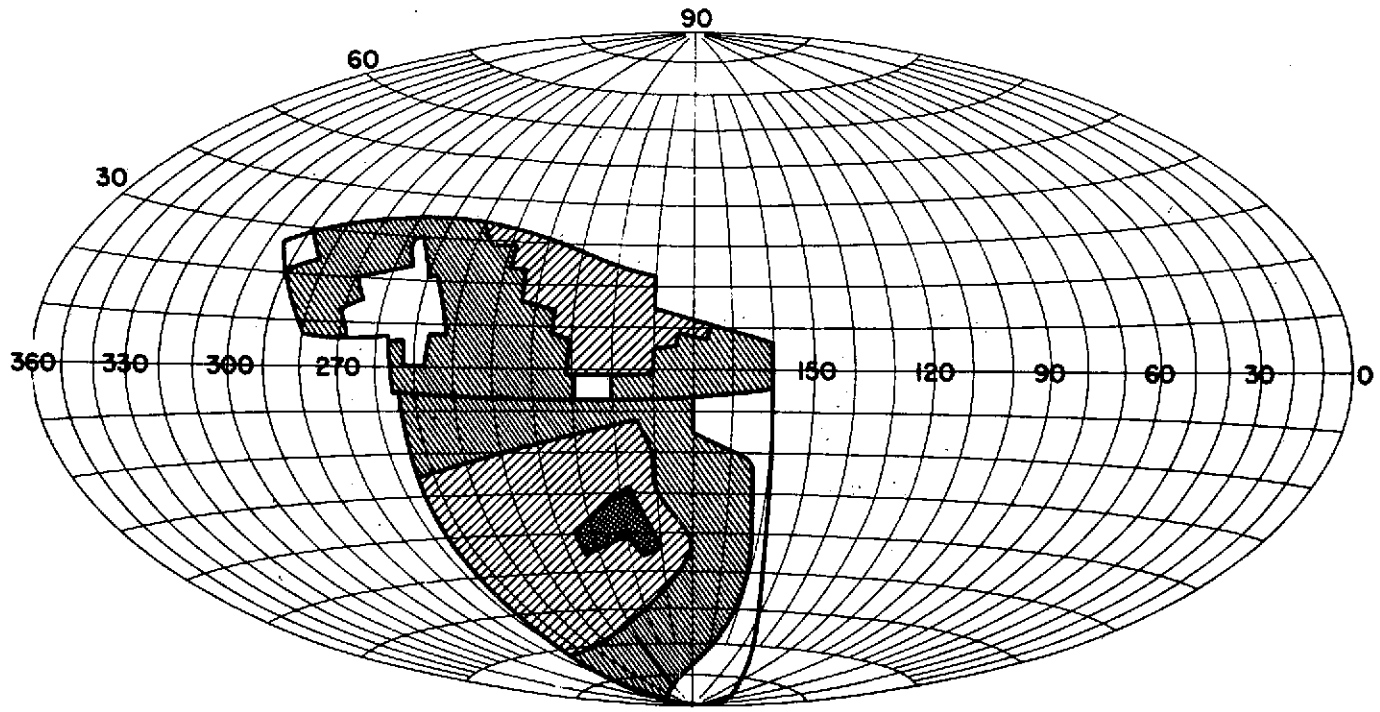
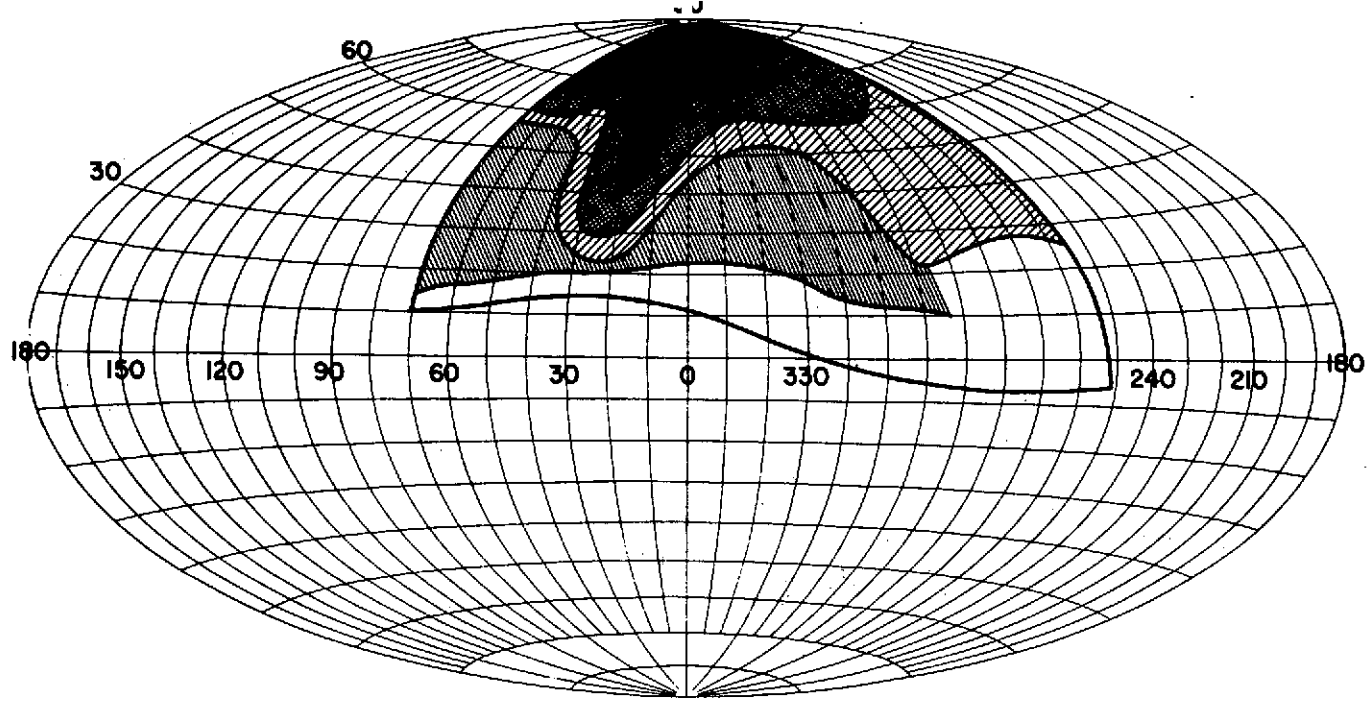


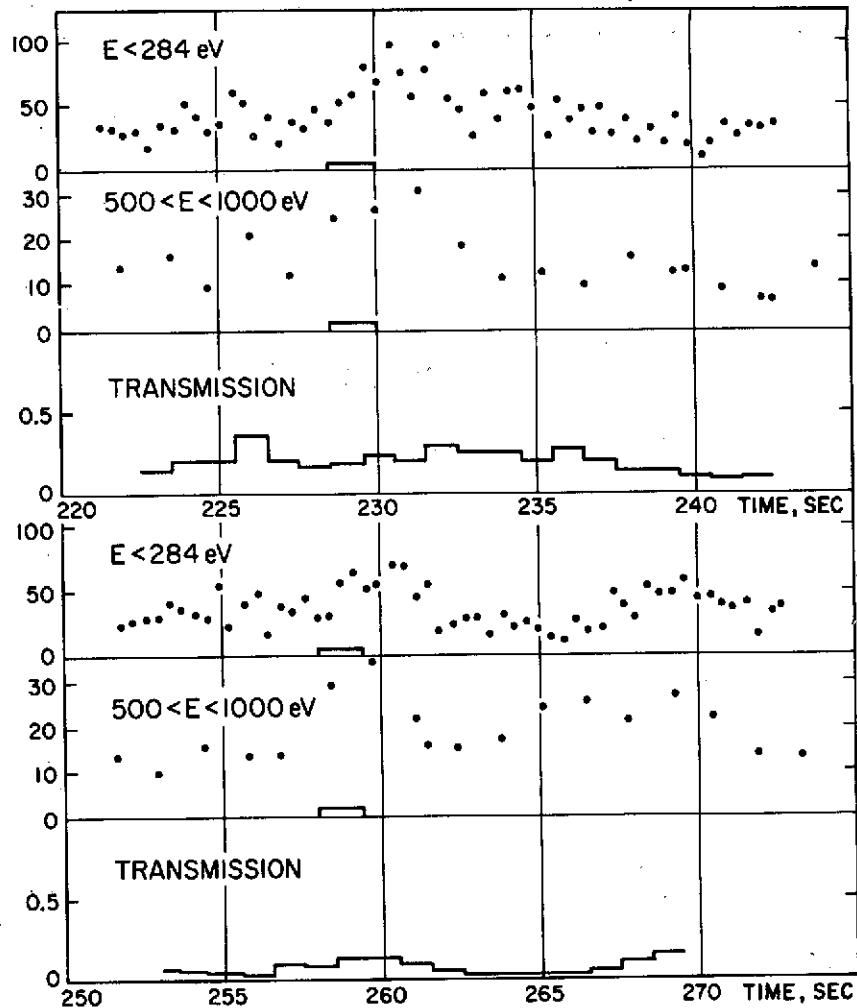
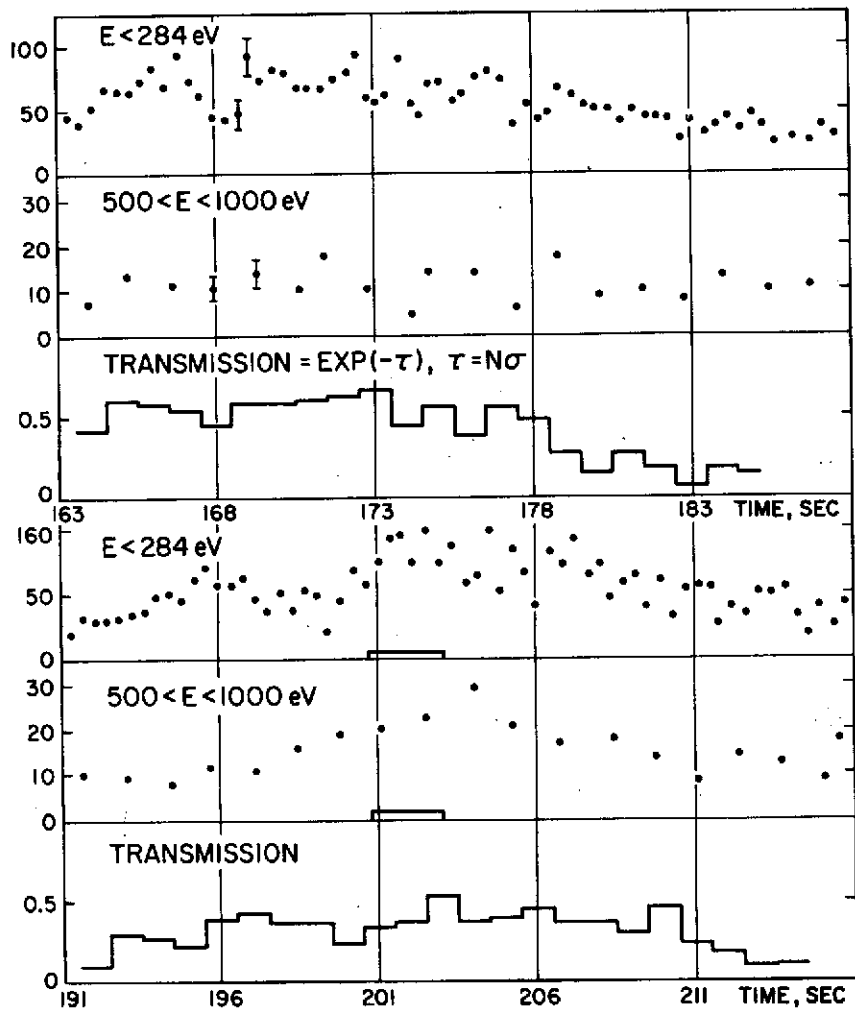


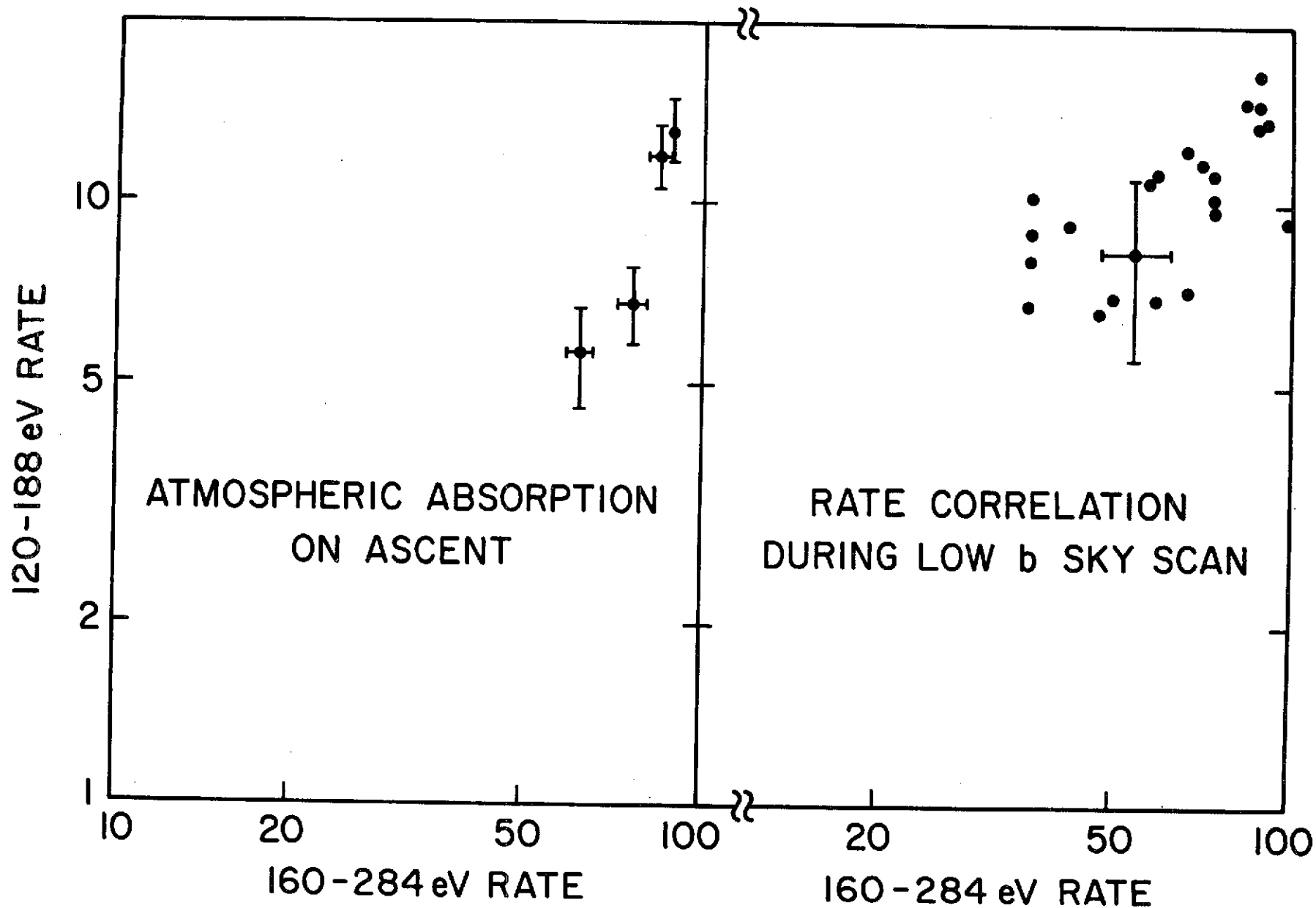
1/2

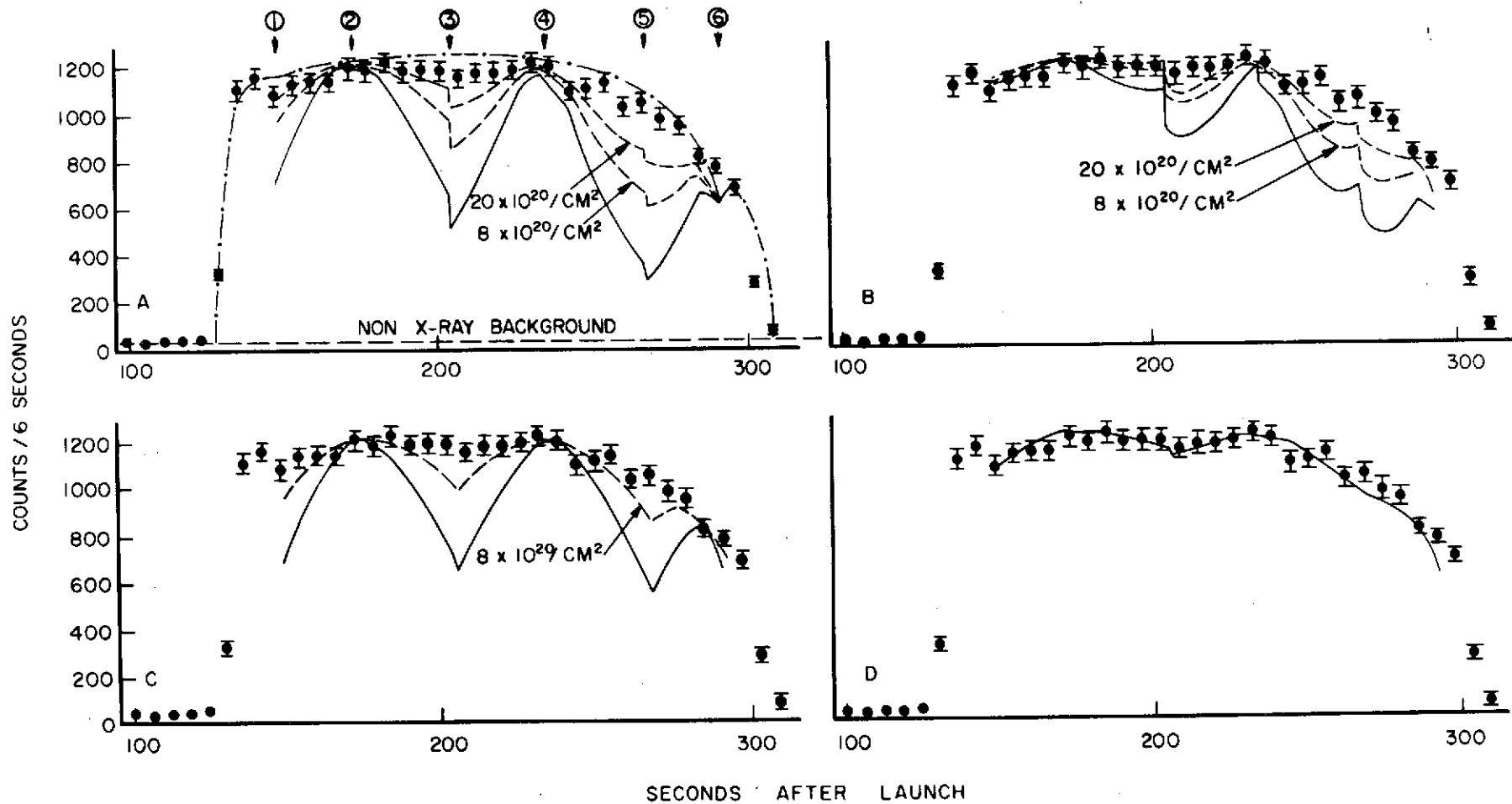


15

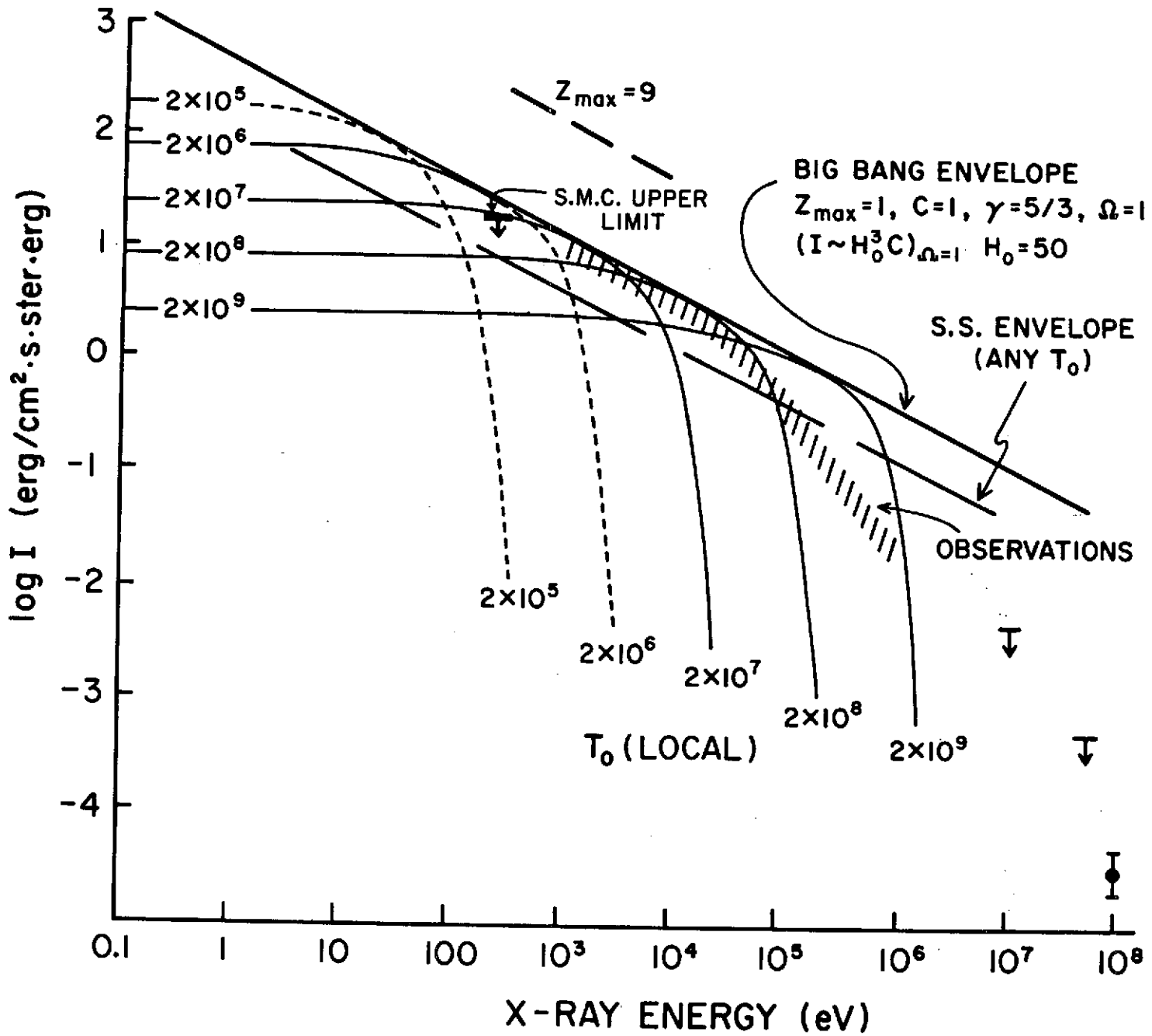








17



1  
N73-28755  
2

THE X-RAY EMISSIVITY OF THE  
UNIVERSE: 2-200 keV

Daniel Schwartz  
Herbert Gursky

American Science and Engineering, Inc.  
Cambridge, Massachusetts 02139

Invited Paper Presented at  
International Symposium and Workshop on Gamma-Ray Astrophysics  
NASA/Goddard Space Flight Center  
Greenbelt, Maryland  
1 May 1973

## I. INTRODUCTION

This paper will discuss observational results on the diffuse X-ray background between 2 and about 200 keV. Appropriately to the sponsorship of this symposium by the Laboratory for Theoretical Studies; we wish to present the results in a form suitable for theoretical discussion; namely, the volume emissivity function  $B(E)$  [ ergs/sec Mpc<sup>3</sup> keV emitted at energy  $E$  ]. The prescription for this is first to establish the spectral intensity  $I(E)$  [ ergs/sec cm<sup>2</sup> ster keV ] measured at the earth, second to subtract the contribution due to known, discrete sources, and third to unfold the equation

$$I(E) = \frac{1}{d\Omega} \int \frac{B(E) dV}{4\pi D^2} \quad (1)$$

which relates the measured intensity to the emissivity.

We may summarize the important characteristics of the diffuse X-ray background on which there is general agreement:

1. A real, cosmic X-ray background exists, which may be truly diffuse or merely composed of discrete sources not yet resolvable. Nothing in this paper will depend on which of those two pictures one adopts.
2. The diffuse X-rays are apparently isotropic over the sky, at least to an extent which precludes a galactic origin.

3. All detailed theories have difficulty accounting for the production of the measured energy into the diffuse spectrum, in the sense that they must hypothesize a rate of electron production, of heating, or of cosmological evolution which is not otherwise observed.

Strictly speaking these three characteristics apply only to the energy range between 2 and 40 keV where the isotropy over the entire sky has been established by the X-ray experiments aboard the Uhuru and OSO-III satellites.

## II. EXPERIMENTAL PROCEDURES

The measurement of the precise spectral flux density of an isotropic diffuse background is extremely difficult. The experimental problem is to determine, as a function of energy, what fraction of the instrumental output is due to internal background, whereby the term "internal" we mean the output which the instrument would have if no diffuse X-rays within the nominal bandwidth entered the aperture. Internal background is also called "non-X-ray background," although in fact X-rays leaking from outside the aperture, or higher energy X-rays which interact with only a partial energy loss both may contribute to internal background. Cosmic rays and geomagnetic particles are the primary ultimate sources of background.

Several basic techniques have been used for estimating internal

background:

1. The earth, assumed to emit no X-rays, has been used as a "shutter" and the entire instrument output obtained when the earth filled the field of view was assumed to be internal;
2. A physical shutter opaque to X-rays has been flown, which either was moved into and out of place over the aperture or else used to cover one of several identical detectors;
3. Different collimator solid angles have been flown, again either by motion of a shutter over one detector or fixed collimators over several identical detectors.

The satellite experiments have allowed an additional technique;

4. Observation of the modulation of the internal background as a function of varying geomagnetic conditions, whereby it can be separated from the constant isotropic X-rays.

By and large, all the above techniques are adequate to give what might be considered "first-order" accuracy by astrophysical standards (i. e., within 25% to 50% errors). However, the photon counting statistics formally imply a much higher precision: for a conservative example, a 200 second rocket flight might count diffuse X-rays at a rate of  $25 \text{ sec}^{-1}$ , and accumulate 5000 counts between 2 and 10 keV. With statistical errors of only a few percent, the following inadequacies of internal background estimation (numbered to correspond to the techniques listed above) become

apparent:

1. Below 10 keV the earth may sporadically emit X-rays due to auroral type events. Above about 30 keV the atmospheric albedo becomes comparable to the diffuse X-ray background.
2. X-rays may be generated by interactions in a mechanical shutter, and produce counts which would not be present when the aperture is open.
3. Data may be contaminated by diffuse geomagnetic electrons, which appear identical to diffuse X-rays. For example, an electron of about 70 keV will on the average penetrate a 1 mil Be window with a few keV residual energy. However, because straggling is a dominant effect for sub-relativistic electrons a wide bandwidth (say 50-100 keV) of incident electrons might be able to contribute counts in the few keV range. These electrons are time variable, either trapped or precipitating, and may occasionally be found even on the L=1 magnetic shell (Schwartz, 1969). Electron fluxes far smaller than are significant for geomagnetic studies, of the order of  $0.01 \text{ (cm}^2 \text{ sec ster keV)}^{-1}$  at 70 keV, can contribute a few percent of the diffuse X-ray counting rate. The existence of electrons of about 10 keV as a severe, sporadic contaminant to 1/4 keV X-rays has been well known (Hill et al., 1970); however, the effect at higher energies in any given rocket flight has generally been ignored.

4. A truly constant internal background component; for example, radioactivity within the detector or vehicle, will not be modulated as a function of geomagnetic conditions.

The reality of effects 1 and 3 as significant considerations for observations between 7 and 40 keV was first shown by the OSO-III experiment. Even when the internal background is measured perfectly accurately, it may simply change between the time it is estimated and the time when diffuse X-ray data is taken. Such changes may be due to motion of the vehicle in space, a change in orientation of the X-ray telescope axis relative to the earth's atmosphere or earth's magnetic field, a change in the configuration of matter around the detector, or temporal changes associated with geomagnetic activity. Table 1 summarizes these background considerations, along with the principal method used and the most likely source of remaining systematic error.

To stress the difficulty of the absolute measurement of a diffuse spectral density, we may digress to a familiar example from the study of the universal microwave background. In radio astronomy an absolute flux is usually presented as the equivalent Rayleigh-Jeans blackbody temperature. Figure 1 illustrates the derivation

of the microwave temperature at 3.2 cm by Roll and Wilkinson (1966). Briefly, that experiment used a Dicke-type radiometer which measured the difference between an antenna horn pointed at the sky, and a cold load maintained near liquid helium temperature. The top bar represents the measured cold load effective temperature. Each lower bar represents the result after applying the correction listed. The key feature here is that most of the corrections are of the same magnitude as the final result, and therefore must be known to the same precision desired for the microwave background. This experiment reported  $T = 3.0 \pm 0.5$  °K, where the error represents an estimate of systematic effects. This 0.5 °K error should be compared to a standard error of 0.06 °K which the authors derived due to the random errors in each correction term. In general, only such random errors are reported for measurements of the X-ray background.

The generalizations discussed above, and the examination of the data presented below, has led us to adopt the following point of view: Most measurements of the flux density at various energies are reliable -- they can be taken at face value with their quoted errors and compared with other results. However, direct measurements of a so-called "spectrum" by a single experiment are much less reliable or useful. The unreliability

results because the uncertain systematic errors invariably are a different function of the energy than the diffuse X-rays. Thus, one or a few data points at one end of the energy range covered by a given experiment systematically distort the overall spectrum, even if many other spectral points are quite accurate. The usefulness of a spectral parameter is minimal for the following reasons: first, information is lost by reporting a few spectral parameters instead of many flux density measurements at various energies; second, the non-linear least squares fits which must be used (due to the complicated spectral response of the typical detectors) do not necessarily give unbiased estimates of the spectral parameters; third, the procedure starts by assuming a general form for the spectrum, such as power law or exponential shape; finally, it is not obvious how to combine spectral parameters from two different experiments spanning slightly different energy ranges -- especially when each of those results has an estimated error which excludes the other. The spectral parameters which we will present below should be interpreted first of all as merely giving a numerical representation of all the data, although one should certainly discuss the physical interpretation of any spectral representation.

### III. Observational Results

Figure 2 presents a selection of published flux density points

9

for the diffuse X-rays between 2 and 200 keV. The plot gives the energy flux in  $\text{keV}/\text{keV cm}^2 \text{ sec ster}$ . Results reported only by giving spectral parameters are not included. Points with reported relative errors larger than 30%, and estimates of upper limits, are also excluded. In general, only the latest results of a given group are shown. Although the points with the smallest error bars tend to be hidden in such a plot, we can see that the bulk of the points do fall within a  $\pm 50\%$  error band, and therefore we may expect the precision of the mean to be still higher. The balloon-borne measurements shown here (except for Manchanda et al. 1972) do not contain additional so-called "Compton scattering" corrections, for reasons discussed below. The total data suggest a gradual steepening of the spectrum from a few keV up to 100 keV -- detailed analysis of several of the experiments confirms this conclusion.

a) Rocket-borne Observations

The key feature of rocket experiments is that they generally operate in the "cleanest" environment with regard to internal background. They are above the secondary cosmic radiation produced in the earth's atmosphere, and below trapped particle populations. (Sporadic electron precipitation events may still affect any one observation.) The major drawback is that the observation lasts at most a few minutes. This usually

does not allow, for example, a program which alternates measurements of diffuse and internal background to verify that the latter is constant.

Consider first the proportional counter observations shown in Figure 2 (LLL: Palmieri et al. 1971; ASE: Gorenstein et al. 1969; GSFC: Boldt et al. 1969; PRL: Prakasarao et al. 1971). In this energy range, 2 to 10 keV, shielding and collimation is easily done with passive structural elements. The fields of view used range from 20 square degrees in the LLL experiment (shown as the eight largest diamonds between 2.4 and 8.7 keV) to 500 square degrees by GSFC. The PRL measurement was carried out at the geomagnetic equator, the GSFC and ASE flights from White Sands occurred at a magnetic shell of approximately  $L = 1.7$  to  $1.8$ . The PRL counters were filled with a xenon/methane mixture, the others with an argon/methane. ASE and LLL determined internal background with a rocket door closed, PRL while looking at the earth, and GSFC by having a movable shutter which gave five different solid angles between 0.125 and 0.17 ster as well as a completely occulted position.

Agreement among the various experiments is rather good.

This may be expected, since proportional counters generally have several hundred  $\text{cm}^2$  areas, and since the X-ray flux

is constantly increasing to the lowest energies. The signal to background ratios obtained were between 3 and 10 to one.

We have omitted two results which suggested spectral line features in the background around 5 and 7 keV (Ducros et al. 1970; Henry et al. 1971). Boldt et al. (1971) have reported an upper limit for such a feature at 7 keV of a factor of ten below the NRL result. This applies to an observation at galactic latitudes from  $+40^{\circ}$  to the North Pole. It is probably fair to say that with the difficulties of establishing a continuum shape accurately, the existence of line fluxes remains to be proven in future experiments. We may comment that the unfolding of spectral data from a proportional counter response is by no means trivial. Such unfolding basically depends on calculation rather than calibration, since both the X-ray and particle spectra in space are very different than in the laboratory.

The proportional counter measurements may be compared with a satellite experiment of LLL (Cunningham et al. 1970; three small diamonds at 4.6, 8, and 12 keV). This involved a NaI crystal with a  $0.76 \text{ cm}^2$  ster telescope factor aboard a

polar orbiting satellite. A mechanical shutter periodically occulted the detector to allow background estimates. Only about 15 minutes of data (apart from solar and discrete source observations) was taken before a failure during the second day of operations.

The results of LLL (intermediate sized diamonds: Toor et al. 1970) and Bologna (Horstman - Moretti et al. 1971) were obtained with rocket-borne NaI counters. These detectors employed passive shielding lined with a plastic anti-coincidence scintillator to define fields of view of about 900 square degrees. The Livermore data are noteworthy because this was the only experiment other than OSO-III to span a range from below 10 keV to above 40 keV. The spectral results were reported as allowing a power law fit, however, the error bars above 30 keV are clearly large enough to be also consistent with a considerable change in slope.

The four data points of the Bologna group (a measurement of  $0.62 \pm 0.04$  at 52 keV is blacked out by other data points) are obtained with an ideal technique: one of four identical detector units is blocked so that internal background measurements are continually taken along with the diffuse X-ray data. Again, we suggest contamination by a sporadic

electron population as the cause of the apparently high points at 90 and 150 keV. This is not an unlikely occurrence at the invariant magnetic latitude of  $38^{\circ}$  ( $L = 1.6$ ) of this observation. The 0.2 mm ( $54 \text{ mg/cm}^2$ ) Al window would allow electrons of roughly 100 - 400 keV initial energy to enter the NaI volume with 50 - 200 keV residual energy, considering straggling. The OSO-III upper limit of  $0.18 \text{ keV}(\text{keV cm}^2 \text{ sec ster})$  at 150 keV, not shown in Figure 2, cannot otherwise be reconciled with this data.

b) Balloon-borne Observations

The dominant feature of the balloon-borne observations is that there exists a significant, diffuse flux of X-rays produced in the atmosphere. These must be separated from the diffuse cosmic X-rays by some indirect line of reasoning. Figure 3 schematically illustrates the observational situation. The top solid curve is the counting rate which a vertically pointed telescope of cone-angle  $9^{\circ}$  to  $20^{\circ}$  (as used in the four experiments plotted on the previous graph) might record as a function of atmospheric depth. The lower solid curve is that which a shuttered detector might record, and is the "internal" background defined earlier. Only

the Leiden-Nagoya group actually used such a shutter, the others effectively lumped internal background along with atmospheric.

At depths below 10 to 20 gm/cm<sup>2</sup>, the difference in the two curves is due entirely to the atmospheric X-rays. (We intend the Figure to show that the atmospheric X-rays may have a different, although similar, dependence on depth compared to the internal background.) Both the internal and atmospheric background originate from the soft component of the energy degradation of the primary cosmic rays, and show the Pfozter transition maximum at about 90 gm/cm<sup>2</sup>.

The turn-up of the rates at altitudes higher than about 10 gm/cm<sup>2</sup> is interpreted as the observation of X-rays external to the atmosphere. X-rays of 30 keV have a mean free path of 3.4 gm/cm<sup>2</sup> for photoelectric absorption, compared to ceiling depths of 3 to 7 gm/cm<sup>2</sup> attained in the various experiments. The dashed curve represents an extrapolation which each experimenter must make for the assumed behavior of the atmospheric X-rays. The difference ( $R_1 - R_2$ ) is then multiplied by the photoelectric attenuation at the given ceiling depth (which may be a factor of 2 to 8 correction) to derive the diffuse flux external to the atmosphere.

There has been some discussion (e.g., Horstman and Horstman-Moretti 1971) that additional corrections need be applied due to single and multiple scattering of diffuse X-rays by the atmosphere, which eventually enter the detector aperture. This discussion is important and valuable since such a physical process must certainly take place. However, it is not appropriate to apply such a correction to  $(R_1 - R_2)$  for the following simple reason: once the diffuse X-ray scatters in the atmosphere it loses its identity, and is no different than an atmospheric X-ray which might be produced by electron bremsstrahlung at the exact same location. But all the atmospheric X-rays have presumably been accounted for by the dashed line extrapolation. One may well ask whether the dashed line is an accurate extrapolation of the atmospheric background, but this is a very different, and very important, problem.

In principle, one could study the difference between  $R_1$  and  $R_2$  as a function of depth, and test whether it changes in the exact manner expected for photoelectric absorption of X-rays external to the atmosphere. In practice this is not decisive because the points below float altitude are only sampled for a relatively brief time during ascent or descent. As  $(R_1 - R_2)$  becomes smaller, the absolute error on this difference becomes

larger and it may be that the data allows anything between zero and infinite absorption.

Strictly speaking, we might say that the true atmospheric X-ray curve could vary considerably from the intuitively simple extrapolations used, and that there might in fact be no diffuse X-rays at all. Returning to Figure 2, we can let the scatter of the data speak for itself in illustrating the intrinsic accuracy which has been obtained. The lowest and highest points, by the Tata Institute (Manchanda et al. 1972) and Saclay (Rothenflug et al. 1968) groups, used an exponential law extrapolation. The Leiden (Bleeker and Deerenberg, 1970) and Physical Research Laboratory (Rangan et al. 1969) groups used a power law extrapolation for the rates vs. depth. Each pair of groups spanned magnetic shells at least from  $L = 1$  to  $L = 1.7$ .

The detectors used in these experiments were all NaI crystals, with some combination of passive shield and plastic anti-coincidence. These give relatively high susceptibility to internal background. As the groups at UCSD, UCB, and MIT have developed detectors with lower internal background by using  $4\pi$  active-anticoincidence techniques, they have systematically tended to stop down

the solid angle and concentrate on discrete source observations.

We may suggest a prescription for obtaining a more objective determination of the atmospheric X-ray contribution at ceiling. This is based on the concept of a source function  $S(E, x)$  (X-rays of energy  $E$  produced  $(\text{cm}^3 \text{ sec})^{-1}$  at a depth  $x$ ). This technique has been used successfully by Peterson, Schwartz and Ling (1973) to interpret counting rates of atmospheric  $\gamma$ -rays as a function of depth. Figure 4 shows the basic geometry. The function  $S$  is strictly a convenient mathematical form, containing a few constants to be determined. With the detector in a fixed orientation at a depth  $h$ , the source function multiplied by the projected detector area  $A(\theta)$  and by the attenuation  $\exp(-\mu r)$  (where  $\mu$  is the total coefficient for any interaction) is integrated over all of space. The unknown constants in  $S$  should be determined while the detector is at large depths  $h$  and/or while it is oriented downward. Then with the detector pointed upward at the float altitude,  $C(E, h)$  would simply be calculated and subtracted from the total output. Physically, of course,  $S$  will contain a contribution from Compton-scattered diffuse X-rays; however, this need not ever be considered explicitly.

#### c) OSO-III Observations

Finally, we will discuss the data points obtained by the UCSD

X-ray telescope aboard OSO-III. These points were relatively inconspicuous in Figure 2 because of their small error bars; yet they are of significance as the only case in which a power law spectrum could not fit the data of one single experiment. Because of this significance, Schwartz and Peterson (1973) have reconsidered the results with regard to some suggested corrections for spallation induced radioactivity, fluorescence radiation from the shield, and energy dependence of the geometry factor, and we have confirmed the inconsistency of a power law with the OSO-III data. The best fit of a power law gives  $X^2 = 20$  for 3 degrees of freedom.

Briefly, the OSO-III experiment was a  $9.5 \text{ cm}^2$  NaI crystal, actively collimated by a CsI annulus to a  $23^\circ$  FWHM conical field of view. The satellite had a 550 km altitude,  $33^\circ$  inclination orbit so that magnetic shells from  $L = 1$  to  $L = 2$  were sampled, and the lower edge of the South Atlantic trapped particle region was traversed during half of the 16 orbits per day. The data was telemetered in 6 logarithmically spaced channels between 8 and 210 keV. Certain integrated and solar-pointing rates were also telemetered.

The most serious contributor to the background was the existence of sporadic, charged particles. Selection criteria

to minimize contamination were developed. These limited the upper threshold integral rate, required  $L \leq 1.2$ , and accepted data only when pointed within the local magnetic loss cone. This caused rejection of about 80 percent of the data.

The next most serious source of background was due to radioactivity which built up when inside the trapped particle regions, and which then decayed until the next traversal of the South Atlantic Anomaly. A 15-hour half life decay curve gave a good fit to the monitor count rates in the interval 30 minutes to 12 hours after penetrating the particle belts. The activation coefficients derived from these monitor rates were used to correct the diffuse counting rates, over the same time span. The diamonds and upper limit in Figure 5 (taken from Schwartz and Peterson, 1973) show the effective spectrum at the NaI detector, due to radioactivity. Phenomenologically, this spectrum is interpreted as Compton scattered  $\gamma$ -rays from the  $Mg^{24}$  daughter produced by the reaction

$$Al^{27} (n, \alpha) Na^{24} \xrightarrow{15 \text{ hour}} Mg^{24} \text{ taking place throughout}$$

the satellite. The solid line is a spallation spectrum measured by Dyer and Morfill (1971), and plotted with an arbitrary normalization. The horizontal bars integrate this spectrum over the OSO-III energy channels, and normalize it to be consistent with the 7.7 - 12.5 keV limit. Thus the spallation

mechanism is probably not significant on this time scale.

This radioactivity correction could be made because it varied on a 15 hour time scale. However, radioactivity with a half life of a week or longer would not decay significantly in one day, and might in principle be a constant, unnoticed contaminant of the data. By subtracting the rates when looking at the earth from the sky rates on day 44 after launch, we show that at least 95 to 90 percent of the reported diffuse flux for the three channels from 7.7 to 38 keV cannot be contaminated by radioactivity. The points between 38 to 110 keV might require further downward correction, but this will only accentuate the inability of a single power law to fit the data.

Examination of the detailed rates vs. time after launch in the 38 - 65 keV channel, compared with the predicted build-up curve using the proton dose by Dyer, Engel, and Quenby (1972) led us to conclude (Schwartz and Peterson 1973) that at most 1/3 of that proton dose would be the appropriate normalization. We have increased the error bars of the upper channels so that such a radioactivity correction (if valid) would only reduce the quoted fluxes by two sigma.

The most significant correction necessary to the previous OSO-III results have been the allowance for K-shell X-radiation escaping from inside of the collimator, as suggested

by Horstman (Dumas et al. 1972). Diffuse X-rays between 35 and a few hundred keV striking the inside of the CsI collimating annulus would not trigger the shield anti-coincidence threshold. A certain fraction of the resultant K-escape X-rays will be emitted into the central detector, causing a spurious contribution to the 22 - 38 keV channel. The Monte Carlo program of J. Matteson, which has been used extensively at UCSD to predict background rates of X-ray and  $\gamma$ -ray detectors, was used to calculate an effective telescope factor (solid angle times area) for such fluorescent X-ray events as a function of the incident photon energy above 34 keV. The product of this telescope factor and the diffuse spectrum  $2200 E^{-3}$  previously estimated (Schwartz et al. 1970) was integrated from 34 to 210 keV. As a result, the point at 30 keV was reduced 17 percent.

d) Summary

In Figure 6 we attempt to summarize the most reliable data selected according to the following criterion: The experiment either operated over a range of geomagnetic conditions, or else incorporated some direct means for assessing effects of electron contamination. The Livermore rocket experiment (Palmieri et al 1971) had a methane-filled anti-coincidence

proportional counter over the entrance to their argon detector. This experiment of all the rocket and satellite observations should be uniquely free of charged particle contamination. The ASE experiment (Gorenstein et al. 1969) incorporated pulse shape discrimination, which is sensitive to relativistic electrons which may deposit only a few keV total energy but spread out over a long path. That experiment also had one counter unit with a 1 mil Be window and three counter units with 3 mil Be windows. These windows would show very different transfer characteristics for the 70 - 100 keV geomagnetic electrons.

The three experiments of the Leiden - Nagoya group (Bleeker and Deerenberg, 1970) provide key evidence for the reality of a diffuse component above 40 keV. The experiments took place at  $20^\circ$ ,  $40^\circ$ , and  $50^\circ$  geomagnetic latitudes. The flux densities at the various latitudes are in reasonable agreement, while the inferred component of 20 - 40 keV atmospheric X-rays is a factor 5 higher at the northern latitude.

The solid curve shows the function

$$I(E) \left[ \text{keV/keV cm}^2 \text{ ster sec} \right] = \begin{cases} 10E^{-0.52} & \text{for } 1 \leq E \leq 23 \text{ keV} \\ 140E^{-1.37} & \text{for } E > 23 \text{ keV,} \end{cases} \quad (2)$$

and the dashed curve is

$$I(E) = 3.3 \exp(-E/34.4), \text{ (c.f. Cowsik and Kobetich, 1972) (3)}$$

The sharp break in the power law representation does not have physical reality - this is merely a minimum parameter power law representation of the data. The key observational conclusion of such a representation is that the overall change in the slope is at least an exponent of 0.9. The errors in the power law indices are roughly  $\pm 0.1$  below 23 keV and  $\pm 0.15$  from 30 - 100 keV. The error in the effective kT of equation 3 is somewhat larger, as we have arbitrarily tried to fit the data only in the 10 - 100 keV range.

In Figure 7 we wish briefly to compare with the data from a few hundred ev to a few Mev. We have not attempted any completeness in the higher and lower energy data. The ASE point at 270 ev was obtained with a focusing collector, and is an upper limit in the sense that Gorenstein and Tucker (1972) argue it might all result from galactic sources. The Wisconsin upper limit is based on the absence of absorption by the Small Magellanic Cloud (McCammon et al, 1970). The Ranger 3 data (Metzger et al, 1964) represent only an energy-loss count rate spectrum, while the Apollo 15 data (Trombka et al, 1972) have been unfolded to a photon spectrum, and corrected for spallation

induced radioactivity.

#### IV. THE EMISSIVITY FUNCTION

If we assume a constant emissivity  $B(E)$  per unit coordinate volume, through which we look a distance  $R_{\max}$ , then equation (1) becomes simply

$$I(\bar{E}) = \frac{1}{4\pi} B(E) R_{\max} \quad (4)$$

Equation (4) holds, to within a factor of 2, for the popular models of Friedman cosmologies, providing there are no significant evolutionary effects, and providing that we take  $R_{\max} = \frac{1}{2} c/H_0$ . We will adopt  $H_0 = 75$  km/sec Mpc. Then from equation 2, we have

$$B(E) = \begin{cases} 2.1 \times 10^{-26} E^{-0.52} \text{ keV}/(\text{cm}^3 \text{ sec keV}) & \text{for } E \leq 25 \text{ keV} \\ 2.9 \times 10^{-25} E^{-1.37} \text{ keV}/(\text{cm}^3 \text{ sec keV}) & \text{for } E \geq 25 \text{ keV}. \end{cases}$$

For the integrated emissivity between 2 and 7 keV,

$B = 2.2 \times 10^{39}$  ergs/sec Mpc<sup>3</sup>. We stress that  $B$  is determined directly from the observations, and subject to the qualifications above it will not change significantly. The redshift will preserve a power law shape.

#### V. CORRECTION FOR DISCRETE SOURCES

Characteristics of the classes of discrete extragalactic sources identified in the 2U catalog (Giacconi et al, 1972) are summarized in Table 2. In Figure 8 we illustrate how they modify

the emissivity function. We must stress that the spectra and total emissivities are very poorly determined for the cases where we only have 1 single object in the class: the Seyfert galaxy NGC 4151, the radio source CEN A, and the quasar 3C 273. We have normalized the total power of each source according to the quantity  $n_{\text{Oj}}$ , and represented its spectrum as the flat end of the range allowed by UHURU in order to obtain the closest agreement to the background shape. The solid curve is the power law representation presented earlier. The higher dashed curve represents the subtraction of the identified extragalactic sources. The bottom dashed curve represents a possible residual emissivity if we hypothesize that the unidentified high latitude sources are a new class of extragalactic object which produce  $1/2$  the background observed from 2 - 7 keV.

## VI. INTERPRETATION AS THERMAL BREMSSTRAHLUNG

Figure 9 replots the data on a semi-log scale. Correction for discrete sources allows the exponential fit to hold above 5 keV. The two solid curves (Field, 1972) are the temperature independent lower limits to radiation from a hot intergalactic plasma of sufficient density to close the universe. In the "Big Bang" model the gas is suddenly heated to a temperature  $T_{\text{O}}$  at an epoch  $z = 1$ , and cools adiabatically with an index  $\gamma = 5/3$ . Field uses a Hubble

constant  $H_0 = 50$  km/sec Mpc. The predicted spectrum is approximately exponential with e-folding energy  $k T_0$ , and would be tangent to the lower limit curve at  $E_0 = (0.57) k T_0$ . The observed radiation falls a factor of 2 below the minimum, and the discrepancy is worse if the intergalactic medium is not smooth.

The disagreement implies one or more of the following:

- 1) The density of intergalactic plasma is  $\sqrt{2}$  less than required for a closed universe, or  $n_0 = 2 \times 10^{-6}$  particle  $\text{cm}^{-3}$ ;
- 2) The Hubble constant is a factor  $\sqrt[3]{2}$  smaller, or  $H_0 = 40$  km/sec Mpc;
- 3) The temperature  $T_0 \leq 3 \times 10^7$  °K.

We hope we have not spent too much time discussing X-ray results at a  $\gamma$  - ray symposium. We have tried to make the point that the X-ray observations have a relatively high level of precision, and that we can start using them to do some interesting physics. We look for many more exciting results and new ideas to come as study of the spectrum and of the isotropy is extended into the MeV region.

## ACKNOWLEDGEMENTS

We acknowledge conversations with L. Peterson, C. Dyer, B. Dennis, and H. Horstman regarding interpretation of the OSO-III X-ray data.

We thank E. Kellogg and S. Murray for discussion of the Uhuru results on extragalactic sources. This research was supported by NASA contract NAS 8 - 27973.

TABLE I

## Internal Background

<u>Method of Deduction</u>	<u>Used by</u>	<u>Contaminant</u>	<u>Might Affect</u>
Earth Occultation	PRL	Albedo	Leiden, PRL, Tata, Saclay
Opaque Shutter	LLL, Bologna, ASE	Production in shutter	ASE, LLL
Variable Solid Angle	GSFC	Precipitating Electrons	GSFC, Bologna, OSO-III, ASE, PRL
Modulation with vehicle motion	OSO-III, Leiden, PRL, Tata, Saclay	Radioactivity	OSO-III, LLL (satellite)

28

TABLE 2

## Contribution of Discrete Sources to the X-Ray Background

<u>Source</u>	<u># in 2 U Catalog</u>	<u>Spectrum (kT, for 1-10 keV range)</u>	<u>Luminosity <math>\langle j \rangle \frac{\text{ergs}}{\text{sec}}</math></u>	<u>Density <math>n_k (\text{Mpc})^{-3}</math></u>	<u>Emissivity <math>B_k \frac{\text{ergs}}{\text{sec} (\text{Mpc})^3}</math></u>	<u>Fraction of Background <math>f</math></u>
Normal Galaxies	3	5 keV	$2 \times 10^{39}$	0.03	$6 \times 10^{37}$	0.027
Giant Radio Galaxies	1	10 - 15	$3 \times 10^{41}$	$3 \times 10^{-5}$	$9 \times 10^{36}$	0.004
Seyfert Galaxies	1	(1.5 - 6.5)	$10^{42}$	$3 \times 10^{-4}$	$3 \times 10^{38}$	0.14
Rich Clusters	5	5 - 8	$3 \times 10^{44}$	$2.5 \times 10^{-7}$	$7.5 \times 10^{37}$	0.034
QSO's	<u>1</u>	(4 - 15)	$3 \times 10^{45}$	$10^{-8}$	<u><math>3 \times 10^{37}</math></u>	<u>0.014</u>
Subtotal	11				$4.8 \times 10^{38}$	0.22
Observed Background		15 - 20			$2.2 \times 10^{39}$	1.0
Unidentified Sources	22	4 - 6	$5 \times 10^{43}$	$10^{-5}$	$5 \times 10^{38}$	0.25 ?

- Manchanda, R. K., Blswas, S., Agrawal, P.C., Gokhale, G.S., Iyengar, V.S., Kunte, P.K., and Sreekantan, B.V., 1972, Ap. and Space Sci., 15, 272.
- McCammon, D., Bunner, A.N., Coleman, P.L., Kraushaar, W.L. 1971, Ap. J. (Letters), 168, L 33.
- Metzger, A. E., Anderson, E. C., Van Dilla, M.A., and Arnold, J. R. 1964, Nature, 204, 766.
- Palmieri, T.M., Burginyon, G.A., Grader, R.J., Hill, R.W., Seward, F.D., and Stoering, J.P. 1971, Ap. J., 169, 33.
- Peterson, L. E., Schwartz, D. A., and Ling, J. C. 1973, J.G.R., (to be published).
- Prakasarao, A.S., Sharma, D. P., Jayanthi, U.B., and Rao, U.R. 1971, Ap. and Space Sci., 10, 150.
- Rangan, K.K., Bhavsar, P.D., and Nerurkar, N.W. 1969, J. Geophys. Res., 74, 5139.
- Roll, P. G. and Wilkinson, D. T. 1966, Phys. Rev. Lett., 16, 405.
- Rothenflug, R., Rocchia, R., Boclet, D., and Durouchoux, P. 1968, Space Res. VIII, 423.
- Schwartz, D. A. 1969, unpublished Ph.D., thesis, University of California at San Diego.
- Schwartz, D.A., Hudson, H.S., and Peterson, L.E. 1970, Ap. J., 162, 431.
- Schwartz, D.A., and Peterson, L.E. 1973, Ap. J., (to be submitted).
- Toor, A., Seward, F. D., Cathey, L. R., and Kunkel, W. E. 1970, Ap. J., 160, 209.
- Trombka, J. I., Metzger, A.E., Arnold, J. R., Matteson, J. L., Reedy, R.C., and Peterson, L. E. 1972, submitted to Ap. J. Letters.

## REFERENCES

- Bleeker, J.A.M., and Deerenberg, A.J.M., 1970, Ap. J., 159, 215.
- Boldt, E.A., Desai, U.D., Holt, S.S., and Serlemitsos, P.J. 1969, Nature, 224, 677.
- Boldt, E.A., Desai, U.D., Holt, S.S. and Serlemitsos, P.J. 1971, Ap. J. (Letters), 167, L 1.
- Cowsik, R., and Kobetich, E.J., Ap. J., 177, 585.
- Cunningham, C., Groves, D., Price, R., Rodrigues, R., Swift, C., and Mark, H. 1970, Ap. J., 160, 1177.
- Ducros, G., Ducros, R., Rocchia, R., and Tarrius, A., 1970, Astr. and Ap., 7, 162.
- Dumas, A., Horstman, H., Horstman-Moretti, E., and Brini, D. 1972, in IAU Symposium No. 55 on Non-Solar X-Ray and Gamma-Ray Astronomy, Madrid (to be published).
- Dyer, C.S., Engel, A.R., and Quenby, J. J. 1972, in IAU Symposium No. 55 on Non-Solar X-Ray and Gamma-Ray Astronomy, Madrid (to be published).
- Dyer, C.S., and Morfill, G. E., 1971, Ap. and Spac. Sci. 14, 243.
- Field, G. 1972, in Annual Review of Astronomy and Astrophysics, Volume 10, (Annual Reviews Inc.: Palo Alto), 227-260.
- Giacconi, R., Murray, S., Gursky, H., Kellogg, E., Schreier, E., and Tananbaum, H. 1972, Ap. J., 178, 281.
- Gorenstein, P., Kellogg, E.M., and Gursky, H. 1969, Ap. J. 156, 315.
- Gorenstein, P., and Tucker, W. 1972, Ap. J., 176, 333.
- Henry, R. C., Fritz, G., Meekins, J. C., Chubb, T., and Friedman, H. 1971, Ap. J. (Letters), 163, L 73.
- Hill, R. W., Grader, R., and Seward, F. D. 1970, J. Geophys. Res., 75, 7267.
- Horstman-Moretti, E., Fuligni, F., and Brini, D., 1971, Il Nuovo Cimento, 6 B, 68.
- Horstman, H. and Horstman-Moretti, E. 1971, Nature (Phys. Sci.), 229, 148.

## FIGURE CAPTIONS

- FIGURE 1 Derivation of the microwave temperature at 3.2 cm in the experiment of Roll and Wilkinson (1966). Several of the corrections have magnitude nearly equal to the final result of  $T = 3.0^{\circ}\text{K}$ . The random errors are an order of magnitude smaller than the estimated systematic effects.
- FIGURE 2 A selection of published energy flux measurements of the diffuse X-ray background. Results presented only by giving spectral parameters, and points with greater than 30 percent error estimates, are excluded. The data show a general consistency, with the high rate points around 10 keV and 150 keV possibly due to electron contamination. The slope increases with higher energy.
- FIGURE 3 Representation of the counting rates of a vertically mounted, wide-aperture telescope. Diffuse X-rays cause the turn-up of the "aperture open" curve. One must estimate the atmospheric contribution (dashed line) to deduce the diffuse intensity.
- FIGURE 4 Geometry for calculating the contribution of atmospheric X-rays to the counting rate  $C(E, h)$  of a detector at depth  $h$  (from Peterson et al, 1973). An empirical volume production rate function

$S(E, x)$  is constructed as a function of depth  $x$ . The integral over the volume of the atmosphere gives the contribution for a fixed detector orientation.

FIGURE 5

Diamonds and upper limit: Effective spectrum of radioactivity background observed by the OSO-III X-ray telescope immediately after emergence from the proton belts. Solid line: an effective spectrum due to spallation measured by Dyer and Morfill (1971) as the difference in CsI crystal output measured 86.5 minutes and 11.2 hours after irradiation. The normalization is arbitrary. Horizontal bars: The same spallation spectrum integrated over the OSO-III energy channels and normalized for consistency with the measured limit at 10 keV (from Schwartz and Peterson 1973).

FIGURE 6

An attempt to select the most reliable experimental data between 2 and 200 keV. The observations either utilized some direct means for assessing effects of electron contamination, or else operated over a range of geomagnetic conditions. The solid curve shows the power law  $10E^{-0.52}$  keV/(keV sec cm<sup>2</sup> ster) below 23 keV and  $140E^{-1.37}$  above 23 keV. The dashed line is the function  $3.3 \exp(-E/34.4)$ .

FIGURE 7

The data and power law fit of figure 6 is shown along with a sample of measurements at higher and lower energies. The Ranger 3 data are only an energy-loss spectrum, while for the Apollo results the true photon spectrum has been unfolded and a correction applied for spallation induced radioactivity.

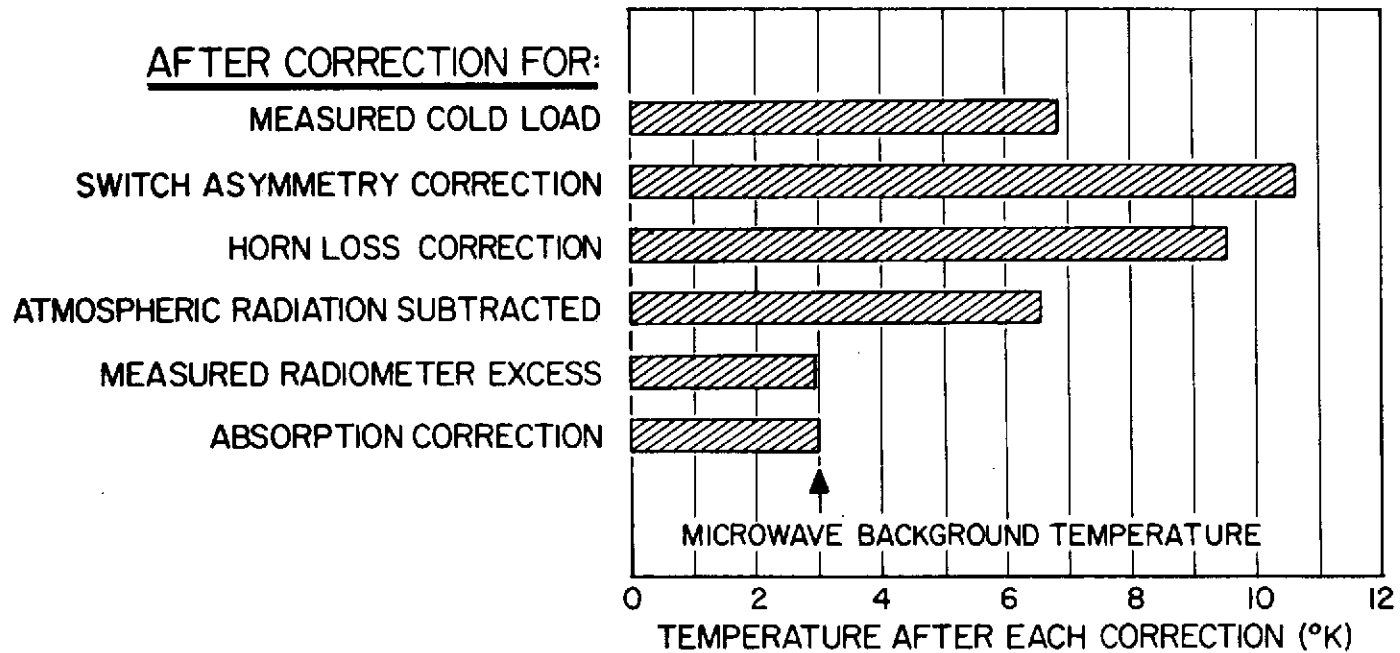
FIGURE 8

Volume emissivity functions. The top solid line shows the emissivity derived from the power law representation of figure 6. The five curves for identified extragalactic sources are derived from estimates of intrinsic luminosity and spectra based on the 2U catalog. The upper dashed curve corrects the diffuse emissivity for these sources. The lower dashed curve represents the resulting diffuse emissivity if we postulate that the unidentified high latitude sources (observed to have a spectrum with  $kT = 5$  keV) comprise 50 percent of the 2 - 7 keV diffuse background. The points at 20 keV are from UCB, and the UCSD OSO-7 experiment.

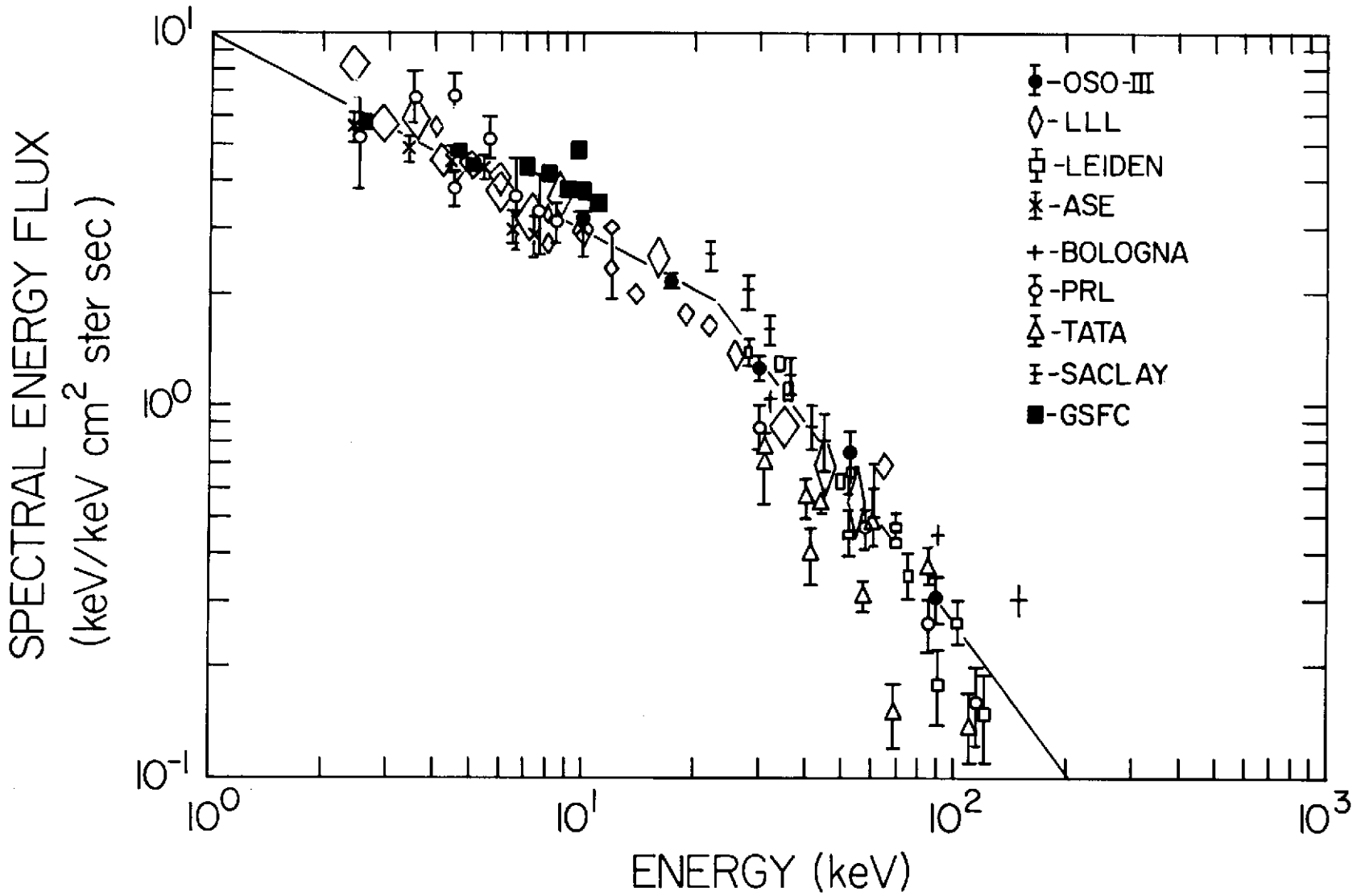
FIGURE 9

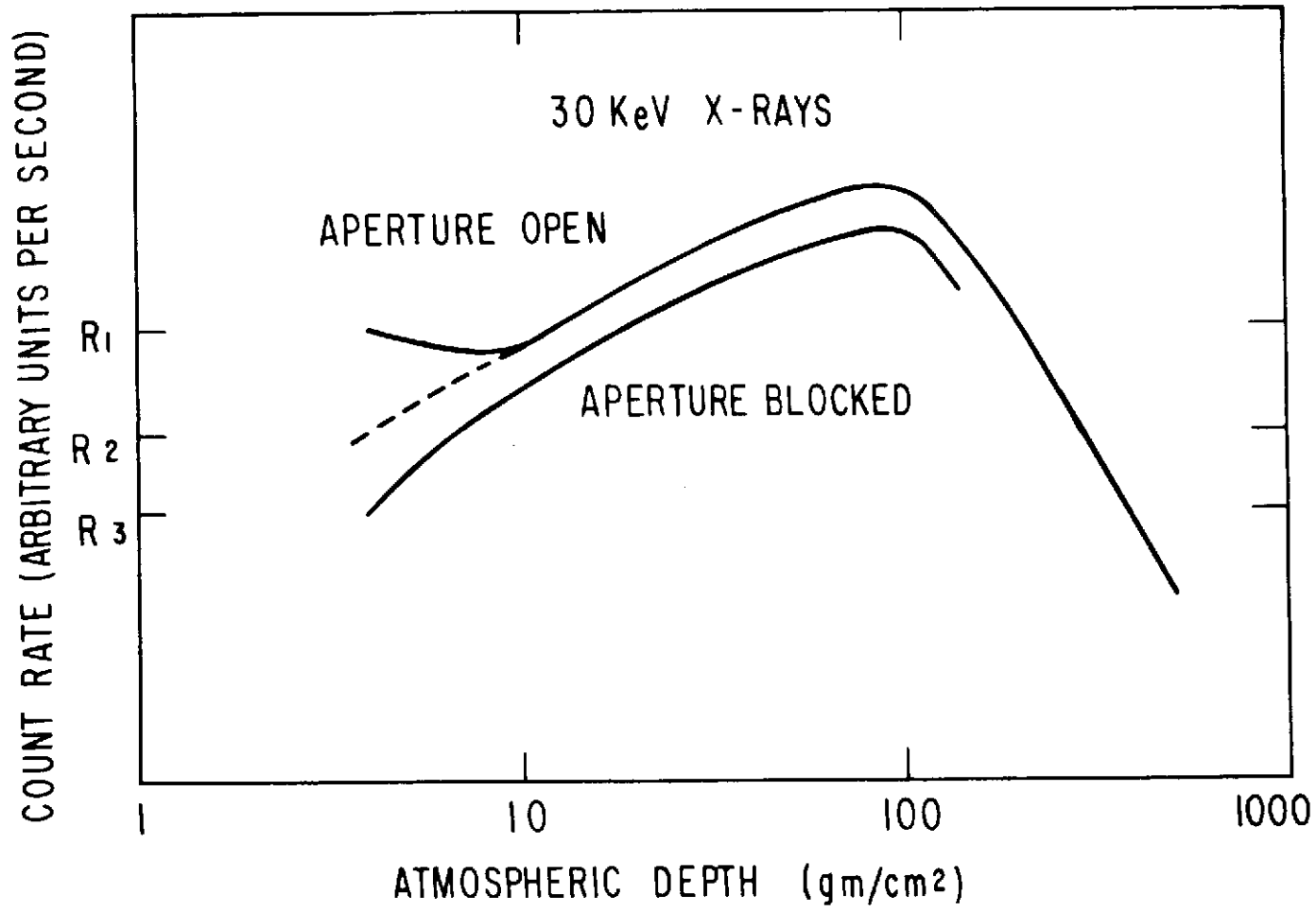
The data from figure 6 are plotted on a semi-log scale. The dashed line is the function  $3.3 \exp(-E/34.4)$ . The solid lines are "lower limits" to the emission from a hot intergalactic plasma of sufficient density to

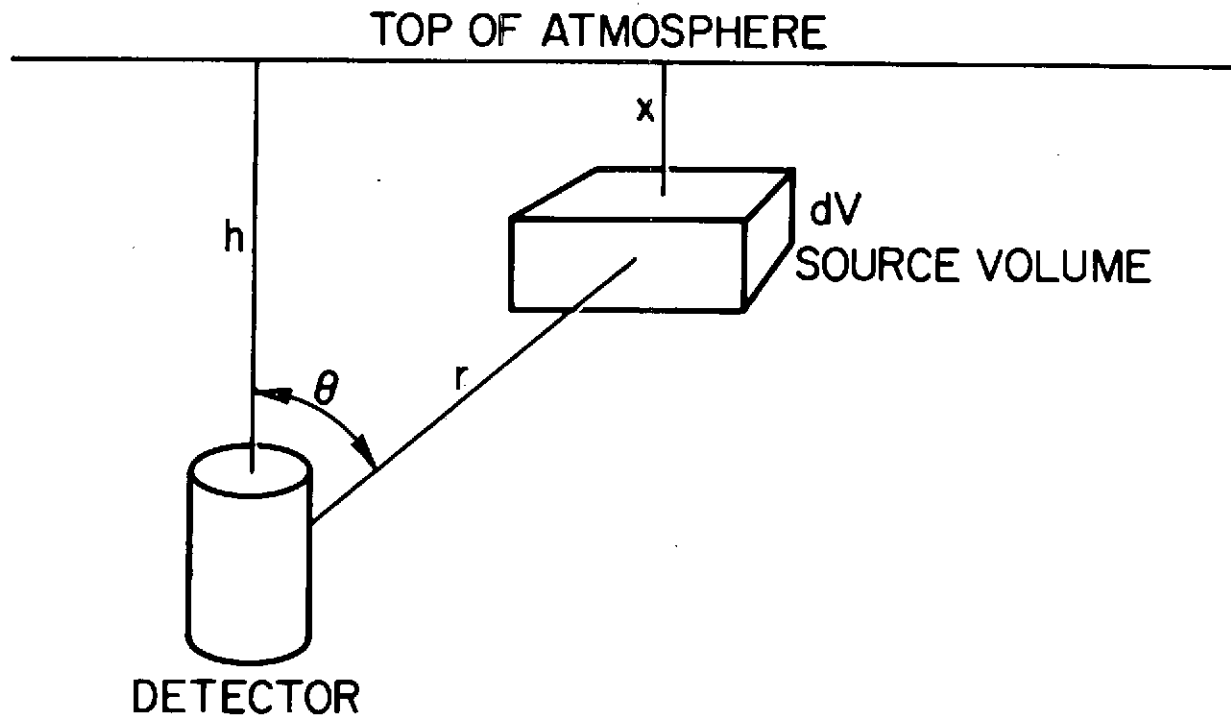
close the universe calculated by Field (1972) with a Hubble constant  $H_0 = 50 \text{ km/sec Mpc}^3$ . The X-ray observations are at least a factor of two discordant with the Big Bang model.



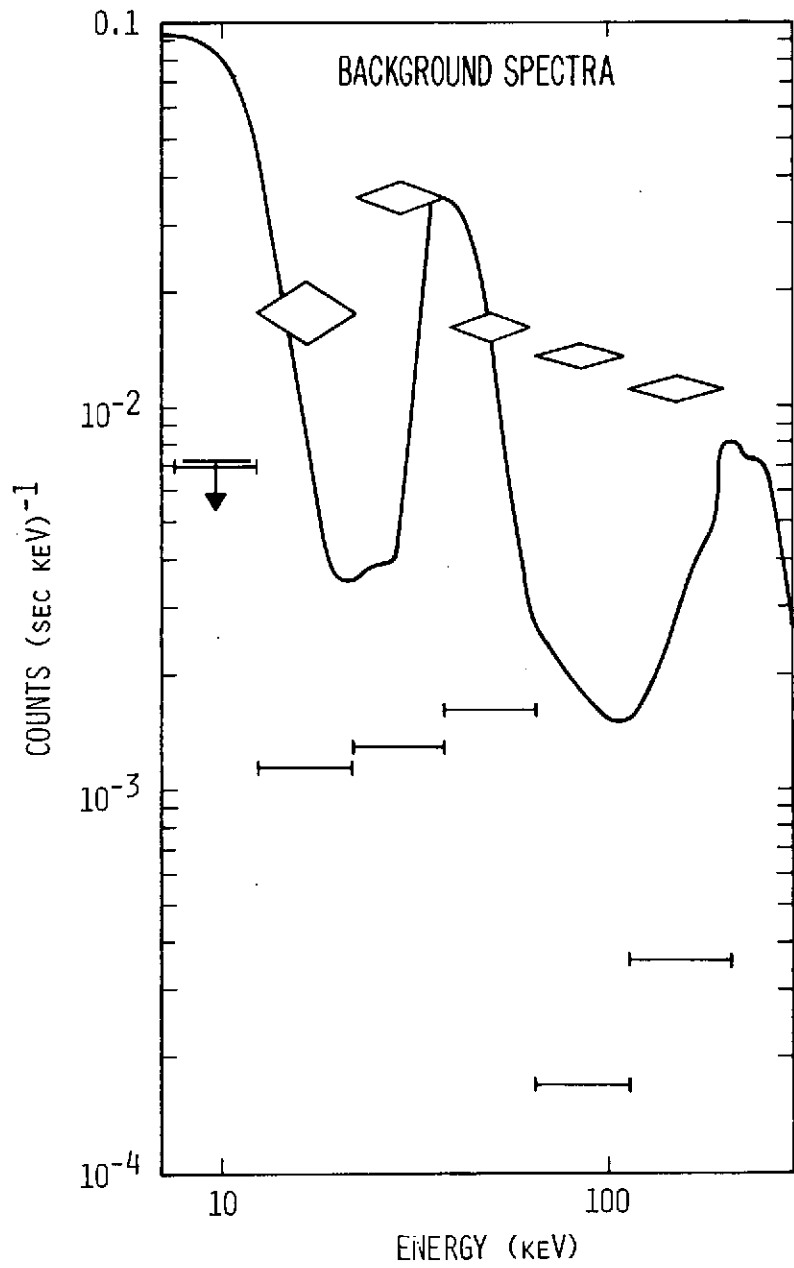
5

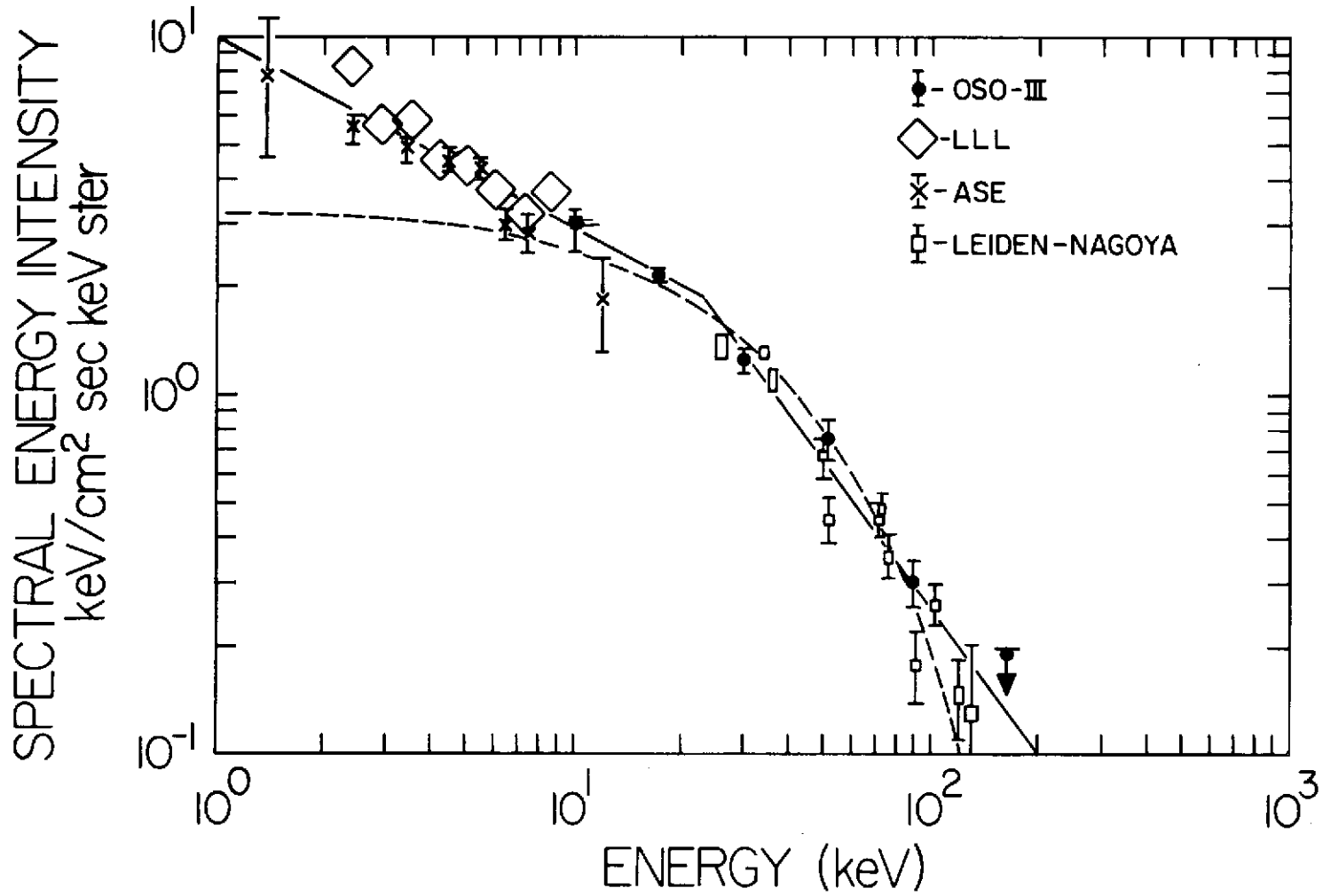


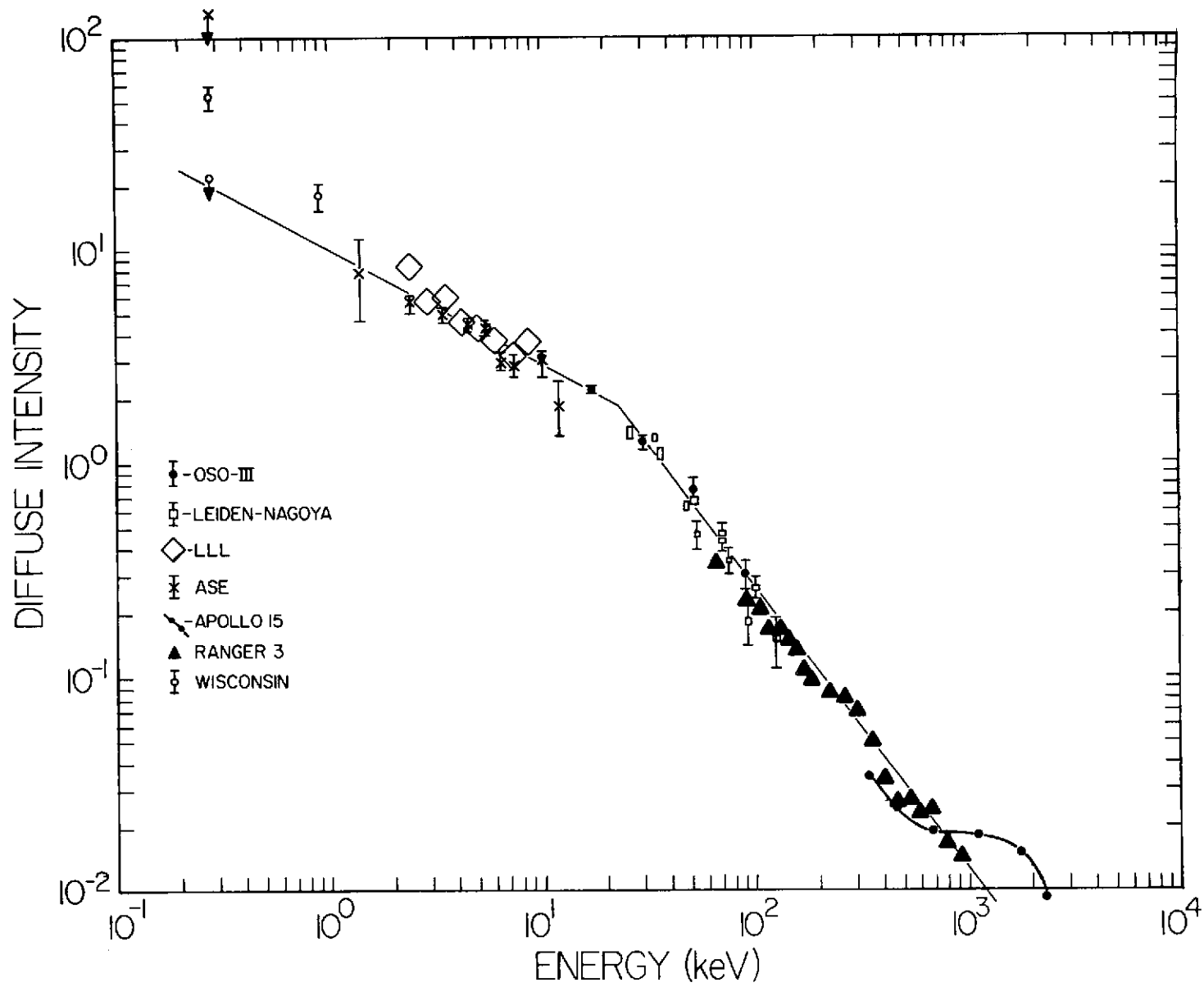


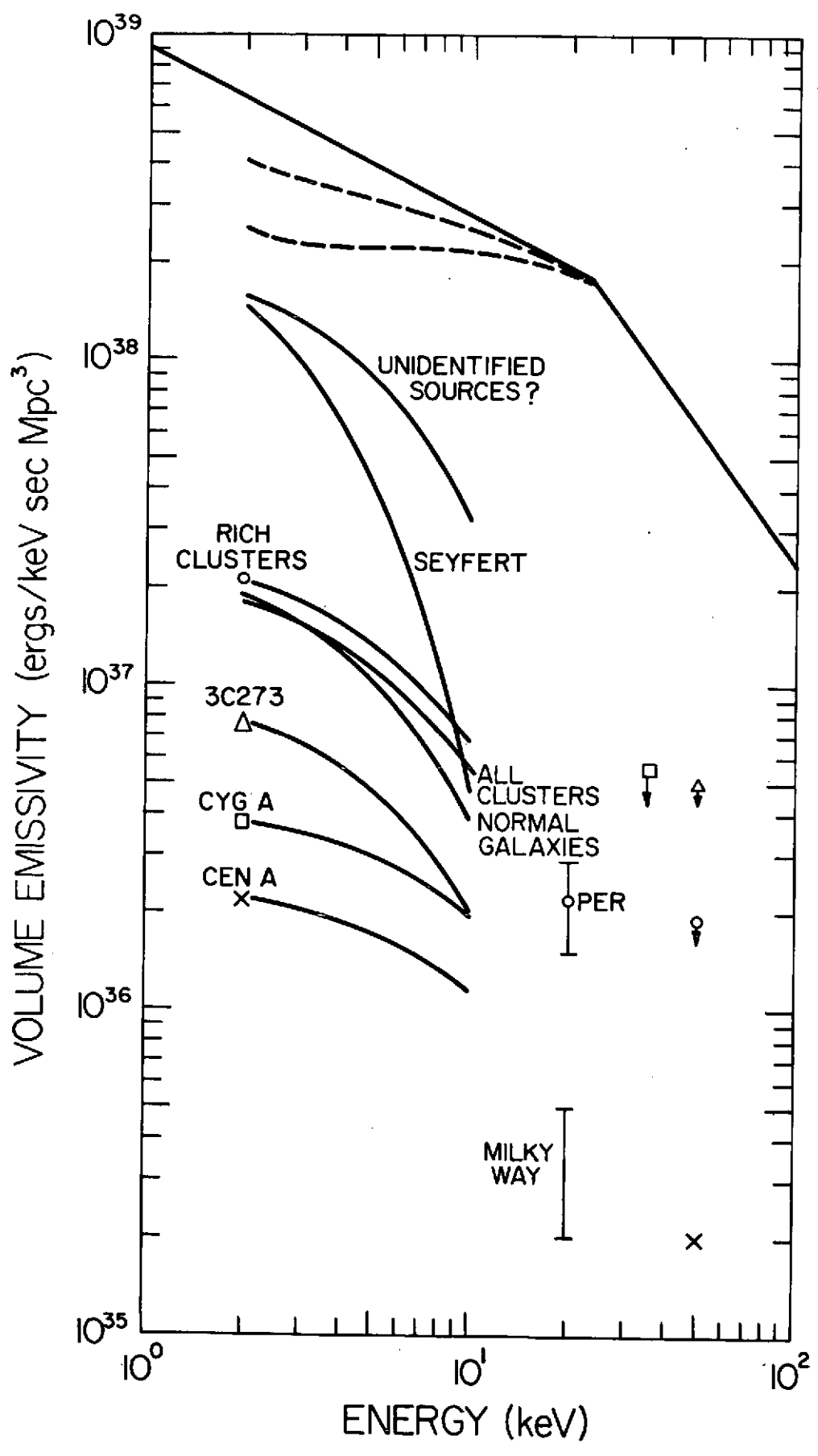


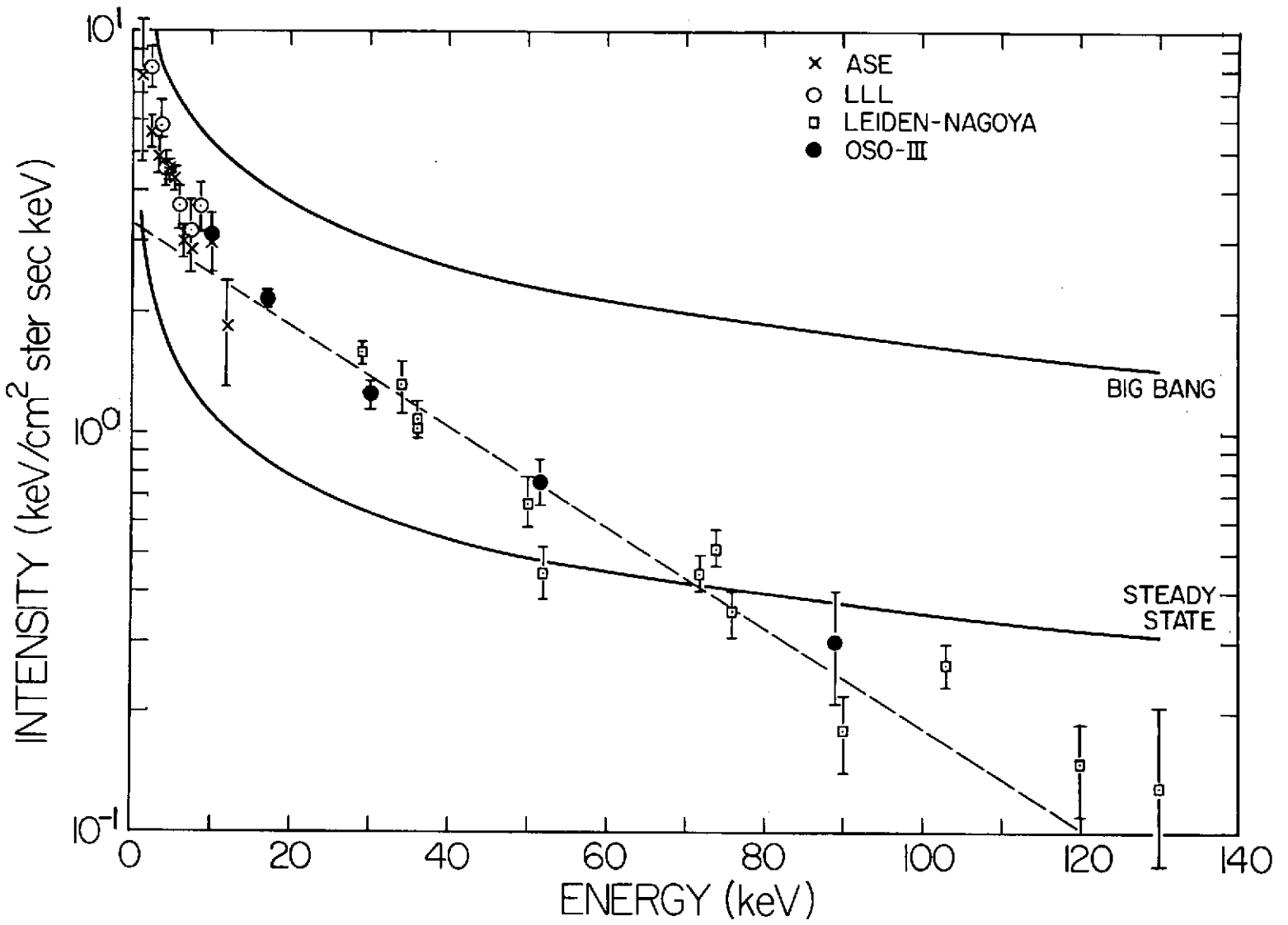
$$C(E, h) = \frac{1}{2} \int_{\forall} A(\theta) S(E, x) e^{-\mu r} \sin \theta \, d\theta \, dr$$











173-28754  
3

The Measurement and Interpretation of the  
Cosmic Gamma-Ray Spectrum Between 0.3 and 27 MeV  
as Obtained During the Apollo Mission

A Review Paper Presented by

L. E. Peterson (UCSD)  
and  
J. I. Trombka (GSFC)\*

\*The work reported here represents the efforts of a team of investigators from the Apollo 15 and 16 missions. Other members of the team are A. E. Metzger (JPL), J. R. Arnold (UCSD), J. I. Matteson (UCSD) and R. C. Reedy (LASL)

## I. INTRODUCTION

During the trans-earth portion of the Apollo 15 and 16 missions, data on the spectrum of the total (diffuse and discrete sources) cosmic  $\gamma$ -ray background over the 0.3 - 27 MeV range was obtained (Reference 1). An uncollimated 7.0 cm x 7.0 cm cylindrical NaI(Tl) scintillation counter located on a boom 7.5 m from the Apollo Service Module was used to perform the measurement. An analysis of the data obtained on Apollo 15 is presented here.

A major source of interference in determining the magnitude and shape of the cosmic gamma spectrum can be attributed to the cosmic-ray induced activation of the NaI(Tl) detector crystal. A NaI(Tl) crystal similar to that used during the Apollo 15 and 16 missions was flown aboard the Apollo 17 Command Module. This crystal was returned to earth and measurements of the induced activity were obtained. Preliminary analysis of the results are now available (Reference 2). Other sources of interference with respect to the determination of the diffuse gamma ray spectrum have also been considered. This interference or background was due to sources aboard the spacecraft and cosmic-ray induced gamma ray emission from the spacecraft and material surrounding the detector. Attempts have been made to correct the measured spectrum for these background effects.

An upper limit measure of the gamma ray flux around .51 MeV was also obtained.

## II. INSTRUMENTATION

The Apollo 15/16 gamma-ray spectrometer (Reference 3) consists

of a 7.0 cm dia x 7.0 cm long NaI(Tl) central detector viewed by a 3" photomultiplier. Except at the photomultiplier end, the crystal is surrounded by a 1 cm thick plastic scintillator shield which detects charged particles. The plastic scintillator is viewed by a 1-1/2" photomultiplier and has a threshold of about 1.0 MeV for generating an anticoincidence event when interactions occur in the most optically unfavorable location. Central detector events with no shield anticoincidence are pulse-height analyzed into 511 channels and are transmitted at a maximum event rate of 369 counts/sec. The shield rate, the coincidence rate, and the livetime are transmitted every 0.328 seconds. The spectrometer and associated electronics are enclosed in a thermal shield and mounted on a boom which could be extended from one side of the Service Module by an astronaut. The components carried on the boom present  $\sim 5 \text{ gm/cm}^2$  averaged over all directions. The astronaut could fully deploy the detector to 7.6 m from the spacecraft edge or position it at intermediate distances using stop-watch timing. Furthermore, he could step the high voltage supply or disable the anticoincidence.

### III. RESULTS

#### (a) Energy Loss Spectra

The data reported here were obtained during portions of the Trans-earth Coast of Apollo 15 from about 2200 4 August to 1500 7 August 1971, and represent  $\sim 4$  hours of operation in the extended position. During this period the earth and moon solid angles were always less than  $10^{-2}$

sr and in the fully extended boom position, the spacecraft subtended  $\sim 0.28$  sr. Spectra were obtained with the detector at various boom positions, with the anti-coincidence both on and off, and with the high voltage set to give several energy ranges up to 27 MeV. Although data were obtained over a 0.16 to 27 MeV range, the analysis reported here is based on energy losses  $> 0.3$  MeV. Calibration was obtained with a  $\text{Hg}^{203}$  source and by means of known, easily identifiable spacecraft background  $\gamma$ -rays. Counting rate anisotropies, if they exist, were averaged out over long runs from which these results were derived, since the Command/Service Module rotated  $\sim 3\text{RPH}$  in the ecliptic plane.

Figure 1 shows energy-loss spectra (for several important data modes) corrected for livetime, channel width, and the isotropic detector geometry factor of  $57.5 \text{ cm}^2$ . Here counts have been summed over channels consistent with the detector energy resolution which was 8.6% at 662 keV. With the exception of the strong line at 0.51 MeV, most of the  $\gamma$ -ray lines measured inboard largely disappear with boom extension, leaving a continuum extending to 27 MeV, on which is superposed a number of weak lines. Since the intensity changed only about a factor of five, while the spacecraft solid angle changed a factor of 20, most of the count rate in the extended position is not of spacecraft origin. From a detailed analysis of the rates vs. solid angle, we estimate  $\sim 6.6 \times 10^{-3} \text{ c}(\text{cm}^2\text{-sec-MeV})^{-1}$  at 2.4 MeV and  $\sim 1.9 \times 10^{-3} \text{ c}(\text{cm}^2\text{-sec-MeV})^{-1}$  at 5 MeV are due to the spacecraft. These are 0.1 and 0.2, respectively, of the spectrum with the boom extended.

The flat energy loss spectrum of  $0.052 \text{ c}(\text{cm}^2\text{-sec-MeV})^{-1}$  above 5 MeV with the anti-coincidence disabled in the extended position agrees with that value expected from the shield rate of 450 c/sec, from which a cosmic-ray flux of  $3.50 (\text{cm}^2\text{-sec})^{-1}$  may be derived. The large ratio of cosmic-ray to photon energy losses near 27 MeV requires effective charged particle rejection, which could not be measured before launch to the required accuracy. However, preliminary results from an identical experiment on the Apollo 16 in April 1972 confirm the Apollo 15 differential energy loss spectrum below 10 MeV to within  $\sim 12$  percent. We interpret this as indicating that there were not systematic differences in the behavior of the instruments.

The energy loss spectrum with the anti-coincidence enabled in the extended position is shown with other measurements obtained in cislunar space in Figure 2. The NaI(Tl) Apollo 15/16 detector is identical in size to the CsI(Tl) detector in Ranger III (Reference 4) both of which differ only slightly from the NaI(Tl) crystal on the ERS-18 (Reference 5). The 8kg mass on the end of the Apollo 15 boom is nearly the same as that system aboard the ERS-18, while the Ranger III detector carried only  $\sim 3$ kg. Clearly, the present data are in good agreement with previous measurements below  $\sim 2$  MeV, but are well below the 3.7 - 6.0 MeV point measured by the ERS-18, which is apparently erroneous.

(b) Equivalent Photon Spectra

The equivalent photon spectra, Figure 3, have been obtained from

the energy loss spectra in Figure 1 and 2 by using a measured response "library" and a matrix inversion technique as described in Reference 3. The  $\gamma$ -ray lines are separated from the continuum by using an iterative procedure, (Reference 6 and 7). Here the pulse-height spectrum is transformed to photon space where lines appear as discontinuities, which may be subtracted by requiring the remaining continuum to vary slowly with energy. This procedure results in the removal of 2.5 c/sec over the 0.6 to 3.5 MeV range due to lines or about 17% of the energy loss spectrum, and leaves a smooth equivalent photon continuum shown in Figure 3.

A few comments on the determination of the measured response "library". The shape and detection efficiency of these library functions strongly depends on the angular distribution of the incident gamma ray flux. To illustrate this point, the detection probability (intrinsic efficiency) for a 7.0 cm x 7.0 cm cylindrical NaI(Tl) detector is given in Figure 4 as a function of energy for two different cases: a parallel beam incident on the face of the crystal (the crystal axis is parallel to the beam), and an isotropic distribution of gamma rays. As can be seen there is significant difference in the detection efficiencies over much of the energy region of interest. The shapes of the pulse height spectra do not seem to change quite as radically as a function of the angular distribution of the incident flux. In order to transform from measurement or energy loss spectra to photon spectra, efforts were made to eliminate all background components in order to isolate the

energy loss spectra characteristic of the diffuse component. The assumption was then made that this component was isotropic and the transformation was then performed using an "isotropic" type response library. From a comparison of our experimental work (Reference 8) with Monte Carlo calculations (Reference 9), we found that the response library function can be calculated theoretically for any energy and geometry needed in the analysis.

(c) Discrete Line Spectra

The discrete line spectrum in the measured cosmic ray spectrum can be mainly attributed to natural radioactivity aboard the spacecraft (K-40 and Th), proton and neutron induced activation in the spacecraft and materials surrounding the detector, and activity induced in the detector itself. Using the technique considered in section (b), the continuous portion of the energy loss spectrum was determined and the continuous spectrum was subtracted from the uncorrected energy spectrum. In this way, the energy loss spectrum characteristic of discrete lines is determined. The results are shown in Figure 5. Identification of certain lines are also indicated. We believe that the following lines can be identified: a) the .51 MeV line due to positron annihilation, b) the .63 and .69 MeV lines due to proton induced activation of the crystal producing  $^{124}\text{I}$  and  $^{126}\text{I}$ , the 1.47 MeV characteristics of  $^{40}\text{K}$ , c) and the 2.6 MeV line of Thorium. Other lines due to Thorium, (n, $\gamma$ ) and (n, n,  $\gamma$ ) reactions on Mg, H, Al, O and Na may also be presented.

(d) Spallation Correction

Fishman (Reference 10) has suggested that radioactive spallation nuclei produced by cosmic-ray interactions in the scintillation crystals may account for a large fraction of the counting rate measured in the 1-3 MeV region. Although a direct measurement of this effect in the cosmic-ray flux is difficult and has not been accomplished, calculations and laboratory measurements by Reference 10 and (Dyer, private communication) have indicated the spectra shape and approximate magnitude of the energy loss spectrum. We have attempted to correct the spectra of Figure 3 for this effect by subtracting from the equivalent energy loss spectrum a spallation model spectrum whose normalization was a free parameter. Since spallation contributes mostly to the energy losses in the 0.6 to 3 MeV range, the normalization was determined, rather arbitrarily, by the criterium that the resultant photon spectrum be relatively smooth. This was found to occur when a spallation spectrum, based on the work of Reference 10 and Dyer and Morfill (Reference 11 and private communication) but of approximately half their intensity was subtracted out. As shown in Table 1, this results in removal of about 16% of the energy loss spectrum in the 0.6 to 3.5 MeV range and a negligible amount at higher energies. Subtracting a much larger spallation component, such as the full Dyer and Morfill value, would give no energy loss spectrum in the 1-2 MeV range, while still requiring an external photon component above 3 MeV which is not physically possible. Although there seems no doubt that a spallation energy loss contribution exists, its spectral

shape and intensity are only approximately known.

The spallation components are always subtracted out in energy loss space. In an attempt to obtain experimental data on the extent of the proton-induced activity, a NaI(Tl) crystal was flown aboard Apollo 17. The crystal assembly was physically identical to that flown aboard Apollo 15 and 16 (Reference 3). The assembly aboard the Apollo 17 CSM did not include the photo-multiplier, the proton anti-coincidence mantle, and the thermal shield. The detector was a 7 cm x 7 cm right cylindrical crystal. A glass plate was optically sealed to the crystal. MgO was used as the optical reflector inside the crystal assembly. This type of assembly permitted the crystal to be hermetically sealed, and allowed for a simple procedure for optically coupling the crystal assembly to a photo-multiplier tube after flight. The crystal and reflector were enclosed in a steel jacket. An identical second crystal assembly which was not flown was used as a control throughout the measurement program. After splashdown, the flight (i.e., activated) crystal was returned to the recovery ship and optically mounted on a photo-multiplier tube and pulse height spectra were obtained. The activated crystal was counted in a large steel low level shield. The crystal counting started about one and a half hours after the Command Module re-entered the earth's atmosphere. Before splashdown the control or unactivated crystal was optically sealed to a photo-multiplier tube and the background was determined in the steel shield. The same photo-multiplier tube was used to count the activated and control crystal

assemblies. After thirty hours of counting aboard the recovery ship, the detector was flown back to the Oak Ridge National Laboratory (ORNL) where measurements were continued. This permitted the observation of the decay of the longer-lived induced activities. Direct measurements of the induced activities were made by again, by optically sealing a photo-multiplier tube to the activated crystal. Indirect measurements using both Ge(Li) detectors and a large scintillation  $4\pi$  detector in a low level counting system at ORNL (Reference 7) were performed in order to determine the spectral distribution and intensity of the emitted radiations. The  $4\pi$  scintillation counter is divided into two halves. Both halves can be operated so as to require that there be coincidence events in both halves before an event is analyzed and recorded (coincidence spectra) or both halves can be operated without the coincidence requirement and events independent of their coincidence can be analyzed and recorded (singles spectra).

To date it has been possible to obtain qualitative identification of the following nuclear species:  $^{22}\text{Na}$  (2.6 yrs.),  $^{24}\text{Na}$  (15 hrs.),  $^{133}\text{I}$  (13 hrs.),  $^{134}\text{I}$  (4 days),  $^{135}\text{I}$  (13 days),  $^{138}\text{I}$  (25 min.), and  $^{127}\text{Xe}$  (34 days). After suitable calibrations, quantitative concentrations of these radionuclides will be obtained. The present results indicate that the induced activity observed after recovery can be attributed mainly to species with half lives of about half a day and longer. Decay products with shorter half lives do not make a large contribution to the post recovery integral count rate. This is not to imply that there are

no short half life components. In fact, the line at 0.44 MeV characteristic of  $^{128}\text{I}$ . There are a few more regions with relatively short half lives (in order of tens of minutes) which have not as yet been identified.

Figure 6 shows the pulse height spectrum obtained during the first hour and a half of counting after recovery. The spectrum has been corrected for background by subtracting the measurements obtained with the control crystal. Peak energies for the nuclides presently identified are indicated. The peak positions of  $^{123}\text{I}$ ,  $^{124}\text{I}$ ,  $^{126}\text{I}$ ,  $^{128}\text{I}$  are displaced 27 keV due to X-ray emission and absorption in the crystal after electron capture.

Measurements of the flight and control crystal carried out at the low level counting laboratory at the Oak Ridge National Laboratory prior to flight, indicated the K and Th content of the flight crystal to be slightly higher than that for the control crystal. Thus, one would expect some indication of these elements after background subtraction. The energy identification for  $^{124}\text{I}$ ,  $^{126}\text{I}$ , and  $^{24}\text{Na}$ , have been verified by measurements made with the Ge(Li) detector and in the low level counting system. Both energy and half life information have been used to determine the presence of these nuclear species. The  $^{123}\text{I}$  and  $^{128}\text{I}$  were identified by use of the spectra obtained on board the carrier from both energy and half life determinations.  $^{22}\text{Na}$  has been tentatively identified based on a preliminary analysis of the data obtained by the coincidence measurements in the low level counting facility.  $^{127}\text{Xe}$  presence has been determined by the identification of energy lines at 0.172 MeV, 0.203 MeV and 0.375 MeV using the Ge(Li) detector.

One factor requiring consideration was the difference in the environment during the Apollo 15 and 16 missions compared with Apollo 17 mission. Firstly, the crystals aboard Apollo 15 and 16 were stowed in the Service Module and extended twenty-five feet away from the vehicle for short periods of time, whereas the Apollo 17 crystal was stowed in the Command Module for the total flight time. Thus, there was a difference in mass around the crystal which might cause a difference in the secondary proton and neutron flux in the region of the stowed crystals. Secondly, the exposure profile of the primary flux both in time and spectral distributions were different. The Apollo 17 crystal passed through the near earth trapped proton flux twice before measurements, while the Apollo 15 and 16 detectors had passed through the trapped belts only once before measurement. The Apollo 15 measurement of diffuse gamma-ray spectrum was made about 250 hours after lift off while the Apollo 17 measurements were made some 305 hours after lift off. It has not as yet been determined how significant these differences are in terms of trying to infer the magnitude of the proton-induced activity in the Apollo 15 and 16 detectors from the Apollo 17 measurements.

The shape of the cosmic ray-induced gamma-ray pulse height spectrum can be divided into two parts: the discrete line spectrum and the continuous spectrum. The discrete line pulse spectrum for activated nuclear species in the crystal is produced by monoenergetic gamma-rays emitted after electron capture. The continuum for such nuclear species

is produced by electrons, positrons, positron annihilation, and gamma rays (other than those emitted after electron capture) interacting in the crystal. If the material surrounding the crystal is radioactive (eg some  $^{24}\text{Na}$ ,  $\text{Th}$ ,  $^{40}\text{K}$ ) then monoenergetic gamma rays independent of the mode of decay can be seen in the crystal as a discrete line pulse height spectrum. In Figure 6, the discrete lines are indicated and the continuous distribution can be seen underneath. The actual energy position should be moved  $\sim 27$  KeV up in energy due to the summing of iodine K X-ray line with the gamma-ray line after K capture.

In the Apollo 15 trans-earth spectrum (Reference 10), the  $^{124}\text{I}$  0.606 MeV, and the  $^{126}\text{I}$  0.66 MeV lines can be identified. It has been calculated that the integrated count rate in this region above the continuum for Apollo 15 is half of that observed in the same region above the continuum for the Apollo 17 mission. This difference cannot be attributed to the difference in exposure time alone. Thus, the difference in local mass and the passage through the near earth trapped radiation belts a second time may be the cause of this increase.

In Figure 6 the magnitude of the continuum and associated error as predicted in Reference 10 is compared with the Apollo 17 measurement taken aboard the recovery ship. The magnitude of the continuum inferred from the Apollo 15 data (Reference 1) is also shown. Its magnitude is consistent with the Apollo 17 results if it is considered that the discrete line magnitude for  $^{124}\text{I}$  and  $^{126}\text{I}$  is down by a factor of two. This also assumes that the shorter half lived nuclides and the prompt gamma-ray

emission is small compared to the longer half lived emitters. Calculations (Reference 11) indicate that short half-lives may be quite important.

(e) Spacecraft Continuum

The following procedures were used to determine the magnitude of the spacecraft continuum.

Spectra were obtained with the detector position at 6 feet, 8 feet, 15 feet and 25 feet away from the spacecraft. An effective solid angle for each position was calculated for these positions. The discrete line spallation backgrounds discussed in sections b and c were then subtracted from the energy loss spectrum at 6 feet and 25 feet. It was then assumed that the 6 foot spectrum characterized the energy loss spectrum of the continuous gamma rays spectrum emitted from the spacecraft. The intensity at 6 feet is reduced by the ratio of the effective solid angle at twenty-five feet to the effective solid angle at six feet. This then is a first estimate of the contribution of the spacecraft continuum at 25 ft. The spacecraft continuum contribution is then subtracted from the residual energy loss spectrum at twenty-five feet and a first estimate of the energy loss spectrum due to the diffuse component is obtained. It is now assumed that the diffuse energy loss spectrum does not depend on the distances of the detector from the spacecraft (i.e. the spacecraft occultation is ignored) and this first approximation is subtracted from the energy loss spectrum at six feet. A second approximation of the continuous energy loss spectrum from the spacecraft at six feet is obtained. This new continuous energy loss

spectrum is corrected for change in solid angle to obtain its contribution at twenty-five feet and then subtracted from the original residual energy loss spectrum at twenty-five feet in order to obtain a second approximation of the diffuse energy loss spectrum. The procedure as described above is continued for another two iterations and it was found that the shape of the diffuse energy loss spectrum did not change significantly between the last two iterations. After the last iteration, the energy loss spectrum was then converted to photon spectrum. The transformation was accomplished using library functions and efficiencies characteristics of isotropic flux distributions.

(f) Cosmic Photon Spectrum

The photon spectrum incident on the central detector, shown in Figure 3 as a dashed line, has also been corrected for the various interferences discussed in sections (a) through (e). The contribution of the various components over the 0.6 - 3.5 MeV and the 3.5 - 9.0 MeV ranges are summarized in Table 1. Despite the many corrections, about 50-75% of the energy losses cannot be accounted for by presently understood local processes and therefore must originate externally. Obtaining the photon spectrum incident isotropically on the spectrometer requires a correction for local matter. Taking this to be equivalent to a uniform shell 5.0 gm/cm<sup>2</sup> thick of Al surrounding the NaI crystal, and correcting for absorption, but not scattering, results in the final photon spectrum shown in Figure 3. We have assumed the photon continuum

extends as  $E^{-2.0}$  above 27 MeV; however, the result is rather independent of this shape.

Systematic errors, which are difficult to estimate, completely dominate the statistical uncertainties in this analysis. Correcting for the spacecraft lines can be done to high precision. The effective solid angle for continuum production in the spacecraft may be less certain. No correction has been made for production in local material, which is believed to be small (Reference 5). We estimate the equivalent photon spectrum, before correction for spallation, to be accurate to about  $\pm 20\%$ . The spallation correction cannot be much larger than that indicated in Figure 3. Correcting for absorption, but not scattering, results in an upper limit to the external flux.

These results may be compared to those of others who have presented spectra at various stages of correction. The Apollo 15 photon equivalent continuum is considerably below that determined from ERS-18, which had no corrections for  $\gamma$ -ray lines, effects of local material, or spallation, and which apparently had an instrumental malfunction at higher energies. The final photon Apollo 15 spectrum is compared direction with balloon and low altitude satellite work (Reference 12, 13, and 14) in Figure 7. The result of the reference is considerably above the other work and is therefore not shown. Although the low latitude observations should not require a significant correction for spallation, they do require an altitude and latitude dependent model to correct for cosmic-ray produced  $\gamma$ -rays, and in some cases, an

additional large correction for counter efficiency.

The new results, in addition to being in reasonable agreement with the more recent work above 1 MeV, also agree with data near 100 keV (Reference 15) when extrapolated as an  $E^{-2}$  power law. Furthermore, the Apollo spectrum is consistent with new data on the diffuse component near 30 MeV (Reference 16 and 17). Figure 7 shows some of these results, as well as at 100 MeV obtained from the OSO-3 (Reference 18).

Also shown in Figure 7 is a single power law which has been suggested (Reference 15) as capable of representing the total cosmic  $\gamma$ -ray spectrum between  $\sim 0.02$  and 1.0 MeV. It is clear that the derived Apollo 15 spectrum is well above this extrapolation and even though we interpret our result as an upper limit, we do not believe that the remaining small corrections and uncertainties can reduce the final cosmic spectrum to the extrapolated value.

#### IV. DISCUSSION

Assuming that the  $\gamma$ -ray fluxes are of extragalactic origin (Reference 19) a number of workers have attempted to account for the spectra shown in Figure 7. Compton scattering of electrons leaking from radio galaxies (Reference 20), redshifted  $\gamma$ -rays from  $\pi^0$  decays produced by cosmic-ray collisions at an early epoch of the expanding Universe (Reference 21), nuclear  $\gamma$ -rays from supernovae in distant galaxies (Reference 22), intergalactic electron bremsstrahlung (Reference 23, 24 and 25) and matter-antimatter annihilation (Reference 25)

have all been suggested. Vette (Reference 5), in attempting to account for the ERS-18 data, fitted a model in which a  $\pi^0$  decay component produced at an epoch with a redshift  $\approx 70$  was superimposed on a Compton scattering X-ray background. Based on the present data, the intensity of the flux required at very early epochs is reduced somewhat. The final spectrum of Apollo 15 does require an additional component above a simple power law. A discussion of the theoretical consequences of these results is given by Stecker elsewhere in these proceedings.

The analysis process used here subtracts out all discrete  $\gamma$ -ray lines and produces a smooth continuum, as presented in Figure 3. Discrete  $\gamma$ -rays of cosmic origin, if they exist, would therefore be removed along with known spacecraft and spallation contributions. Only considerable further analysis can separate these components, and place valid limits on possible cosmic components.

The  $\gamma$ -ray line near 0.51 MeV has an intensity after correction for spacecraft production and local absorption estimated to be  $3.0 \pm 1.5 \times 10^{-2}$  photons  $(\text{cm}^2\text{-sec})^{-1}$ . The uncertainty is an estimate of the effect of systematic errors in the correction for weak  $\gamma$ -ray features near this energy and for detector efficiency and absorption. The 0.51 MeV  $\gamma$ -ray measured on Apollo 15 cannot originate in the spacecraft since this component decreases less rapidly with spacecraft solid angle than the continuum. The intensity of the line seems

inconsistent with upper limits on the cosmic flux at 0.51 MeV of  $< 10^{-2}$  photons  $(\text{cm}^2\text{-sec})^{-1}$  obtained from balloon measurements (Reference 26) and on the Ranger III (Reference 4). Since the Ranger III, which also measured in interplanetary space, had considerably less matter locally to the detector, it may be possible to attribute the flux to annihilation of positrons produced by cosmic-rays or spallation  $\beta^+$  decays in the local mass. It is also possible that low energy positrons of either solar or cosmic origin with a flux of  $\sim 10^{-2}$   $(\text{cm}^2\text{-sec})^{-1}$  could stop and annihilate in the inert matter surrounding the detector. Such a mechanism has been suggested by Stephens (private communication) and is in fact consistent with the interplanetary medium flux of  $2 \times 10^{-2}$  positrons  $(\text{cm}^2\text{-sec})^{-1}$  at  $\sim 2$  MeV reported in Reference 27. Haymes (Reference 28) has reported a  $\gamma$ -ray line at  $\sim 470$  keV whose intensity is  $2 \times 10^{-3}$  photons  $(\text{cm}^2\text{-sec})^{-1}$  originating from the galactic center. The  $\gamma$ -ray line measured on Apollo 15 is definitely at  $0.511 \pm 0.012$  MeV, and the  $2\sigma$  upper limit to a  $\gamma$ -ray at 0.47 MeV is  $\sim 2 \times 10^{-3}$  photons  $(\text{cm}^2\text{-sec})^{-1}$ , based on the analysis of four hours of data.

## BIBLIOGRAPHY

1. Trombka, J. I., Metzger, A. E., Arnold, J. R., Matteson, J. L., Reedy, R. C., and Peterson, L. E., Ap. J. 181, 737-746, 1973.
2. Trombka, J. I. Schmadebeck, R. L., Bielefeld, M., O'Kelley, G. D., Eldredge, J. S., Northcutt, K. J. Metzger, A. E., Schonfeld, E., Peterson, L. E., Arnold, J. R., and Reedy, R. C., Apollo 17 Preliminary Science Report (In press).
3. Adler, I., and Trombka, J. I., 1970, Physics and Chemistry in Space, Vol. 3, ed. J. G. Roederer and J. Zahringer (New York: Springer-Verlag).
4. Metzger, A. E., Anderson, E. C., Van Dilla, M. A., and Arnold, J. R., 1964, Nature, 204, 766.
5. Vette, J. I., Gruber, D., Matteson, J. L., and Peterson, L. E., 1970, Ap. J. (Letters), 160, L161.
6. Trombka, J. I., Senftle, F., and Schmadebeck, R., 1970, Nuc. Inst. and Methods, 87, 37.
7. Reedy, R. C., Arnold, J. R., and Trombka, J. I., 1973, (accepted for publication in J.G.R.).
8. Trombka, J. I., Eller, E., Osswald, G. A., Berger, M. J., and Seltzer, S. M., USAEC Report Conf. - T10402, Vol. III, III-43, 1971.
9. Sletzer, S. M., and Berger, M. J., ANS Transactions, 14, No. 1, 124, 1971.
10. Fishman, G. J., 1972, Ap. J., 171, 163.
11. Dyer, C. S., and Morfill, G. E., 1971, Astrophys. and Sp. Sci., 14, 243.

12. Golenetskii, S. V., Mazets, E. P., Il'inskii, V. N., Aptekar, R. L., Bredov, M. M., Gur'yan, Yu. A., and Panov, V. N., 1971, Astro. Letters, 9, 69.
13. Vedrene, G., Albernhe, F., Martin, I., and Talon, R., 1971, Astron. & Astrophys., 15, 50.
14. Damle, S. V., Daniel, R. R., Joseph, G., and Lavakare, P. J., 1971, Astrophys. and Sp. Sci., 14, 473.
15. Pal, Y., 1972, Proceedings of IAU Symposium #55, Madrid, Spain (in press).
16. Mayer-Hasselwander, H. A., Pfeffermann, E., Pinkau, K., Rothermel, H., and Sommer, M., 1972, Ap. J. (Letters), 175, L23.
17. Shore, G. H., Kinzer, R. L., and Seeman, N., 1972 Proceedings of IAU Symposium #55, Madrid, Spain, (in press).
18. Kraushaar, W. L., Clark, G. W., Garmire, G. P., Borken, R., Higbee, P., Leong, C., and Thorsos, T., 1972, preprint (submitted to Ap. J.).
19. Stecker, F. W., Vette, J. I., and Trombka, J. I., 1971, Nature, 231, 122.
20. Brecher, K., and Morrison, P., 1969, Phys. Rev. Letters, 23, 802.
21. Stecker, F. W., 1971, Nature, 229, 105.
22. Clayton, D. D., and Silk, J., 1969, Ap. J. (Letters), 158, L43.
23. Arons, J., McCray, R., and Silk, J., 1971, Ap. J., 170, 431.
24. Stecker, F. W., and Morgan, D. L., Jr., 1972, Ap. J., 171, 201.
25. Stecker, F. W., Morgan, D. L., Jr., and Bredekamp, J., 1971, Phys. Rev. Letters, 27, 1469.

26. Chupp, E. L., Forrest, D. J., Sarkady, A. A., and Lavakare, P. J.,  
1970, Planetary and Space Science, 18, 939.
27. Cline, T. L., and Hones, E. W., 1970, ACTA Phys., 29, Supp 1, 159.
28. Johnson, W. N., III, Harnden, F. R., Jr., and Haymes, R. C., 1972,  
Ap. J. (Letters), 172, L1.

FIGURE CAPTIONS

Figure 1. Energy loss spectra in the 7.0 cm dia x 7.0 cm long NaI(Tl) scintillation counter measured on Apollo 15 during Trans-earth Coast. Since the rates decreased only a factor of about 5 when the detector was extended to 7.6 m, while the solid angle subtended by the spacecraft decreased a factor of 20, we interpret most of the rate in the extended position to be associated with cosmic  $\gamma$ -rays. The spectrum with the anticoincidence disabled agrees that expected from cosmic-rays passing through the crystal edges.

Figure 2. Energy loss spectra are compared directly with other measurements obtained outside the magnetosphere. These data were obtained with counters that differ only slightly in geometry and materials.

Figure 3. Equivalent photon spectra derived from the Apollo 15 are shown at various stages of data correction. First all component due to discrete  $\gamma$ -ray lines are removed, then the spacecraft continuum contribution, and an estimate of energy losses due to spallation nuclei are subtracted. The final result contains a correction for absorption of local material, assuming all energy losses at this stage are due to an external isotropic  $\gamma$ -ray flux.

Figure 4. Intrinsic efficiencies as a function of energy for a 7 cm x 7 cm NaI(Tl) detector. Both parallel beam and isotropic gamma ray fluxes are considered.

Figure 5. Discrete line energy loss Spectrum Apollo 15.

Figure 6. Proton induced activity in 7 cm x 7 cm NaI(Tl) crystal 1-1/2 hours after re-entry. The background has been subtracted. Counting time was 1800 seconds. The spectrum measurement started an hour and a half after re-entry. The spectrum was obtained by direct internal counting of the activated crystal.

Figure 7. The cosmic photon spectrum derived from the Apollo 15 data agrees with previous results below 1 MeV, but is well below that determined from the ERS-18 at higher energies. Limits derived from balloon and low altitude satellite work, despite large corrections for efficiency and cosmic-ray produced  $\gamma$ -rays, are in agreement with the Apollo results.

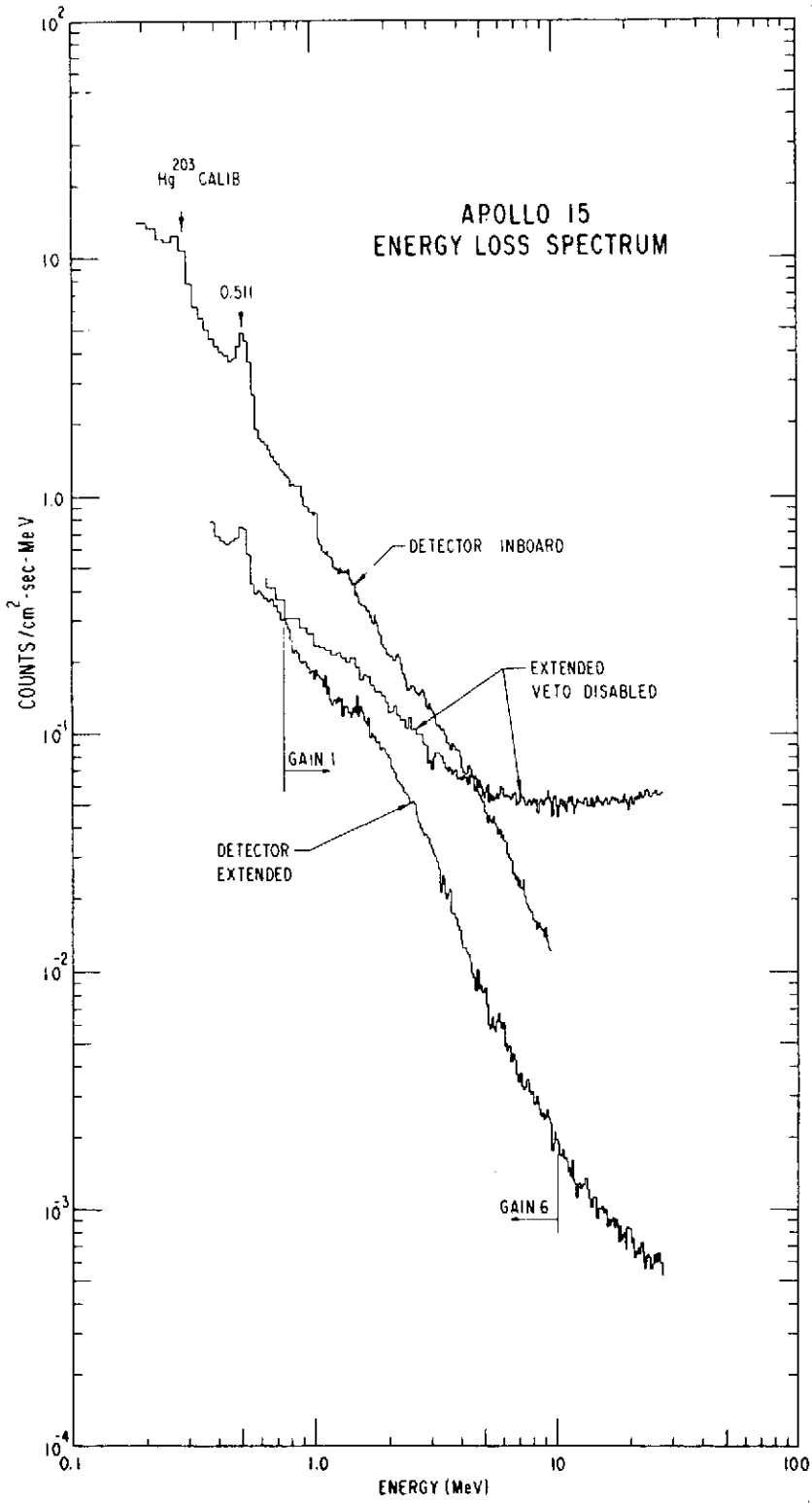


Figure 1.

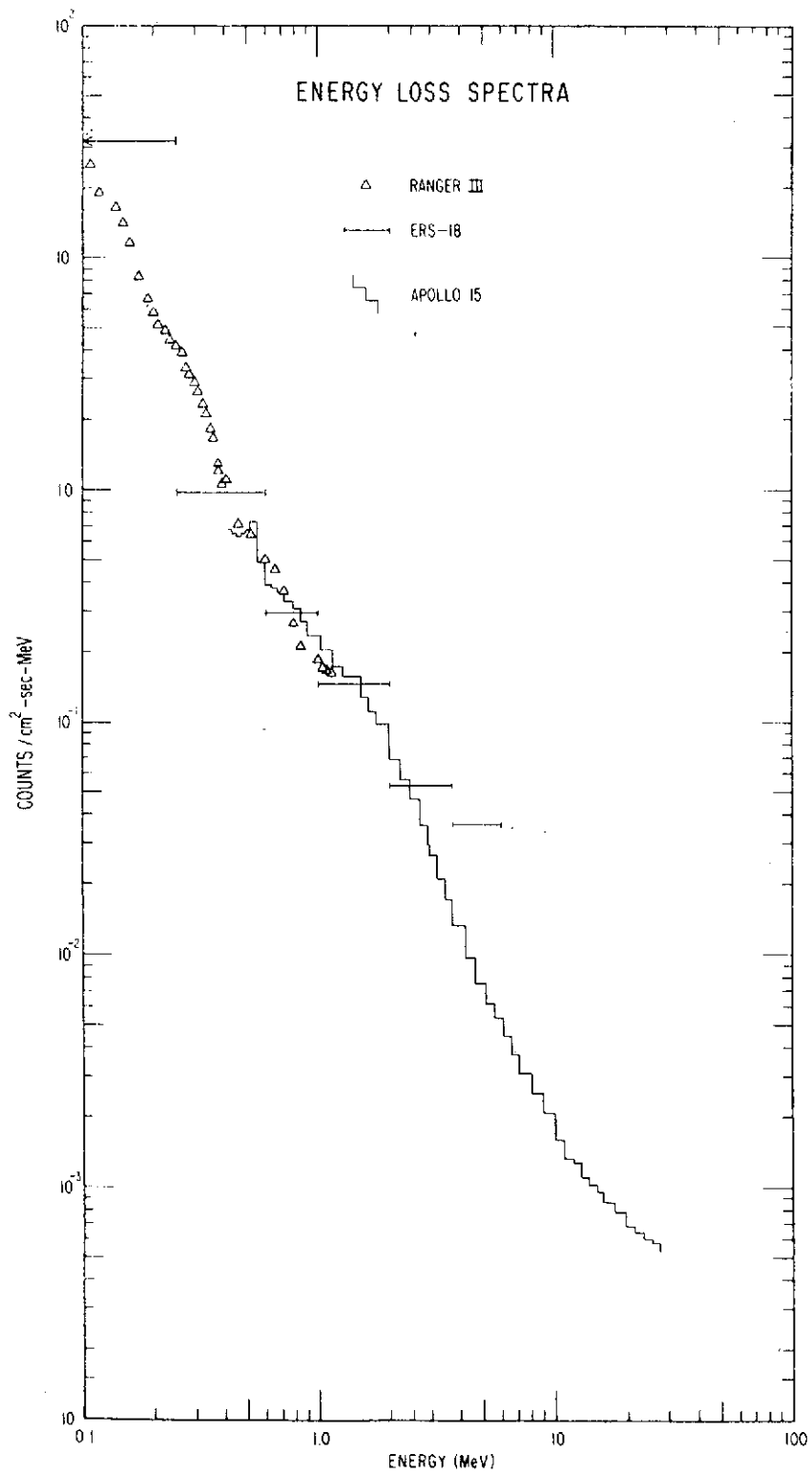


Figure 2.

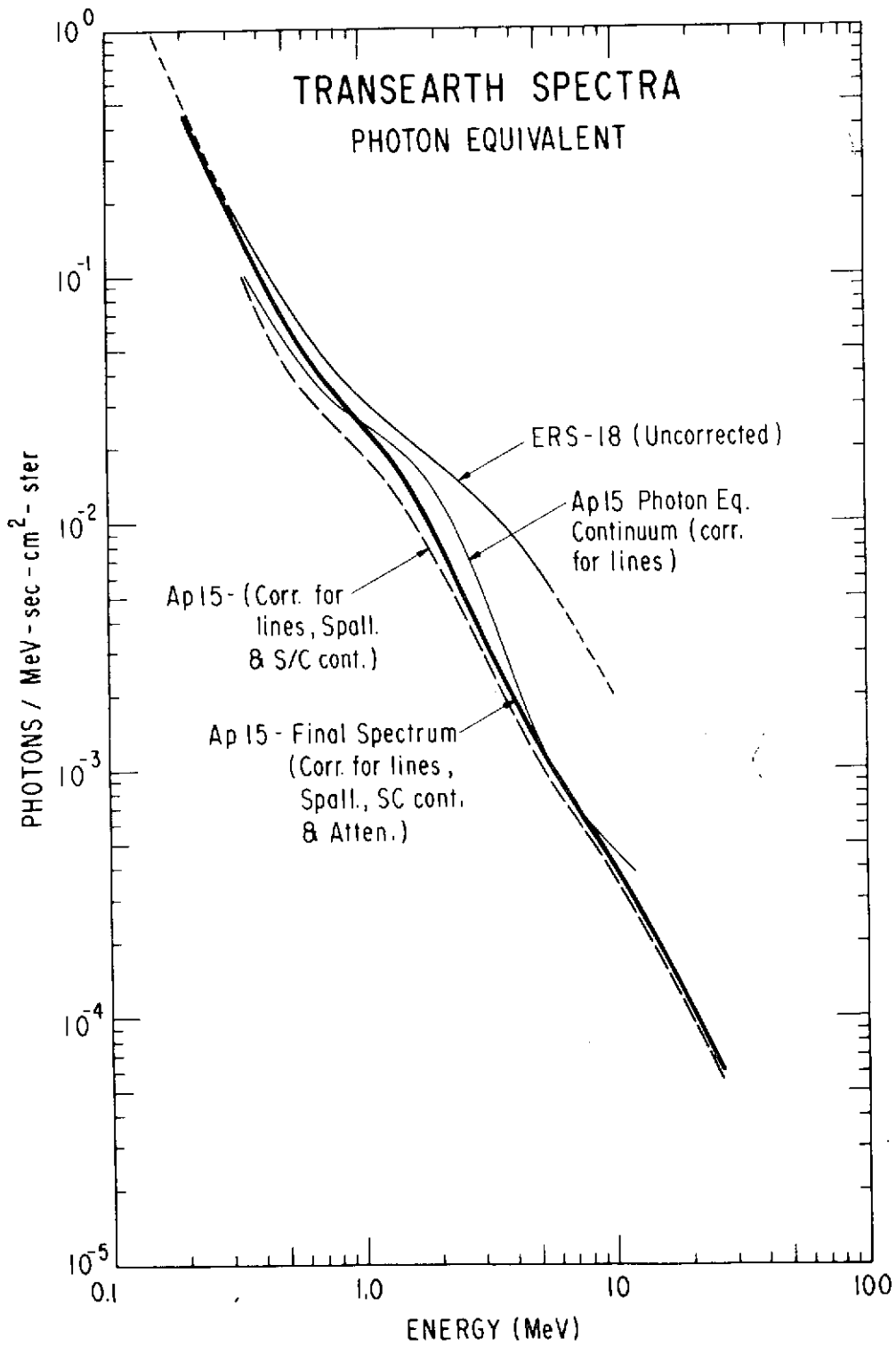


Figure 3.

# INTRINSIC EFFICIENCIES

2 3/4" x 2 3/4" NaI

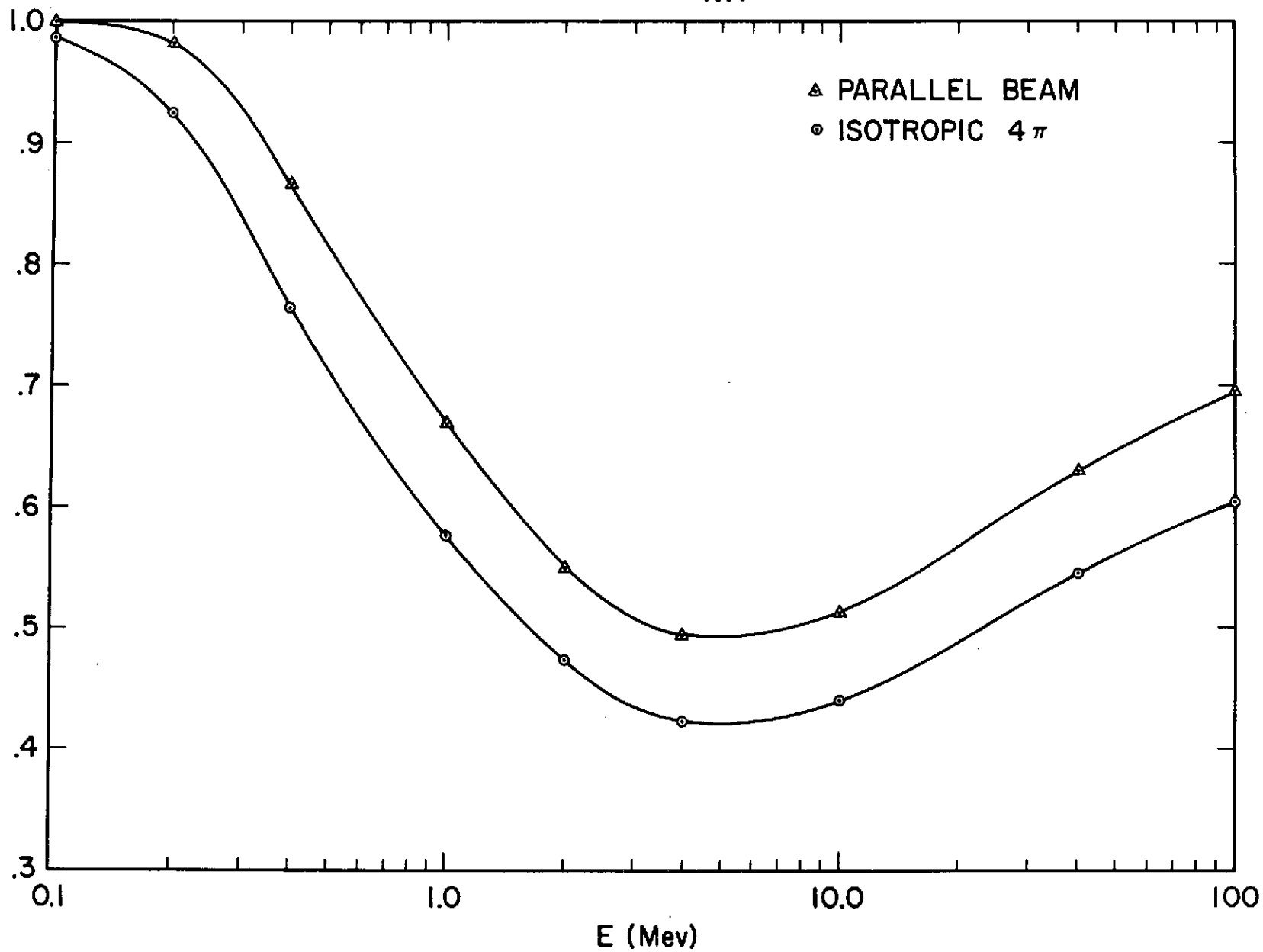


Figure 4.

# PULSE HEIGHT SPECTRUM

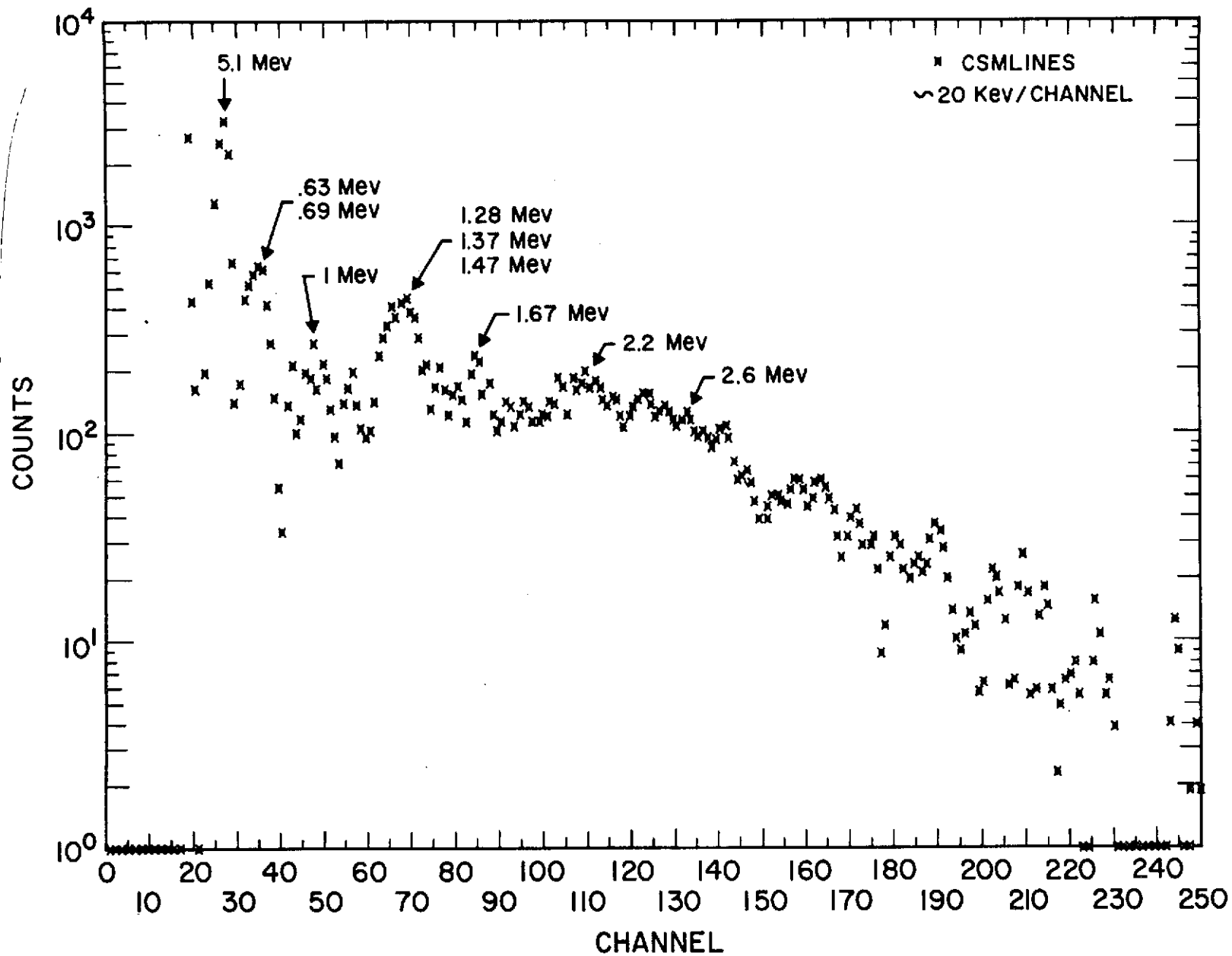


Figure 5.

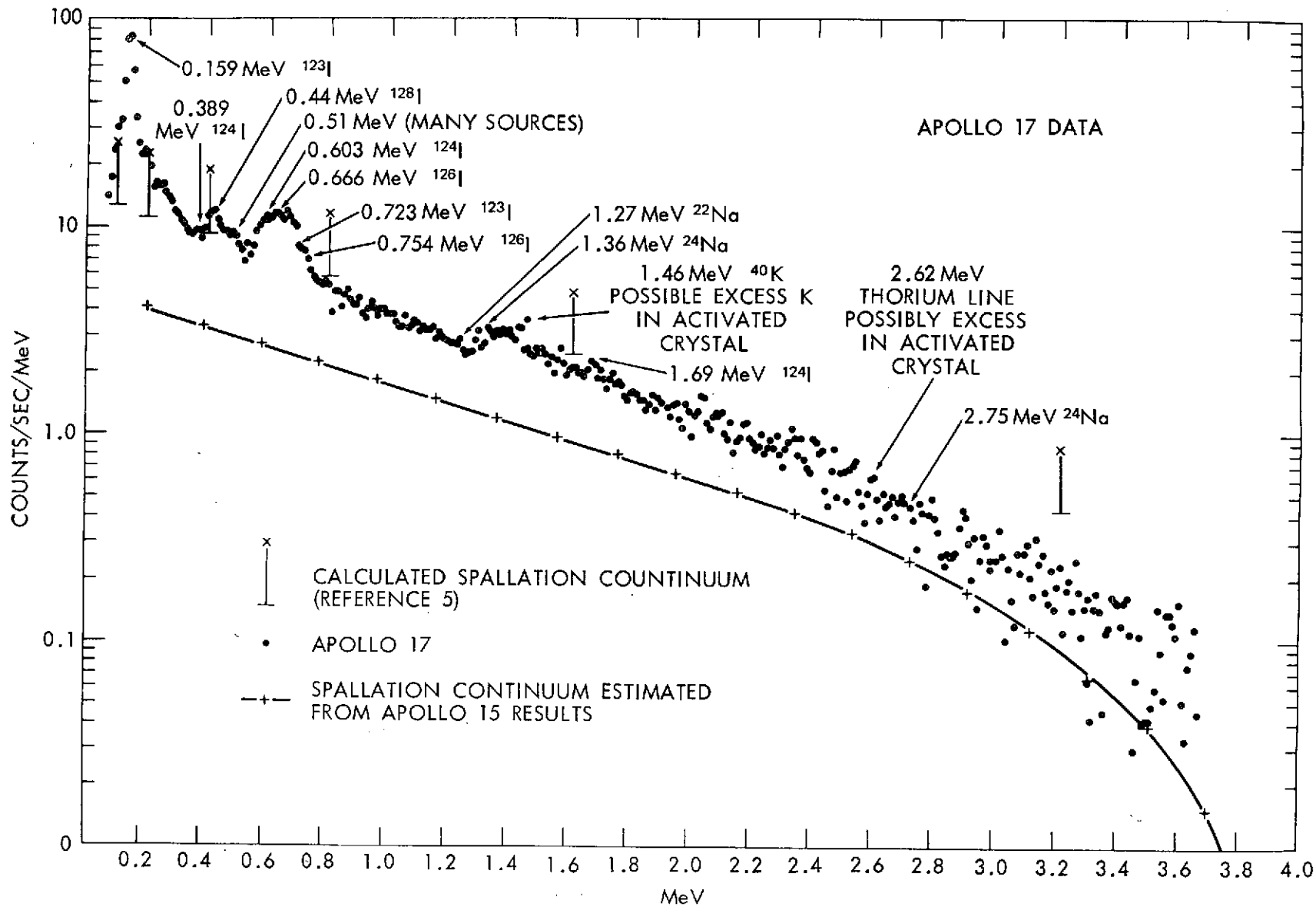


Figure 6.

20

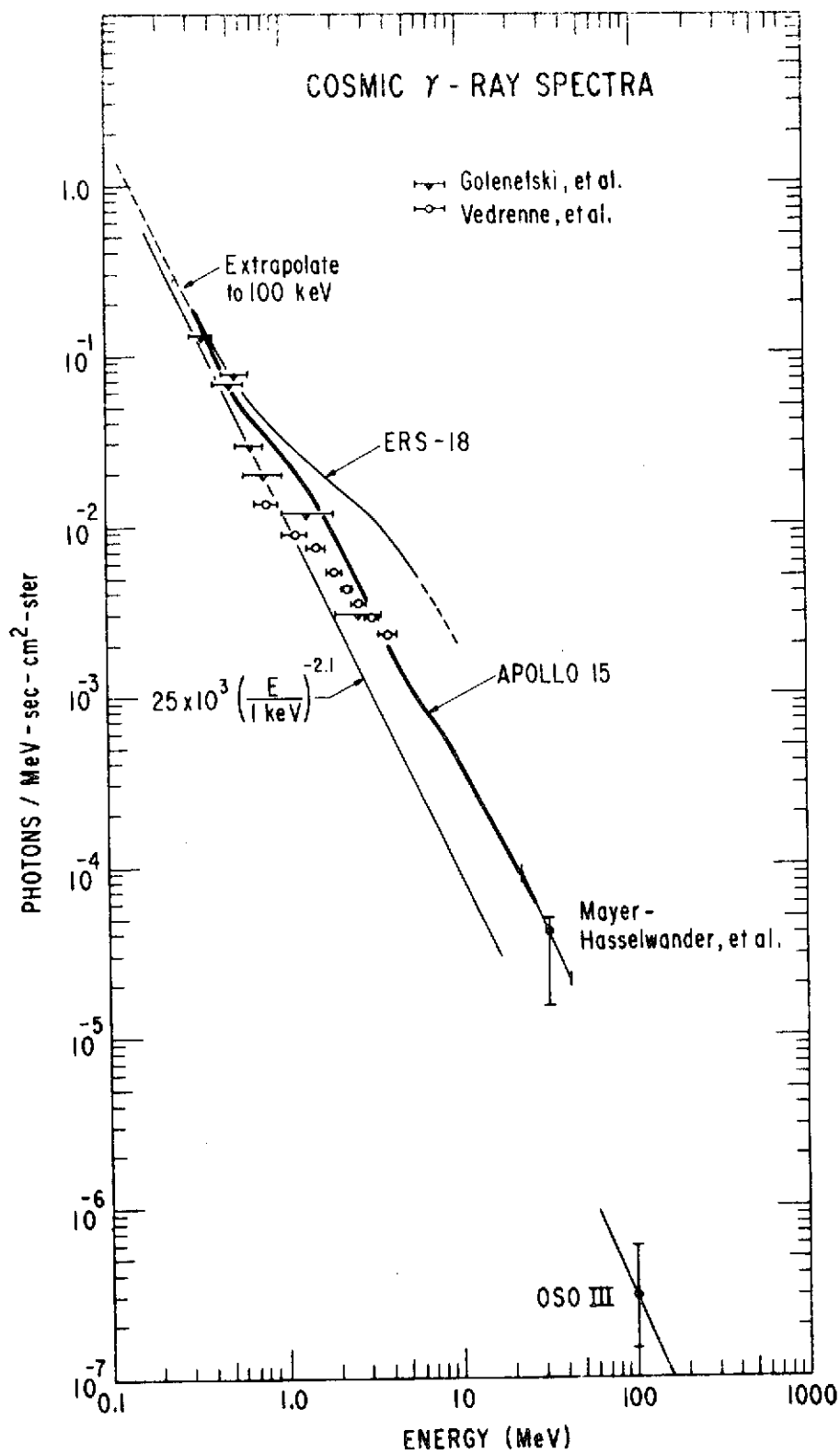


Figure 7.

1  
N73-28757

RECENT OBSERVATIONS OF COSMIC  
GAMMA RAYS FROM 10 MeV TO 1 GeV\*

GERALD H. SHARE

Laboratory for Cosmic Ray Physics  
Naval Research Laboratory, Washington, D. C. 20375, U.S.A.

---

\*Invited paper presented at the International Symposium and Workshop on Gamma-Ray Astrophysics, April 1973.

Introduction

Radio astronomy was born in the 1930's when Karl G. Jansky (1932;1933) discovered a "steady hiss type static of unknown origin" which he concluded "is fixed in space, i.e., that the waves come from some source outside the solar system." The source was in the direction of the center of the galaxy. From further observations Jansky demonstrated that radio emission is also observed, but with diminished intensity, when other regions of the Milky Way passed within the field of view of his antenna. Some 30 years later the newest branch of astronomy was born when a detector on board the OSO-3 satellite found that  $\gamma$ -ray photons  $10^{16}$  times more energetic than the radio waves were also emitted from the plane of the galaxy (Clark, Garmire and Kraushaar 1968). However, the similarity in the early histories of these two disciplines stops right there. Whereas Jansky discovered extraterrestrial radio emission while studying the arrival direction of thunderstorm static, the discovery of cosmic  $\gamma$ -rays came after more than a decade of intensive investigation by various laboratories.

In this paper I shall discuss recent observations of cosmic  $\gamma$ -rays made subsequent to the discovery of energetic photons from the galactic plane. An extensive review of the field prior to 1971 has been compiled by Gal'per et al. (1972; also Fazio 1973 and Pal 1973). I shall treat three main areas under current investigation: a)  $\gamma$ -ray emission from the plane of the galaxy, with emphasis on observations made in the vicinity of the galactic center; b)  $\gamma$ -ray emission from the Crab Nebula and its pulsar; and c) diffuse  $\gamma$ -radiation.

Gamma Radiation from the Plane of the Galaxy

The OSO-3 telescope measured detectable intensities of  $\gamma$ -radiation emitted along the galactic equator at all galactic longitudes. These

measurements are summarized in Figure 1, taken from a final report on the observations (Kraushaar et al. 1972). The variation in counting rate of the instrument is shown as a function of galactic latitude for six  $60^\circ$  intervals of galactic longitude. For comparison the authors have indicated by the histogram the expected rates, assuming that the radiation originated in collisions of cosmic-ray nuclei with interstellar gas. The galactic distribution of gas was obtained from 21 cm measurements of neutral hydrogen. The agreement between the expected intensity and their observations is good, with the exception of the region near the galactic center. In this region, they found that the measured intensity was significantly above the calculated value. Because the radiation appeared to be associated with diffuse emission from the plane, they expressed it in terms of an equivalent line intensity ( $\gamma/\text{cm}^2\text{-sec-rad}$ ) for an apparent width of  $\pm 15^\circ$  in latitude. For longitudes  $30^\circ < \ell_{\text{II}} < 330^\circ$ , they measured an average integral intensity of  $(3.4 \pm 1.0) \times 10^{-5} \gamma/\text{cm}^2\text{-sec-rad}$  for energies above 100 MeV; whereas in the vicinity of the galactic center, they found a broad maximum along the plane with an intensity of  $(1.1 \pm 0.3) \times 10^{-4} \gamma/\text{cm}^2\text{-sec-rad}$ .

As the angular resolution of the detector of OSO-3 was about  $\pm 15^\circ$ , the width of the apparent band of emission in directions away from the galactic center could have been almost entirely due to instrumental effects. However, the broad maximum in intensity, observed along the galactic equator in the direction of the center, could not be attributed entirely to instrumental effects.

Ögelman (1969) suggested that the distribution of  $\gamma$ -ray emission from the plane could be accounted for by the distribution of known X-ray sources, assuming that they emitted photons with a hard spectrum,  $\propto E^{-2}$  in differential intensity. This suggestion could not be tested in greater detail by the OSO-3 detector because of its limited angular resolution.

Initial measurements at higher angular resolution were made predominantly in the northern hemisphere. Most of these instruments employed multi-plate spark chambers as their prime detector, which permitted angular resolutions better than  $\pm 3^\circ$ . In some early reports, evidence was presented for emission of  $\gamma$ -rays from the plane of the galaxy in the vicinity of Cygnus (e.g., Valdez and Waddington 1969, Frye and Wang 1969, and Hutchinson et al. 1969). However, these measurements were of marginal statistical significance and furthermore, indicated an intensity considerably above the revised intensity measured on OSO-3 (Kraushaar et al. 1972).

The higher intensities observed in the direction of the center of the galaxy prompted balloon expeditions to the southern hemisphere by various groups. Using a wire spark chamber with magnetic-core readout, the group at the Goddard Space Flight Center investigated the galactic center region with an estimated angular resolution of  $\sim 2^\circ$  at 100 MeV. Their instrument was a prototype version of the SAS-B  $\gamma$ -ray telescope which was launched late in 1972. From a balloon flight conducted over Australia in 1969, Kniffen and Fichtel (1970; also Fichtel et al. 1972) confirmed the high  $\gamma$ -ray intensity in the vicinity of the galactic center ( $-25^\circ \leq \ell^{\text{II}} \leq +20^\circ$ ). Their results are summarized in Figure 2, where they have summed their data in  $2^\circ$  and  $6^\circ$  bands of latitude. On comparing the observed distribution with what they would have expected for atmospheric  $\gamma$ -rays, they found about a four standard deviation excess within  $\pm 6^\circ$  of the galactic equator. The measured "line intensity"  $> 100$  MeV,  $(2.0 \pm 0.6) \times 10^{-4}$   $\gamma/\text{cm}^2\text{-sec-rad}$ , is in agreement with that obtained from OSO-3. Fichtel et al. also set an upper limit on the galactic flux emitted between 50 MeV and 100 MeV. This limit led them to conclude that at least 50% of the galactic flux comes from the decay of  $\pi^0$ -mesons produced in cosmic-ray collisions. They also searched for possible point sources in this vicinity and were unable to detect any at a sensitivity of about  $3 \times 10^{-5}$   $\gamma/\text{cm}^2\text{-sec}$  above 50 MeV.

Three groups using balloon-borne instruments sensitive to photons  $> 100$  MeV have failed to detect diffuse emission from the galactic plane near the galactic center. The first group, a collaborative effort between Case-Western Reserve University and the University of Melbourne, has reported results from a series of 3 balloon flights over Australia, during an investigation of  $\gamma$ -rays in the southern hemisphere (Frye et al. 1971a). Their investigation was performed with a multi-plate spark chamber, and data were recorded on photographic film. They estimate their angular resolution to be  $\sim 2^\circ$  averaged over a typical spectrum for energies  $> 100$  MeV. The intensity of  $\gamma$ -rays observed during these flights is shown plotted against the sine of galactic latitude in Figure 3, where the bin widths have been corrected for exposure and atmospheric contributions. Events specified as "R" refer to those exhibiting a straight single track emerging from one of the conversion layers in the spark chamber. The summed data for the 3 flights are shown in parts G and H of the figure and are compared with the enhancement expected along the galactic equator, based on the intensity reported by Fichtel et al. With the sensitivity of these measurements, it is difficult to explain why the galactic emission was not detected.

Another observation, which has recently been published, was performed by the group at Minnesota (Dahlbacka et al. 1973). They used an instrument incorporating a nuclear emulsion stack as a converter for the  $\gamma$ -rays and a narrow-gap spark chamber to identify the proper events in the emulsion. With this technique an angular resolution better than  $1^\circ$  at energies  $> 100$  MeV can be achieved. The region of the galactic center was investigated during a balloon-flight over Australia in 1970. The number of events observed as a function of galactic latitude near the galactic center is shown in Figure 4. The upper plot was derived from measurements made on events located in the emulsion stack, whereas the lower plot was obtained from measurements of the

spark chamber photographs ( $\sim 3^\circ$  resolution). Shown by the dashed curves are the expected numbers of events, assuming that they are atmospheric in origin. The distributions do not provide any evidence for emission from the galactic plane, although the upper limits set by the observations are not inconsistent with the intensities reported by Kraushaar et al. and Fichtel et al.

The third group, from the University of Southampton (Browning, Ramsden and Wright 1972), has reported evidence for point sources of  $\gamma$ -rays along the galactic plane near the center. They claim that these sources can account for the apparent diffuse intensity observed from the plane, and furthermore, that there is no residual diffuse intensity after the sources are subtracted. I shall return to these results later.

The above discussion indicates that there still appears to be some disagreement between the various experiments. Two recent measurements, made at energies significantly below those we have discussed, have helped to clarify the situation. Both were made over Argentina in the late fall of 1971 during the expedition "Galaxia '71." The first was performed by H. Helmken and J. Hoffman of the Smithsonian Astrophysical Observatory using a large area gas Cerenkov counter which employed a plastic scintillator as the converter for photons above 15 MeV. Although the instrument has good rejection properties for various backgrounds, it suffers from its relatively poor angular resolution,  $\sim 30^\circ$  FWHM. This requires that in searching for continuous emission from a possible gamma-ray source, measurements must be made both on and off the source in order to determine the background level. From two balloon flights, Helmken and Hoffman (1973) have reported that they detected a  $3.8 \sigma$  excess from the direction of the galactic center. Due to their detector's broad angular resolution, they were unable to determine whether the excess came from point sources near the center, or whether it could be attributed to emission from along the galactic plane.

The other experiment was performed by R. L. Kinzer, N. Seeman and myself at the Cosmic-Ray Laboratory (Chief Scientist, M. M. Shapiro) at NRL. (A detailed description of this experiment will be published in Ap. J. and can also be found in the Proceedings of the 13th International Cosmic Ray Conference.) Our experiment was similar in design to that flown by the Minnesota group; it incorporated a stack of nuclear emulsions with a wide-gap spark chamber in order to unambiguously identify the gamma-ray interaction, as well as to provide an angular resolution of  $\sim 1\frac{1}{2}^\circ$ . The difference between this instrument and the one flown by the Minnesota group resides in its energy range. Whereas the Minnesota detector had a threshold energy of about 100 MeV, our instrument had a low-energy threshold near 10 MeV and was relatively insensitive to photons  $\geq 200$  MeV. The lower threshold was attained by design features which restricted the amount of material between the spark chamber and nuclear emulsion stack, reducing the scattering of the particles considerably and permitting low-energy electrons to be followed back into the emulsion.

The NRL experiment was flown to an atmospheric depth of  $2.5 \text{ g-cm}^{-2}$  and was pointed in the direction of the galactic center. The distribution of  $\gamma$ -rays as a function of galactic latitude was obtained from a partial analysis of events located in the stack of emulsion and is shown in Figure 5. Plotted are the number of  $\gamma$ -rays observed as a function of galactic latitude for  $3^\circ$  and  $1^\circ$  intervals. The curves superimposed on the histogram were normalized for  $\left| b^{\text{II}} \right| > 6^\circ$  and show the expected number of events, assuming the  $\gamma$ -rays were entirely of atmospheric origin. Evident is a significant excess of events within  $\pm 3^\circ$  of the galactic equator; 32 events were observed whereas only 13 were expected. The probability of randomly obtaining this excess of events is less than  $10^{-5}$ . The distribution of  $\gamma$ -radiation along the plane appears to be considerably narrower ( $\sim 3^\circ$  wide) than measured by either the OSO-3 or Goddard detectors.

From the measurements which I have discussed above, an integral spectrum for  $\gamma$ -rays emitted along the galactic equator in the vicinity of the galactic center can be constructed. This spectrum is shown in Figure 6. There is good agreement between the intensities measured by Kraushaar et al. and Fichtel et al. near 100 MeV. As mentioned earlier, the upper limit set by Minnesota is consistent with these measurements. Plotted at 15 MeV are the integral fluxes determined from the NRL observations for two assumed emission spectra,  $\pi^0$ -decay from cosmic-ray collisions with interstellar gas and a power-law representative of Compton collisions of high-energy electrons on starlight and microwave radiation. Due to its design, the NRL instrument is more sensitive to lower energy photons; therefore the estimated flux for a power-law spectrum is lower than that for the harder  $\pi^0$ -spectrum. Shown by the dashed lines are extrapolations of these measurements to higher energies. Within the uncertainties, our measurements and those at higher energies indicate that the  $\pi^0$ -mechanism can account for the observed emission; however, as shown by the dotted-dashed curve, a spectrum with equal contributions from both  $\pi^0$  and power-law production mechanisms provides a better fit to the observations. The flux measured by Helmken and Hoffman, if attributed entirely to emission from the plane, is higher than our observations and requires a much larger contribution from Compton collisions or Bremsstrahlung.

The upper limit set by Frye et al. is in apparent contradiction with the other observations above 100 MeV, assuming that the emission comes from a narrow band along the galactic equator. This upper limit is consistent with our measurements at lower energies only for a fairly steep energy spectrum. However, preliminary spectral information obtained from our data appears inconsistent with such a steep spectrum.

Suggested Point Sources of  $\gamma$ -rays in the Vicinity of the Galactic Center

Frye et al. (1969) reported the first evidence for emission from a point source in the vicinity of the galactic center. The source was designated Sgr  $\gamma$ -1 and was reported to have been observed on each of 3 balloon-flights (Frye et al. 1971a). The combined statistical significance for all three observations was about four standard deviations. Subsequently, this group reported the observation of three additional sources, designated as G $\gamma$  2+3, G $\gamma$  3 $\frac{1}{2}$ +1 and Libra  $\gamma$ -1. The first two had a combined significance of about  $4\sigma$  over background, after data from all three flights were summed. The third source was observed with a significance of  $6\sigma$  during one of their flights, but had not been observed by them during an earlier exposure. Table 1 summarizes the data on these possible sources. Other possible sources in the vicinity of the galactic center have been reported by the group in Southampton (Browning et al. 1972); however, their evidence is of marginal statistical significance. Data on these possible sources, as well as one mentioned by Dahlbacka et al. (1973) are also given in the Table.

The region about the galactic center was investigated with the NRL telescope for emission of  $\gamma$ -rays with energies  $> 15$  MeV from point sources. A galactic map of the arrival directions of the observed  $\gamma$ -rays is shown in Figure 7. There is a concentration of events along the galactic equator between  $350^\circ$  and  $360^\circ$  in longitude, but limited statistics preclude the possibility of attributing, with certainty, this concentration to one or more point sources. However, if it were due to two equally intense point sources, their estimated fluxes above 15 MeV would each be  $\sim 6 \times 10^{-5}$   $\gamma/\text{cm}^2\text{-sec}$ . This same region is known, however, to contain an enhanced columnar density of atomic hydrogen (see e.g. Garmire and Kraushaar 1965) and therefore might be expected to exhibit an increased emission of  $\pi^0$ -decay  $\gamma$ -rays resulting from collisions with high-energy cosmic-rays.

Table 1

## SUSPECTED POINT SOURCES NEAR GALACTIC CENTER

Reported by	Identification	Galactic Coordinates		Flux > 100 MeV (x 10 <sup>+5</sup> γ/cm <sup>2</sup> s)	NRL Results (x 10 <sup>+5</sup> γ/cm <sup>2</sup> s)	
		<i>l</i> <sup>II</sup>	<i>b</i> <sup>II</sup>		> 10 MeV*	> 15 MeV**
Case - Melbourne	Sgr. γ-1	0°	- 18°	1.5 ± 0.5	< 16	< 10
(Frye et al.)	Gγ 2+3 (GX 1+4?)	2°	+ 3°	1.5 ± 0.5	< 22	< 6
	Gγ 341+1 (GX 340-2?)	341°	+ 1°	1.6 ± 0.5	< 36	< 12
	Libra γ-1 (PKS 1514-24?)	340°	+ 30°	2.4 ± 0.6 < 1.5	< 25	< 8
Southampton	2U 1833-05?	26.5°	+ 1.5°	2.9 ± 0.8	< 35	< 12
(Browning et al.)	2U 1813-14?	17.5°	+ 3.5°	1.8 ± 0.4	< 43	< 8
	2U 1728-16?	9.5°	+ 6.5°	2.1 ± 0.6	< 47	< 6
Minnesota (Dahlbacka et al.)	?	352°	+ 16°	2 - 5	< 32	< 8

\* Angular resolution ~ 10°

\*\* Angular resolution ~ 1½°

None of the locations listed in Table 1 for possible  $\gamma$ -ray sources shows a significant concentration of events in Figure 7 (excluding Libra  $\gamma$ -1). A map of events obtained from a separate exposure to Libra  $\gamma$ -1 is shown in Figure 8. Again, there is no evidence for an excess in the direction of the suspected source. These exposures, therefore, failed to confirm the existence of any of the suspected sources. Upper limits (95% confidence level) placed on their intensities  $> 15$  MeV are given in the Table. Limits placed on the fluxes above 10 MeV, also shown in the Table, were derived from a broad resolution survey ( $\sim 10^0$ ) using only measurements from the NRL spark chamber. These limits indicate that if the sources are real, they must either be variable or their differential emission spectra must be significantly harder than a power-law in energy  $\propto E^{-2}$ .

O'Mongain (1973; see also Hearn 1969) has recently studied the statistical methods employed in analyzing data for sources of  $\gamma$ -ray emission. He concludes that in many cases authors have underestimated the probability that the suspected sources could have been generated by statistical fluctuations.

#### The Crab Nebula and its Pulsar

The Crab Nebula has been a target of  $\gamma$ -ray investigations for many years. However, prior to the discovery of the pulsar near the center of the Nebula, these investigations had failed to detect a significant signal from the Crab. Upper limits to the continuous emission above 100 MeV were placed at about  $2 \times 10^{-5}$   $\gamma/\text{cm}^2\text{-sec}$  (see e.g. Frye and Wang 1969).

The existence of the pulsar gave  $\gamma$ -ray astronomers an added dimension to investigate. Assuming that a large fraction of the energy emitted by the Crab was pulsed, then measurements performed at  $\sim 1$  msec resolution would benefit from the reduced background. In 1969, about one month after the observed "glitch" in the pulsar frequency, our group at NRL searched for emission of pulsed  $\gamma$ -rays above 10 MeV during a balloon flight over Texas (Kinzer et al.,

1971a). The initial study was performed at about  $10^0$  resolution and provided evidence that pulsed  $\gamma$ -rays were emitted in phase with the optical peaks. Results from this study are shown in Figure 9, where the time of arrival of events originating  $< 10^0$  from the Crab are plotted in part a) against the pulsar's optical phase; for comparison, the time of arrival of "background" events ( $> 10^0$  from the Crab) is shown in part b). The evidence was of marginal statistical significance and prompted a more detailed study of the data at higher angular resolution using the stack of emulsions actively incorporated into the design of the telescope. The directions of  $\sim 50\%$  of the events occurring close to the times of arrival of both the primary and secondary optical peaks were determined to within about  $2^0$  from measurements in the emulsion; however there wasn't a significant concentration near the Crab (Kinzer et al. 1971b). This apparent disagreement with our earlier suggestion could be explained, however, as being due to the differing energy thresholds of the two samples of data. Indeed, a subsequent study of only low-energy events observed in the spark chamber confirmed the evidence for pulsation and furthermore, indicated that the pulsed emission at  $\gamma$ -ray energies may exhibit sub-structure with widths of  $\sim 0.5$  msec. (Kinzer et al. 1973).

This suggestion of emission at the lower  $\gamma$ -ray energies prompted Albats et al. (1972) to alter their telescope in order to permit  $\gamma$ -rays with energies as low as 10 MeV to be detected. Their results from an exposure to the Crab are shown in Figure 10 for  $\gamma$ -rays with energies between about 10 and 30 MeV. Two samples of data are shown which have slightly different selection criteria. Both exhibit a striking excess within about 1 msec of the primary radio peak. Conspicuous by its absence, however, is any evidence of a pulse in the vicinity of the secondary radio peak. This is to be contrasted with measurements in the 100-400 keV region shown in Figure 11 and obtained by Kurfess (Kurfess and Share 1973). In this lower-energy domain the secondary peak and interpulse

region between the primary and secondary pulses contribute a substantial fraction of the X-rays emitted by the pulsar. The primary X-ray peak is found to occur within 0.5 msec of the primary optical peak. This suggests that the radiation emitted, from the radio band up to the high energy X-ray band originates from a region no greater than about 150 km in extent; this distance is about ten percent of the radius of the speed of light cylinder.

The close relationship in the phase of the primary peak appears to persist up to photon energies near 1 GeV and perhaps higher. Recent results from an experiment performed by the group at Cornell are shown in Figure 12 (McBreen et al. 1973). The measurements were made at energies above  $\sim 200$  MeV using a gas Cerenkov counter having a sensitive area of about  $45,000 \text{ cm}^2$ . In the energy range above 700 MeV, significant peaks were observed at both the location of the primary optical peak and secondary peak. In addition the peak coincident with the primary optical pulse appeared to have an intrinsic width  $\sim 0.7$  msec. This is narrower than has been observed at optical and X-ray energies. Similar structure is also apparent in the lower energy range between 240-700 MeV, but is less significant statistically. The authors point out the possible existence of pulse structure in the interpulse region between the main and secondary peaks. Additional evidence for structure outside of the main peaks was reported by our group at NRL (Kinzer et al. 1973).

Although questions remain concerning the shape of the pulsation and possible variability, evidence is mounting supporting the existence of  $\gamma$ -ray pulsations from the Crab. In order to illustrate the compelling nature of the evidence, I have summed in phase the 1 msec resolution data of NRL, Case-Melbourne and Cornell. This summation is shown in Figure 13 where the data have been combined in 3 msec bins centered on the main optical peak. The ratio of the average number of events in 3 msec bins in the pulsed region to the average number in the background region is  $1.30 \pm 0.08$ . Furthermore, the

bin centered on the main optical peak stands more than 7 standard deviations above the background level.

Measurements of the intensity of pulsed  $\gamma$ -rays are summarized in Figure 14. The dashed line represents an extrapolation of a power-law fit to X-ray observations of the total emission from the Crab. The low-energy data, up to a few MeV, come from measurements with large area NaI crystals or plastic scintillators. At higher energies visual techniques using spark chambers were employed, with the exception of the recent measurements by Helmken and Hoffman (private communication) and McBreen et al. (1973) in which gas Čerenkov counters were used. In contrast to their measurement between 10 and 30 MeV, the higher energy measurement of Albats et al. does not show a significant pulse within 1 msec of the main radio peak; it does, however, show an excess in the broad pulsed region. Our upper limit plotted at 40 MeV comes from the emulsion analysis (Kinzer et al. 1971b). The upper limit above 100 MeV previously reported by the Saclay-Palermo-Milan collaboration (Leray et al. 1972) has been superseded by a recent measurement giving evidence for pulsed emission above 20 MeV (Parlier et al. 1973). It is apparent from the mixture of upper limits ( $2\sigma$ ) and claimed observations, that the sensitivity of the individual experiments require about an order of magnitude improvement in order to permit detailed studies of the Pulsar.

Observations in the hundred MeV region by the Cornell group (McBreen et al. 1973) indicate that the total emission of the Crab Nebula is consistent with the power-law shown in the Figure. This suggests that about half of the 0.1 - 1 GeV emission from the Crab Nebula comes directly from the Pulsar. In the 10-100 MeV region only upper limits or marginal evidence for continuous emission from the Crab have been obtained (see e.g., Frye and Wang 1969, Kinzer et al. 1971c, and Parlier et al. 1973). These limits are consistent with the

power-law extrapolation and also suggest that the pulsed emission represents a large fraction of the total emission from the Crab.

### Diffuse Cosmic Gamma Radiation

One of the most difficult areas of experimental  $\gamma$ -ray astronomy is the investigation of the primary diffuse radiation. The non-visual detectors, such as NaI and CsI crystals, which are used at low energies are susceptible to various backgrounds. These backgrounds can be caused, for example, by inefficiencies in anticoincidence counters, as well as by radioactive buildup from proton spallation and neutron interactions in the crystal and surrounding material, (see e.g., Pal 1973, Kasturiranjana and Rao 1971, Dyer and Morfill 1971, and Fishman 1972). At energies above 10 MeV, where both "non-visual" counter telescopes and "visual" spark-chamber telescopes have been employed, background contamination is still a problem. Inefficiencies in anti-coincidence counters, which reject the intense fluxes of charged particles, can be a major problem in counter telescopes (see e.g., Valentine et al. 1970). Although spark-chamber telescopes are capable of discriminating against this type of background, they may be susceptible to other more subtle forms, for example, local production of  $\gamma$ -radiation. In addition, detectors flown from balloons within the atmosphere, or from low orbiting satellites, must contend with the secondary atmospheric  $\gamma$ -radiation.

However, evidence continues to be compiled indicating the existence of a general diffuse glow of photons from the keV region up to energies of a few hundred MeV. A power-law in energy is capable of fitting the general shape of the spectrum up to about one MeV, but there are suggestions of some departures from this spectrum. These departures include a possible steepening in the spectrum near 40 keV (Schwartz, Hudson, and Peterson 1970) and a possible flattening above 1 MeV (Trombka et al. 1973).

In this section, I shall summarize the measurements made at energies above 10 MeV. Until recently, only upper limits to the intensity of the isotropic component of cosmic  $\gamma$ -rays had been reported (Clark, Garmire and Kraushaar 1968; Frye and Wang 1969; Bratolyubova-Tsulukidze et al. 1970; Valentine, Kaplon and Badhwar 1970; Kinzer, et al. 1971c). Further analysis of the data from OSO-3 has convinced Kraushaar et al. (1972) that the residual rate that their detector observed in directions away from the galactic plane was due to cosmic  $\gamma$ -radiation. The fact that this residual rate remained constant over a wide range of geomagnetic cut-off rigidities, and therefore charged particle intensities, was an important consideration in the conclusion of Kraushaar et al. Their detector also provided an indication that the spectrum of the radiation was softer than the spectrum from either the horizon of the earth or from the galactic plane, both believed to arise predominantly from  $\pi^0$ -decay  $\gamma$ -rays.

A recent measurement from within the atmosphere using a balloon-borne telescope has led to the suggestion by the group at the Max Planck Institute (Mayer-Hasselwander et al. 1972) that the intensity of diffuse  $\gamma$ -rays in the vicinity of 30-50 MeV is considerably above an extrapolation made between X-ray data and the 100 MeV observation of Kraushaar et al. The detector flown by the Max Planck group incorporated a multiplate spark chamber with magnetic core readout. During two balloon flights over Texas in 1971, their detector measured the intensity of  $\gamma$ -rays as a function of atmospheric depth. These measurements are plotted in Figure 15 and provide evidence for a departure from the expected growth curve of atmospheric  $\gamma$ -rays. By extrapolating the measurements made between  $\sim 50 \text{ g-cm}^{-2}$  and  $\sim 2 \text{ g-cm}^{-2}$  to the top of the atmosphere, the authors found a residual rate over 10 standard deviations above zero. There were some differences in the absolute intensities measured during the two flights; in addition a fairly large uncertainty, about  $0.5 \text{ g-cm}^{-2}$ ,

was present in the measurement of the atmospheric depth. However, the authors did not feel that these uncertainties affected their conclusions concerning the existence of a cosmic diffuse component. They also presented evidence that the spectrum of this component was appreciably softer than the atmospheric spectrum. This conclusion was reached on the basis of measurements made on the distribution of the opening angles of pairs observed in the spark chamber. However, the observed increase in the average opening angle appears to occur abruptly, at depths less than about  $3 \text{ g-cm}^{-2}$ , and is therefore suspicious.

During the NRL balloon flight over Argentina in 1971, an investigation was also made of the growth of atmospheric  $\gamma$ -rays as a function of depth, in an attempt to establish the existence of the primary diffuse component. Advantage was taken of the increased cutoff rigidity (11.5 GV), which reduced the intensity of secondary radiation. The data are shown in Figure 16, where the counting rate of electron pairs is given in the left ordinate and the estimated intensity of vertically incident  $\gamma$ -rays is shown on the right. Data obtained over Texas ( $R \geq 4.5 \text{ GV}$ ) are also displayed for comparison. A linear extrapolation of the data over Argentina gave evidence for a residual rate above the atmosphere which was about  $3.5 \sigma$  above zero (Share, Kinzer and Seeman 1972 and preprint 1972). An upper limit obtained from our Texas data (Kinzer et al. 1971c) is consistent with this residual rate.

Due to the difficulties in making measurements of this kind, we made a detailed investigation of various possible sources of background which might have simulated this residue. Among those investigated were local sources for producing the residual photons, such as the pressure vessel enclosing the system, and atmospheric  $\gamma$ -rays incident from the horizon. From our investigations we concluded that these sources were not likely to have contributed appreciably to the residue.

A schematic drawing of the NRL telescope is shown in Figure 17. Downward  $\gamma$ -rays are detected after they convert in a stack of nuclear emulsion and produce either Compton electrons or electron pairs which trigger the proportional counter (P) and two scintillators (B), without the presence of an accompanying particle in any of the anticoincidence scintillators (A). The absorption-Cerenkov counter (C) restricts detected  $\gamma$ -rays to those below  $\sim 200$  MeV; it also rejects about 50% of upward moving  $\gamma$ -rays converting in the Plexiglas block (C) and producing upward-moving low-energy electrons which can also trigger the telescope. The remaining upward-moving electrons are a likely source for the residual rate of  $\gamma$ -rays which we observed. However, as I mentioned above, only events appearing to be downward-moving electron-pairs were used in our growth curve. How then can these upward-moving electrons simulate downward-moving pairs? If the electrons are of low-energy, they can be scattered appreciably in the emulsion and then emerge in the downward direction; the event would then appear to be a downward pair of low energy.

Another source for these low-energy electrons which can enter the detector's geometry is the splash albedo from the atmosphere. These electrons can pass through the space between the active walls of the spark chamber and the anticoincidence cup surrounding the Plexiglas block. They will be detected and appear as downward pairs if they are scattered back out of the emulsion and have sufficient energy to reach the bottom coincidence counters (B).

We estimate that the combined rate from both of these types of events, which imitate downward electron-pairs, can contribute appreciably to our residual rate of pairs above the atmosphere. For this reason, we have concluded that our measurement must be interpreted only as an upper limit to the true diffuse  $\gamma$ -ray intensity.

The measurements of diffuse  $\gamma$ -radiation above 1 MeV are summarized in Figure 18. The solid line represents an extrapolation of the fit of X-ray data to a power-law spectrum (Kasturirangan and Rao, 1972), while the dotted-dashed curves represent the uncertainty in this extrapolation. Measurements above 10 MeV are typically obtained over a wide range in energy; this range is shown by the dashed lines and the points have been plotted at the median energy photon detected for an assumed  $E^{-2}$  spectrum. The data above 1 MeV from ERS-18 (Vette et al. 1970) were found to have been in error and have been superseded by measurements from Apollo 15 (Trombka et al. 1973; see also Trombka and Peterson in this volume). The measurements from Apollo 15 indicate that the energy spectrum of low-energy  $\gamma$ -rays flattens above about 500 keV; above 1 MeV their measured intensities are still higher than the upper limits reported by Bratolyubova-Tsulukidze et al. (1970) and by Daniel, Joseph, and Lavakare (1972).

The intensity reported by Mayer-Hasselwander et al. at higher energies appears consistent with the data from Apollo 15. However, there may be a systematic error in the intensity given by Mayer-Hasselwander et al. They report that their measurement of the atmospheric  $\gamma$ -ray intensity is about 60% of the value calculated by Beuermann (1969); however, measurements by other groups indicate that the calculated flux may be too low (e.g. Fichtel, Kniffen and Ogelmann 1969; and Seeman, Share and Kinzer 1973). This suggests that the primary diffuse intensity reported by Mayer-Hasselwander et al. may therefore be low by about a factor of two.

The upper limit determined by our measurement over Argentina, although consistent with the reported intensities, suggests that the flux of diffuse  $\gamma$ -rays near 30 MeV is lower than reported by either Trombka et al. or Mayer-Hasselwander et al. The fluxes reported by these authors are considerably above a power-law spectrum fit to both the X-ray observations and the 100 MeV

measurements of Kraushaar et al. 1972. This had led to suggestions that an additional component may be needed to explain the results from 1-50 MeV. Theoretical models for generating this additional component have been recently summarized by Silk (preprint 1973), Stecker (1973), and Strong et al. (1973). Further discussion can also be found in other sections of this volume.

### Future Observations

Gamma-ray astronomy has finally emerged as an observational science. However, as is apparent from this summary of recent measurements, an improvement in sensitivity is required in order to permit more detailed investigations. The new generation of satellite detectors, ESRO's TD-1A and COS-B, and NASA's SAS-B represent the first step in providing the increased sensitivity. This is primarily due to the longer observation periods and lower  $\gamma$ -ray background intrinsic in satellite observations.

These detectors should be able to measure the energy spectrum of the diffuse radiation  $\geq 30$  MeV and to begin to investigate its spatial isotropy. They should also have the sensitivity to verify the existence of the various possible point sources of  $\gamma$ -rays reported from balloon-borne observations and, furthermore, to study their energy spectra and to establish whether or not they are variable. There is also little doubt that these detectors will be able to investigate emission of diffuse  $\gamma$ -radiation from the galactic plane and to map its distribution at resolutions of  $\sim 3^\circ$ . These measurements of high-energy photons from the galactic disc, like the ones made 25 years earlier in the radio band, will substantially further our knowledge of the distribution of matter, magnetic field strengths and cosmic-ray fluxes in the galaxy.

Continued work at balloon altitudes should be encouraged, especially in the light of the reduced funding for "expensive" satellite programs. These balloon-borne instruments should be designed with improved resolution in energy, angle and timing in order to help compensate for the atmospheric background and to permit continued investigation of periodically pulsing objects such as the Crab Pulsar. Improved sensitivity for balloon-borne detectors should follow naturally from the development of high-altitude super-pressure balloons and from observations conducted at high geomagnetic cutoff rigidities.

## REFERENCES

- Albats, P., Frye, G. M., Jr., Zych, A. D., Mace, O. B., Hopper, V. D., and Thomas, J. A. 1972, *Nature*, 240, 221.
- Bennett, K., Penengo, P., Rochester, G. K., Sanderson, T. R., and Sood, R. K. 1972, *Nature*, 238, 31.
- Beuermann, K. P. 1971, *J. Geophys. Res.*, 76, 4291.
- Bratolyubova-Tsulukidze, L. I., Grigorov, N. L., Kalinkin, L. F., Melioransky, A. S., Pryakhin, E. A., Savenko, I. A., and Yufarkin, V. Ya. 1970, *Acta Phys.*, 29 Suppl. 1, 123.
- Browning, R., Ramsden, D., and Wright, P. J. 1971, *Nature Phys. Sci.*, 232, 99.
- Browning, R., Ramsden, D., and Wright, P. J. 1972, *Nature*, 238, 138.
- Clark, G. W., Garmire, G. P., and Kraushaar, W. L. 1968, *Ap. J. (Letters)*, 153, L203.
- Dahlbacka, G. H., Freier, P. S., and Waddington, C. J. 1973, *Ap. J.*, 180, 371.
- Damle, S. V., Daniel, R. R., Joseph, G., Lavakare, P. J. 1971, *Ap. and Space Sci.*, 14, 473.
- Daniel, R. R., Joseph, G., and Lavakare, P. J. 1972, *Ap. and Space Sci.*, 18, 462.
- Dyer, C. S. and Morfill, G. E. 1971, *Ap. and Space Sci.*, 14, 243.
- Fazio, G. G. 1973, *Proceedings of IAU Symposium #55 on X-Ray and Gamma-Ray Astronomy*, H. Bradt ed. (in press).
- Fichtel, C. E., Hartman, R. C., Kniffen, D. A., and Sommer, M. 1972, *Ap. J.*, 171, 31.
- Fichtel, C. E., Kniffen, D. A., and Ogelman, H. B. 1969, *Ap. J.*, 158, 193.
- Fishman, G. J. 1972, *Ap. J.*, 171, 163.
- Frye, G. M., Jr., Albats, P. A., Zych, A. D., Staib, J. A., Hopper, V. D., Rawlinson, W. R., and Thomas, J. A. 1971a, *Nature*, 231, 372.
- 1971b, *Nature*, 233, 466.
- Frye, G. M., Jr., Staib, J. A., Zych, A. D., Hopper, V. D., Rawlinson, W. R., and Thomas, J. A. 1969, *Nature*, 223, 1320.
- Frye, G. M., Jr. and Wang, C. P. 1969, *Ap. J.*, 158, 925.
- Gal'per, A. M., Kirillov-Ugryumov, V. G., Luchkov, B. I., and Prilutskii, O. F. 1972, *Soviet Phys. Uspekhi*, 14, 630.
- Garmire, G. and Kraushaar, W. L. 1965, *Space Sci. Rev.*, 4, 123.
- Golenetskii, S. V., Mazets, E. P., Ill'inskii, V. N., Aptekar', R. L., Bredov, M. M., Gur'yan, Yu. A., and Panov, V. N. 1971, *Ap. Letters*, 9, 69.
- Hearn, D. 1969, *Nucl. Inst. and Meth.*, 70, 200.
- Helmken, H. F. and Hoffman, J. A. 1973, *Nature Phys. Sci.*, 243, 6.
- Hillier, R. R., Jackson, W. R., Murray, A., Redfern, R. M., and Sale, R. G. 1970, *Ap. J. (Letters)*, 162, L177.
- Hutchinson, G. W., Pearce, A. J., Ramsden, D., and Wills, R. D. 1969, *Acta Phys.* 29, Suppl. 1, 87.
- Jansky, K. G. 1932, *Proc. IRE*, 20, 1920.
- Jansky, K. G. 1933, *Proc. IRE*, 21, 1387.
- Kasturirangan, K. and Rao, U. R. 1972, *Ap. and Space Sci.*, 15, 161.
- Kettenring, G., Mayer-Hasselwander, H. A., Pfeffermann, E., Pinkau, K., Rothermal, H., and Sommer, M. 1971, *Proc. 12th Int. Conf. Cosmic Rays*, Hobart, 1, 57.
- Kinzer, R. L., Noggle, R. C., Seeman, N., and Share, G. H. 1971a, *Nature*, 229, 187.
- Kinzer, R. L., Seeman, N., and Share, G. H. 1971b, *Proc. 12th Int. Conf. Cosmic Rays*, Hobart, 1, 45.
- Kinzer, R. L., Seeman, N., and Share, G. H. 1971c, *Proc. 12th Int. Conf. Cosmic Rays*, Hobart, 1, 51.

- Kinzer, R. L., Share, G. H., and Seeman, N. 1973, Ap. J., 180, 547.
- Kniffen, D. A. and Fichtel, C. E. 1970, Ap. J., 161, L157.
- Kraushaar, W. L., Clark, G. W., Garmire, G. P., Borken, R., Higbie, P., Leong, C., and Thorsos, T. 1972, Ap. J., 177, 341.
- Kurfess, J. D. 1971, Ap. J. (Letters), 168, L39.
- Kurfess, J. D. and Share, G. H. 1973, preprint.
- Leray, J. P., Vasseur, J., Paul, J., Parlier, B., Forichon, M., Agrinier, B., Boella, G., Maraschi, L., Treves, A., Buccheri, L., Cuccia, A., and Scarsi, L. 1972, Astr. and Ap., 16, 443.
- Mayer-Hasselwander, H. A., Pfeffermann, E., Pinkau, K., Rothermel, H., and Sommer, M. 1972, Ap. J. (Letters), 175, L23.
- McBreen, B., Ball, S. E., Jr., Campbell, M., Greisen, K., and Koch, D. 1973, .. Preprint to be published in Ap. J.
- Ogelman, H. 1969, Nature 221, 753.
- O'Mongain, E. 1973, Nature, 241, 376.
- Orwig, L. E., Chupp, E. L., and Forrest, D. J. 1971, Nature, 231, 171.
- Pal, Y. 1973, Proceedings of IAU Symposium #55 on X-Ray and Gamma-Ray Astronomy, H. Bradt ed. (in press).
- Parlier, B., Agrinier, B., Forichon, M., Leray, J. P., Boella, G., Maraschi, L., Buccheri, R., Robba, N. R., and Scarsi, L. 1973, Nature Phys. Sci., 242, 117.
- Schwartz, D. A., Hudson, H.S., and Peterson, L. E. 1970, Ap. J., 162, 431.
- Seeman, N., Share, G. H., and Kinzer, R. L. 1973, Proc. 13th Int. Cosmic-Ray Conf.
- Share, G. H., Kinzer, R. L., and Seeman, N. 1972, Bull. A.P.S., 17, 524.
- Share, G. H., Kinzer, R. L., and Seeman, N. 1973, Proc. 13th Int. Cosmic-Ray Conf.
- Stecker, F. W. 1973, Nature, 241, 74.
- Strong, A. W., Wolfendale, A. W., and Wdowczyk, J. 1973, Nature, 241, 109.
- Trombka, J. I., Metzger, A. E., Arnold, J. R., Matteson, J. L., Reedy, R. C., and Peterson, L. E. 1973, Ap. J., 181, 737.
- Valdez, J. V. and Waddington, C. J. 1969, Ap. J. (Letters), 156, L85.
- Valentine, D., Kaplon, M. F., and Badhwar, G. 1970, Acta Phys., 29, Supp. 1, 101.
- Vedrenne, G., Albernhe, F., Martin, I., and Talon, R. 1971, Astr. and Ap., 15, 50.
- Vette, J. I., Gruber, D., Matteson, J. L., Peterson, L. E. 1970, Ap. J. (Letters), 160, L161.

Figure Captions

- Figure 1 Variation of the counting rate of cosmic  $\gamma$ -rays observed from OSO-3 as a function of galactic latitude for successive  $60^\circ$ -intervals of galactic longitude.
- Figure 2 Ratio of observed line intensity of  $> 100$  MeV  $\gamma$ -rays to expected background intensity for  $-25^\circ \leq l^{\text{II}} \leq +20^\circ$ , plotted as a function of galactic latitude,  $b^{\text{II}}$  (from Fichtel et al. 1972).
- Figure 3 Variation in  $\gamma$ -ray intensity scanned across the galactic equator near the galactic center by Frye et al. (1971a). The dashed curves in parts G and H represent the intensity reported by Fichtel et al. (1972).
- Figure 4 A histogram of the number of  $\gamma$ -ray events in strips parallel to the galactic plane reported by Dahlbacka et al. (1973). The upper histogram is for events found in the emulsion and the lower one is for events observed in the spark chamber. The dashed curves represent the expected shape if there were no excess of emission from the galactic plane.
- Figure 5 Distribution of observed  $\gamma$ -rays within a)  $3^\circ$  and b)  $1^\circ$  bands of galactic latitude for  $320^\circ < l^{\text{II}} < 40^\circ$  as reported by the NRL group. The curves are normalized to the observed events for  $|b^{\text{II}}| > 6^\circ$  and represent the distribution expected for  $\gamma$ -rays of atmospheric origin.
- Figure 6 Measurements of the flux of  $\gamma$ -rays from the galactic plane near the center of the galaxy. The NRL measurements are given for three assumed spectra and are extrapolated to higher energies.

- Figure 7 Galactic map of arrival directions of  $\gamma$ -rays reported by the NRL group. The RMS uncertainty in arrival direction is shown by the open circles. Regions within the dashed curves had relative exposures  $> 75\%$  and  $> 50\%$ .
- Figure 8 Map of arrival directions of  $\gamma$ -rays observed in a search by the NRL group for the variable source Libra  $\gamma$ -1.
- Figure 9 Number of  $\gamma$ -ray events  $\geq 10$  MeV observed by Kinzer et al. (1971) relative to the optical phase of NPO532. a) Events pointing within  $10^\circ$  of the Crab; b) events pointing outside  $10^\circ$  from the Crab. The dashed lines give the mean numbers ( $N$ ) of  $\gamma$ -rays/time-bin and the errors shown are  $\pm \sqrt{N}$ .
- Figure 10 Number of  $\gamma$ -ray events 10-30 MeV observed by Albats et al. (1972) within  $15^\circ$  of the Crab plotted relative to the radio phase of NPO532.
- Figure 11 The X-ray "light curves" for photons from the Crab Pulsar between 100-400 keV observed by Kurfess (1971) during two balloon flights on a) Oct. 10, 1970 and b) Oct. 21, 1970.
- Figure 12 Phase histograms of two independent samples of  $\gamma$ -ray events observed with the Cornell  $4.5 \text{ m}^2$  Čerenkov telescope (McBreen et al. 1973). The events in the upper histogram originated within  $2^\circ$  of the Crab Nebula, while those in the lower histogram within  $1^\circ$  of the Crab. The arrival times of the optical main pulse and secondary pulse are shown. The indicated background levels were derived from the events recorded in the intervals 0-9 and 24-33 msec.
- Figure 13 Summed phase histogram of  $\gamma$ -ray observations of the Crab Pulsar taken from Figures 9, 11, and 12. The original data were plotted at 1 msec resolution, but are summed here in 3 msec bins in order to display the broad features of the observations.

- Figure 14 Measurements of the time-averaged pulsed intensity of NP0532. The straight line represents an extrapolation of a power-law fit to the total emission spectrum of the Crab at X-ray energies.
- Figure 15 Counting rates of electron pairs as a function of residual atmosphere observed during two balloon flights conducted by the Max Planck Institute over Texas. The full lines are fits to the data deep in the atmosphere and represent the growth of secondary  $\gamma$ -rays. The dashed curves are fits to all the data obtained at depths  $\leq 50 \text{ g-cm}^{-2}$ , assuming the presence of an extraterrestrial component of  $\gamma$ -rays.
- Figure 16 Vertical intensities of  $\gamma$ -rays  $10 < E < 200 \text{ MeV}$  at rigidities  $> 4.5 \text{ GV}$  and  $> 11.5 \text{ GV}$  as determined by the NRL group from the counting rates of "electron pairs" observed in its wide-gap spark chamber as a function of atmospheric depth. The lines are least squares fits and the errors shown are statistical. (Not shown in the rate  $100 \pm 13/\text{min}$  observed at  $55 \text{ g-cm}^{-2}$  for  $R > 4.5 \text{ GV}$ .)
- Figure 17 Drawing of the detector used by the NRL group showing an electron pair in the wide-gap spark chamber (S.C.). (A) plastic anti-coincidence counters; (E) emulsion stack  $650 \text{ cm}^2 \times 1.25 \text{ cm}$ ; (P) multiwire proportional counter; (B) 2 plastic coincidence counters; (c) absorption - Čerenkov counter of clear Plexiglas ( $15 \text{ g-cm}^{-2}$ ). Čerenkov light from up-coming particles is reflected by (R) onto phototubes (not shown) imbedded in the block.
- Figure 18 Measurements of diffuse cosmic  $\gamma$ -radiation. Energy ranges for observations  $> 10 \text{ MeV}$  are shown and the fluxes are plotted at the median energy photon detected for an assumed  $E^{-2}$  spectrum.

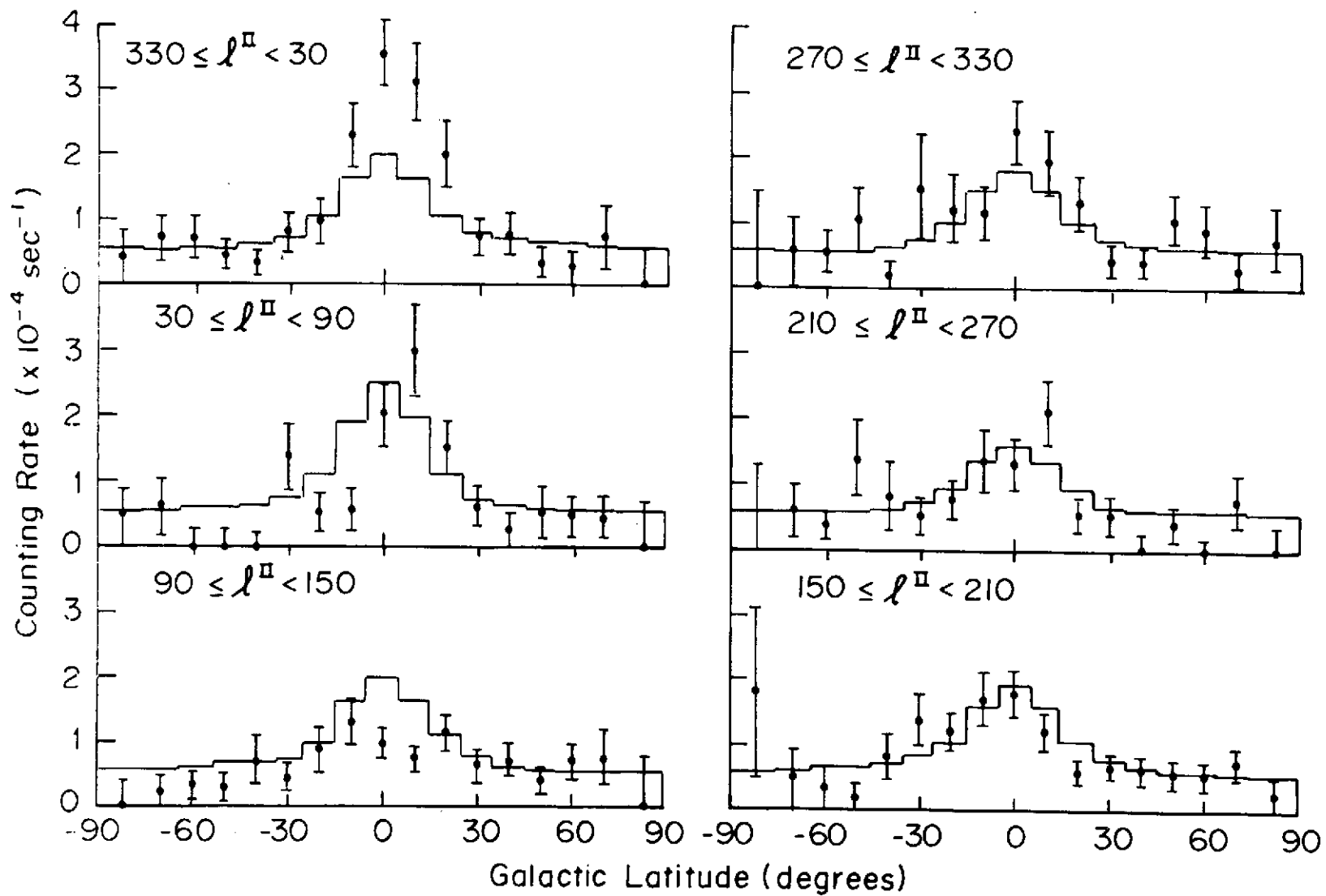


Figure 1

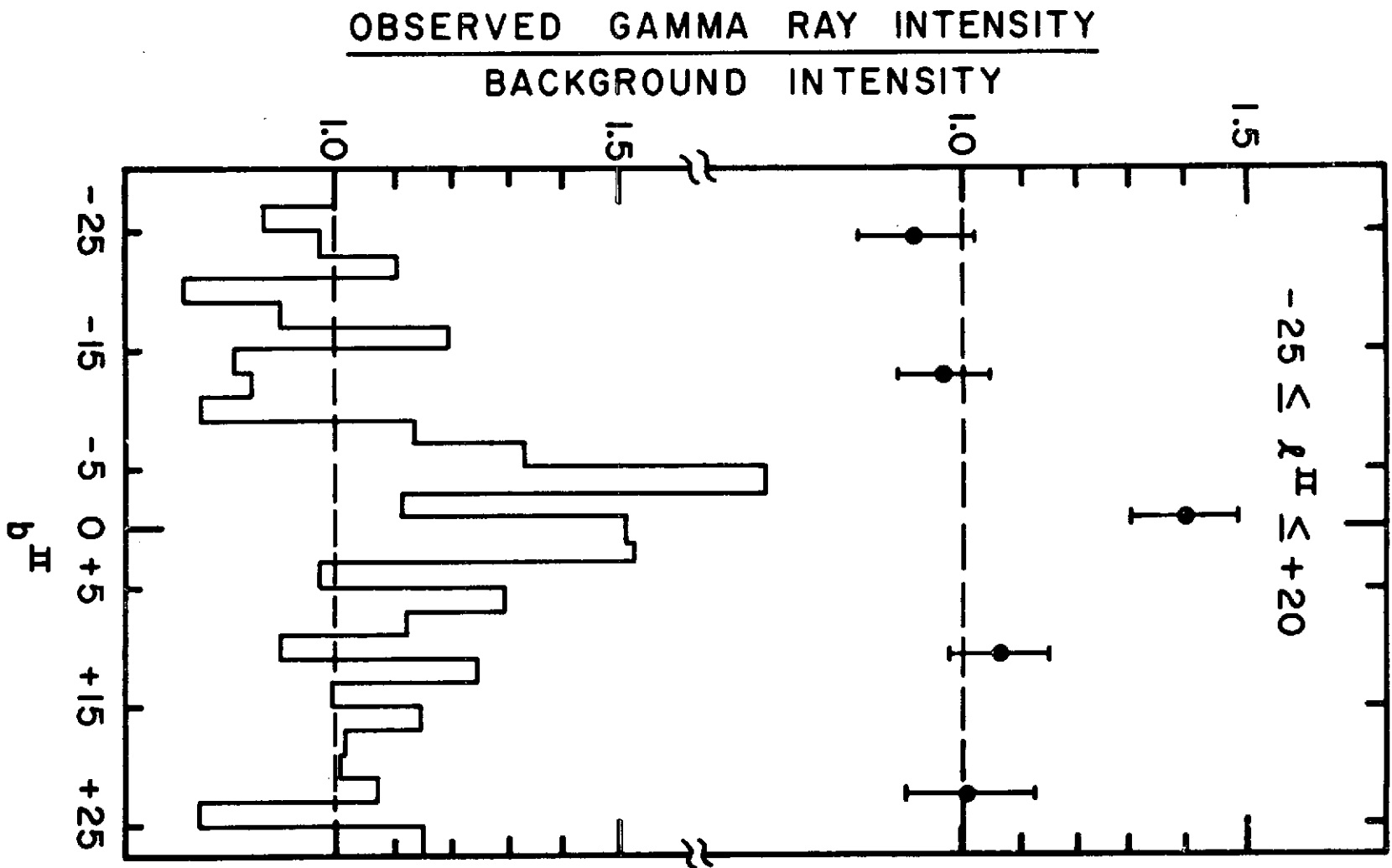


Figure 2

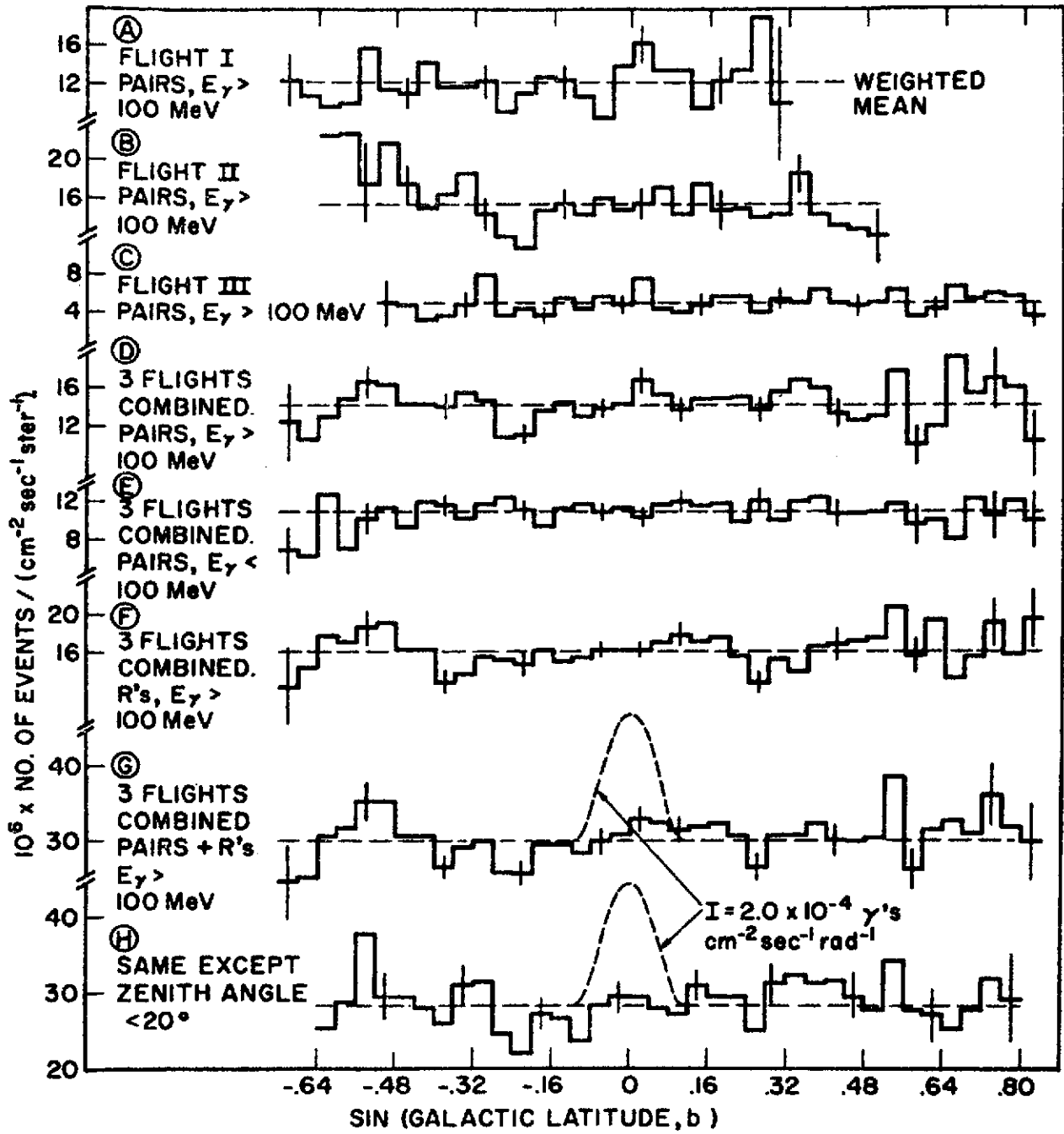


Figure 3

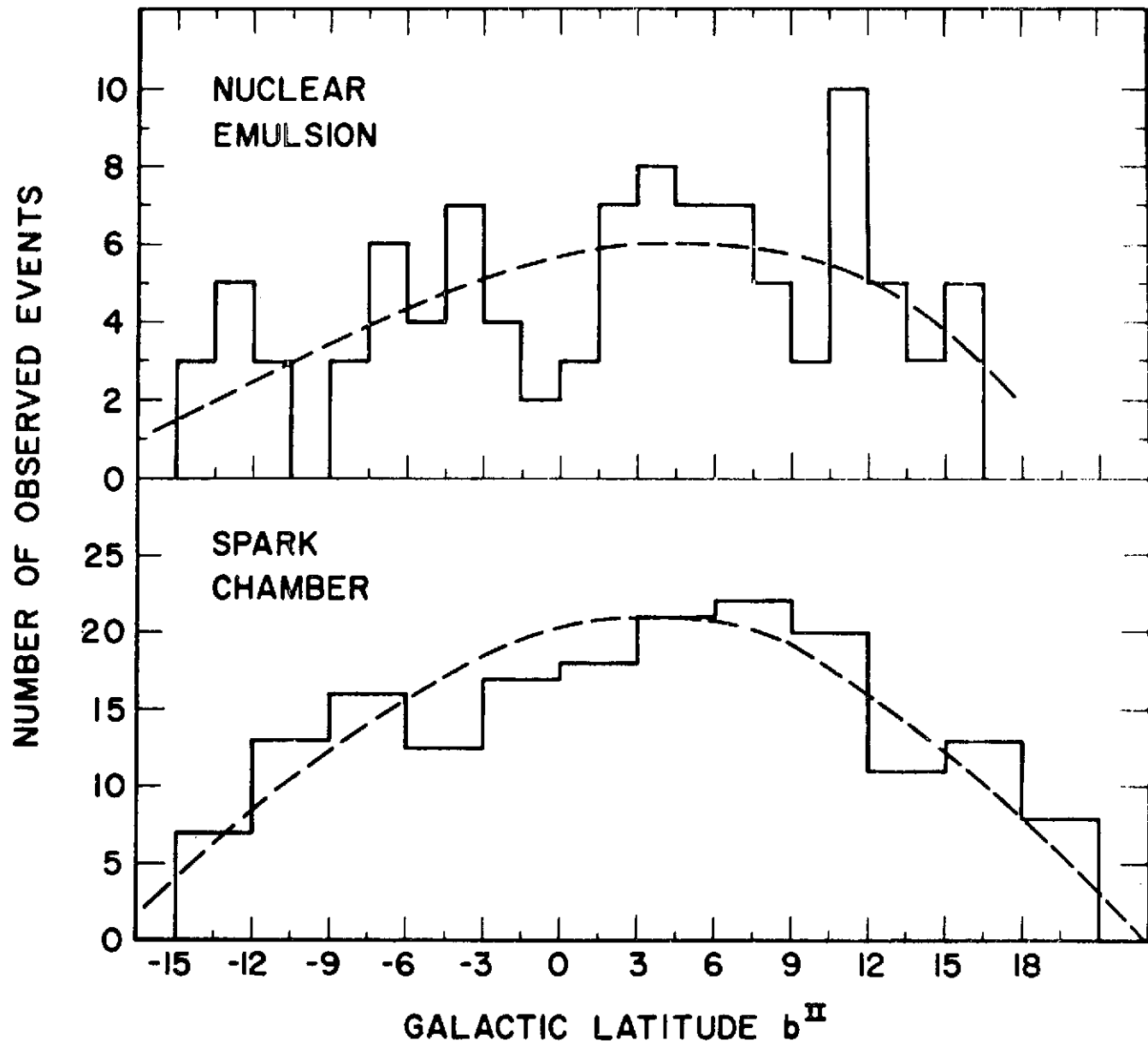


Figure 4

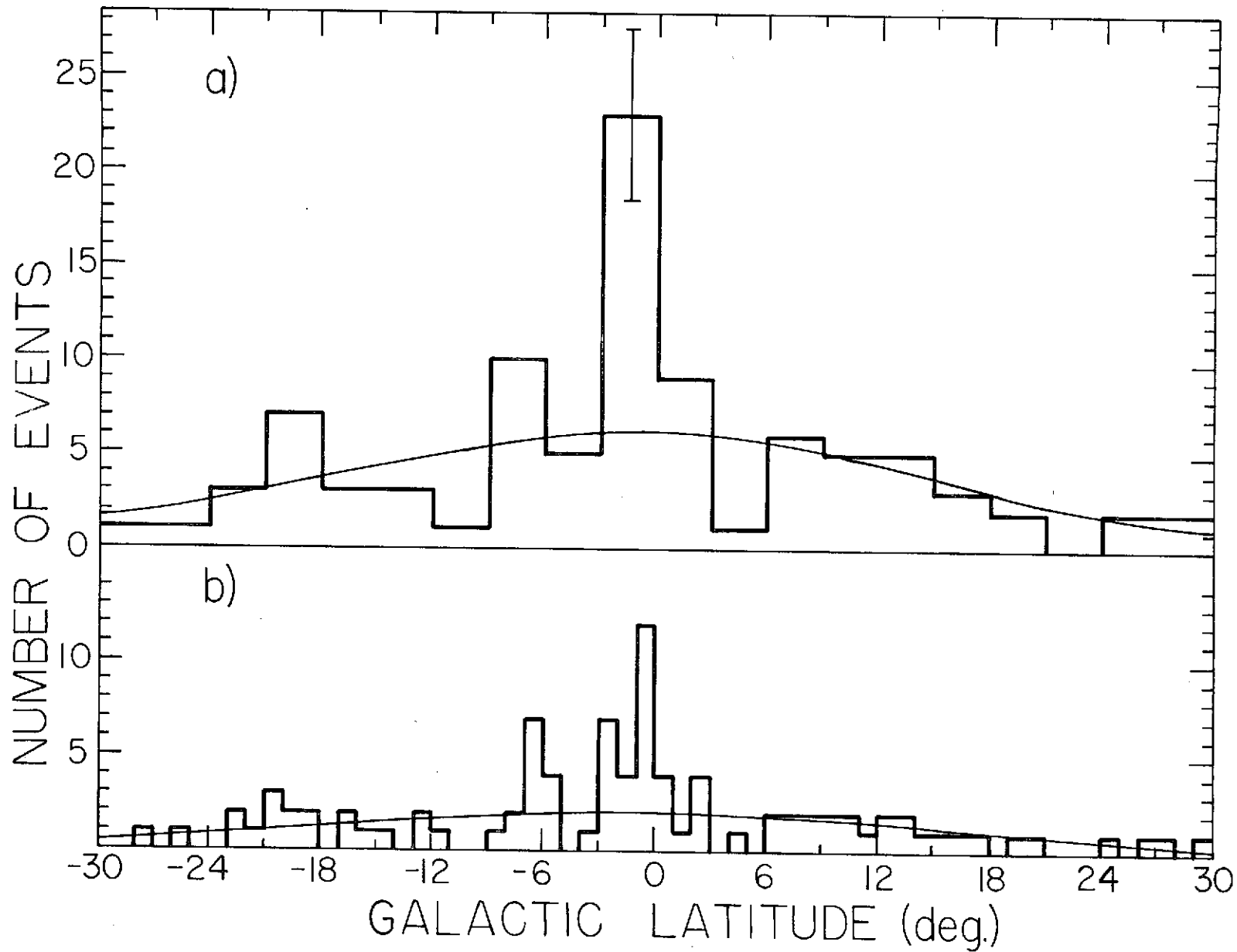


Figure 5

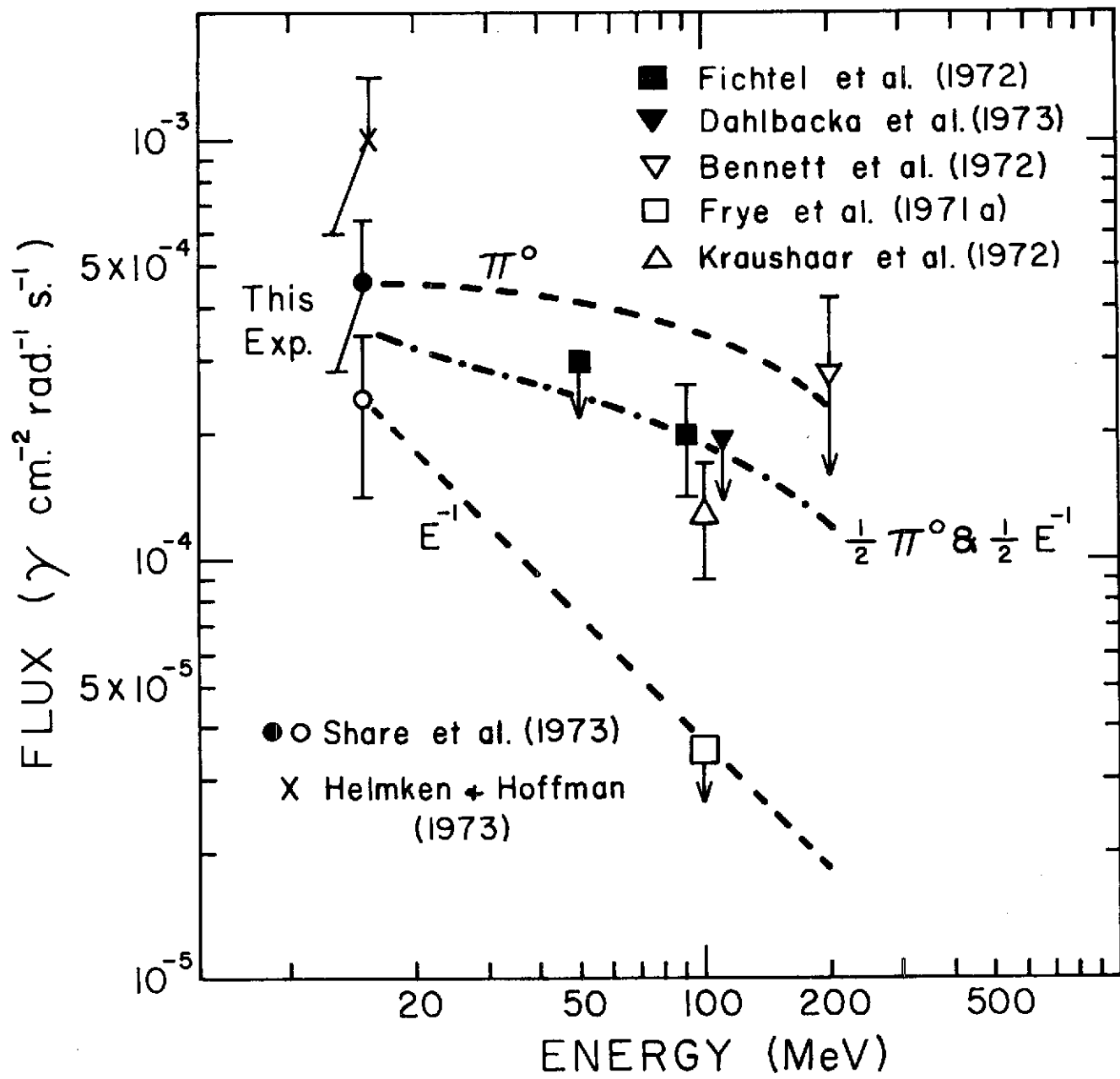


Figure 6

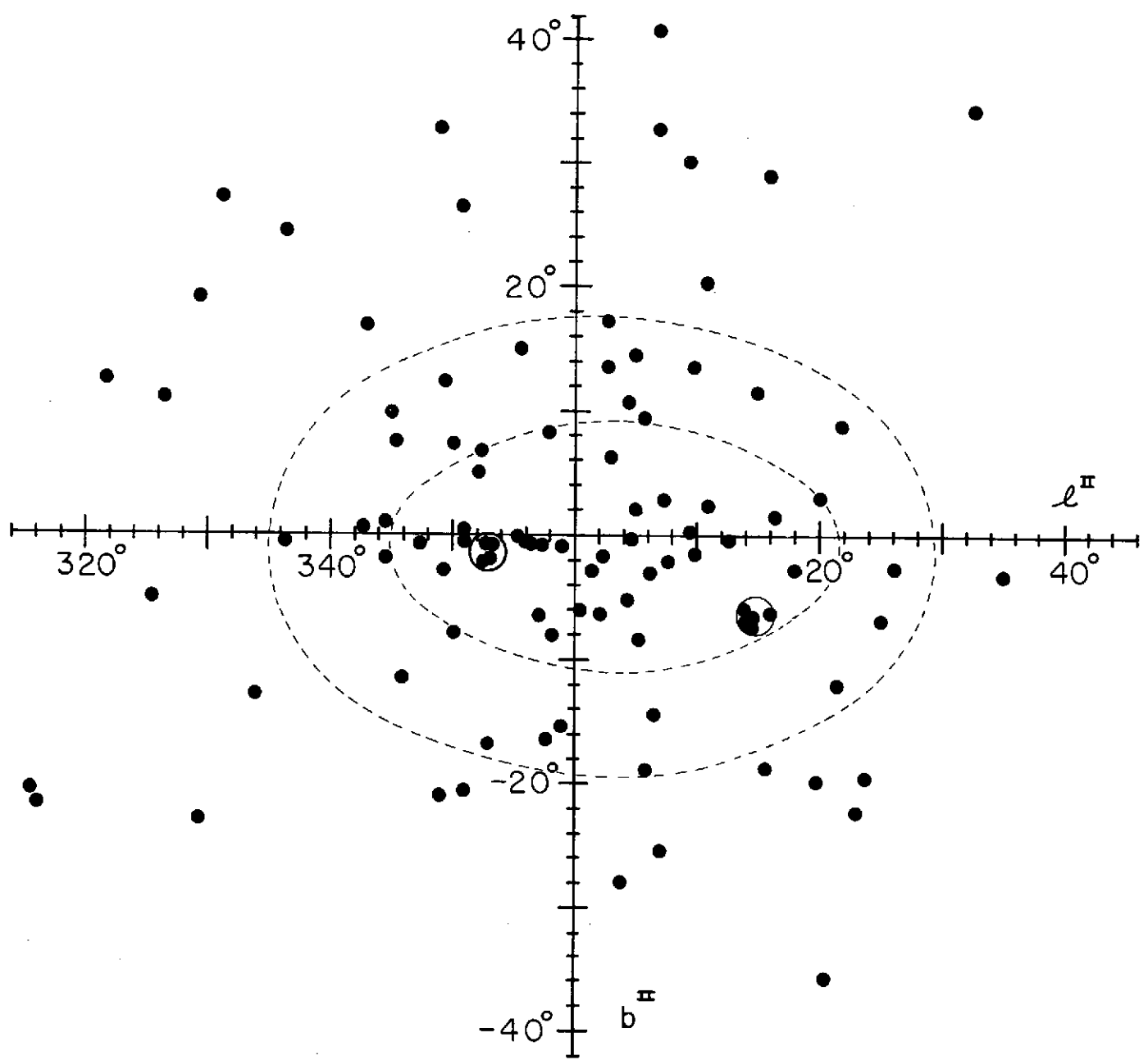


Figure 7

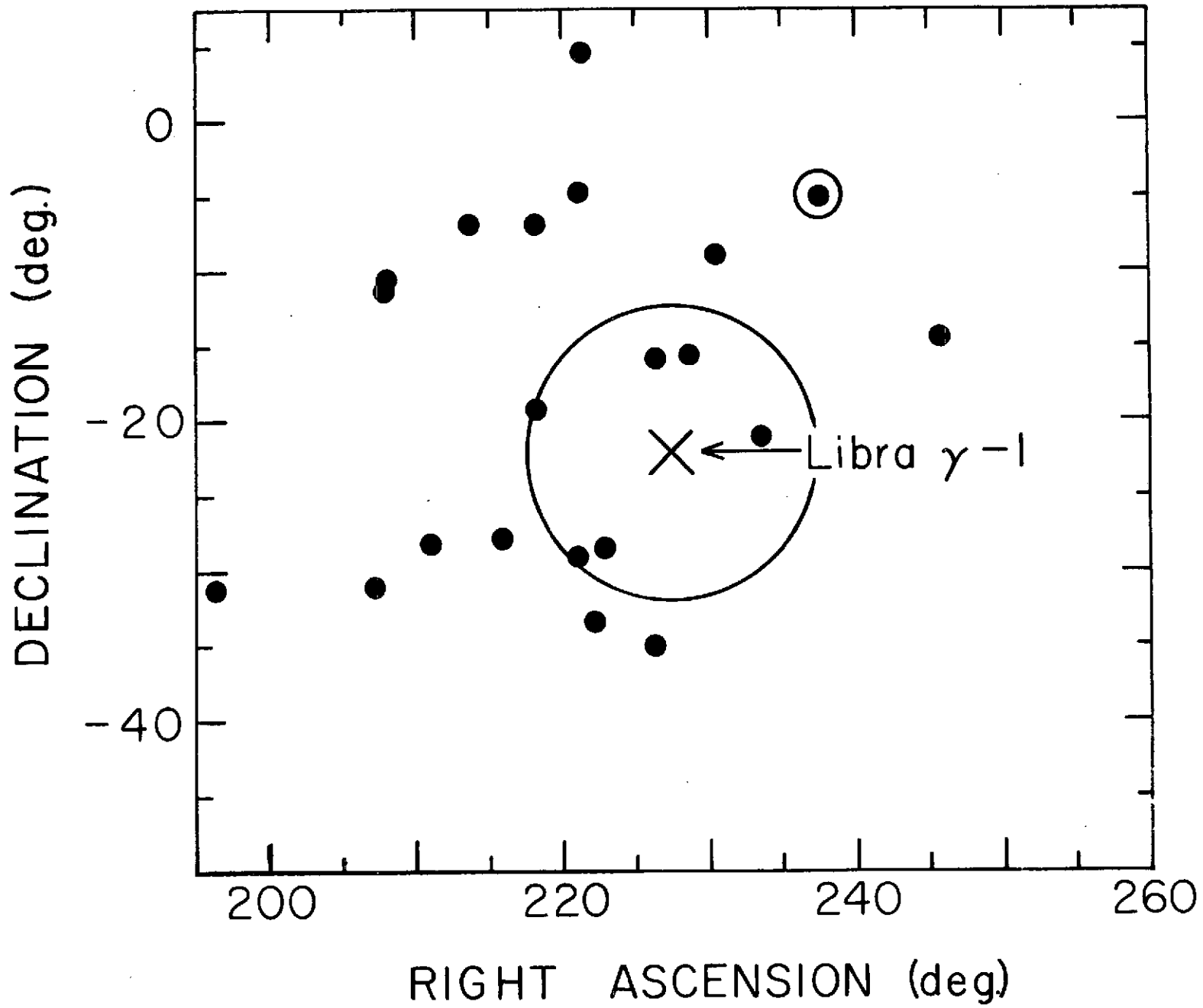


Figure 8

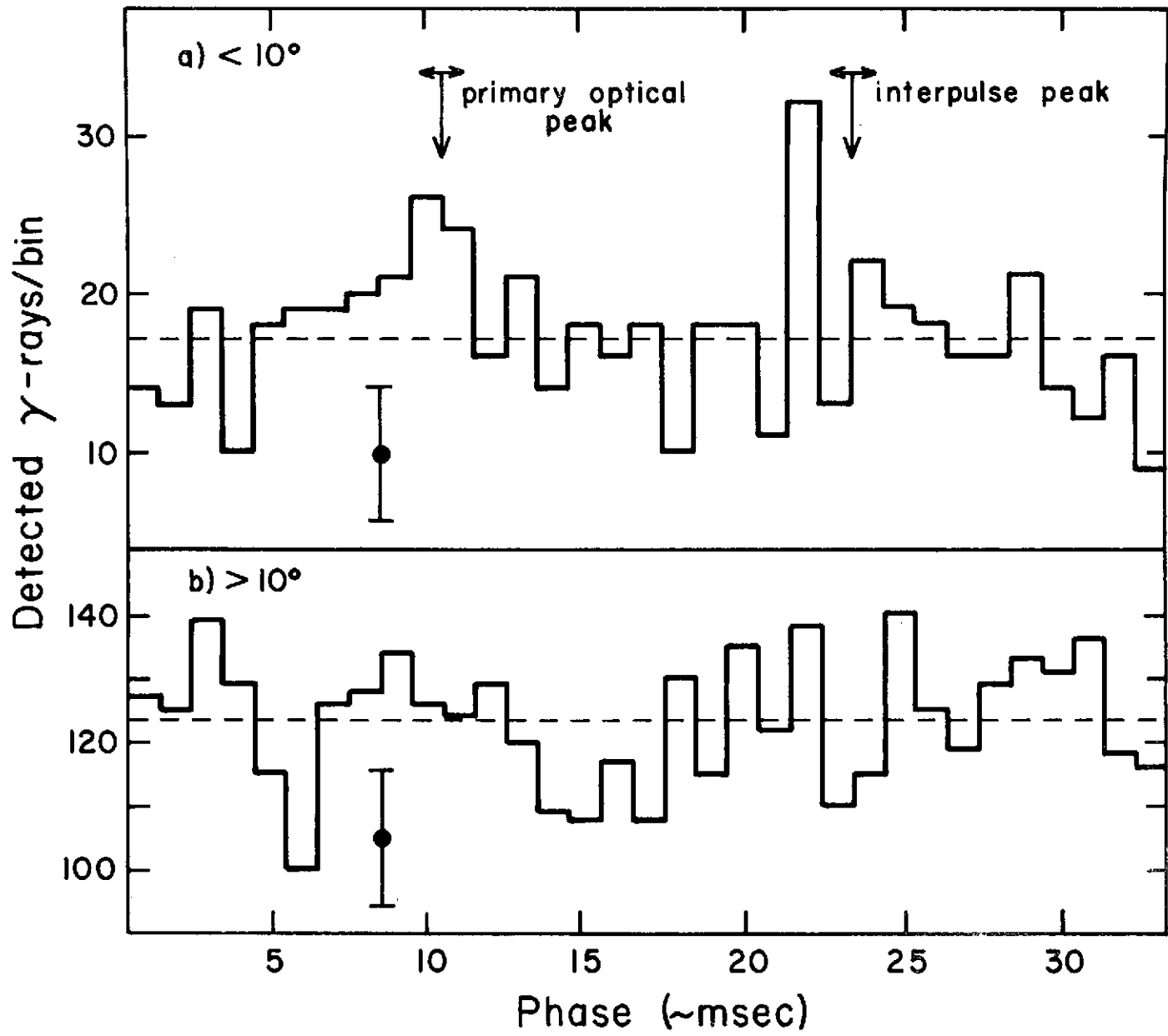


Figure 9

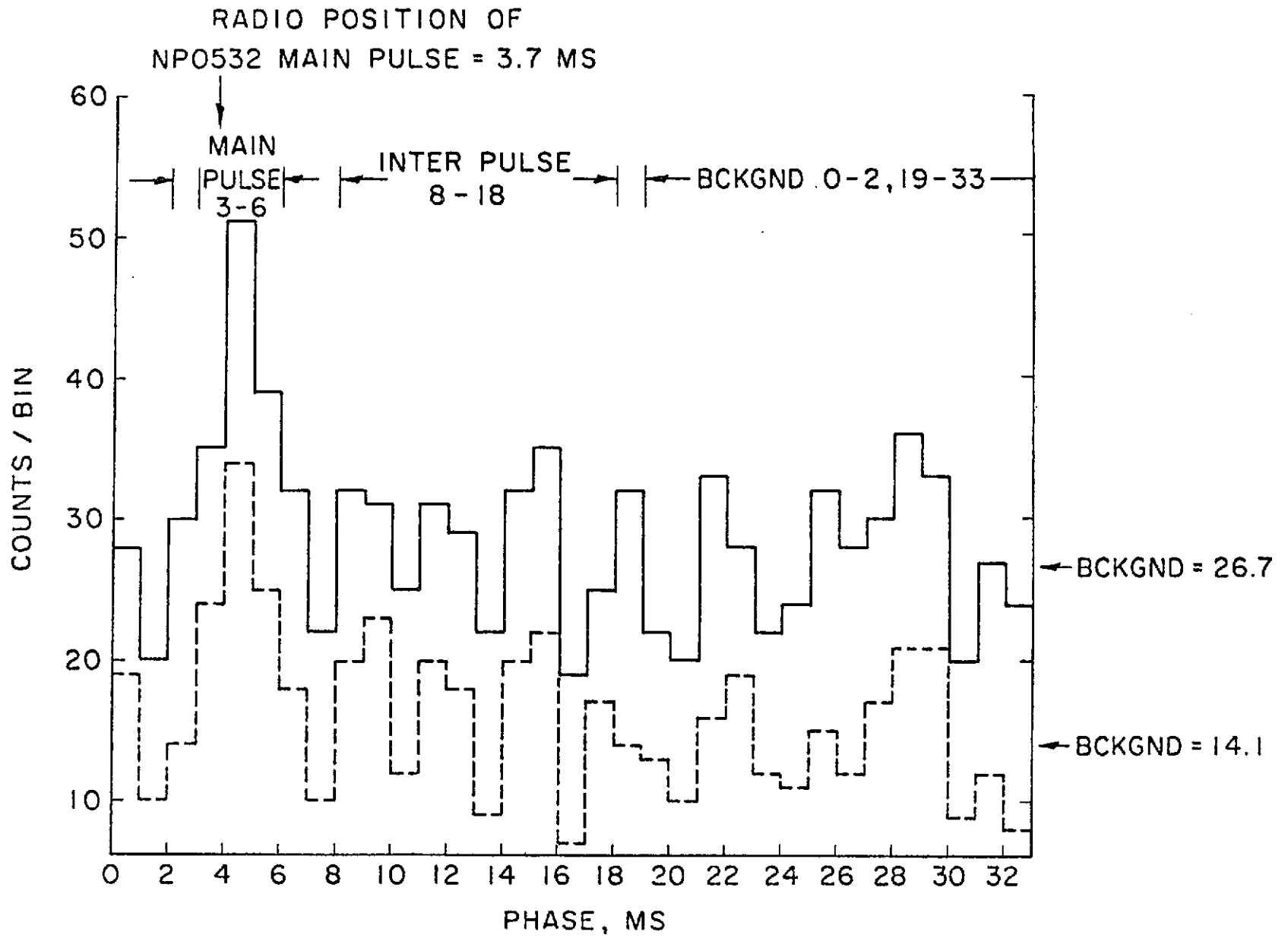


Figure 10

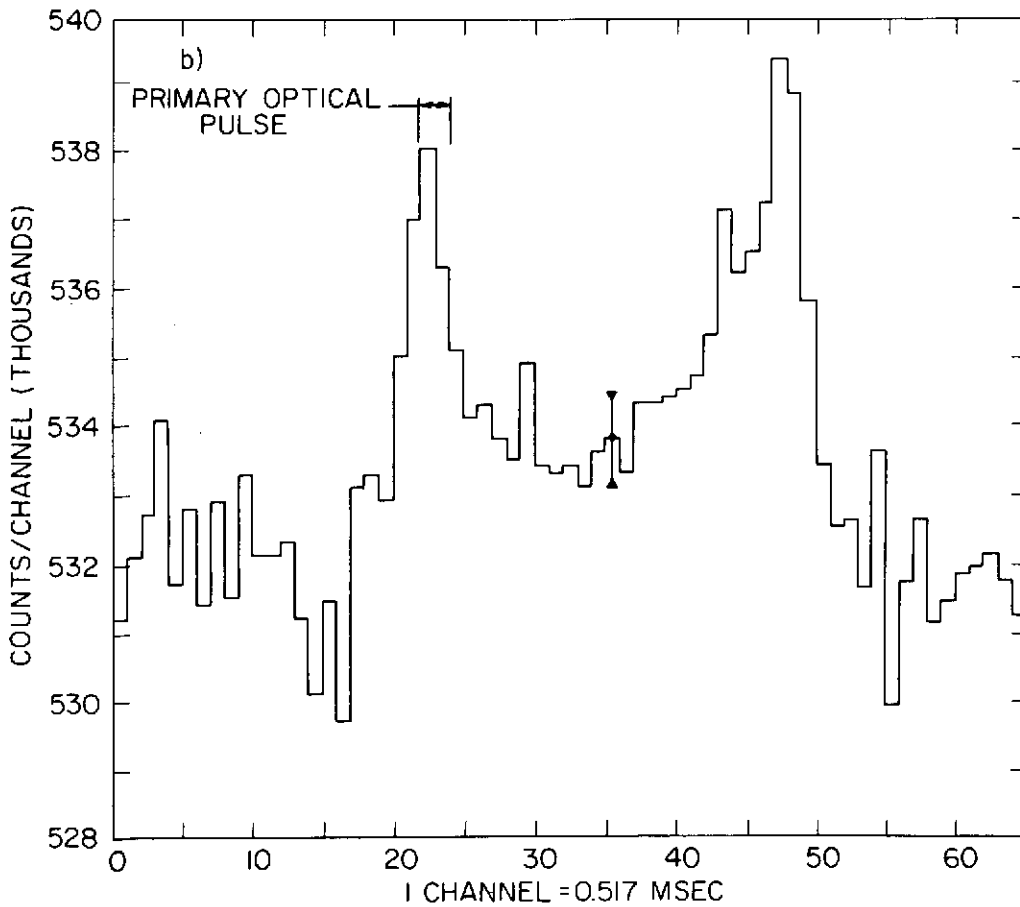
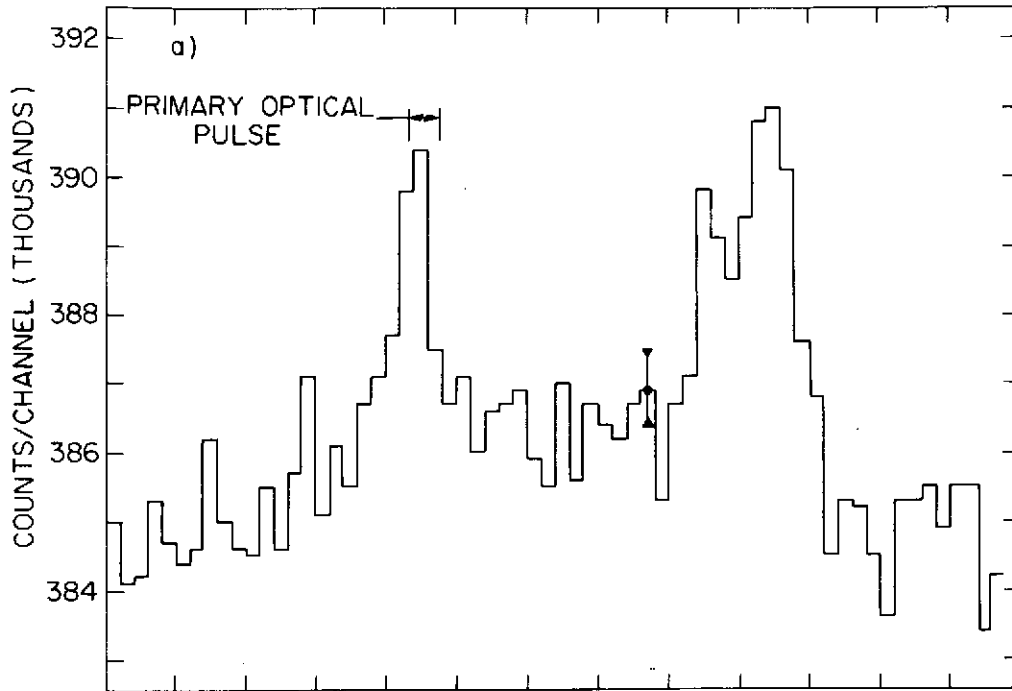
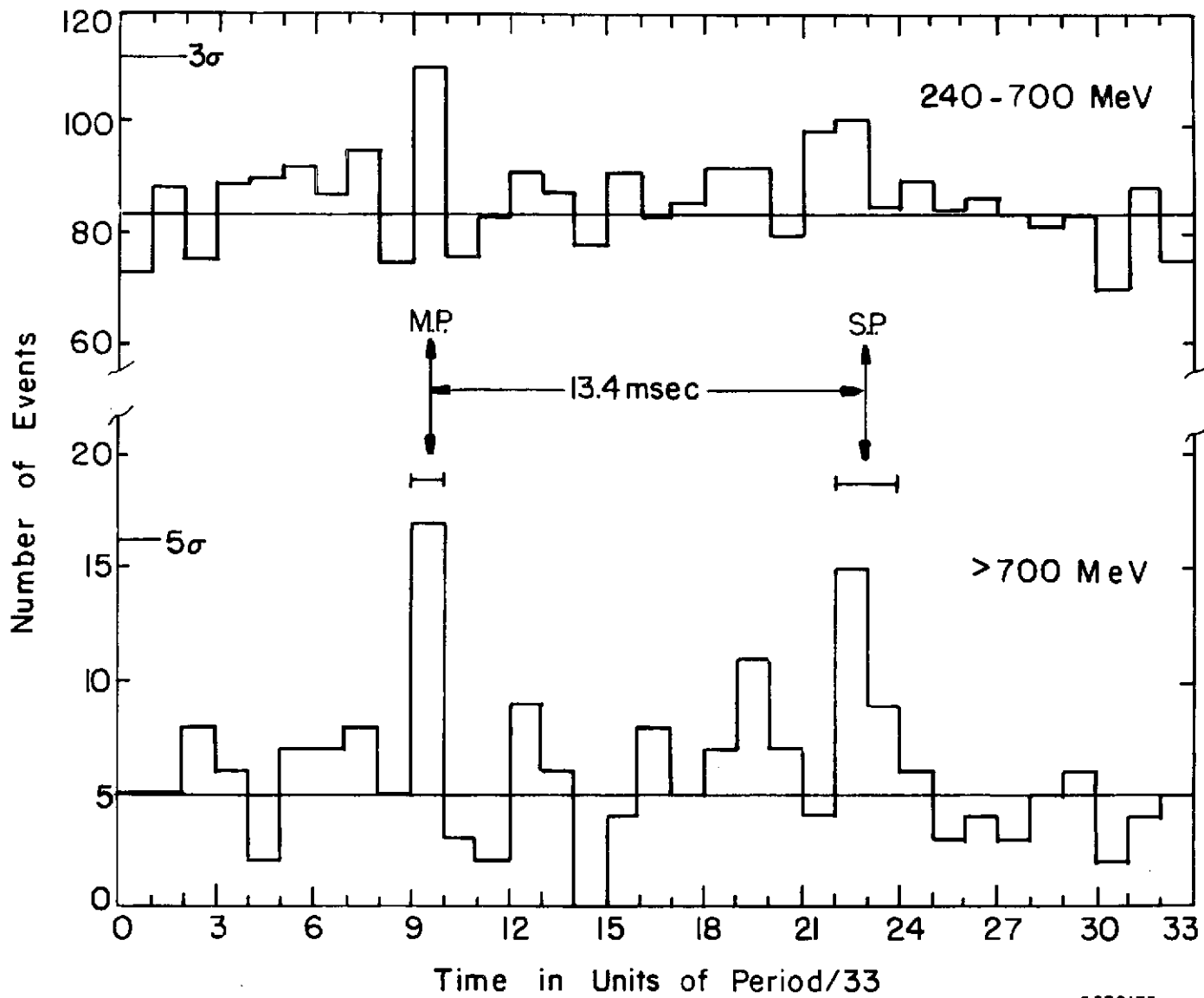


Figure 11



0270173

Figure 12

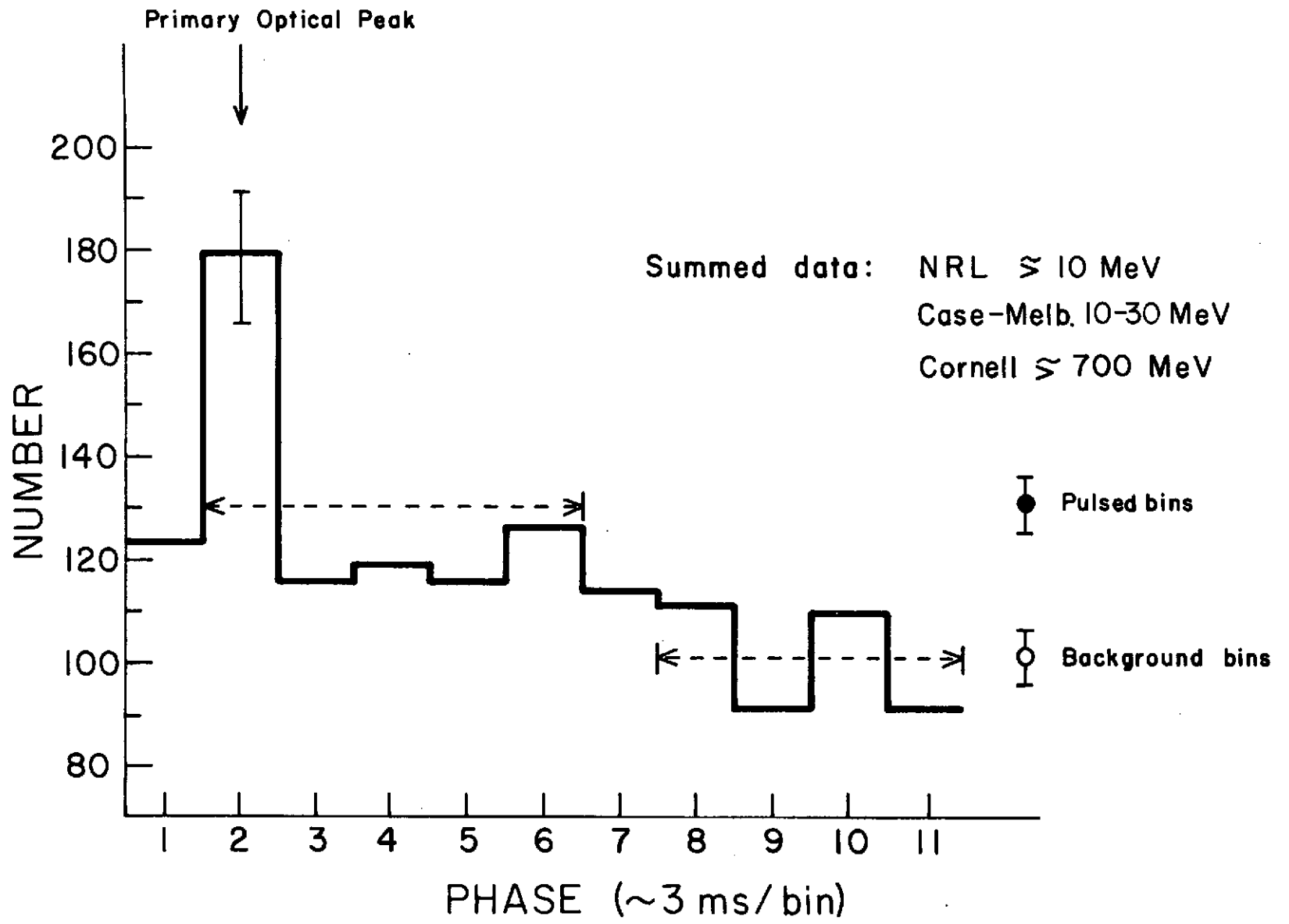


Figure 13

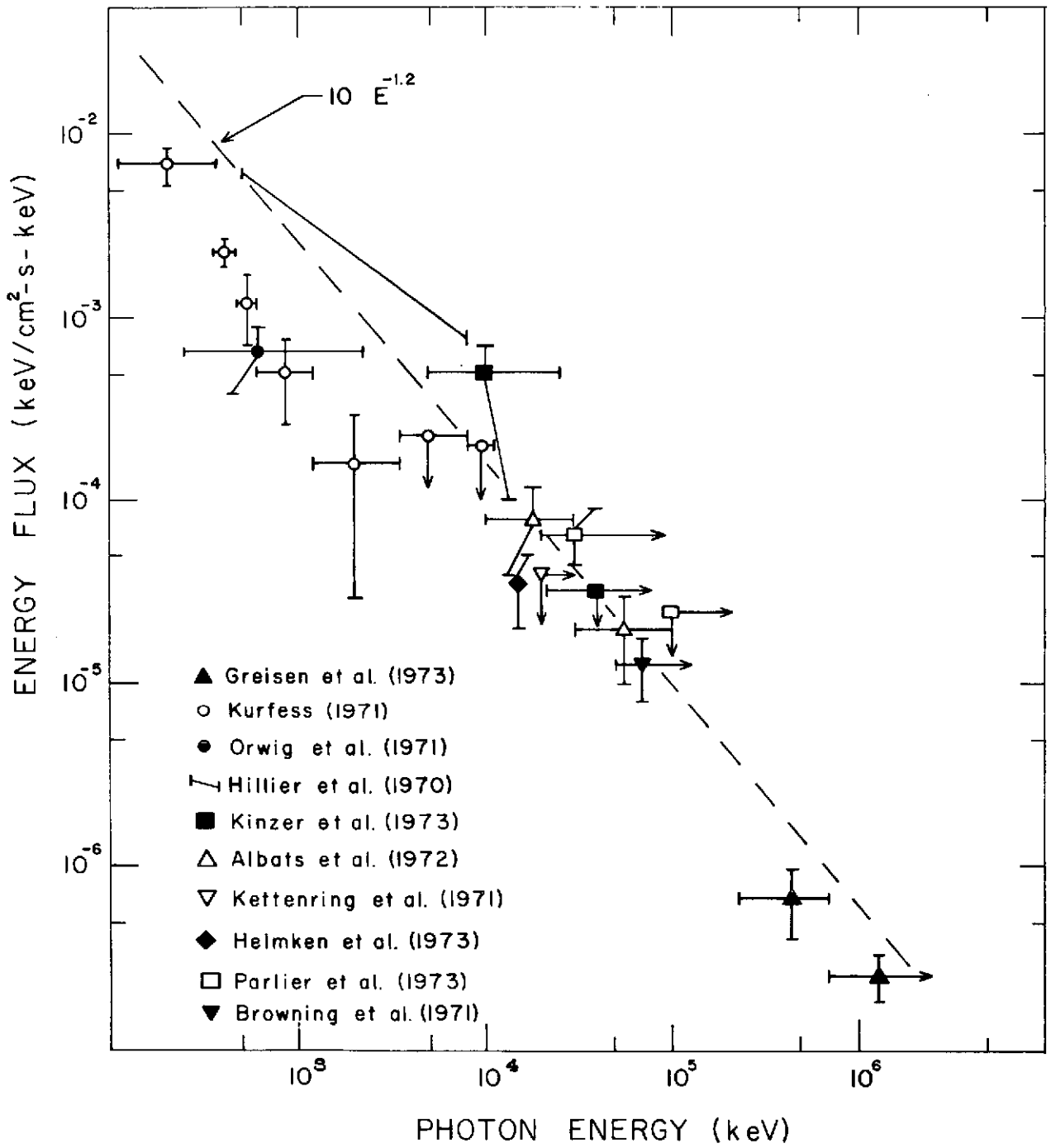


Figure 14

Figure 15

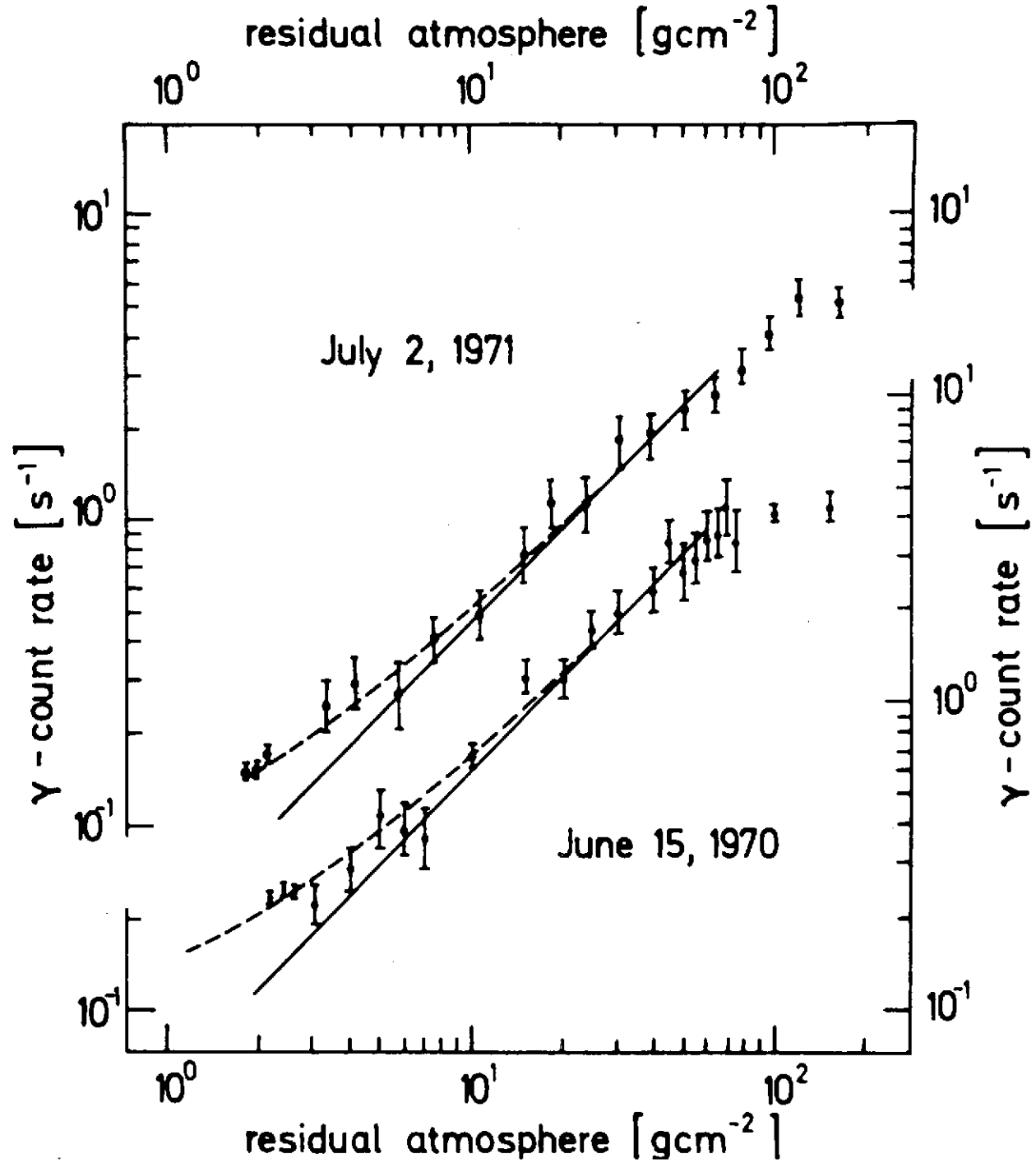
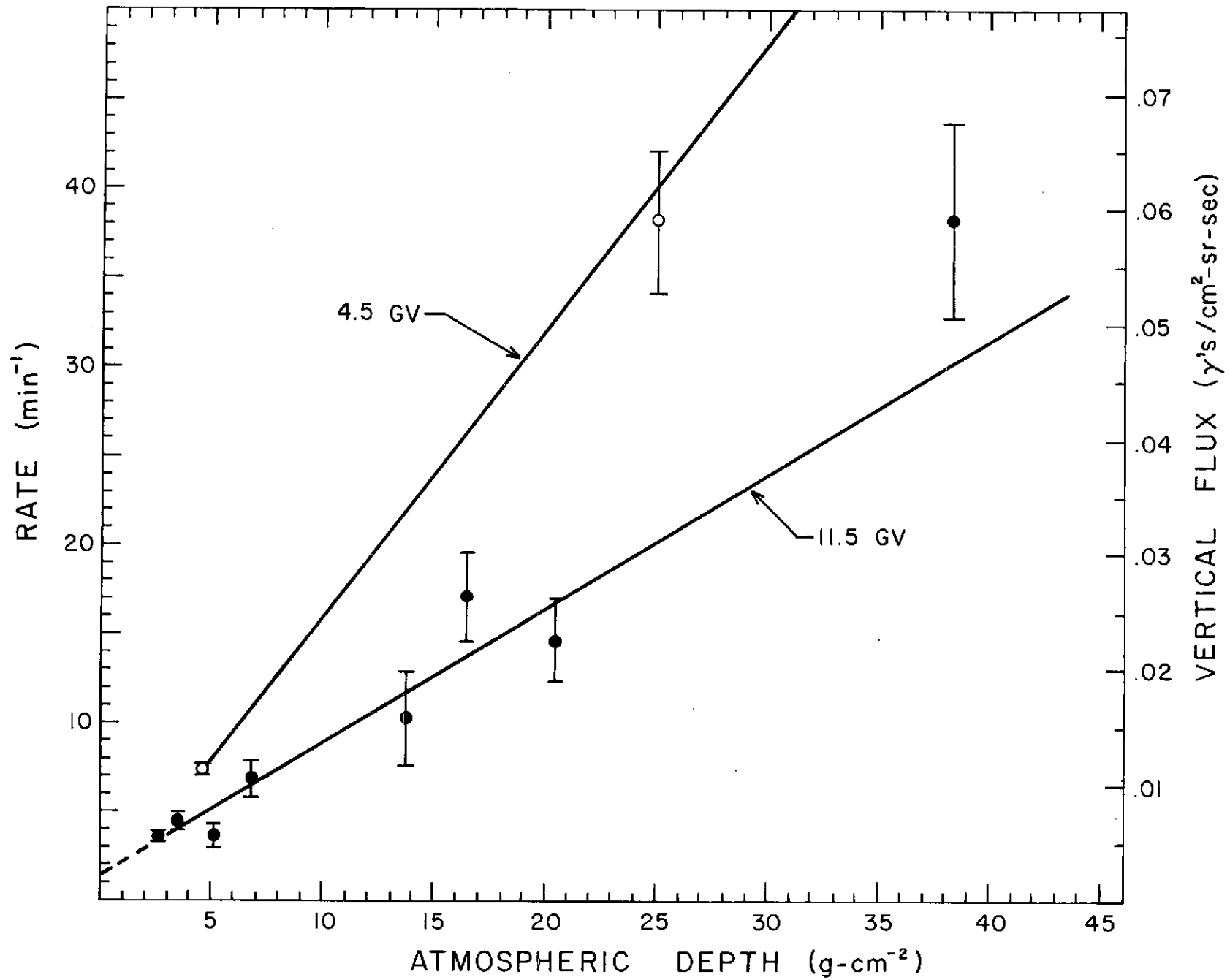
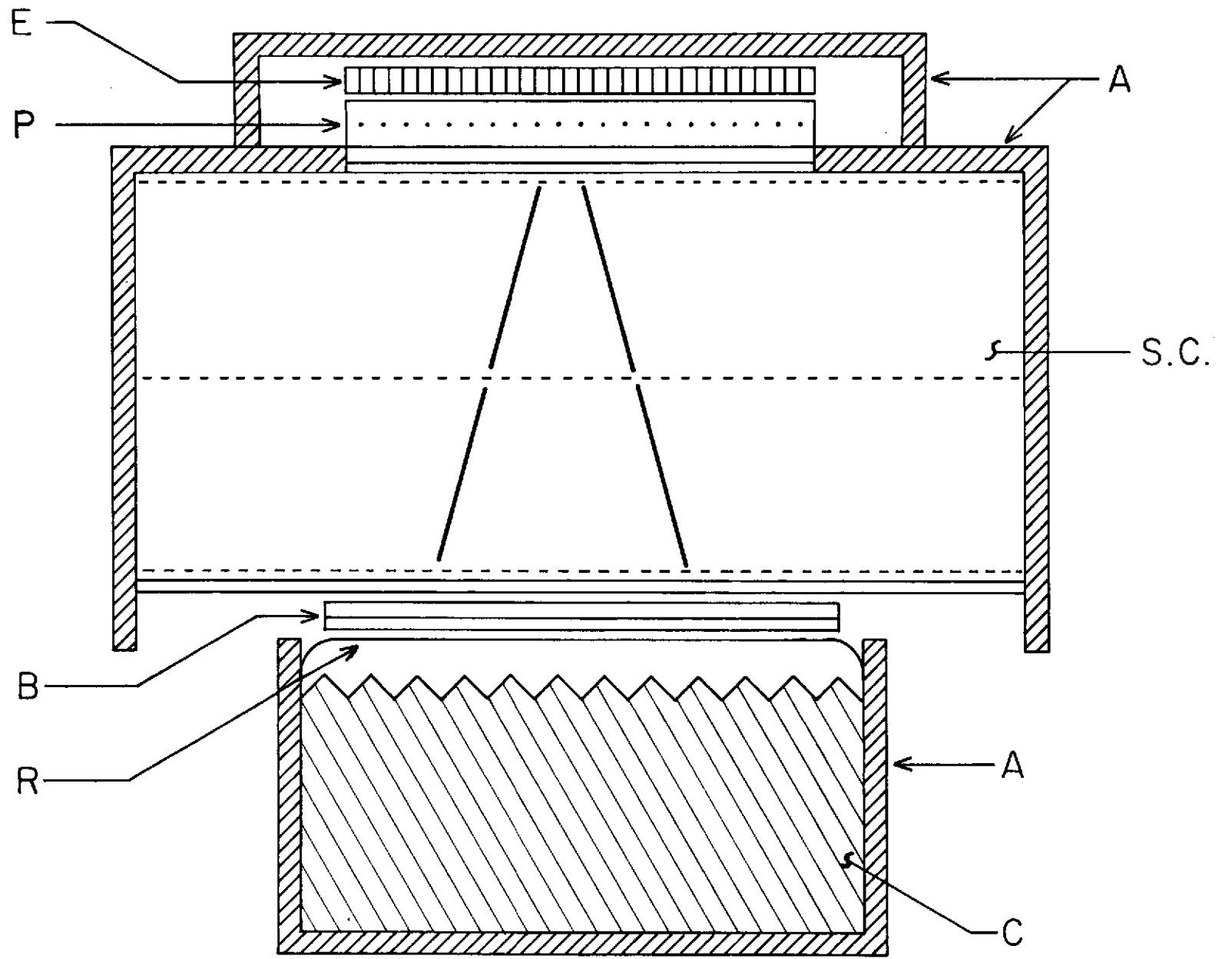


Figure 16





10 cm.

Figure 17

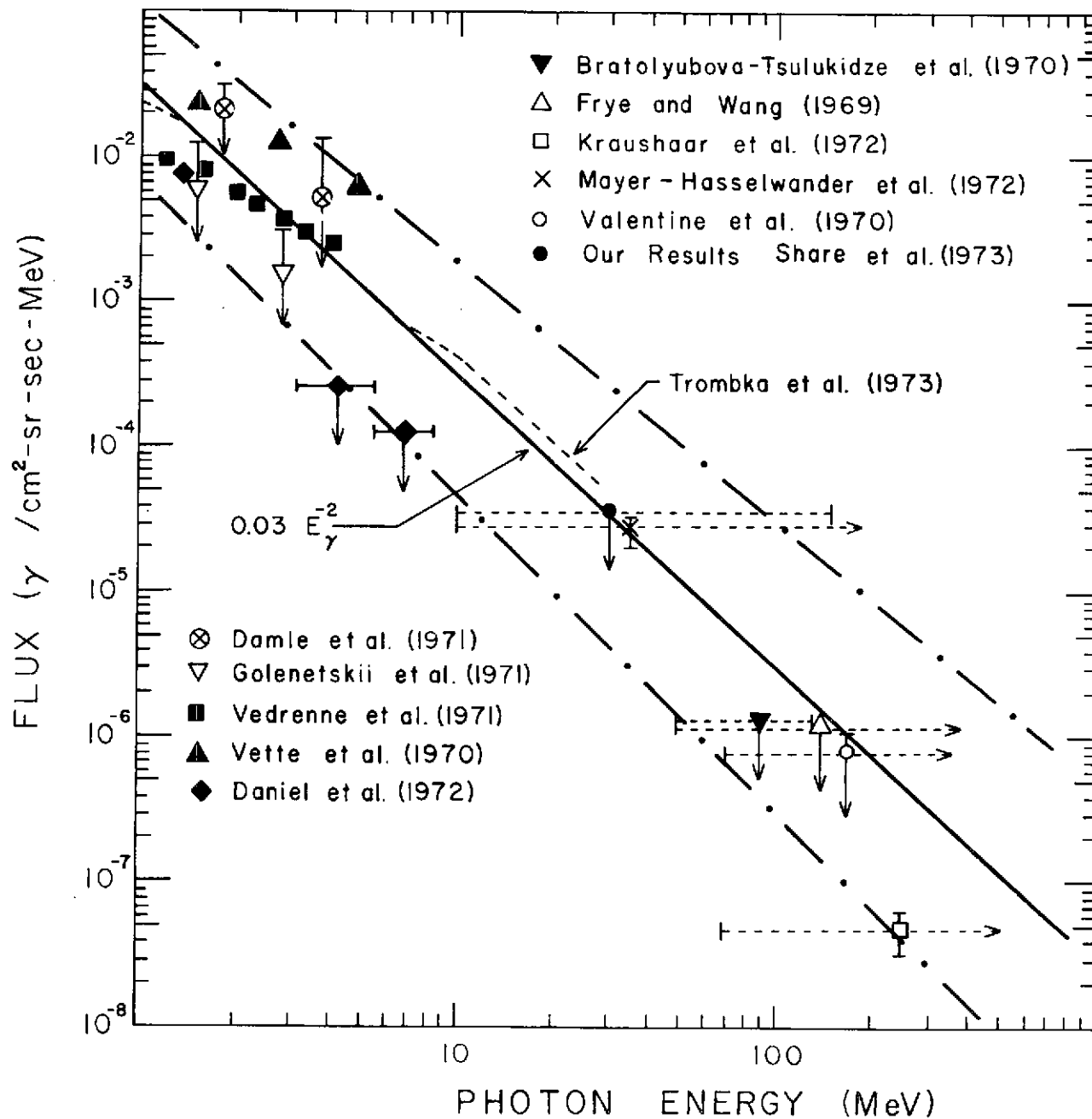


Figure 18

1173-28758

Report to the Goddard Workshop on Gamma Ray Astronomy Results  
obtained in Europe since the IAU-Symposium No.55

K. Pinkau

Max-Planck-Institut für Physik und Astrophysik  
Institut für extraterrestrische Physik  
8046 Garching bei München, Germany

(April 25, 1973)

Introduction

Since the IAU-Symposium No. 55 in Madrid, 1972 (Yash Pal, 1973, G.G. Fazio, 1973), only little progress has been made in obtaining new results on celestial gamma rays in Europe.

The gamma ray experiment S-133 on board ESRO's TD-1 satellite has worked through its first period of operational life from March 1972 to October 1972, when the satellite went into hibernation. The experiment has been activated again in February 1973 for a second all-sky scan. For this second scan, the trigger counter thresholds have been raised. It is hoped to thereby increase the gamma ray energy required to trigger the experiment, thus providing a kind of "two-color" all-sky scan in gamma rays together with the 1972-data.

Data analysis of this experiment has been very slow and tedious and is not as yet in such a state that first results could be presented. This is, in part, due to the fact that TD-1's tape recorders failed after the first two months of operational life and the tapes of the very good real-time coverage provided by ESRO were slow in arriving. A more serious problem, however, was the severe background problem encountered. This requires that all spark chamber images be visually inspected and this work has as yet not been finished.

In what follows, the results on measurements of the diffuse flux, and on the Crab pulsar NP 0532 are updated. The various reports on point sources discovered are, in the author's opinion, of a preliminary nature and require confirmation by independent measurement with good statistics.

## Diffuse Flux

The present status of gamma ray measurements concerning the diffuse flux is well illustrated by Fig. 1 (taken from Trombka et al., 1972), where the results of Vedrenne et al. (1971) and Mayer-Hasselwander et al. (1972) are compared with the results of Golenetskii et al. (1971), OSO-III (Kraushaar et al., 1972), and Apollo 15 (Trombka et al., 1972). (See also the paper of Peterson and Trombka, these proceedings.)

Apart from OSO-III, the results seem to indicate that these authors find diffuse gamma ray fluxes in excess of the  $25 \times 10^3 \left(\frac{E}{1 \text{ keV}}\right)^{-2.1}$  spectrum proposed by Yash Pal (1973). It appears to be too early to speculate in detail about the physical significance of this at present still rather uncertain result. If all these findings are confirmed, the diffuse gamma ray spectrum would exhibit a shoulder below 100 MeV, as pointed out by Yash Pal (1973). It is interesting to note that gamma ray production through the  $\pi^0$ -process at various redshifts in the past should integrate up to just such a shoulder (See paper of Stecker, these proceedings).

In this context, a remark concerning the analysis of gamma ray data appears justified. In the domain where pair production is dominant ( $\geq 20$  MeV), gamma ray astronomy experiments are triggered by the diverging beam of electron-positron pairs that are created close to the trigger-telescope. Multiple scattering causes these electrons to diverge, and the solid angle of such an instrument is not well defined.

Furthermore, if P is the probability that one of the two electrons triggers the instrument, the total triggering probability will be  $1 - (1-P)^2$  thus causing a significant enhancement of the probability that a gamma ray incident at large zenith angles will actually trigger the counter because one of the electrons was scattered into the sensitive cone of the telescope.

These considerations show that the energy-angle response function  $a(E, \theta)$  of a gamma ray counter telescope cannot be separated into one function of energy and another one dependent on angle only, as was assumed in the case of the OSO-III data analysis (Kraushaar et al., 1972). Rather, the effective solid angle  $\Omega$  defined as

$$\Omega = \frac{\int 2\pi \sin \theta a(E, \theta) d\theta}{a(E, \theta = 0)}$$

will remain a function of energy, increasing with decreasing energy. This has the interesting consequence that the ratio of line flux factor to isotropic flux factor  $G_{\text{line}}/G_{\text{iso}}$  as defined by Kraushaar et al. (1972) will depend upon energy and thus on the assumptions on the line flux and isotropic flux energy spectra, respectively. This has to be borne in mind when comparing the results of OSO-III of the galactic plane emission with that of high galactic latitudes.

#### Crab Pulsar NP 0532

In recent months, two results have been published that appear to establish the Crab pulsar spectrum in the 10-100 MeV energy range. They are the measurements of Albats et al. (1972), and of Parlier et al. (1972). Fig. 2 shows the Crab pulsar spectrum as presented in the paper of the Saclay-Milan-Palermo group (Parlier et al. 1972, see there for the references. Measurement point no ②0 is that of Albats et al., 1972).

These results are significant in two respects:

First, the ratio of the continuous to pulsed flux from the Crab is about a factor of 6 at .1 MeV, and this decreases to less than half that value at 20 MeV. Indeed, all the flux  $> 20$  MeV could be pulsed.

Secondly, while the interpulse appears to be dominant in the low energy gamma ray domain (Kurfess, 1971), both Albats et al. (1972) and Parlier et al. (1972) claim that the main pulse is dominant in their results. It would certainly be very interesting to study, with good statistics, the transition between these two different results in the 1-10 MeV region.

( See also papers of Fazio, Kniffen and Share, these proceedings.)

### Conclusion

Gamma ray astronomy has been, and still is, a slowly developing branch of science. This is due to the very great experimental difficulties. Furthermore, gamma ray observations cannot be carried out from very simple, or small, spacecraft. It appears that the development of the field has also been slowed down by the comparatively large amount of time lost in the effort to obtain access to satellite space.

### References

- Albats, P., Frye, G.M., Zych, A.D., Mace, O.B., Hopper, V.D., Thomas, J.A., *Nature*, 240, November 24 (1972).
- Fazio, G.G., IAU-Symposium No. 55, eds. H. Bradt and R. Giacconi, D. Reidel Publ. Co. Dordrecht (1973).
- Golenetskii, S.V., Mazets, E.P., Il'inskii, V.N., Aptekar, R.L., Bredov, M.M., Gur'yan, Yu.A., and Panov, V.N., *Astro. Letters*, 9, 69 (1971).
- Kraushaar, W.L., Clark, G.W., Garmire, G.P., Boriken, R., Higbie, P., Leong, C., and Thorsos, T., *Ap. J.*, 177, 341 (1972).
- Kurfess, J.D., *Astrophys. J.*, 168, L39 (1971).
- Mayer-Hasselwander, H.A., Pfeffermann, E., Pinkau, K., Rothermel, H., and Sommer, M., *Ap.J. Letters*, 175, L23 (1972).
- Parlier, B., Agrinier, B., Forichon, M., Leray, J.P., Boella, G., Marashi, L., Buccheri, R., Robba, R., Scarsi, L., (1972), to be published in *Nature Physical Science*.
- Trombka, J.I., Metzger, A.E., Arnold, J.R., Matteson, J.L., Reedy, R.C., Peterson, L.E., Preprint, Goddard Space Flight Center X-641-72-421 (1972).
- Vedrenne, G., Albernhe, F., Martin, I., and Talon, R., *Astron. & Astrophys.*, 15, 50 (1971).
- Yash Pal, IAU-Symposium No. 55, eds. H. Bradt and R. Giacconi, D. Reidel Publ. Co. Dordrecht (1973).

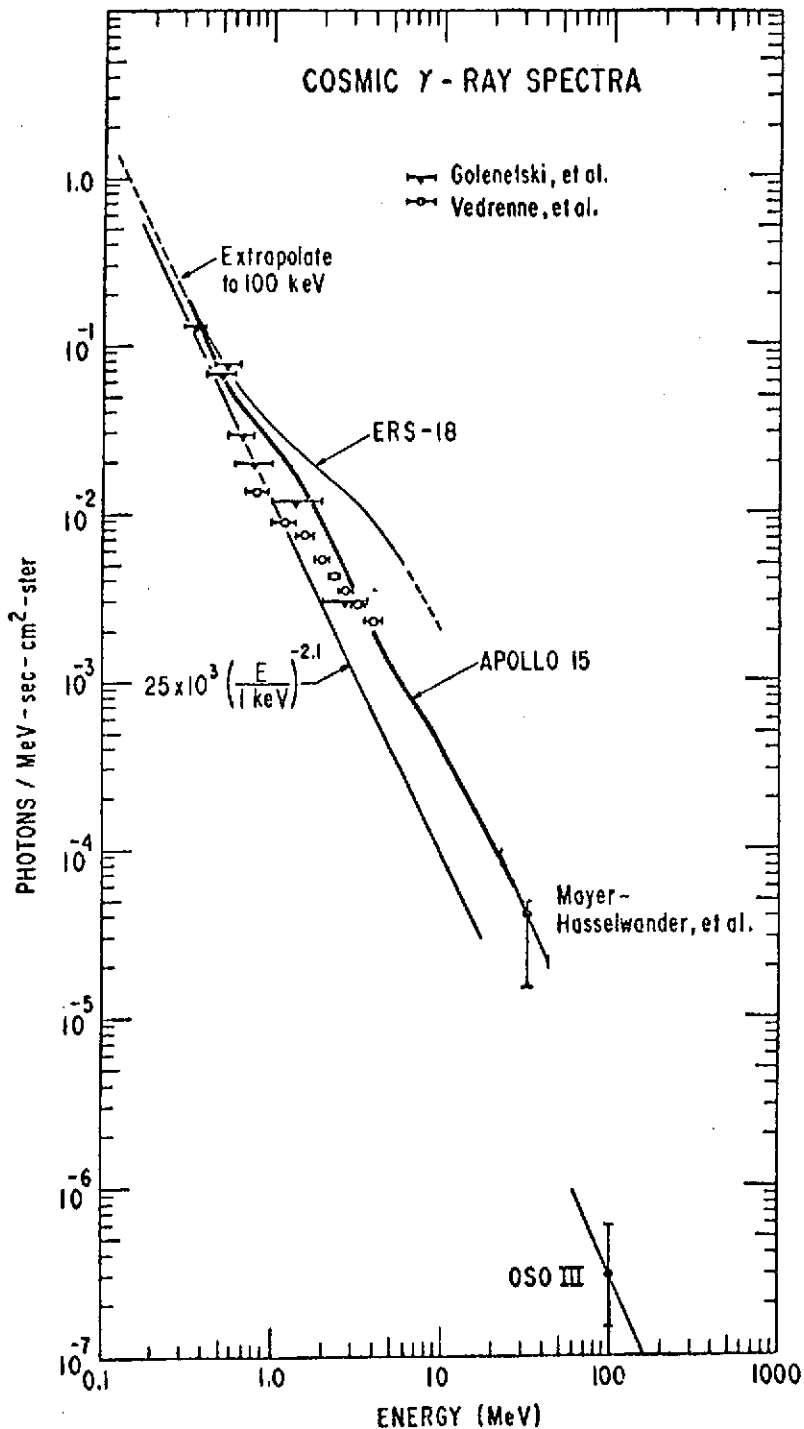


Fig. 1 The cosmic photon spectrum derived from the Apollo 15 data agrees with previous results below 1 MeV, but is well below that determined from the ERS-18 at higher energies. Limits derived from balloon and low altitude satellite work, despite large corrections for efficiency and cosmic-ray produced  $\gamma$ -rays, are in agreement with the Apollo results.

(From Trombka et al. , 1972)

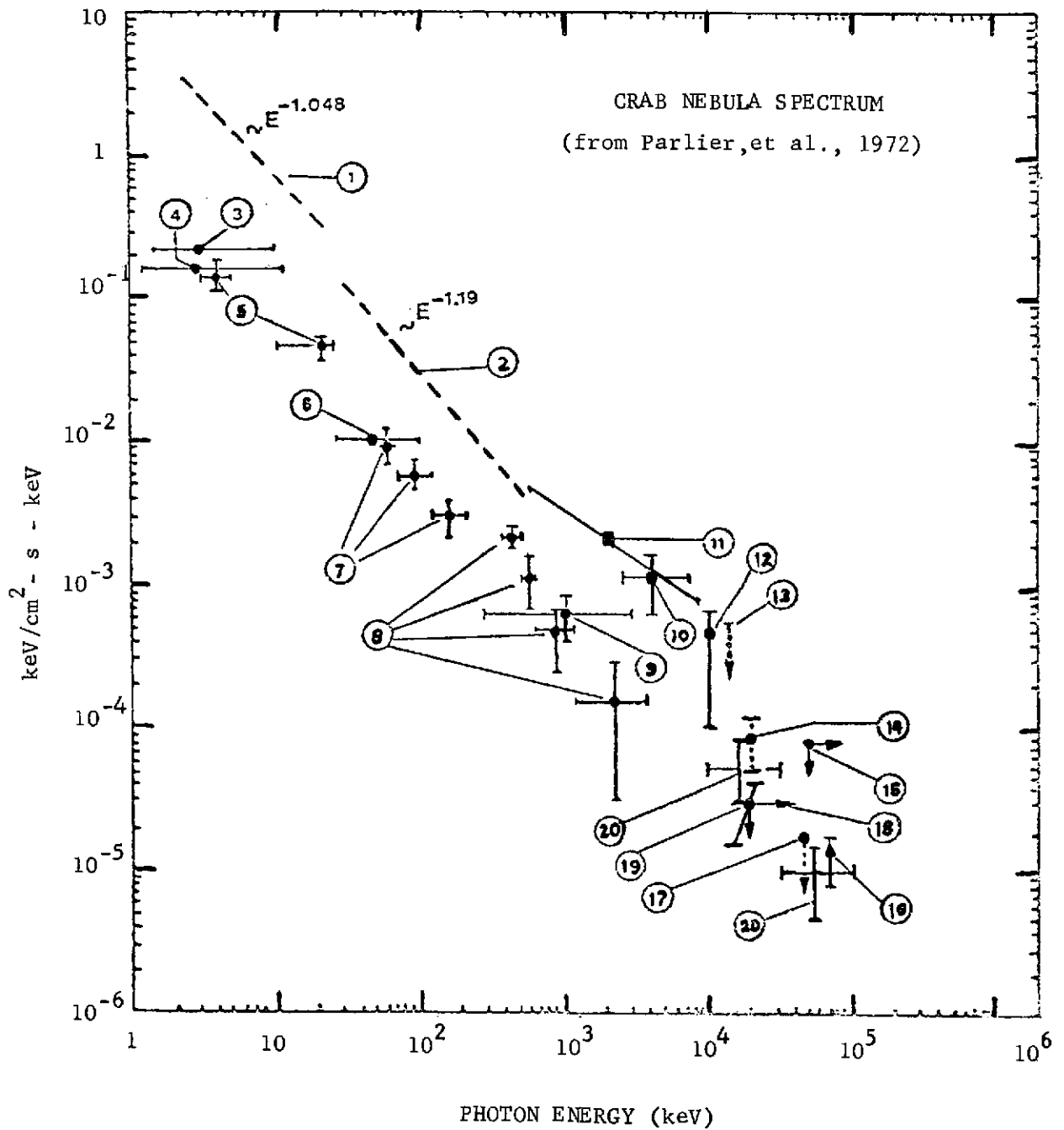


Fig. 2

N73-28 259

Preliminary Results on SAS-II Observations  
of  $> 30$  MeV Gamma Radiation

D. A. Kniffen, C. E. Fichtel, and R. C. Hartman

NASA/Goddard Space Flight Center  
Greenbelt, Md. 20771

1. Introduction. It was Morrison (1958) who first pointed out that the low interaction cross section of the high energy gamma ray make it a unique and valuable medium for obtaining information on many of the major energy transfers which take place in the Universe. Furthermore, its chargeless state allows the information to be related to the regions in which the processes are occurring. In papers presented at this conference Stecker, Ginzburg and Clayton have pointed out that the spectra obtained from the observations of energetic gamma radiation may provide most important information concerning a number of astrophysical problems. These problems include the study of the distribution of high energy nuclei in the Universe in space and time, the possible existence of antimatter on a universal scale, the origin of the  $> 50$  MeV galactic emission observed by Kraushaar, Clark and Garmire (1973), and other phenomena unique to large scale astrophysical bodies. In addition, the field of high energy gamma ray astronomy provides an opportunity to extend our knowledge of the electromagnetic phenomena for diffuse and discrete source X-ray emission to high energies.

Within our own galaxy; high energy gamma rays speak directly to the presence of energetic protons within discrete sources and in the galaxy

as a whole through the broadly peaked but distinctive spectrum of gamma rays produced by the high energy nucleons interacting with other nucleons. In this way, the cosmic ray distribution throughout the galaxy may be studied as well as the high energy particle gas surrounding individual objects from which cosmic rays have come. The picture which emerges will significantly aid in the understanding of the dynamics of our galaxy and the origin of energetic charged particle cosmic rays.

Beyond our galaxy gamma ray observations serve as an indicator of conditions existing in the cosmological past. In an expanding model of the Universe, the density of matter is much greater in the past than it is observed to be in the present epoch. Two of the processes expected to be most likely producers of gamma radiation on the Universal scale are nuclear interactions of energetic cosmic radiation with the intergalactic gas and nucleon-antinucleon annihilation. Both processes produce a characteristic  $\pi^0$ -decay gamma ray spectrum in the rest frame, but the energy is degraded by the cosmological redshift caused by the expansion of the Universe. Hence, gamma ray astronomy can address itself directly to the subject of cosmology.

Also expected to be important contributors to gamma ray production are the electromagnetic interactions important in X-ray astronomy, including the interactions of energetic electrons with matter (bremsstrahlung), with cosmic photon fields (Compton scattering) and with magnetic fields (bremsstrahlung).

Within discrete stellar objects, in addition to these mechanisms there are other processes unique to the objects which may produce

detectable levels of gamma radiation. Examples of such possibilities are the radioactive decay of the nucleosynthesis products as they are explosively ejected in supernovae (Clayton, 1973) and short intense burst of energetic photons emitted in the hydromagnetic shock wave following a stellar collapse (Colgate, 1968). The detection of gamma rays and the determination of their spectral characteristics during such events would provide most important clues to the validity of the theories which predict them.

The potential significance of gamma ray observations has led a large number of groups to develop a variety of detectors for the search of this rare photon in a very high background of energetic charged particle cosmic rays. The first unambiguous positive observations of extraterrestrial gamma rays above a few tens of MeV was made by Kraushaar, Clark and Garmire (1973) with their OSO-3 gamma ray detector, launched in 1968. This pioneering experiment measured a general diffuse flux and an enhanced emission from the galactic disk gamma radiation above 50 MeV. Theoretical models for the origin of these observation fluxes have been difficult to obtain because of the limited angular and spectral resolution of the OSO-3 experiment. Share (1973) has reviewed other results obtained from a large number detectors flown from balloons and satellites. Positive observations have been obtained for the diffuse flux, the galactic disk emission and a large number of discrete sources, but conflicting evidence between experiments in some cases and marginal statistics in others has left a generally uncertain picture with the possible exception of pulsed gamma ray emission from the Crab nebula pulsar NP 0532 and the galactic plane emission.

In March of 1972, the first of the second generation of satellite gamma-ray experiments was launched aboard the ESRO TD-1. The experiment consisted of a 9-deck vidicon spark chamber gamma ray telescope. On November 15, 1972, the SAS-II was launched into orbit with a larger 32 deck magnetic core digitized spark chamber. These instruments should provide the sensitivity and angular and spectral resolution with the inherently low background of a satellite experiment needed to address many of the important questions in gamma ray astronomy.

In this paper we will give a description of the SAS-II detector and present some of the preliminary results we have obtained.

2. Experiment. Fig. 1 is a schematic view of the SAS-II telescope, a thirty-two deck spark chamber with a scintillator-Cerenkov counter charged particle triggering telescope and a large plastic scintillator anticoincidence dome surrounding the entire experiment. Each spark chamber module is separated from the next by a .03 radiation length tungsten pair production plate. The tungsten plates serve as scattering plates for the electrons following their formation, allowing the energy of each electron and hence of the incoming gamma ray, to be determined by analysis of the multiple scattering. This information is also used to obtain a weighted bisector of the pair for determining its arrival direction in spark chamber coordinates. A large number of thin plates are used so that the electron pair can be clearly identified and the arrival direction of the gamma ray can be accurately measured. The signature required for a trigger of the spark chambers is for a particle to pass undetected through the anticoincidence dome

and to pass simultaneously (within about 500 ns) through the two elements of one of the four scintillator-Cerenkov charged particle telescopes. This coincidence triggers the application of high voltage across the spark chambers and initiates the readout system.

Fig. 2 shows a photograph of a single wire grid module containing two planes of 200 wires each on opposite sides of the frame. The wires within a plane are parallel and orthogonal to the wires on the opposite plane. Each grid wire is threaded through a ferrite core contained on a shelf on the side of the frame. Two additional wires are threaded through each core to readout those set during an event. As a spark breaks down along the ion path remaining along the trajectory of a charged particle, current flows along one or more affected wires in each plane of the grid, setting one or more cores. The readout of such set cores thus provides the coordinates of the charged particle passage through that modular deck.

If the distribution of set cores is plotted separately for each of the two orthogonal planes, a picture is obtained such as that shown in the Fig. 3, which is a reproduction of a 16 mm microfilm frame of the two orthogonal views of a gamma ray pair production event. The scale for the vertical axis is compressed by a factor of those relative to the horizontal so incoming angles are exaggerated.

The flight unit was given a preflight calibration at a tagged photon facility established for this purpose at the 170 MeV electron synchrotron at the National Bureau of Standards in Gaithersburg. The beam provides monoenergetic photons selectable over the 30-150 MeV

energy interval. A very extensive calibration is currently underway using the essentially identical flight spare experiment unit. Until this calibration is complete the results must be considered preliminary and flux and intensity values should be considered to be no better than about a factor of 1.5.

The characteristics of the telescope include an area of about  $540 \text{ cm}^2$ , a solid angle of about  $1/3$  steradian, and an asymptotic high energy pair production efficiency of 29 percent. Timing accuracy of about 1 to 2 milliseconds allows a search for periodic emission. Arrival directions for 100 MeV gamma rays may be measured to about two degrees at 100 MeV. The energy threshold is about 30 MeV, although it is not sharp. Differential energy measurements may be made on 30-200 MeV gamma rays, and integral fluxes obtained for  $> 200$  MeV gamma rays. A more detailed description of the experiment has been given by Derdeyn et al. (1972).

The experiment was launched as the sole experiment aboard the second of the Small Astronomy Satellites on November 15, 1972. The orbital trajectory is essentially equatorial and approximately circular at a height ranging from 440 to 610 km above the Earth's surface. Fig. 4 gives an artist's concept of the telescope, surrounded by a gold colored thermal blanket, sitting atop the spacecraft control section. The satellite is spin stabilized with magnetic torquing of commandable electromagnets against the Earth's magnetic field providing steering to any selectable point on the sky. Attitude is determined by a magnetometer-sun sensor combination, and to more

precision by a star sensor, which is capable of determining the telescope pointing direction to about a quarter of a degree, thus allowing the directions of the gamma rays in spark chamber coordinates to be transformed into celestial and galactic coordinates.

The viewing program has been chosen so as to examine each portion of the sky with about a one week exposure, with early emphasis on those regions of the sky expected to be most interesting in gamma rays.

Fig. 5 gives a view of the sky with the regions of the sky examined to date with the  $1/3$  steradian field of view denoted by the cross hatched area, with those regions for which extensive analysis has been completely denoted by the double cross-hatching. Second week exposures have already been obtained on the galactic center region as well as the anti-center, Crab nebula region. The sensitivity of the exposure to each of these points is determined by an analytical program which takes into account all variable functions of the experiment which affect the exposure, as well as the occultation by the earth and folds these together with the angular response function and projects them onto equal solid angle bins on the sky.

3. Data Analysis and Reduction. SAS-II data is recorded at a one kilobit per second rate on redundant onboard continuous loop tape recorders. Once per orbit the recorded data is transmitted at a 20 kilobit per second rate to a tracking station located near Quito, Ecuador. Real time data taken before and after the recorder playback is used to

correlate the spacecraft clock with the station clock. This provides time in the data stream accurate to better than two milliseconds in absolute time.

The data stream contains, in addition to spacecraft time, the spark chamber event data, experiment and spacecraft control section housekeeping data (counter rates, voltages, currents, temperatures, pressures, etc.) and aspect data from a digital solar aspect sensor, two fluxgate magnetometers and an N-slit star sensor. Three orbits of data per day are transmitted via transmission links directly to the Goddard Space Flight Center (GSFC) to determine the aspect for the purposes of planning any necessary maneuvers. Maneuvers of the spin stabilized spacecraft are accomplished by command of electromagnet torquing coils which provide fields which interact with the terrestrial field to provide maneuvering rates of up to about 5.0 degrees a minute. Analog magnetic tapes of the remaining orbits are shipped to GSFC where time is correlated and the data placed in proper time sequence with any overlapping data eliminated. The magnetometer, sun sensors and star sensors are used to determine the spark chamber pointing direction to an accuracy of about .25 degrees.

Analysis of the spark chamber data is made by an automatic pattern recognition designed to recognize the readout patterns produced as gamma rays interact in the tungsten plates to create electron-positron pairs (See Fig. 3). An alternate mode for analysis of the event data is made by interactive editing of the events with a graphics display unit. Most of the results available at the present time have been obtained using the latter mode.

Events selected for editing have been carefully chosen to insure that no ambiguities will be introduced into the measured fluxes by misidentification of spark chamber events. The selection is based on the following criteria: (1) only intervals which contain data taken when the spark chamber axis points away from the Earth are chosen for analysis; (2) only gamma-ray pair events are selected; (3) events which may masquerade as pair events as a result of interactions in the material of the sidewalls of the spark chamber are rejected for analysis; (4) Events which set cores in the top grid are rejected to provide a veto for the rare events which form in the small amount of material between the coincidence counter and the spark chambers, and (5) gamma rays arriving at very large angles with respect to the detector axis are not included in the analysis. Edited events are automatically processed to obtain the energy and chamber arrival direction of each observed gamma ray according to procedures developed in the analysis of balloon data as described by Fichtel et al. (1972). The directional information is then combined with attitude and orbit data to provide the gamma ray arrival direction in celestial, galactic, geographic and geomagnetic coordinates. Events with zenith angles greater than 90 degrees with respect to the outward radius vector of the satellite position are rejected from further consideration for the celestial analysis, safely avoiding the terrestrial horizon which lies at zenith angles greater than  $110.0^\circ$ .

The sensitivity of the telescope to each region of the sky is determined by an automatic analytic program which checks against all

status conditions which affect sensitivity. In addition the accumulation is made differentially in time in order to include instantaneous detector live time and to exclude those portions of the sky occulted by the Earth.

4. Results. The results may be classified into three categories: diffuse, presumably extragalactic gamma rays coming from regions of the sky not associated with the galactic plane; gamma radiation from the galactic plane; and discrete sources of energetic gamma rays.

(a) Diffuse gamma radiation. For the regions of the celestial sphere which we have examined thus far, there seems to be a weak, but finite component of high energy gamma rays which exists for regions away from the galactic center. OSO-III, even with its much smaller sensitivity  $1.6 \text{ (cm}^2 \text{ sr efficiency)}$  compared to about  $30 \text{ (cm}^2 \text{ sr efficiency)}$  for SAS-II above 100 MeV, also indicated a finite, apparently constant diffuse flux for regions of the sky which were far enough from the galactic plane that no portion of the relative wide angle of the OSO-III detector ( $\sim 35^\circ$ ) overlapped the galactic plane. From observations that SAS-II has made, it now appears that in the region  $-20^\circ < l_{11} < +20^\circ$ , and  $b_{11} > 0^\circ$ , the flux is already at the background level at about  $b_{11} = +15^\circ$ . Data to be reported here comes from the region of the sky centered at  $(l_{11} = 0, b_{11} = +25)$ . The diffuse energy spectrum is presented in Fig. 6. Notice that the spectrum is quite steep, steeper than other gamma ray spectra observed on SAS-II or the earlier balloon work of the Goddard group (e.g. Fichtel

et al., 1969 and 1972), including the galactic center region, the Crab, and the atmospheric secondary spectrum, upward or downward. The integral flux above 100 MeV is  $(3.9 \pm 1.1) \times 10^{-5} / (\text{cm}^2 \text{sr sec})$  consistent with the OSO-III result of  $(3.0 \pm 0.9) \times 10^{-5} / (\text{cm}^2 \text{sr. sec.})$  averaged over all regions of the sky (Kraushaar et al., 1973). (Value corrected according to private communication with G. W. Clark, 1973.) The OSO-III experiment did not measure the energy spectral shape.

(b) The Galactic Plane. SAS-II has confirmed the high intensity of gamma rays coming from the galactic center region. The region extends along the galactic plane for  $60^\circ$  to  $70^\circ$  in the vicinity of the galactic center and is no wider than  $9^\circ$  full width half maximum for 100 MeV gamma rays and could be narrower, since there is still a final correction to be applied to the SAS-II attitude data. The general intensity level is about  $1.2 \times 10^{-4} / (\text{cm}^2 \text{ rad sec})$ , to which an uncertainty factor of 1.5 is attached until the SAS-II calibration is complete. Whereas the average energy spectrum from this region is much harder than the diffuse radiation, the number of gamma rays between 30 and 60 MeV relative to the number above 100 MeV is inconsistent with a pure  $\pi^0$ -decay component. Apparently, there are other components with softer spectra. Because the SAS-II aspect has not yet been solved with sufficient accuracy, at present the SAS-II data would allow either a diffuse radiation or a sum of point sources for the soft component; however, there would, have to be several (at least about six) point sources, or there would have been a greater non-uniformity than observed.

(c) Discrete sources. High quality attitude data is not yet available for a detailed study of discrete sources with SAS-II. However, a positive flux is detected for the Crab nebula on the basis of an analysis of a sixth of the data available. A complete analysis of the data combined with accurate attitude data will allow a study of the energy spectrum of the Crab nebula emission and the possible periodic pulsations from NPO532.

No evidence is obtained for gamma ray emission from Sco X-1, with 95 percent confidence limits based on about a fourth of the data of  $1.7 \times 10^{-6}/(\text{cm}^2\text{sec})$  for gamma rays above 40 MeV and  $1.0 \times 10^{-6}/(\text{cm}^2\text{sec})$  above 100 MeV. A full analysis of a typical one week exposure will allow 95 percent confidence limits of about  $2 - 3 \times 10^{-7}/(\text{cm}^2\text{sec})$  for sources for which no positive indication is obtained.

## 5. Discussion.

(a) Diffuse Radiation. Fig. 7 shows that the isotropic gamma radiation for  $|b_{11}| > 20^\circ$  exhibits an enhancement relative to the single extension of the power law spectrum valid in the X-ray region from 1 to 20 MeV and then a rapid decrease in intensity in the region from 40 to 200 MeV with an apparently reasonably smooth curve through the entire gamma ray region. Until more SAS-II data from many regions of the sky have been analyzed with the full angular resolution, it is not possible to say that the radiation is truly uniform over the sky, and uniform also on a fine scale. However, it seems a plausible

hypothesis to assume that the regions examined thus far by SAS-II are representative and consider the possible origin of the radiation.

There is, of course, the possibility that radiation is the sum of many, many weak sources of unknown origin. However, there are at least two other possibilities, one that the radiation comes from diffuse electrons interacting with matter, photons, or magnetic fields and the other is that the gamma rays are of cosmological origin.

With regard to the diffuse electron possibility, bremsstrahlung seems unlikely because, at an energy where an increased slope would be expected, 1 to 10 MeV, due to an increasing rate of energy loss, the inverse is observed. For both Synchrotron and Compton radiation, a power law electron energy spectrum leads to a power law photon, spectrum, but with a different electron spectrum which would have at least as sharp features. There is no reason to expect such a spectral shape for diffuse electrons, although there is no experimental knowledge of the electron spectrum in the relevant energy range. Further, especially in the synchrotron case, the intensity seems too high to be consistent with reasonable estimates of the interstellar parameters.

Of the pure gamma ray cosmological hypothesis, there are two of which the authors are aware that seem to be possible candidates. They are the cosmic ray interstellar matter interaction model and the particle-anti-particle annihilation in the baryon symmetry steady state model. In both theories, the resulting gamma ray spectrum, which is primarily due to  $\pi^0$  decay, is red-shifted substantially over the age of the expansion of the universe. They are discussed by Stecker, et al. (1971) and Stecker (1973).

In an expanding model of the Universe, the density of matter is much greater in the cosmological past than it is observed to be in the present. However, since the produced gamma radiation reaches us from large distances, the energy of the photons is degraded by the cosmological redshift caused by the expansion of the Universe. One curve developed by Stecker (1969) involving red-shifts up to about 100 is shown in Fig. 7. The theoretical curve is seen to agree with experimental data reasonably well.

An alternate attempt to explain the gamma radiation through red-shifted gamma rays from  $\pi^0$  decay arises from the big bang theory of cosmology with the principal of baryon-symmetry. Harrison (1967) was one of the first to propose a model of this type. Omnes (1969), following Gamow (1948) considers a big-bang model which is initially at a very high temperature and density, and then shows that, if the universe is baryon-symmetric, a separation of matter from anti-matter occurred at  $T > 30$  MeV. The initial phase separation of matter and anti-matter leads ultimately to regions of pure matter and pure anti-matter containing masses of the size of galaxy clusters. Stecker, Morgan, and Bredekamp (1971) have predicted the gamma ray spectrum which would be expected from annihilation at the boundaries of such clusters from the beginning of their existence. This spectrum is very similar to the one shown in Fig. 7 in the energy range for which data exists, and is not included in the figure for that reason.

(b) Galactic Plane Radiation. Since the final attitude data do not exist for SAS-II at the time of writing of this article, discussion

of the galactic center region must be limited to a summary of the broad features observed by SAS-II. (1) the enhancement of the galactic radiation in the region of the galactic center observed by OSO-III is confirmed. (2) It is  $60^\circ$  to  $70^\circ$  in length along the plane and no more than  $9^\circ$  wide. (3) The energy spectrum is not a pure  $\pi^\circ$  spectrum, but rather it also contains an enhanced flux below 70 MeV relative to that expected from a  $\pi^\circ$  spectrum. (4) The enhancement is not due just to a few point sources, although it could, of course, be due to a large number of point sources.

(c) Discrete Sources. A discussion of the significance of discrete sources must await further data analysis, however the sensitivity of SAS-II should allow the study in detail of a number of discrete sources and limits on objects with no emission almost two orders of magnitude greater than existing ones.

6. References.

- Clayton, D. 1973. These Proceedings.
- Colgate, S.A., Canadian J. Phys. 46, S476.
- Derdeyn, S.M., Ehrmann, C.H., Fichtel, C.E., Kniffen, D.A., and Ross, R.W. 1972, Nuclear Instruments and Methods 98, 557.
- Fichtel, C.E., Hartman, R.C., Kniffen, D.A. and Sommer, M., 1972, Astrophys. J. 171, 31.
- Gamow, G. 1948. Phys. Rev. 74, 505.
- Ginzburg, V.L. 1973. These Proceedings.
- Golenetskii, S.V., Mazets, E.P., Il'inskii, V.N., Aptekar', R.L., Bredov, M.M., Guryah, Yu.A. and Panov, V.N. 1971. Astr. Letters 9, 69.
- Harrison, E.R. 1967. Phys. Rev. Letters 18, 1011.
- Hartman, R.C., Fichtel, C.E., Kniffen, D.A., Thomson, D.J., Ogelman, H.B. and Tumer, T. 1973. Proc. 13th International Cosmic Ray Conference, paper no. 262.
- Kniffen, D.A., Fichtel, C.E., and Hartman 1973. Proc. 13th International Cosmic Ray Conference, paper no. 263.
- Kraushaar, W.L., Clark, G.W., Garmire, G.P., Borken, R., Higbie, P., Leong, V., and Thorsos, T. 1973. Astrophys. J. 177, 341.
- Morrison, P. 1958. Il Nuovo Cimento 7, 858.
- Mayer-Hasselwander, H.A., Pfeffermann, E., Pinkau, K., Rothermel, H., and Sommer, M. 1972. Astrophys. J. Letters 175, L23.
- Omnes, R. 1969. Phys. Rev. Letters 23, 38.

Share, G. 1973. These Proceedings.

Stecker, F.W. 1969. Astrophys.J. 157, 507.

Stecker, F.W. 1973. These Proceedings.

Stecker, F.W., Morgan, D.L. and Bredekamp, J. 1971. Phys.Rev.Letters 27, 1469.

Trombka, J.I., Metzger, A.E., Arnold, J.R., Matteson, J.L., Reedy, R.C. and

Peterson, L.E. 1973. Astrophys.J. 181, 737.

Vedrenne, G., Albernhe, F., Martin, I., and Talon, R. 1971. Astr. and Astrophys.

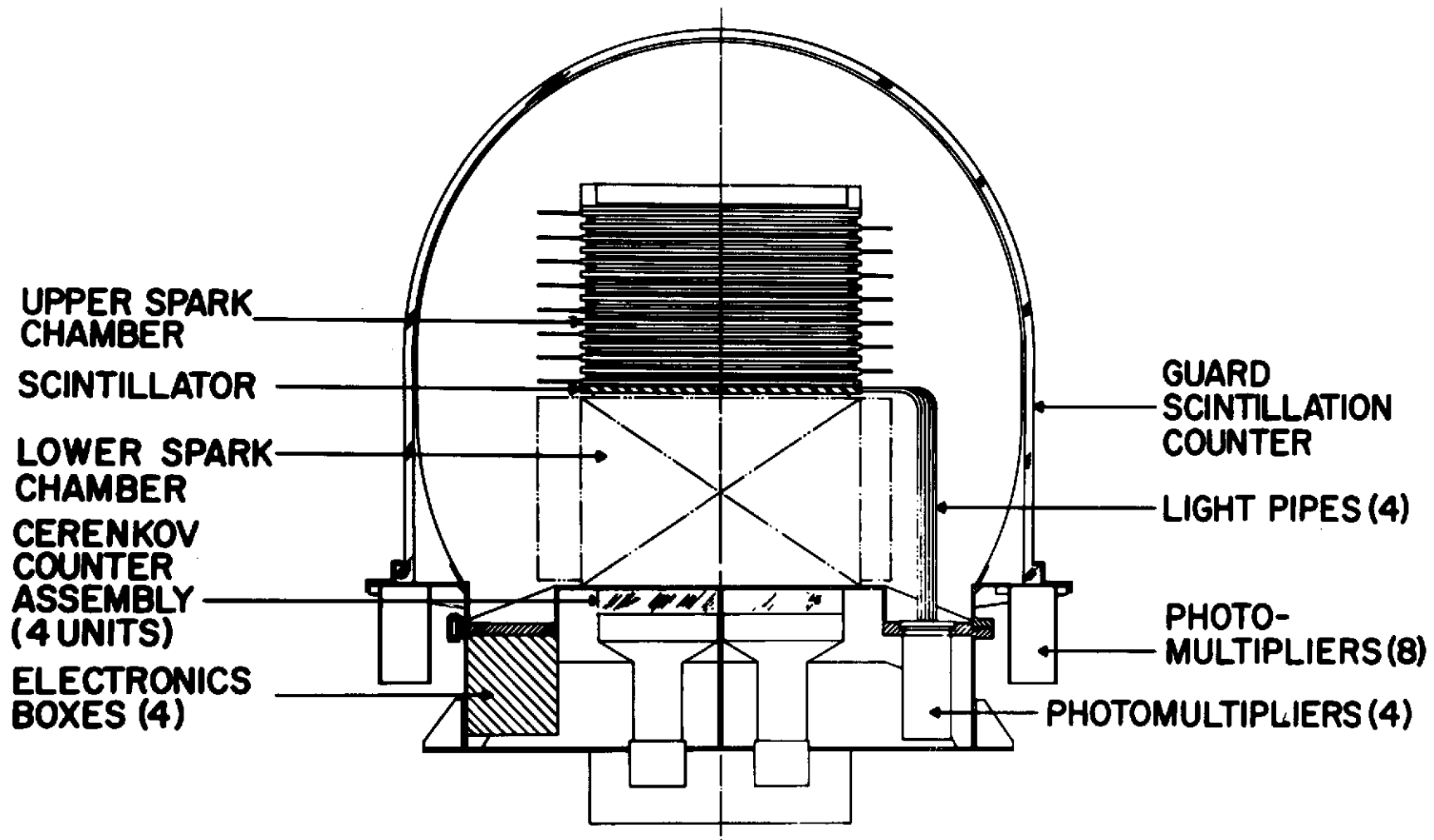
15, 50.

Figure Captions

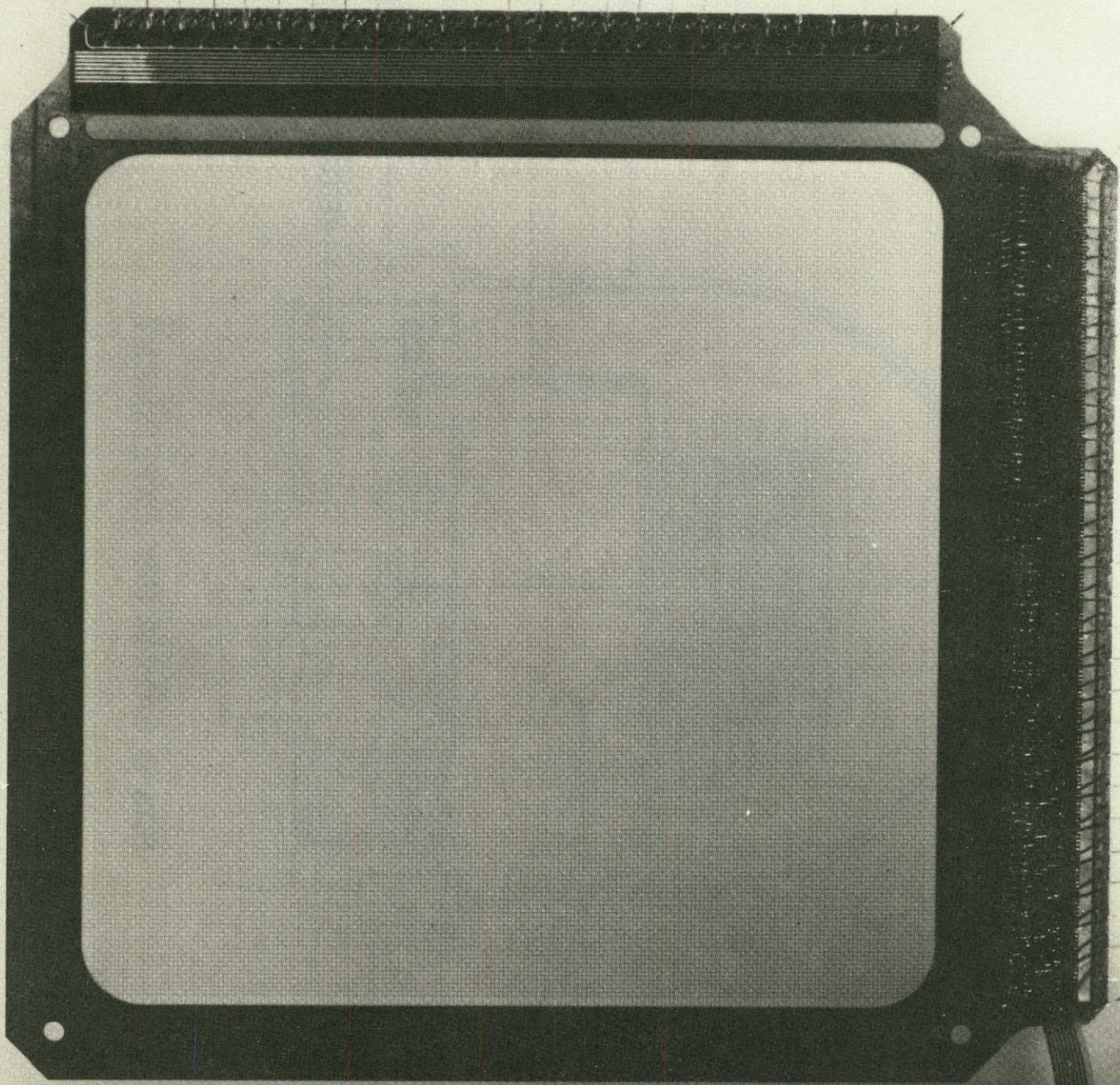
- Figure 1. Schematic diagram of the SAS-2 Gamma-ray spark chamber telescope.
- Figure 2. Photograph of a single wire grid spark chamber module with two planes of two hundred parallel wires. The direction of the wires in one plane is orthogonal to that in the opposite plane. Each wire is terminated through a ferrite core.
- Figure 3. A microfilm plot of an event which presents two orthogonal views of the digitized trajectory of a pair of electrons produced by a gamma-ray interacting with one of the tungsten plates between the 32 spark chamber modules. the x's and y's denote cores set due to the passage of charges particles in the two orthogonal views. The vertical axis is compressed by nearly a factor of three relative to the horizontal, causing angles to be overemphasized.
- Figure 4. An artists concept of the Small Astronomy Satellite (SAS)-2 in orbit. The experiment surrounded by a thermal blanket sits atop the spin stabilized spacecraft. Altitude is controlled by magnetic torquing.
- Figure 5. Regions of the sky in galactic coordinates viewed by SAS-2 through May 21, 1973. The cross hatched regions are those viewed during the first five weeks after launch. See text for further details.
- Figure 6. The diffuse gamma-ray spectrum measured by SAS-2 for regions of the sky analyzed with  $|b_{II}| > 20^\circ$ . See text for a discussion of the specific region. For the present, a factor of uncertainty of 1.5

should be attached for each point.

Figure 7. Diffuse radiation observed by several experiments. Also shown is the linear extrapolation of the X-ray data (solid line) and the spectrum predicted by Stecker, et al.(1971) for gamma-rays produced by the decay of neutral pions resulting from cosmic ray interactions with interstellar matter in the cosmological past. See text for discussion.



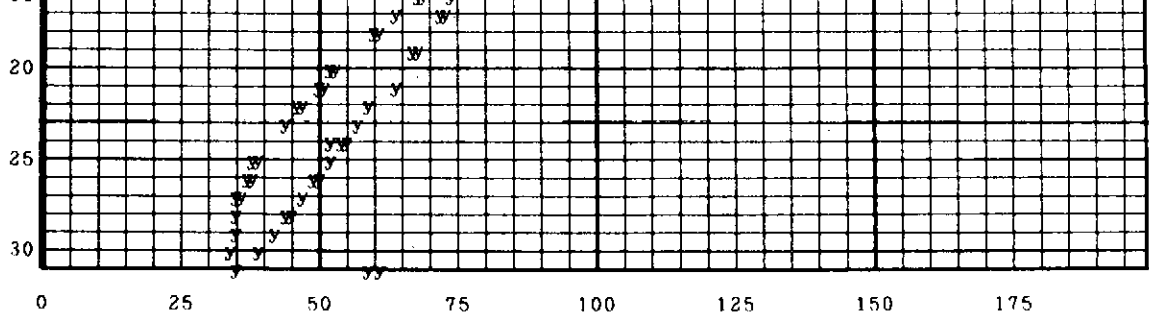
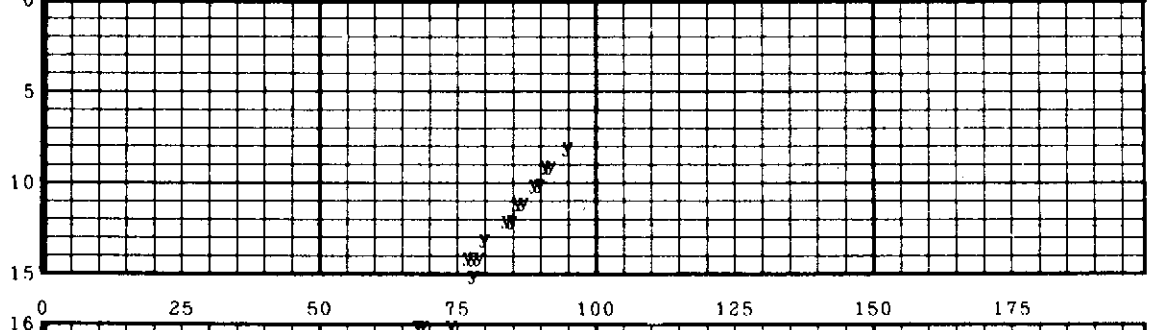
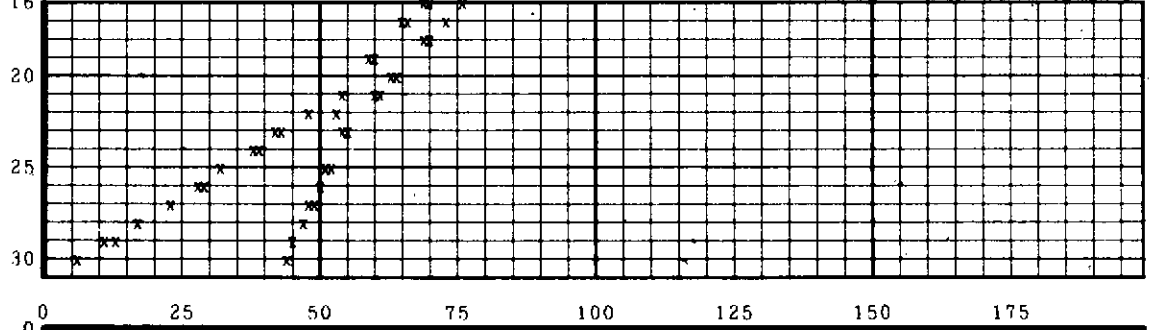
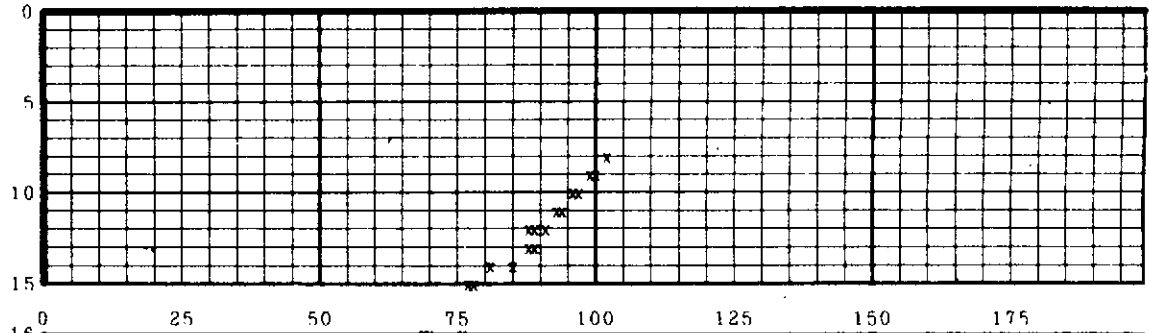
SAS-B GAMMA RAY EXPERIMENT



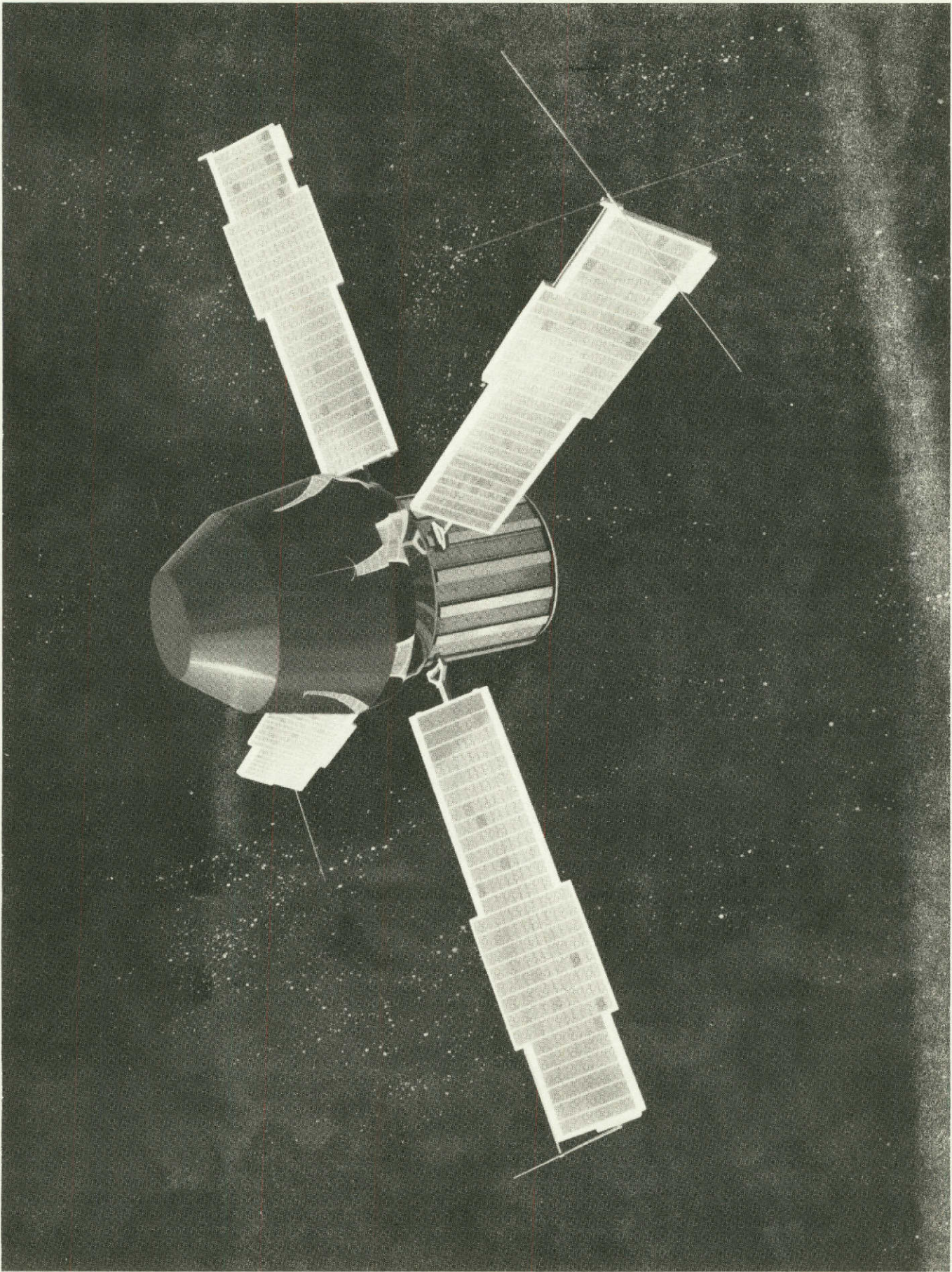
EVENT  
\*\*\*\*  
YEAR  
72  
MO  
12  
DAY  
21  
HR  
22  
MIN  
50  
SEC  
9  
MSEC  
520

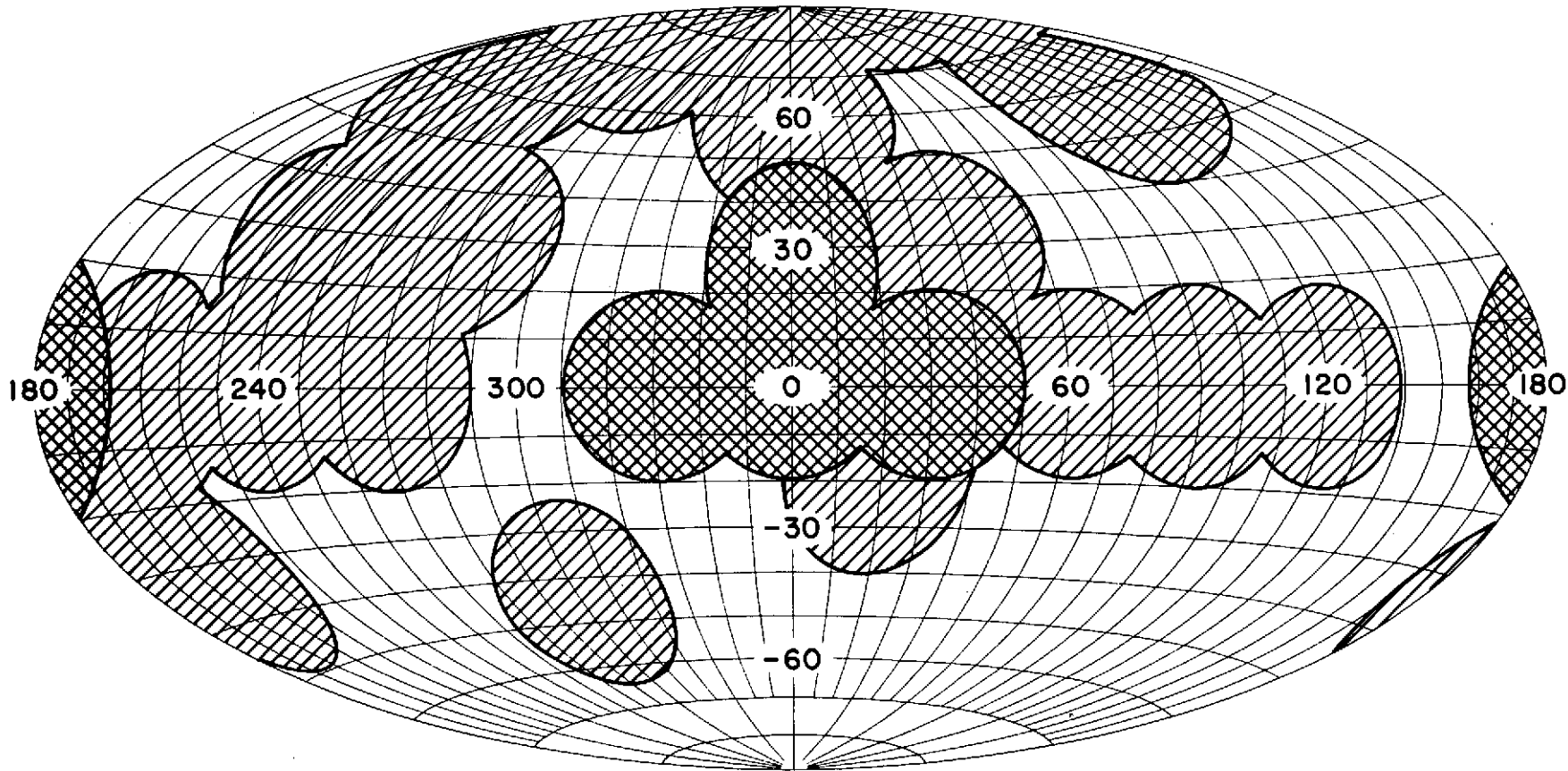
X ARRAY

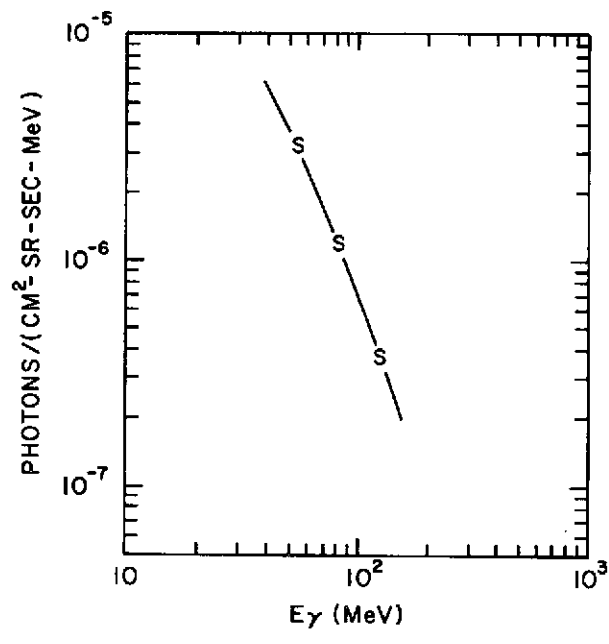
Y ARRAY

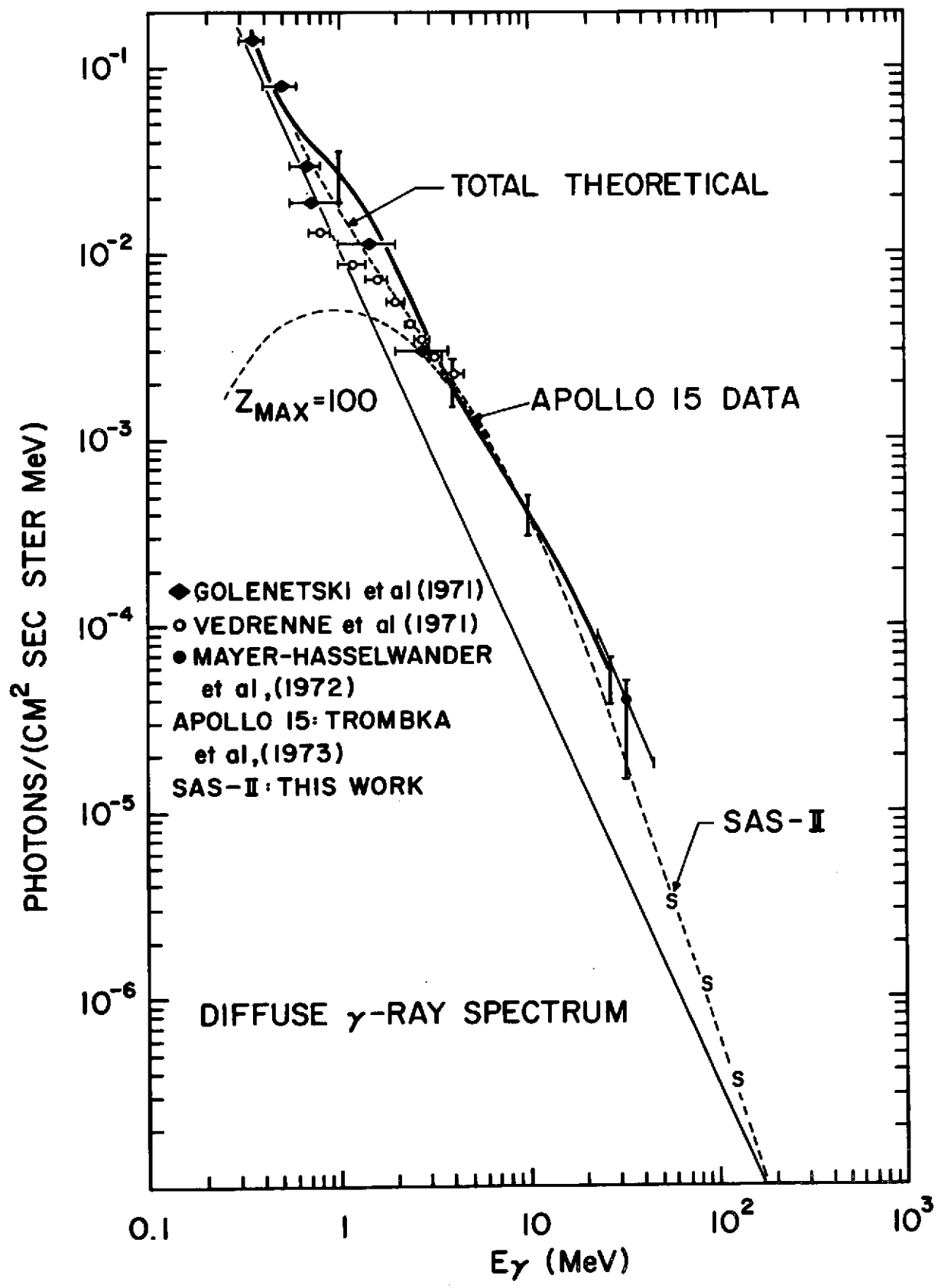


22









OBSERVATIONS OF HIGH-ENERGY GAMMA RAYS<sup>1</sup>

G. G. Fazio

Smithsonian Astrophysical Observatory and Harvard College Observatory  
Cambridge, Massachusetts

## I. INTRODUCTION

At energies above  $10^{11}$  eV, the predicted fluxes of cosmic gamma rays from discrete sources are so small ( $< 1 \text{ m}^2 \text{ day}^{-1}$ ) that it becomes impractical to measure these fluxes with detectors in high-altitude balloons and satellites. However, this radiation can be observed, indirectly, with ground-based instruments. When high-energy cosmic gamma rays strike the Earth's atmosphere, they generate a shower of particles that in turn emit a burst of Cerenkov light. In principle, a ground-based observer, using rather simple apparatus, can record the intensity and direction of either the particles or the Cerenkov light, or both, and hence determine the energy and arrival direction of the incident gamma-ray photon. In the energy region between  $10^{11}$  and  $10^{13}$  eV, the shower particles are absorbed

---

<sup>1</sup>An invited paper presented at the International Symposium and Workshop on Gamma-Ray Astrophysics, National Aeronautics and Space Administration, Goddard Space Flight Center, May 1973.

in the atmosphere, and therefore only the Cerenkov light technique can be used. It is this energy region in which most experiments are done and about which I will describe our recent results. Let me begin by first describing the instrumentation used in these experiments, as it has bearing on the interpretation of the results.

## II. INSTRUMENTATION

In the absence of sufficiently strong sources of cosmic gamma rays, the design of experiments must be based on theoretical models of the properties of the Cerenkov light generated by air showers. These studies have been done by Zatsepin and Chudakov (1962), Zatsepin (1965), Long (1967), Rieke (1969), and Bosia, Maringelli, and Navorra (1972). In general, at  $10^{11}$  eV, these light bursts of 3-nsec duration have angular diameters of the order of  $0.5^\circ$  but, when viewed away from the shower axis, are elongated and displaced in angle toward the shower maximum. The number of Cerenkov photons per unit area at ground level is rather constant within 130 m of the shower core and falls rapidly beyond this radius. Therefore, a light detector with sufficient sensitivity will be able to detect showers over an area of  $5 \times 10^4 \text{ m}^2$ . Thus, the principal advantages of this technique are the combination of a large sensitive area with good angular resolution.

There are also disadvantages. The basic one is that there is no equivalent of the anticoincidence counter to remove those showers generated by charged cosmic-ray particles; these are at least several hundred times

more numerous. Another disadvantage is that the technique can be used only on clear, moonless nights.

To obtain the maximum possible light-collecting power and hence the minimum possible threshold energy, the Smithsonian Astrophysical Observatory (SAO) constructed a light reflector of 10-m aperture, mounted on an alt-azimuth antenna positioner. The reflector is located at the 2300-m level of Mount Hopkins, Arizona (Fig. 1). Based on theoretical calculations, the reflector, when used as a gamma-ray detector pointed to the zenith, has a threshold energy of  $9 \times 10^{10}$  eV, an effective sensitive area of  $1.3 \times 10^4 \text{ m}^2$ , and an effective angular resolution of  $1^\circ$ . The maximum shower count rate at the zenith is about  $400 \text{ min}^{-1}$ . At angles away from the zenith, the threshold energy and the effective collecting area increase. There is no energy resolution in the integral counting mode other than this method of varying the threshold energy. Attempts are being made to achieve energy resolution by measuring the intensity of each Cerenkov light burst.

The primary cosmic radiation generates an isotropic background source of Cerenkov light bursts; hence, a gamma-ray source can be distinguished by an increase in the number of showers detected in the direction of the suspected source. Two observational techniques have been used to detect this anisotropy, the drift-scan mode and the tracking mode. In the drift-scan mode, the reflector is aligned 20–30 min of right ascension ahead of the suspected source; the Earth's rotation then sweeps the field of view of the detectors over the source. Many drift scans must be accumulated on

each object, since the expected anisotropy is less than 1 percent. Although the drift-scan mode has advantages in terms of stability and ease of operation, it is most inefficient because less than 20 percent of the observing time is spent on the source. To increase the on-source observing time, the tracking mode was developed. In this mode, two phototubes are located at the focus of the reflector and separated by  $4^{\circ} 2'$ . The reflector then tracks the source in such a manner that one phototube views the source while the other phototube views the background shower rate "off" source. Every 10 min, the fields of view are reversed. In this mode, approximately 90 percent of the time is spent observing the source.

The major limitation to the sensitivity of these experiments is the isotropic cosmic-ray background owing primarily to proton-initiated air showers (P-EAS). Several groups have sought to distinguish gamma-ray-initiated showers (G-EAS) from P-EAS by making use of subtle differences in the light distributions from the two types of showers (Tornabene and Cusimano, 1968; O'Mongain et al., 1968).

However, the most successful experiments in distinguishing the origin of the air shower have been performed by Grindlay (1971a, b). He has presented evidence that he has been able to distinguish the Cerenkov light from the electrons at the maximum of the shower's electromagnetic cascade (height  $h_{\text{max}}$ ) from the Cerenkov light owing to the unscattered, penetrating shower "core" of predominantly pions, muons, and secondary electrons. These latter particles would be present only in P-EAS. The technique

uses two searchlight-mirror detectors operated in coincidence mode and separated by 70 m, with each mirror rotated inward from the source direction by an angle  $\theta$  so that each is pointed at the shower maximum (figs. 2 and 3); for a gamma-ray energy of  $10^{12}$  eV,  $h_{\text{max}} = 6.2$  km and  $\theta = 0^\circ 35'$ . A third mirror system is used to detect the penetrating shower core ( $h = 3.5$  km,  $\theta = 0^\circ 65'$ ). Because the light from the lower component is relatively nearby, it is rich in the ultraviolet component and hence can be distinguished from light at the shower maximum. A G-EAS is registered only when light from shower maximum is seen not accompanied by light from the lower level.

With this technique, Grindlay has been able to reach an average rejection ratio of 70%. For gamma-ray energies  $\geq 5 \times 10^{11}$  eV, the combined effects of P-EAS rejection and increased angular resolution have made possible an order-of-magnitude increase in sensitivity over mirrors of the same size used in the normal modes. The drift-scan mode was used in these experiments, and the complicated pointing geometry permitted only 5 percent of the operating time on source. Recent experiments using the 10-m reflector and a 5-foot searchlight mirror on an alt-azimuth antenna positioner permitted operation in the tracking mode and a considerable increase in operating time on source.

Grindlay, in cooperation with Prof. R. Hanbury Brown's group at the University of Sydney, has converted the two 22-foot reflectors of the stellar interferometer at Narrabri, Australia, for use as atmospheric Cerenkov light detectors (fig. 4). P-EAS rejection was obtained with a second phototube located in an off-axis position on one of the reflectors,

and the reflectors were operated in the tracking mode. Several discrete sources in the Southern Hemisphere were investigated for the first time in 1972.

### III. OBSERVATIONS AND RESULTS

Since 1968, the 10-m reflector has been used to search for cosmic gamma rays from more than 27 discrete sources, including supernova remnants, pulsars, X-ray sources, magnetic variables, radio galaxies, and quasars. With the exception of the Crab Nebula, none of these sources was detected (Weekes *et al.*, 1972). For gamma-ray energies greater than  $2 \times 10^{11}$  eV, the upper limits to the flux were of the order of  $10^{-10}$  photon  $\text{cm}^{-2} \text{sec}^{-1}$ . It takes approximately 10 hours of observation on source to reach these limits. An extrapolation of the X-ray spectrum of some of these sources would indicate a gamma-ray flux in excess of this value. Simple Compton-synchrotron models for producing gamma rays in radio sources also predict fluxes above this value. Where enough information is known about these radio sources, the upper limits place important constraints on the source parameters, particularly the average magnetic field in the source.

Although other groups in the past have reported evidence for discrete gamma-ray sources in this energy range (e. g., Stepanian, Vladimirovsky, and Fomin, 1972), we have investigated these same sources and have found no evidence of gamma-ray emission.

During 1972, Grindlay's observations with the Narrabri reflectors in the Southern Hemisphere yielded preliminary evidence for gamma rays from several sources, but no radiation above  $2 \times 10^{11}$  eV from the discrete source Sgr A at the galactic center nor from several of the 100-MeV gamma-ray sources reported by Frye et al. (1971). These results are very tentative and further observations are currently being performed during April-June 1973.

The Crab Nebula is a very special case. Observations with the 10-m reflector over the years 1969-1972 indicate an average flux of gamma rays of  $4.4 \pm 1.4 \times 10^{-11}$  photon  $\text{cm}^{-2} \text{sec}^{-1}$  with energy above  $2.5 \times 10^{11}$  eV at the  $3.1 \sigma$  level (Fazio et al., 1972). This flux corresponds to an emission of  $6 \times 10^{33}$  ergs/sec, which is significantly less than the X-ray emission of the Nebula. However, the gamma-ray flux may vary with time, and the most significant flux ( $1.21 \pm 0.24 \times 10^{-10}$  photon  $\text{cm}^{-2} \text{sec}^{-1}$ ) may occur 60 - 120 days after a major spin-up of the pulsar NP 0532. This increase was observed on three different occasions and if only the flux in these intervals is used, the effect is at the  $5 \sigma$  level. The total gamma-ray energy observed on each occasion was  $\sim 10^{41}$  ergs, an energy approximately equal to the energy of the pulsar spin-up.

The average gamma-ray flux detected can be explained easily by a Compton-synchrotron model of the Crab Nebula, in which the gamma rays are produced by Compton scattering of relativistic electrons on their own synchrotron radiation (Gould, 1965; Rieke and Weekes, 1969; Grindlay and Hoffman, 1971). The primary unknown variable in this theory is the

magnetic field in the Nebula; and, hence, a measurement of the gamma-ray flux is a way of determining the average magnetic field. Figure 5 shows the current data along with the exact Compton-synchrotron model of Grindlay and Hoffman (1971). The data are best fitted with a value of  $\langle B_{\perp} \rangle = 2.5 \times 10^{-4}$  gauss in the uniform field model of the Nebula and by a value of  $B_{1\theta_0} = 10^{-3}$  gauss for a model based on a  $1/r$  field, where  $B_{1\theta_0}$  is the value of the field at the inner edge of the first wisp surrounding the pulsar.

The variability of the gamma-ray flux is more difficult to explain. In a Compton-scattering process, the electrons have too long a lifetime. The synchrotron process requires electrons of the order of  $10^{17}$  eV in a field of  $10^{-3}$  gauss; these electrons have a lifetime of  $\sim 10^3$  sec, and hence this process seems more feasible. The number of  $10^{17}$  eV electrons required is small compared to the total number of electrons injected into the Nebula. The 60-day delay and the 60–120-day duration may be due either to a time delay in the electron-acceleration process, e.g., in the wisps, or, assuming that the particles stream out from the pulsar, to the light-travel time in the geometry of the region where the synchrotron radiation is produced.

Because of this possible variation in the gamma-ray flux from the Crab Nebula, it is important that the SAS-B experiment monitor the 100-MeV flux from the Nebula for time variations. If, indeed, the 10-m reflector has detected a continuous flux of gamma rays at  $10^{11}$  eV from the Crab Nebula, it becomes particularly interesting to determine to what

extent this flux is pulsed. Grindlay (1971c), using the proton-shower-rejection technique, first reported a pulsed flux of gamma rays from NP 0532 based on 42 drift scans in January 1971.

Ninety-nine additional scans were obtained in November-December 1971, which also showed evidence of a pulsed effect (Grindlay, 1972). Later, it was discovered that the November-December data were analyzed with the wrong period, owing to a computer-program error. Reanalysis of this data resulted in even more significant evidence of having detected a pulsed effect from NP 0532. The sum of all 141 drift scans exhibited a  $4.2 \sigma$  effect, but the primary and interpulse both appear to be 1.7 msec early with respect to the corresponding optical peaks. These data correspond to a pulsed flux above  $6 \times 10^{11}$  eV of  $8 \pm 6.5 \times 10^{-12}$  photon  $\text{cm}^{-2} \text{sec}^{-1}$ .

Grindlay repeated the observations in 1973, by using the tracking mode to increase the observing time on source. Preliminary analysis of the data again showed evidence of pulsed gamma rays, but the primary peak of the radiation may be delayed in phase from the optical pulse by 1.7 msec (Grindlay et al., 1973). This repeated positive effect is most interesting, and it is still possible that Grindlay, using the proton-shower-rejection technique, has detected a pulsed gamma-ray flux from NP 0532 but the present results do not give unambiguous proof.

Helmken et al. (1973), by using data on the Crab Nebula obtained with the 10-m reflector, have analyzed the arrival times of air showers for over 200 hours of these observations; the arrival times were recorded to a

precision of 200  $\mu\text{sec}$ . An analysis of the data by use of the optical pulsar period and phase revealed no statistical excess at the primary pulse of the interpulse. A typical upper limit to the flux at  $1.8 \times 10^{11}$  eV for a 1.3-msec bin width and  $E^{-1.1}$  spectrum was  $1.4 \times 10^{-11}$  eV  $\text{cm}^{-2}$   $\text{sec}^{-1}$   $\text{ev}^{-1}$ . Upper limits to the flux were also obtained at energies of  $3.0 \times 10^{11}$  eV and  $4.7 \times 10^{11}$  eV (fig. 5).

The lower energy X- and gamma-ray data are best fitted by a curve of the form  $1.0 E^{-1.1}$ . Extrapolated to the  $10^{11}$  eV energy region, the curve lies 2 orders of magnitude above the current upper limits. The extrapolated flux, if true, would be verified in less than 20 min of observations. Thus, an important result of this work is that the upper limits to the gamma-ray flux indicate a major break in the pulsar spectrum between 1 and 100 GeV. When the previously reported positive continuous flux is taken with the present upper limits to the pulsed flux, it places an additional upper limit of 30 percent on the ratio of the pulsed-to-continuous component at  $10^{11}$  eV. This is a reversal of the trend at lower energies.

The University College, Dublin-Harwell group (N. Porter, private communication, 1972) also have evidence for a periodic flux of  $2 \times 10^{12}$  eV gamma rays from the pulsar, but, again, the primary pulse is not in phase with the optical pulse. If real, the effect would correspond to a flux of  $2 \times 10^{-12}$  photon  $\text{cm}^{-2}$   $\text{sec}^{-1}$ .

#### IV. FUTURE EXPERIMENTS

It is particularly important to continue observations on the Crab Nebula for two reasons: a) To determine if an increase in the continuous gamma-ray flux is associated with the pulsar spin-up, and b) to determine if Grindlay's technique of rejection of proton-induced showers has detected a pulsed flux from NP 0532.

The next priority would go to observation of the sources seen in the 100-MeV-1-GeV region with balloon-borne detectors, e. g., the sources reported by Frye et al. (1971) and with the SAS-B and TD-1 satellite detectors.

The sensitivity achieved in the current experiments has been the result of many hours of observation on a limited number of sources. It is still possible that there exist sources of detectable intensity that were not included in our survey or that were not observed in other regions of the spectrum. Therefore, Weekes et al. (1972) have proposed an all-sky survey of the Northern Hemisphere. Very few observations have been made in the Southern Hemisphere.

It is also possible that the gamma-ray sources examined are time variable, which makes verification even more difficult. Delays between balloon-borne gamma-ray detector flights are of the order of 6 months. One advantage of the atmospheric Cerenkov light technique is that

immediate observations can be made on a suspected source. In view of this, we ask groups that have discovered a possible source of cosmic gamma rays to communicate the information to us as soon as possible.

In all the above programs, an increase in detector sensitivity would be most helpful. In theory, the proton-shower-rejection technique used by Grindlay should significantly increase the sensitivity. Hence, it appears that the design of any future detectors should use this technique. One possibility is the construction of a second large reflector near the 10-m reflector at Mount Hopkins. Another tack one could follow would be to lower the gamma-ray threshold energy ( $E_t$ ) of the 10-m reflector. The current reflector mount could support a second 10-m reflector. Since  $E_t \propto A^{-1/2}$ , where  $A$  is the area of the reflector, doubling the area would reduce the threshold energy only by a factor of 0.7, but additional reductions could be made by increasing the frequency bandwidth and operating in the coincidence mode.

Continued studies of the structure of the Cerenkov light bursts produced in air showers are also necessary to maximize the efficiency of present detectors. For example, N. Porter has suggested that the geomagnetic field can have important effects on the angular distribution of Cerenkov light from extensive air showers.

## V. ACKNOWLEDGMENTS

The results described in this paper, obtained with the 10-m reflector, have been produced through the efforts of many people. Trevor C. Weekes has been primarily responsible for the operation of the 10-m reflector with the assistance of Ed Horine. The pulsar data analysis was done through the very patient efforts of Henry Helmken. George Rieke and Eon O'Mongain assisted in many of the observations and in the interpretation of the data. Jonathan Grindlay performed the compton-synchrotron model calculations.

## REFERENCES

- Bosia, G., Maringelli, M., and Navorra, G., 1972, Il Nuovo Cimento, 9B, 201.
- Fazio, G. G., Helmken, H. F., O'Mongain, E., and Weekes, T. C., 1972, Ap. J. (Letters), 175, L117.
- Frye, G. M., Albats, P. A., Zych, A. D., Staib, J. A., Hopper, V. D., Rawlinson, W. R., and Thomas, J. A., 1971, 12th Intl. Conf. on Cosmic Rays, Hobart, Tasmania, paper OG-24.
- Gould, R. J., 1965, Phys. Rev. Lett., 15, 577.
- Grindlay, J. E., 1971a, Il Nuovo Cimento, 2B, 119.
- \_\_\_\_\_, 1971b, Smithsonian Ap. Obs. Spec. Rept. No. 334.
- \_\_\_\_\_, 1971c, Nature (Physical Science), 234, 153.
- \_\_\_\_\_, 1972, Ap. J. (Letters), 174, L9.
- Grindlay, J. E., Helmken, H. F., Weekes, T. C., Fazio, G. G., Boley, F., 1973, preprint submitted to 13th Intl. Cosmic Ray Conf., Denver, June.

- Grindlay, J. E., and Hoffman, J. A., 1971, Ap. J. (Letters), 8, 209.
- Helmken, H. F., Fazio, G. G., O'Mongain, E., and Weekes, T. C.,  
1973, Ap. J. (in press).
- Long, C. D., 1967, Ph.D. thesis, National Univ. of Ireland.
- McBreen, S., Ball, S. E., Jr., Campbell, M., Greisen, K., and  
Koch, M., 1973, submitted to Ap. J. (Letters).
- O'Mongain, E. P., Porter, N. A., White, J., Fegan, D. J., Jennings,  
D. M., and Lawless, B. G., 1968, Nature, 219, 1348.
- Rieke, G. H., 1969, Smithsonian Ap. Obs. Spec. Rept. No. 301.
- Rieke, G. H., and Weekes, T. C., 1969, Ap. J., 155, 429.
- Stepanian, A. A., Vladimirovsky, B. M., and Fomin, V. P., 1972,  
Nature (Physical Science), 239, 40.
- Tornabene, H. S., and Cusimano, F. J., 1968, Canadian J. Phys., 46,  
S81.
- Weekes, T. C., Fazio, G. G., Helmken, H. F., O'Mongain, E., and  
Rieke, G. H., 1972, Ap. J., 174, 165.
- Zatsepin, V. I., 1962, Soviet Phys. - JETP, 15, 1126.
- \_\_\_\_\_, 1965, Soviet Phys. - JETP, 20, 459.

## LIST OF FIGURE CAPTIONS

Fig. 1. The 10-m optical reflector located at the 2300-m level of Mount Hopkins, Arizona.

Fig. 2. Simplified geometry of the detection technique used by Grindlay to reject proton-initiated extensive air showers.

Fig. 3. Photograph of the series of 5-foot searchlight mirrors used by Grindlay at Mount Hopkins, Arizona.

Fig. 4. One of the 22-foot reflectors at Narrabri, Australia.

Fig. 5. Graph of recent results of the pulsed and continuous flux from the Crab Nebula. The solid lines represent the Compton-synchrotron model computed by Grindlay and Hoffman (1971) for a uniform magnetic-field model and for a field proportional to  $1/r$ .

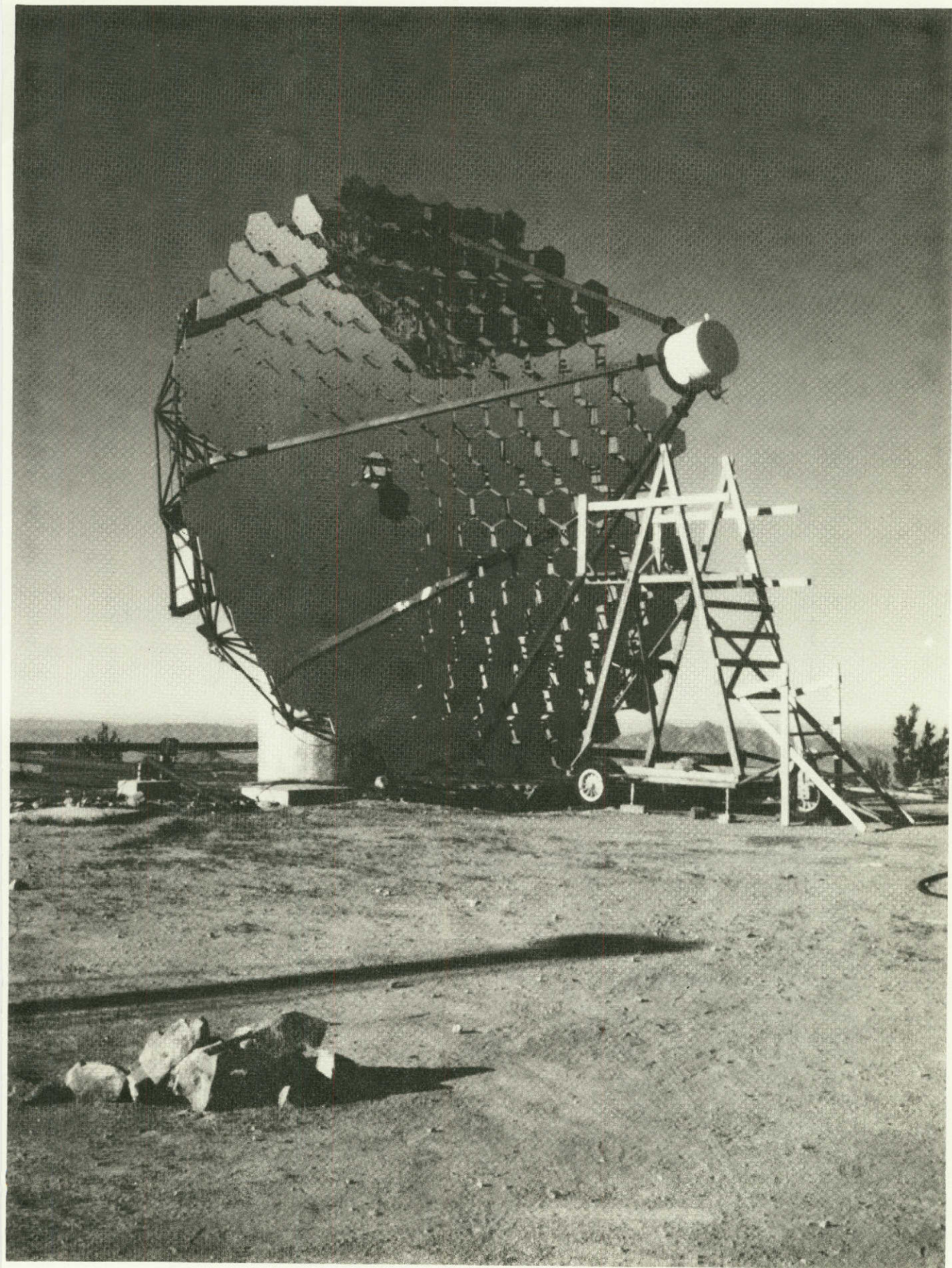


Figure 1

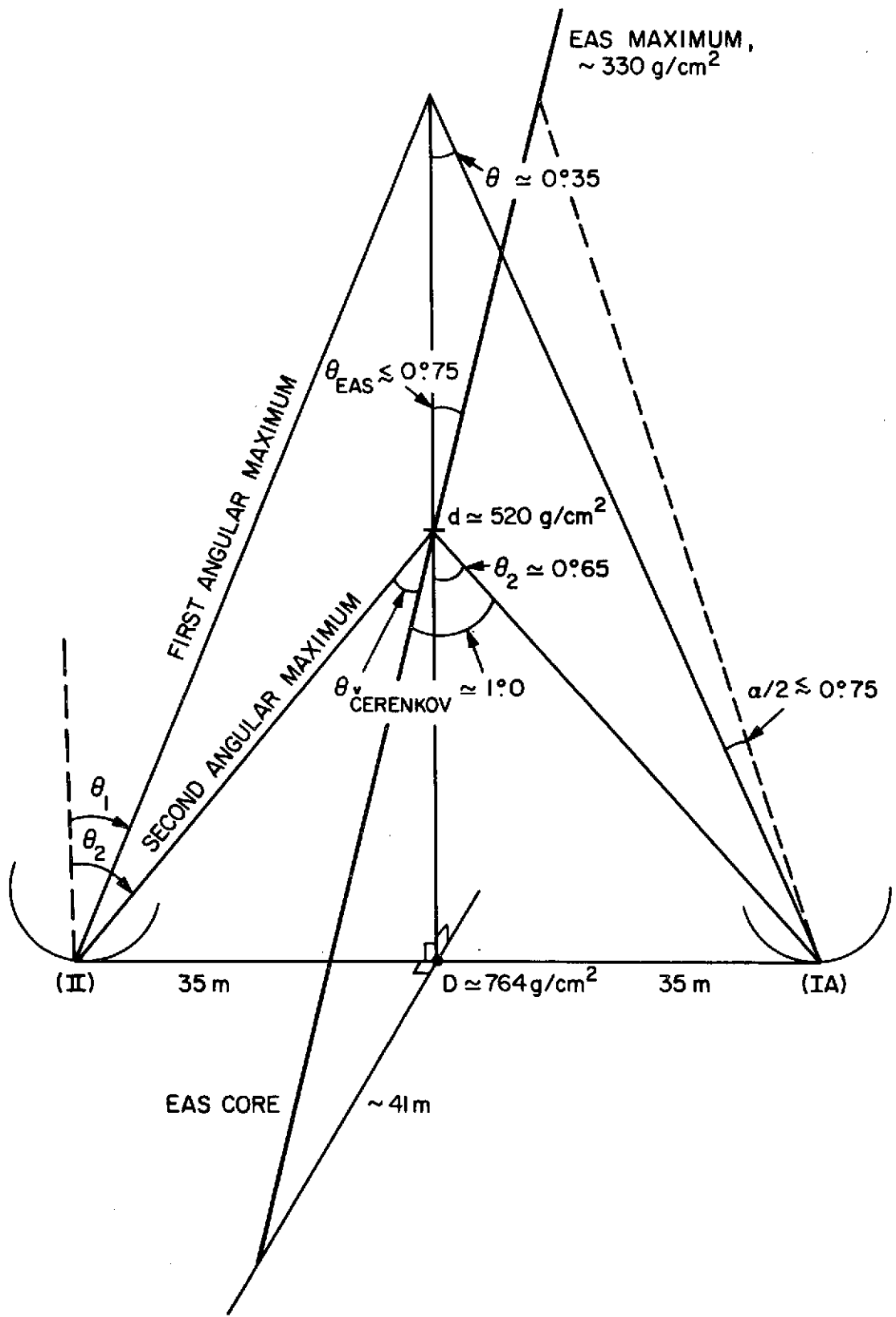
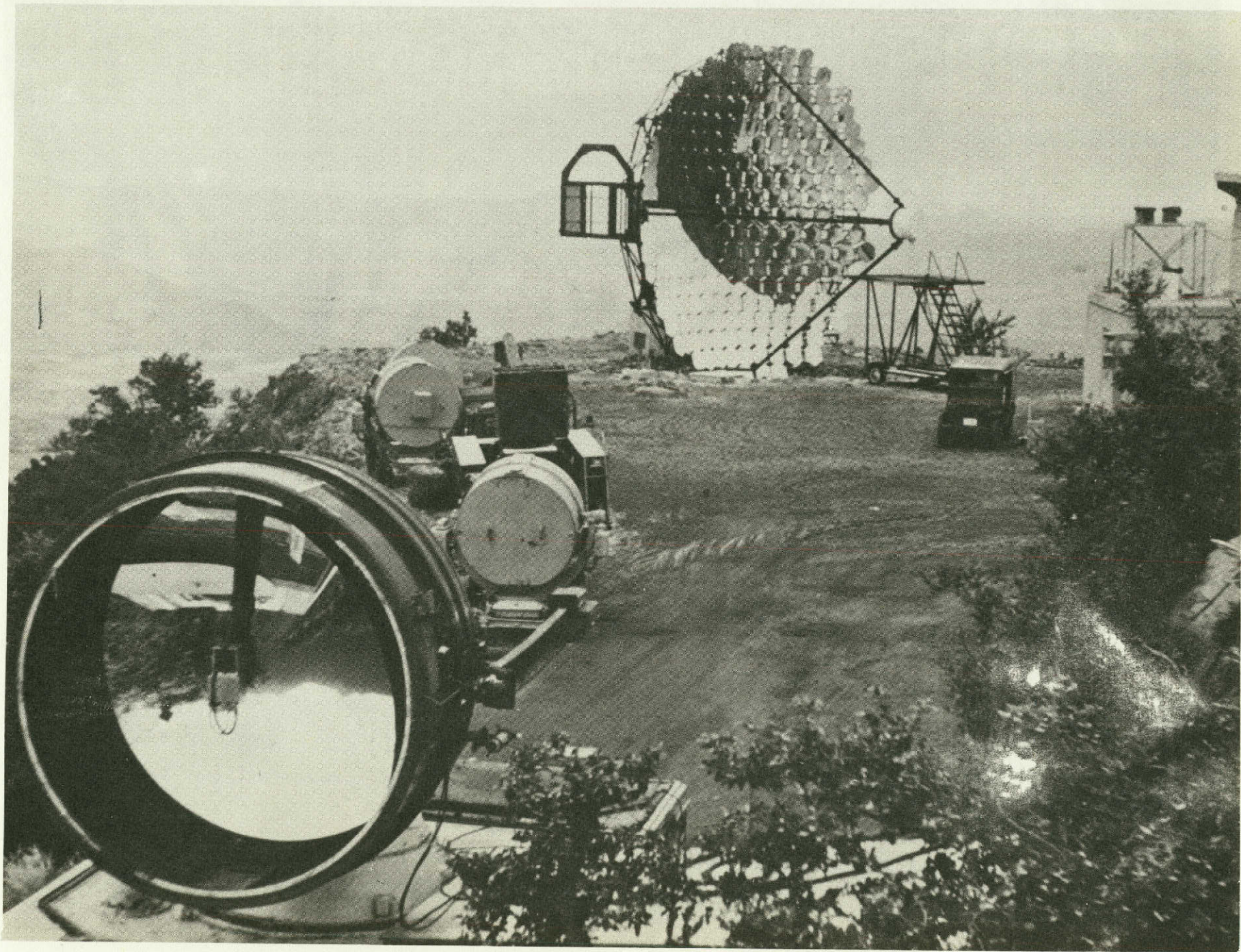


Figure 2

Figure 3



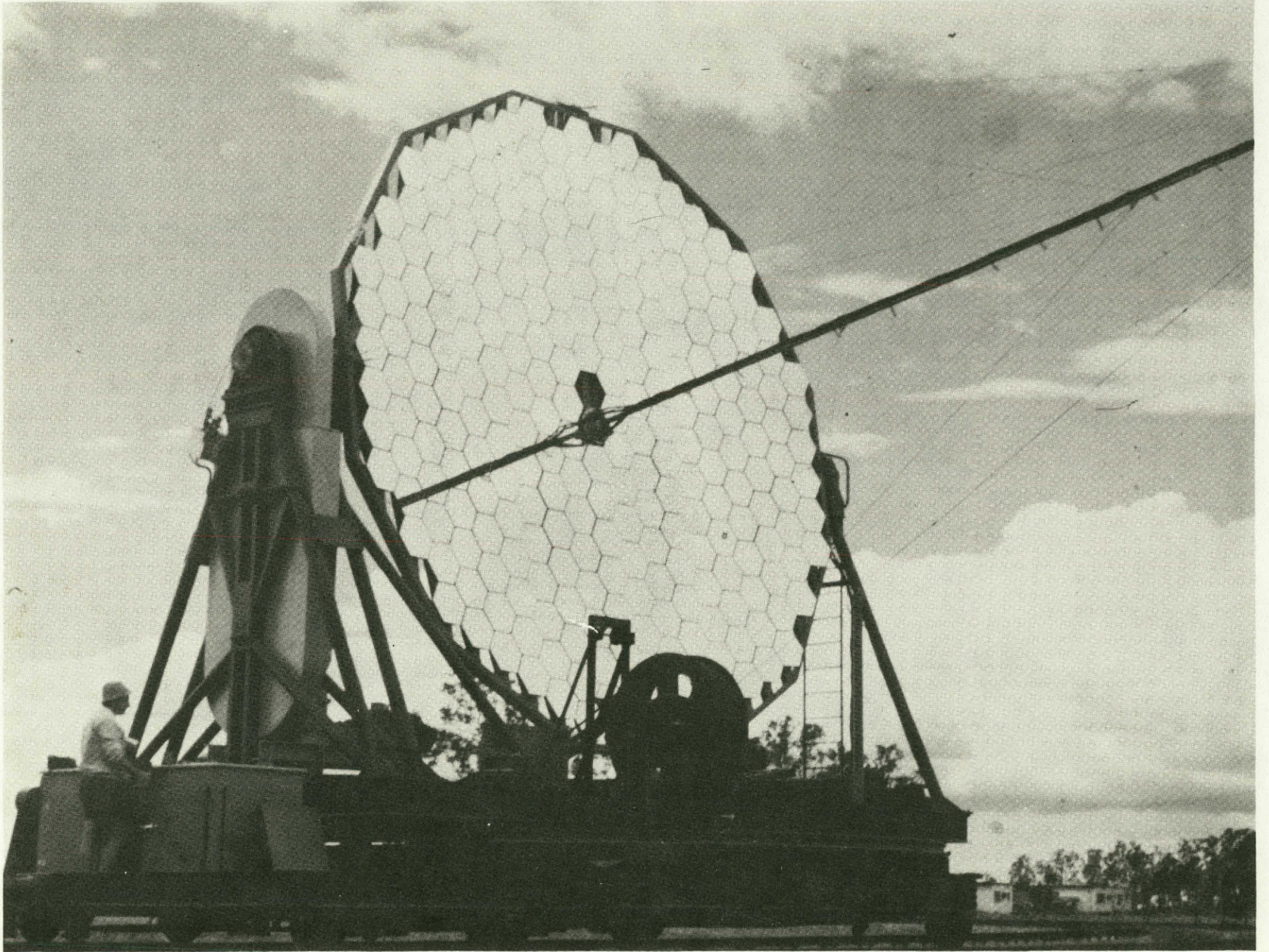


Figure 4

03

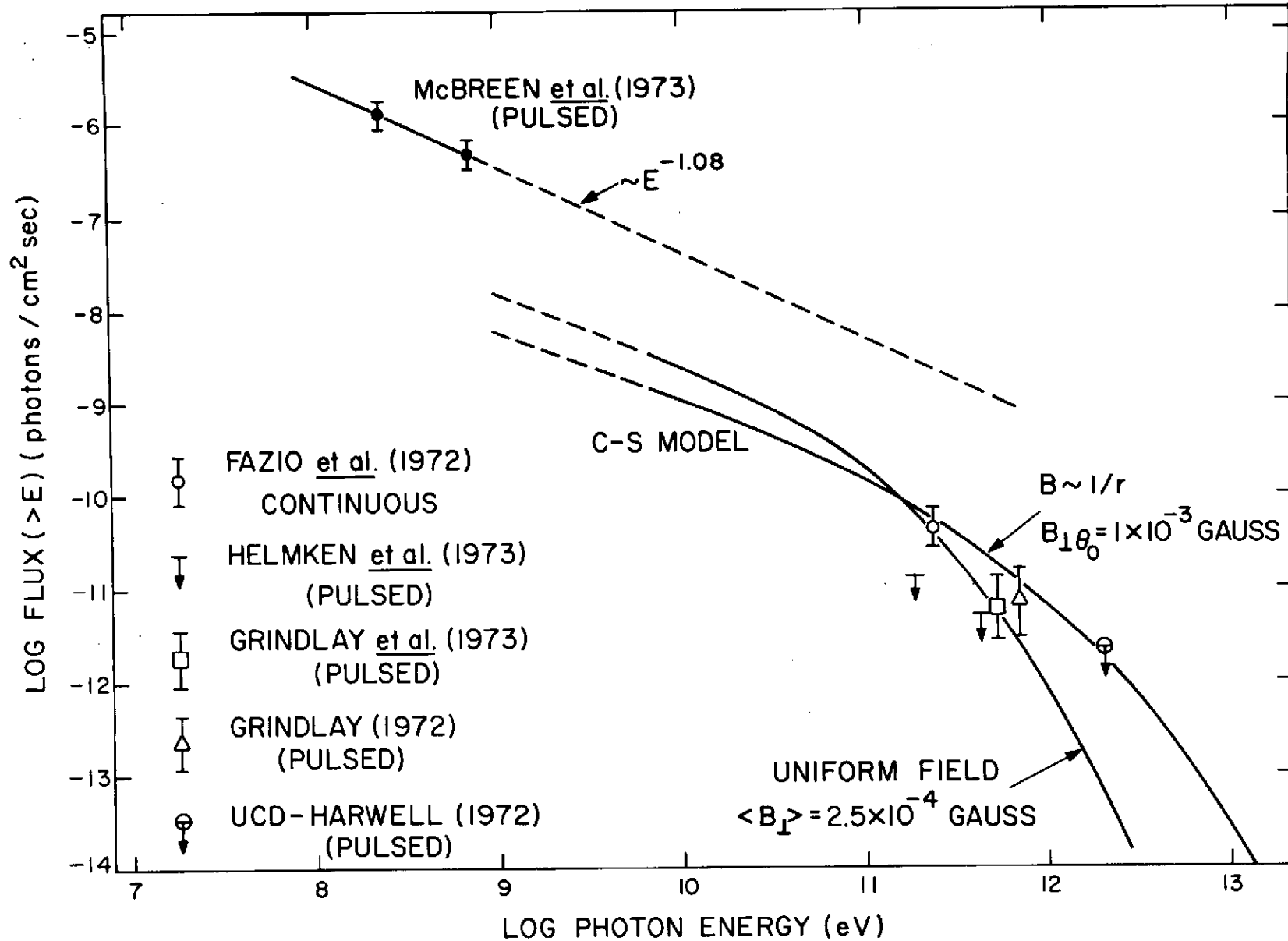


Figure 5

Observations of Gamma-Ray Emission in Solar Flares\*

D. J. Forrest, E. L. Chupp++, A. N. Suri, and C. Reppin+++  
Department of Physics, University of New Hampshire  
Durham, New Hampshire (USA) 03824

Abstract

This paper reviews the observations of gamma-ray emission made from the OSO-7 satellite in connection with two solar flares in early August 1972. The details of the measurements and a preliminary interpretation of some of the observed features are given.

---

\* This work was supported by NASA under Contract Nas 5-11054.

† Invited paper presented at the International Symposium and Workshop on Gamma-Ray Astrophysics held at Goddard Space Flight Center (Greenbelt, Maryland), April - May 1973.

++ Alexander von Humboldt and Fulbright-Hayes Scholar on leave at the Max-Planck-Institute for Extra-terrestrial Physics, Munich, Germany.

+++ On leave from the Max-Planck-Institute for Extra-terrestrial Physics, Munich, Germany.

## Introduction

The primary purpose of this paper is to review the observations of solar flare-associated gamma rays. Some preliminary discussion of the features of the measurements will be given even though the full interpretation of the measurements is not complete, as far as understanding the physics of solar flares is concerned. The observations discussed here were first presented at the NASA Symposium on High Energy Phenomena on the Sun (Chupp et al., 1972), and a more detailed report has been published (Chupp, et al., 1973).

The University of New Hampshire gamma-ray detector, which is situated in the wheel section of the OSO-7 spacecraft, has been described in detail by Higbie et al., 1973. Briefly, it consists of a 7.6-cm by 7.6-cm NaI scintillator surrounded by and in anticoincidence with an active CsI shield. It is calibrated by a gated radioactive source (Forrest et al., 1972) twice each orbit and has an energy resolution of  $\approx 8$  percent FWHM at 662 keV. Two independent pulse height spectra covering the energy range 0.3 - 9 MeV are simultaneously accumulated over an 180-second interval; one in the solar direction, and one in the antisolar or background direction. An auxiliary 7.9-cm<sup>2</sup> NaI X-ray detector is also included in the instrument. It covers the energy range 7.5 - 120 keV in four energy bands, and a complete X-ray spectra is taken every 30 seconds.

### Gamma-Ray Observations

Figure 1 shows the counting rate versus time in several energy bands covering the range 7.5 keV - 8 MeV observed during the 3B H $\alpha$  flare that began at ~0621 UT on 4 August 1972. Also shown is the radio burst at 19,000 MHz as reported in UAG-21 (Lincoln and Leighton, 1972). The rates in the energy interval 7.5 - 120 keV are from the X-ray detector, and the rate in the 0.35 - 8 MeV interval is from the central gamma-ray detector. As can be seen, OSO-7 was eclipsed by the earth before the event was over, but according to the radio burst, most of the flash phase was observed. The time correspondence between the radio, X-ray, and gamma-ray continuum is self-evident. Figure 2 shows some of the same rates on an expanded time scale. All of the rates were observed to increase above their preflare values at 0621 $\pm$ 1 UT. Although the lower energy channels quickly reached their instrumental saturation level, the two higher energy channels did not. These channels indicate that the rates continually increase over a 200-second interval and then appeared to level off until the eclipse at 0632 UT. The pulse height spectra that was observed in the time interval 0623 - 0632 UT is shown in Figure 3. As can be seen, there is an increase in the energy continuum that extends above 3 MeV and two pronounced photopeaks at 0.5 and 2.2 MeV in the solar quadrant. The two peaks at 1.17 and 1.33 MeV are leakage peaks from the onboard Co<sup>60</sup> calibration source. The two peaks at 0.5 and 2.2 MeV have been interpreted as resulting from positron annihilation at 511 keV and neutron capture in hydrogen at

2.23 MeV. The time history of the counting rates in the two photopeaks are shown in Figure 4 where the 60 - 120 keV rate (X-ray Channel 4) is reproduced for comparison. Although the photopeak counting statistics in the individual 180-second scans are not sufficient to determine a detailed time history, it can be seen that the rates in the photopeaks follow the time history of the high energy continuum quite closely.

The counting rate observed in association with the 3B Ha flare that started at ~1517 UT on 7 August is shown in Figure 5. Also shown is the radio flux at 15,400 MHz (Solar Geophysical Data Report No. 342, February 1973). The OSO-7 spacecraft was in eclipse during the flash phase of the flare and no continuum X-rays with energies greater than 120 keV were observed after the spacecraft came out from eclipse at 1538 UT. However, evidence for line emission at 0.5 and 2.2 MeV was observed between 1538 -1547 UT.

The time-averaged fluxes at these two energies observed on 4 and 7 August are given in Table 1. Also given are the fluxes observed at 4.4 and 6.1 MeV on 4 August. These latter two lines have been interpreted as arising from  $C^{12*}$  and  $O^{16*}$ .

### Interpretation

The gamma-ray lines observed from the flare on 4 August, namely, at 0.51, 2.23, 4.43, and 6.13 MeV (from positron annihilation, neutron capture on hydrogen, and excited states of  $C^{12}$  and  $O^{16}$ , respectively) have been predicted to be the most intense

lines based on known cross sections, solar abundances, and assuming nuclear interaction of the energetic solar particles with the solar atmosphere (Lingenfelter and Ramaty, 1967). The ratio of the observed lines are those predicted to result from a spectrum of energetic solar particles of the form

$$N(>P) = N_0 \exp(-P/P_0)$$

where the characteristic rigidity  $P_0$  is in the range 60 - 80 Mv. The spectrum of energetic particles measured on satellite detectors near 1 AU between 4 and 8 August agree with this spectral shape (Ramaty and Lingenfelter, 1973). However, there is at least one reference to a ground level effect from this flare (Pomerantz and Duggal, 1973). If this is true, then at least a portion of the energetic solar particles must have had a much higher characteristic rigidity. The absolute intensity of the observed gamma-ray line fluxes, however, is much lower (by a factor of  $10^2 - 10^3$ ) than was predicted from a flare of this magnitude. The intensity of the gamma rays is based mainly on the solar atmospheric density in the region where the particles interact and the number of energetic particles accelerated and released. In the past the only estimate of the total number of particles accelerated and released was based on measurements near 1 AU and model-dependent extrapolations back to the sun.

If the observed 200-second risetime of the very hard X-ray continuum is interpreted to be the time history of the rate of nuclear reactions producing the positrons and neutrons, then several other interesting results can be derived. First, unless the electrons and protons are accelerated and stored very high in the atmosphere and what we are seeing is the dump of these

particles into the denser lower atmosphere, then the time scale for converting some form of potential energy into the kinetic energy of relativistic particles is also 200 seconds. Second, a study of the risetime of the 2.2-MeV line flux indicates that the neutrons must have been captured in a region where the density was  $\approx 2 \times 10^{17}$  protons/cm<sup>2</sup> (Reppin et al., 1973). This is the photosphere and is expected since the neutrons, being uncharged, can easily escape from the region where they are produced to the higher density regions where they can be slowed down and captured. Last, the observed risetime of the 511-keV line cannot be more than 200 seconds. This together with the known cross section for annihilation implies that the density in the region where the positrons annihilate must be greater than  $2 \times 10^{11}$  electrons/cm<sup>3</sup>. A study of the line width of the 511-keV line observed on 4 August has lead to an upper limit temperature in this same region of  $\approx 7 \times 10^6$ °K (Dunphy et al., 1973). Because the positron is charged, it is reasonable to assume that the positrons are trapped in the region where they are produced and that the above temperature is an upper limit for this region.

The observations of line emission on 7 August after the flash phase is over is expected because of the  $\approx 200$ -second annihilation time for the positrons; some of the positrons are produced from radioactive isotopes with long half lives and the 100-second capture time for neutrons in the photosphere.

### Conclusion

The solar flare gamma-ray observations reported here appear to be in general agreement with models and calculations proposed by Lingenfelter and Ramaty, 1967. Further study of these observations together with other observations of the same flare of other wavelengths and particles should lead to a rather specific acceleration and interaction model for these flares. Of particular interest is the reported  $\text{He}^3$  measurements (McDonald et al., 1973).  $\text{He}^3$  in the intensities reported must have been produced in the same sort of nuclear reactions that produced the gamma rays.

### References

Chupp, E. L., D. J. Forrest, and A. N. Suri, in Proceedings of Symposium on High Energy Phenomena on the Sun held at Goddard Space Flight Center, Greenbelt, Maryland, 28-30 September 1972. Edited by R. Ramaty, to be published.

Chupp, E. L., D. J. Forrest, P. R. Higbie, A. N. Suri, C. Tsai, and P. P. Dunphy, Nature 241, 33 (1973).

Dunphy, P., E. L. Chupp, D. J. Forrest, and A. N. Suri, Bull. Am. Phys. Soc. 18, 695 (1973).

Forrest, D. J., P. R. Higbie, L. E. Orwig, and E. L. Chupp, Nucl. Instr. and Meth. 101, 567 (1972).

Higbie, P. R., E. L. Chupp, D. J. Forrest, and I. U. Gleske, IEEE Trans. Nucl. Sci. NS-19, No. 1, 606 (1972).

Lincoln, J., Virginia and Hope I. Leighton, World Data Center A, Report UAG-21; U.S. Department of Commerce, NOAA, Environmental Data Service, Ashville, North Carolina, November 1972.

Lingenfelter, R. E. and R. Ramaty, High Energy Nuclear Reactions in Astrophysics, edited by B. S. P. Stern, Benjamin, New York (1967).

McDonald, F. B., B. J. Teegarden, J. H. Trainor, W. R. Webber, and E. C. Roelof, Bull. Am. Phys. Soc. 18, 697 (1973).

Pomerantz, P. and S. P. Duggal, Nature 241, 33 (1973).

Ramaty, R., and R. E. Lingenfelter, in Proceedings of Symposium on High Energy Phenomena on the Sun held at Goddard Space Flight Center, Greenbelt, Maryland, 28-30 September 1972. Edited by R. Ramaty, to be published.

Reppin, C., E. L. Chupp, D. J. Forrest, and A. N. Suri, in Proceedings of International Conference on Cosmic Rays, Denver, Colorado, 17-30 August 1973, to be published.

Figure Captions

- Figure 1            Counting rates and radio flux versus time for  
the flare on 4 August 1972.
- Figure 2            Counting rates on an expanded time scale for  
the flare on 4 August.
- Figure 3            Pulse height spectra recorded in the time  
interval 0623 - 0632 UT on 4 August.
- Figure 4            Time history of the photopeak counting rate  
on 4 August.
- Figure 5            Counting rates and radio flux versus time  
for the flare on 7 August 1972.

Table 1

OSO-7 August 1972

Associated Flare and the time of Observations	Designations and Solar Flux at 1 AU Photons $\text{cm}^{-2}\text{sec}^{-1}$			
	0.5 MeV	2.2 MeV	4.4 MeV	6.1 MeV
3B (H $\alpha$ ) 4 Aug 1972 0624 - 0633 UT (Before H $\alpha$ Max)	$(7 \pm 1.5) \times 10^{-2}$	$(2.2 \pm 0.2) \times 10^{-1}$	$(3 \pm 1) \times 10^{-2}$	$(3 \pm 1) \times 10^{-2}$
3B (H $\alpha$ ) 7 Aug 1972 1538 - 1547 UT (After H $\alpha$ Max)	$(3.7 \pm 0.9) \times 10^{-2}$	$(4.8 \pm 1) \times 10^{-2}$	$< 2 \times 10^{-2}$	$< 2 \times 10^{-2}$

8-A

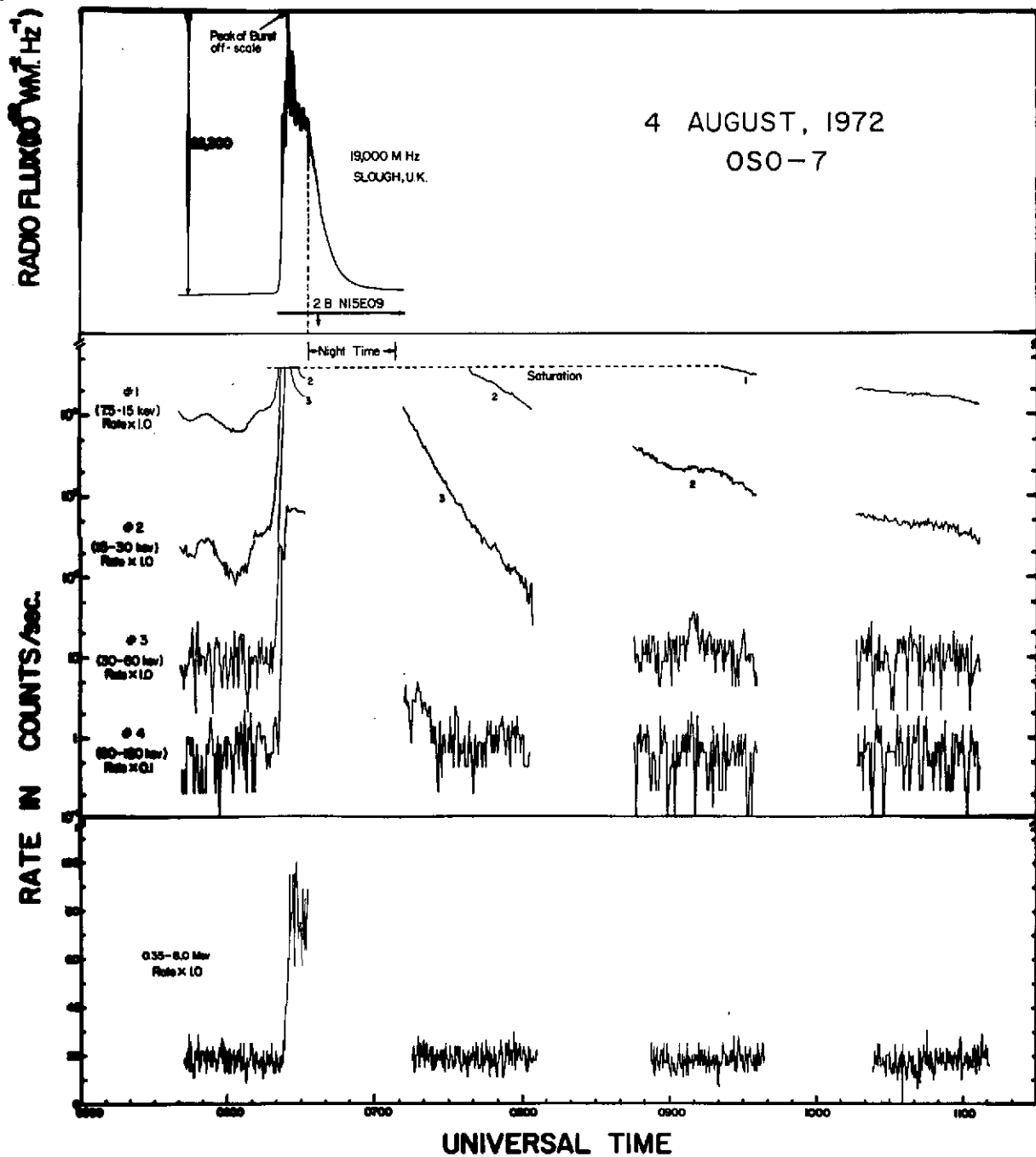


Figure 1

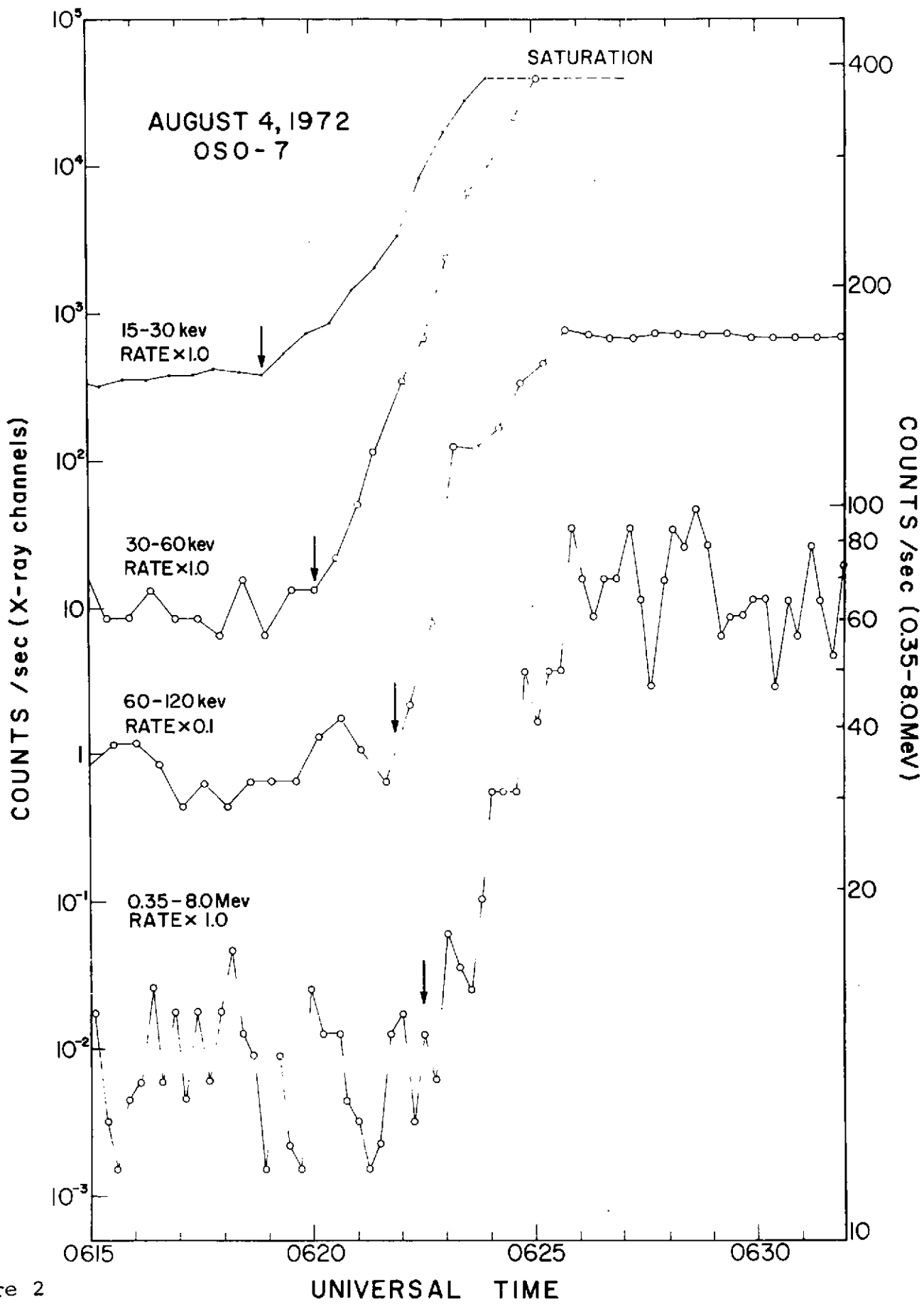


Figure 2

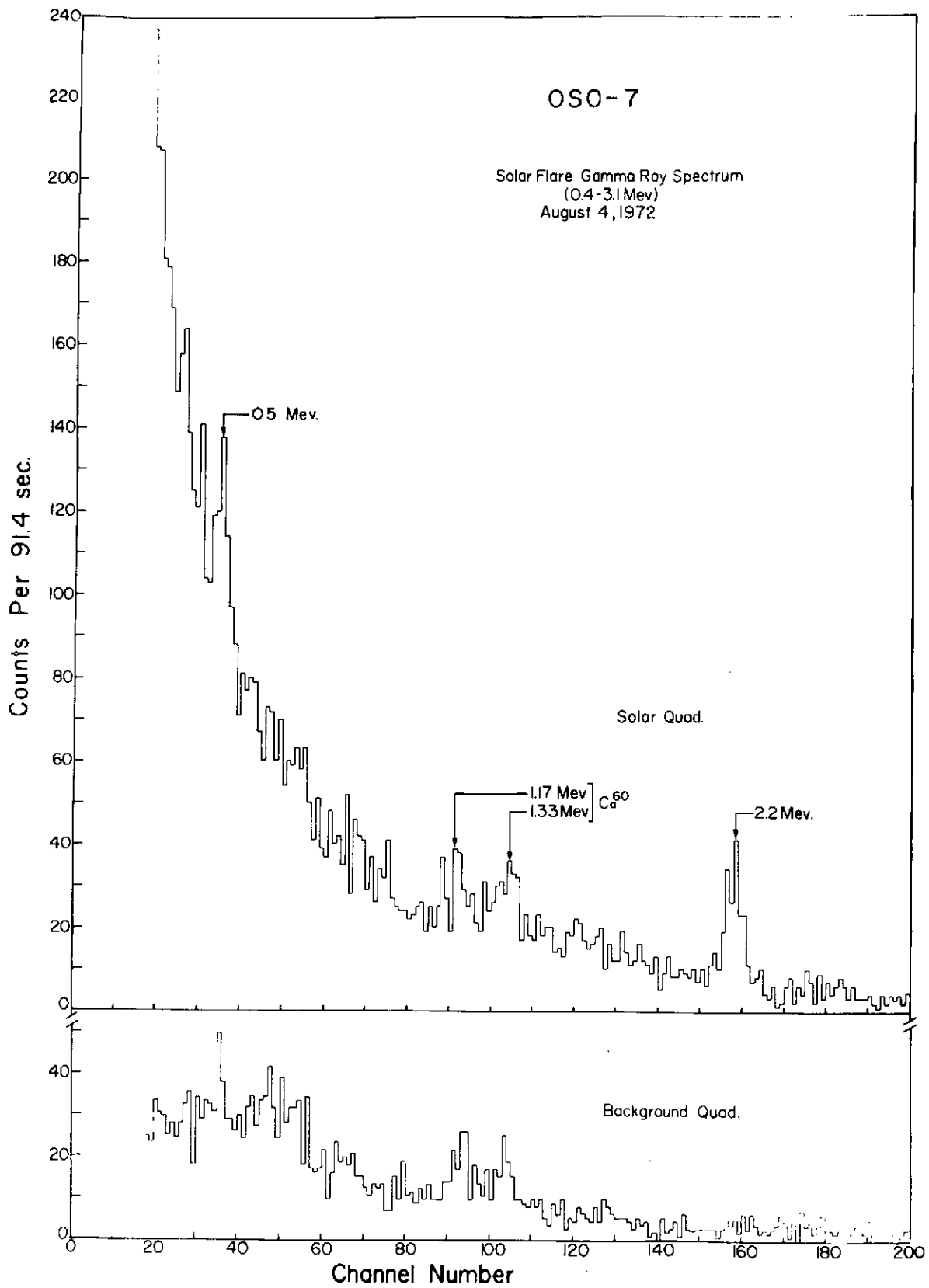


Figure 3

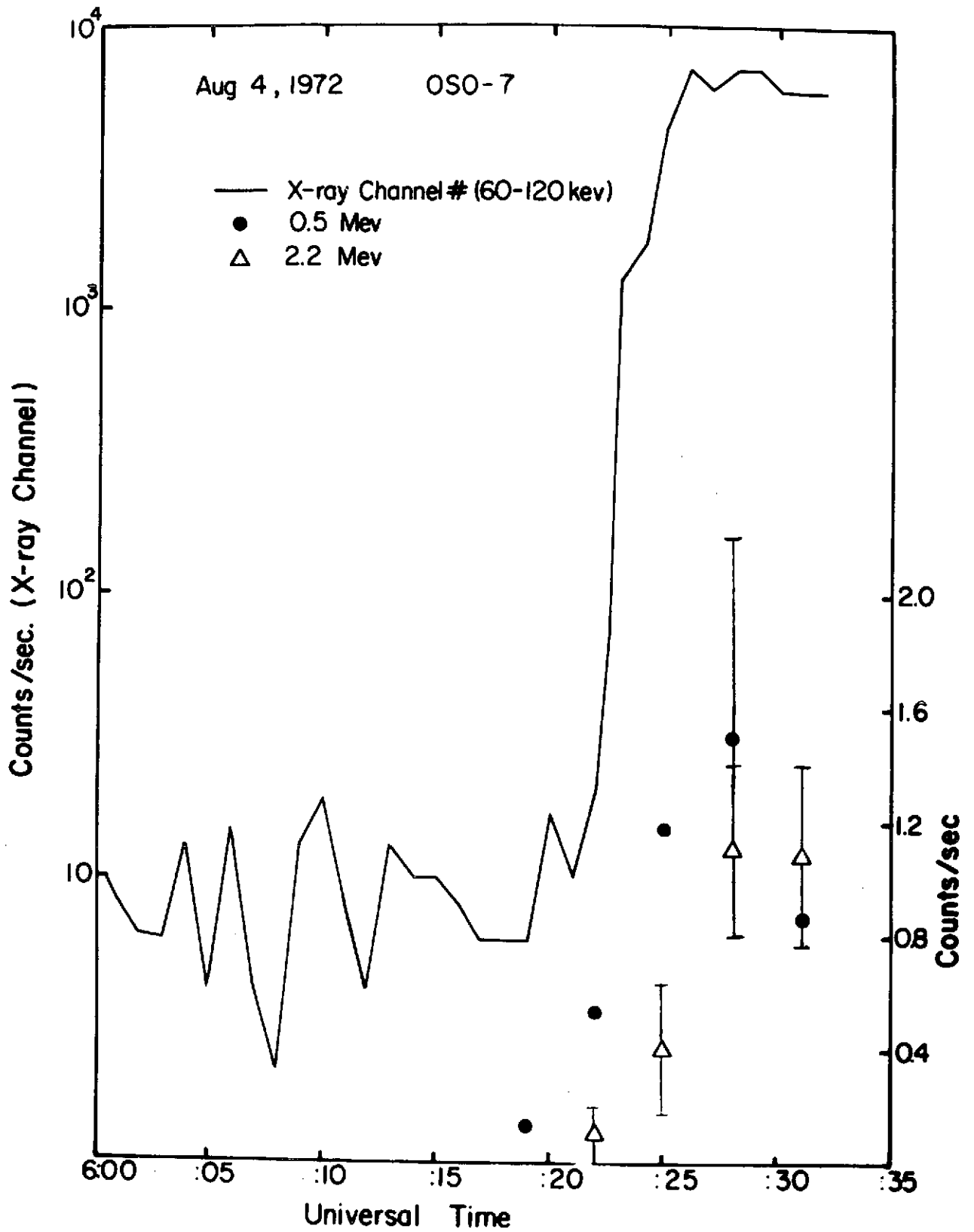


Figure 4

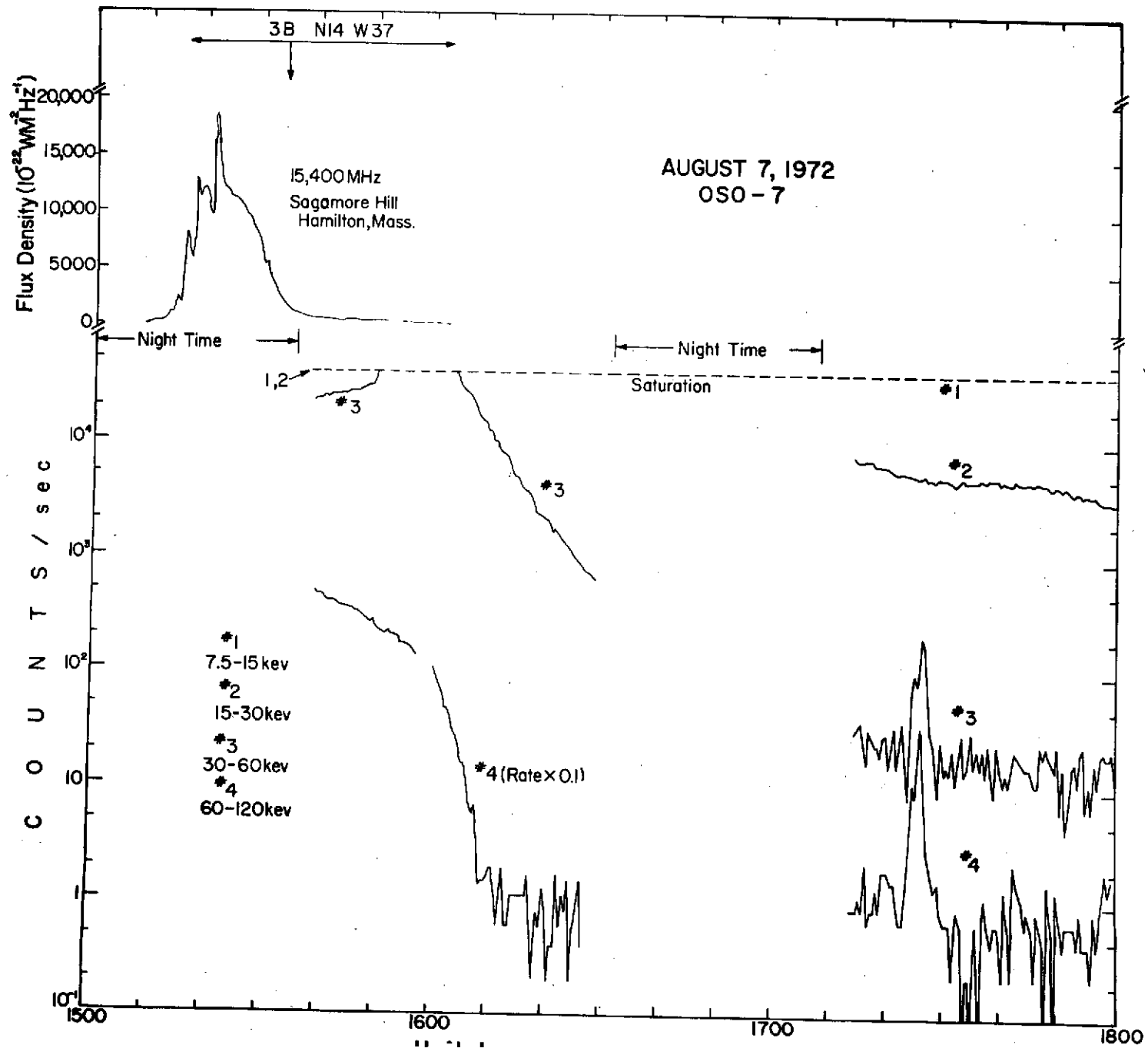


Figure 5

N73-28762<sub>9</sub>

THE ASTROPHYSICS OF THE DIFFUSE BACKGROUND  
OF X-RAYS AND GAMMA RAYS

Ramanath Cowsik

Department of Physics, University of California\*  
Berkeley, California 94720

I. INTRODUCTION

Studies in the field of x-ray and gamma ray astronomy have given rise to new insights into the structure and composition of our galaxy, the intergalactic space and the universe itself. Since there have been many comprehensive reviews (Silk 1970, Silk 1973, Felten 1972) on the subject, we will describe here only our views on the origin of the diffuse x-ray and gamma ray background and some of the astrophysical implications of such a radiation background. In the same spirit detailed references to all existing literature is not made and one may refer to the comprehensive reviews for this purpose.

The range of energies that is of interest here extends from  $10^2$  eV to  $10^8$  eV, over 6 decades, and a variety of processes contribute to the generation of a diffuse background. In order to make statements about the distribution of the sources of the radiation background, we appeal primarily to the angular distributions of the radiations about us. Considerations based on plausibility of models of origin and on minimizing the energy requirements in the sources supplement the classification of the sources either as Galactic or extragalactic. Our views on the origin of the various components are summarized in Table 1.

---

\*The address starting 1 October 1973 will be Max Planck Institute,  
8046 Garching bei Munchen, Germany.

Table 1. Origin of the Diffuse X-ray and  $\gamma$ -Ray Background

Energy Range	Process	Source Region	Discussed in Section No.
~250 eV - 2 keV	Thermal Bremsstrahlung	Our Galaxy and the external galaxies	III
	Compton scattering of the 2.7°K photons	Intergalactic space	
-2 keV - 200 keV	Thermal Bremsstrahlung	Intergalactic space	IV
-0.2 MeV-10 MeV	Compton scattering of $\sim 10^4$ °K photons	Cosmic ray sources in the Galaxy	V
$\geq 100$ MeV	Compton scattering of starlight	Central regions of Galaxy (extended source at the Galactic Center)	VI
	$\pi^0 \rightarrow 2\gamma$	Galactic disc (line source)	
	$\pi^0 \rightarrow 2\gamma$ ?	Galactic Halo? (isotropic background)	

Finally, in Section VII it is shown that the measured  $\gamma$ -ray fluxes at  $\sim 100$  MeV from the galactic disc place a rather stringent upper limit on the energy density of any background at submillimeter wavelengths.

## II. SOME IMPORTANT MECHANISMS FOR GENERATION OF X-RAYS AND $\gamma$ -RAYS

### 1. Thermal Bremsstrahlung

A high temperature plasma emits x-rays mainly through free-free transitions. Here the electrons which have a thermal energy distribution emit bremsstrahlung photons in the field of the ions. This process is weakly dependent on the exact chemical composition of the plasma and the rate of x-ray emission by an optically thin plasma is given by (Hayakawa 1969)

$$\begin{aligned}
 P_{\text{ff}}(E_x) &= \frac{1}{6\pi^3} \frac{e^2}{hc} \sigma_{\text{th}} c n_e \left( \frac{mc^2}{kT} \right)^{1/2} \left[ \sum Z n_Z \bar{g}_{\text{ff}}(Z, T, E_x) \right] \\
 &\quad \times \frac{1}{E_x} \exp(-E_x/kT) \\
 &= 0.81 \times 10^{-12} n_e^2 T^{-1/2} g_{\text{eff}} \frac{1}{E_x} \exp(-E_x/kT)
 \end{aligned} \tag{1}$$

For a plasma of solar composition the effective Gaunt factor,  $g_{\text{eff}}$  is approximately equal to unity. Equation 1 integrates easily to yield a cooling time

$$\tau \approx 1.96 \times 10^{11} T^{1/2} / n_e \text{ sec.} \quad (2)$$

In galaxies clouds of hot plasma may be created continuously, for example by supernova explosions. These will cool continuously emitting radiation. Then at any time there will be an equilibrium distribution temperature of these clouds extending up to  $T_{\text{max}}$ , the maximum temperature of generation of these clouds. If all clouds are created at  $T_{\text{max}}$  and they cool mainly through the free-free process, then the integrated emission of all the clouds can be approximated by

$$p(E_x) \sim \frac{1}{E_x^2} \exp(-E_x/kT_{\text{max}}) \quad (3)$$

Notice that this is steeper than the single temperature case by a factor  $\frac{1}{E_x}$ , indicating that there is less emission at high energies.

Besides free-free emission there would be free-bound and bound-bound transitions which will lead to sharp edges and lines in the emitted spectrum depending on the elemental abundances in the plasma.

## 2. Decay of Neutral Pions

Neutral pions would be produced in the interaction of nuclear cosmic rays with ambient matter, and these pions decay almost instantaneously to two gamma rays. This subject has been studied extensively by Stecker (1972) and in Figure 1 we show the spectrum of  $\gamma$ -rays generated through this process. It has a very flat spectrum in the region of  $\sim 70$  MeV and has a spectral slope identical to the cosmic ray beam at high energies.

## 3. Compton Scattering of Thermal Photons

The importance of this process under astrophysical conditions has

been made clear by the work of Morrison and his co-workers (see for example Brecher and Morrison 1969). In this process a highly relativistic electron scatters a low energy thermal photon into the x-ray energy region. Cowsik and Kobetich (1971,1972) have made a detailed calculation of this process; this calculation is briefly outlined below.

Under most astrophysical conditions the spectral distribution of background low energy photons can be taken to be the Planck function

$$K(\epsilon) = \frac{8\pi}{h^3 c^3} \frac{\epsilon^2}{\exp(\epsilon/kT)-1} \quad (4)$$

The angular distribution of these photons is isotropic, i.e.

$$\frac{dn}{d\cos\theta} = \text{constant} \quad (5)$$

The exact expression for the differential Compton-scattering cross-section is quite involved. However, simplification occurs because the mean energy of the x-ray generated by this process is usually much smaller than the energy of the electron involved in the scattering. Accordingly, the differential scattering cross-section for the emission of an x-ray photon of energy  $E_x$  in a collision of an electron of energy  $E$  with a photon of energy  $\epsilon$  integrated over the angular distribution of the incoming and outgoing photons becomes (Hayakawa 1969)

$$\sigma_c(E, \epsilon, E_x) = \frac{\pi}{4} r_e^2 \frac{(mc^2)^4}{E^3 \epsilon^2} \left[ 2 \frac{E_x}{E} - \frac{(mc^2)^2 E_x^2}{E^3 \epsilon} + \frac{4E_x}{E} \ln \frac{(mc^2)^2 E_x}{4 E^2 \epsilon} + \frac{8E\epsilon}{(mc^2)^2} \right] \quad (6)$$

On making the substitutions

$$B = (mc^2)^2, \quad D = \pi r_e^2/4 \quad \text{and} \quad x = \frac{B E_x}{4 E^2 \epsilon} \quad (7)$$

this reduces to (Blumenthal and Gould 1970)

$$\sigma_c = \frac{8DB}{E^2 \epsilon} (1 + x - 2x^2 + 2x \ln x) \quad (8)$$

Consider now a delta-function spectrum of electrons,  $\delta(E-E_0)$ , generating x-rays by Compton scattering against a thermal photon field (eq. 4)

This x-ray spectrum is shown in Figure 2. In view of the fact that the universal thermal background of microwave photons is the most relevant to the discussion of the isotropic component of the x-ray background, the plot in Figure 2 corresponds to  $T=2.7^\circ\text{K}$ . The spectral shape for any other temperature is obtained by simple sliding the same curve by a factor  $\frac{T}{2.7^\circ}$  along the X-axis on a log-log paper.

The most important feature that is to be noticed in this figure is that the emission by electrons of single energy is over a very wide band width, extending over a factor of 20 <sup>in x-ray energies,</sup> at half-maximum. Because of this large band-width any kink or peak or other spectral feature in the electrons <sup>energy</sup> is smeared out over an extremely broad <sup>energy</sup> region of the x-ray spectrum. Apart from the broad band-width, the mean energy of the x-ray depends quadratically on the electron energy. This relationship further contributes to the smoothing of the x-ray spectrum relative to the electron spectrum.

The Compton scattering of  $2.7^\circ\text{K}$  photons in the intergalactic space by cosmic-ray electrons leaking from galaxies could lead to an important contribution to the x-ray background (Brecher and Morrison 1969). In view of this we calculate the spectral shape of the electrons in the intergalactic space using the radio data of Lang and Terzian (1969). The expected x-ray spectrum is shown in Figure 3 marked as  $L_{ig}$ . The normalization of this curve is arbitrary.

### III. DIFFUSE X-RAYS BELOW A FEW keV.

Since the early observations by Boyer et al (1968), there has been a substantial progress in our understanding of the diffuse flux at  $\sim 250$  eV. The observations and related theoretical considerations are reviewed comprehensively by Silk (1973).

The comparison of the Compton x-ray flux from the intergalactic space ( $L_{IG}$  in Figure 3) with the observed data indicates that this process may contribute significantly to the background below a few keV. However, since the normalization of this curve is somewhat arbitrary it is reasonable to expect that only a part of the observed flux indeed arises through this process. In view of the fact that our own galaxy emits significantly in this band width one may expect that the diffuse background is generated as a superposition of emission of all the galaxies in the universe. This suggestion was first made perhaps by Silk (1970) and has had much experimental confirmation due to the observation of several extragalactic sources using the Uhuru satellite (Gursky et al 1972, Giacconi et al 1972). We show in Table 2 (taken from Silk 1973) the contribution of various types of extragalactic objects to the x-ray background at  $\sim 2$  keV.

Summing up the last column of the table shows that the sources contribute significantly at  $\sim 2$  keV. What is the spectrum of emission to be expected? If we try to fit a thermal bremsstrahlung spectrum to individual sources the maximum temperature that is encountered in these extragalactic sources is  $\sim 2 \times 10^7$ °K. Following our discussion in Section I (eq. 2) the cooling time of a plasma at this temperature is

$$\tau \approx \frac{1.96 \times 10^{11} (2 \times 10^7)^{1/2}}{n_e} \approx 10^{15} \text{ sec} \approx 3 \times 10^7 \text{ yrs.}$$

taking  $n_e=1$ . This cooling time is much smaller than  $\frac{1}{H_0}$  so that there would be a broad temperature distribution in the temperatures of the plasma leading to a spectral shape as given by eq. 3. Viz

$$p(E_x) \sim \frac{1}{E_x^2} \exp(-E_x/kT_{\max})$$

with  $T_{\max} \approx 2 \times 10^7$ °K. This spectral shape fits excellently the results

Table 2. Contribution of Identified Extragalactic Sources to the Isotropic X-Ray Background<sup>a</sup>

Class	Source	$L_x$ (2-10 keV) $\frac{\text{erg}}{\text{sec}}$	Local space density $n$ ( $N=0.03 \text{ Mpc}^{-3}$ )	Flux $\frac{c}{4\pi H_0} nL$ (keV/cm <sup>2</sup> sec ster)
Small galaxies	LMC	$4 \times 10^{38}$		
	SMC	$1 \times 10^{38}$		
	<u>Adopted mean</u>	$2 \times 10^{38}$	10 N	1.9
Normal galaxies	M31	$3 \times 10^{39}$		
	Our galaxy <sup>d</sup>	$5 \times 10^{39}$		
	<u>Adopted mean</u>	$4 \times 10^{39}$	N	3.8
Radio galaxy	Cen A	$8 \times 10^{41}$	$10^{-3} N$	0.74
Seyfert galaxy	NGC 4151	$2 \times 10^{41}$	0.02 N	3.8
Abell I clusters <sup>b,c</sup>	Centaurus	$4 \times 10^{43}$		
	Virgo	$1.5 \times 10^{43}$		
	<u>Adopted mean</u>	$3 \times 10^{43}$	$2 \times 10^{-5} N$	0.57
Abell II clusters <sup>b</sup>	Coma	$5 \times 10^{44}$		
	Perseus	$1 \times 10^{45}$		
	Abell 2256	$1 \times 10^{45}$		
	<u>Adopted mean</u>	$8 \times 10^{44}$	$5 \times 10^{-6} N$	3.8
Quasar	3C273	$7 \times 10^{45}$	$3 \times 10^{-8} N$	0.18

<sup>a</sup>Data are taken from the Uhuru catalogue (Giacconi et al 1972);  $H_0$  is set equal to  $50 \text{ km sec}^{-1} \text{ Mpc}^{-1}$ .

<sup>b</sup>Only those sources identified with clusters and known to be extended are included.

<sup>c</sup>The Centaurus and Virgo clusters are not in Abell's (1958) catalogue; however they approximately correspond to Abell's richness class I.

<sup>d</sup>Estimated x-ray luminosity of our galaxy (Seward et al 1972).

below a few keV. Therefore, we conclude that free-free emission from the various extragalactic sources would contribute significantly to the x-ray background below few keV. However, the spectral shape is too steep to contribute significantly at higher energies.

#### IV. THE 2-200 keV REGION AND POSSIBLE THERMAL BREMSSTRAHLUNG OF THE INTERGALACTIC GAS.

Investigating the possible origin of the x-rays in this energy band we noticed (Cowsik 1971) that thermal bremsstrahlung of a tenuous plasma at a temperature of  $3 \times 10^8$  K had the right spectral form to fit the observations. An emission measure,  $\int n_e^2 d\ell \approx 1.3 \times 10^{17}/\text{cm}^5$  was required to give the observed intensities. Assuming no clumping (i.e.  $n_e$  independent of  $\ell$ ) and taking  $\int d\ell = \frac{2c}{3H_0} \approx 10^{28}$  cm, one gets  $n_e \approx 3 \times 10^{-6} \text{ cm}^{-3} = m_{\text{crit}} \approx \frac{3H_0}{8\pi G m_{\text{H}}}$ , for  $H_0 = 50$  km/sec. Mpc. Therefore we suggested the possibility of a hot intergalactic plasma as a possible source of this background (Cowsik 1971, Cowsik and Kobetich 1972). The thermal bremsstrahlung fit to the experimental data after plausible subtractions of other emission mechanisms below 2 keV (Sec. III) and above 200 keV (Sec. V) is shown in Figure 4.

That a hot intergalactic medium could be the source in this region has been independently pointed out by Field (1972). Of course, the idea of a hot intergalactic medium is not new. It has been discussed in the context of continuous creation of matter in the form of neutrons in the steady state cosmology by Gold and Hoyle (1959) and by Gould and Burbidge (1963). However, Petrosian and Ramaty (1972) have provided arguments based on excessive production of hard x-rays through the radiative decay of the neutron that continuous creation of matter as neutrons is forbidden by x-ray

observations. The x-ray spectral observations in the region of 2-20 keV yield merely the temperature and emission measure of the radiating plasma. Therefore, the question arises as to whether the emission indeed comes from a hot intergalactic medium or from hot gas in various galaxies.

We believe that there are indeed reasons that indicate that the hot intergalactic medium is the most plausible explanation of this emission. The high degree of isotropy as measured by Schwartz (1970) has been analyzed by Silk (1973) to show that one needs at least  $10^7$  sources in the sky to yield the required degree of isotropy. This means that a reasonable fraction of the galaxies should contain hot plasma at  $3 \times 10^8$ °K. In order that the spectrum of emission is not transformed by free-free cooling (see Sec. 1. eq. 2,3)

$$\frac{1.96 \times 10^{11} (3 \times 10^8)^{1/2}}{n_e} > \frac{1}{H_0} > 3 \times 10^{17} \text{sec} \quad (8)$$

which yield  $n_e \sim 10^{-2}/\text{cm}^3$ . Even if one takes  $n_e \sim 10^{-2}$  one finds that about 5% of all visible galactic matter should be at a temperature of  $\sim 3 \times 10^8$ °K in order to generate an emission measure of  $\sim 1.3 \times 10^{17} \text{ cm}^{-5}$ . Firstly, most of the mass of the galaxies is concentrated in stars (temperature  $\sim 10^4$ °K), with gas contributing to less than 10% of the total mass. The galaxies would definitely be unable to contain gravitationally such a large amount of hot plasma.

There is a second argument in favor of a critical mass density existing in the form of a hot intergalactic plasma. This argument essentially invokes the intergalactic medium as a heat sink for the energy released during the synthesis of heavy elements in supernovae exploding in the galaxies. It has been pointed out that in our galaxy with a mass of  $\sim 10^{11}$  solar masses

one needs  $\sim 10^9$  supernovae to generate the heavy elements. How much energy is released in this process? We may estimate that about one solar mass collapses to a neutron star in each event yielding an energy of  $\frac{G(1/2 M_{\odot})}{R}$ . Thus the energy generated per unit mass of the galaxy

$$u = 10^9 \frac{G M_{\odot}^2}{R} \cdot \frac{1}{10^{11} M_{\odot}} = \frac{G M_{\odot}}{100R} \approx 2 \times 10^{18} \text{ erg/g}$$

using  $R = 10^6$  cm. This released energy is not seen as electromagnetic radiation in any frequency band, and this energy must therefore have gone into the kinetic energy of matter.  $5 \times 10^9$  ergs/gm corresponds to a temperature of  $\sim 10^{10}$  K. This shows that we need to have approximately 100 times as much intergalactic matter as in the galaxies to absorb this energy so that the mean temperature of the universe may not be too high. With a hot intergalactic plasma of critical density (equal to  $\sim 50$  times the mass density contributed by the galaxies) one has a hot universe at  $\sim 3 \times 10^8$  K.

#### V. 0.3 - 3 MeV GAMMA RAYS.

Stecker, Morgan and Bredekamp (1971) have attempted to explain this flux of gamma-rays as due to annihilation of matter and antimatter at  $Z=100$  in a baryon symmetric universe. However, neither the absolute intensity nor the isotropy of this radiation has been established. Therefore, we wish to investigate here the possibility that this radiation could be of local, galactic origin. In fact, there are indications in the cosmic-ray electron spectrum that such emission could be taking place from our galaxy. Before discussing this galactic source in detail we must emphasize that the burden of proof lies with experiments. Should they show that the radiation is indeed isotropic one has to give away the Galactic model,

which is discussed below.

The cosmic-ray electron spectrum is well measured in the region of ~100 MeV to ~100 GeV; it is shown in Figure 5 after correcting for solar modulation effects. The spectrum below a few GeV has a spectral index of -1.6, but steepens to an index of ~-2.6 above a few GeV. This is not the true electron spectrum that is injected into the interstellar space by the cosmic ray sources but is contaminated by interstellar secondaries generated by the nuclear component of cosmic rays. The positron flux gives a very good estimate as to the amount of this contamination. After subtracting the secondaries the spectrum of electrons injected by the sources is shown in Figure 6. Since the processes of cosmic ray acceleration are electromagnetic in nature, one may safely assume that the spectrum of electrons accelerated by the sources is a simple power law with an index of 2.6 similar to that of the nuclear component. The difference in the energy between the accelerated spectrum and the injection spectrum must have been radiated away. If part of this radiation is due to Compton scattering against optical frequency photons then one obtains a gamma ray luminosity (Cowsik 1971)

$$L(E_\gamma) = \frac{5}{(\beta-1)} \sqrt{\frac{3}{16 E_\gamma \epsilon}} \left[ E_H^{p-1} + \left( \frac{m}{2} \sqrt{\frac{3E}{\epsilon}} \right)^{p-1} \right]^{-\frac{\beta-1}{p-1}} - \left[ E_\gamma^{p-1} + \left( \frac{m}{2} \sqrt{\frac{3E_\gamma}{\epsilon}} \right)^{p-1} \right]^{-\frac{\beta-1}{p-1}} \quad (9)$$

$\beta$ ,  $S$ ,  $E_H$ ,  $E_T$  and  $p$  are constants derived from the electron spectrum and  $\epsilon = 3 \times 10^{-6}$  MeV is the assumed mean energy of the optical photon. The intensity as seen by a detector having isotropic response is shown in Figure 7. One notices that the spectrum is insensitive to the parameter  $p$ . The general shape of the curve is essentially determined by  $\beta \approx 2.6$ , the

spectral index of the cosmic ray electrons at low and high energies respectively. Despite this elegant fit to the data one has to wait for measurements of angular distribution in this energy region before the Galactic nature of the MeV gamma ray fluxes can be established.

## VI. GAMMA-RAYS IN THE 100 MeV RANGE

The pioneering work of Clark, Garmire and Kraushaar (1969) established the existence of a line source coincident with the galactic disc with an enhancement around the galactic center, and a possible isotropic component. The measured intensity in the direction of the center is  $\sim 10^{-4}\gamma/\text{cm}^2$  sec rad, the line source elsewhere is about a third of this  $\sim 2-3 \times 10^{-5}\gamma/\text{cm}^2$  sec rad. The line source has been explained by Stecker (1969) as due to production and subsequent decay of neutral pions by cosmic rays. If the same mechanism should yield the enhancement of the intensities near the center one needs a substantially large enhancement of gas density near the central regions of the galaxy. There is no evidence, direct or indirect for such an enhancement. On the other hand, there is evidence that the density of stars increases considerably towards the galactic center. The density distribution of stars as a function of Galacto-centric distance  $\omega$ , is shown in Figure 8. (Perek 1962). The increase in mass distribution of stars towards the center is  $\sim \frac{1}{\omega^3}$ , and so would be that of the distribution of starlight. With such enhanced starlight density, the Compton scattering of the cosmic ray electrons of these photons would provide an intense gamma ray source. Preliminary calculations of the angular distribution expected through this process is shown in Figure 9 (Cowsik and Hutcheon 1971). The actual calculations yielded only 70% of the intensity towards the galactic center as due to this process. If one

adds the line source due to  $\pi^0 \rightarrow 2\gamma$  decay contributing ~30% with a flat dependence on galactic longitude (Stecker 1969) then the emission from the galactic disc can be explained completely.

What is the spectrum of  $\gamma$ -rays generated through the Compton scattering of starlight? The cosmic ray electron spectrum has a spectral slope of  $\beta_1 = 1.6$  below ~3 GeV and a slope of  $\beta_2 = 2.6$  above ~3 GeV. The maximum and the mean energies of the scattered photons in the Compton process are given by

$$E_{\gamma\text{max}} = 4 \left( \frac{E_e}{m} \right)^2 \epsilon \quad (10)$$

and

$$\langle E_\gamma \rangle = \frac{4}{3} \left( \frac{E_e}{m} \right)^2 \epsilon$$

The spectral slope of Compton gamma-rays will be  $\alpha_1 = (\beta_1 - 1)/2 = 0.3$  at low energies and  $\alpha_2 = (\beta_2 - 1)/2 = 0.8$  at high energies. The typical  $\gamma$ -ray energy at which the transition takes place can be calculated by using eq. 10, with  $E_e \approx 3$  GeV, and the mean energy of the starlight photon ~3 eV (corresponding to a temperature of  $10^4$ °K).

$$E_{\gamma\text{-transition}} \approx \frac{4}{3} \frac{3 \times 10^9}{5 \times 10^5} \times 3 \text{ eV}$$

$$\approx 150 \text{ MeV}$$

This means that below ~150 MeV the spectral slope would be ~0.3 and as such would be very difficult to distinguish from a  $\pi^0$  source. We now wish to emphasize the inevitability of the existence of a Compton source of  $\gamma$ -rays in the central regions of our galaxy. There is evidence both for the existence of high density of starlight near the galactic center (as discussed before) and for the relativistic electrons through their synchrotron emission; thus the Compton scattering must occur leading to significant  $\gamma$ -ray flux from the region of the galactic center. Detailed

spectral shapes and sky maps due to this process will be presented at the Cosmic Ray Conference at Denver (Sullivan and Cowsik 1973).

The isotropic component at  $\sim 100$  MeV has an intensity of  $\sim 10^{-5} \gamma/\text{cm}^2 \text{ sec ster}$ . At this moment it is hard to pinpoint a precise source for this radiation. We wish to add that the existence of an extended halo to our galaxy may contribute significantly to this flux and also that a truly extragalactic component in this energy region cannot be excluded.

#### VII. THE 100 MeV GAMMA-RAY FLUX AND A LIMIT ON THE ENERGY DENSITY IN THE SUBMILLIMETER BACKGROUND

As pointed out in the last section, the line source of  $\gamma$ -rays away from the galactic center can be completely explained as due to the decay of  $\pi^0$ 's produced by nuclear cosmic rays (Stecker 1969). This means that any other source of  $\gamma$ -rays must be very weak indeed. One such could be provided by the existence of intense submillimeter radiation which would then be scattered to  $\gamma$ -ray energies by cosmic ray electrons. Thus, one may use the gamma ray fluxes to put stringent limits on the microwave background. This is done in Table 3 taken from Cowsik (1972). From this table it is clear that the energy density in any radiation background over and above the universal thermal background at  $2.7^\circ\text{K}$  should be less than  $0.6 \text{ ev}/\text{cm}^3$ . In Figure 10 this limit is shown in comparison with observations at microwavelengths.

Table 3. Gamma-ray Fluxes at  $E_\gamma > 100$  MeV: Theory and Experiment\*

Source	Region of sky scanned	
	$60^\circ < l < 30^\circ, b = 0^\circ$ (disc) Flux $(\text{cm}^2 \text{s rad})^{-1}$	$b = \pi/2$ (halo) Flux $(\text{cm}^2 \text{s sr})^{-1}$
Experiment	$(3.4 \pm 0.6) \times 10^{-5}$	$(3 \pm 0.4) \times 10^{-5}$
$p + \bar{p} \rightarrow \pi^0 \rightarrow 2\gamma$	$> 2.6 \times 10^{-5}$	$3.7 \times 10^{-6}$
$e + \bar{e} (2.7^\circ) \rightarrow e + \gamma$	$> 1.1 \times 10^{-5}$	$1.1 \times 10^{-5}$
Residual	$< 0.9 \times 10^{-5}$	$2.3 \times 10^{-5}$
$e + \bar{e} (\text{sub-mm}) \rightarrow e + \gamma$	$4.5 n_{\text{ph}} \times 10^{-8}$	$4.4 n_{\text{ph}} \times 10^{-8}$
Maximum number density of sub-mm quanta	$= n_{\text{ph}} < 200 \text{ cm}^{-3}$	$n_{\text{ph}} < 500 \text{ cm}^{-3}$
Corresponding energy density	$= \rho(\text{sub-mm}) = N_{\text{ph}} \epsilon < 0.25 \text{ eV}$	$\rho < 0.6 \text{ eV/cm}^3$

\*The radio disc is assumed to extend up to  $\sim 1$  kpc above the galactic plane in making the theoretical estimates.

Because of the Gaussian response of the detector with angles, the expected counting rates increase slower than linearly with the assumed thickness of the disc. Note that the estimates from the "halo" direction are uncertain and are to be given much lower weight.

#### VIII. SUMMARY

Thus it appears that one has a reasonable explanation for a good part of the diffuse x-ray and  $\gamma$ -ray background that is observed over 6 decades in energy. Thermal sources seem to dominate up to an energy of  $\sim 200$  keV. Angular distribution measurements are essential in choosing between galactic and universal models for the intensities in the MeV region. The source of 100 MeV gamma rays from the disc and galactic center seem to be well understood as due to the decay of neutral pions and Compton scattering of starlight respectively. These observations put a

stringent limit on the energy density in any possible radiation background at submillimeter wave lengths.

I cannot close this review more effectively than by making a call for all experimentalists in the field to measure the angular distribution of photons in the MeV range which is of very great astrophysical and cosmological importance, for it relates either to the cosmic ray sources in our Galaxy or to annihilation of antimatter in baryon symmetric cosmologies.

Acknowledgements.

I want to thank Professor P. Buford Price and the members of his group for their active interest in this work. This work has been supported in part by NASA grant NGR 05-003-376.

## References

- Anand, K.C., Daniel, R.R., and Stephens, S.A. 1969, TIFR Preprint NE-69-14 (Published in Proc. Indian Acad. Sci.)
- Anad, K.C., Joseph, G. and Lvaakare, P.J. 1969, Proc. Indian Acad. Sci. 71, 225.
- Blumenthal, G.R., and Gould, R.J. 1970, Rev. Mod. Phys. 42, 237.
- Bowyer, C.S., Field, G.B., and Mack, J. 1969, Nature 223.
- Brecher, K., and Morrison, P. 1969, Phys. Rev. Letters 23, 802.
- Clark, G.W., Garmire, G.P., and Kraushaar, W.L. 1972, preprint (also see Proc. IAU Symp. No. 37, Rome 1970).
- Cowsik, R. 1971, Talk presented at 12th Int. Conf. on Cosmic Rays (Hobart, Tasmania).
- Cowsik, R. 1971, Proc. 12th Int. Conf. on Cosmic Rays 1, 334.
- Cowsik, R. 1972, Nature Phys. Sci. 239, 41.
- Cowsik, R. 1971, Proc. 12th Int. Conf. on Cosmic Rays 1, 334.
- Cowsik, R. and Hutcheon, I.D. 1971, Ibid 1, 102.
- Cowsik, R. and Kobetich, E.J. 1971, Ibid 1, 38.
- Cowsik, R. and Kobetich, E.J. 1972, Astrophys. J. 177, 585.
- Damle, S.V., Daniel, R.R., Joseph, G. and Lavakore, P.J. 1971, Proc. 12th Int. Conf. Cosmic Rays 1, 84.
- Felten, J.E. 1972, Proc. of IAU Symposium (Madrid).
- Field, G.B. 1972, Ann. Rev. Astron. and Astrophys. 10, 227.
- Giacconi et al 1972, preprint.
- Gold, T. and Hoyle, F. 1959, Paris Symp. on Radio Astronomy (ed. Bracewell) IAU Symp. 9, 583.
- Gould, R.J. and Burbidge, G.R. 1963, Astrophys. J. 138, 969.
- Gursky, H., Matilsky, T., Kellogg, E., Tananbaum, H. and Giacconi, R. 1972, preprint.

- Hayakawa, S. 1969, Cosmic Ray Physics (John Wiley and Sons, New York),  
p. 609.
- Lang, R.R. and Tergian, Y. 1969, Astrophys. J. Letters 3, 29.
- Perek, L. 1962, Adv. in Astron. and Astrophys. 1, 165.
- Petrosian, V. and Ramaty, R. 1972, Astrophys. J. Letters 173, 83.
- Seward, F.D., Burginyon, G.A., Grader, R.J. and Palmieri 1972, Astrophys.  
J.
- Schwartz, D.A. 1970, Astrophys. J. 162, 439.
- Silk, J. 1970, Space Sci. Rev. 11, 671.
- Silk, J. 1973, preprint.
- Stecker, W.F. 1969a, Astrophys. J. 157, 507.  
b, Nature 224, 870.
- Stecker, F.W. 1971, Cosmic Gamma Rays (Mono Book Corp., Baltimore).
- Stecker, F.W., Morgan, D.L., and Bredekemp, J. 1971, Phys. Rev. Letters  
27, 1469.

## Figure Captions

- Figure 1. The integral spectrum of gamma rays generated by cosmic ray interactions with interstellar matter. Nuclei heavier than helium do not contribute significantly (Stecker 1970).
- Figure 2. The x-ray flux emitted in collisions of electrons of energy  $E_0$  with the 2.7°K photon field is plotted as a function of x-ray energy. Notice that the full width at half maximum is a factor of ~20 wide; also the mean x-ray energies related quadratically with the electron energy. These effects tend to yield an x-ray spectrum which is very much smoother than the electron spectrum. This fact was used to show that Compton scattering of the 2.7°K photons is not a significant source at ~30 KeV (Cowsik and Kobetich 1972).
- Figure 3. The x-ray energy flux is plotted as a function of x-ray energy and compared with experimental data. Curve 1 is our calculation of the inverse Compton-scattering; curve 2 is calculated using the galactic  $\gamma$ -ray model of Cowsik (1971); and curve 3 is the sum of the two contributions. The experimental data for x-ray energies  $E_x < 0.17$  MeV and  $E_x \geq 10$  MeV were taken from the review paper by Silk (1970) and for  $0.17$  MeV  $< E_x < 10$  MeV were taken from Damle et al (1971) and Golenetskii et al (1971). The enhanced emission at  $2 \text{ keV} < E_x < 200 \text{ keV}$  is attributed to a hot ( $3 \times 10^8 \text{°K}$ ) intergalactic gas.
- Figure 4. The difference between the observed energy flux and the calculated flux (see Figure 3) in the energy interval  $2 \text{ keV} < E_x < 200 \text{ keV}$  is plotted as a function of x-ray energy. The line represents

the thermal bremsstrahlung emission for a hydrogen plasma at  $3.3 \times 10^8 \text{K}$ . The line of sight integral  $\int N_e N_p dl$  for this emission is  $1.3 \times 10^{17} / \text{cm}^5$ . If one assumes no clumping and  $\int dl = 10^{28} \text{ cms}$ , one gets  $N_e = N_p = 3 \times 10^{-6} / \text{cm}^3$ . Such a density is adequate to close the universe if  $H_0 = 55 \text{ km/sec Mpc}$ .

Figure 5. Electronic component of cosmic rays in the interstellar space. The secondary electron flux generated by the nuclear component is normalized using positrons.

Figure 6. The injection spectrum of primary cosmic ray neutrons. Hatched area indicates uncertainties in the estimate. The predictions of the model are for  $p = 2$  (.-.-.-) and  $p = 3$  (——);  $E_c = 0.5, 0.7, 1.0 \text{ GeV}$  starting from top. Since it is the difference between the accelerated powerlaw spectrum  $\sim E^{-2.6}$  and the injection spectrum that governs the  $\gamma$ -ray intensities the uncertainty in the  $\gamma$ -ray fluxes are within a factor of  $\sim 2$ .

Figure 7. A well defined background  $\gamma$ -ray flux (absolute normalization within  $\times 2$  is predicted by model. For  $E_\gamma \ll 1 \text{ MeV}$ , there is a large flux of intergalactic origin. The model predicts correctly the primary gamma ray slope and intensity that would generate the experimental response shown (Anand et al 1969; data from Silk 1970).

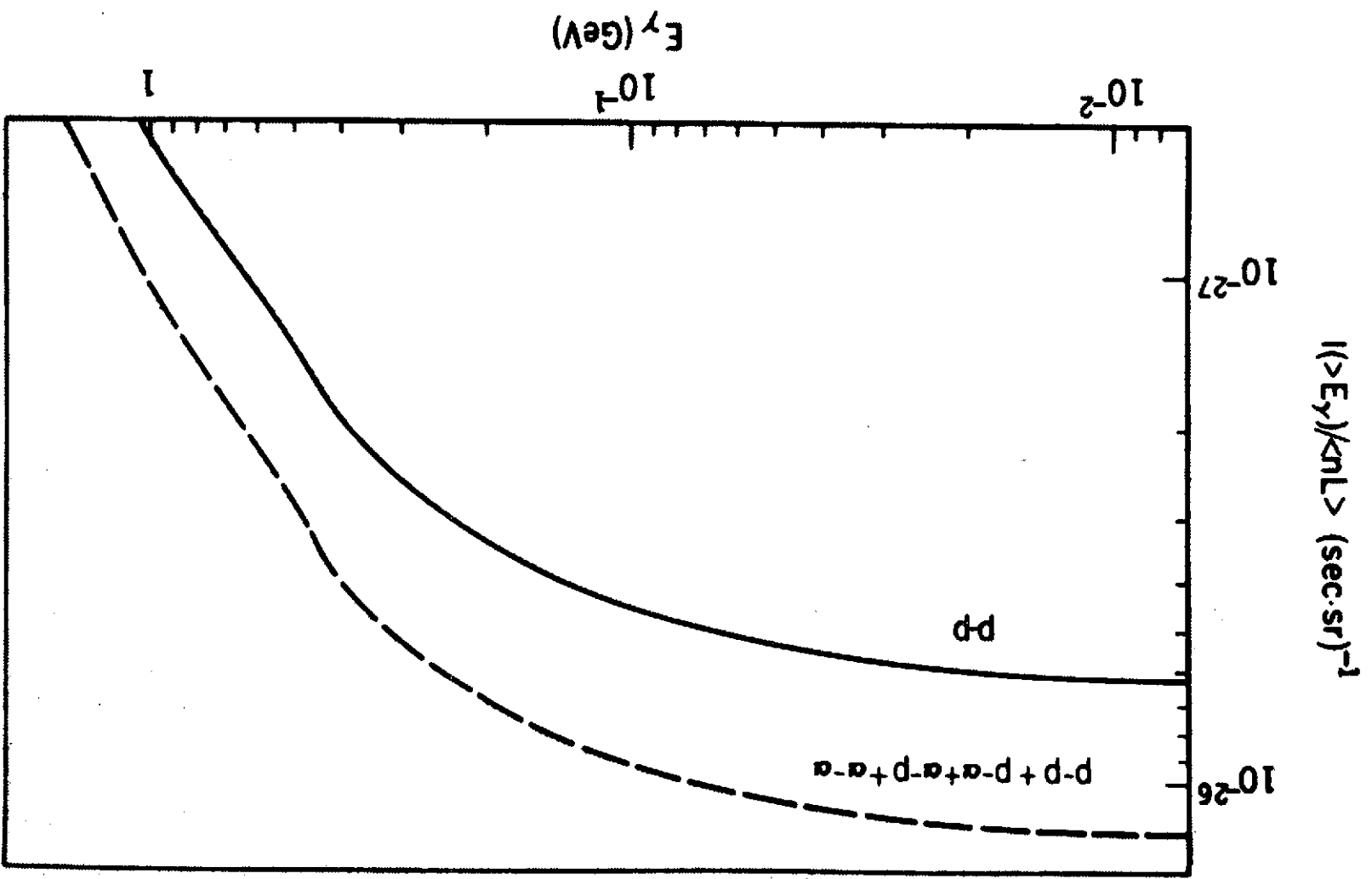
Figure 8. The mass distribution in the galaxy in units of  $M_\odot / \text{pc}^3$  is shown as a function of cylindrical coordinates centered at the Galactic center (taken from Perek 1972).

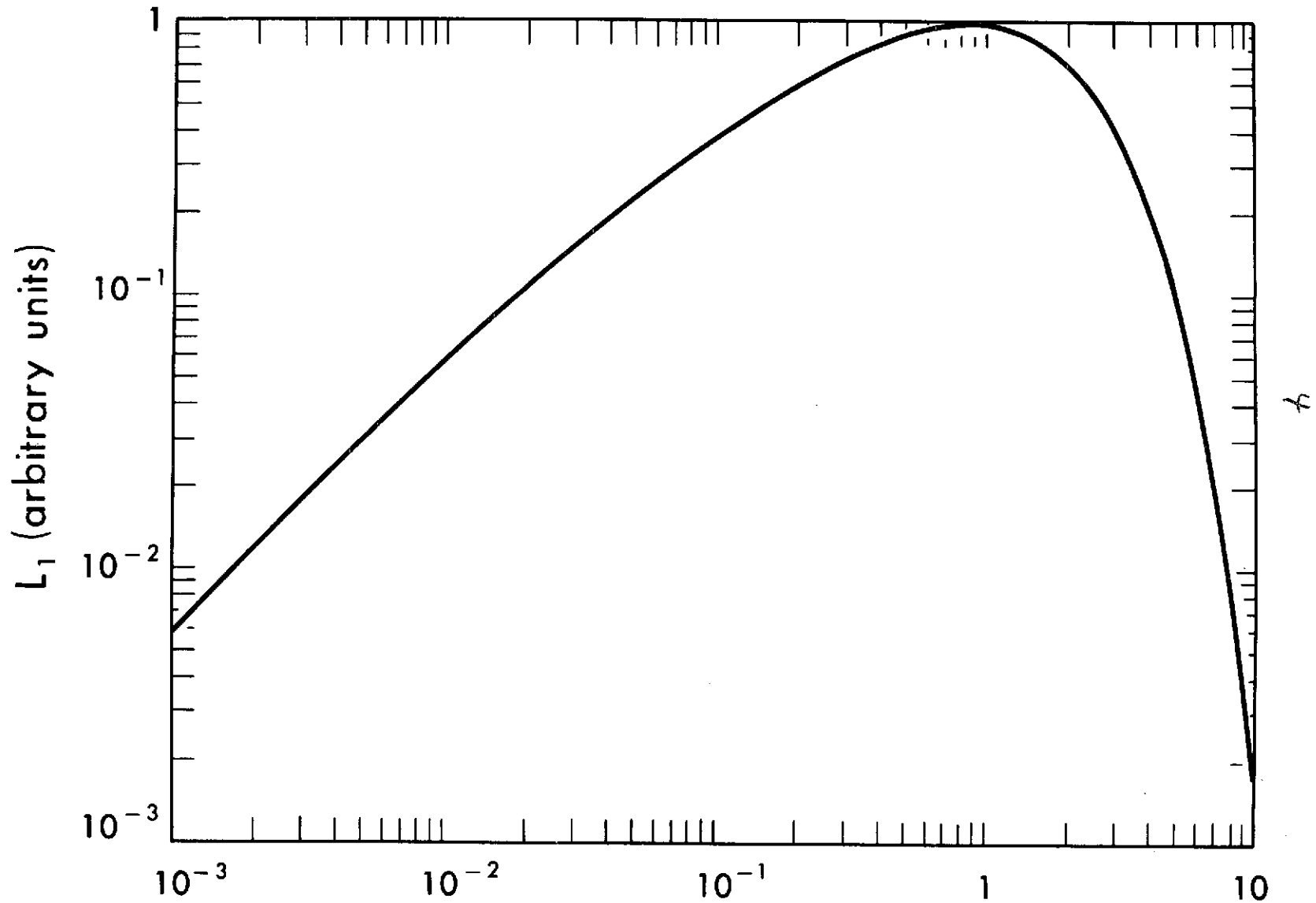
Figure 9. The gamma ray intensities that are calculated using starlight distribution implied by Figure 8 are compared with results of Clark et al (1972). The preliminary theoretical estimates

are multiplied by  $\sim 1.4$  and then averaged over the aperture of the detector. It is seen that the Compton scattering of starlight contributes negligibly beyond  $\sim 60^\circ$  galactic longitude. Beyond this point the  $\Pi^0 \rightarrow 2\gamma$  process discussed by Stecker (1969) dominates and should be added to the Compton fluxes to make a detailed fit to

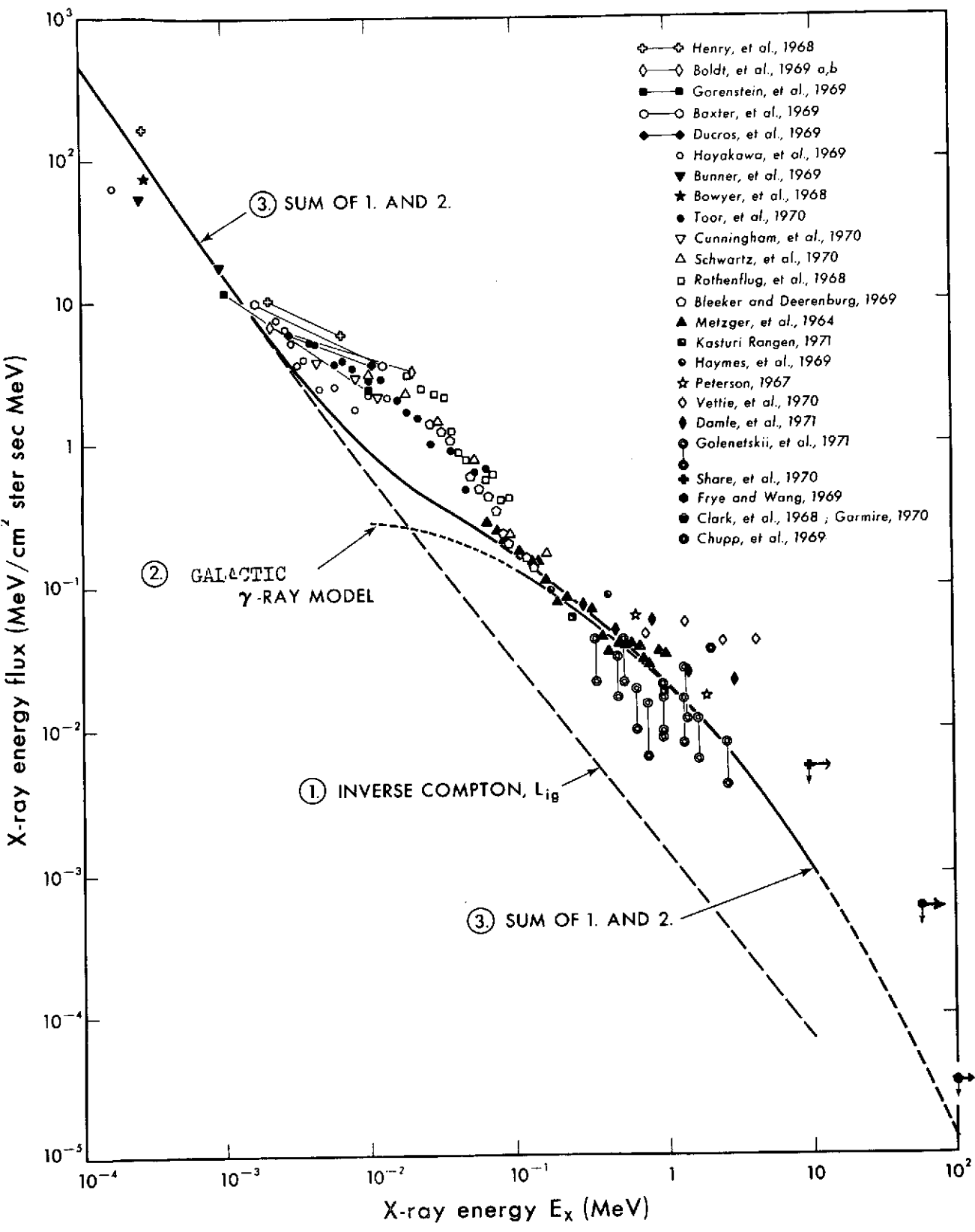
Figure 10. Measured background radiation fluxes are compared with that expected from a black body at  $2.7^\circ\text{K}$ . The  $\gamma$ -ray fluxes measured by Clark et al (1972) put a stringent limit on the intensities allowable at submillimeter wave lengths. In plotting our upper limit of  $\sim 0.6 \text{ eV/cm}^3$  we have assumed that the background radiation has a band width equal to that of the detector of the Cornell instrument.

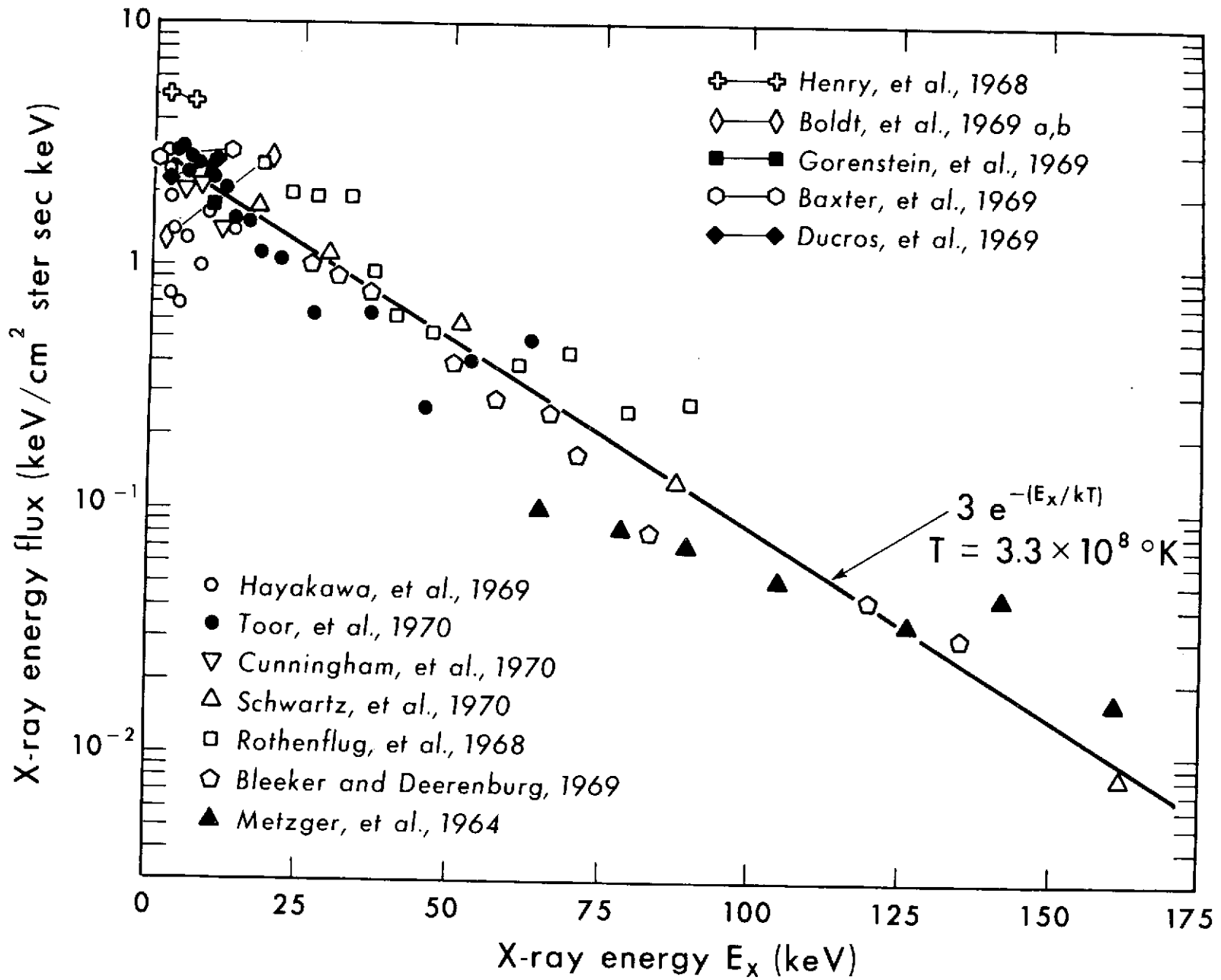
2

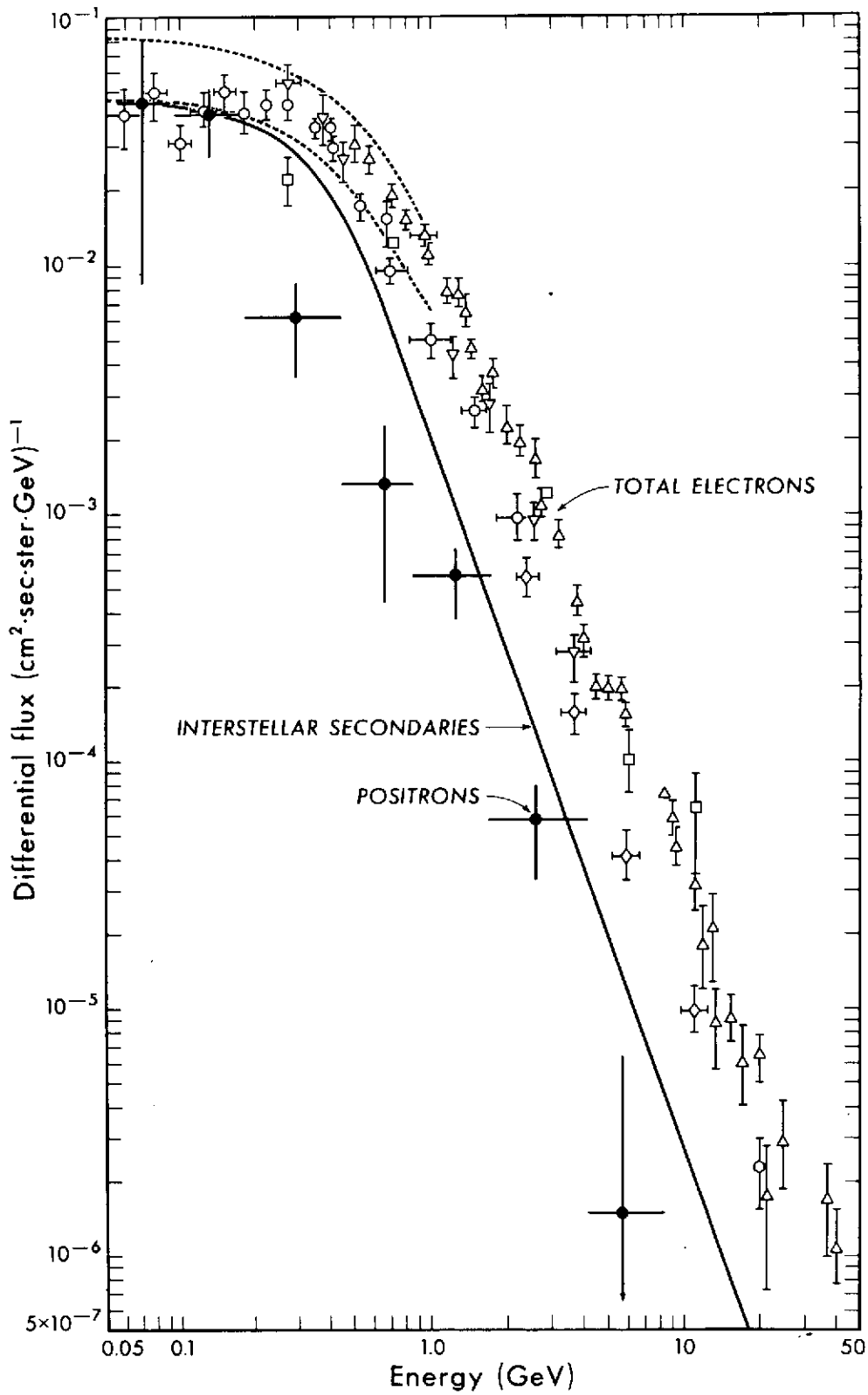


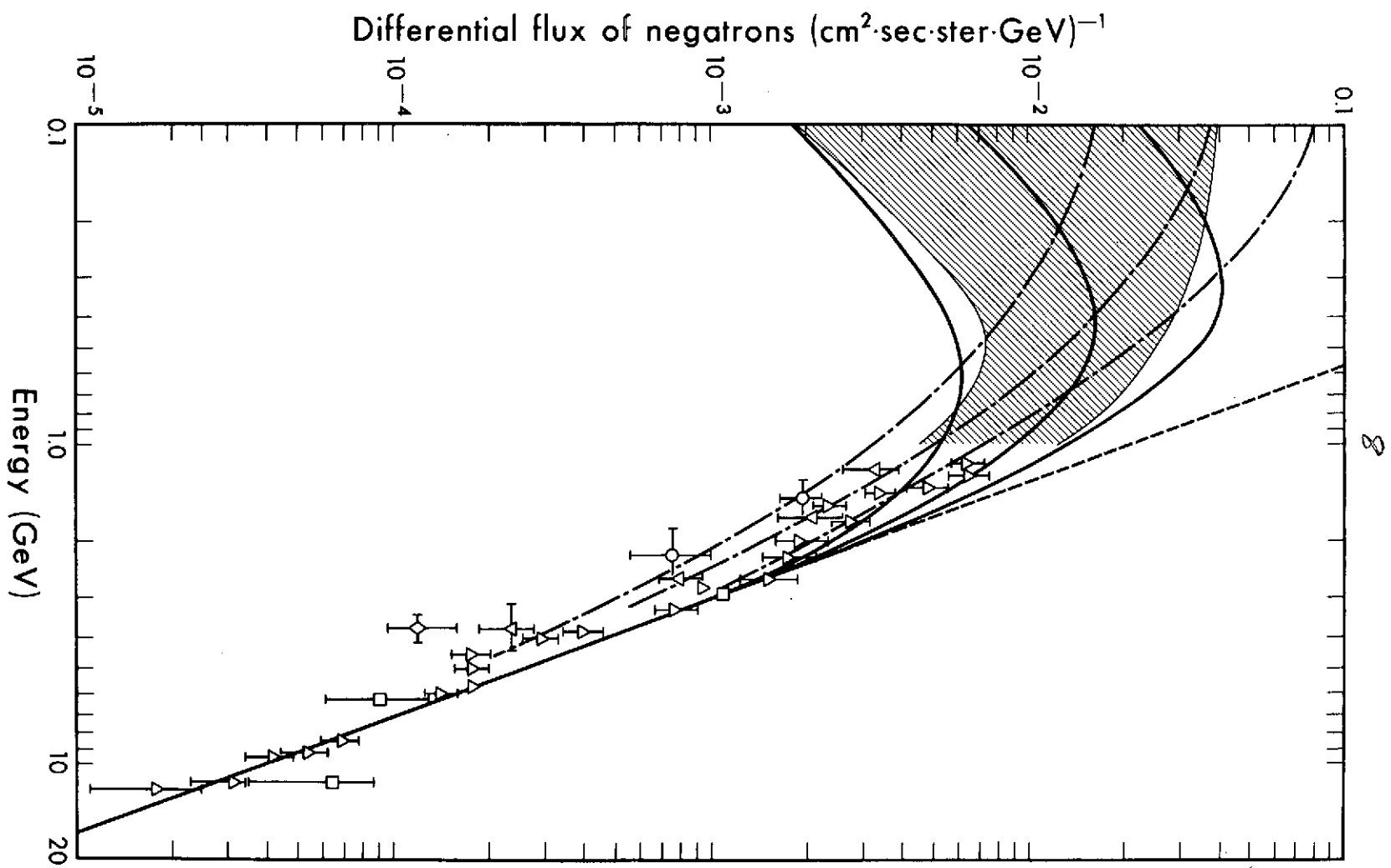


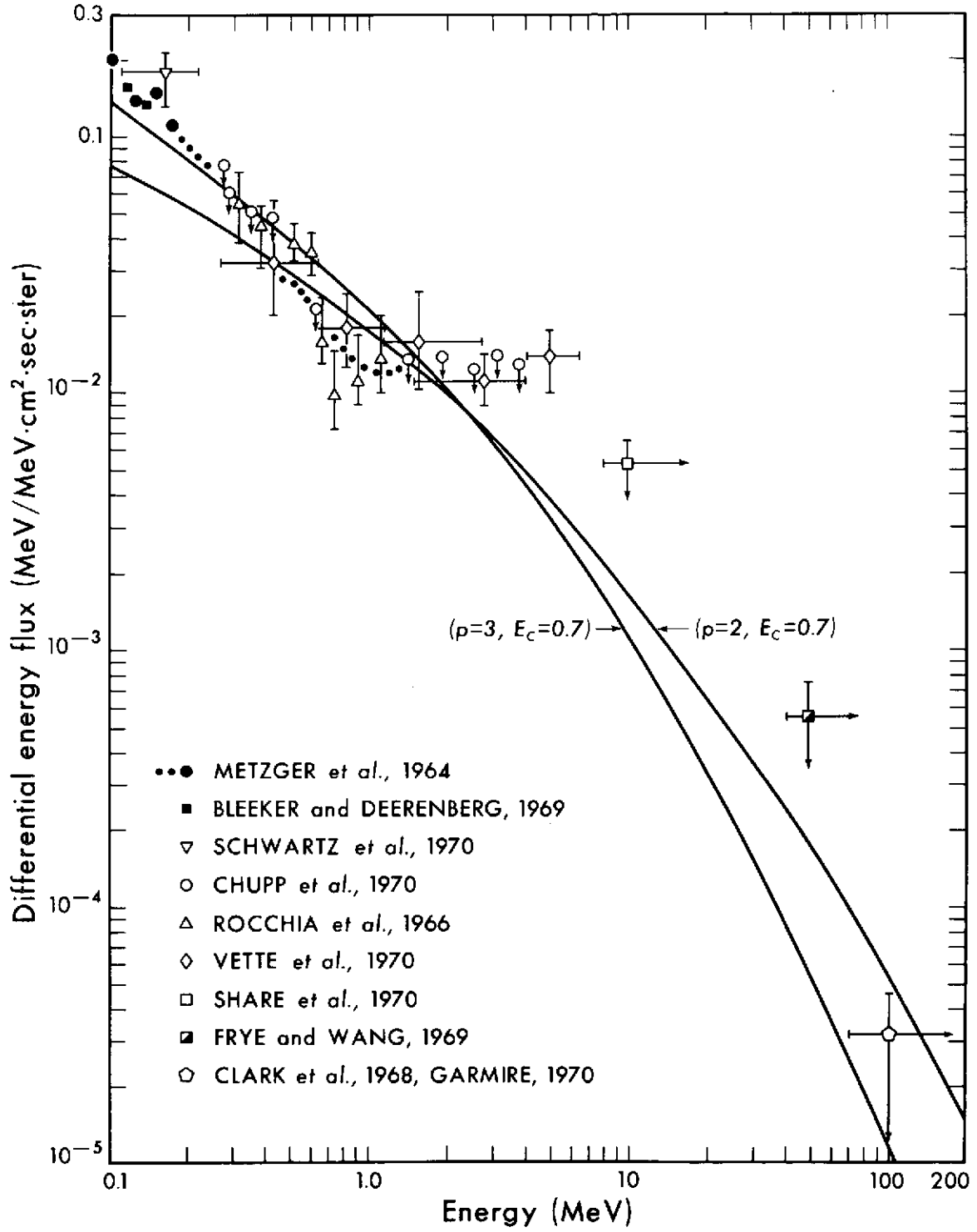
$$X = a \frac{E_x}{E_0^2}, \quad a = 2.8 \times 10^8 \text{ MeV}$$

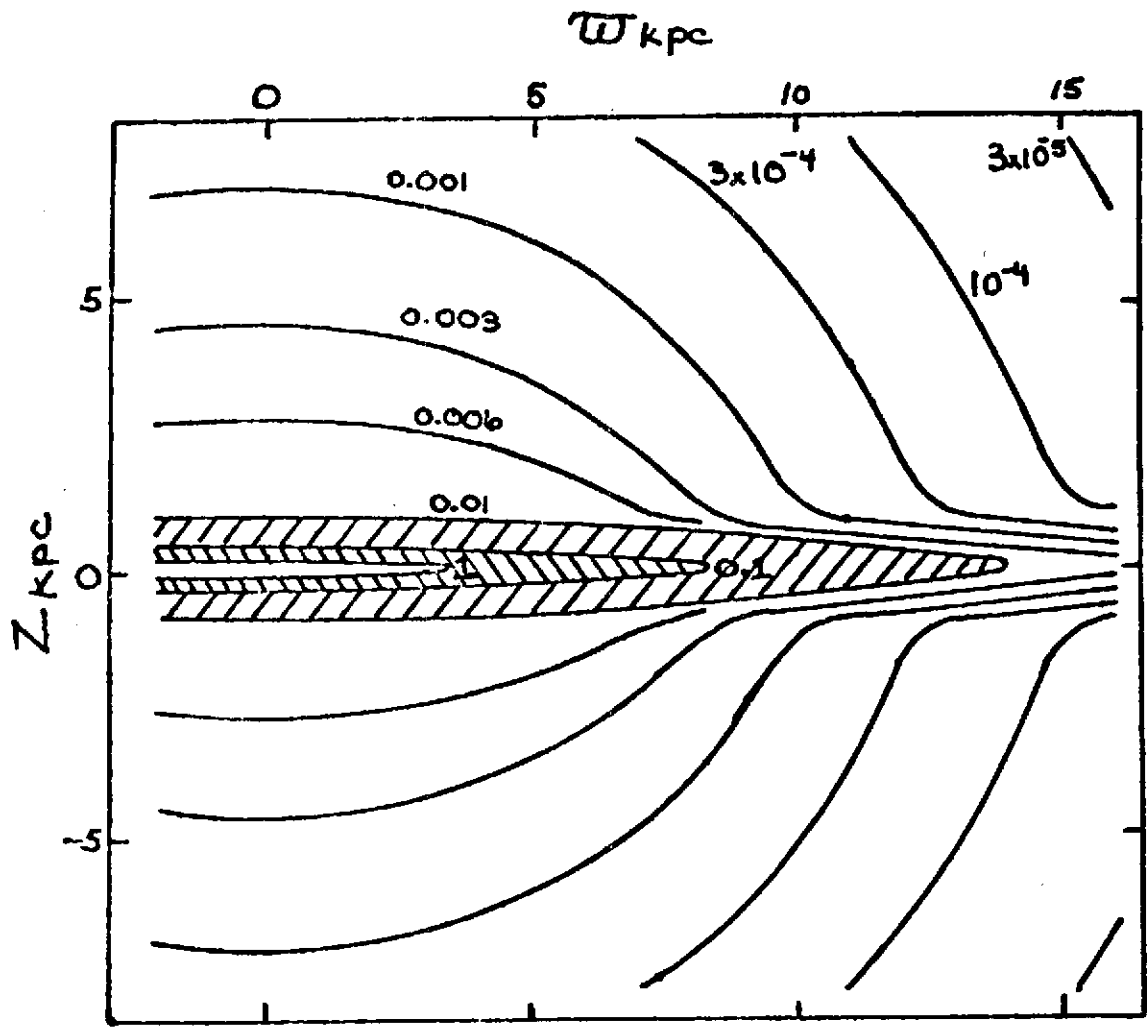


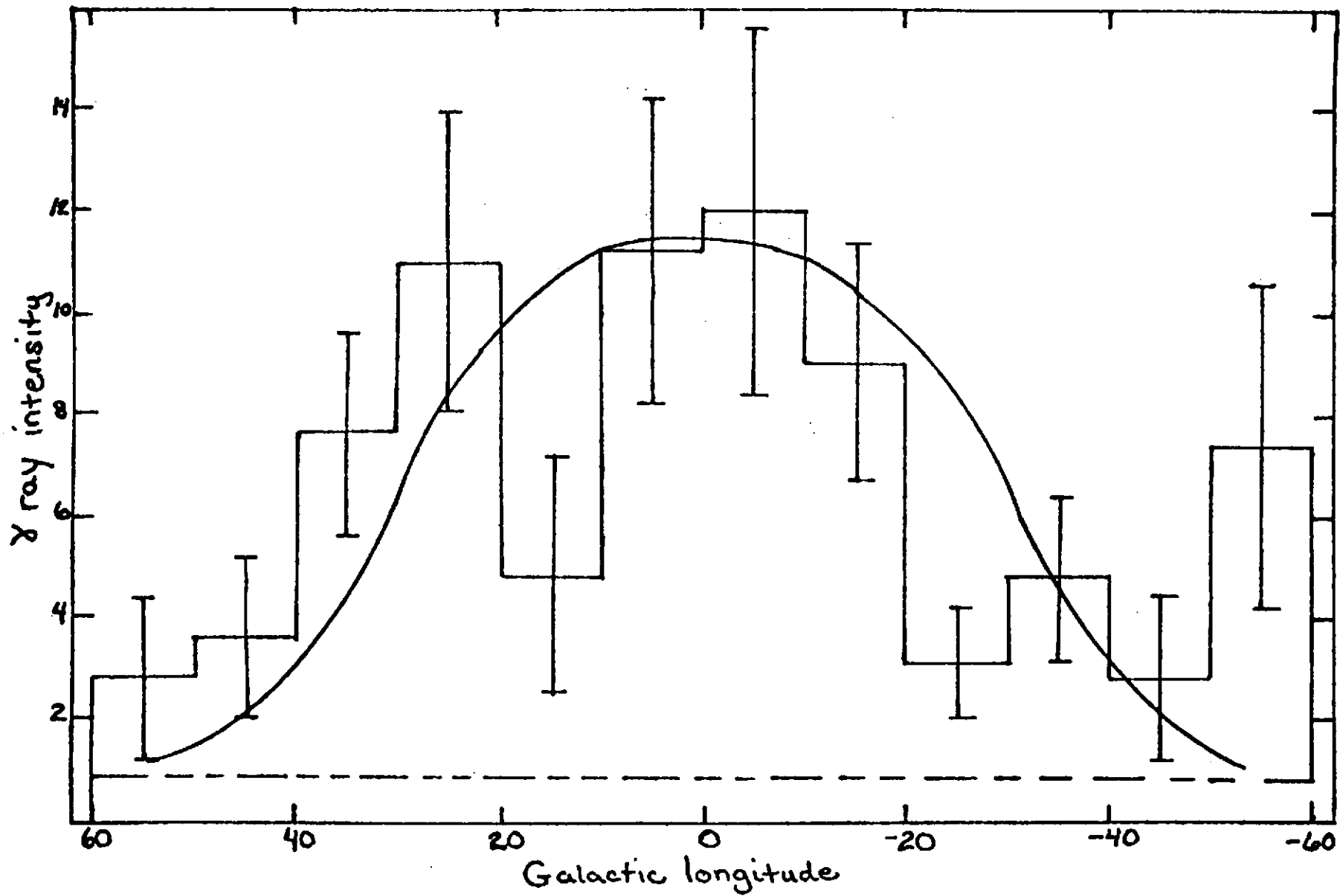


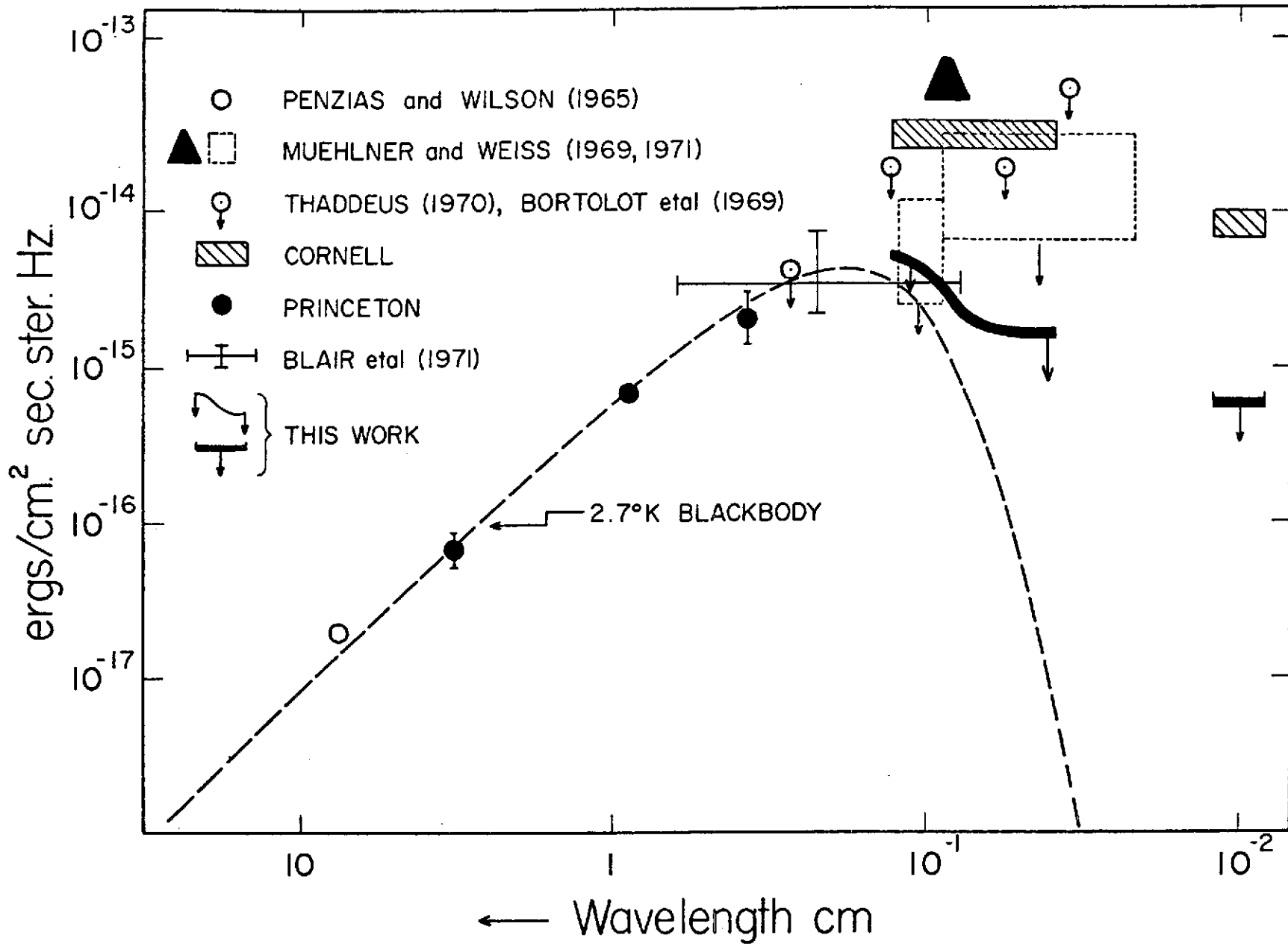












MECHANISMS FOR PRODUCTION OF THE DIFFUSE  
 $\gamma$ -RAY CONTINUUM RADIATION

F.W. Stecker  
Theoretical Studies Branch  
Laboratory for Space Physics  
NASA Goddard Space Flight Center  
Greenbelt, Maryland 20771

AN INVITED PAPER PRESENTED AT THE INTERNATIONAL SYMPOSIUM  
AND WORKSHOP ON GAMMA RAY ASTROPHYSICS, NASA GODDARD SPACE  
FLIGHT CENTER, APRIL 30- MAY 2, 1973.

MECHANISMS FOR PRODUCTION OF THE DIFFUSE  
 $\gamma$ -RAY CONTINUUM RADIATION

F.W. Stecker  
Theoretical Studies Branch  
Laboratory for Space Physics  
NASA Goddard Space Flight Center  
Greenbelt, Maryland 20771

The basic mechanisms expected to be important in the production of cosmic  $\gamma$ -radiation were suggested by Morrison in a classic paper in Nuovo Cimento in 1958. They are Compton interactions with low-energy photons, bremsstrahlung interactions, cosmic-ray induced  $\pi^0$  production, and matter-antimatter annihilation. Of these four mechanisms, the first two involve cosmic-ray electrons and are electromagnetic processes whereas the last two involve nucleons, mainly protons, and are strong interactions processes. Above 511 keV, the  $\gamma$ -radiation from matter-antimatter annihilation arises mainly from the decay of  $\pi^0$ -mesons produced in the annihilation process so that the kinematics involved in the last two processes is similar. Since this paper will be concerned mainly with diffuse continuum radiation rather than line radiation or radiation from point sources, the discussion here will be restricted mainly to the above four processes. (For a treatment of the theory of the production of cosmic line radiation, see the paper of Clayton;

these proceedings.)

The most astrophysically significant role which Compton interactions are expected to play in cosmic  $\gamma$ -ray production involves the interactions of relativistic cosmic-ray electrons with low-energy photons of the universal 2.7 microwave blackbody radiation field. The microwave photons have an average energy near  $10^{-3}$  eV and a number density of  $\sim 400$  per  $\text{cm}^3$  considered to be uniformly distributed throughout the universe. Compton interactions with cosmic-ray electrons can then produce  $\gamma$ -rays with typical energies of

$$\langle E_\gamma \rangle \approx 10^{-3} \gamma^2 \text{ eV} \quad (1)$$

where  $\gamma = (E_e/m_e c^2)$  is the Lorentz factor of the cosmic-ray electron. Thus a 50 GeV electron with a Lorentz factor of  $\sim 10^5$  will typically produce  $\gamma$ -rays of energy  $\sim 10$  MeV through Compton interactions with 2.7K photons. We can define the "spectrum" of  $\gamma$ -rays from a single Compton interaction as the normalized probability distribution of  $\gamma$ -rays of energy  $E_\gamma$  expected to be produced by an electron of energy  $E_e$ . Such a spectrum turns out to be flat and rather broad around the average energy  $\langle E_\gamma \rangle$  (Heitler 1954, Jones 1965). Because  $\langle E_\gamma \rangle \propto \gamma^2$ , the spectrum of  $\gamma$ -rays produced by a power-law cosmic-ray electron spectrum of the form  $K_e E_e^{-\Gamma_e} e$  will also have a power-law form  $K_\gamma E_\gamma^{-\Gamma_\gamma}$  but with  $\Gamma_\gamma = (\Gamma_e + 1)/2$ . In fact, for interactions with a blackbody spectrum of low-energy

photons at temperature  $T$ , the Compton-generated  $\gamma$ -ray spectrum is given by

$$I(E_\gamma) \approx 6.22 \times 10^{-21} L [10^{-2.962\Gamma_e} f(\Gamma_e)] K_e T^{(\Gamma_e+5)/2} E_\gamma^{-(\Gamma_e+1)/2} \quad (2)$$

with the factor  $f(\Gamma_e) \sim 1$  given by Ginzburg and Syrovatskii (1964). If for example,  $\Gamma_e \sim 2.6$ , then  $\Gamma_\gamma \sim 1.8$  for galactic cosmic-ray electrons. Because the 2.7K blackbody radiation is believed to be universal, Compton interactions have been invoked to explain the cosmic X-ray background spectrum where the observed  $\Gamma_\gamma \sim 2$  and to set limits on the metagalactic cosmic-ray electron intensity  $w_{Mg,e}$  to show that it must be much less than the galactic value, i.e.,  $w_{Mg,e} \ll w_{G,e}$  (Felten 1965, Gould 1965, Fazio, Stecker and Wright 1966, Felten and Morrison 1966; see also the papers of Cowsik and Ginzburg; these proceedings).

Bremsstrahlung interactions are expected to take place between cosmic-ray electrons and interstellar and intergalactic gas and may be significant in producing low-energy  $\gamma$ -rays and X-rays both in the galaxy and in intergalactic space (see paper of Cowsik; these proceedings). The probability distribution spectrum for  $\gamma$ -rays from bremsstrahlung of a cosmic-ray electron of energy  $E_e$  is quite flat and may be approximated by

$$f(E_\gamma | E_e) \approx \begin{cases} E_e^{-1} & \text{for } 0 \leq E_\gamma \leq E_e \\ 0 & \text{otherwise} \end{cases} \quad (3)$$

so that the  $\gamma$ -ray production spectrum is given by

$$I_b(E_\gamma) = X^{-1} \int_0^L dr \langle \rho(\vec{r}) \rangle \frac{I_e(>E_\gamma)}{E_\gamma} \quad (4)$$

where  $\rho$  is the matter-density of the gas in  $\text{g/cm}^3$  and  $X$  is the average radiation length for interstellar matter and is  $\sim 65 \text{ g/cm}^2$ . We may also write equation (4) in terms of the atomic density  $n$  and the path along the line-of-sight  $L$  so that

$$I_b(E_\gamma) = 3.4 \times 10^{-26} nL \frac{I_e(>E_\gamma)}{E_\gamma} \quad (5)$$

It follows from equation (5) that for bremsstrahlung from cosmic-ray electrons following a power-law spectrum  $K_e E_e^{-\Gamma} e$ ,  $\Gamma_\gamma = \Gamma_e$  (for relativistic electrons) so that, in general, the  $\gamma$ -ray spectrum from bremsstrahlung is steeper than that from Compton interactions.

We next discuss the  $\gamma$ -radiation from the decay of  $\pi^0$ -mesons produced by cosmic-ray interactions between high-energy nucleons and gas nuclei in interstellar and intergalactic space. Because it now appears that  $\pi^0$ -decay  $\gamma$ -rays from cosmic-ray interactions may account for almost all of the  $\gamma$ -radiation above 100 MeV observed in our galaxy (Fichtel, et al. 1972, Clark, et al. 1968, Stecker 1969a, Stecher and Stecker 1970, Cavallo and Gould 1971, see also the paper of Ginzburg; these proceedings), because it has long been recognized as an important process for cosmic  $\gamma$ -ray

production (see e.g., Morrison 1958, Pollack and Fazio 1963, Ginzburg and Syrovatskii 1964), and because it has the most difficult spectrum to calculate theoretically (Hayakawa, et al. 1964, Dilworth, et al. 1968, Stecker 1970, Cavallo and Gould 1971, Levy and Goldsmith 1972) and various theoretical calculations are somewhat contradictory, this process has received the most attention. I do not intend to break the tradition here, in fact, I hope to help resolve here some of the contradictions that have arisen between the theoretical calculations.

Figure 1 shows the type of  $\gamma$ -ray spectra obtained from the decay of  $\pi^0$ -mesons with various simple energy spectra  $f(E_\pi)$ . Typically the spectrum is flat near  $m_\pi c^2/2 \sim 70$  MeV and symmetric about this value on a logarithmic energy plot. These characteristics can be easily shown from the kinematics of  $\pi^0$ -decay (see, for example the thorough discussion by the author (Stecker 1971a)) and we will not repeat them here. Figure 2 shows how a typical  $\pi^0$ -decay  $\gamma$ -ray spectrum may be built up from an arbitrary pion-energy spectrum and that the spectrum always has a maximum at  $\sim 70$  MeV. Figure 3 shows the differential  $\gamma$ -ray spectrum obtained by Stecker (1970), illustrating the various expected characteristics. Figure 4 shows a comparison of the integral spectra obtained by Stecker (1970) and Cavallo and Gould (1971) normalized to compare the shapes obtained. The wiggles in the spectrum

represent artifacts of the assumed pion-production models and should not be taken too seriously. The shapes of the two spectra are in good agreement and probably represent an accurate approximation to reality within the uncertainty indicated by the wiggles.

The largest discrepancy between the various calculations is in the total  $\gamma$ -ray production rates calculated by various workers and compared in Table 1.

Pollack and Fazio (1963) and Dilworth, et al. (1968) obtained a total  $\gamma$ -ray production rate per hydrogen atom which would be equivalent to roughly  $1.1 \times 10^{-25} \text{s}^{-1}$  and  $1.0 \times 10^{-25} \text{s}^{-1}$  respectively for energies above 100 MeV. This corresponds to the quantity

$$Q_{\gamma, \pi^0} (>100\text{MeV}) \equiv 4\pi I_{\gamma} (>100\text{MeV}) / \langle nL \rangle \quad (6)$$

Pollack and Fazio used the observed cosmic-ray spectrum at the earth for their calculations. Stecker (1970) used a demodulated cosmic-ray spectrum to estimate the galactic cosmic-ray spectrum and, for this reason, obtained a slightly higher value of  $1.3 \times 10^{-25} \text{s}^{-1}$  for  $Q$  (see following discussion). Kraushaar, et al. (1972) from the OSO-3 satellite observations, obtained an upper limit for  $Q$  of  $1.6 \times 10^{-25} \text{s}^{-1}$  and recently the author (Stecker 1973) obtained a theoretical upper limit of  $\sim 1.5 \times 10^{-25} \text{s}^{-1}$  assuming a maximum solar demodulation effect to obtain a

maximum galactic cosmic-ray spectrum as deduced by Comstock, et al. Thus, all of the above values for  $Q_{\gamma, \pi^0}$  are basically consistent. The value obtained by Cavallo and Gould (1971) appears to be somewhat high compared with the others, but a value of  $\sim 1.3 \times 10^{-25} \text{s}^{-1}$  falls within their 30% error bracket. It is the author's opinion, as will be presently discussed, that a value of  $1.3 \times 10^{-25} \text{s}^{-1}$  is close to a "best value" for  $Q_{\gamma, \pi^0}$ . The value of Levy and Goldsmith (1972) is a factor of  $\sim 2.5$  higher and requires some discussion.

Figure 5 shows an up-to-date summary of the accelerator data on total cross section ( $\sigma$ ) times multiplicity ( $\zeta$ ) for neutral pion production in p-p interactions for energies up to  $\sim 1500$  GeV shown as a function of kinetic energy (T) (Stecker 1973). These data are well approximated by the broken power-law

$$\sigma_{\pi^0}(T) \zeta_{\pi^0}(T) \approx \begin{cases} 10^{-2} \text{s} T^{7.64} \text{cm}^2 & 0.4 \leq T \leq 0.7 \text{GeV} \\ 8.4 \times 10^{-27} T^{0.53} \text{cm}^2 & T \geq 0.7 \text{GeV} \end{cases} \quad (7)$$

as the reader can verify from the figure. Taking the cosmic-ray spectrum  $I(T) = 0.15 T^{-2.2} \text{cm}^{-2} \text{s}^{-1} \text{Sr}^{-1} \text{GeV}^{-1}$  used by Levy and Goldsmith (1972), the total  $\gamma$ -ray production rate from p-p interactions is given by

$$\begin{aligned}
 q_{\gamma H} &= 8\pi \int dT I(T) \sigma_{\pi^0}(T) \zeta_{\pi^0}(T) \\
 &= 3.77 \times 10^{-25} \int_{0.4}^{0.7} T^{5.44} dT + 3.17 \times 10^{-26} \int_{0.7}^{\infty} T^{-1.67} dT \quad (8) \\
 &= 0.66 \times 10^{-25} s^{-1}
 \end{aligned}$$

Adding in the contribution from p- $\alpha$ ,  $\alpha$ -p and  $\alpha$ - $\alpha$  interactions in the galaxy brings the total production rate per hydrogen atom up to  $\sim 10^{-25} s^{-1}$ . There is, of course, some uncertainty in the assumption of the true "demodulated" galactic cosmic-ray spectrum as distinguished from that observed at the earth. However, using the upper-limit to the demodulated cosmic-ray spectrum given by Comstock, et al. (1972), an upper-limit on the  $\gamma$ -ray production rate is obtained of  $(1.51 \pm 0.23) \times 10^{-25} s^{-1}$  with the error bracket reflecting the experimental error in the accelerator data on  $\sigma_{\zeta}$ . The above value is consistent with the value of  $1.6 \times 10^{-25} s^{-1}$  given by Kraushaar, et al. (1972), which also represents an upper limit since it does not take account of the additional contribution from cool H and H<sub>2</sub> which may be adding to the observed flux.

Why then is there such a large discrepancy between the results presented here and those obtained by Levy and Goldsmith? The answer appears to lie in the difference between assumptions on the total cross section for  $\pi^0$  - production as a function of energy and the multiplicity  $\zeta$  assumed.

While we have chosen to rely on measurements from accelerator experiments, Levy and Goldsmith adopt a theoretical multiplicity law based on the Feynman scaling hypothesis which may hold above 100 GeV. The logarithmic multiplicity law adopted by Levy and Goldsmith has some empirical support in cosmic-ray measurements above 70 GeV cited by Levy and Goldsmith but is contradicted in other cosmic-ray measurements so that the situation at high energies is not as yet clear (see review by Sreekantan 1972). The logarithmic multiplicity law based on the scaling prediction is based on arguments which hold asymptotically in the high-energy limit and which do not appear to be valid below 50 GeV although they may begin to be valid within the 50-300 GeV energy range as evidenced by data obtained at the accelerator facilities at Serpukhov and Batavia (Slattery 1972).

Figure 6 shows a solid-line fit to the data given in Figure 5 in comparison with the dashed line which shows the product  $\sigma_{\pi} \circ \zeta_{\pi} \circ$  based on the assumptions of Levy and Goldsmith for proton kinetic energies greater than 1 GeV. The Levy-Goldsmith assumptions show a reasonable fit to the data above 100 GeV where the scaling prediction may hold. However, below 100 GeV the dashed curve is, in all cases, above the data points. Figure 7 shows the  $\pi^0$ -production function for pp interactions given by the product  $\sigma_{\pi} \circ \zeta_{\pi} \circ I_p$  based on the data given in Figure 5. This figure shows

clearly that almost all of the  $\pi^0$ -mesons produced in cosmic-ray pp interactions involve cosmic-ray energies between 1 and 10 GeV. Figure 8, shows the integral  $\gamma$ -ray production function which is proportional to the integral of the curve shown in Figure 3 and is defined such that  $Q_\gamma^{(pp)}(<\infty)$  corresponds to the total  $\gamma$ -ray production rate per hydrogen atom per second from pp-interactions alone (the number  $q_{\gamma H}$ ) given in the previous approximate calculation. It can be seen from Figure 8 that only 10% of the  $\gamma$ -ray production occurs in interactions involving protons below 1 GeV and perhaps another 10% occurs in interactions above 30 GeV. This means that (1) since cosmic-ray modulation effects are only important below 1 GeV, the uncertainty in the true cosmic-ray spectrum due to modulation effects produces only a small uncertainty in the total calculated  $\gamma$ -ray production rate, and (2) the uncertainty in the exact form of the pion-multiplicity law  $\zeta_\pi(T)$  above 30 GeV produces little uncertainty in the total  $\gamma$ -ray production rate. Indeed, 90% of the  $\gamma$ -rays are produced in interactions below 30 GeV where the form of the multiplicity law used by Levy and Goldsmith does not hold. Figure 8 also shows that the median proton energy for  $\pi^0$ -production is  $\sim 3$  GeV. If we compare the values of  $\sigma_{\pi^0}\zeta_{\pi^0}$  used by Levy and Goldsmith with those used here (as shown in Figure 6) at the median  $\pi^0$ -production energy of 3.3 GeV, we obtain a ratio of 2.5 which just corresponds to the ratio between the values for

the total  $\gamma$ -ray production rate given by Levy and Goldsmith (1972) and the author (Stecker 1970). Thus, the discrepancy between the two values is accounted for. The conclusion is that the Levy-Goldsmith value appears to be too high because it is based on an asymptotic multiplicity law which does not hold in the energy range where at least 90% of the  $\gamma$ -rays are produced.

Mesons and hyperons are also produced in strong inelastic nucleon-nucleon interactions at somewhat higher energies and their important decay modes leading to  $\gamma$ -ray production are summarized in Table 2. In addition, nucleon resonances can be formed which lead to decay chains involving  $\pi^0$ -mesons in particular. These processes have been discussed in detail by the author (Stecker 1971a), with particular regard to the  $\gamma$ -ray spectra produced. In particular, it is found from accelerator measurements that hyperons and baryon resonances formed in p-p interactions, tend to carry off a roughly constant fraction (~60%) of the energy of the incident proton and from this it can be shown that the resulting  $\gamma$ -ray spectra from the decay of these "excited baryon states" maintains the same power-law form as the incident cosmic-rays at high energies, i.e., if  $I_{cr} = K_{cr} E_{cr}^{-\Gamma}$ , than  $I_{\gamma, N, Y} \sim K_{\gamma} E_{\gamma}^{-\Gamma}$ . In particular, if  $\pi^0$ -mesons are produced by a process leading to a multiplicity law  $\zeta \propto E_{cr}^a$  and given an average energy  $\propto E_{cr}^b$  where  $b = 1-a$ , the resulting  $\gamma$ -ray

spectrum has the form (at high energies)

$$I_{\pi}(E_{\gamma}) = K_0 E_{\gamma}^{-\Gamma_0} \quad (9)$$

where

$$\Gamma_0 = \frac{(\Gamma_{cr} + b) - (a+1)}{b} \quad (10)$$

and

$$K_0 = \frac{2nLK_{\rho} \sigma_0 \chi_0 [\Gamma_{cr}^{-(a+1)}] / b}{(\Gamma_{cr} + b) - (a+1)} \quad (11)$$

For the decay of  $\Sigma^0$ -hyperons, the spectrum is given by

$$I_{\Sigma^0}(E_{\gamma}) = K_{\Sigma^0} E_{\gamma}^{-\Gamma_{cr}} \quad (12)$$

with

$$K_{\Sigma^0} = \frac{K_{cr}}{2\Gamma_{cr}} nL\sigma_{\Sigma^0} \left( \chi_{\Sigma^0} \frac{M_{\Sigma}^2 - M_{\lambda}^2}{M_{\Sigma}^2} \right)^{(\Gamma_{cr} - 1)} \quad (13)$$

and for nucleon resonances (isobars)

$$I_i(E_{\gamma}) = K_i E_{\gamma}^{-\Gamma_{cr}} \quad (14)$$

with

$$K_i = \frac{2K_{cr} R_i nL}{\Gamma_{cr}^2} (2\chi_i)^{(\Gamma_{cr} - 1)} \xi_i E_{\gamma}^{-\Gamma_{cr}} \quad (15)$$

where  $\xi_i$  typically  $10^{-1}$ - $10^{-2}$

(Stecker 1971a). The relevant data for hyperons and isobars are given in Tables 3-5. Table 6 shows the relevant data for the "fireball" models of pion production (Stecker 1971) and the resultant differential  $\gamma$ -ray spectra at high energies are shown in Figures 9 and 10. The "scaling" hypothesis

predicts a logarithmic increase in pion multiplicity with energy but the resultant form of the  $\gamma$ -ray spectrum at high energies should be close to the result given in Figure 10.

Gamma-rays produced from the decay of  $\pi^0$ -mesons produced in nucleon-antinucleon annihilations have spectral characteristics typical of pion-decay  $\gamma$ -rays, i.e., a maximum at  $m_\pi c^2/2 \sim 70$  MeV and a nearly flat spectrum in the vicinity of the maximum which is symmetric on a  $\log E_\gamma$  plot about the point  $m_\pi c^2/2$ . However, if the annihilations are assumed to occur near rest in the laboratory system (i.e., in the universe) the spectrum is bounded between a maximum  $\gamma$ -ray energy of  $\sim 919$  MeV and a minimum energy of about 5 MeV. This is because the maximum energy given to a  $\pi^0$ -meson occurs in the three particle annihilation



and is 923 MeV (two-particle annihilations involving  $\pi^0$ -mesons being forbidden by selection rules involving conservation of G-parity, see discussion in Stecker (1971a)).

Frye and Smith (1966) using accelerator data, and independently Stecker (1967, 1971a) using a theoretical pion-production model in  $p\bar{p}$  annihilation have calculated the resultant  $\gamma$ -ray spectrum from  $p\bar{p}$  annihilation at rest. There is excellent agreement between the two calculations and the resultant spectrum, on a logarithmic energy plot, is shown in Figure 11.

We now turn to a discussion of the isotropic  $\gamma$ -ray background spectrum which is expected to be of cosmological origin.\* Figure 12 shows schematically the results of recent observations of this background spectrum by Trombka, et al. (1973), Mayer-Hasselwander, et al. (1972), Share, et al. (1972) and Kraushaar, et al. (1972) (see the papers of Trombka, Share and Kniffen; these proceedings).

Because of the cosmological aspects relating to studies a the diffuse isotropic  $\gamma$ -ray background, it is necessary to discuss the physics of  $\gamma$ -ray production in past epochs (such radiation may be reaching us today from distances of the order of  $\sim 15$  billion light years. According to big-bang cosmology, the universe was in a smaller, denser state in the distant past and has been continually expanding. This general expansion has caused all electromagnetic radiation to be Doppler shifted to the red (i.e., to longer wavelengths which implies lower energies). The red-shift is usually designated by  $z \equiv \Delta\lambda/\lambda$ .

This implies that a spectrum of  $\gamma$ -rays for example from  $\pi^0$ -decay (either from annihilation or cosmic-ray interactions) which has a maximum at  $\sim 70$  MeV locally, would have that maximum shifted to a lower energy if such radiation were produced at an epoch corresponding to a significant red-shift. To find the total spectrum expected to be observed, we must

Footnote to top of page 14:--~~q~~

Results from the OSO-3 detector in the 10 to 100 keV energy range have shown that the background radiation in this range is isotropic to better than 5 per cent over angular scales of  $10^{\circ}$  (Schwartz, D. 1970, *Astrophys. J.* 162, 439). In the energy range between 0.2 and 4 MeV, Damle, et al. 1972 (*Nature* 235, 319) have found evidence for the isotropy of the diffuse background flux. Above 50 MeV, the results from SAS-2 and OSO-3 (See papers of Share and Kniffen, et al. in these proceedings) indicate that there is a relatively hard component of  $\gamma$ -radiation of galactic origin and a true diffuse extragalactic background component observed at high galactic latitudes which is soft ( $\sim E_{\gamma}^{-3}$ ) and which connects smoothly with the Apollo data below 30 MeV (see figures 12, 16 and 17). The evidence would thus seem compelling that the spectrum represented in figure 12 is of extragalactic origin and is therefore not consistent with the galactic-origin hypothesis suggested by Cowsik elsewhere in these proceedings.

integrate over all red-shifts where  $\gamma$ -rays were being produced and weigh the integration with various factors of the quantity  $(1+z)$ , (for a complete discussion, see Stecker, 1971a, Chapters 9-14). Also, for  $z \gtrsim 100$ , Compton interactions between  $\gamma$ -rays and intergalactic gas may result in energy loss for the  $\gamma$ -rays so that, in general, an integrodifferential transport equation involving  $E_\gamma$  and  $z$  must be solved in order to obtain the expected total  $\gamma$ -ray spectrum resulting from high-red-shift processes such as matter-antimatter annihilation (Stecker, et al. 1971). Absorption processes such as pair-production mechanisms involving intergalactic gas and 2.7K blackbody photons eliminate  $\gamma$ -rays from large red-shifts from various parts of the observed spectrum. Gamma-rays arising from any pion-decay process at cosmological distances contribute significantly to the isotropic background only above 1 MeV, because  $\gamma$ -rays at lower energies have been red-shifted by a factor of  $\gtrsim 70$ . Such a red-shift corresponds to an epoch when the universe was opaque to  $\gamma$ -rays and absorption effects were important. The basic equation to be solved, which we have called the CPT (cosmological photon transport) equation is of the form

$$\frac{\partial \mathcal{L}}{\partial t} + \frac{\partial}{\partial E} [-E H(z) \mathcal{L}] = \mathcal{Q}_{\text{ANN}}(E, z) - \kappa_{\text{AB}}^{(z)} \mathcal{L} + \int_E^{E(E)} dE' \kappa_{\text{SC}}^{(z)}(E|E') \mathcal{L}(E') \quad (17)$$

where  $E$  is the photon energy,  $\kappa_{AB}$  and  $\kappa_{SC}$  are the photon absorption and scattering rates (which are a function of  $z$  because the intergalactic gas density is assumed to scale as  $(1+z)^3$  because of the expansion of the universe. The script quantities for the  $\gamma$ -ray intensity and production rate

$$\mathcal{I}(E, z) \equiv (1+z)^{-3} I(E, z)$$

and

$$\mathcal{Q}(E, z) \equiv (1+z)^{-3} Q_{ANN}(E, z) \tag{18}$$

are quantities co-moving with the expansion, defined so that their red-shift-density dependence cancels out.  $\mathcal{E}(E)$  is an upper limit on the scattering integral defined by the Compton process and  $H(z)$  is the Hubble parameter which, in terms of the Hubble constant  $H_0$ , is given by the relation

$$H(z) = H_0 (1+z) [1 + \Omega z]^{1/2} \tag{19}$$

where  $\Omega$  is the ratio of the mean gas density in the universe to the density needed to close the universe gravitationally.

The term

$$\frac{\partial \mathcal{I}}{\partial t} = -(1+z)H(z) \frac{\partial \mathcal{I}}{\partial z} \tag{20}$$

and the second term in equation (17) expresses the energy loss of the  $\gamma$ -rays because of the expansion-red-shift.

Between  $\sim 5$  and  $\sim 50$  MeV, equation (17) reduces to a power-law form  $I(E) \propto E_{\gamma}^{-\Gamma_{ANN}}$  (see Figures 13 and 14) with the value for  $\Gamma_{ANN}$  estimated by Stecker and Puget (1972) to be  $\sim 2.5 < \Gamma_{ANN} < \sim 3.5$ .

In the vicinity of  $\sim 1$  MeV and below, absorption effects due to Compton scattering become important and cause the spectrum to bend over as shown in Figures 13 and 14. Figure 15 shows the critical red-shift for absorption of  $\gamma$ -radiation as a function of observed energy. At lower energies absorption is due to Compton interactions with intergalactic matter; in the intermediate range absorption is due to pair-production interactions with intergalactic matter (Arons and McCray 1969, Rees 1969). At the higher energies absorption is due to pair-production interactions with blackbody photons (Fazio and Stecker 1970). There is a natural "window" between  $\sim 1$  MeV and  $\sim 10$  GeV which is optimal for studying cosmological gamma-rays. Absorption effects come in below 1 MeV and above 10 GeV.

Figure 16 shows a two component model normalized for a best-fit to the observations involving the production of intergalactic gamma-rays from cosmic-ray interactions with intergalactic gas producing  $\pi^0$ -mesons out to a maximum red-shift of 100 (Stecker 1969b,c, 1971b). Three problems arise with this explanation: 1) even with a relatively steep assumed cosmic-ray spectrum ( $\sim E^{-2.7}$ ) the bulge in the theoretical spectrum may be too large to fit the observations, although this discrepancy may not be too serious considering observational uncertainties, 2) large amounts of energy are needed in cosmic-rays at high-red-shifts\*, and

Footnote for bottom of page 17:-A

\* In later private discussion between the author and P. Morrison, it became apparent that the energy problems may not be too great with this (protar) hypothesis if, indeed, spinars existed at such redshifts of about 70-100 (Stecker 1971b). If it is considered that each spinar produces approximately  $10^{62}$  ergs over a time scale of  $10^7$ - $10^8$  years ( P. Morrison 1969. *Astrophys.J.* 157, L75.), a time comparable to the Hubble time at these redshifts, then at most 20 per cent of the presently observed galaxies are needed to have arisen from this early spinar state in order to provide the cosmic-ray energy needed to account for the diffuse  $\gamma$ -radiation above 1 MeV. At a redshift of about 70, the free-fall time for forming spinars from gas clouds is comparable to the Hubble time. This may provide a natural upper limit to the redshift,  $z_{MAX}$ , for primordial cosmic-ray production in the spinar model. (It should, however, be noted that such spinars may arise in other ways (see Stecker 1971b) and that they may now be a class of moribund objects unrelated to galaxies as we see them now).

3) the maximum red-shift for cosmic-ray production ( $Z_{MAX}$ ) is a free-parameter chosen to fit the observations. The matter-antimatter annihilation hypothesis does not suffer from the above mentioned problems. The parameter  $Z_{MAX}$  does not enter into the theory; annihilations occur at all red-shifts and the 1 Mev-flattening is an absorption effect as discussed earlier. The transport equation (17) was solved to determine the exact form of the spectrum. Energy considerations do not present a problem. Another advantage of the theory is that it arises as a natural effect in a cosmology such as that suggested by Omnes (see papers of Omnes, Schatzman and Puget; these proceedings). Figure 17 shows a detailed comparison of the annihilation hypothesis spectrum with present observations assuming  $\Gamma_{ANN} \approx 2.5$  (see discussion of Stecker and Puget (1972)). The two component model shown presents an excellent fit to the observational data.

Several other models of isotropic  $\gamma$ -ray production have been put forward recently. One suggestion is that the whole spectrum in the  $10^{-3}$ - $10^2$  MeV range is due to Compton interactions of intergalactic electrons with the universal black-body radiation (Felten 1965, Gould 1965, Hoyle 1965, Fazio, Stecker and Wright 1966, Felten and Morrison 1966). In its most recent version Brecher and Morrison (1969) have attempted to explain the observed spectral features using the Compton hypothesis, vis., the steepening in the spectrum at  $\sim 40$  KeV

and flattening above 1 MeV. The Brecher-Morrison spectrum is shown in Figure 18, superimposed on the "data-curve" of Figure 12. The fit is reasonable except at the extreme high and low energy ends of the energy range. However, Cowsik and Kobetich (1972) have recently recalculated the Brecher-Morrison spectrum using a true blackbody target spectrum and a more realistic energy distribution for Compton scattered photons (rather than the  $\delta$ -function approximations used by Brecher and Morrison). The result is a smearing out of the spectral features of the Brecher-Morrison model into a smooth power-law spectrum. Other problems with the Brecher-Morrison model stem from the fact that in order to get a large enough flux generated, electrons are required to leak out of normal galaxies in a time much shorter than the  $\sim 10^7$  y deduced for protons on the basis of cosmic-ray isotropy measurements.

Another hypothesis which attempts to account for the whole photon spectrum is the electron-bremsstrahlung hypothesis. Figure 19, which compares the spectrum generated by this process with the observations shows an excellent fit with the theoretical spectrum based on calculations by Arons, McCray and Silk (1971) below 1 MeV and Stecker and Morgan (1972) above 1 MeV. The break at  $\sim 3.5$  MeV is due to energy loss by cosmic-ray electrons interacting with the 2.7K blackbody radiation. Unfortunately, we again have severe

energetic problems with this process, bremsstrahlung being an inherently inefficient  $\gamma$ -ray generating mechanism. Another problem lies in getting galaxies to leak low-energy non-relativistic electrons at a fast enough rate. Assuming this could be done, an electron spectrum would be distorted by heating the intergalactic medium to  $10^9$  K. The problems with this mechanism have been discussed by Setti and Rees (1970), Prilutskii and Rozental (1971) and Cowsik and Pal (1971). (See paper of Cowsik; these proceedings.)

One additional mechanism for producing a second component of  $\gamma$ -radiation was suggested by Syunyaev (1970), viz., thermal bremsstrahlung from relativistic electrons in a 20 MeV plasma in such objects as the nuclei of Seyfert galaxies. This, of course, immediately presents the problem of having enough Seyfert Galaxies to account for the observed flux. However, a much more serious problem with the fundamental physics of the mechanism has been pointed out by Prilutskii, et al. (1971). They notice that in order to contain the hot relativistic plasma, a magnetic field is required of a strength such that

$$\frac{H^2}{8\pi} \geq n_e kT \quad (2)$$

In that case, the ratio,  $R$ , of the electron energy loss rate from synchrotron radiation to that from bremsstrahlung is of the order of

$$R \approx \frac{\sigma_T c (H^2/8\pi) (kT_e/m_e c^2)^2}{\alpha \sigma_T c n_e kT_e} \approx \alpha^{-1} (kT_e/m_e c^2)^2 \gg 1 \quad (22)$$

for a relativistic plasma where  $kT_e > m_e c^2$  and  $\alpha^{-1} \approx 137$  ( $\sigma_T$  is the Thomson cross section). In fact, for a plasma of temperature  $T_{\text{MeV}}$  given in MeV,

$$R \approx 500 T_{\text{MeV}}^2 \quad (23)$$

Thus, in an optically thin plasma, the synchrotron loss rate is the dominant loss term in the energy-equilibrium equation determining the equilibrium electron spectrum which will insure that the electrons have a non-thermal spectrum and produce non-thermal radiation. In addition, the 20 MeV cutoff in the electron spectrum suggested by Sunyaev will not exist. The details of the argument are further described by Prilutskii, et al. (1971).

It is the opinion of the author, based on the previous discussion, that the most promising theoretical interpretation of the unexpected increase in the observed background flux of  $\gamma$ -radiation above 1 MeV at present is that this radiation has arisen from the annihilation of nucleons and antinucleons, primarily at high red-shifts, on the boundaries between regions of matter and antimatter (Stecker, et al. 1971, Stecker and Puget 1972; see papers of Omnes, Schatzman and Puget; these proceedings). This conclusion is, of course, conditional upon future observations and theoretical investigations.

The argument presented in the paper of Steigmen elsewhere in these proceedings put restrictions on baryon-symmetric cosmologies, but nonetheless are not in conflict with the particular cosmological model discussed here and in the papers of Omnes, Schatzman and Puget (these proceedings).

Tables 7 and 8 summarize some of the significant aspects and spectral attributes of the various mechanisms important for the production of the diffuse cosmic  $\gamma$ -radiation. The last column in table 7 lists the cosmic domains where the various mechanisms probably play an important role. The results from OSO 3 and SAS 2, as summarized in these proceedings in the papers of Share and Kniffen, et al., indicate that in the energy range above 50 MeV there is a distinct hard component of galactic origin and a much softer, high galactic latitude component, of extragalactic origin. The galactic component appears to be predominantly ( i.e., greater than 50 per cent) of  $\pi^0$  - decay origin and therefore is small relative to the steep extragalactic component much below 50 MeV. The extragalactic component fits onto the Apollo data (see paper of Peterson and Trombka, these proceedings) below 30 MeV so that all indications are that the flux below 30 MeV is overwhelmingly extragalactic. Because the galactic flux is much harder above 100 MeV than the extragalactic flux, the galaxy stands out well above the ex-

tragalactic background at these energies. However, below 30 MeV, the galaxy becomes relatively dim and blends into background as only a small perturbation. These conclusions are contrary to the galactic origin hypothesis for 0.2 to 10 MeV  $\gamma$ -radiation discussed by Cowsik in these proceedings, but appear to be at present more consistent with recent satellite observations as presented at this conference.

If the galactic disk component of  $\gamma$ -radiation is primarily of  $\pi^0$ -decay origin, I will stand by my previous arguments (Stecker 1969a, Stecher and Stecker 1970, Stecher 1971a, Chapter 8) that the OSO-3 measurements of Kraushaar, et al. (1972) and those obtained by SAS-2 (Kniffen, et al., these proceedings) indicate that there must be a substantial amount of molecular hydrogen in the galaxy. These are implied by my recent calculations of the  $\gamma$ -ray production rate (Stecker 1973) which confirm my earlier calculations of  $1.3 \pm 0.2 \times 10^{-25} \text{ s}^{-1}$  (see Table 1), but are now on a much more solid basis. The cosmic-ray isotropy measurements do not suggest a large gradient over the galactic disk, in which case the intensity in our region may be typical of the galactic intensity. Forthcoming results from SAS -2 and Copernicus should settle the question in the near future.

In the galactic center region, we expect the flux to be somewhat softer than in the disk as a whole because of a significant component from Compton interactions (Stecker and Stecker 1970, Stecker 1971a, Chapter 8). Preliminary observational results suggest that this is the case (see papers of Share and Kniffen et al. these proceedings). Again, here we await the final results from SAS-2.

The note of anticipation here is a good note to end on because, it seems, that at the time of this first international  $\gamma$ -ray astrophysics symposium we are all on the threshold of a new era of observational  $\gamma$ -ray astronomy.

REFERENCES

- Arons, J. and McCray, R. 1969. *Astrophys. J. Lett.* 158, L91.
- Arons, J., McCray, R., and Silk, J. 1971. *Astrophys. J.* 170, 431.
- Brecher, K., and Morrison, P. 1969. *Phys. Rev. Lett.* 23, 802.
- Cavallo, G., and Gould, R.J. 1971. *Nuovo Cimento* 2 B, 77.
- Clark, G.W. Garmire, G.P., and Kraushaar, W.L. 1968, *Astrophys. J. Lett.* 153, L203.
- Comstock, G.M., Hsieh, K.C., and Simpson, J.A. 1972. *Astrophys. J.* 173, 691.
- Cowsik, R., and Kobetich, E.J. 1972. *Astrophys. J.* 177, 585.
- Cowsik, R., and Pal, Y. 1971. Cosmic Ray Astrophysics (Tata Institute Press, Bombay).
- Dilworth, C., Maraschi, L., and Perola, G.C. 1968. *Nuovo Cimento* 56 B, 334.
- Fazio, G.G., and Stecker, F.W. 1970. *Nature* 226, 135.
- Fazio, G.G., Stecker, F.W., and Wright, J.P. 1966. *Astrophys. J.* 144, 611.
- Felten, J.E. 1965. *Phys. Rev. Lett.* 15, 1003.
- Felten, R.J., and Morrison, P. 1966. *Astrophys. J.* 146, 686.
- Fichtel, C.E., Hartman, R.C., Kniffen, D.A., and Sommer, M. 1972. *Astrophys. J.* 171, 31.
- Frye, G.M. and Smith, L.H. 1966. *Phys. Rev. Lett.* 17, 733.
- Heitler, W. 1960. Quantum Theory of Radiation (London, Oxford Press).
- Hoyle, F. 1965. *Phys. Rev. Lett.* 15, 131.
- Jones, F.C. 1965. *Phys. Rev.* 137, B1306.

- Kraushaar, W.L., Clark, G.W., Garmire, G.P., Boriken, R.,  
Higbie, P., Leong, C., and Thorsos, T. 1972. *Astrophys. J.* 177, 341.
- Levy, D.J., and Goldsmith, D.W. 1972. *Astrophys. J.* 177, 643.
- Mayer-Hasselwander, H.A., Pfefferman, E., Pinkau, K.,  
Rothermel, H., and Sommer, M. 1972. *Astrophys. J. Lett.*  
175, L23.
- Morrison, P. 1958. *Nuovo Cimento* 7, 858.
- Pollack, J.B. and Fazio, G.G. 1963. *Phys. Rev.* 131, 2684.
- Prilutskii, O.F., Ochelkov, Y.P., Rozental, I.L., and  
Shukalov, I.B. 1971. *Izvestia Akademii Nauk SSSR* 35, 2453.
- Prilutskii, O.F., and Rozental, I.L. 1971. *Aston. Zh.* 48, 489.
- Rees, M.J. 1969. *Astrophys. Lett.* 4, 61 and 113.
- Share, G.H., Kinzer, R.L., and Seeman, N. 1972. *Proc. I.A.U.*  
*Symp. No. 55*, in press.
- Slattery, P. 1972. *Phys. Rev. Lett.* 29, 1624.
- Sreekantan, B.V. 1972. *Space Sci. Rev.* 14, 103.
- Stecker, T.P., and Stecker, F.W. 1970. *Nature* 226, 1234.
- Stecker, F.W. 1967. Smithsonian Astrophys. Observ. Special  
Report. No. 261.
- Stecker, F.W. 1969a. *Nature* 222, 865.
- Stecker, F.W. 1969b. *Astrophys. J.* 157, 507.
- Stecker, F.W. 1969c. *Nature* 224, 870.
- Stecker, F.W. 1970. *Astrophys. and Space Sci.* 6, 377.
- Stecker, F.W. 1971a. Cosmic Gamma Rays NASA SP 249 (Washington,  
U.S. Gov't Print. Off.).
- Stecker, F.W. 1971b. *Nature* 229, 105.
- Stecker, F.W. 1973. *Astrophys. J.* 185, in press.

- ~~Stecker, F.W., and Morgan, D.L. 1972. Astrophys. J. 171, 201.~~
- Stecker, F.W., Morgan, D.L. and Bredekamp, J. 1971. Phys. Rev. Lett. 27, 1469.
- Stecker, F.W., and Puget, J.L. 1972. Astrophys. J. 178, 57.
- Sunyaev, R.A. 1970. Pis'ma Zh. Eksp. Teor. Fiz. 12, 381.
- Trombka, J.I., Metzger, A.E., Arnold, J.R., Matteson, J.L., Reedy, R.C., and Peterson, L.E. 1973. Astrophys. J. 181, 737.

TABLE 1.

**$\gamma$ -RAY PRODUCTION RATE  
FROM THE DECAY OF  $\pi^0$ -MESONS  
PRODUCED IN INTERSTELLAR pp, p $\alpha$ ,  $\alpha$ p  
COSMIC-RAY INTERACTIONS**

<u>REFERENCE</u>	<u>ENERGY RANGE</u>	<u>RATE PER H ATOM (<math>\times 10^{25}</math>) S<sup>-1</sup></u>
POLLACK AND FAZIO (1963)	>0 MeV	1.2
DILWORTH, et al. (1968)	>50 MeV	1.1
STECKER (1970)	>100 MeV	1.3 $\pm$ 0.2
CAVALLO AND GOULD (1971)	>100 MeV	1.8 $\pm$ 0.54
LEVY AND GOLDSMITH (1972)	>100 MeV	3.2
KRAUSHAAR, et al. (1972)*	>100 MeV	<1.6
STECKER (1973)	>100 MeV	<(1.51 $\pm$ 0.23)

28

**TABLE 2. GAMMA-RAY MULTIPLICITY AND BRANCHING RATIOS FROM HYPERON AND MESON DECAYS**

DECAY MODE	BRANCHING RATIO (R)	MULTIPLICITY( $\xi_\gamma$ )	$R\xi_\gamma$
$\pi^0 \rightarrow 2\gamma$	1.00	2	2.00
$\Sigma^0 \rightarrow \Lambda + \gamma$	1.00	1	1.00
$K^\pm \rightarrow \pi^\pm + \pi^0$	0.215	2	0.430
$K_1^0 \rightarrow 2\pi^0$	$\frac{1}{2}(0.311)$	4	0.622
$K_2^0 \rightarrow 3\pi^0$	$\frac{1}{2}(0.265)$	6	0.795
$K_2^0 \rightarrow \pi^+ + \pi^- + \pi^0$	$\frac{1}{2}(0.114)$	2	0.114
$\Lambda \rightarrow n + \pi^0$	0.331	2	0.662
$\Sigma^+ \rightarrow p + \pi^0$	0.510	2	1.02

29

### TABLE 3 HYPERON CROSS-SECTION DATA

PROTON MOMENTUM (GeV/c)	LAMBDA CROSS SECTION (mb)	NEUTRAL SIGMA CROSS SECTION (mb)	POSITIVE SIGMA CROSS SECTION (mb)
4.7	0.051	0.049	0.083
6	0.259	0.077	
10	0.472	0.196	0.239
23.1	LAMBDA + NEUTRAL SIGMA CROSS SECTION = 0.77 LAMBDA + NEUTRAL SIGMA CROSS SECTION = 1.13		
24.5			

### TABLE 4. ISOBAR CROSS-SECTION DATA

INCIDENT MOMENTUM (GeV/c)	CROSS SECTION (mb)				
	Δ (1.237)	N (1.410)	N (1.518)	N (1.688)	Δ (2.190)
2.85	3.8	-	-	-	-
4.55	1.5	0.63	0.68	0.7	-
6	0.376	-	-	-	-
6.06	0.6	0.65	0.45	0.5	-
7.88	0.41	0.45	0.31	0.46	-
10	0.184	0.544	0.196	0.562	-
15	0.142	0.602	0.160	0.638	-
20	-	0.660	0.170	0.560	0.128
30	-	0.744	0.166	0.576	0.108

20

**TABLE 5. PRODUCTION AND DECAY PARAMETERS  
FOR  $\Lambda$ ,  $\Sigma^+$ ,  $\Sigma^0$ , N (1.410), AND N (1.688)**

PARTICLE	DECAY SCHEME	MASS (GeV)	PRODUCTION THRESHOLD ENERGY (GeV) IN P-P COLLISION	BRANCHING RATIO FOR $\gamma$ -PRODUCING MODES	ASSUMED PRODUCTION CROSS SECTION AT HIGH ENERGIES (mb)	DECAY TIME (sec)
N (1.688)	$N^+ (1.688) \rightarrow N + \pi^0$	1.688	1.80	0.33†	0.6	$\sim 10^{-23}$
N (1.410)	$N^+ (1.410) \rightarrow N + \pi^0$	1.410	1.24	0.33†	0.6	$< 10^{-23}$
$\Sigma^+$	$\Sigma^+ \rightarrow p + \pi^0$	1.189	1.90	0.510	0.8	$\sim 10^{-10}$
$\Sigma^0$	$\Sigma^0 \rightarrow \Lambda + \gamma$	1.192	1.90	1.00	0.4	$< 10^{-14}$
$\Lambda$	$\Lambda \rightarrow n + \pi^0$	1.115	1.70	0.331	0.4	$\sim 10^{-10}$

† FOR SIMPLICITY, IT IS ASSUMED THAT ALL DECAYS OCCUR VIA THE i-PROCESS. MORE PRECISELY,  $\sim 10$  TO 15% OF THE DECAYS OCCUR VIA THE PRODUCTION OF TWO PIONS.

31

**TABLE 6. PARAMETERS FOR DETERMINING GAMMA-RAY SPECTRA FROM VARIOUS PIONIZATION MODELS**

MODEL	VALID ENERGY RANGE	a	b	g/b		
				$\Gamma = 2.5$	$\Gamma = 2.7$	$\Gamma = 3.2$
FERMI'S MODEL (FERMI, 1951)	ALL $E_p$	0.25	0.75	2.67	2.93	3.6
ONE-FIREBALL MODEL	$E_p < 150 \text{ GeV}$	0.5	0.5	3.0	3.4	NOT APPLICABLE
TWO-FIREBALL MODEL	$E_p > 10^3 \text{ GeV}$	0.25	0.75	NOT APPLICABLE	2.93	3.6
LANDAU'S MODEL	ALL $E_p$	-	-	GAMMA-RAY SPECTRUM PROPORTIONAL TO $E_\gamma^{-3.2}$		

TABLE 7.

MECHANISM	PARTICLE PRIMARILY INVOLVED	INTERACTION TYPE	PROBABLE IMPORTANCE
COMPTON INTERACTIONS	COSMIC-RAY ELECTRONS AND LOW ENERGY PHOTONS	ELECTROMAGNETIC	EXTRAGALACTIC INTERACTIONS WITH 2.7 K BLACKBODY PHOTONS
BREMSSTRAHLUNG INTERACTIONS	COSMIC-RAY ELECTRONS AND COSMIC GAS	ELECTROMAGNETIC	EXTRAGALACTIC, POSSIBLY GALACTIC BELOW 10 MeV
NEUTRAL PION PRODUCTION (INELASTIC COSMIC-RAY INTERACTIONS)	COSMIC-RAY PROTONS AND COSMIC GAS	STRONG	GALACTIC, POSSIBLY EXTRAGALACTIC
NEUTRAL PION PRODUCTION IN MATTER-ANTIMATTER ANNIHILATION.	PROTONS AND ANTIPROTONS	STRONG	EXTRAGALACTIC, COSMOLOGICAL

63  
55

TABLE 8.

MECHANISM	$\gamma$ -RAY SPECTRUM CHARACTERISTICS		
	SINGLE INTERACTION	GALACTIC SPECTRUM	COSMOLOGICAL SPECTRUM
COMPTON INTERACTIONS	FLAT AT TYPICAL COSMIC-RAY ENERGIES PEAKED TOWARD HIGH PHOTON ENERGY AT ULTRAHIGH ENERGIES. (KLEIN-NISHINA THEORY)	POWER-LAW ROUGHLY $I(E_\gamma) \sim E_\gamma^{-2}$ RELATION BETWEEN EXPONENTS $\Gamma_c = (\Gamma_e + 1) / 2$	POWER-LAW ROUGHLY $I(E_\gamma) \sim E_\gamma^{-2}$ RELATION BETWEEN EXPONENTS $\Gamma_c = (\Gamma_e + 1) / 2$
BREMSSTRAHLUNG INTERACTIONS	FLAT AT RELATIVISTIC ENERGIES. PEAKED TOWARD LOW PHOTON ENERGY AT NON-RELATIVISTIC ENERGIES.	POWER-LAW ROUGHLY $I \sim E_\gamma^{-3}$ $\Gamma_b = \Gamma_e$ (RELATIVISTIC) $\Gamma_b = (\Gamma_e + 1)$ , NON-REL.	POWER-LAW WITH POSSIBLE CHANGES OF EXPONENT AT $\sim 0.04$ , $\sim 1$ , and $\sim 3.5$ MeV.
NEUTRAL PION PRODUCTION (INELASTIC COSMIC-RAY INTERACTIONS)	FLAT AND SYMMETRIC AROUND $m_\pi c^2 / 2$ ON A LOG $E_\gamma$ GRAPH (FOR DECAY OF A SINGLE PION)	MAXIMUM AT $m_\pi c^2 / 2$ . NEARLY FLAT NEAR MAXIMUM AND SYMMETRIC ON A LOG $E_\gamma$ GRAPH. POWER-LAW ROUGHLY $I \sim E_\gamma^{-3}$ ABOVE A FEW HUNDRED MeV.	MAXIMUM IS REDSHIFTED TO SOME ENERGY BETWEEN $\sim 1$ AND $\sim 70$ MeV. (NOTE: $m_\pi c^2 / 2 \approx 70$ MeV). POWER-LAW AT HIGHER ENERGIES.
NEUTRAL PION PRODUCTION IN MATTER-ANTIMATTER ANNIHILATION.	FLAT AND SYMMETRIC AROUND $m_\pi c^2 / 2$ ON A LOG $E_\gamma$ GRAPH (FOR DECAY OF A SINGLE PION)	EXPECT NONEXISTENT	SPECTRUM POWER-LAW BETWEEN $\sim 5$ AND $\sim 50$ MeV, TURNS OVER BELOW 5 MeV AND FALLS OFF MORE SHARPLY ABOVE 50 MeV.

34

## FIGURE CAPTIONS

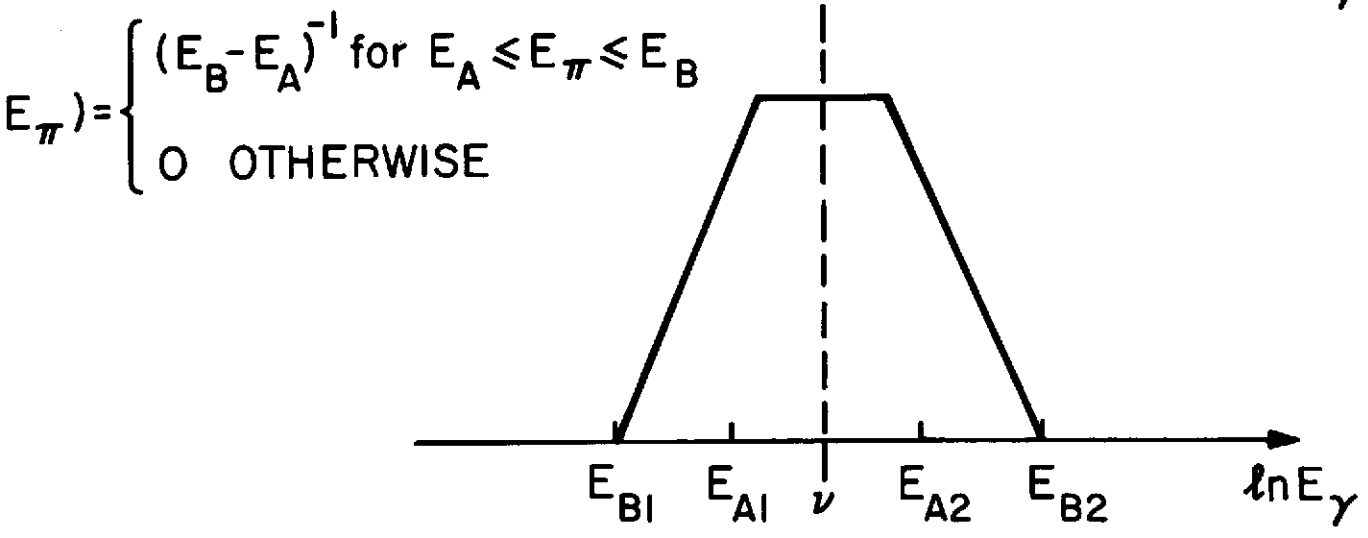
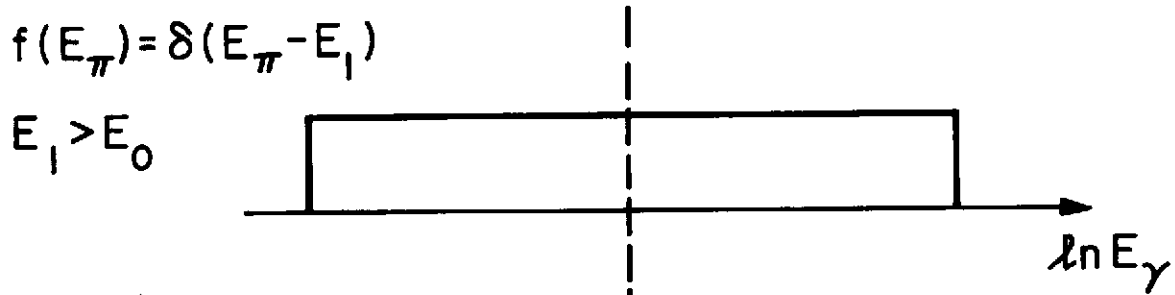
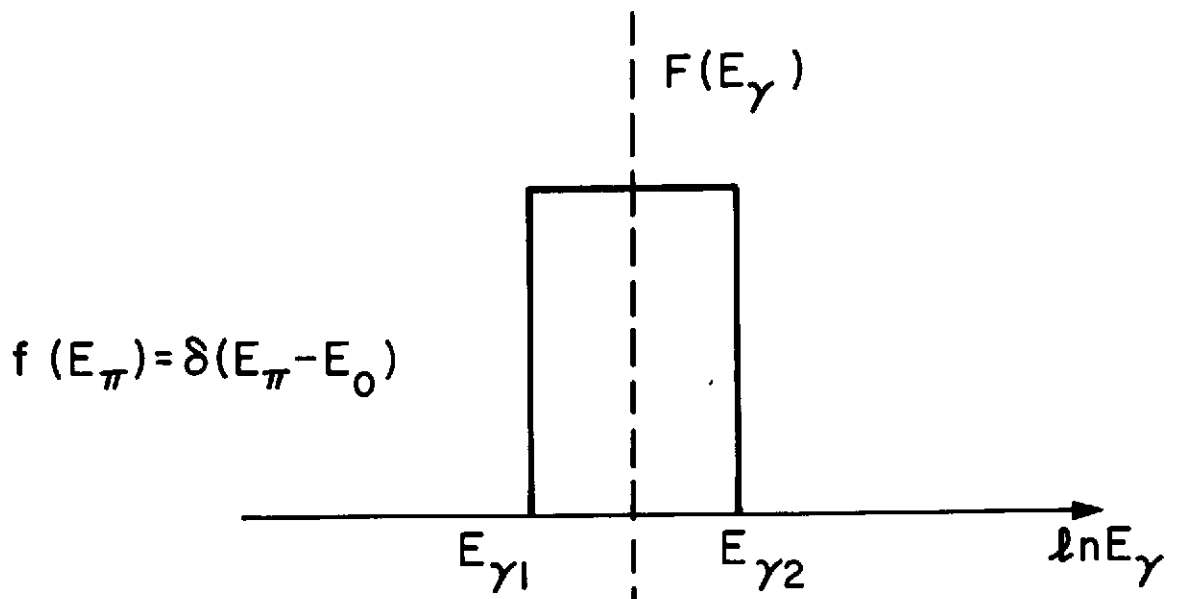
- Figure 1. Gamma-ray spectra from the decay of neutral pions for various simple pion energy distributions.
- Figure 2. Idealized superposition of  $\gamma$ -ray spectra from the decay of pions having various energy distributions.
- Figure 3. The calculated differential production spectrum of  $\gamma$ -rays produced in cosmic-ray interactions in the galaxy based on the "isobar (i)-plus-fireball (f)" model of Stecker (1970).
- Figure 4. A comparison of the shapes of the integral galactic pion-decay energy spectra calculated by Stecker (1970) and Cavallo and Gould (1971). The total production rate is normalized to unity.
- Figure 5. Cross section times multiplicity for neutral pion production in p-p interactions as a function of incident kinetic energy.
- Figure 6. Comparison of accelerator data from Figure 5 with the assumptions made by Levy and Goldsmith (1972).
- Figure 7. Differential neutral pion production function from p-p interactions.
- Figure 8. Integral  $\gamma$ -ray production function from the decay of neutral pions produced in p-p interactions.
- Figure 9. Calculated  $\gamma$ -ray spectra from various secondary particles produced in galactic cosmic-ray interactions (Stecker 1971).

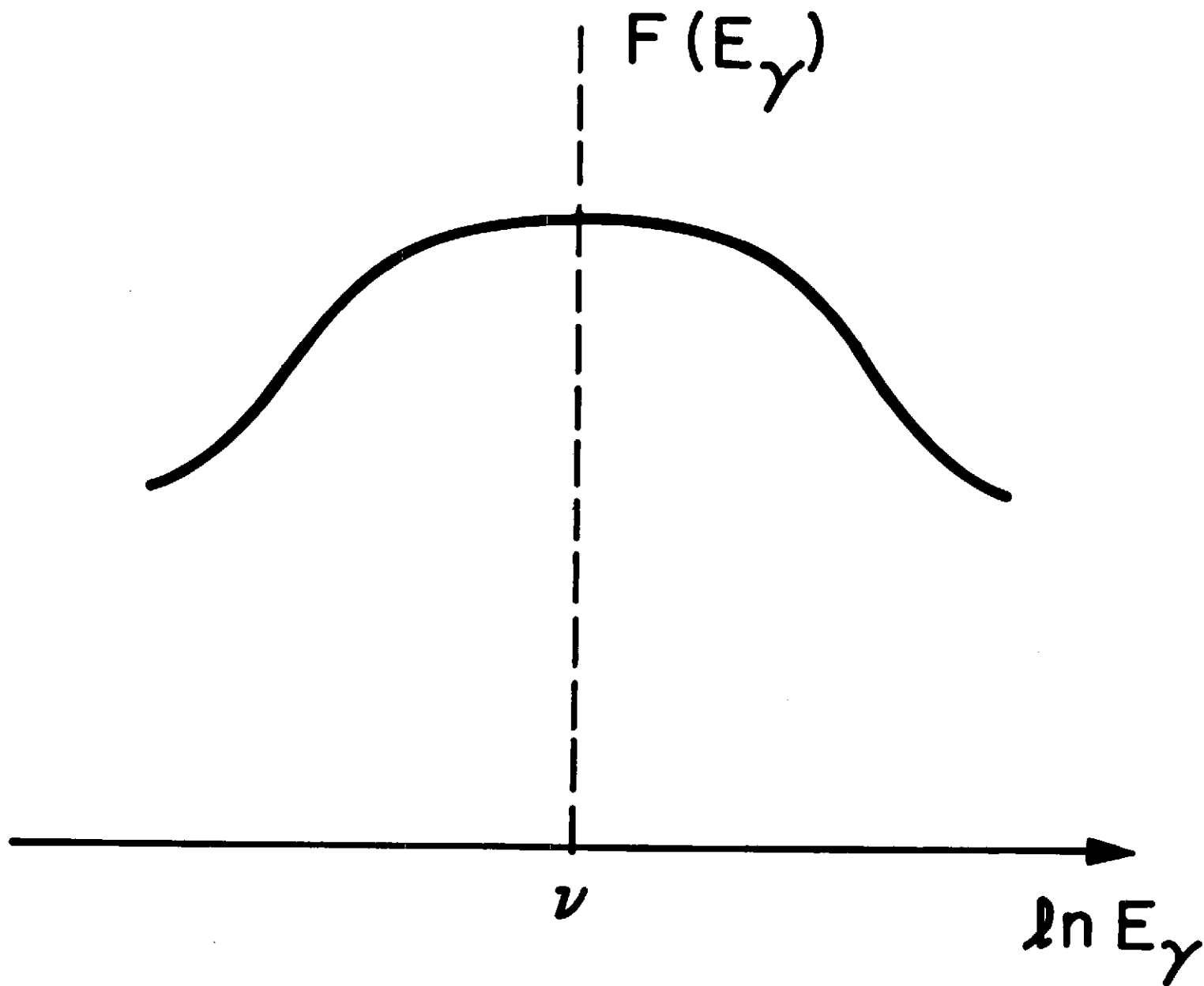
- Figure 10. Total calculated galactic  $\gamma$ -ray production spectrum from cosmic-ray interactions (Stecker 1971).
- Figure 11. Normalized local differential  $\gamma$ -ray spectrum from  $p\bar{p}$  annihilation at rest.
- Figure 12. Recent observational results on the cosmic  $\gamma$ -ray background spectrum.
- Figure 13. The cosmological  $\gamma$ -ray spectrum from matter-anti-matter annihilation calculated by solving the CPT equation numerically for  $\Omega = 1$ . The solid line represents the complete solution. The other curves represent the effect of neglecting the absorption and scattering (transport) terms in equation (17).
- Figure 14. The effect of absorption of  $\gamma$ -rays at high redshifts by the protogalactic gas.
- Figure 15. The critical redshift for absorption of  $\gamma$ -radiation as a function of observed  $\gamma$ -ray energy.
- Figure 16. Comparison of the observed background with a two-component model involving the production and decay of neutral pions produced in intergalactic cosmic-ray interactions at redshifts up to 100.
- Figure 17. Comparison of the observed background spectrum with a two-component model involving the matter-antimatter hypothesis as discussed in the text.

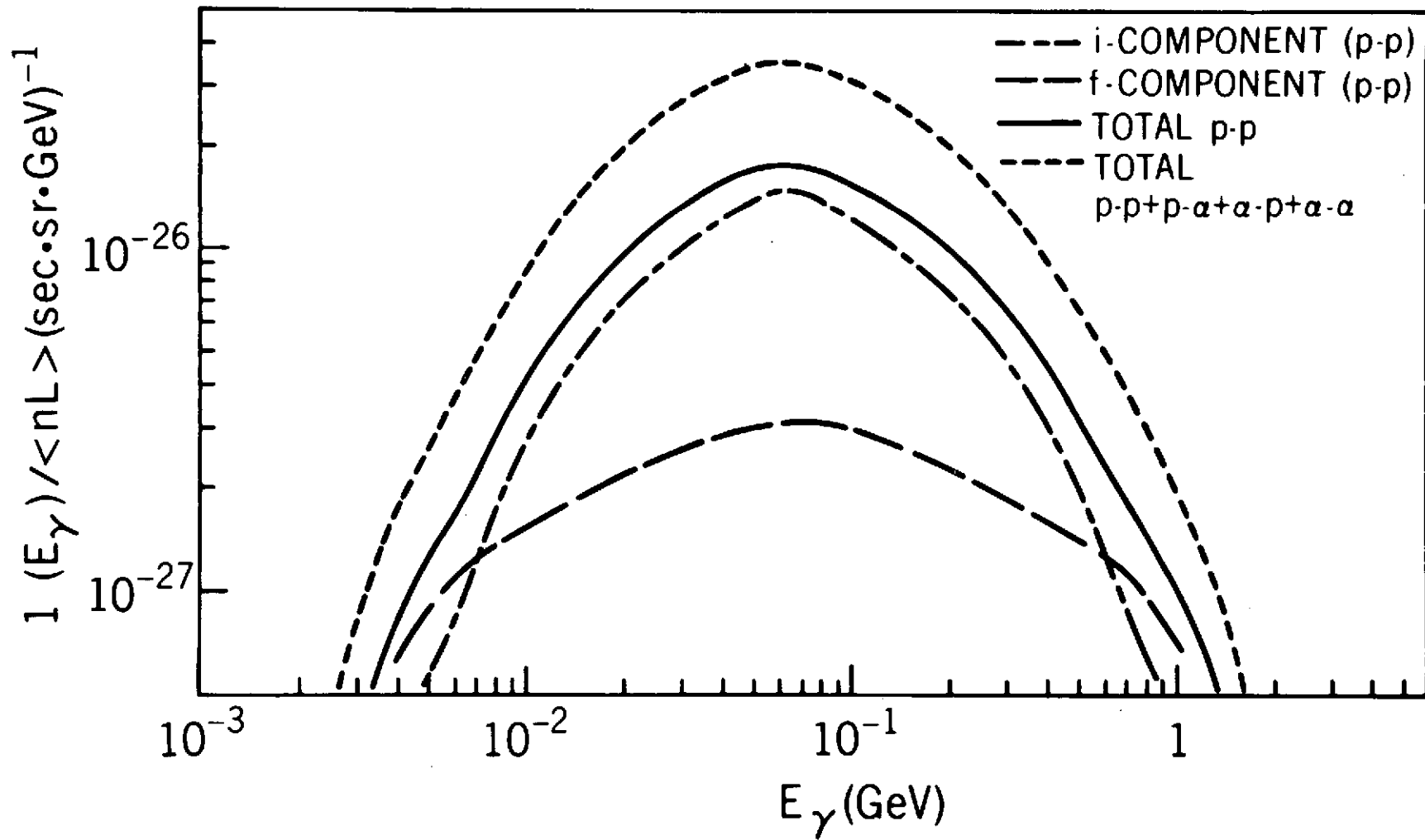
Figure 18. Comparison of the observed background spectrum with the Brecher-Morrison model.

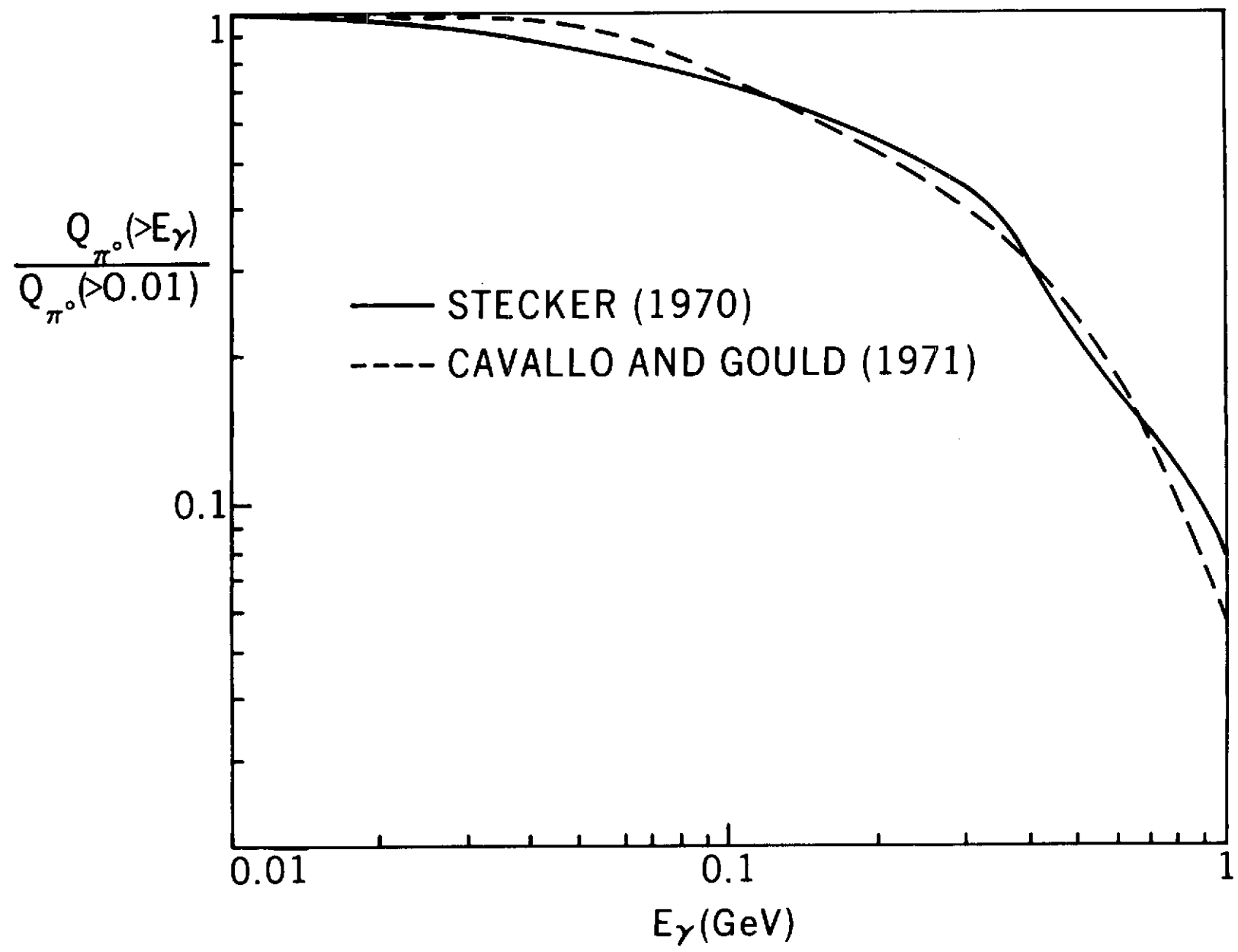
Figure 19. Comparison of the observed background spectrum with the electron bremsstrahlung model as discussed by Arons, et al. (1971) and Stecker and Morgan (1972) with a spectral break at  $E_B = 3.5$  MeV as discussed by Stecker and Morgan.

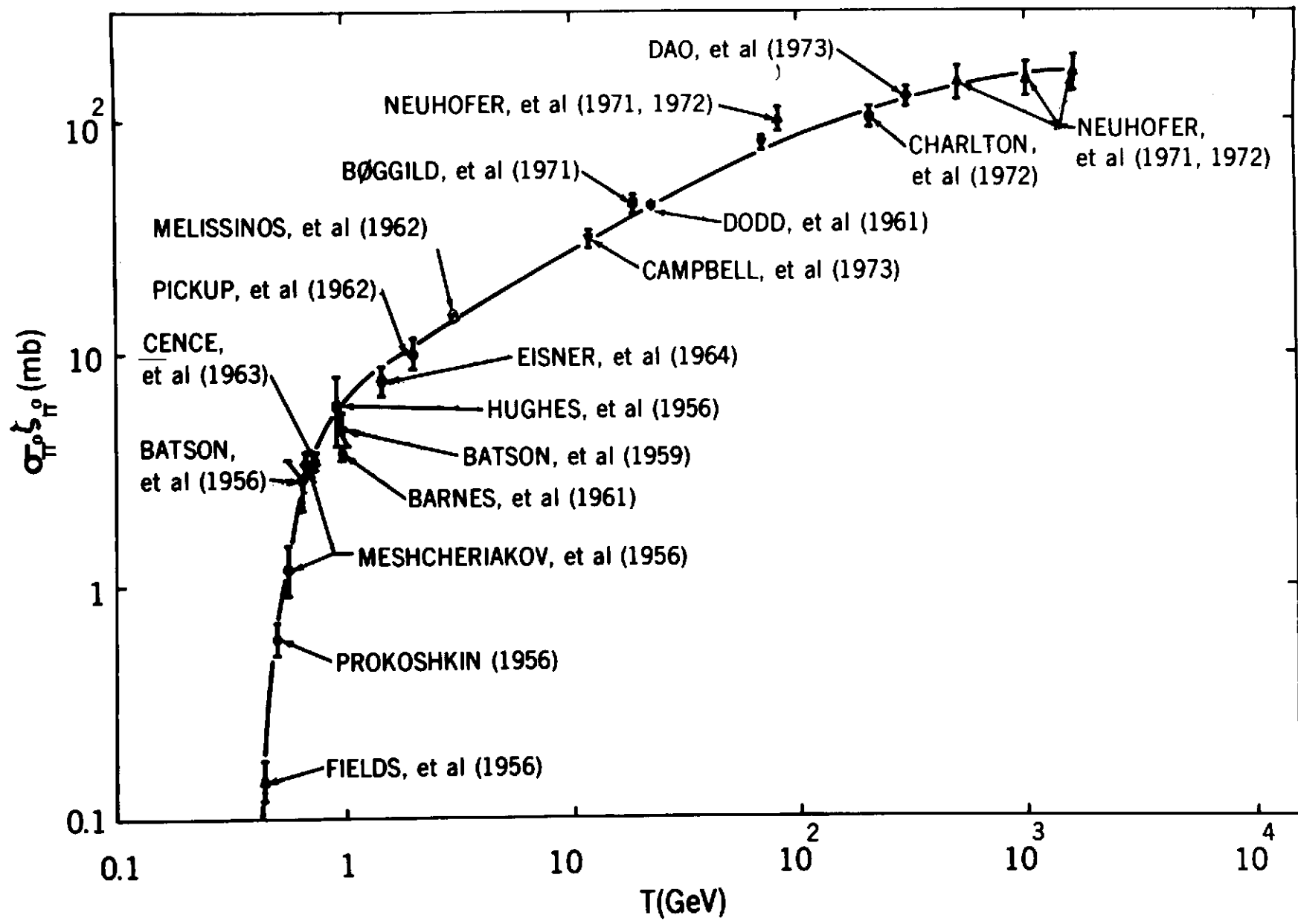
Fig. 1











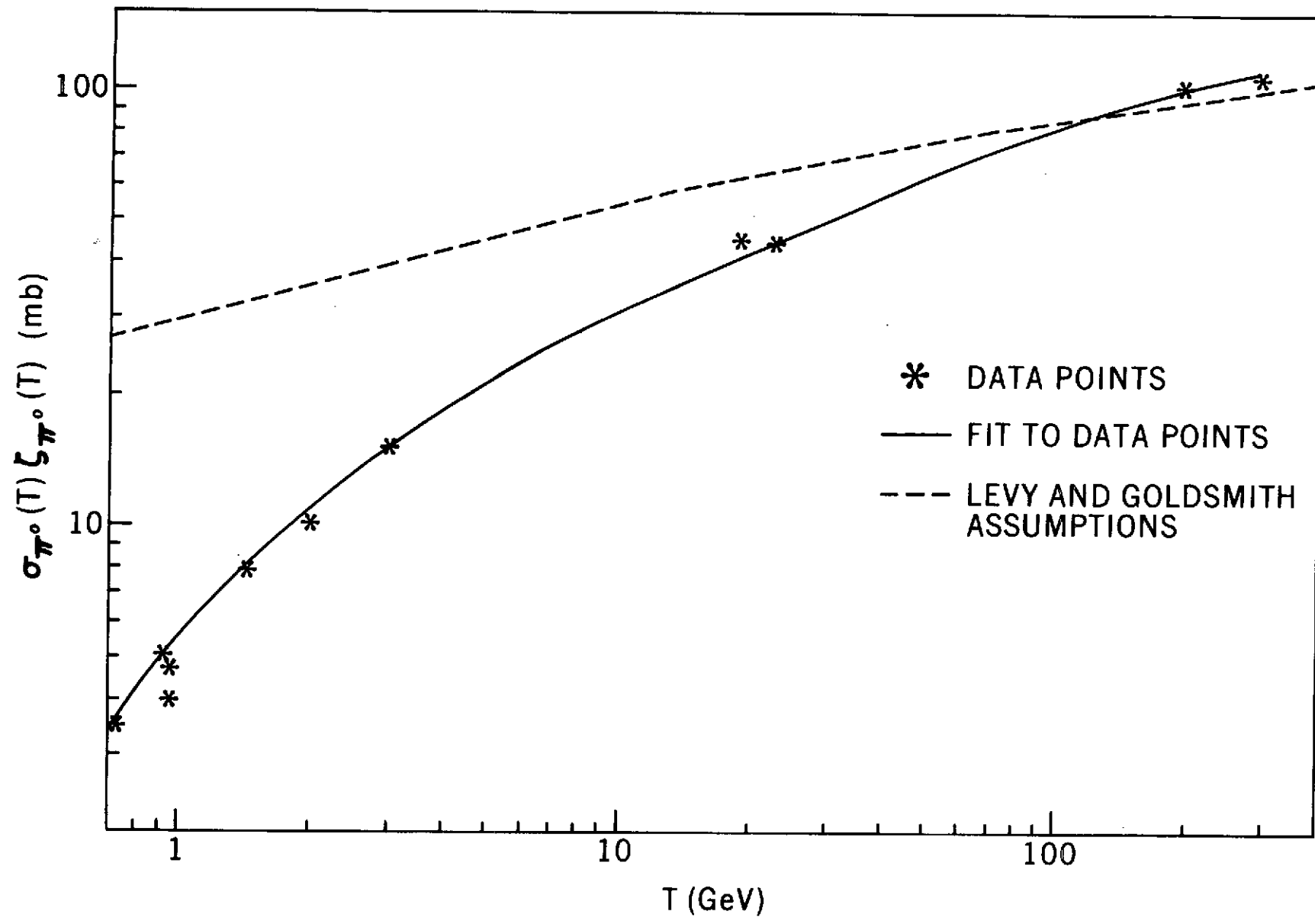
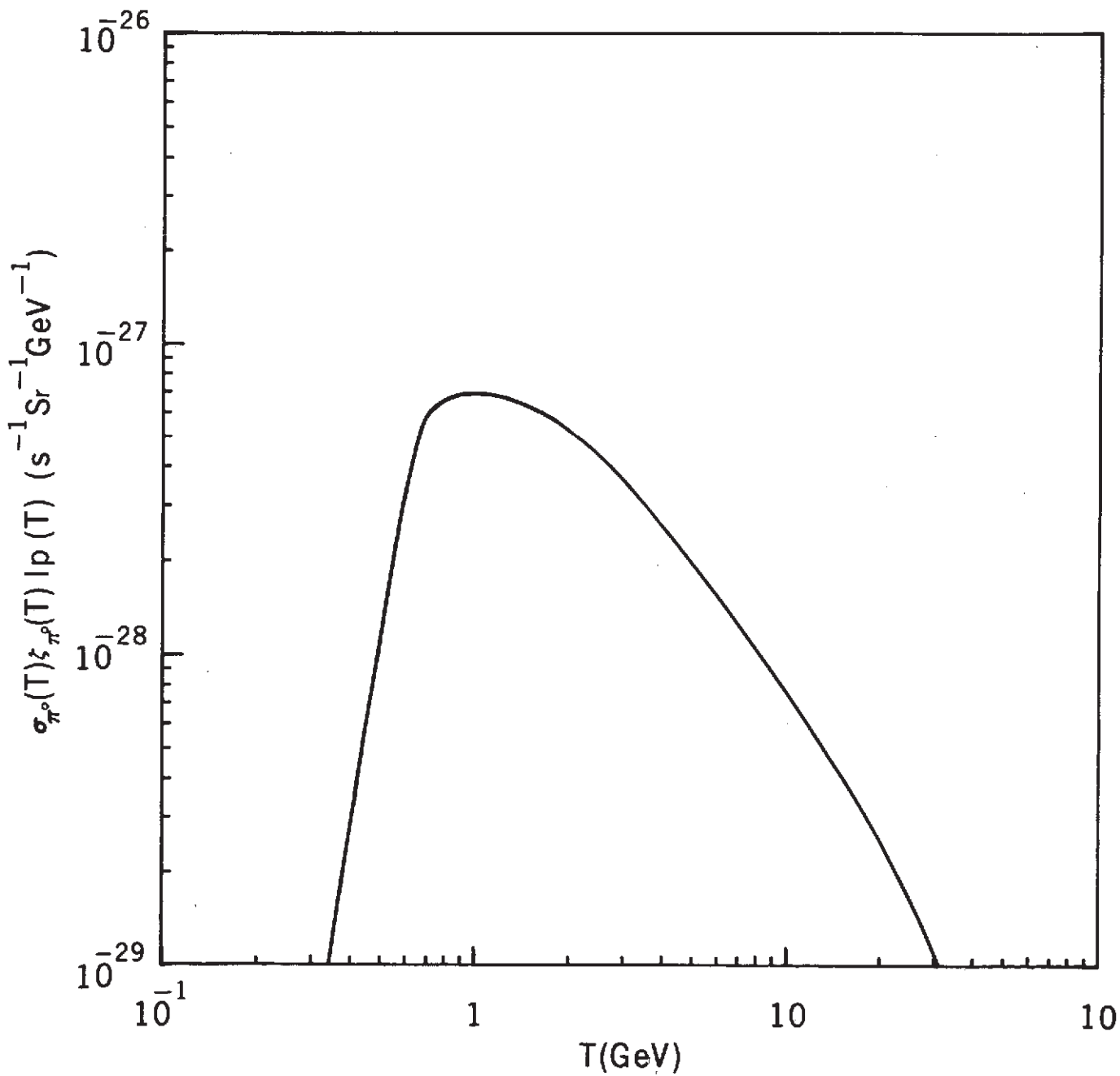


Fig. 7

$\pi^0$  - PRODUCTION FUNCTION FROM pp INTERACTIONS ONLY



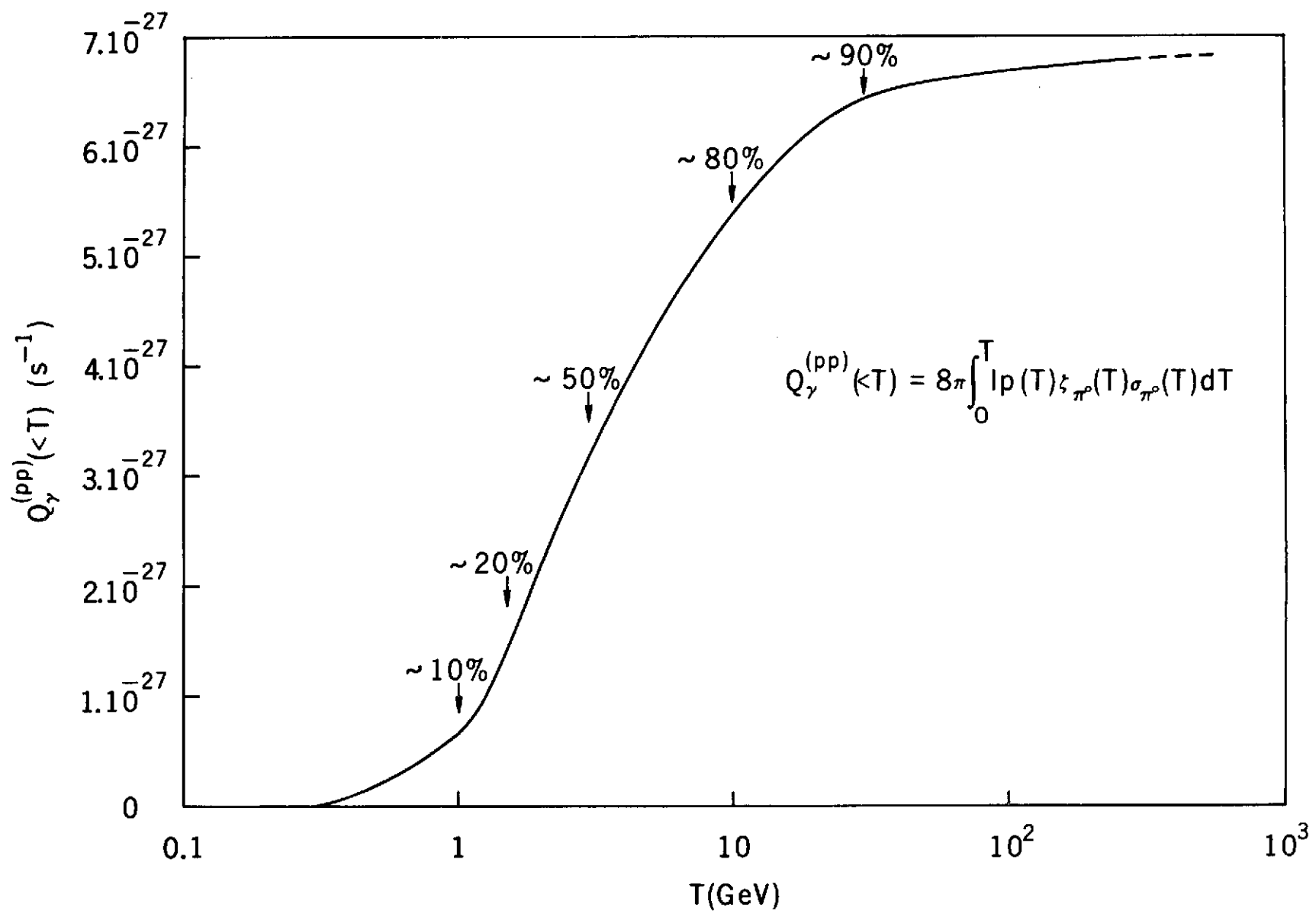


Fig. 9

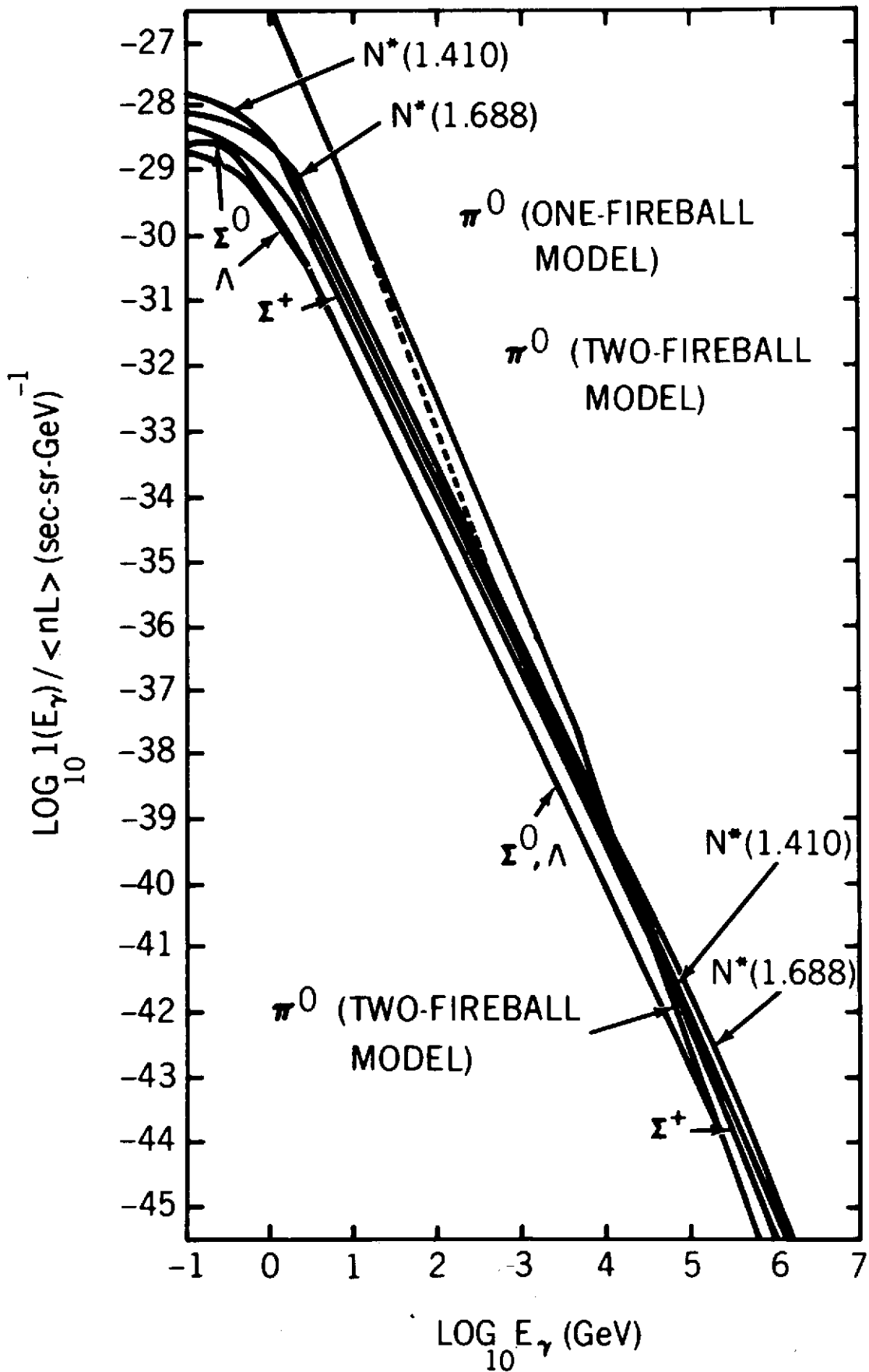
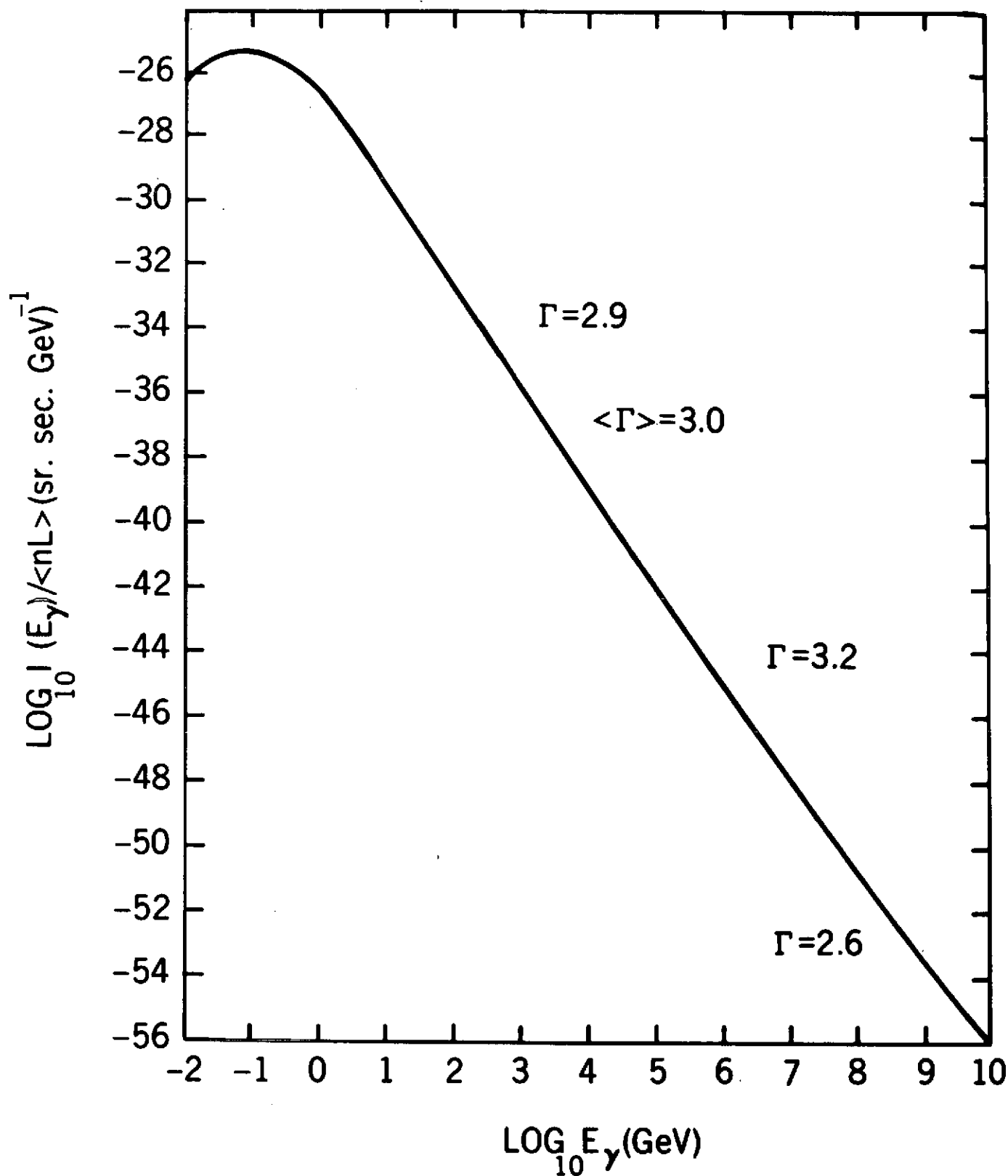


Fig. 10



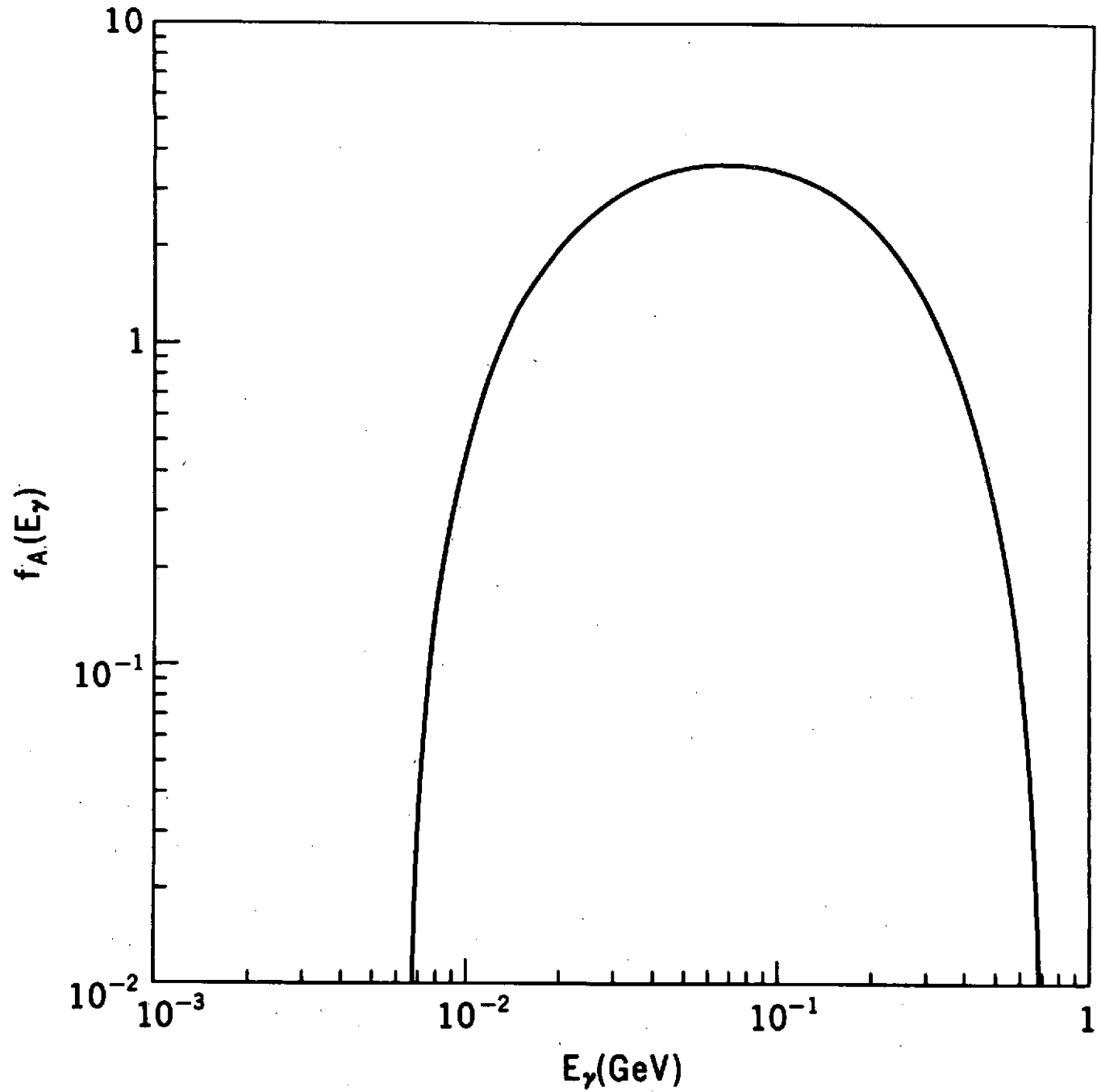


Fig. 12

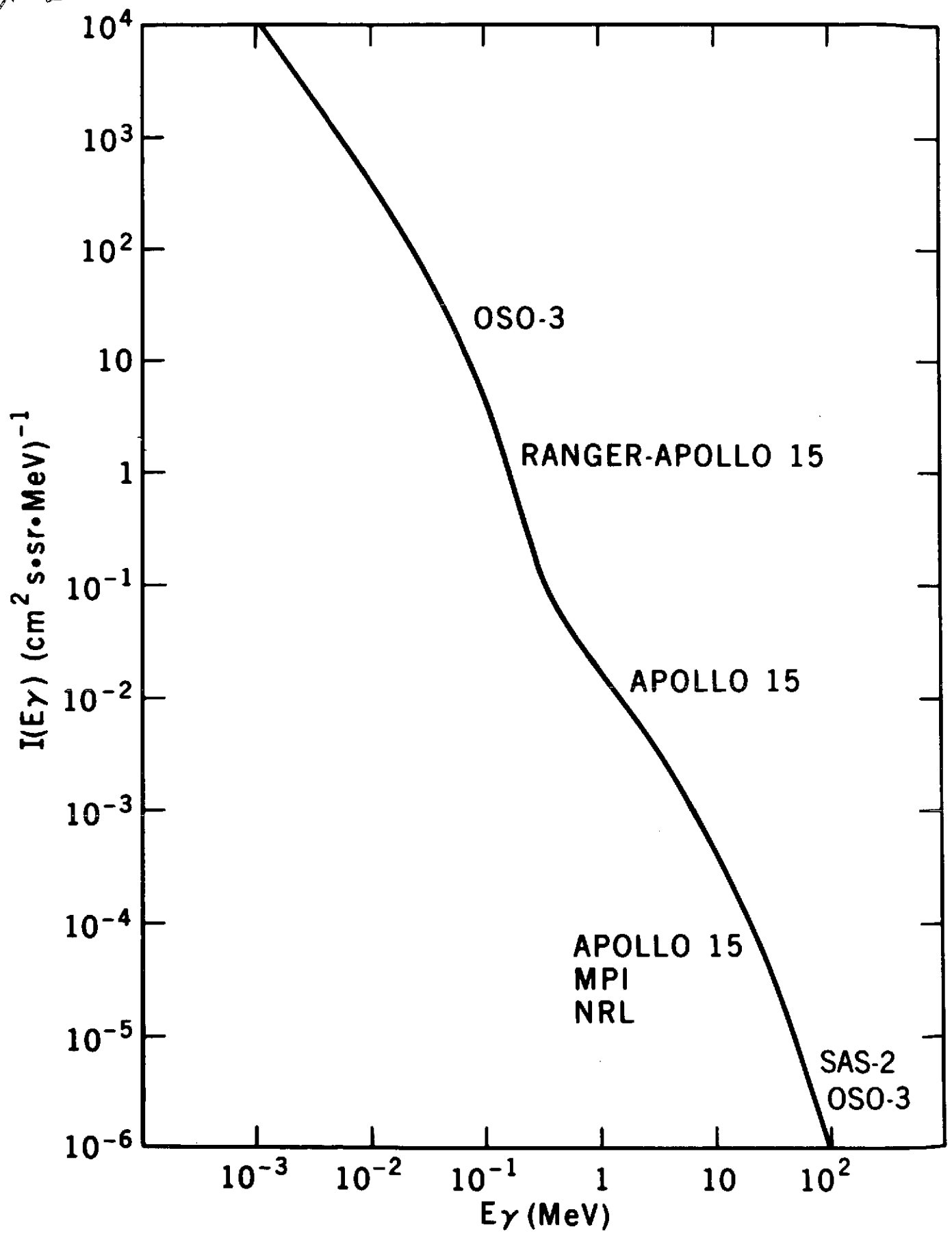


Fig. 13

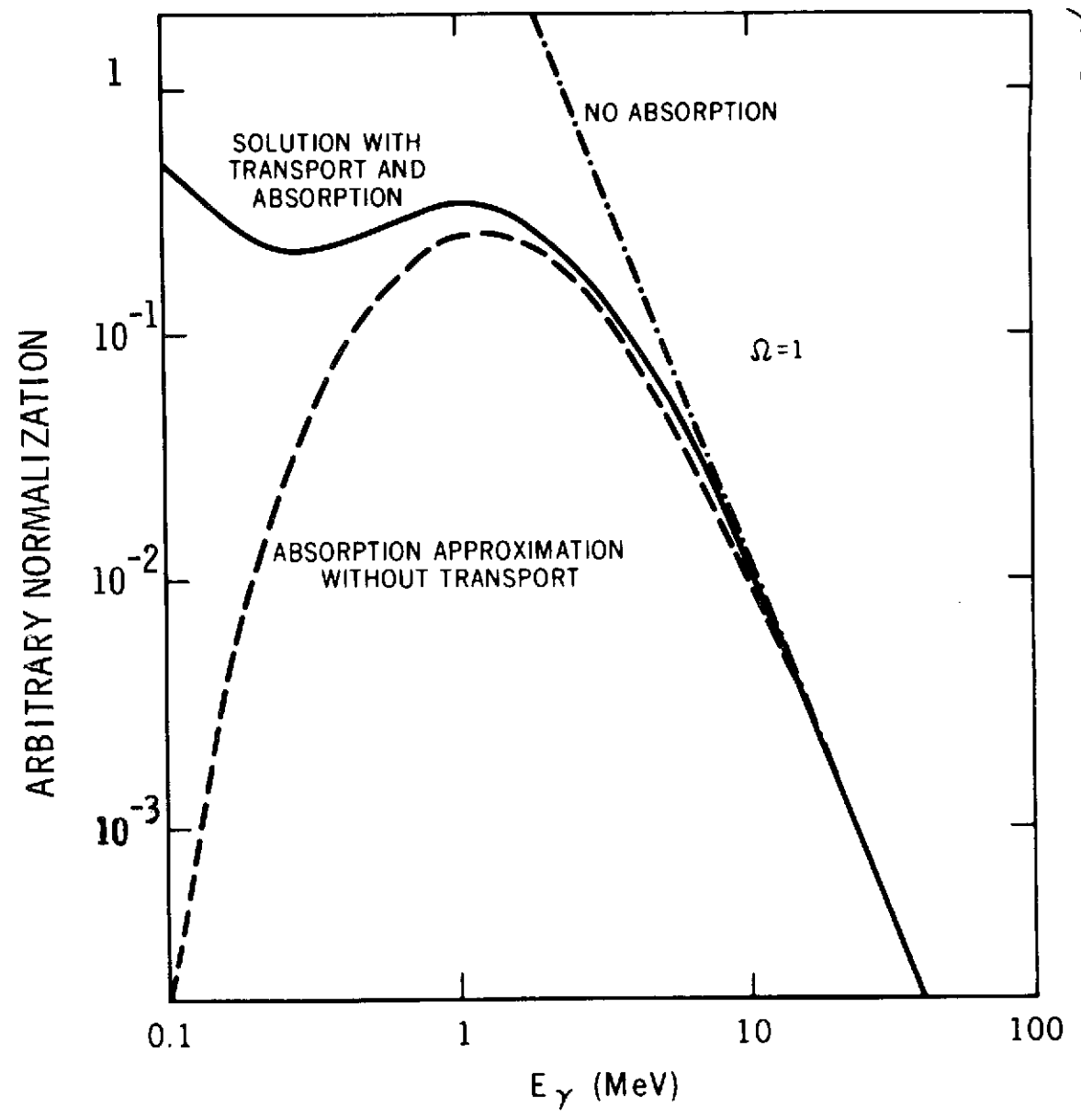
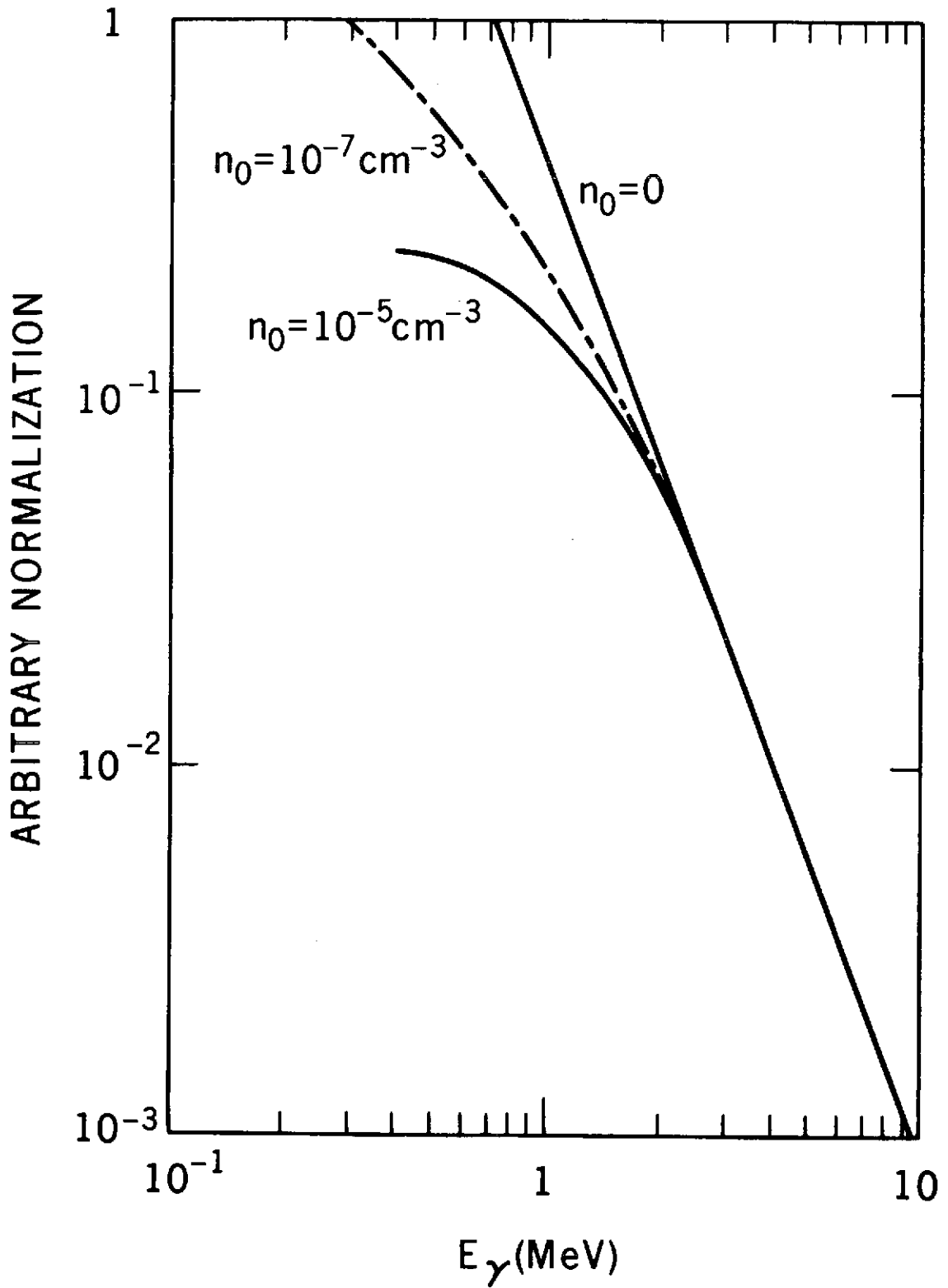


Fig. 14



### REDSHIFT AT WHICH THE UNIVERSE BECOMES OPAQUE TO PHOTONS

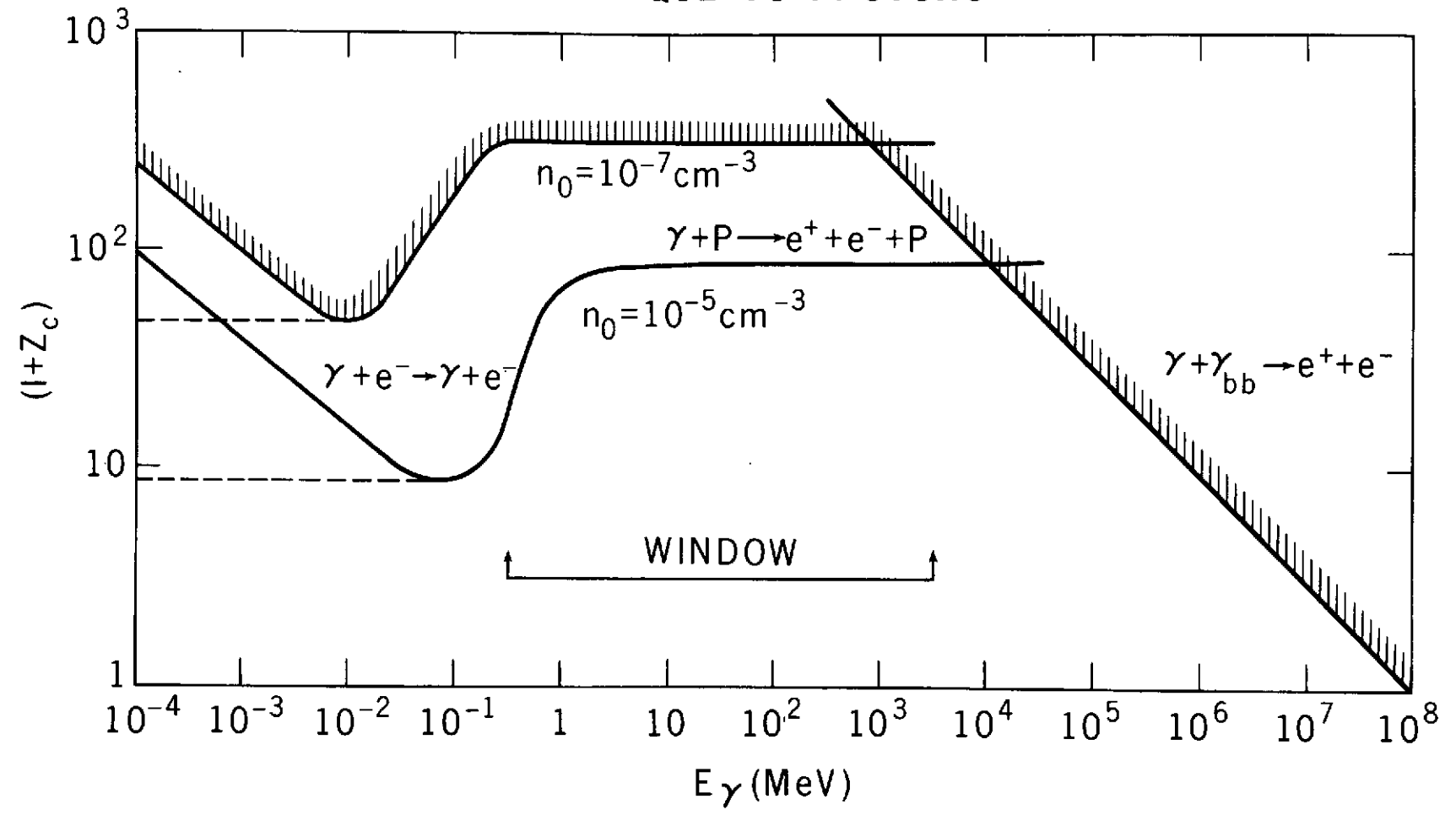


Fig. 16

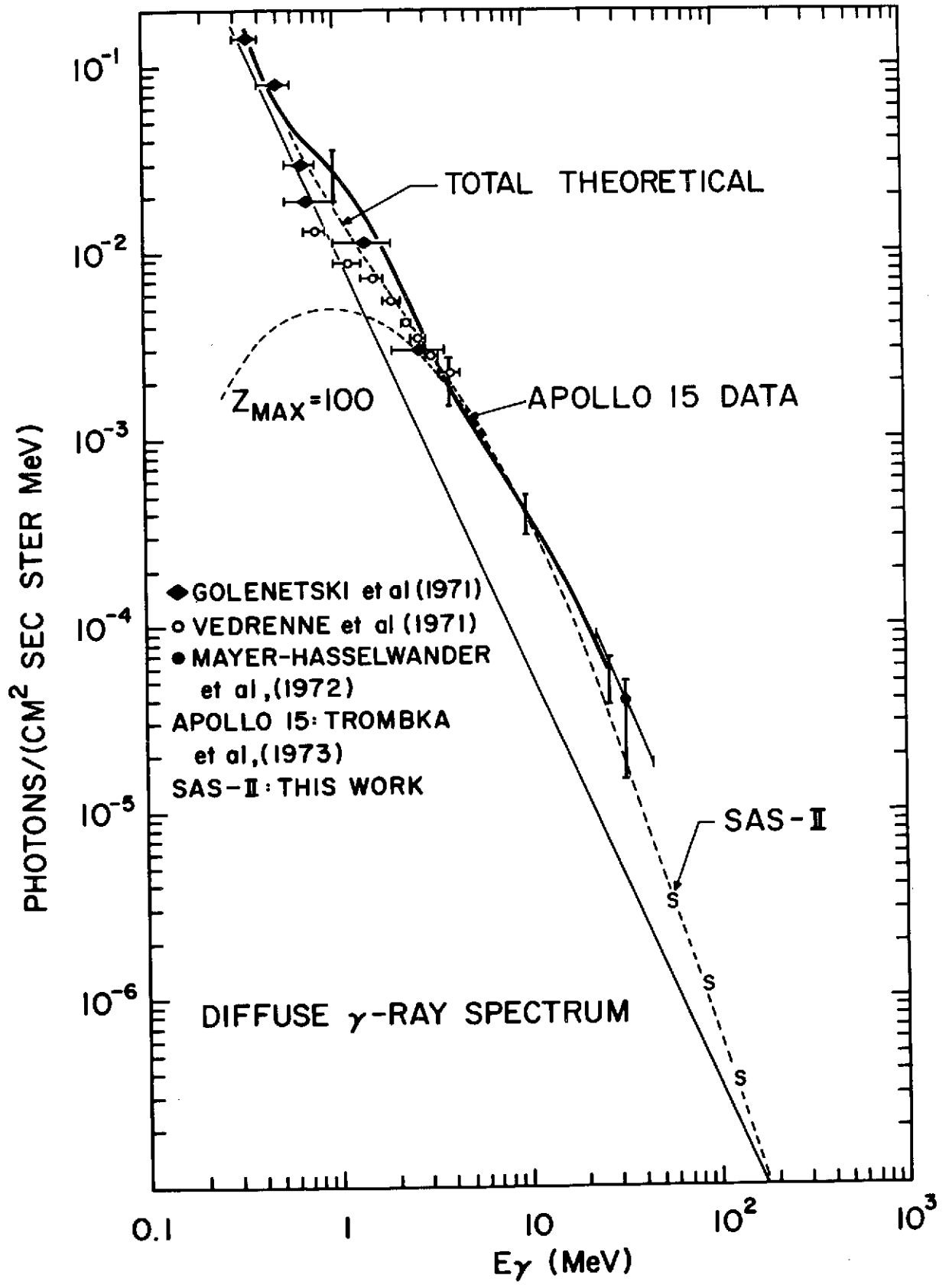
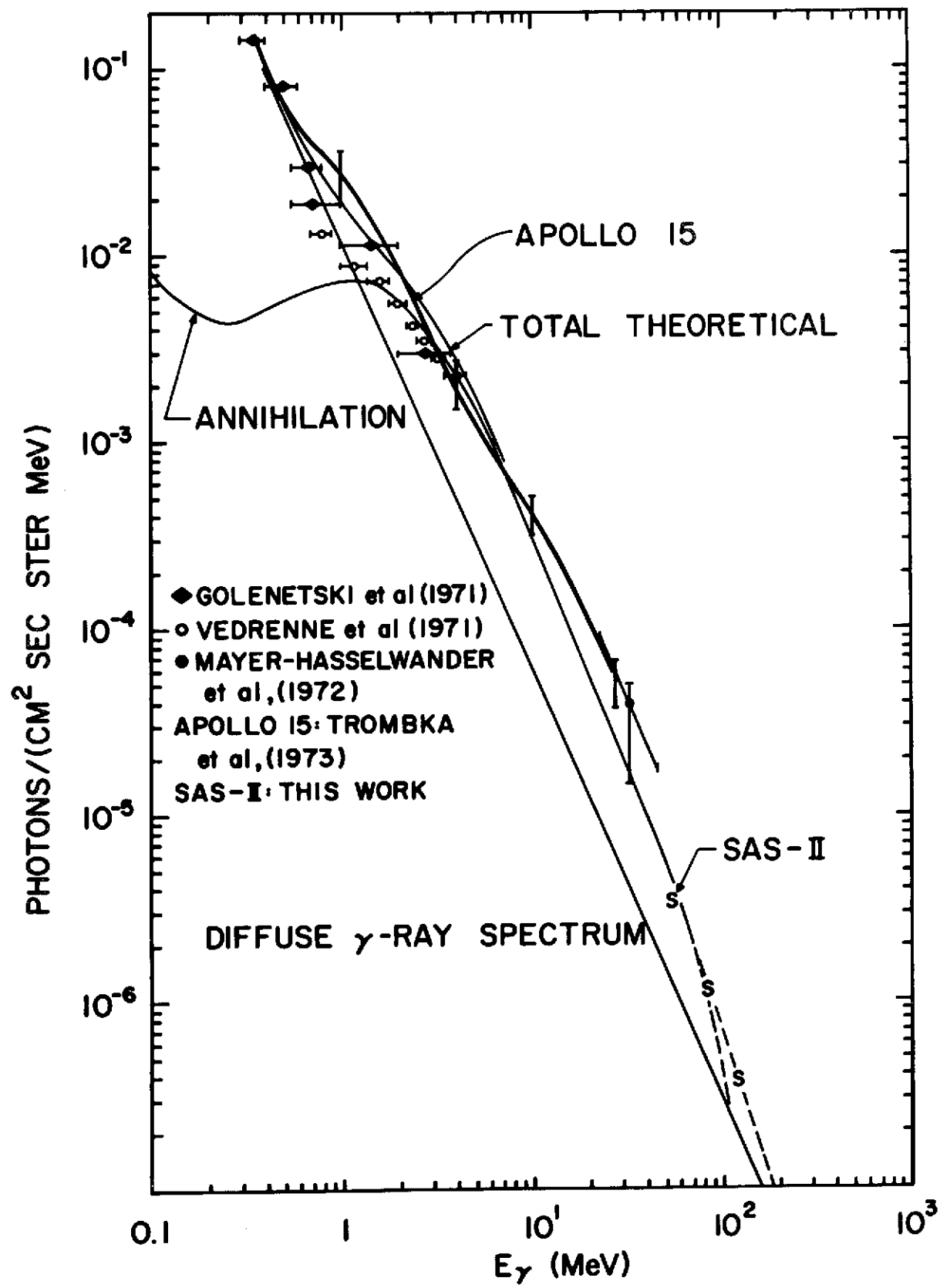


Fig. 17



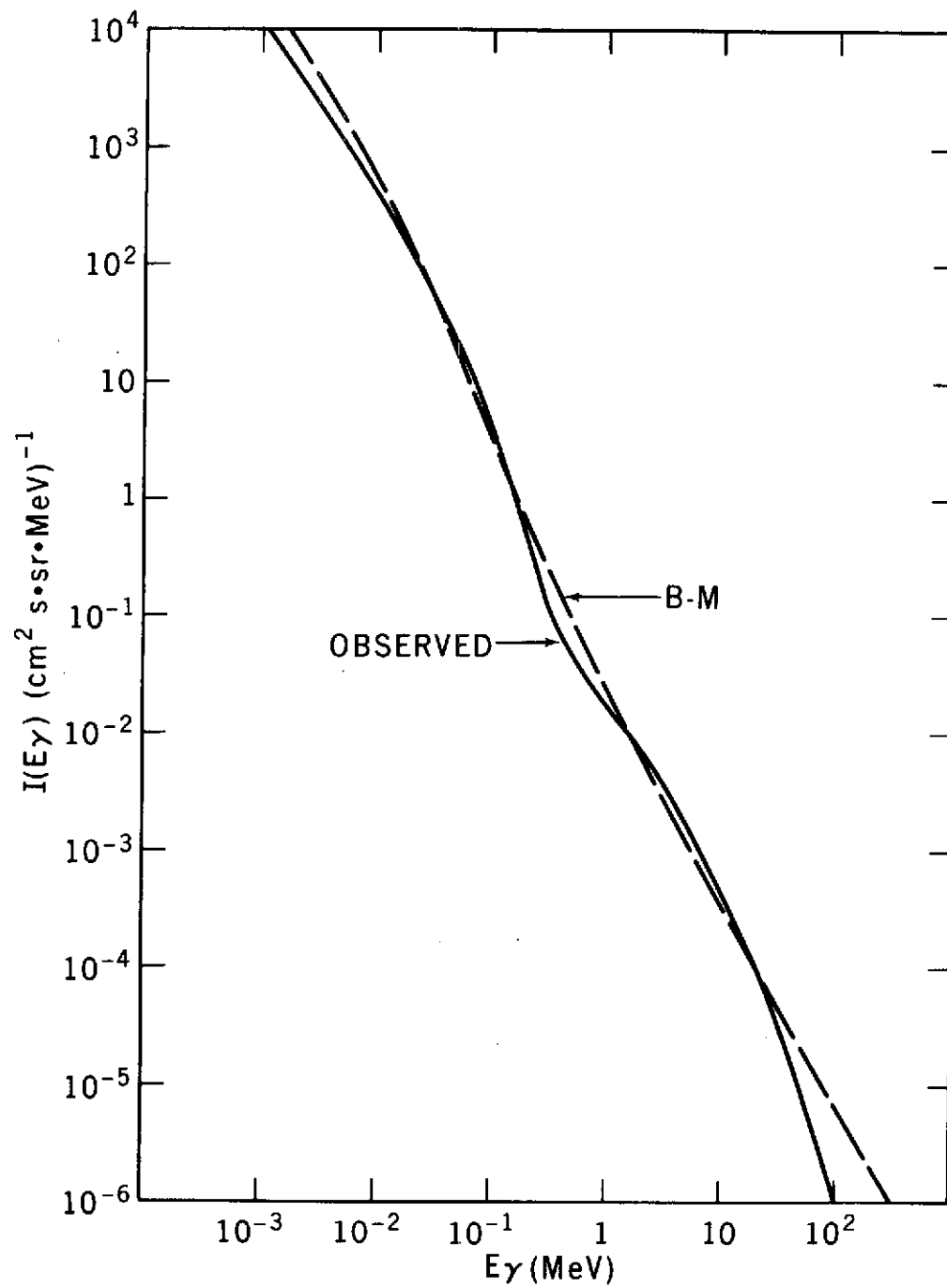
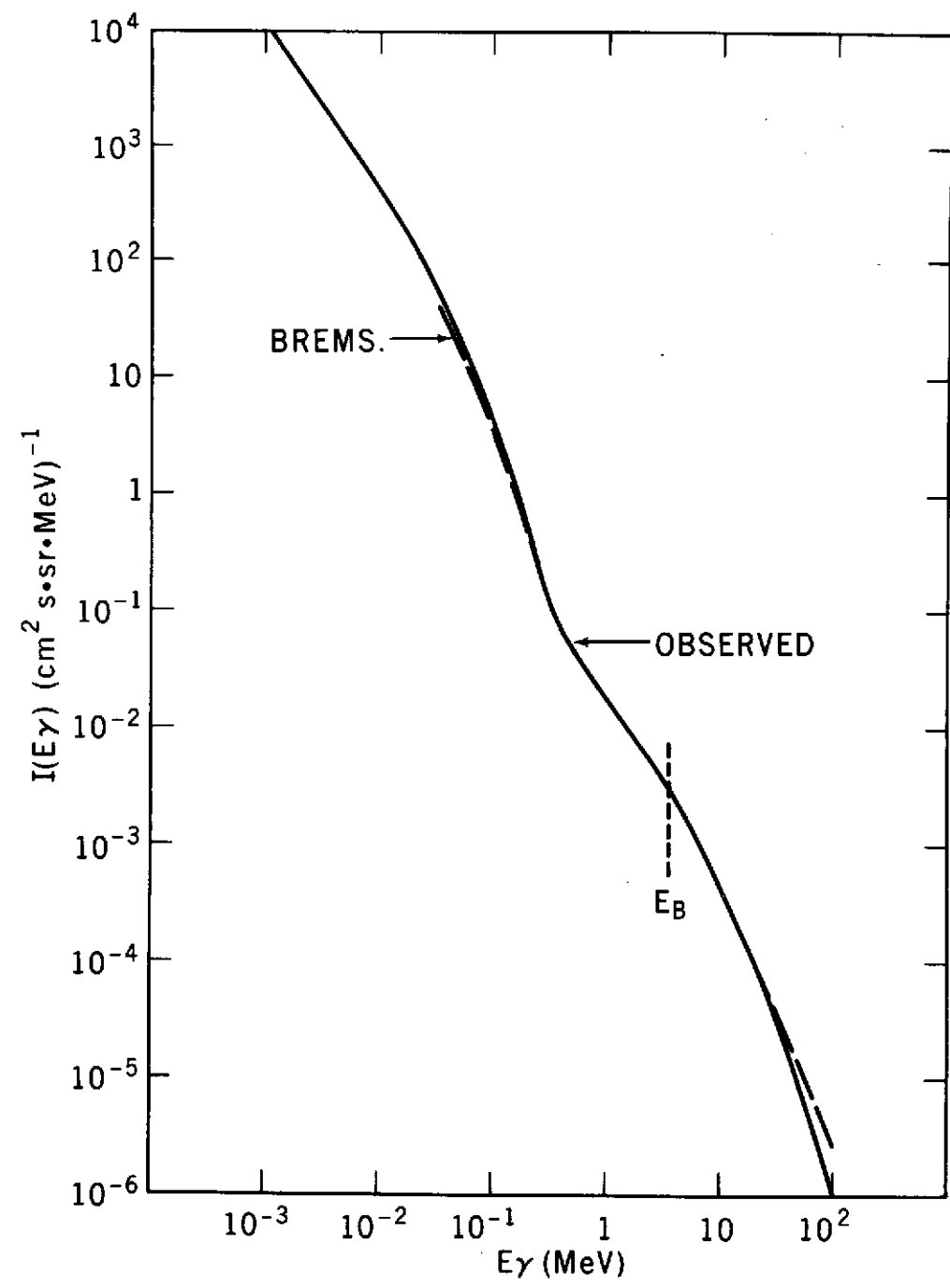


Fig. 18  
8/9/64



## Gamma-Ray Astronomy and Cosmic-Ray Origin Theory

V. L. Ginzburg  
 P. N. Lebedev Physical Institute  
 Academy of Sciences of USSR  
 Moscow, USSR

The science of  $\gamma$ -ray astronomy will yield entirely new information which cannot be obtained by optical, radio, or X-ray astronomy and which will be important for the whole study of high energy astrophysics, including the astrophysics of cosmic rays and the problem of their origin. Indeed, only  $\gamma$ -ray astronomy allows us to study the nuclear component of cosmic rays far from the Earth. (We will refer to the nuclear component here as "cosmic rays" and the electron-positron component as "relativistic electrons".)

Before the present  $\gamma$ -ray observations, we had only indirect knowledge about the cosmic-rays far from the Earth, this knowledge obtained mainly by radio observations. The radioastronomical data, as is well known, enable us to obtain the form of the relativistic electron spectrum, but the spectrum itself, and the corresponding energy density of the electrons,  $w_e$ , can be deduced only by making an additional assumption about the strength of the magnetic field  $H$  in the radiating region. To estimate the energy density of the cosmic rays,  $w_{cr}$ , we have also to assume a relation between  $w_{cr}$  and  $w_e$ . In fact, it is usually assumed that they are proportional, i.e.

$$w_{cr} = \kappa_r w_e = \kappa_H^{-1} (H^2/8\pi)V \quad (1)$$

Here  $w_{cr} = w_{cr}V$ ,  $W_e = w_eV$  and  $(H^2/8\pi)V$  are respectively the energy of the cosmic rays, the relativistic electrons and the magnetic field in the source of volume  $V$ ,  $\kappa_r = (w_{cr}/w_e)$  and  $\kappa_H = (H^2/8\pi w_{cr})$ .

Thus, from radio astronomy observations (and also knowing the distance to the source,  $R$ ) we can determine the quantities  $w_{cr}$ ,  $w_e$ , and  $H$  only by fixing the values of  $\kappa_r$  and  $\kappa_H$ . Near the Earth,  $\kappa_r \sim 100$ , and in quasiequilibrium conditions, probably  $\kappa_H \sim 1$ . These values are usually assumed, but in doing this two far-reaching assumptions are made. In nonstationary sources of cosmic rays, it is entirely possible that  $\kappa_H < 1$  or even  $\ll 1$ . Close to strong sources of infrared and optical radiation it may turn out that  $\kappa_r \gg 100$  because electrons undergo rapid energy loss. It is possible that in some cases, if mainly electrons are accelerated,  $\kappa_r \ll 100$ .

It is, in principle, possible to use radio and X-ray data together to determine the magnetic field strength,  $H$ , itself (or the quantity  $\kappa_r \kappa_H$ ) if the radio emission mechanism is synchrotron radiation and the X-radiation is produced by inverse Compton scattering of the same relativistic electrons in a known radiation field. But, here too, we cannot find the energy of the cosmic rays  $w_{cr}$  directly without assuming the values of  $\kappa_r$  or  $\kappa_H$ .

A vital question has not yet been answered concerning the energy density of cosmic rays  $w_{cr,Mg} = w_{Mg}$  in the metagalaxy (or the metagalactic region close to the galaxy). Metagalactic models for the origin of cosmic rays are still being discussed (Setti and Woltjer 1971, Burbidge and Brecher 1971, Shklovskii 1971) and are sometimes even considered preferable to galactic models for the origin of

cosmic rays. In the metagalactic models,  $w_{Mg} \approx w_G$  and  $w_G \equiv w_{cr,G} \sim 10^{-12}$  erg/cm<sup>3</sup>, is the energy density of cosmic rays at the earth and, we may also assume, in a considerable part of the galaxy. I have previously given my views on the origin of cosmic rays on many occasions (Ginzburg 1970, 1971; Ginzburg and Syrovatskii 1964, 1967, 1971). I feel that the metagalactic models are much less likely than the galactic models of the origin of cosmic rays. The main arguments rely on energy considerations and are also connected with  $\gamma$ -ray observations. However, these and other arguments are not yet conclusive, especially in regard to local metagalactic models in which  $w_{Mg} \approx w_G$  only in a restricted region in the vicinity of the galaxy.

Since we assume fewer relativistic electrons in the metagalaxy than at the earth (cf. Ginzburg 1970), in the metagalactic models far from the galaxy,  $\kappa_r \gg 100$ . It is also hard to doubt that in intergalactic space  $\kappa_H \ll 1$  since for  $\kappa_H \sim 1$ ,  $H_{Mg} \sim 5 \times 10^{-6}$  oe. Therefore, we cannot rely on radio and X-ray data to determine the cosmic ray intensity in remote regions of the galaxy and in radiogalaxies and determine the validity of the metagalactic models; it is necessary to find a new, independent method. Such a method is provided by  $\gamma$ -ray astronomy (see for instance Ginzburg and Syrovatskii 1964, 1965, Clark, Garmire and Kraushaar 1968, 1970, Fazio 1968, Stecker 1971, Cavallo and Gould 1971, Fichtel et al. 1972).

Protons and nuclei in cosmic rays collide with protons and nuclei of intergalactic and interstellar gas. As the result of these collisions, various particles are produced. Of particular importance here are the secondary  $\pi^0$ -mesons and  $\Sigma^0$ -hyperons which quickly decay to produce  $\gamma$ -rays. The probabilities and kinematics of all the essential reactions are fairly well known (Stecker 1971, Cavallo and Gould 1971) and enable us to calculate the spectrum of  $\gamma$ -rays with an accuracy which is entirely sufficient from the point of view of cosmic-ray origin theory (see the paper by Stecker, these proceedings). The integral flux of  $\gamma$ -rays from a discrete source is given by the expression

$$F_{\gamma}(>E_{\gamma}) = \int_{\Omega} I_{\gamma}(>E_{\gamma}) d\Omega \approx \frac{5 \times 10^{23} (\overline{\sigma I}_{cr}) M}{R^2} \text{ photons/cm}^2\text{s} \quad (2)$$

where  $\Omega$  is the solid angle subtended by the source,  $R$  is the distance to the source (in cm) and  $M$  is the mass of gas in the source in grams. The chemical abundances in the source are assumed to be the same as the common abundances of the elements (especially in the case of He) and thus the average mass of a gas nucleus is taken to be  $2 \times 10^{-24}$ g. The value for  $(\overline{\sigma I}_G)_{E_{\gamma} = 100 \text{ MeV}}$  is taken from Figure 1 to be  $10^{-26} \text{ S}^{-1}\text{Sr}^{-1}$  as given by Stecker (1971). Therefore

$$F_{\gamma}(>E_{\gamma}) = \frac{5 \times 10^{-3} M (w_{cr}/w_G)}{R^2} \text{ photons/cm}^2\text{s} \quad (3)$$

where  $w_{cr}$  is the cosmic-ray energy density in the source, assuming that the form of their spectrum is the same as that observed near the Earth. Within the limits of this approximation, for sources like the galaxy, where nonionized atomic hydrogen predominates,  $M = 1.2 M_{HI}$ , where  $M_{HI}$  is the mass of neutral atomic hydrogen.

The spectrum of  $\gamma$ -rays from  $\pi^0$ -decay, is concentrated mainly in the energy range above 50-100 MeV (where the  $\gamma$ -rays do not originate in highly redshifted sources). (See Figure 1 and also the paper by Stecker, these proceedings.) For  $\gamma$ -rays from pion-decay, we find

$$\xi = \frac{F_{\gamma}(E_{\gamma} > 50 \text{ MeV}) - F_{\gamma}(E_{\gamma} > 100 \text{ MeV})}{F_{\gamma}(E_{\gamma} > 100 \text{ MeV})} = 0.12 \quad (4)$$

In the case of bremsstrahlung radiation from relativistic electrons with the spectrum  $I_e(E) = KE^{-2.6}$ ,  $\xi = 2.03$ , and for the case of synchrotron radiation or inverse Compton scattering from relativistic electrons  $\xi = 0.74$ . Thus, spectral measurements of the  $\gamma$ -ray flux allow us, in principle, to distinguish between the various production processes and establish the "nuclear" nature of the  $\gamma$ -radiation. Once this is done, measurements of the flux allow us to determine the quantity  $w_{cr}/w_G$  in the source. (Here we have assumed that the cosmic-ray spectrum in the source is similar to the spectrum observed near the earth. This determination even by the method given above, would represent an important step forward and, I feel, would be a very important achievement for high-energy astrophysics.

I wish to illustrate my remarks with two examples of the potential for  $\gamma$ -ray observations of specific astronomical objects, viz., the Magellanic clouds and the galactic center. Observations of the Magellanic clouds provide a potential test for the local metagalactic origin model as well as other metagalactic models of the origin of cosmic rays. If  $w_{Mg} \ll w_G \sim 10^{-12}$  erg/cm<sup>3</sup> the metagalactic models can be discarded (Ginzburg 1972). For the Large Magellanic Cloud (LMC) and the Small Magellanic Cloud (SMC), their distances and neutral-hydrogen masses are approximately equal and are given by (Bok 1966).

$$R(\text{LMC}) = 55 \text{ kpc}, R(\text{SMC}) = 63 \text{ kpc},$$
$$M_{\text{HI}}(\text{LMC}) = 1.1 \times 10^{42} \text{ g}, M_{\text{HI}}(\text{SMC}) = 0.8 \times 10^{42} \text{ g}.$$

Therefore, if  $w_{\text{cr}} = w_G$ ,

$$F_{\gamma, \text{LMC}}(> 100 \text{ MeV}) \approx 2 \times 10^{-7}, F_{\gamma, \text{SMC}}(> 100 \text{ MeV}) \approx 1 \times 10^{-7} \text{ photons/cm}^2\text{s} \quad (5)$$

It is important here to note that the fluxes given above follow immediately for any metagalactic model because for these models, by definition, for the Magellanic clouds as well as for the galaxy, the role played by their internal cosmic-ray sources is unimportant and therefore  $w_{Mg} \approx w_G \approx w_{\text{LMC}} \approx w_{\text{SMC}}$ .

For the galactic models, on the contrary, there is no reason to expect the above quality to hold. Even assuming similar activity of cosmic-ray sources in our galaxy and the Magellanic clouds, it is probable that  $w_G > w_{\text{LMC}} > w_{\text{SMC}}$  because of the smaller sizes of the

clouds and the correspondingly more rapid escape of cosmic rays from them. Besides, in our galaxy there is apparently a strong central source of cosmic rays (which will be presently discussed), but in the clouds there is probably no such source.

Thus, if the metagalactic models are valid, the flux from both Magellanic clouds should be  $\gtrsim 3 \times 10^{-7}$  photons/cm<sup>2</sup>s. (Any additional "non-nuclear" sources of  $\gamma$ -radiation in the clouds would only serve to increase the flux.)

I now turn to the important question of  $\gamma$ -radiation from the region of the galactic center. Such radiation has already been observed (see elsewhere in these proceedings). Using the values given by Clark, Garmire and Kraushaar 1970 and Fichtel, et al. (1972), we find

$$F_{\gamma}(E_{\gamma} > 100 \text{ MeV}) = (3-10) \times 10^{-5} \text{ photons/cm}^2\text{s} \quad (6)$$

On the basis of spectral measurements (Fichtel et al. 1972) and from several indirect observations, it seems likely that we are observing  $\gamma$ -rays from the galactic center region which were produced by cosmic rays and are the products of the decay of  $\pi^0$ -mesons. Accepting this interpretation, we shall draw several conclusions (Ginzburg and Khazan 1972). By inserting the result (6) into equation (3), we conclude that the galactic center region contains a cosmic-ray component of total energy

$$W_c = w_c V_c \approx (3-10) \times 10^{56} (w_c/n_c) \sim (3-10) \times 10^{54}/n_c \text{ erg} \quad (7)$$

taking  $R = 10$  kpc. If we assume that the central source is larger than 300 pc, we cannot assume that the gas density is much greater than  $\sim 1 \text{ cm}^{-3}$ . (If  $L_c \sim 10^{21} \text{ cm}$ ,  $V_c \sim 10^{63} \text{ cm}^3$  and  $M_c \sim 2 \times 10^{39} n_c \sim 10^6 n_c M_\odot$  where  $M_\odot$  is the mass of the sun. If  $n_c \sim 10 \text{ cm}^{-3}$ ,  $M_c \sim 10^7 M_\odot$  which is probably an upper limit for an area of this size.) For  $n_c \sim 1 \text{ cm}^{-3}$ , it follows from equation (7) that  $W_c \sim (3-10) \times 10^{54}$  erg, which is only an order of magnitude smaller than the total energy of cosmic rays in the galaxy (Ginzburg 1969, Ginzburg and Syrovatskii 1971, Ginzburg 1970).

On the other hand, a result of the order of  $10^{55}$  erg is obtained from an analysis of astronomical data indicating that there was an explosion in the region of the galactic nucleus approximately  $10^7$  years ago (Oort 1971, van der Kruit 1971). A similar number for the energy of cosmic rays produced in an explosion of the galactic nucleus was used in Ginzburg and Syrovatskii (1964).

If the size of the central  $\gamma$ -ray source is less than 200-300 pc, then  $n_c$  can be greater than  $10 \text{ cm}^{-3}$ . We then obtain a smaller estimate for  $W_c$  from equation (7), but the intensity of cosmic rays  $I_{cr,c} \equiv I_c$  is not diminished. For example, if  $n_c = 10 \text{ cm}^{-3}$  and  $V_c = 10^{63} \text{ cm}^3$ ,  $W_c \sim (3-10) \times 10^{53}$  and  $I_c/I_G = W_c/W_G \sim (3-10) \times 10^2$ . It seems that it would be rather difficult to confine cosmic-rays within a smaller volume for  $10^7$  years. Therefore the value of  $W_c \sim 3 \times 10^{53}$  erg would seem to represent a lower limit and it is more likely that  $W_c \gtrsim 3 \times 10^{54}$  erg. If this is the case, the central cosmic-ray source would be

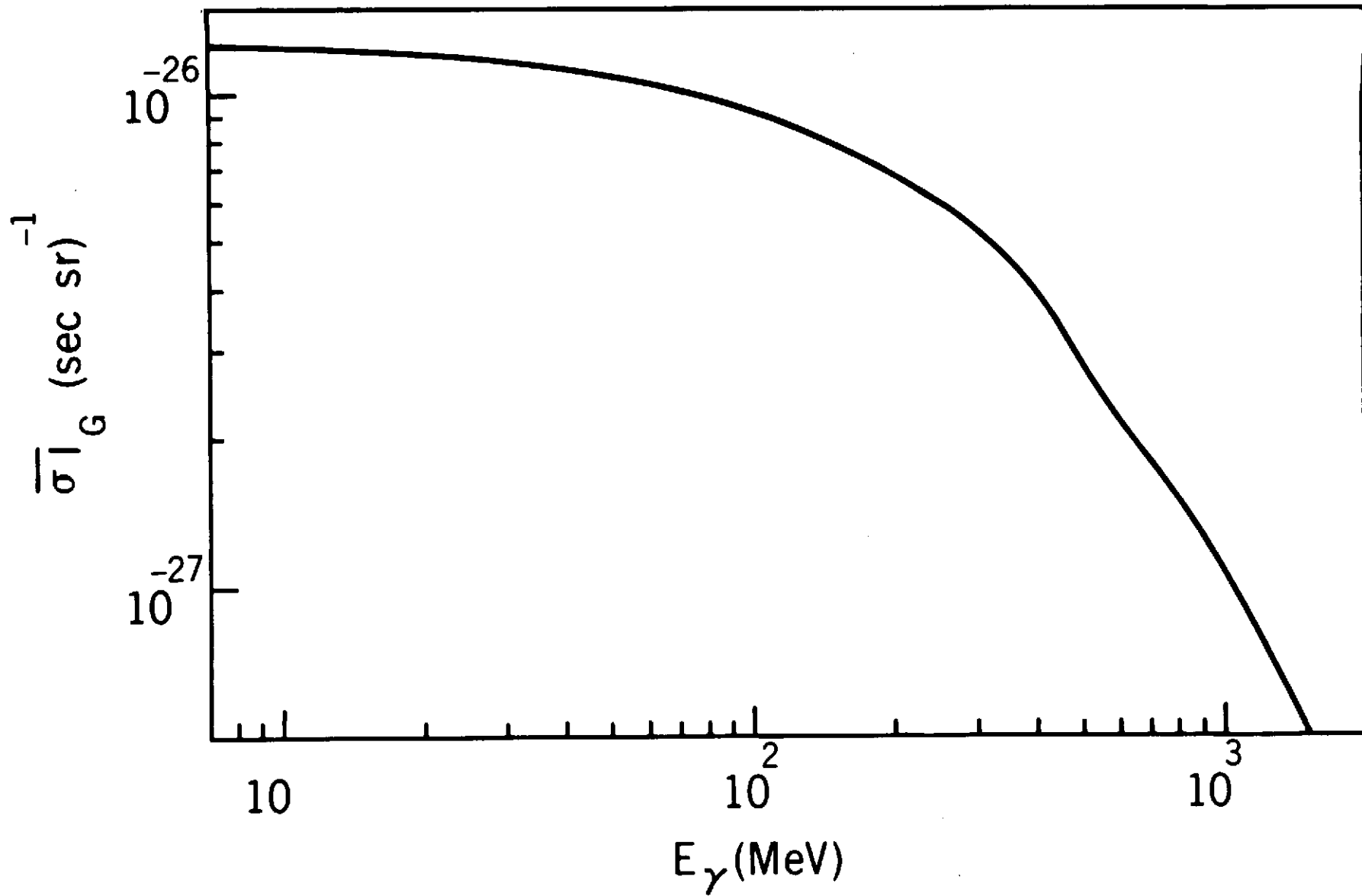
essential from the point of view of the total energy balance of cosmic rays in the galaxy. The average power of injection would be  $U_c \sim W_c/T_c \gtrsim 10^{40}$  erg/s with  $T_c = 10^7$  years). The number is of the same order of magnitude as the total power of injection used in the galactic-origin models (Ginzburg and Syrovatskii 1964, Ginzburg 1969, 1970).

If future measurements confirm the existence of a central galactic  $\gamma$ -ray source of  $\pi^0$ -decay origin, then we will have one more important argument against the metagalactic models for the origin of cosmic rays, since our own galaxy will then prove sufficient to supply a considerable part of the observed cosmic rays as opposed to other galaxies and quasars which would be the predominant source of cosmic rays in the metagalactic models. This would be true without even taking into account the production of cosmic rays in supernovae and pulsars. (In fact, I feel that the role of supernovae is essential.) The assumption of metagalactic sources for cosmic rays will thus become superfluous.

## References

- Bok, B. J., 1966, *Ann. Rev. Astron. and Astrophys.* 4, 95.
- Burbidge, G. and Brecher, K., 1971, *Comm. Astrophys. and Space Sci.*  
3, 140.
- Cavallo, G. and Gould, R. J., 1971, *Nuovo Cimento* B2, 77.
- Clark, G. W., Garmire, G. P. and Kraushaar, W. L., 1968, *Astrophys. J. (Lett.)* 153, 1203.
- Clark, G. W., Garmire, G. P. and Kraushaar, W. L., 1970, *Bull. Amer. Phys. Soc.* 15, 564.
- Fazio, G. G., 1968, *Ann. Rev. Astron. and Astrophys.* 5, 481.
- Fichtel, C., Hartman, R., Kniffen, D., and Sommer, N., 1972,  
*Astrophys. J.* 171, 31.
- Ginzburg, V. L., 1970, *Comm. Astrophys. and Space Phys.* 2; 1.
- Ginzburg, V. L., 1971, *Proc. 12th Int'l. Conf. on Cosmic Rays.*
- Ginzburg, V. L., 1972, *Nature Phys. Sci.* 239, 8.
- Ginzburg, V. L. and Khazan, Ya.M., *Astrophys. Lett.* 12, 155.
- Ginzburg, V. L. and Syrovatskii, S. I., 1964, *The Origin of Cosmic Rays* (New York; Pergamon Press).
- Ginzburg, V. L. and Syrovatskii, S. I., 1965, *Uspekhi. Fiz. Nank* 87,  
65.
- Ginzburg, V. L. and Syrovatskii, S. I., 1967, *Proc. IAU Symp. No. 31*,  
*Radio Astron. and the Galactic System* (H. van Woerden, ed.)  
(New York, Academic Press).
- Ginzburg, V. L. and Syrovatskii, S. I., 1971, *Proc. 12th Int'l. Conf. on Cosmic Rays*, pg. 53.

- Oort, J. H., 1971, Les Noyau des Galaxies, Pontifical Academia Scientiarum, p. 321.
- Setti, G. and Woltjer, L., 1971, Nature Phys. Sci. 231, 57.
- Shklovskii, 1971, Astron. Tsirkulyar SSSR 661, 1.
- Stecker, F. W., 1971, Cosmic Gamma Rays, NASA SP-249 (Washington, D. C.; U.S. Government Printing Office).
- Van der Kruit, P. C., 1971, Astron. and Astrophys. B, 405.



12

1  
N73-28765  
12

PROSPECTS FOR NUCLEAR-GAMMA-RAY ASTRONOMY\*

Donald D. Clayton  
Rice University, Houston 77001

ABSTRACT

Gamma rays emitted as a form of nuclear deexcitation offer hope of another new astronomy. I consider such gamma rays coming from two sources outside the solar system: (1) radioactive decay of fresh nuclear products of explosive nucleosynthesis, and (2) scattering of low-energy cosmic rays. The former should be detectable and will provide a factual base for many suppositions about the site and history of nucleosynthesis. The latter may be detectable and, if so, will probably provide factual information about high-flux regions of cosmic radiation.

\*Invited address to "International Symposium and workshop on Gamma-Ray Astrophysics", NASA Goddard, May 1973

## I. INTRODUCTION

Each new astronomy has provided us with new types of information. Radiations of vastly differing wavelengths tend naturally to have their origins in differing physical processes of emission, so that the different astronomies record, by and large, differing types of events. The enrichment of astronomical knowledge is obvious. If history is any reliable guide, we may expect to detect gamma-ray lines emitted during the electromagnetic deexcitation of nuclei. Their observation will confirm that excited states of nuclei are being produced, and the fluxes and spectra will identify the specific nuclei and their rate of excitation. Because extreme physical circumstances are required for the production of excited nuclei at low densities where they can be seen, unique information about the source regions will be obtainable.

In this paper I consider prospects for two sources of gamma rays from outside the solar system. Both radioactive decay and inelastic collisions produce nuclei in excited states. As Rutherford emphasized from the beginning, the radioactivity would have all passed away were it not being continually replenished. Therefore radioactive gamma-ray sources in space will be associated with events of nucleosynthesis-- probably supernova explosions of some type. The fluxes and spectra will depend on the yield of radioactive nuclei, their gamma-ray emission lines, and their halflives. Inelastic collisions with high-energy cosmic rays are probably not important sources as far as nuclear-deexcitation gamma rays are concerned. The average high-energy fluxes are known to be too small. The best prospect here is for much larger fluxes

of MeV particles, especially near the source regions. My attention will fall outside the solar system, thereby intentionally passing over the sun, moon and planets as interesting special sources.

## II. EXPLOSIVE NUCLEOSYNTHESIS

The idea that the common intermediate-mass nuclei are synthesized during their explosive ejection (Arnett and Clayton 1970) from stars, rather than before it, has one extremely important observational consequence. Several abundant nuclei are ejected in the form of radioactive progenitors, and their decay outside the star can clarify many unproven hypotheses concerning nucleosynthesis. Specifically, if the gamma-ray lines from radioactivity in supernova ejecta and in the accumulated background of the universe can be detected (and the anticipated fluxes are promising) it will be possible to:

- (1) Prove supernovae eject new nuclei and measure the supernova yield
- (2) Prove nucleosynthesis occurs during the explosion rather than prior to it
- (3) Measure the supernova structure by the profiles of the lines and their Compton tails
- (4) Discover Galactic supernova remnants
- (5) Demonstrate that nucleosynthesis is occurring today in the universe and measure its average rate today in the isotropic background
- (6) Determine whether the average rate of nucleosynthesis has been relatively constant or peaks in the distant past
- (7) Gain additional information about the average density in the universe

(8) Evaluate evolving versus steady-state cosmologies. That is a lot to promise; if it is correct, these observations will be as entertaining and profound as other great experiments in astronomy, such as the solar neutrino experiment and the microwave background experiment, for example. My object will be to outline these possibilities as a guide to the chances of successful detection.

(a) The Radioactive Species

The most abundant species having a radioactive progenitor is  $^{56}\text{Fe}$ . Bodansky, Clayton and Fowler (1968) showed that ejecta in the process of silicon burning resemble the solar abundances between  $A = 28$  and  $A = 57$  if they contain roughly equal amounts of  $^{28}\text{Si}$  and  $^{56}\text{Ni}$ . This result suggested that several prominent nuclei, primarily  $^{44}\text{Ca}$ ,  $^{48}\text{Ti}$  and  $^{56}\text{Fe}$  were ejected as radioactive  $^{44}\text{Ti}$ ,  $^{48}\text{Cr}$  and  $^{56}\text{Ni}$  respectively. Clayton and Woosley (1969) strengthened that result by showing that if the silicon burning had occurred slowly enough for beta decays to raise the neutron excess to a value for which  $^{56}\text{Fe}$  itself could be ejected during silicon burning, implausible overabundances of key species would result. They further strengthened the case for  $^{56}\text{Ni}$  by showing that something similar to an  $e$ -process centered on  $^{56}\text{Ni}$  would also synthesize otherwise troublesome  $^{58}\text{Ni}$ , especially if the free-particle densities were somewhat in excess of their equilibrium values. Clayton, Colgate and Fishman (1969) used these discoveries to make the first estimates of the importance of  $^{44}\text{Ti}$ ,  $^{48}\text{Cr}$  and  $^{56}\text{Ni}$  to the gamma-ray astronomy of young supernova remnants. Because of the centrality of the  $^{56}\text{Ni}$  vs.  $^{56}\text{Fe}$  argument, Hainebach, Arnett, Woosley and Clayton (1973) have pursued the evidence favoring  $^{56}\text{Ni}$  even further. They show that two-or-three-component  $e$ -processes with differing neutron enrichments

(and with freezeout corrections) overwhelmingly select  $^{56}\text{Ni}$  production when asked to produce the solar abundances by superposition. I think the evidence now makes it virtually certain that  $^{56}\text{Fe}$  was ejected dynamically from the synthesizing events as  $^{56}\text{Ni}$ . The preference for low- $\eta$  solutions [Arnett and Clayton (1970); Arnett (1971); Woosley, Arnett and Clayton (1973)] in explosive burning of carbon, oxygen, and silicon and continuity arguments strongly suggest that  $^{44}\text{Ca}$  and  $^{48}\text{Ti}$  were also ejected as  $^{44}\text{Ti}$  and  $^{48}\text{Cr}$ . The solar mass fractions of these species, their half lives, and the prominent gamma-ray lines emitted during their decay are included in Table 1. The  $^{56}\text{Co} \rightarrow ^{56}\text{Fe}$  decay should be, because of its rich spectrum, high abundance, and 77 day half life, the single most important radioactive decay for gamma-ray astronomy. It remains possible, however, that a less abundant product may prove to be easier to detect if the exploding remnants remain opaque too long.

Clayton (1971) discovered that a significant fraction of  $^{60}\text{Ni}$  was probably synthesized as radioactive  $^{60}\text{Fe}$ , with  $\tau_{\frac{1}{2}} = 3 \times 10^5$  yr, or perhaps as  $^{60}\text{Co}$ , with  $\tau_{\frac{1}{2}} = 5.26$ yr. In either case gamma rays of 1.17 MeV and 1.33 MeV are subsequently emitted. The arguments for and against  $^{60}\text{Fe}$  synthesis are complex and by no means certain. About 1% of  $^{60}\text{Ni}$  could be synthesized by arresting about half of the Cr seed at  $^{60}\text{Cr}$  (which decays to  $^{60}\text{Fe}$ ) in the rapid neutron-induced reactions on seed nuclei during explosive carbon burning (Howard, Arnett, Clayton and Woosley 1971, 1972). Several-to-fifty percent of  $^{60}\text{Ni}$  may have been synthesized as  $^{60}\text{Fe}$  directly from  $^{56}\text{Fe}$  seed nuclei in the same event. Clayton (1971) has made the intriguing observation in this regard that only  $^{60}\text{Ni}$  is abundant enough to have absorbed the  $^{56}\text{Fe}$  seed in explosive carbon

burning, thereby suggesting that much of the iron seed has been arrested at  $^{60}\text{Fe}$ . Because of the strong (p,n) flows during high temperature carbon burning, it also seems plausible that a percent or so of the  $^{60}\text{Ni}$  is due to  $^{60}\text{Co}$  nuclei ejected in the explosion. Although  $^{60}\text{Co}$  synthesis should be less efficient than  $^{60}\text{Fe}$  synthesis, it may nonetheless be more important in young remnants because of its favorable half-life, which is long enough to assure transparency yet short enough to have a detectably high decay rate. Without going in to the matter further here, I let  $p_{60}$  be the percentage (i.e. fraction  $\times 100$ ) of  $^{60}\text{Ni}$  nuclei synthesized as  $^{60}\text{Fe}$  nuclei and  $p'_{60}$  be the percentage synthesized as  $^{60}\text{Co}$ , and I expect

$$1 > p_{60}(\%) < 50$$

$$0.1 < p'_{60}(\%) < 5$$

I note here that Clayton (1971) did not explicitly include  $^{60}\text{Co}$  in his considerations. However, there do appear to be circumstances in which the gamma rays due to  $^{60}\text{Co}$  synthesis could, for many years, exceed those due to synthesis of all other nuclei.

The r-process synthesizes many heavy radioactive nuclei, which are expected to have unfortunately small yields. Clayton and Craddock (1965) considered the flux expected from supernova remnants if the r-process yield were great enough for the "californium hypothesis" of Type I light curves to be correct. In particular they calculated the expectations of the Crab nebula in that regard. There is a large range of half-lives present in initial transbismuth debris, however, so their conclusions on the 920 year-old Crab (that the strongest line should be no greater than  $10^{-4} \text{ cm}^{-2} \text{ sec}^{-1}$ ) would require re-

Table 1. Average Supernova Yield ( $1.7 \times 10^9$  SN)

Nucleus	$X_{\odot}$	Progenitor	$\tau_{1/2}$	$Y_{SN}$	$E_Y$ (%) MeV
$^{56}\text{Fe}$	$1.3 \times 10^{-3}$	$^{56}\text{Co}$	77d	$3.0 \times 10^{54}$	0.84(100), 1.24(67), 2.60(17), 1.03(16), 1.76(14), 3.26(13), 2.02(11), $e^+$ (20)
$^{56}\text{Co}$	$1.3 \times 10^{-3}$	$^{56}\text{Ni}$	6.1d	$3.0 \times 10^{54}$	0.812(85), 0.748(51), 0.472(34), 1.56(15)
$^{48}\text{Ti}$	$2.3 \times 10^{-6}$	$^{48}\text{Cr} \rightarrow ^{48}\text{V}$	16d	$6.2 \times 10^{51}$	0.983(100), 1.31(97), $e^+$ (50)
$^{44}\text{Ca}$	$1.9 \times 10^{-6}$	$^{44}\text{Ti} \rightarrow ^{44}\text{Sc}$	48yr	$5.6 \times 10^{51}$	1.156(100), $e^+$ (94)
$^{60}\text{Ni}$	$2.0 \times 10^{-5}$	$^{60}\text{Fe}(\%p_{60})$ $^{60}\text{Co}(\%p'_{60})$	$3 \times 10^5$ yr 5.26yr	$4.4 \times 10^{52}$	1.17(100), 1.33(100)
$^{238}\text{U}$ (example)	$1.3 \times 10^{-10}$	r-process (example)	$4.5 \times 10^9$ yr	$1.3 \times 10^{47}$	Transuranic plus daughters (many weak possibilities)
$^{57}\text{Fe}$	$3.3 \times 10^{-5}$	$^{57}\text{Ni} \rightarrow ^{57}\text{Co}$	270 d	$7.5 \times 10^{52}$	0.122(98), 0.136(98)

calculation for remnants having different ages and distances. The main problems with this idea would seem to be that it requires the r-process to be concentrated in relatively rare events in order that these nuclei not be greatly overproduced and that there seems to be no compelling reason to associate the Type I light curves with radioactivity. I therefore currently hold little hope for this gamma-ray source, although additional clarifying remarks will be made later.

(b) Typical Supernova Yield

In the absence of more certain knowledge, I take a simple model of galactic nucleosynthesis in supernovae. Arnett and Clayton (1970) and, more specifically, Arnett (1971) have described the conceptual framework more accurately; however, my aim is only to extract typical numbers for the typical supernova event. Let the explosively synthesized nuclei be coproduced in the same abundance ratios that we find in the solar system in identical supernova events occurring at the Galactic rate

$$\dot{N}_{SN} = R e^{-t/T_R}. \quad (1)$$

Fowler (1972) finds that  $T_R \approx 4 \times 10^9$  yr and Galactic age  $A_G = 12 \times 10^9$  yr are not unreasonable caricatures of r-process nucleosynthesis (which I take here to characterize all explosive nucleosynthesis). Taking a current supernova rate  $N_{SN}^0$  (today) =  $0.025 \text{ yr}^{-1}$  then gives  $R = 0.5 \text{ yr}^{-1}$ . The initial supernova rate would, with these particular parametric values, have been twenty times greater.

Let the average yield of the typical event be such that its product with the total number of events prior to the birth of the sun shall have produced a galactic mass having solar composition. The total number of such events is

$$N_{SN} = \int_0^{t_{\odot}} \dot{N}_{SN} dt = \dot{N}_{SN}^0 T_R \left[ 1 - e^{-t_{\odot}/T_R} \right] e^{A_G/T_R} \quad (2)$$

where  $t_{\odot}$  is the time of solar formation (approximately  $7 \times 10^9$  yrs). The number of events is nearly exponential in  $A_G/T_R$  and multiplied by  $T_R$  if  $T_R < t_{\odot}$ , as seems likely. With the specific choice of parameter values taken above,  $A_G/T_R = 3$  and the number of events would have been  $N_{SN} = 1.7 \times 10^9$ .

If the mass of the Galaxy is  $1.8 \times 10^{11} M_{\odot}$  (Schmidt 1965) and the mass fraction of iron in the sun is  $X_{\odot} = 1.3 \times 10^{-3}$  (Cameron 1968), and if the average composition of the galaxy at that time was solar, the galaxy would have contained  $2.3 \times 10^8 M_{\odot}$  of  $^{56}\text{Fe}$ . The average yield for each of the  $1.7 \times 10^9$  contributing events would have been

$$M_{SN}(^{56}\text{Fe}) = \frac{2.3 \times 10^8 M_{\odot} \text{ of } ^{56}\text{Fe}}{1.7 \times 10^9 \text{ SN events}} = 0.14 M_{\odot}/\text{SN}. \quad (3)$$

The corresponding number of  $^{56}\text{Fe}$  atoms per event is

$$Y_{SN}(^{56}\text{Fe}) = \frac{0.14 (2.0 \times 10^{33}) (6.0 \times 10^{23})}{56} = 3.0 \times 10^{54} \quad (4)$$

which would have been ejected initially as  $^{56}\text{Ni}$  atoms. These numbers for several interesting abundances formed explosively as radioactive progenitors are shown in Table 1.

It is not difficult to question the appropriateness of many of the assumptions leading to this estimate. However, my point of view is that the simplest reasonable argument is the most appropriate one for gearing our expectations.

Table 1 shows the total yield of  $^{60}\text{Ni}$  to be  $Y_{\text{SN}}(^{60}\text{Ni}) = 4.4 \times 10^{52}$  atoms persupernova. According to the earlier discussion, the yields of  $^{60}\text{Fe}$  and  $^{60}\text{Co}$  are evaluated as

$$\begin{aligned} Y_{\text{SN}}(^{60}\text{Fe}) &= 4.4 \times 10^{50} P_{60} \\ Y_{\text{SN}}(^{60}\text{Co}) &= 4.4 \times 10^{50} P'_{60} \end{aligned} \quad (5)$$

The yield of  $^{238}\text{U}$  under these assumptions is listed in Table 1 only as an example of transbismuth r-process yield rather than as a nucleus of particular importance for gamma-ray astronomy. Indeed, Clayton and Craddock found that the most important nuclei for the Crab were likely to be  $^{249}\text{Cf}$  and  $^{214}\text{Bi}$ . Nonetheless it is instructive to note that this "typical  $^{238}\text{U}$  yield" is about four orders of magnitude too small for that required for the californium hypothesis of the light curve. If the latter hypothesis is correct, the r-process will have to have occurred in events about  $10^4$  times less numerous than the typical supernovae we are considering in this section. Whereas this is possible, it suggests that all Type I events are not r-process events, in which case the original hypothesis loses its raison d'etre.

### (c) Typical Line Fluxes

If species Z decays with mean lifetime  $\tau(Z) = 1/\lambda_Z$ , and if each decay is accompanied by  $g_i$  photons of type i, then the flux of those gamma rays at the earth due to a nearby

supernova is

$$F_i = g_i \frac{\lambda_z Y_{SN}(Z)}{4\pi R^2} e^{-\lambda_z t} \quad (6)$$

where R is the distance to the supernova and t is the time since its detonation. This formula neglects attenuation due to absorption or scattering in the source and will, therefore, be correct only for times long enough that the expanding remnant has become transparent to gamma rays.

Using information from Table 1 one obtains

$$F_i(^{56}\text{Ni}) = g_i \frac{3.3 \times 10^4}{R^2(\text{kpc})} e^{-(t/8.8\text{d})} \text{cm}^{-2} \text{s}^{-1} \quad (7)$$

$$F_i(^{56}\text{Co}) = g_i \frac{2.6 \times 10^3}{R^2(\text{kpc})} e^{-(t/111\text{d})} \text{cm}^{-2} \text{s}^{-1} \quad (8)$$

$$F_i(^{48}\text{V}) = g_i \frac{26}{R^2(\text{kpc})} e^{-(t/23\text{d})} \text{cm}^{-2} \text{s}^{-1} \quad (9)$$

$$F_i(^{44}\text{Ti}) = g_i \frac{2.1 \times 10^{-2}}{R^2(\text{kpc})} e^{-(t/69\text{yr})} \text{cm}^{-2} \text{s}^{-1} \quad (10)$$

$$F_i(^{60}\text{Fe}) = g_i \frac{2.7 \times 10^{-7} p_{60}}{R^2(\text{kpc})} e^{-(t/4.3 \times 10^5 \text{yr})} \text{cm}^{-2} \text{s}^{-1} \quad (11)$$

$$F_i(^{60}\text{Co}) = g_i \frac{1.6 \times 10^{-2} p'_{60}}{R^2(\text{kpc})} e^{-(t/7.6\text{yr})} \text{cm}^{-2} \text{s}^{-1} \quad (12)$$

Several of these fluxes are shown in Figure 1 as a function of time. The supernova itself has been placed at  $R = 10^3$  kpc to emphasize that the A = 56 lines may even be observable from supernovae in other galaxies. A supernova in M31, for example,

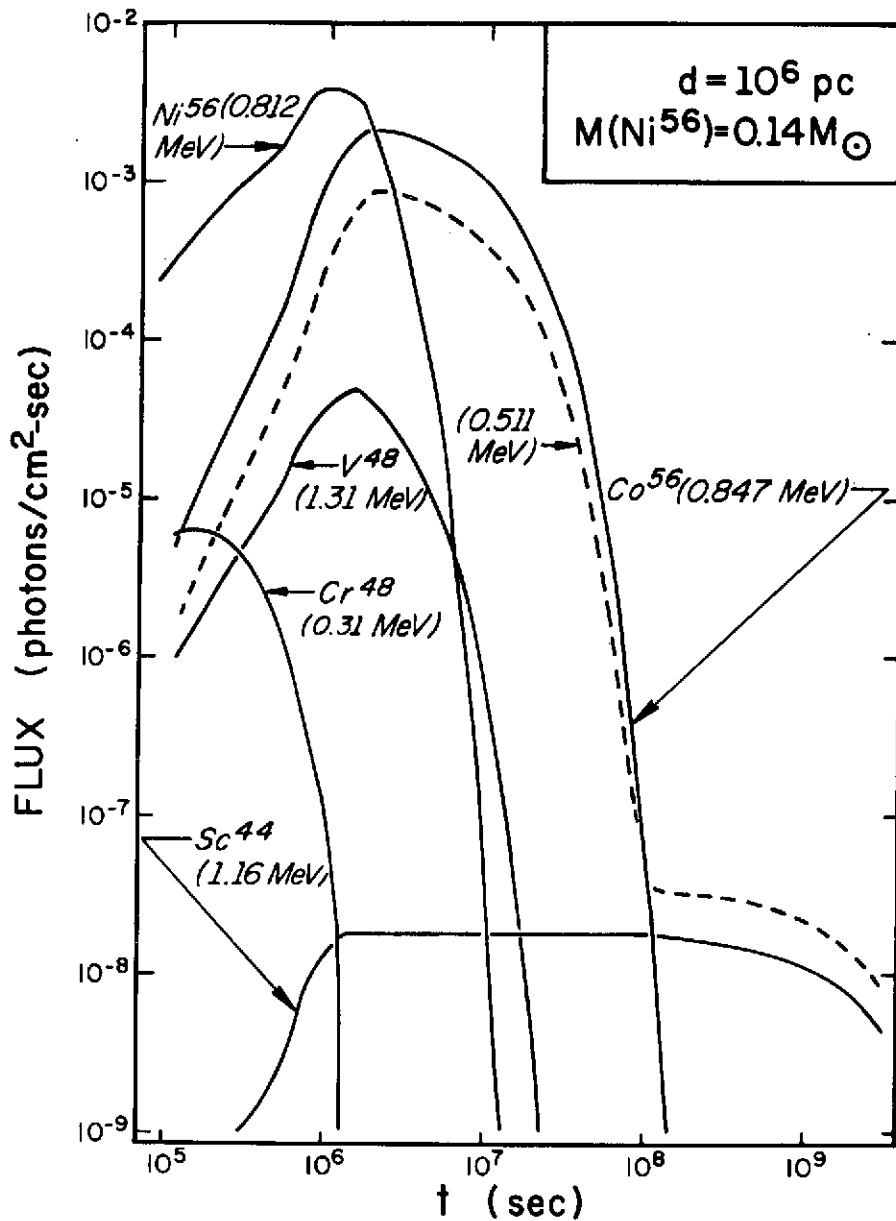


Figure 1. Prominent medium-lifetime gamma-ray line fluxes as a function of time from a distant ( $d=10^6$  pc) supernova ejecting  $0.14M_{\odot}$  of  $^{56}\text{Ni}$  and  $2.0 \times 10^{-4} M_{\odot}$  of  $^{44}\text{Ti}$ . The early growth reflects the increasing transparency of an expanding model (Clayton et al 1969)

would present a  $^{56}\text{Co}$  line flux above the detectable level of about  $10^{-4} \text{ cm}^{-2} \text{ sec}^{-1}$  for more than a year. These lines show a rise time, rather than a pure exponential decay, because a specific model was adopted by Clayton et al. (1969) for the transparency of the expanding supernova. They took a rather optimistic (in light of recent nucleosynthesis theory) model-- a  $0.5 M_{\odot}$  ball of iron expanding at  $1.7 \times 10^9 \text{ cm/sec}$  so that the product of mean density times radius is

$$\bar{\rho}(t) R(t) \approx 8 \times 10^{13} t^{-2} \text{ gm cm}^{-2} \quad (13)$$

which falls below  $10 \text{ gm cm}^{-2}$  (a rough estimate of the optical depth for gamma rays) for  $t > 3 \times 10^6 \text{ sec}$ . Thus at best the lines will be poorly visible for the first month. Even then it is clear that Compton scattering will have a serious effect on the gamma-ray spectrum near those times when they begin to emerge. Brown (1973) has calculated this effect for some special cases similar to those considered by Clayton et al. (1969). Figure 2 shows one of his results, when 3.5 MeV and 1.25 MeV lines are emitted isotropically from a depth of  $18.6 \text{ gm cm}^{-2}$  within an iron sphere of radius  $37.2 \text{ gm cm}^{-2}$ . The total mass of such a sphere depends upon its metric radius, of course, so with  $R(t) = 1.7 \times 10^9 t$  we find that the mass whose line spectrum corresponds to Figure 2 is

$$M(\text{Fig. 2}) = \left( \frac{t}{2 \times 10^6 \text{ sec}} \right)^2 M_{\odot} \quad (14)$$

Therefore the total mass of that example could be any reasonable multiple of the solar mass at time of order a few months. The question of the mass of layers over-lying the CO core at the time of detonation is even more uncertain, but it will

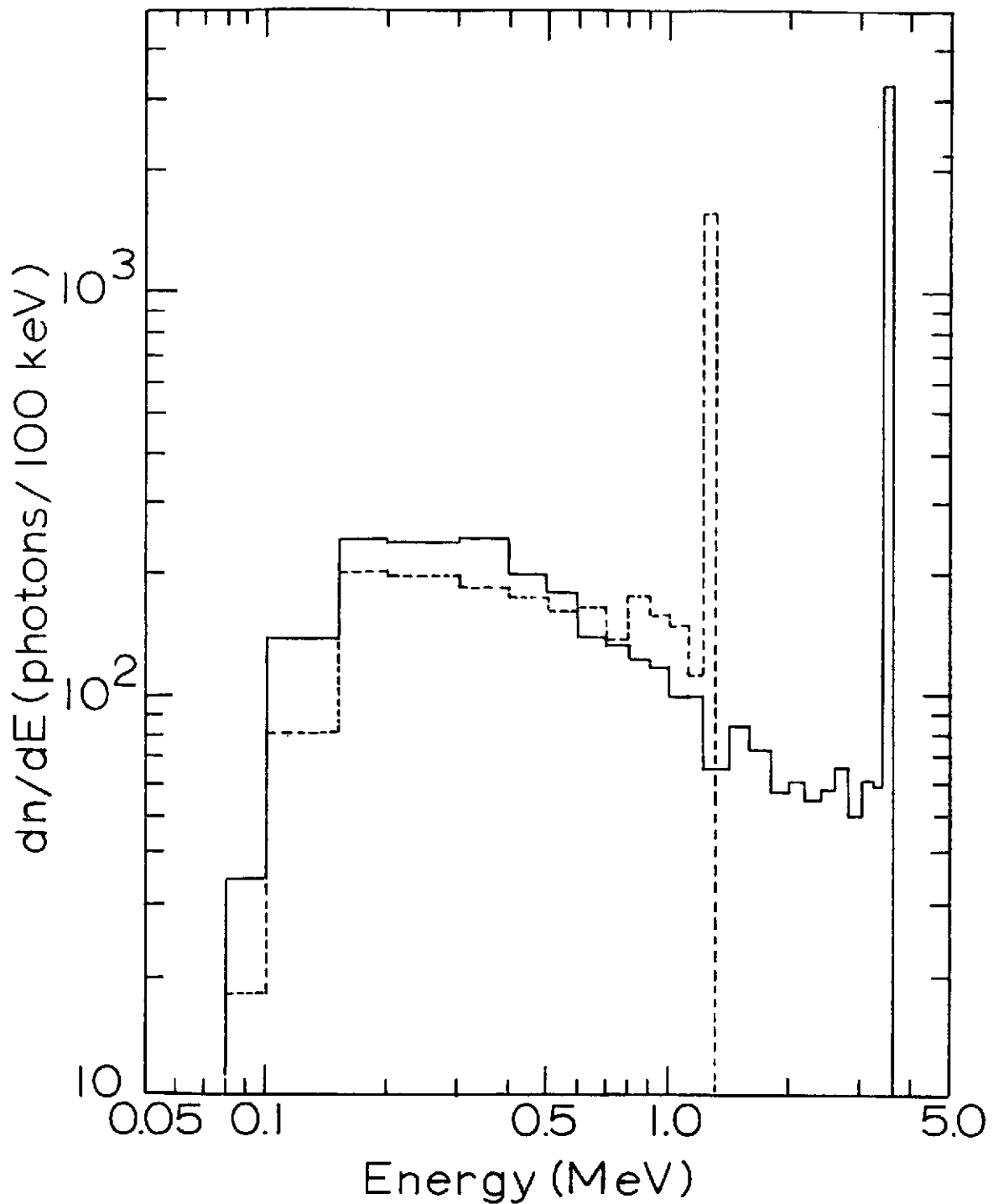


Fig.2. Effect of Compton scattering on 3.5 MeV lines (solid histogram) and 1.25 MeV lines (dashed histogram) emitted isotropically from a point at a depth of  $18.6 \text{ gm cm}^{-2}$  from the surface of an Fe sphere of radius  $37.2 \text{ gm cm}^{-2}$  (Brown 1973).

clearly be worthwhile to evaluate dynamic models of gamma-ray opacity for exploding massive evolved stars. For the time being I wish only to emphasize that whether the  $^{56}\text{Ni}$  lines emerge at all (they did in Fig. 1) depends on the structure and dynamics of the exploding object. Ideally we may one day watch these and the  $^{56}\text{Co}$  lines rise to peak intensity before beginning their decay, and the rise time of these fluxes will be a crucial measure of the structure of the exploding object. The 270-day  $^{57}\text{Co}$  lines from  $^{57}\text{Ni}$  progenitors may also play an important role in this problem (Clayton 1973), although I have not included them here due to their relatively low energies (136 keV and 122 keV). This astronomy will allow us to measure that structure somewhat analogously to the way neutrino astronomy has allowed us to measure the interior of the sun -- and probably with all the surprises!

The 1.16 MeV line emitted subsequent to the decay of the  $^{44}\text{Ti}$  could be quite strong in several present Galactic remnants, and will surely emerge even if the A = 56 lines should happen not to get out. In this sense the  $^{44}\text{Ti}$  synthesis may prove to be extremely important. The real need, of course, is for the Galaxy to arrange a visible supernova, preferably after (if ever) instruments like HEAOB are operational. The A = 48 lines, on the other hand, seem likely to be of no special importance, because they are both weaker and shorter lived than the  $^{56}\text{Co}$  lines.

The  $^{60}\text{Co}$  lines have not been entered on Figure 1, but a comparison of Eqs. (12) and (10) show that they are comparable to those of  $^{44}\text{Ti}$  for about 10 years if  $p'_{60}$  is around unity (i.e. about 1% of  $^{60}\text{Ni}$  is due to synthesis of  $^{60}\text{Co}$ , which requires about 2% of  $^{56}\text{Fe}$  seed to reside at  $^{60}\text{Co}$  at completion of explosive carbon burning). Remnants throughout the Galaxy ( $R < 20$  kpc) should ultimately prove detectable for a decade.

The  $^{60}\text{Fe}$  lines (actually the same as the  $^{60}\text{Co}$  lines but with a much longer half-life) are also not shown in Figure 1.

They are a special case due to the long  $3 \times 10^5$  yr halflife, which insures that many radiating remnants exist but they may have large angular size due to the long time available for dispersal. For the flux to exceed a detectable  $10^{-4} \text{ cm}^{-2} \text{ sec}^{-1}$  requires  $R \leq 160$  pc if 10% of  $^{60}\text{Ni}$  is due to synthesis of  $^{60}\text{Fe}$ . A circle of 160pc radius constitutes about  $10^{-4}$  of the area of the Galactic disk, and should thus contain one of the approximately  $10^4$  supernovae that should have occurred during the lifetime of  $^{60}\text{Fe}$ . The size of a remnant  $10^5$  years old might cover a significant fraction (even half!) the sky for an event about 100pc away, however, so simple on-source-off-source differences will have to be measured with this in mind. The radiation from such sources seems more likely to appear as a general galactic background. The general flux from a wide angle containing the galactic center would be

$$F_{60} (\text{Galactic}) \approx 3 \times 10^{-4} \text{ cm}^{-2} \text{ sec}^{-1} \quad (15)$$

if  $p_{60}$  is about 10%. This is also about the same as the average flux from the Galaxy due to the  $^{44}\text{Ti}$  lines (Clayton 1971), but in this case the actual flux depends on the details of the positions and times of the last few Galactic supernovae.

As a very crude estimate of transbismuth fluxes, I will assume that every transbismuth species is synthesized with a yield  $Y_{\text{SN}}$  equal to that listed for  $^{238}\text{U}$  in Table 1. There are so many different halflives in the r-process ejecta, moreover, that one may roughly assume that, whatever the age of the remnant, there exists one gamma producing nucleus with a halflife approximately equal to the age of the remnant. This species produces the largest flux. In this case Eq. (6) becomes

$$F_i (\lambda_i = t^{-1}) = g_i \frac{Y_{\text{SN}}(r)}{4\pi R^2} \frac{e^{-1}}{t} \quad (16)$$

which has the approximate value

$$\overline{F}_r = \frac{1.25 \times 10^{-5}}{R^2 (\text{kpc}) t (\text{yrs})} \text{ cm}^{-2} \text{ s}^{-1} \quad (17)$$

It is obvious that these fluxes will not commonly be observable unless the r-process is restricted to much rarer events, thereby raising the yield of each event. This conclusion, stated earlier, renders this particular prospect unlikely. Clayton and Craddock (1965) took a yield four orders of magnitude greater to provide radioactive power for the Crab light curve and were thereby able to calculate marginally detectable lines from the Crab. Equation (17) yields only  $\overline{F}_r \approx 10^{-8} \text{ cm}^{-2} \text{ s}^{-1}$  from the Crab, and is probably a more realistic estimate. The site of the r-process is so poorly understood, however, that a great surprise would come as no shock.

#### (d) The Universal Background

One need only appreciate that the average Galactic luminosity due to radioactive gamma rays has been  $3 \times 10^{40} \text{ erg sec}^{-1}$  to realize that their contribution to the isotropic background radiation may be significant. The cosmological principle allows us to estimate their flux very easily. Taking  $H_0 = 55 \text{ km sec}^{-1} \text{ Mpc}^{-1}$  (Sandage 1972), the observed universal density of matter is  $\rho = 1.7 \times 10^{-31} \text{ gm cm}^{-3}$  (Oort 1958). If the average mass fraction of  $^{56}\text{Fe}$  is  $X_{\odot} (^{56}\text{Fe}) = 1.3 \times 10^{-3}$ , this corresponds to  $2.2 \times 10^{-34} \text{ gm cm}^{-3}$  of  $^{56}\text{Fe}$ . Consequently, the average iron number density in the observed universe is

$$n(^{56}\text{Fe}) = 2.3 \times 10^{-12} \text{ cm}^{-3} \quad (18)$$

The flux of these gamma rays per steradian is (Clayton and Silk 1969)

$$\frac{\partial F}{\partial \Omega} = \frac{c}{4\pi} g_{\gamma} n(^{56}\text{Fe}) \quad (19)$$

where  $g_{\gamma}$  is the number of gamma rays emitted per  $^{56}\text{Fe}$  nucleus synthesized. The value of  $g_{\gamma}$  is 2.8 for only  $^{56}\text{Co}$  decays and  $g_{\gamma} = 4.9$  if both  $^{56}\text{Ni}$  and  $^{56}\text{Co}$  decays are used. Taking the latter value yields

$$\frac{\partial F}{\partial \Omega} = 2.7 \times 10^{-2} \text{ cm}^{-2} \text{ ster}^{-1} \text{ sec}^{-1} \text{ ,} \quad (20)$$

To emphasize the size of this flux, Clayton and Silk pointed out that it is as large as the total integrated universal background at photon energies in excess of 300 keV! Clearly it must be an important component of that background unless the  $A = 56$  lines do not escape from their sources. Because this estimate is based on the observed mass density, it will be proportionately greater if the universe contains "hidden matter" that has also synthesized  $^{56}\text{Fe}$ .

The simple density argument does not determine the frequency distribution of the photons comprising the flux in equation (19). For those  $^{56}\text{Fe}$  nuclei synthesized early in the universe, the associated gamma rays will now have been considerably redshifted. It is just this feature that allows the spectrum to carry a wholly new astrophysical datum; i.e. the redshift distribution in the gamma-ray spectrum measures the distribution of the ages of  $^{56}\text{Fe}$  nuclei. Hidden in it is the chronological account of the rate of nucleosynthesis.

Let  $f(t)$  be the rate per unit of cosmic time at which  $^{56}\text{Fe}$  nuclei were (and are being) synthesized. Let it be normalized such that

$$\int_0^{t_0} f(t) dt = 1 \quad (21)$$

so that  $f(t)dt$  is the fraction of all  $^{56}\text{Fe}$  nuclei that were synthesized at cosmic time  $t$  in the interval  $dt$  ( $t_0 =$  cosmic time today). It follows that  $f(t)dt$  is also the fraction of  $A = 56$  gamma rays whose travel times are  $t_0 - t$  in the interval  $dt$ . In any standard cosmological model the travel time  $t_0 - t$  is some function of the redshift  $z$ . Thus  $f(t) = f(z)$  and  $f(t)(dt/dz)dz$  becomes the fraction of the photons having redshift  $z$  in the interval  $dz$ . The gamma-ray source function per unit time per unit  $^{56}\text{Fe}$  nucleus per unit energy interval in the rest frame is just

$$\mathbf{P}(E, t) = \sum_i P_i(E, t) = \sum_i g_i \delta(E - E_i) f(t) \quad (22)$$

where the sum is over the lines of type  $i$  emitted with rest energy  $E_i$  at the rate of  $g_i$  gammas per  $^{56}\text{Fe}$  nucleus synthesized. The differential flux today due to gamma rays of type  $i$  is

$$\begin{aligned} \frac{\partial^2 F_i}{\partial E \partial \Omega} &= \frac{c}{4\pi} n(^{56}\text{Fe}) \int_0^{t_0} \frac{R(t_0)}{R(t)} P_i \left[ \frac{R(t_0)}{R(t)} E, t \right] dt \\ &= \frac{c}{4\pi} n(^{56}\text{Fe}) \int_0^\infty (1+z) P_i \left[ (1+z)E, t \right] \frac{dt}{dz} dz \quad (23) \end{aligned}$$

where  $E$  is the energy today of the photon and  $R(t)$  is the scale factor of the universe. [e.g., McVittie 1965].

Because

$$\frac{E}{E_i} = \frac{R(t)}{R(t_0)} = \frac{1}{1+z} \quad (24)$$

the integral over cosmic emission time can also be expressed as an integral over received energies:

$$dt = \frac{R(t_0)}{R(t)} \frac{dE}{E_i} \quad (25)$$

This integral is easily done due to the  $\delta$ -function nature of  $P_i$  to give

$$\frac{\partial^2 F_i}{\partial E \partial \Omega} = \frac{c}{4\pi} \frac{g_i n(^{56}\text{Fe})}{E_i} \frac{R(t_0)}{R(t_E)} f(t_E) \quad (26)$$

where the time  $t_E$  is the solution of Eq.(24). In the Friedman dust models one has [e.g. Weinberg 1972]

$$\frac{R(t_E)}{R(t_0)} = \frac{E_i}{E} H_0 \left[ 1 - 2q_0 + 2q_0 \frac{E_i}{E} \right]^{\frac{1}{2}} \quad (27)$$

so that Eq.(26) reads

$$\frac{\partial^2 F_i}{\partial E \partial \Omega} = \frac{c}{4\pi} \frac{g_i n(^{56}\text{Fe})}{E_i H_0} f(t_E) \left[ 1 - 2q_0 + 2q_0 \frac{E_i}{E} \right]^{-\frac{1}{2}} \quad (28)$$

Clayton and Silk (1969) evaluated the flux in a simpler form for the two cases where

$$R(t) \propto t^{1/\gamma} \quad (29)$$

They are the low-density universe ( $q_0 \approx 0$ ,  $\gamma \approx 1$ ) and the Einstein-de Sitter universe ( $q_0 = \frac{1}{2}$ ,  $\gamma = 3/2$ ). In those

cases Eq.(24) can be explicitly solved for  $t_E$  and, furthermore, the factor involving  $q_0$  simplifies:

$$\frac{\partial^2 F_i}{\partial E \partial \Omega} = \frac{c}{4\pi} \frac{g_i n(^{56}\text{Fe})}{E_i H_0} f\left[t_0 \left(\frac{E}{E_i}\right)^\gamma\right] \left(\frac{E}{E_i}\right)^{\gamma-1} . \quad (30)$$

It is straightforward to confirm with Eq.(28) or Eq.(30) that

$$\int_0^{E_i} \frac{\partial^2 F_i}{\partial E \partial \Omega} dE = \frac{c}{4\pi} g_i n(^{56}\text{Fe}) \quad (31)$$

as required by photon conservation.

The spectrum due to each line is characterized by a step at the rest energy

$$\Delta \left( \frac{\partial^2 F_i}{\partial E \partial \Omega} \right)_{E=E_i} = \frac{c}{4\pi} \frac{g_i n(^{56}\text{Fe})}{E_i H_0} f(t_0) \quad (32)$$

that is directly proportional to the average rate of nucleosynthesis today in the universe. Detection of the series of correlated rest edges will confirm that nucleosynthesis is still occurring and measure its present rate  $f(t_0)$ . Each rest edge is followed at immediately lower energies by identical redshifted continua, whose shape and extent depend upon the cosmological model and the history  $f(t)$  of galactic nucleosynthesis. It is interesting to note that the ratio  $f(t_0)/H_0$  is a ratio of characteristic times:  $1/H_0$  is approximately the age of the universe and  $1/f(t_0)$  would be the time required to synthesize  $X_0(^{56}\text{Fe})$  at a constant rate  $f(t_0)$ .

Some simple profiles for the  $^{56}\text{Co}$  line of 1.24 MeV are shown in Figure 3. If nucleosynthesis has occurred within galaxies at a constant rate up to the present time  $t_0$  since it began at some time  $t_*$ , then  $f(t) = (t_0 - t)^{-1}$  between  $t_*$  and  $t_0$  and is zero elsewhere. The left half of Figure 3 shows that case

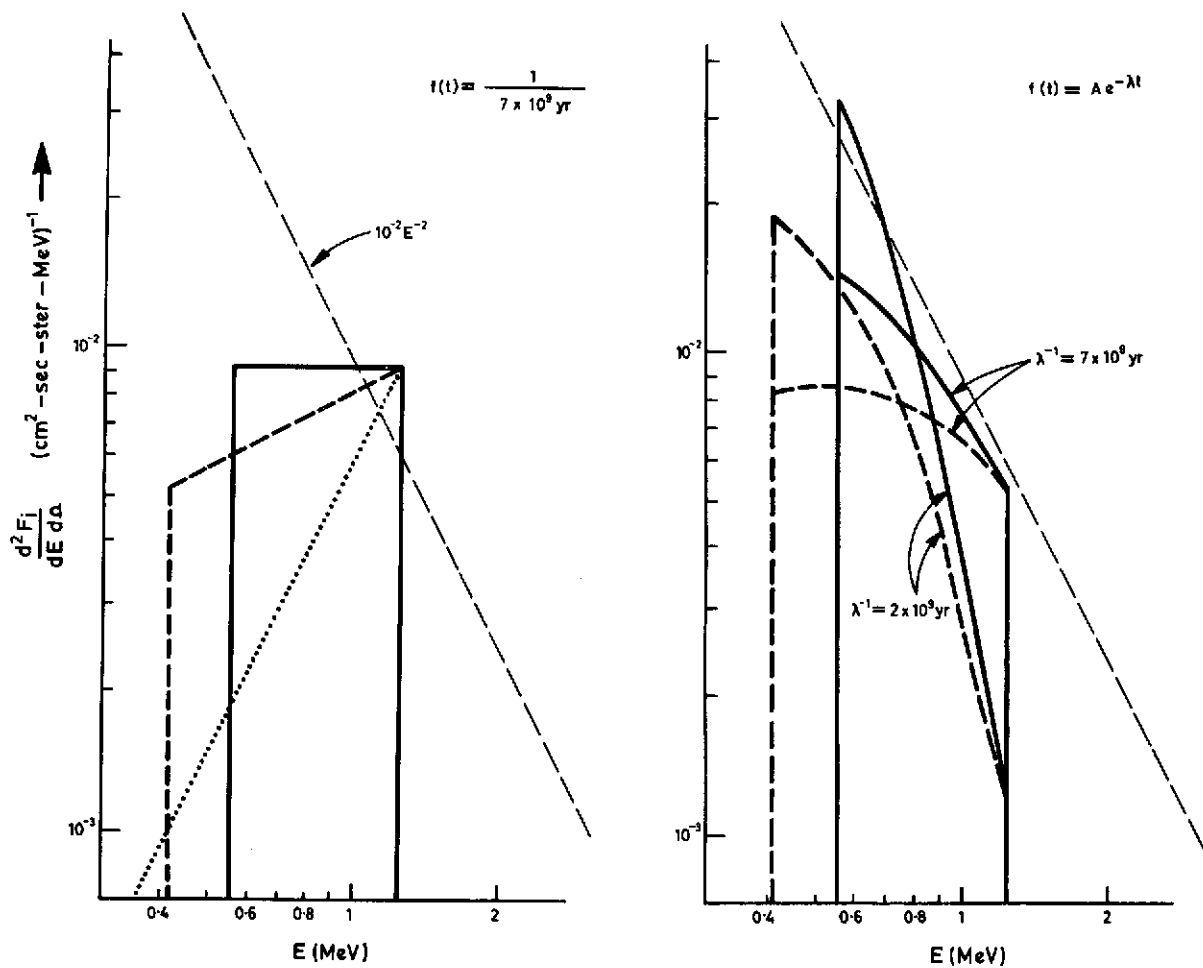


Figure 3. Differential flux due to a single line ( $^{56}\text{Co}$  at 1.24 MeV). Models of constant galactic synthesis of  $^{56}\text{Fe}$  over a period of  $7 \times 10^9$  yr are shown on the left, and models of exponentially decreasing nucleosynthesis are shown on the right. This rather short duration of galactic nucleosynthesis was chosen only for ease of comparison, so that it could fit in the age of the Einstein-de Sitter universe with  $H_0 = 75$  km/sec/Mpc. The low density universe is shown as a solid line and the Einstein-de Sitter as a dashed line. The steady-state-universe line profile is dotted on the left figure. The line  $10^{-2} E^{-2}$  is also shown to indicate the approximate level of the observed diffuse background. (Clayton and Silk 1969)

from Clayton and Silk (1969), who took  $t_0 - t_*$  =  $7 \times 10^9$  yrs so that it could fit easily within the Einstein-de Sitter universe based on  $H_0 = 75$  km/sec/Mpc. The right half of Figure 3 shows this line profile for exponential nucleosynthesis  $f(t) = A \exp[-\lambda(t-t_*)]$ , where  $A$  is a normalization constant and  $\lambda = 1/T_R$  from Eq. (1). The two choices of  $\lambda$  shown there give different relative strengths to present-day nucleosynthesis in comparison with the initial galactic rates. The rest edges are still detectable here, but smaller than for the case of constant nucleosynthesis.

It is worth noting here that these figures are applicable to Sandage's (1972) value  $H_0 = 55$  km/sec/Mpc if one only increases  $t_0 - t_*$  by the factor  $75/55$ , giving the more reasonable  $t_0 - t_* = 9.6 \times 10^9$  yr, and if the value of the flux is reduced by the factor  $(55/75)^2$ . The latter comes about because  $n(^{56}\text{Fe}) \propto H_0^2$  and  $f(t) \propto H_0$  if we require  $t_0 - t_* \propto H_0^{-1}$ . It is clear that the flux at this rest edge may well be comparable to the isotropic background, whose approximate value is shown for comparison. The model  $T_R = 4 \times 10^9$  yr and  $A_G = 12 \times 10^9$  yr used in estimating the typical supernova yield resembles the curve labeled  $\lambda = (2 \times 10^9 \text{ yr})^{-1}$  in Figure 3. Its rest edge is the smallest shown -- about 15 percent of the observed background. Such small edges would go undetected unless observers design detectors and use data reduction methods designed to extract the steps from the continuous background.

The steady-state universe, shown as a dotted line in Figure 3, affords a somewhat different problem. To maintain a constant iron density requires a creation rate

$$c = 3Hn(^{56}\text{Fe}) = \text{constant}, \quad (33)$$

so the gamma rays are created at the rate  $g_i C$ . The age distribution of  $^{56}\text{Fe}$  nuclei is no longer given by the galactic production function  $f(t)$ , because galaxies of all differing ages coexist. The density of nuclei having age  $t_0 - t$  in the interval  $dt$  is simply

$$dN(t_0 - t) = 3Hn(^{56}\text{Fe}) e^{-3H(t_0-t)} dt. \quad (34)$$

Both results follow directly from the fact that the scale factor for the proper distance between comoving-coordinate points is

$$\frac{R(t_0)}{R(t)} = e^{H(t_0-t)} = 1+z \quad (35)$$

where  $z$  is the redshift of a photon whose travel time is  $t_0 - t$ . Since Eq.(35) is also the ratio of the rest energy  $E_i$  to the received energy  $E$ , Eq.(34) is easily rewritten as a distribution in energy of photons of type  $i$ :

$$dN_i(E) = 3g_i n(^{56}\text{Fe}) \left(\frac{E}{E_i}\right)^2 \frac{dE}{E_i} \quad (36)$$

and the differential flux is, as before,

$$\frac{\partial^2 F_i}{\partial E \partial \Omega} = \frac{c}{4\pi} \frac{dN_i(E)}{dE} \quad (37)$$

The flux is independent of both the Hubble constant and the details  $f(t)$  of galactic production, and the spectrum is proportional to  $E^2$  up to the rest edge  $E_i$ . This spectrum is the dotted one in Figure 3. It is of interest to note that Eq.(32) for the size of the rest edge gives the correct answer in this

case also if the present production rate  $f(t_0)$  is replaced by  $3H$  according to Eq. (33):

$$\Delta \left( \frac{\partial^2 F_i}{\partial E \partial \Omega} \right)_{E=E_i} = \frac{c}{4\pi} \frac{3g_i n(^{56}\text{Fe})}{E_i} \quad (38)$$

In setting this rest edge equal to those of the evolving universe in Figure 3 we have been somewhat arbitrary, because  $f(t_0)/H_0 \approx 2$  for the evolving models in the left side of the figure, whereas the steady state gives the slightly larger value 3. However, the average proper density  $n(^{56}\text{Fe})$  could also differ slightly from the value inferred from the solar composition--but not much, because the average galactic age  $(3H_0)^{-1} \approx 6 \times 10^9$  yrs is also approximately the age our Galaxy had when the solar system formed.

The main point of the steady-state cosmology is that the strong rest edge and the  $(E/E_i)^2$  spectrum remain even if the Galactic production function  $f(t)$  were strongly peaked in the past, as in the evolving cosmologies in the right. If the lines emerge unscattered from the sources, a strict steady-state universe will have very strong rest edges--like saw teeth.

Figure 4 illustrates the entire A=56 spectrum for the Einstein-de Sitter case. Two points need be made: (1) the rest edges are clearly more prominent in the case of constant galactic nucleosynthesis than they are in the  $e^{-2}$ -exponential case, but (2) the general shape of the continuum feature produced is quite similar for the two cases. The Einstein-de Sitter universe requires thirty times more mass than has been observed in galaxies, but Figure 4 assumes that only the observed galaxies contain  $^{56}\text{Fe}$ . If nonvisible matter has undergone nucleosynthesis the spectrum normalization would have to be increased. One

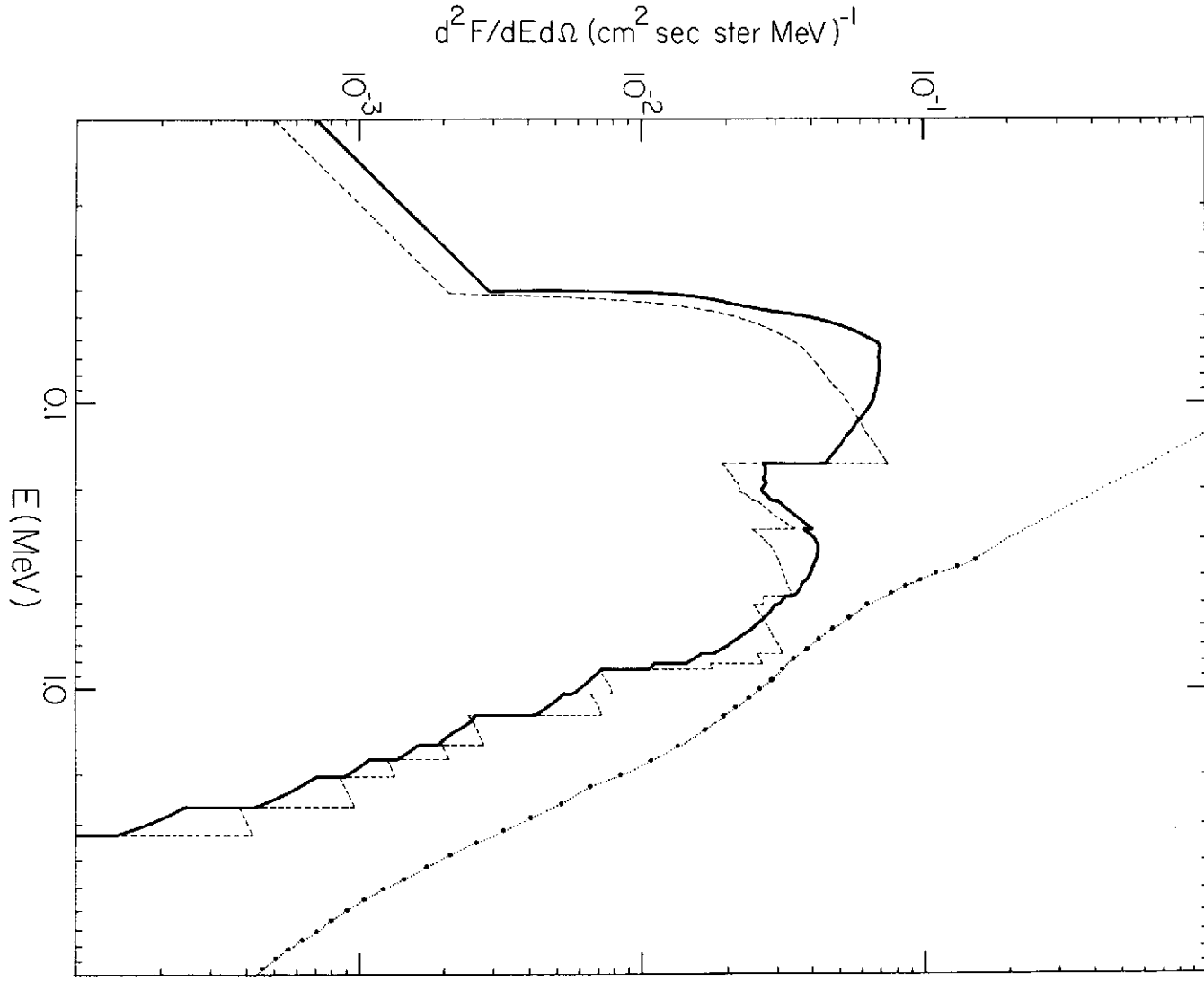


Figure 4. The composite  $^{56}\text{Ni}$ - $^{56}\text{Co}$ - $^{56}\text{Fe}$  gamma-ray spectrum in a specific Einstein-de Sitter universe. The age of this universe is  $11.8 \times 10^9$  years, and nucleosynthesis in galaxies began at  $t = 2 \times 10^9$  years, corresponding to  $z = 2.5$ . The solid line represents an exponentially decreasing rate of nucleosynthesis per galaxy which is today  $e^{-2}$  of the initial rate, whereas the dashed line represents a constant rate of nucleosynthesis per galaxy. The spectrum has series of rest-frequency edges and redshifted continua. The rest edges, which are calculated without Compton scattering in the source, are smallest for nucleosynthesis peaked in the early galactic history. The dotted line, shown for comparison, is the background spectrum observed on the Apollo 15 spacecraft by Trombka et al -- the heavy solid dots being their data points. The number of photons in the radioactivity background is obviously significant, but higher-energy-resolution observations will be needed to extract the presence of detailed structure. Although the density required for  $q_0 = \frac{1}{2}$  with  $H_0 = 55$  km/sec Mpc is  $\rho_c = 5.9 \times 10^{-30}$  gm  $\text{cm}^{-3}$ , this figure assumes that only the galaxies, with density  $\rho_G = 0.028 \rho_c$ , contain  $^{56}\text{Fe}$ . This calculation (Clayton and Ward) is thus a lower limit to the anticipated gamma-ray density.

already sees that it cannot be increased very much, and I tentatively conclude that the density of  $^{56}\text{Fe}$  does not exceed the observed density by more than a factor of two unless the A=56 lines are trapped in their sources. The fascinating thing about the Apollo 15 points of Trombka, Metzger, Arnold, Matteson, Reedy and Peterson (1973) is the way they show a positive curvatures near 400 keV.

↙ This suggests a multisource spectrum, and it is quite conceivable that the radioactivity spectrum may be significant in the over-all shape. Certainly the changes of second derivative will, if they remain after further experimental scrutiny, be important keys to the origins of this spectrum. The radioactivity spectrum may be less visible if the exploding source remains opaque for several months. Compton scattering as extensive as that in Figure 2 would remove at least half of the photons from the rest frequency at the source and redistribute them at energies of 0.5 MeV or so. If this source function were employed in Figure 4, the rest edges would be smaller by a factor of two or so, and the whole high-energy slope would be diminished in importance. At present no firm conclusion can be made, because the NaI(Tl) scintillator aboard Apollo 15 had not the energy resolution to detect structure like that in Figure 4. Nonetheless, such structure should be detectable.

#### (e) Discussion

It is within scientific grasp to learn the answers to many or all of the questions about nucleosynthesis enumerated in the introduction. What is needed is a gamma-ray telescope with high energy resolution, moderately good angular resolution, and long operation times outside the earth's atmosphere while responsive to ground command. Of primary importance is energy

resolution of a few percent or better to extract lines from continua and to detect rest edges in the universal continuum. Because the rest energies of the gamma rays and their relative production rates are known from laboratory studies, relatively sophisticated data analyses can be performed: one could sum the counting rates just before and just after each rest edge, for example, and compare the decrement with that at arbitrary energies in the spectrum. The angular resolution is needed to identify specific radiating objects (supernovae). As far as I know, the best type of instrument for accomplishing these two needs would be one like I described in the NASA x-and- $\gamma$ -Ray Committee Study of November 1965 -- a honeycomb of parallel holes drilled through actively collimating CsI or NaI with solid-state (say Li-drifted Ge) gamma detectors at the bottom of each hole. Operation outside the earth's atmosphere is necessary to reduce the emission background of the earth's atmosphere and its opacity. Ground command will be necessary for viewing different objects and for extracting the isotropic component. Last but by no means least, we need nature's cooperation in presenting us with a new Galactic supernova, preferably a visible one, although an invisible one could be immediately recognized by a large increase of the A=56 lines [See Eqs.(7) and (8)]. Good observation of at least one supernova is needed to measure what fraction of a gamma lines emerge unscattered from their source, for without this calibration the interpretation of the universal background will remain insecure. With a little bit of luck, the entire science of explosive nucleosynthesis will gain a firm observational footing from these very special photons. Like all photons, they tell us that an electromagnetic deexcitation occurred; unlike any other photons, they alone tell us that a new nucleus was just born.

### III. INELASTIC SCATTERING

When particles collide with energies in excess of those of their nuclear excited states, nuclear excitation is possible by the process of inelastic scattering. Let us not consider here the interesting problems of fast particles impinging on special dense objects like the earth's atmosphere, the moon, or the sun's outer atmosphere. Gamma rays from all three sources have been observed, but I will be concerned with radiation from outside the solar system. I also wish to set aside gamma rays from the surfaces of stars and collapsed objects, although both may present some observable sources. By design I will restrict myself to some remarks concerning the interstellar medium and its interaction with fast particles--either a general cosmic-ray flux or special regions of high flux near sources of fast particles. The point to be made at once is that "fast particles" rather than "cosmic rays" may be a more appropriate nomenclature, because the largest cross sections and the largest fluxes may be found in the region of several MeV.

Let  $F_i$  be the gamma-ray flux at the earth within a solid angle  $\Omega$  due to collisions



The center-of-mass kinetic energy before the collision is  $E$ , and after the collision is  $E - E_i$ . Let the cross section for this process be designated by  $\sigma_{AB}^i(E)$ . In practice one of these particles will be a nearly stationary constituent of interstellar or circumstellar plasma, and its number density  $N_A(\underline{x}, t)$  is a function of time and place; the other particle will be regarded

as the fast one with flux  $\phi_B(\underline{x}, t)$  that is also a function of time and place. Then

$$F_i = \frac{1}{4\pi} \int_{E_i}^{\infty} \int_{V(\Omega)} r^{-2} N_A \phi_B(E) \sigma_{AB}^i(E) dE dV \quad (40)$$

where the integral is over center-of-mass energies  $E > E_i$  and  $V(\Omega)$  is the volume of interstellar gas viewed by the solid angle  $\Omega$ . I will suppress the time dependence, although the arguments are evaluated at  $t - r/c$  if the flux is measured at  $t$ . Euclidean geometry is consistent with the assumption that the only gamma-ray lines of this type we are likely to see come from the Galaxy. For an infinitesimal pencil of directions  $d\Omega$ ,  $N_A(\underline{x})$  will be constant over the volume element  $dV = r^2 d\Omega dr$  so that the differential flux is

$$dF_i = \frac{d\Omega}{4\pi} \int_{E_i}^{\infty} \int_0^{\infty} N_A(\underline{x}) \phi_B(\underline{x}, E) \sigma_{AB}^i(E) dE dr \quad (41)$$

and if the position dependence of the fast-particle flux is ignored, this integral becomes a product of the integrated number of particles per unit area along the line of sight times the integral over the energy of the cross section times the flux.

One thing to notice immediately is that there should be another term involving the product  $N_B \phi_A(E)$  in the integrand, and, if the chemical composition of the gas were identical to that of the fast particles at fixed velocity, both integrals would give the same number of gamma rays. In the second case, however, the energy of the received gamma may be significantly Doppler shifted if the particles A were moving at significant fractions of  $c$ . (I will not concern myself at all with truly

relativistic velocities, where pion production dominates gamma-ray considerations and where, in any case, the fluxes are too small to produce detectable low-energy gamma rays.) The Doppler broadening in the second case might make the lines harder to resolve.

Let us make an order of magnitude estimate in order to define the ballpark. Imagine a telescope viewing the galactic disk. Let the solid angle  $\Omega$  contain interstellar gas equal to  $p_g$  percent of the Galactic mass (the total interstellar gas being about  $p_g = 10\%$ ) in the Galactic disk. Let  $p_A$  and  $p'_B$  be the percentages of interstellar particles and of fast particles having identities A and B respectively, so that  $N_A = \left(\frac{p_A}{100}\right)N$  and  $\phi_B = \left(\frac{p'_B}{100}\right)\phi$ . (Throughout I have chosen to express unknown parameters in percentages in order that they have expected values nearer unity in resulting expressions.) Assuming the emissivity of the disk to be nearly uniform means that the flux is comparable to the value it would have if the emission within  $V(\Omega)$  were all from the Galactic center, about 10 kpc away. For that case

$$F_i(\text{Galaxy}) \approx p_g (p_A p'_B + p_B p'_A) 1.8 \times 10^{-11} \bar{\phi} \bar{\sigma}_{AB} (\text{mb}) \text{cm}^{-2} \text{s}^{-1} \quad (42)$$

where  $\bar{\phi}(>E_i)$  the total flux above threshold and  $\bar{\sigma}(\text{mb})$  is the average cross section in units of millibarns. For example if we consider that the 6.1 MeV radiation from  $^{16}\text{O}$  has a proton cross section of about 100 mb above its threshold (effectively about 8 MeV), and if the flux above 8 MeV is  $\bar{\phi}(>8) \approx 50 \text{ cm}^{-2} \text{sec}^{-1}$ , a not unreasonable extrapolation from observations above 30 MeV, then with  $p_{16} = .07$ ,  $p'_H = .90$ ,  $p_H = .90$ ,  $p'_{16} = .3$  [Cameron (1968); Shapiro and Silberberg (1970)] gives

$$F_{16}(\text{Galaxy}) \approx 3 \times 10^{-6} \text{ cm}^{-2} \text{sec}^{-1}$$

if the gas in  $V(\Omega)$  is  $p_g = 1\%$  of the Galactic mass. This corresponds to a total production of about  $10^{41}$  gamma rays per second from the entire Galactic gas, in rough agreement with the estimate of Fowler, Reeves and Silk (1970), and a flux of about  $3 \times 10^{-5} \text{ cm}^{-2} \text{ sec}^{-1}$  with an omnidirectional counter. I do not want to argue this as the best calculation of the emissivity of the Galactic disk. My point is that line fluxes of order  $10^{-5} \text{ cm}^{-2} \text{ sec}^{-1}$  will be expected from  $^{16}\text{O}^*$ , and that this detection will be only marginally possible. That is, this prospect lies near an uncertain edge of detectability.

What basic features of the estimate could be plausibly altered to obtain a larger gamma-ray flux at the earth? One idea would be a discrete source nearby. However, one readily calculates that if a mass  $mM_\odot$  of gas concentrated at a distance  $d(\text{pc})$  is irradiated, the flux of gammas at earth is

$$F_i(\text{source}) = \frac{0.8 \times 10^{-12}}{d(\text{pc})^2} m\bar{\sigma}(\text{mb}) \bar{\phi} (p_A p'_B + p_B p'_A) \quad (43)$$

so that for  $d = m = 1$  the  $^{16}\text{O}^*$  gamma-ray flux, for example, would be  $F_{16}(\text{discrete}) = 3 \times 10^{-9} \bar{\phi} (>8 \text{ MeV})$ . Thus the flux from a discrete source can hardly be much greater than that of the disk as a whole, unless the fast particle flux  $\bar{\phi}$  is very much greater (say  $\bar{\phi} > 10^5 \text{ cm}^{-2} \text{ s}^{-1}$ ) than in the general cosmic radiation. This might occur for a short while following a supernova explosion, or it might occur for long times around a rapidly rotating collapsed object.

Another attractive idea is that fast-particle flux  $\phi(E)$  could be a very steep function of energy. The solar modulation is thought to be (Goldstein, Fisk and Ramaty 1970) so severe for  $E < 30 \text{ MeV/nucleon}$  that measurements at earth give little insight

into the general interstellar flux. If we should be so fortunate that  $\phi(E) \propto E^{-n}$  with  $n > 2$ , a great deal of special information can be extracted from sources. The high fluxes will give observable counting rates and the steep energy dependence will produce informative threshold-dependent features. We may perhaps even expect this near the sources, because Braddy, Chan and Price (1973) have found that big solar flares produce a very steep spectrum having  $n \approx 3.7$  with preferential acceleration of heavy ions. Of course solar flares are not the origins of cosmic rays, but let us make do with what we have and suppose that, like flares, the acceleration mechanisms for cosmic rays also produce a steep low-energy spectrum. If it is as steep as  $n=2$ , the nuclei having low excitation thresholds can be excited more strongly than more abundant nuclei having higher excitation thresholds. This point is illustrated in Figure 5, which shows the relative abundances of cosmic-ray nuclei (assuming terrestrial isotope ratios) as a function of the excitation energy  $E_i = E(A^*)$  of their first excited states. There is a general positive slope of approximately  $E_i^{+1}$  in these abundances, which reflects only the fact that the most abundant nuclei tend to be the most stable, and those in turn tend to have the largest excitation energies.

First consider an example of how gamma-ray astronomy could measure the exponent  $n$  in the fast-particle spectrum. The  $^{14}\text{N}$  nucleus has excited states at 2.31 and 3.94 MeV with "effective thresholds" of about 3.3 and 4.9 MeV (to allow the outgoing proton at least 1 MeV to beat the Coulomb barrier). The excitation of the 3.95 MeV level results (96%) in a cascade of 1.6 and 2.3 MeV gamma rays, whereas the excitation of the 2.31 MeV level results only in the 2.3 MeV gamma ray. Thus the relative gamma-ray

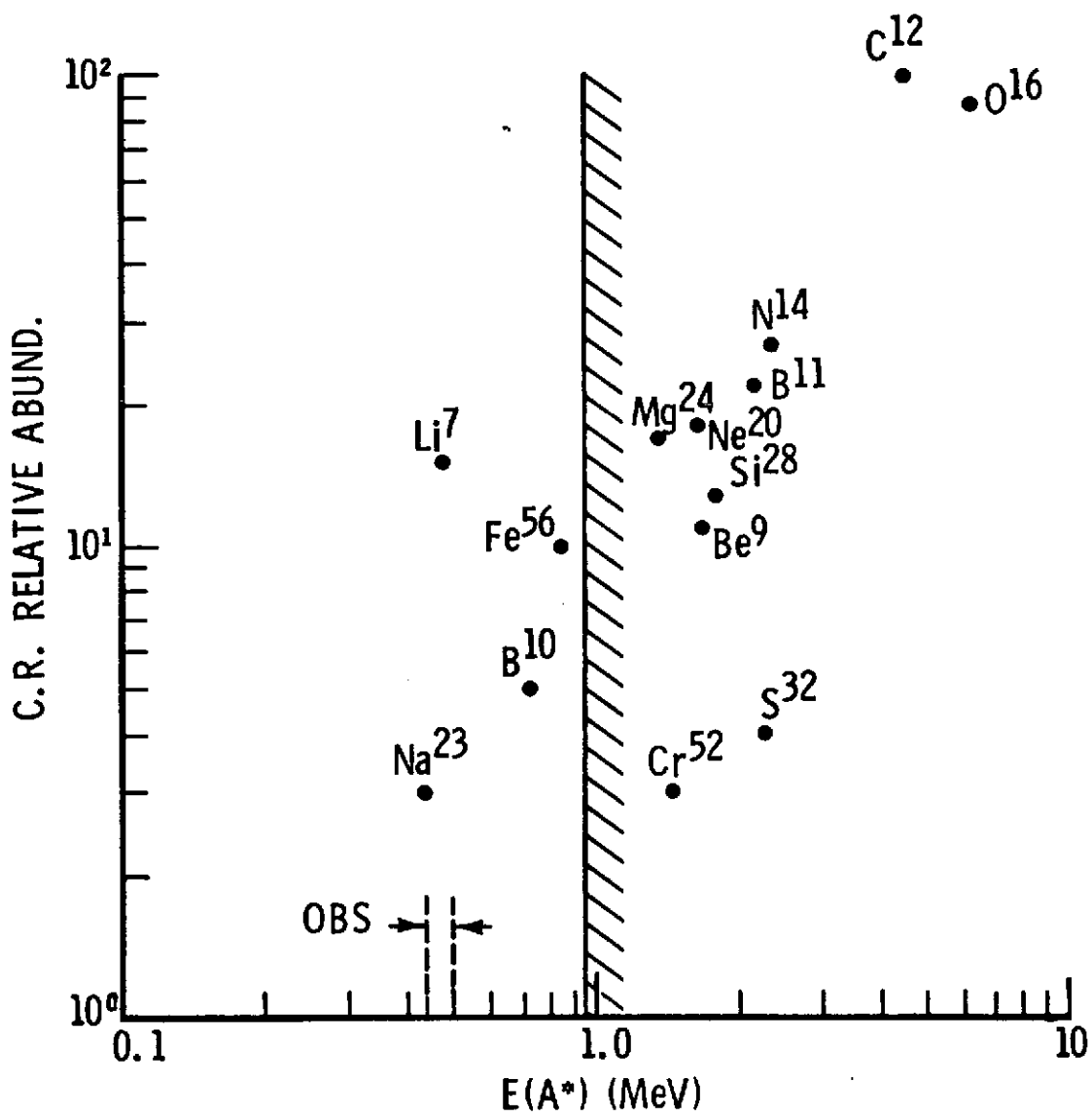


FIGURE 5

fluxes should be

$$\frac{F_{2.3}}{F_{1.6}} \approx \frac{\int_{3.3}^{\infty} E^{-n} \sigma_{pN}^{2.31}(E) dE}{\int_{4.9}^{\infty} E^{-n} \sigma_{pN}^{3.95}(E) dE} + 1 \quad (44)$$

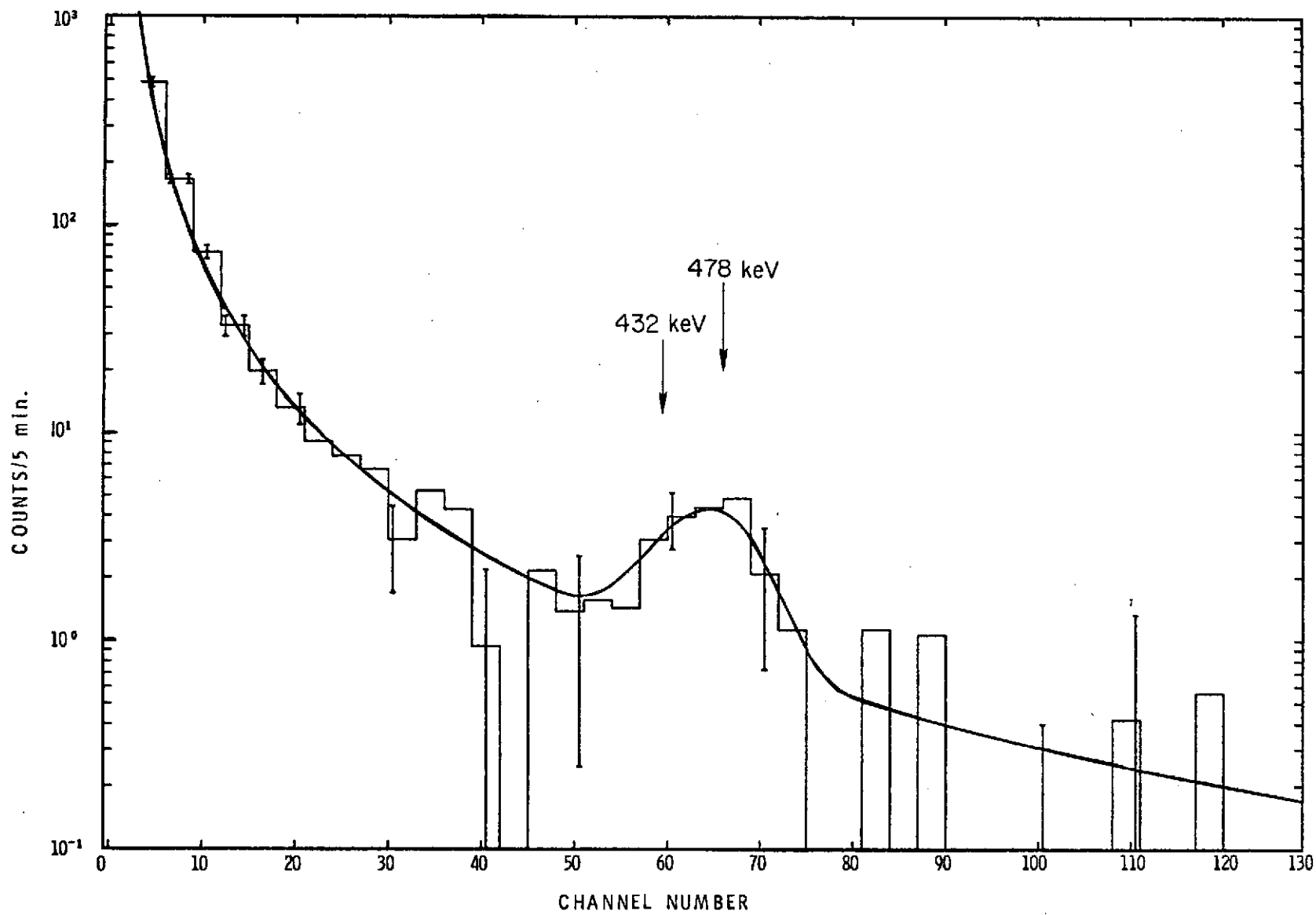
I can foresee a need for tabulations of nuclear cross sections of this type; however, if we only assume for simplicity that the ratio of these two averaged cross sections is near unity, then the n dependence is proportional to the ratio of fast-particle fluxes :

$$\frac{F_{2.3}}{F_{1.6}} \propto \left(\frac{4.9}{3.3}\right)^{n-1} + 1 = 3.8 \text{ for } n = 3.5,$$

whereas the corresponding ratio would be near two if there were a deficiency rather than an excess of MeV particles. One could also compare the first excited-state lines of  $^{12}\text{C}$  and  $^{16}\text{O}$ , but then the abundance ratio in the source would be an unknown. If many different lines of many different species can be observed, an interesting picture of the abundances and energy spectrum could be assembled. A related type of problem was extensively discussed by Lingenfelter and Ramaty (1967) for the case of solar flares, and many of their conclusions pass directly to extra-solar gamma-ray astronomy. Now that some of these solar-flare gamma rays have been seen by OSO-7, we may expect further clarifications on prospects for the future of Galactic astronomy. For fast particles more energetic than 10 MeV, the most prominent astronomical lines should be the pair annihilation line, the 2.23 MeV radiative neutron capture by hydrogen, and the excited states of C,N,O and Ne nuclei. Fowler, Reeves and Silk (1970) emphasized for these particles, however, that the gamma-ray flux

is limited by the requirement that the accompanying spallation reactions not overproduce Li, Be and B abundances. They find that the rate of production of  $^{12}\text{C}$  and  $^{16}\text{O}$  gamma rays is less than  $10^{-26} \text{ sec}^{-1}$  per interstellar H atom. This limit is an average over time and place, however, and could be greatly exceeded in limited regions for limited times.

Figure 5 shows those nuclei that will be most exciteable by low-energy fast particles, so let us turn our attention to the possibility that large fluxes of particles with  $E < 5 \text{ MeV}$  may be common. In addition to the solar-flare observations to motivate this hypothesis, we have <sup>the</sup><sub>A</sub> fact that if the HI regions are heated by fast particles, they must surely lie in the MeV region. If the fast-particle spectrum is steeper than  $E^{-2}$ , the nuclei with low excited states are excited more frequently than the more abundant nuclei. Of all these,  $^7\text{Li}$  is anomalous in that its cosmic-ray abundance is very much greater than the general line through Figure 5. In a steep fast-particle spectrum, the 478 keV line of  $^7\text{Li}^*$  should be the most prominent if the fast particles have the relative abundances of the cosmic rays. This peculiar fact was used by Fishman and Clayton (1972) in their attempt to account for the spectral feature observed toward the Galactic center by Johnson, Harnden and Haymes (1972). They point out that a 432 KeV gamma ray due to  $^7\text{Li}(p,n)^7\text{Be}^*(432)$  should accompany the main  $^7\text{Li}$  radiation with about 1/3 its intensity. Their fit to the data of Johnson et al is shown in Figure 6. The computed solid curve is a simple power-law continuum plus the  $^7\text{Li}$  doublet feature at an intensity comparable to the observed counting rate. The fit is basically quite good, so the explanation could be correct. Fishman and Clayton used  $p_g = 2\%$  and  $p'_{\text{Li}} = 0.08\%$



500

Figure 6

Figure 5

Relative abundances of cosmic-ray nuclei (Shapiro and Silberberg 1970) plotted as a function of the energy of their first excitation level. Terrestrial isotope ratios have been assumed. The energy range of the line feature observed from the Galactic center region (Johnson et al 1972) is indicated. No observations have been made above 0.93 MeV. From Fishman and Clayton (1972).

Figure 6

The curve shows the shape of the  ${}^7\text{Li}$  -inelastic-scattering feature superimposed on a smooth power-law continuum (Fishman and Clayton 1972). The profile was computed for an energy resolution equal to that of the detector used by Johnson et al. Because of the limited resolution, the line at 432 keV due to  ${}^7\text{Li} (p,n) {}^7\text{Be}^*$  is not physically separated from the line at 478 keV due to  ${}^7\text{Li} (p,p') {}^7\text{Li}^*$  which is three times stronger. The histograms are the data of Johnson et al (1972) with their energy channels summed in groups of three adjacent channels to reduce statistical fluctuations. The consistency of their feature with the one proposed by Fishman and Clayton is evident.

in Eq. (42) to conclude that if the radiation was from this much gas toward the Galactic center, one gets  $\bar{\phi} \approx 5 \times 10^4 \text{ cm}^{-2} \text{ sec}^{-1}$  between about 2 and 10 MeV/nucleon. This is a much larger flux than one is accustomed to think of in cosmic rays, but it is not out of line with  $E^{-3.5}$  spectra like those of a solar flare; with  $n = 3.5$  one has  $\phi(>2) \approx 900 \phi(>30)$ . The large energy density of over  $100 \text{ eV cm}^{-3}$  would create dynamic instabilities were it a Galacticwide phenomenon, however, so it must exist instead in bottles of high-flux regions. Nonetheless, our calculation requires the amount of irradiated gas to be large to obtain the observed flux, so there are strong astrophysical problems here. Another problem is that the high  ${}^7\text{Li}$  abundance is usually assumed to be spallogenic from high-energy cosmic rays, so that large low-energy fluxes of this nucleus might not be expected from that point of view. My philosophy is that observational gamma-ray astronomy is quite capable of teaching us the truth in these matters, so elaborate models for or against this particular explanation may not be appropriate at present. We also need much better evidence of the cosmic-ray flux at the solar system, because the Goldstein, Fisk and Ramaty (1970) calculations show that the particles at earth's orbit having 30 MeV/nucleon are three to four orders of magnitude less abundant than their 50-100 MeV progenitors at the boundaries of the solar system. Perhaps Pioneer 10 will give us badly needed facts on this modulation problem.

This work was partially supported by the National Science Foundation GP-18335.

REFERENCES

- Arnett, W. D. and Clayton, D. D. 1970, Nature, 227, 780.
- Arnett, W. D. and 1971, Ap. J., 166, 153.
- Bodansky, D., Clayton, D. D., and Fowler, W. A. 1968,  
Ap. J. Suppl. 16, 299.
- Braddy, D., Chan, J. and Price, P. B. 1973, Phys. Rev. Letters  
30, 669.
- Brown, R. T. 1973, Ap. J., 179, 607.
- Cameron, A. G. W. 1968 in Origin and Distribution of the  
Elements, L. H. Ahrens, ed., (New York: Pergamon Press)  
p.125.
- Clayton, D. D. 1971, Nature, 234, 291.
- Clayton, D. D. 1973, Science, 000, 000.
- Clayton, D. D. and Craddock, W. 1965, Ap. J., 142, 189.
- Clayton, D. D., Colgate, S., and Fishman, G. J. 1969,  
Ap. J., 155, 75.
- Clayton, D. D. and Silk, J. 1969, Ap. J., 158, L43.
- Clayton, D. D. and Woosley, S. E. 1969, Ap. J., 157,  
1381.
- Fishman, G. J. and Clayton, D. D. 1972, Ap. J., 178, 337.
- Fowler, W. A. 1972, in Cosmology, Fusion, and Other Matters,  
ed. F. Reines, (Boulder: Univ. of Colorado Press) p.67.
- Fowler, W. A., Reeves, H., and Silk, J. 1970, Ap. J., 162,  
49.
- Goldstein, M. L., Fisk, L. A., and Ramaty, R. 1970, Phys.  
Rev. Letters, 25, 832.

- Hainebach, K., Arnett, W. D., Woosley, S. E. and Clayton, D. D. 1973, in preparation.
- Howard, W. M., Arnett, W. D., Clayton, D. D. and Woosley, S. E. 1971, Phys. Rev. Letters, 27, 1607; 1972, Ap. J., 175, 201.
- Johnson III, W. N., Harnden, F. R., and Haymes, R. C. 1972, Ap. J. (Letters), 172, L1.
- Lingenfelter, R. E. and Ramty, R. 1967, in High Energy Nuclear Reactions in Astrophysics, B. Shen, ed. (New York: W.A. Benjamin, Inc.)
- McVittie, G. C. 1965, General Relativity and Cosmology (Urbana: Univ. Illinois Press)
- Oort, J. H. 1958, in Solvay Conference on Structure and Evolution of the Universe (Brussels: R. Stoops)
- Sandage, A. 1972, Ap. J., 178, 1.
- Schmidt, M. 1965, in Galactic Structure, A. Blaauw and M. Schmidt, eds. p.528 (Chicago: University of Chicago Press).
- Shapiro, M. M. and Silberberg, R., 1970, Ann. Rev. of Nuclear Science, 20, 323.
- Trombka, J. I., Metzger, A. E., Arnold, J. R., Matteson, J. L., Reedy, R. C. and Peterson, L. E. 1973, "The Cosmic  $\gamma$ -Ray Spectrum Between 0.3 and 27 MeV Measured on the Apollo 15", preprint and private communication.
- Weinberg, S. 1972, Gravitation and Cosmology (New York: John Wiley) p.495.

N73-28766  
13

INTERNATIONAL SYMPOSIUM ON GAMMA-RAY ASTROPHYSICS

GODDARD SPACE FLIGHT CENTER, APRIL 30 - MAY 2, 1973

ULTRA HIGH ENERGY GAMMA-RAYS

by

A.W. Strong, J. Wdowczyk\* and A.W. Wolfendale  
Physics Department, University of Durham, U.K.

(\* On leave from Institute of Nuclear Research, Lodz, Poland).

A B S T R A C T

An analysis is made of the interactions of very high energy cosmic ray protons with the relict radiation in extragalactic space. Two situations are examined: gamma rays derived from  $\pi^0$ -mesons produced in collisions in a non-evolutionary situation and gamma rays from electron pairs produced at early epochs. It is shown that the ultra high energy  $\gamma$ -rays ( $E_\gamma > 10^{19}$  eV) could conceivably be of high enough intensity to be detected. The flux of  $\gamma$ -rays from the second process ( $E_\gamma < 10^9$  eV) is not far from the diffuse background that has been reported.

## §1. Introduction

The problem of the origin of the cosmic radiation is well known. Although there are many potential sources in the galaxy: novae, supernovae, pulsars, the Galactic nucleus, etc., there is great difficulty in explaining the observed isotropy of the radiation above  $10^{17}$  eV where the galactic magnetic field is not strong enough to randomise the particle directions and considerable anisotropies should result. The suggestion of an extragalactic origin for all the radiation demands a rather high energy density of this component throughout the Universe ( $\sim 1\text{eV cm}^{-3}$ ) but if only particles above  $10^{15}$  eV or so come predominantly from outside the Galaxy this difficulty disappears.

If these very energetic primaries are indeed of extragalactic origin, their interaction with the radiations in space, principally the relict radiation (Penzias and Wilson, 1965, and later papers), becomes a process of importance. The protons will lose energy by way of interaction with this radiation and produce, successively as the energy is increased,  $e^+e^-$  pairs and pions. In turn, the energy loss would be expected to show up as an increase in slope of the energy spectrum of protons recorded at the earth.

There is the well known increase of slope at  $\sim 3 \times 10^{15}$  eV and it is conceivable that this arises from just such interactions, principally  $e^+e^-$  production, at early stages of the evolution of the Universe when the relict radiation was at a higher temperature than its present value of 2.7K (Hillas, 1968, Strong et al., 1973). The latter authors have calculated the flux of  $\gamma$ -rays expected to result from such interactions and, although they are hardly of 'ultra-high' energy, they will be considered briefly later because their origin is similar to that of the much higher  $\gamma$ -rays which are the main subject of this work.

If cosmic ray protons did not start to be produced until comparatively late stages in the evolution of the Universe, when the temperature of the relict radiation was close to its present value,  $e^+e^-$  production would cause a reduction of primary proton intensity by a factor  $\sim 3$  above  $\sim 3.10^{18}$  eV and pion production would cause a reduction starting at  $\sim 5.10^{19}$  eV and reaching a factor  $\sim 100$  above  $\sim 2.10^{20}$  eV. Now such a reduction does not appear to have been detected experimentally (although at the energies in question the numbers of events detected, extensive air showers, is small and errors of energy determination are not negligible). A possible way out of the problem is to assume that the production spectrum of primary protons above  $10^{19}$  eV is flatter than that at lower energies so that after attenuation the spectrum at the earth has roughly the same slope as that below  $10^{19}$  eV. Although this idea is perhaps improbable, it is by no means impossible. Clearly in this case there will be significant energy going into pions and electrons, and eventually  $\gamma$ -rays and these will be, in principle, detectable. The details to be described in the following sections are taken largely from the work of Wdowczyk et al. (1971, 1972, referred to as I).

## §2. Interaction of Protons with the Relict Radiation.

### 2.1 The attenuation length for photomeson production

The interaction process has been considered by a number of authors, starting with Greisen (1966) and Zatsepin and Kuzmin (1966) and an accurate analysis has been given by Stecker (1968). This author has summarised experimental data on the total photomeson production cross section and inelasticity for high energy protons in the relict radiation as a function of  $\gamma$ -ray energy in the proton rest system and used the data in the derivation of  $\lambda_a$  ( $\lambda_a = (K_p n_\gamma \sigma)_{\text{eff}}^{-1}$  where  $K_p$  is the inelasticity of the interaction

$n_\gamma$  is the photon density and  $\sigma$  the meson production cross section. The values of  $\lambda_a$  derived in this way are given in Figure 1. Kuzmin and Zatsepin (1967) and Adcock (1970, private communication) have derived values of the interaction length,  $\lambda_1$ , as a function of  $E_p$  and these values are close to what would be expected from Stecker's results.

### 2.2 Energy spectrum of protons

Wdowczyk et al. (1972) considered two limiting forms for the energy spectrum of protons at the earth, as shown in Figure 2. The higher intensities (A) come from the work of Linsley et al. (1963) and the lower spectrum (B) is that due to Andrews et al. (1971). Although the latter seems more probable, results for both will be given so that interpolation (or extrapolation) may be made if results are needed for some other spectrum.

### 2.3 Energy spectrum of $\gamma$ -rays on production

In I, use was made of Stecker's data to calculate the production spectra of  $\pi^0$ -mesons, and in turn that of  $\gamma$ -rays, with the results shown in Figure 2. An important datum is the total energy going into  $\gamma$ -rays: for A this is

$$\begin{aligned} &7 \times 10^{-25} \text{ eV cm}^{-3} \text{ s}^{-1} \text{ from } \pi^0\text{-mesons, together with} \\ &4 \times 10^{-25} \text{ eV cm}^{-3} \text{ s}^{-1} \text{ from } e^+e^- \text{ pairs.} \end{aligned}$$

For spectrum B the corresponding figures are

$$\begin{aligned} &6 \times 10^{-26} \text{ eV cm}^{-3} \text{ s}^{-1} \text{ from } \pi^0\text{-mesons and} \\ &\approx 4 \times 10^{-25} \text{ eV cm}^{-3} \text{ s}^{-1} \text{ from } e^+e^- \text{ pairs (the spectra A and B are} \\ &\text{very similar in the energy region where pair production is important).} \end{aligned}$$

With spectrum A and assuming a residence time for photons in the Universe of  $T = 13 \times 10^9 \text{ y} = 4 \times 10^{17} \text{ s}$ , the integrated  $\gamma$ -ray intensity is

$7 \times 10^2 \text{ eV cm}^{-2} \text{ s}^{-1} \text{ sr}^{-1}$  and the energy density is  $3 \times 10^{-7} \text{ eV cm}^{-3}$ .

This energy density can be compared with that in the proton spectrum at the earth above  $5 \times 10^{19} \text{ eV}$  of  $\sim 3 \times 10^{-10} \text{ eV cm}^{-3}$ . The large disparity is because of the fact mentioned in §1 that the proton spectrum on production must be much flatter than that observed. Essentially, the detected protons come from within one attenuation length ( $\sim 3 \times 10^{25} \text{ cm}$  at a mean energy of  $3 \times 10^{20} \text{ eV}$ ) whereas  $\gamma$ -rays come from the whole of the Universe ( $\sim 10^{28} \text{ cm}$ ).

The production spectra in Figure 2 are close to those given by Stecker (1973, private communication) for the same alternative proton spectra.

### §3. Propagation of $\gamma$ -rays through the Universe

#### 3.1 Extragalactic radiation fields

Summaries of the radiation fields and the corresponding interaction mean free paths for  $\gamma$ - $\gamma$  collisions have been given by a number of authors, notably Gould and Schreder (1967a, b), Stecker (1971) and I. There is, understandably, agreement for the relict radiation but a small disparity for starlight and I.R. and a large disparity for the radio background. A comparison is made in Figure 1 between the results of I - full line, and that of Stecker (1971 - an updating of Gould and Schreder, 1967a, b) - dotted line. Of importance for the propagation of  $\gamma$ -rays above  $10^{20} \text{ eV}$  is the difference in the radio background and this needs to be considered. The problem of measuring the isotropic component of the radio background at the earth is severe and experimental differences are rather great. The authors of I used the measurements of Clark et al. (1970), which show a fall off in intensity at photon energies below  $10^{-8} \text{ eV}$ , and insofar as these measurements are later than those used by the other authors their analysis will be used here. It is interesting to note that if the shorter

interaction lengths are valid for  $E > 10^{20}$  eV then the result will be a reduction in the intensity of such  $\gamma$ -rays at the earth but an increase in intensity at energies just below this value.

### 3.2 The interaction process

The generated high energy photons will interact with the photons of the various radiation fields to produce electron pairs,  $\gamma + \gamma \rightarrow e^+ + e^-$ . Muon pairs can also be produced if the energy is high enough ( $E_\gamma > 10^{19}$  eV for relict radiation) and the mean free paths for muon pair and electron pair production eventually become equal; however, in the energy region where a significant effect would occur, the radio background takes over.

The interaction process has been examined in some detail by Bonometto and Lucchin (1971), Allcock and Wdowczyk (1972) and by Wdowczyk et al. (1972). The authors have pointed out the important fact that at high photon energies the angular distribution of the electrons peaks in the forward and backward directions so that in the laboratory system one of the electrons takes an increasingly large fraction of the energetic photon energy. In the absence of an extragalactic magnetic field of magnitude above  $\sim 10^{-11}$  gauss (see I), the electrons produced will collide with the relict photons and produce further energetic photons by the inverse Compton effect and in this way a  $\gamma$ -ray cascade will be built up.

### 3.3 First generation $\gamma$ -spectrum

Whether or not magnetic fields are present, the  $\gamma$ -ray spectrum of Figure 2 will be generated and a first generation spectrum  $I_1(E_\gamma) = \frac{1}{4\pi} W(E_\gamma) \lambda(E_\gamma)$  will be formed. This spectrum has been calculated in I for proton spectra A and B with the result shown in Figure 3.

### 3.4 Cascading in the absence of galactic magnetic fields

The cascading problem is one of some complexity and the only calculations reported to date appear to be those in I. An order of magnitude

estimate of the upper limit to the intensity at low energies (where most of the energy will eventually lie) can be obtained from energy conservation. For example, if starlight were to be disregarded (i.e.  $\lambda_i$  for starlight  $> 10^{28}$  cm) then very roughly the intensity would have an average value below  $10^{14}$  eV (Figure 1) of  $I_c (< 10^{14}$  eV) given by

$$\int_{E_0}^{10^{14} \text{ eV}} E_\gamma I_c(E_\gamma) dE_\gamma \approx 7 \times 10^2 \text{ eV cm}^{-2} \text{ s}^{-1} \text{ sr}^{-1} \quad \text{for proton}$$

spectrum A; (where  $E_0 \ll 10^{14}$  eV) i.e.

$$I_c(E_\gamma < 10^{14} \text{ eV}) \approx 10^{-25} \text{ cm}^{-2} \text{ s}^{-1} \text{ sr}^{-1} \text{ eV}^{-1}$$

Similarly, in the presence of considerable starlight but no radiation causing attenuation below  $10^{11}$  eV, we would expect

$$I_c(E_\gamma < 10^{11} \text{ eV}) \approx 10^{-19} \text{ cm}^{-2} \text{ s}^{-1} \text{ sr}^{-1} \text{ eV}^{-1}$$

again for proton spectrum A.

The diffusion equations were solved in I giving the energy spectra shown in Figures 4 and 5. It can be seen that the intensities at low energies are not inconsistent with what would be expected from the remarks in the previous paragraph.

### 3.5 Cascading in the presence of galactic magnetic fields

The presence of significant fields causes the electrons produced in  $\gamma$ - $\gamma$  collisions to lose energy by synchrotron radiation and thus give rise to 'low' energy  $\gamma$ 's rather than to transfer most of their energy to a single photon by I.C.E. The problem was considered in I and results were

given for what might be a reasonable field:  $\langle B \rangle = 10^{-9}$  gauss. Not surprisingly, perhaps, the synchrotron spectrum so derived is rather similar to that from cascading, below  $10^{15}$  eV. However, a note of caution is necessary, because of the effect of the field on the proton spectrum. It is possible to envisage a situation where the proton spectrum is higher elsewhere and the  $\gamma/p$  ratio at the earth would be correspondingly higher.

#### §4. Summary of Predictions concerning $\gamma$ -rays above $10^{12}$ eV.

The intensities of  $\gamma$ -rays shown in Figures 4 and 5 (for the case of  $\langle B \rangle \approx 10^{-11}$  gauss) have been used to give the  $\gamma/p$  ratios shown in Figure 6.

It will be noticed that the ratios are approaching measurable fractions at energies above  $10^{19}$  eV. Of particular interest is the peak in the region of  $2 \times 10^{19}$  eV which comes from the effect of the transition from domination by relict radiation to that by the radio background at this energy (Figure 1). An approximate analysis was made in I of the upper limit that can be set on this ratio from studies of extensive air showers ( $\gamma$ -initiated showers would be poor in muons compared with proton-initiated showers). It can be seen that so far the experimental limit is significantly higher than the maximum predicted ratio. However, there are sufficient uncertainties in our knowledge of extragalactic parameters to make it possible that detectable fluxes of very energetic  $\gamma$ 's do exist and it is urged that systematic searches be made. One point that should be stressed in this connexion is the possibility of a non-uniform radio background; this could produce a transition effect which would concentrate  $\gamma$ -ray energy in a particular region to an even greater extent than in the present case and give rise to a much higher ratio.

## §5. $\gamma$ -rays in an evolving Universe

As remarked in the Introduction there is the possibility that the kink in the proton spectrum at  $3 \times 10^{15}$  eV is connected with electron pair-production on the relict radiation at early epochs. The  $\gamma$ -rays expected from these interactions may allow constraints to be put on models in which the primary spectrum above  $10^{14}$  eV is of extragalactic origin and this topic therefore has relevance to the ultra high energy  $\gamma$ -region.

Strong et al. (1973a, b) have examined the problem in detail and their derived  $\gamma$ -spectrum at the earth is given in Figure 7. As will be appreciated, although the total energy in the spectrum will be constant (it is  $\sim 1.7 \times 10^5$  eV cm<sup>-2</sup> s<sup>-1</sup> sr<sup>-1</sup>) the spectral shape will depend on the energy density of extragalactic starlight. The  $\gamma$ -ray spectra in Figure 7 correspond to different assumptions about the variation of starlight density with epoch.

The experimental situation is not clear. There appear to be a number of intensities below the expected spectra and if these are correct then the suggested origin of the proton spectrum kink is not correct (although this does not preclude the very energetic protons of this energy being of extragalactic origin). However, the recent measurements of Mayer-Hasselwander et al. (1972) are in good agreement with the prediction.

A firm conclusion cannot be made at this stage, therefore, although with new measurements being made at the present time, this problem, at least, should be solved rather soon.

### Acknowledgements

The authors wish to thank the Science Research Council of the U.K. for the provision of research grants to support this work.

R E F E R E N C E S

- Allcock, M.C. and Wdowczyk, J., 1972, *Nuovo Cimento*, 9, 315.
- Andrews, D. et al., 1971, *Proc. 12th Int. Conf. on Cosmic Rays, Hobart*, 3, 995.
- Bonometto, S.A. and Lucchin, F., 1971, *Lett. Nuovo Cim.*, 2, 1299.
- Bratolubova-Tsulukidze, L.K., et al., 1970, *Acta Phys. Hung.* 29, Suppl. 1, 123.
- Clark, G.W., Garmire, G.P. and Kraushaar, W.L., 1971, *Proc. 12th Int. Conf. on Cosmic Rays, Hobart*, 1, 91.
- Clark, T.A. et al., 1970, *Nature, Lond.*, 228, 847.
- Daniel, R.R., Joseph, G. and Lavakare, P.J., 1972, *IAU/COSPAR Symposium No. 55, Madrid (in the press)*.
- Goletskii, S.V., 1971, *Astrophys. Lett.*, 9, 69.
- Gould, R.J., and Schreder, G.P., 1967a, *Phys. Rev.* 155, 1404.  
1967b, *Phys. Rev.* 155, 1408.
- Greisen, K., 1966, *Phys. Rev. Lett.*, 16, 748.
- Hillas, A.M., 1968, *Canad. J. Phys.* 46, S623.
- Kuzmin, V.A. and Zatsepin, G.T., 1968, *Canad. J. Phys.*, 46, S617.
- Linsley, J., 1963, *Proc. Int. Conf. on Cosmic Rays, Jaipur*, 4, 77.
- Mayer-Hasselwander, H.A. et al., 1972, *Astrophys. J. Lett.* 175, L23.
- Penzias, A.A. and Wilson, R.W., 1965, *Astrophys. J.*, 142, 19.
- Stecker, F.W., 1968, *Phys. Rev. Lett.*, 21, 1016.
- Stecker, F.W., 1971, "Cosmic Gamma Rays", *Mono Book Corp., Baltimore, U.S.A.*
- Strong, A.W., Wdowczyk, J. and Wolfendale, A.W., 1973a, *Nature*, 241, 109.  
1973b, (to be published).
- Vette, J. et al., 1970, *Astrophys. J. Lett.*, 160, L161.
- Wdowczyk, J., Tkaczyk, W. and Wolfendale, A.W., 1972, *J. Phys. A.*, 5, 1419.
- Zatsepin, G.T. and Kuzmin, V.A., 1966, *Zh. Eksperim, Teor. Fiz. Lett.*, 4, 114.

CAPTIONS TO FIGURES

- Figure 1 Interaction length against photon energy for collisions of energetic photons with photons of the various photon fields ( $e^+e^-$  production only). The full lines represent the calculations of Wdowczyk et al. (1972) and the dotted lines those of Stecker (1971). Also shown (top right hand corner) is the attenuation length for protons in the relict radiation from the work of Stecker (1968).
- Figure 2 Alternative primary proton spectra  $j_A$  and  $j_B$  and the corresponding  $\gamma$  production spectra,  $W(E_\gamma)$ , from I.
- Figure 3 First generation production spectra from I. If the mean extragalactic magnetic field exceeds  $10^{-10}$  gauss or so, cascading will be inhibited and these will be the spectra of  $\gamma$ -rays above  $\sim 10^{18}$  eV.
- Figure 4  $\gamma$ -ray spectra over the whole energy range, from I. The diffuse X-ray spectra summarised by Ipavich and Lenchek (1970) are also shown, as is primary proton spectrum A.
- Figure 5  $\gamma$ -ray spectrum for primary proton spectrum B, from I. (approximate - relaxed from Figure 4).
- Figure 6  $\gamma/p$  ratio from reference I.

Figure 7

Comparison of observed, and predicted, isotropic flux of  $\gamma$ -rays. The predicted intensities are from the work of Strong et al. (1973), with (1) representing the more probable situation.

Key to observational points:-

	OSO-III	Clark et al. (1971)
	COSMOS - 208	Bratolubova-Tsulukidze et al. (1970)
	PROTON - 2	ibid
	COSMOS - 163	Golenetskii et al. (1971)
	ERS - 18	Vette et al. (1970)
	Mayer-Hasselwander et al. (1972)	
	Daniel et al. (1972).	

Fig 1

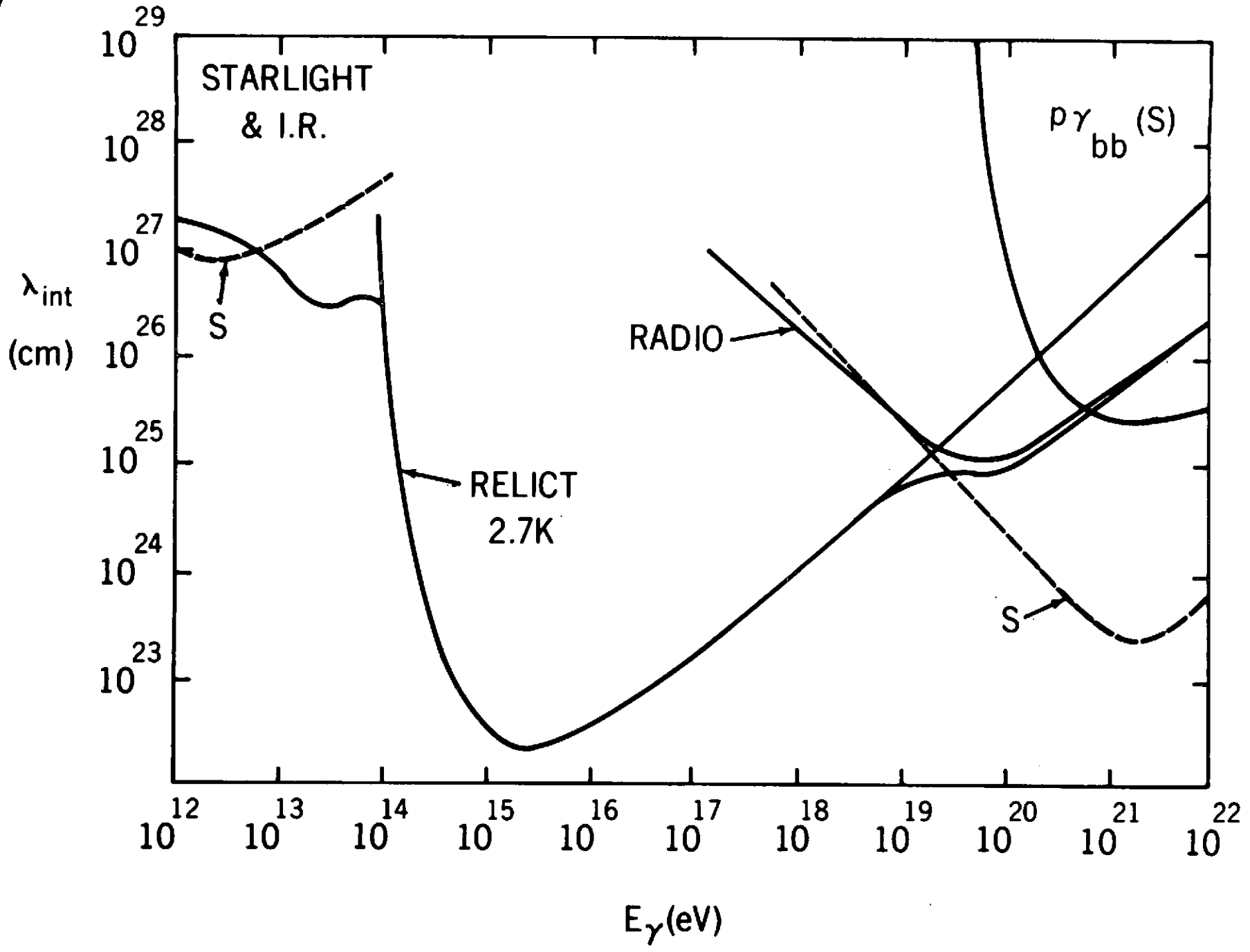


FIG 2

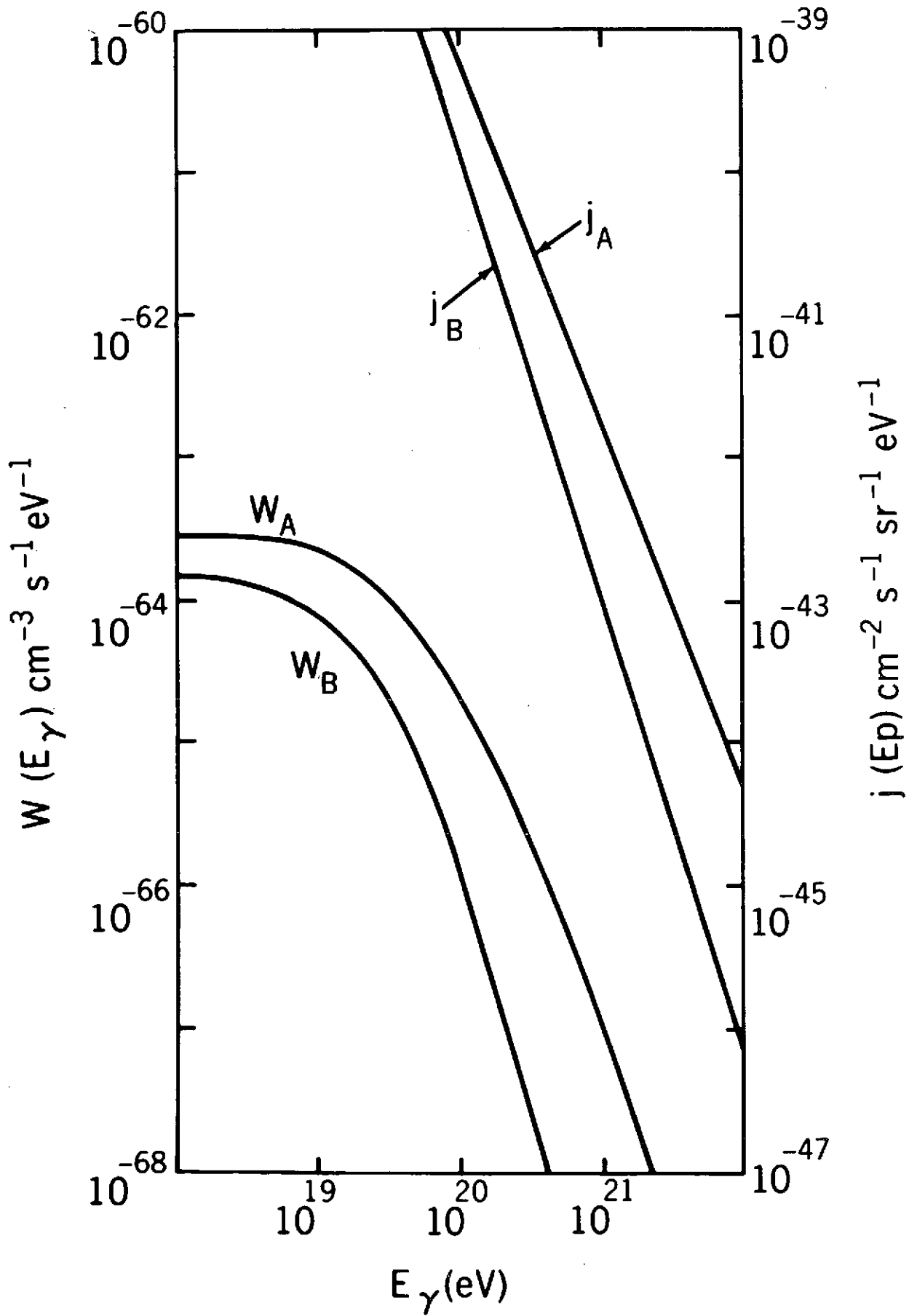
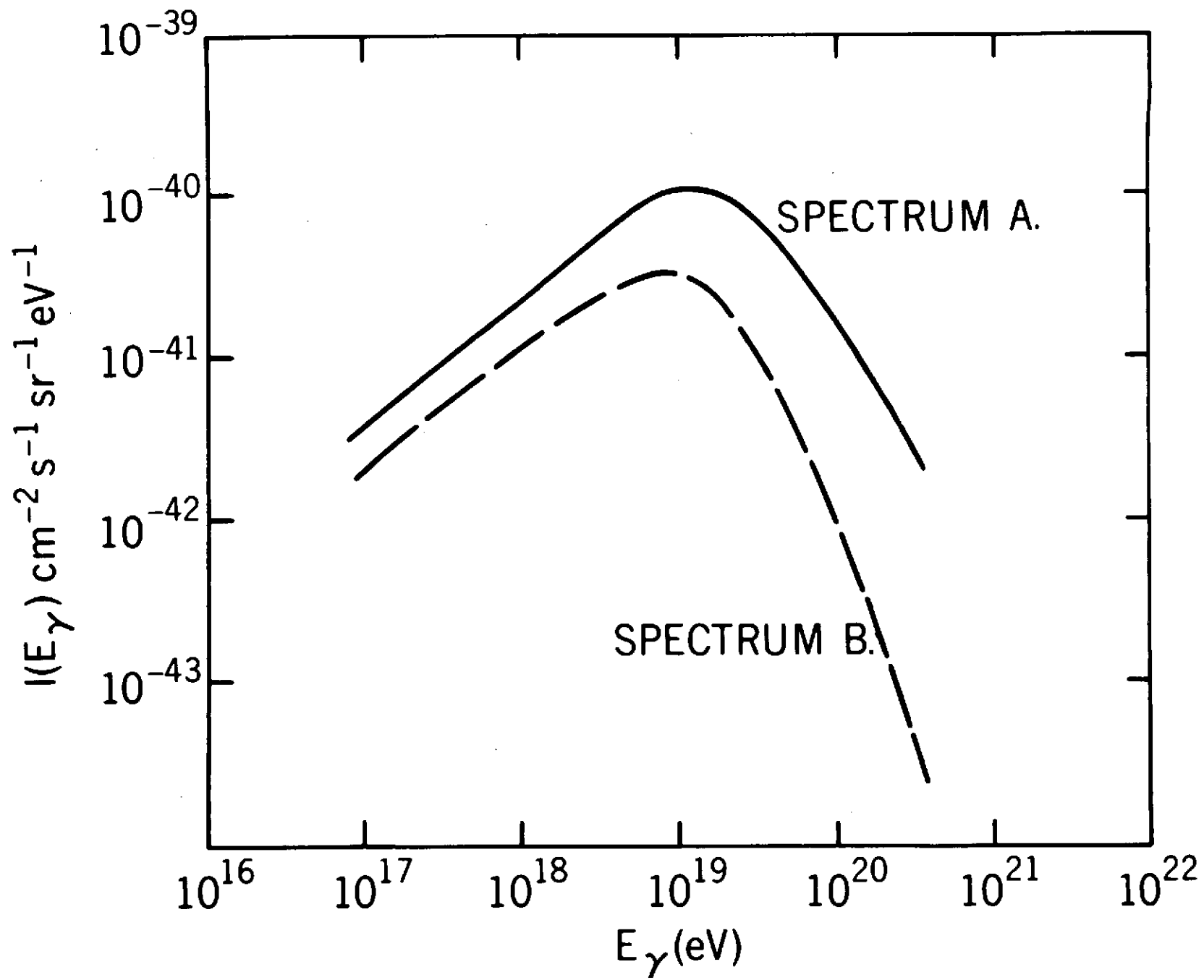


FIG 3



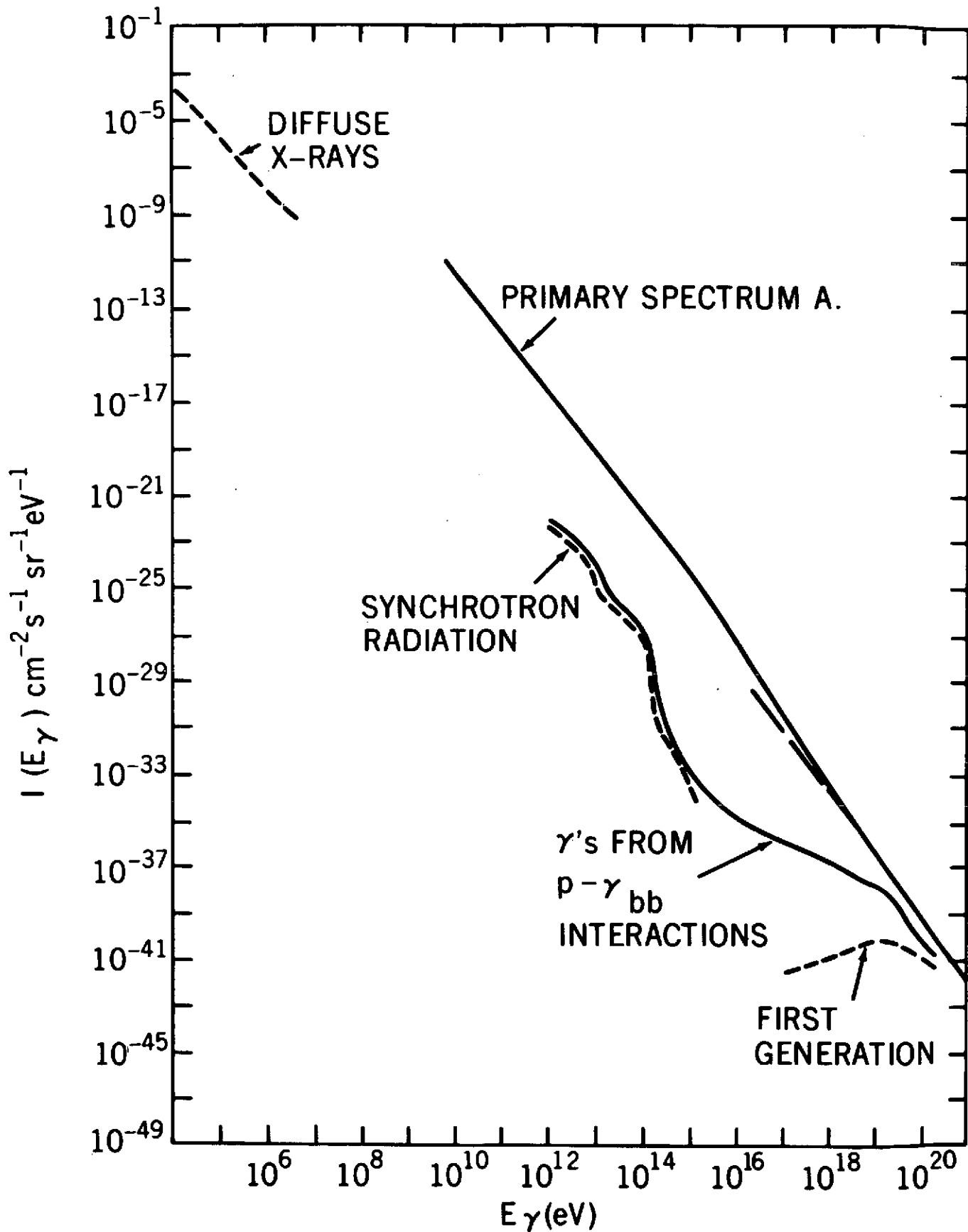


FIG 4

FIG 5

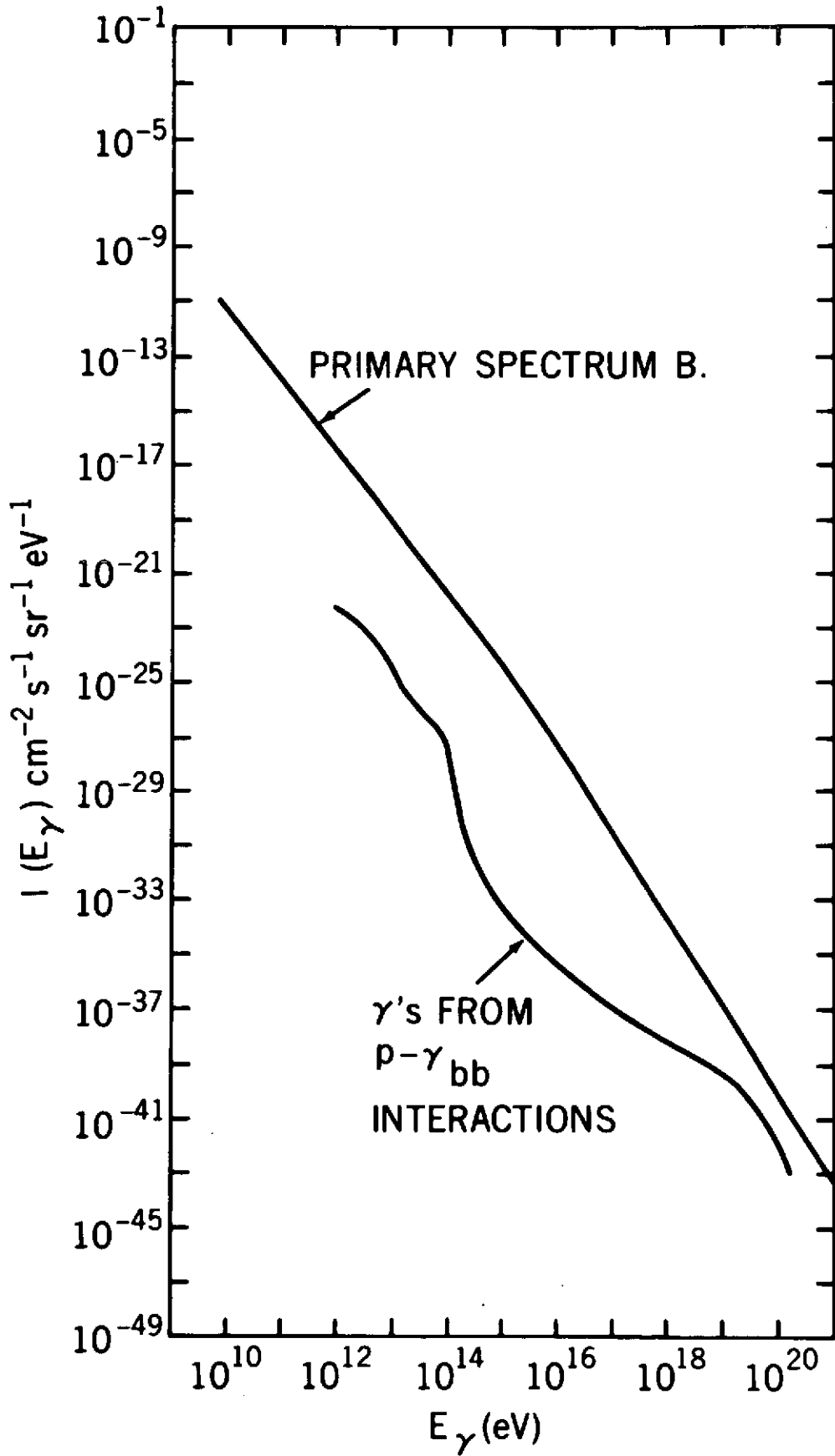


FIG 6

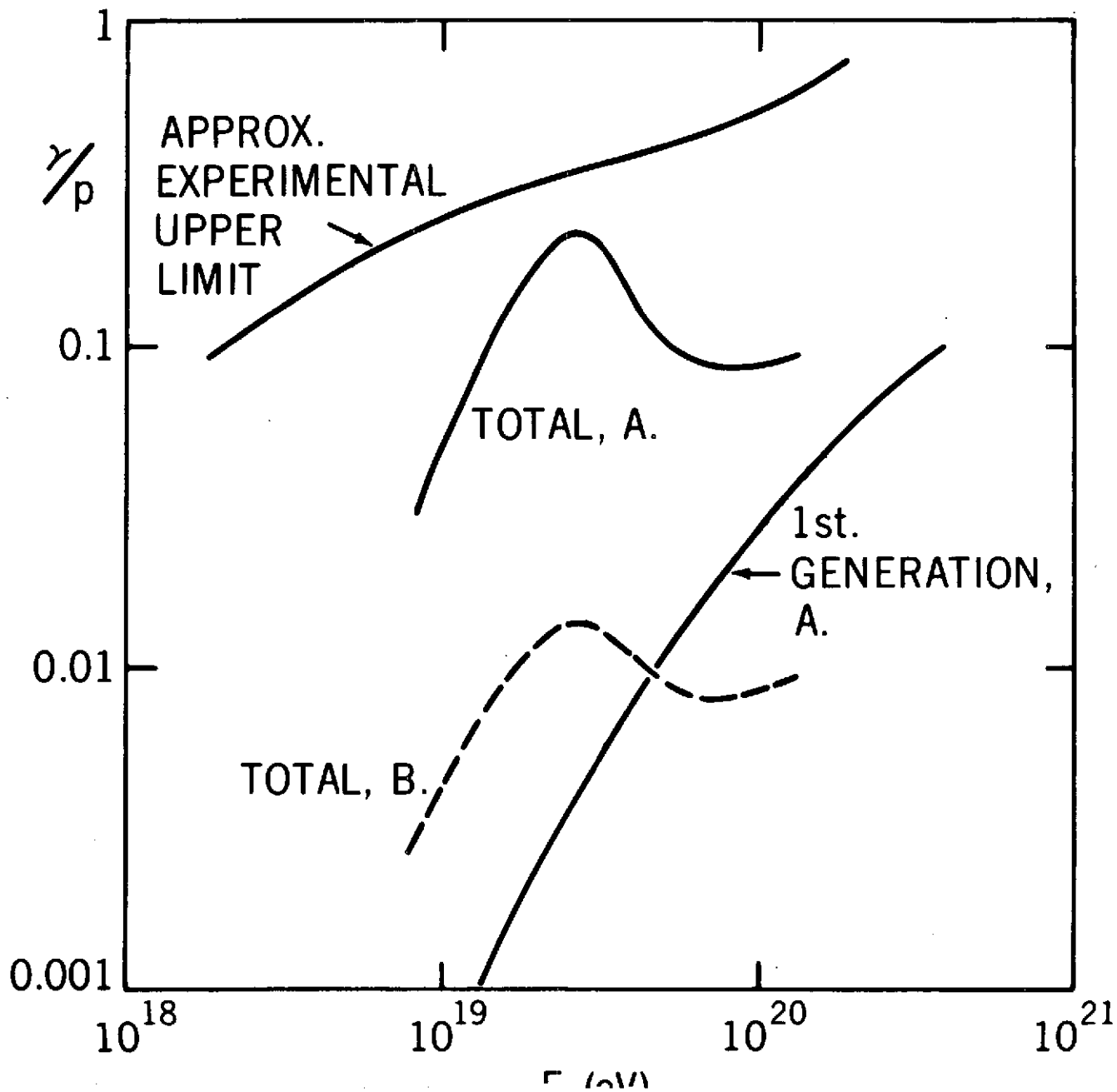
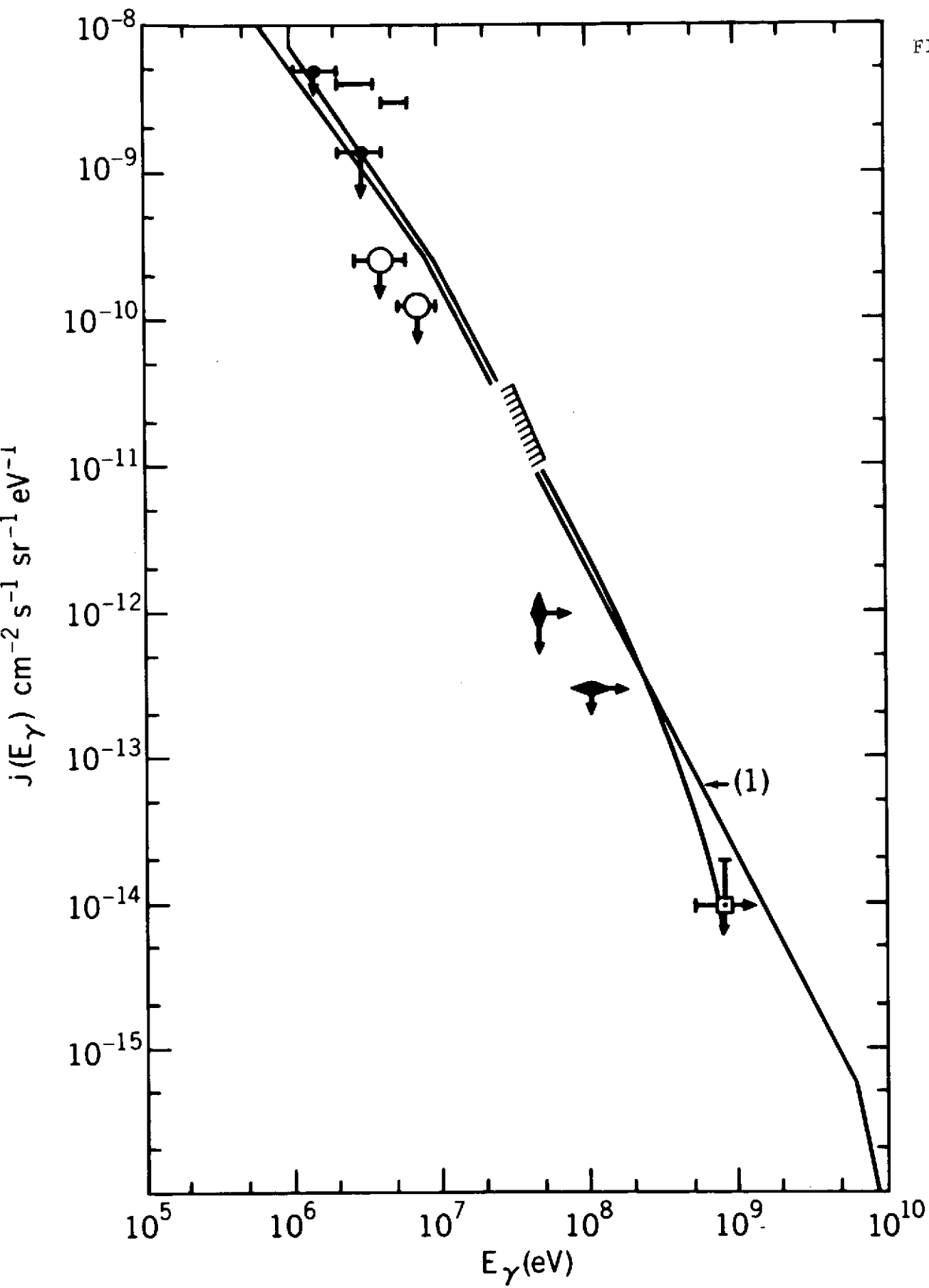


FIG 7



MATTER - ANTIMATTER COSMOLOGY

R. Omnès

Laboratoire de Physique Théorique et Hautes  
Energies

Université de Paris-Sud, 91405 Orsay, France

Congrès d'Astrophysique des Rayons  
Gamma organisé par la NASA au  
"Goddard Space Flight Centre"  
de Greenbelt, 30 avril - 2 mai 1973

Antimatter is quite a relevant subject for a meeting dealing with cosmic gamma rays since annihilation is an important potential source of hard photons. Therefore I am glad to have this occasion to report upon some recent work concerning the possible existence of anti-matter on a large scale.

The starting point of these investigations was an attempt to understand the origin of matter as being essentially analogous to the origin of the background thermal radiation. This background radiation is probably a remnant of a prior situation where the Universe was hot and space was much more compact than it is now. It was noticed long ago <sup>(1)(2)</sup> that, according to general relativity, an isotropic Universe had to pass through conditions where the temperature at early times was very high (this is the hot big bang cosmology). When the temperature was somewhat higher than 100 MeV, thermal radiation contained all kinds of elementary particles including among others nucleons and anti-nucleons. It is therefore tempting to wonder whether matter is a remnant of these particles. Preliminary investigations of this question showed however that a sufficiently efficient separation could not come from statistical fluctuations <sup>(3-4)</sup>. More precisely, if we introduce the basic parameter  $\eta = N/N_\gamma$  which is invariant under expansion (where  $N$  is the present particle density of matter and  $N_\gamma$  the density of thermal photons), one finds that statistical fluctuations give (ref. 4)

$$\eta \leq 10^{-18}$$

whereas the observed value is

$$\eta = 10^{-8} \text{ to } 10^{-10} \tag{1)-A}$$

Therefore some mechanism of separation between matter and antimatter, more efficient than mere fluctuations, had to be found.

A few years ago, it was noticed that nucleon-antinucleon interactions at intermediate energy (less than 1 GeV) could produce such a separation<sup>(5)</sup>. The basic idea is the following : According to the mesonic theory of nuclear forces<sup>(6)</sup>, it turns out that the S-wave scattering of nucleons and antinucleons is repulsive, i.e. the scattering lengths are positive. The same result is also found from a phenomenological analysis of nucleon-antinucleon interactions<sup>(7)</sup>. This important feature can in principle be checked experimentally by measuring with enough precision the energy of X rays emitted by the protonium ( $p\bar{p}$ ) atom<sup>(8)</sup> and this experiment is now under way at CERN<sup>(9)</sup>. If this effective low-energy repulsion between nucleons and antinucleons turns out to be correct, it could in principle induce a separation between nucleons and antinucleons among the particles constituting thermal radiation at high temperatures.

This hypothesis has been analyzed theoretically, by using a variety of different models<sup>(5,10-13)</sup>, with the following conclusion : Separation could indeed be the result of a phase separation occurring above a critical temperature which is of the order of 300 MeV. Some approximations had to be made in all of these models so that this conclusion can only be considered as tentative. I shall not deal in detail with this question to-day.

A detailed study of the Universe evolution when the temperature drops from 300 MeV to 30 keV has been performed recently<sup>(14)</sup> with the following results :

- The parameter  $\eta$  is essentially stabilized after a period

of intense annihilation at  $T = 1$  MeV at the value

$$\eta \geq 10^{-9} \quad (2)$$

(only a lower limit could be obtained).

- The system of matter and antimatter constitutes an emulsion (i.e. a three-dimensional maze). The size of such an emulsion can be characterized by the ratio  $L$  between a large volume  $V$  and the area of the matter-antimatter boundary  $S$  enclosed in this volume

$$L = \left\langle \frac{V}{S} \right\rangle. \quad (3)$$

$L$  is equal to  $10^{4.5}$  cm when  $T = 1$  MeV and a volume  $L^3$  contains at that time a mass of matter of the order of  $10^{13}$  g.

- Neutrons are lost by annihilation around 1 MeV so that there is no helium formation at this stage.

Here again, I shall not deal with the details of this analysis.

### Coalescence

I come now to the first subject of this talk which is to show how annihilation along the matter-antimatter boundary can induce important fluid motions by the effect of which the emulsion size  $L$  will grow tremendously during the radiative period. This effect has been called coalescence<sup>(15-16)</sup>.

First, let me stress that this effect is relevant for any antimatter model of the Universe. Even if the separation effect described above were but a theoretician's dream, coalescence would still be the essential feature of a model where matter and antimatter would be given in separate regions in the initial conditions at time zero<sup>(17)</sup>

or any other conceivable model.

This investigation has been carried out by Aldrovandi, Caser, Puget and Omnès (to be published).

The basic idea is the following : along the matter-antimatter boundary, annihilation produces high-energy particles : photons, electrons and positrons. These particles, together with secondary particles which they put into motion by collisions, carry their momentum to the fluid which is made of matter (or antimatter) and radiation over some distance  $\lambda$ . Let us consider the case where the boundary has a curvature radius  $R$  and  $\lambda \ll R$ . Since as many particles are generated by annihilation which are going towards matter or towards antimatter, the pressure they exert on both sides of the boundary is inversely proportional to the area of the effective surface where they are stopped. These areas are proportional to  $(R + \lambda)^2$  and  $(R - \lambda)^2$  so that a discontinuity pressure  $[p]$  appears along the boundary :

$$[p] = 2 p_a \frac{\lambda}{R} \quad (4)$$

where  $p_a$  is the annihilation pressure carried by the high-energy particles.

Formula (4) is of a well-known type : it is essentially the Laplace-Kelvin formula which gives the discontinuity pressure associated with a surface tension with coefficient

$$\alpha = 2 p_a \lambda \quad (5)$$

so that we expect it to reduce the boundary area, i.e., according to Eq. (3), to increase  $L$ . This is coalescence.

Perhaps it should be mentioned at this stage that the amount of matter or antimatter connected within the emulsion is infinite

despite the finite value of  $L$  (i.e. you can go to infinity by staying within the maze)<sup>(18)</sup>. As a result, coalescence is but an unfolding of the boundary.

### The theory of coalescence

The details of the analysis look a bit different when the temperature is respectively larger or smaller than 100 eV because in the first case high-energy photons have a small mean free path (because of the reaction  $\gamma + \text{thermal photon} \rightarrow e^+ e^-$ ). Below  $T = 100$  eV, this mean free path becomes larger than  $L$  so that primary photons (due to  $\pi^0$ 's annihilation) do not contribute to coalescence. I shall restrict myself to this last case.

In order to treat quantitatively the coalescence effect, one performs an analysis of the transfer and thermalization of particles. High-energy particles as well as thermal photons and matter electrons are described by a set of Boltzmann equations.

Primary high-energy electrons (generated by  $\pi^- \rightarrow \mu^- \rightarrow e^-$ ) first give their momentum to thermal photons by Compton scattering. Thereby they give rise to X-rays which carry the momentum. These X rays travel along a distance  $\lambda_0 = (N \sigma_T)^{-1}$  and give all their momentum to some electrons by Compton scattering. After this first collision they travel a distance much longer than  $L$  before being thermalized so that their energy is homogeneously distributed over the emulsion and does not affect the motion of the fluid. The second-generation electrons transfer their momentum, partly to thermal photons through Compton collisions (say a fraction  $\xi$  of this momentum) and partly to the matter plasma by Coulomb collisions (i.e. a fraction  $1 - \xi$ ).

It is a somewhat trivial but tedious exercise to compute the particles spectra and to write the Boltzmann equations which describe these processes. Once we have these Boltzmann equations, we can write hydrodynamical equations by taking as usual the first few moments of the particles distributions. For the plasma we get an equation of motion which is

$$\rho_m \frac{d\vec{v}}{dt} = (1 - \xi) \frac{\vec{J}}{\lambda_0} - \frac{\rho_m \vec{v}}{\zeta_D} + \frac{\vec{P}}{\zeta_0} - \vec{\nabla} p_m \quad (6)$$

where  $\rho_m$  is the plasma mass density.  $\vec{J}_c$  is the momentum density of X rays.  $\vec{P}$  is the density of momentum of thermal photons so that the third term in the r.h.s. represents the momentum given by radiation to the plasma. The second term represents the inverse effect : The plasma transfers its momentum to photons within a time of drag  $\zeta_D$ . One has

$$\zeta_0 = \lambda_0/c \quad \zeta_D = \frac{3}{4} \frac{\rho_m}{\rho_\gamma} \zeta_0 \quad (7)$$

The last term in Eq. (6) represents the effect of the plasma pressure which is in general negligible except near the boundary where annihilation creates a loss in particles.

The equations for thermal photons need not be written here because, even when they are written in a form involving hydrodynamical motion plus diffusion, they are still ugly. Let us note only that for distances larger than  $\lambda_0$  (the thermal photons mean free path), the system plasma + radiation behaves like a unique fluid obeying the equation of motion :

$$\rho \frac{d\vec{V}}{dt} = - \vec{\nabla} \frac{E}{3} + \frac{\vec{J}}{\lambda_0} + \eta_V [\vec{\nabla}^2 \vec{V} + \frac{1}{3} \vec{\nabla} (\vec{\nabla} \cdot \vec{V})] \quad (8)$$

Here  $E$  is the energy density of thermal radiation ( $E/3$  is the pressure)

and  $\eta_V$  is the viscosity coefficient

$$\eta_V = \frac{8}{27} \frac{\lambda_0 E}{c} . \quad (9)$$

Eq. (8) must be supplemented by an equation for the energy transfer which is

$$\frac{\partial E}{\partial t} + \vec{\nabla} \cdot (\vec{J}c + D \vec{\nabla} E + \frac{4}{3} E \vec{V}) = 0 . \quad (10)$$

These equations of motion must be completed by a boundary condition which gives the pressure discontinuity across the boundary. The basic idea has already been given and the passage from kinetic equations to discontinuity follows the lines provided by the kinetic theory of surface tension<sup>(19)</sup>. One gets

$$\left[ \frac{E}{3} \right] = \frac{4}{3} \frac{J(0) \lambda_0}{R} = \frac{\alpha}{R} . \quad (11)$$

### The annihilation rate

The annihilation pressure  $p_a$  or the momentum density  $cJ(0)$  are determined by the rate of annihilation at the boundary. To compute it, one can use Eq. (6). Essentially what happens is the following : annihilation creates a dip in the plasma density which tends to be filled under the effect of the plasma pressure gradient  $\vec{\nabla} p_m$  while the corresponding flow of matter is slowed down by the drag of plasma against radiation. This gives

$$J(0) \simeq N \left[ \frac{kT}{4 \pi m_p} \frac{\tau_p}{t} \right]^{\frac{1}{2}} m_p c . \quad (12)$$

As a result, it is found that only a small fraction of matter ( $\ll 10^{-2}$ ) is annihilated during the coalescence period so that  $\eta$  does

not decrease appreciably.

The rate of coalescence

Given the hydrodynamical equations together with the boundary condition (11), one can compute the rate of change of  $L$  with time. In fact, the extreme geometrical complexity of the emulsion can be turned into advantage by averaging the equations over a large volume  $V$ . This leads to a simple equation for the variation of  $L$  :

$$\ddot{L} = \frac{\alpha(t)}{\rho(t)} L^{-2} \quad (13)$$

which can be explicitly solved, taking into account the rate of change of  $\alpha$  and  $\rho$  with time which is due to expansion. The result is again quite simple, namely

$$L^3 = \frac{16}{5} \frac{\alpha}{\rho} t^2 . \quad (14)$$

It is found therefore that  $L$  increases with time, which is coalescence.

For numerical purposes, one can compute the mass  $M$  contained within a typical volume  $V$  of the emulsion. We have chosen for  $V$  the average volume which is seen from an interior point, which turns out to be given by

$$V = 8 \pi L^3 \quad (15)$$

so that

$$M = \rho_m V . \quad (16)$$

For  $T = 3000^\circ\text{K}$ ,  $t = 10^{13}$  sec (the conventional end of the radiative period), one gets

$$M \approx 10^{43} \text{ g} \quad (17)$$

i.e. a galactic mass.

The size of inhomogeneities. Galaxy formation.

We have found that coalescence generates quite naturally inhomogeneities of matter and antimatter which can be at the origin of galaxies.

In fact, things are not that simple : Because of annihilation, matter is kept ionized in the symmetric Universe a much longer time than in the conventional hot big bang model, so that coalescence can still go on during this long recombination period and generate much higher masses. Moreover drag becomes less effective, which tends to increase the rate of coalescence. Furthermore the viscosity becomes much smaller so that turbulence can be generated.

The study of this long recombination period is still incomplete. I believe Puget and Stecker will say more about it in this meeting<sup>(20)</sup>. The masses of matter will be larger than before, i.e. rather in the range of mass of clusters and matter will have a turbulent motion (i.e. the kind of situation first envisioned by Ozernoy<sup>(21)</sup>). The main difficulty ordinarily found with turbulence (i.e. its dissipation at the end of the radiative period)<sup>(22)</sup> is much reduced here since turbulence would be generated by the coalescence motion itself.

Antimatter and gamma rays

Coming back to the subject of this meeting, it is interesting to consider the consequences of this model as far as gamma ray detection is concerned. For the sake of <sup>the</sup> argument, we shall consider the Puget-

Stecker model where whole clusters are made of only one type of matter. These clusters are born from the largest eddies generated by coalescence.

In such a case<sup>(20,23)</sup> annihilation on the boundaries of clusters is too weak to be detectable at the present level. Apparently, the only detectable gamma rays come from early annihilation and could be seen in the isotropic background around 1 MeV after being red-shifted<sup>(24)</sup>. This effect will be described in a communication by Stecker.

#### What is the evidence for antimatter ?

Except for the 1 MeV bump in the X-ray background, the present model has behaved somewhat like a hat from which a rabbit was drawn: The correct amount of matter in the Universe has been computed, Puget and Stecker claim that the model gives the right kind of turbulence (i.e. the right size for the largest eddies and the right velocities) to agree with the parameters of clusters and galaxies (i.e. their mass and angular momentum), so that it gives exactly those cosmological parameters which up to now had been hidden in the initial conditions. Furthermore, the model has also shown a remarkable knack for embodying past objections<sup>(24)</sup> and using them for progress : the hat is still being brushed but the rabbit is well alive<sup>(14-16)</sup>.

However, one feels quite frustrated to find how difficult it is to show experimentally the existence of antimatter.

I am now going to describe briefly one conceivable type of consequence. It concerns a possible mechanism for the activity of quasars and Seyfert galaxies which is yet far from being properly analyzed. In fact, I only mention it here because of its possible relevance to gamma-ray astronomy and my excuse for releasing it too early will be the

occasion provided by this meeting.

An oecumenic model of quasars

Many models of quasars have already been proposed. Let us recall a few of them<sup>(25-28)</sup> :

- Quasars have been tentatively identified with supermassive stars<sup>(29,30)</sup>. The main difficulty for this theory comes from the star temperature which is too low for nuclear energy to be produced efficiently. One must therefore appeal to rotational energy, but this raises difficult problems of conversion<sup>(31-35)</sup>.

- A non relativistically rotating supermassive star tends to collapse rapidly. This has led to a variety of models for quasars where some stabilization is provided by rotation<sup>(31-35)</sup>, turbulence or magnetic fields<sup>(36,37)</sup>. These last two agents are good stabilizers, but turbulence should be continuously generated by a process which has not yet been found, up to my knowledge.

- Several models of quasars identify them with star clusters<sup>(38-42)</sup>. For our purpose, the basic aspect of this class of models is the importance it lays on collisions.

- One has suggested antimatter as an efficient source of energy for quasars<sup>(43-45)</sup>. Here the difficulty is to propose a specific structure for the matter-antimatter system<sup>(46-47)</sup>. One must also be aware of the limitations imposed to annihilation by the observation of high-energy gamma rays<sup>(48,49)</sup>.

I shall briefly describe here another model of quasars which has been suggested by the matter-antimatter symmetric cosmology. Because it reconciles many features of already existing proposals, it might be

called an oecumenic model. A convenient consequence of this character is that most relevant calculations have already been done in the literature.

Let us now state the model : A supermassive star  $\Sigma$  made of antimatter is located within the nucleus of a matter galaxy. Energy is generated by the annihilation of accreting matter and impinging stars. Heat being thus produced in a stochastic manner, large <sup>temperature</sup> differences are produced between the regions where annihilation is taking place and the average temperature. Turbulent convection is therefore continuously generated. On the other hand high magnetic fields are expected.

There are reasons derived from our cosmological model to expect the occurrence of such a peculiar object. It is conceivable (albeit not yet quite clear nor necessary) that, by effect of the coalescence motions, some amount of antimatter may be trapped within matter. The general characteristics of coalescence as described above shows that the mass of this inclusion cannot be too small as compared to a galactic mass, say  $M \gtrsim 10^8 M_{\odot}$ . The contraction of such a mass of antimatter will take place after recombination as a consequence of annihilation pressure (i.e. the high-energy electrons and positrons produced by annihilation communicate their momentum to matter and antimatter if there is a magnetic field. Such a strong boundary pressure can induce contraction<sup>(50)</sup>). In this way we expect that a supermassive star such as  $\Sigma$  could be produced.

It may be that  $\Sigma$  has a hard early life and there are a few unsolved problems concerning this period : it is necessary that stabilization by turbulence or magnetic fields occur very soon after the birth of  $\Sigma$  to avoid collapse and this point has not been clarified

(although we expect in this model galaxies to contract at the same epoch as  $\Sigma$  because of the same mechanism). Also one does not know why  $\Sigma$  should stand in the galactic nucleus : maybe its large mass could serve to start the initial condensation of the galaxy or its motion in the galaxy would lead it to the center either by gravitational effects<sup>(51)</sup> or because of a specific viscosity generated by annihilation<sup>(52)</sup>.

Assuming the existence of such an object, we will now show that it behaves in many ways like a quasar. For the sake of definiteness, we shall consider an object  $\Sigma$  with mass  $10^8 M_{\odot}$  with a radius  $R = 1$  pc. situated at the center of a galactic nucleus. We shall use data concerning our galaxy for the environment density so that most accreting matter is probably in the form of stars<sup>(53)</sup>. One finds that 2.2 stars (with a solar mass) are entering into  $\Sigma$  every year with a velocity 1000 km/sec. The average particle density  $\langle N \rangle$  in  $\Sigma$  is  $10^9$  antiprotons per cc, and the average mass density  $\langle \rho \rangle$  is  $10^{-15}$  g per cc.

The characteristics of  $\Sigma$  are well known<sup>(25)</sup>. Its density profile is that of a polytrope with index  $n = 3$ . The temperature  $T$  is related to the density  $\rho$  by

$$T = 1.97 \times 10^7 \text{ } ^{\circ}\text{K} \left( \frac{M}{M_{\odot}} \right)^{1/6} \rho^{1/3}_{\text{c.g.s.}} \quad (18)$$

The thermal luminosity is given by

$$L_{\text{th}} = 1.3 \times 10^{38} \left( \frac{M}{M_{\odot}} \right) \text{ erg/sec.} \quad (19)$$

However, it should be pointed out that this value for  $L_{\text{th}}$  may be over-estimated if large magnetic fields contribute to the pressure near the surface. If it were left to itself,  $\Sigma$  would start gravitational collapse when it reaches a critical state corresponding to a central density

and a radius

$$\rho_c \approx 2 \times 10^{18} \left( \frac{M}{M_\odot} \right)^{-7/2} \text{ g/cc.} \quad (20)$$

$$R_c (M/M_\odot = 10^8) = 3 \times 10^{-2} \text{ pc.} \quad (21)$$

(if one assumes  $\Sigma$  to be made of pure hydrogen).

The energy of  $\Sigma$  is then independent of its mass

$$E_c = -4 \times 10^{54} \text{ ergs.} \quad (22)$$

An important quantity is the evolution time of  $\Sigma$ , which can be quite small if  $\Sigma$  is not stabilized otherwise, namely

$$t_c = -\frac{E_c}{L_{th}} \geq 10^9 \left( \frac{M}{M_\odot} \right)^{-1} \text{ years.} \quad (23)$$

$\Sigma$  is heated by infalling stars which begin to annihilate when they penetrate antimatter. Their initial velocity is  $(GM/R)^{1/2} = V$ . The star surface is heated by annihilation: an energy flux is produced which is essentially given by  $\dot{q} = VN mc^2$  where  $m$  is the proton mass. (When  $V$  is reduced, this flux becomes of the order of  $V_s N mc^2$  where  $V_s$  is the local sound velocity). The cascade of thermalizing particles has been analyzed in another context<sup>(16)</sup>. First X rays are produced, by the products of annihilation ( $\gamma, e^\pm$ ), via pair production, Compton effect and the reactions  $\gamma + \text{thermal photon} \rightarrow X$  and  $e + \text{thermal photon} \rightarrow X$ . These X rays are later on thermalized by Compton effect. Large quantities of energy are accumulated near the surface of the star where the particle density is much larger than  $N$ . Two cases are possible which have been only analyzed grossly and both lead to the same result: either strong convective motions take place which blow off the star envelope, or energy is transported by diffusion over a distance of the order of

CS

the star radius. In that case, the local temperature becomes larger than  $10^7$  °K. Once again this leads to a blowing off of the envelope by evaporation.

The long-distance transport of energy in  $\Sigma$ , in which the main pressure is radiative, will take place through shock waves. These shock waves will leave a complicated pressure distribution resulting into turbulence. Altogether, the annihilation process appears to be rather complicated and violent and it is very difficult to analyze it in detail. The only simple relation which can be derived comes from energy balance :

$$2 \pi R^2 n v M_{\odot} c^2 = \langle L \rangle . \quad (7)$$

Here  $n$  is the star density around  $\Sigma$  and  $\langle L \rangle$  the average luminosity, in general higher than  $L_{th}$ . Many parameters are free here, so that it is no surprise that the highest known quasar luminosities are easily obtained.

One will not detect the original products of annihilation. Gamma rays produced by  $\pi^0$ 's will be stopped on a short distance by several processes (pair production upon protons and electrons, Compton effect, pair production by collision with thermal photons) so that this model does not contradict the limit set upon annihilation by gamma ray astronomy<sup>(48)</sup>.

The most difficult question that is raised by this model is to describe the kind of average equilibrium which will take place in  $\Sigma$ . It is only locally heated by annihilation in a random way and the energy is carried mostly by turbulence and shock waves. It would obviously be essential to analyze this kind of processes and see what limitations can be imposed on the radius (by star penetration) and on the encounter frequency (by the evolution time of  $\Sigma$ ). We have not yet done this work because we

were not able to master the problems of transfer which are involved. Let us note only a favourable circumstance: strong fluid motions should be continuously generated, which would tend to stabilize  $\Sigma$ . (36,37)

Another unsolved problem concerns magnetic fields. It is a general consensus that annihilation can produce large magnetic fields, although only preliminary studies of this effect have been made (54-56). Large scale magnetic fields can also be present in  $\Sigma$  since the origin or be produced by relative motions (including differential rotation).

Things are complicated by the violent events which the model predicts. Too much local energy generation can result into instabilities, ejection of antimatter, rejection of matter, even disruption of  $\Sigma$  (considering the small value of  $E_c$ ). However  $\Sigma$  will not suffer fragmentation (57). Despite the nightmarish character such a system may have for a theoretician, it does not look incompatible with what is observed.

An important new feature of this kind of model concerns the lifetime of quasars. Typical values of  $M = 10^8 M_\odot$  and  $\langle L \rangle = 10^{46}$  ergs/sec. give a lifetime  $\tau \approx 10^9$  years. Values of  $M/M_\odot$  up to  $10^2$  times higher are still compatible with the model. This shows that quasars have been active since the origin of galaxies. The highest red-shifts of quasars provide therefore an important cosmological information. Furthermore a strong evolution towards decay is predicted with the right order of lifetime (58).

To conclude, let us now list what relations can be made between the model and observations.

1) Evolution (58)

2) The validity of the Christmas tree behaviour for compact radio sources

(refs. 59, 68). The individual flashes corresponding here to a new star or a new cloud annihilating.

- 3) The analogy between Seyfert galaxies and quasars. In this model, the difference is only quantitative. All quasars should be in a galaxy<sup>(61)</sup>, even if it is only a dwarf one, as one would expect if the ratio between the masses of matter and antimatter is not far from one.
- 4) The ejected matter, in the form of dust and gas, has a stellar composition. Such ejected matter constitutes the atmosphere of  $\Sigma$ , which agrees with the characteristics of the emission lines<sup>(26)</sup>.
- 5) Multiple absorption red-shifts are probably due to gas ejected by radiation pressure and quenched by line-locking<sup>(62)</sup>.
- 6) Infra-red emission might be due to synchrotron emission by annihilation electrons in a high magnetic field<sup>(63)</sup>, but most probably it is due to external dust. Indeed, such dust should be abundant near a region where stars explode.
- 7) The origin of extended radio sources frequently associated with quasars and of the cosmic electrons radiating in these sources would be explained in this model as previously suggested by Layzer and Ozernoy<sup>(36,37)</sup>

Important observations to test the model might come from X-ray and gamma-ray observations of quasars with a low density central star, if it turns out that enough lower-energy gamma-rays from annihilation can escape. A cut-off in the energy of these gamma rays could be seen at a value related to the temperature existing in the annihilation region.

References

- (1) G. Gamow, Phys. Rev. 74, 505 (1948); Nature 162, 680 (1948);  
R.A. Alpher, H.A. Bethe and G. Gamow, Phys. Rev. 73, 803 (1948);  
R.A. Alpher, Phys. Rev. 74, 1577 (1948);  
R.A. Alpher and R. Herman, Phys. Rev. 74, 1737 (1948); Nature 162, 774  
(1948); Phys. Rev. 75, 1089 (1949);  
R.A. Alpher and R. Herman, Rev. Mod. Phys. 22, 153 (1950); Phys. Rev. 84,  
60 (1951); Annual Review of Nuclear Science 2, 1 (1953);  
R.A. Alpher, R. Herman and G. Gamow, Phys. Rev. 74, 1198 (1948); 75, 3321  
(1949);  
R.A. Alpher, J.W. Follin and R.C. Herman, Phys. Rev. 92, 1347 (1953);  
R.A. Alpher, G. Gamow and R. Herman, Proc. Nat. Acad. Sci. 58, 2179 (1967).
- (2) See for instance the recent books by Peebles and Weinberg.
- (3) M. Goldhaber, Science 124, 218 (1956).
- (4) Ya. B. Zel'dovitch, Advances Astron. Astrophys., Ed. Z. Kopal, 3, 241 (1965).
- (5) R. Omnès, Phys. Rev. Letters 23, 38 (1969); Phys. Rev. Comments and Addenda,  
Phys. Rev. 1, 723 (1970).
- (6) J.S. Ball, A. Scotti and D.Y. Wong, Phys. Rev. 142, 1000 (1969)  
R. Aldrovandi and S. Caser, Nuclear Physics B 39, 306 (1972)
- (7) R.A. Bryan and <sup>R.J.N.</sup>Phillips, Nuclear Physics 85 (1968) 201
- (8) S. Caser and R. Omnès, Physics Letters 39 B, 364 (1972)
- (9) G. Backenstoss, private communication
- (10) R. Omnès, Physics Reports 30, 1 (1972)
- (11) R. Aldrovandi and S. Caser, Nuclear Physics B 38 (1972) 593
- (12) A. Cisneros, Phys. Rev. 1973
- (13) R. Omnès, Proceedings of the I.A.U. Meeting on dense matter, Boulder, 1972.

- (14) R. Aldrovandi, J.J. Aly, S. Caser, R. Omnès, J.L. Puget, G. Valladas, unpublished.
- (15) R. Omnès, *Astronomy and Astrophysics* 11, 450 (1971); 10, 228 (1971); 15, 275 (1971)
- (16) R. Aldrovandi, S. Caser, R. Omnès, J.L. Puget, to be published, preprint LPTHE Orsay, Feb. 1973)
- (17) E.R. Harrison, *Mon. Not. Roy. Astr. Soc.* 142, 129 (1968); *Commun. Math. Phys.* 18, 301 (1970)
- (18) P.G. de Gennes, P. Lafore and J.P. Millot, *J. de Physique et le Radium* 20, 624 (1959); S.R. Broadbent and J.M. Hammersley, *Proc. Camb. Phil. Soc.* 53, 629 (1957).
- (19) *Handbuch der Physik*
- (20) F. Stecker and J.L. Puget, *Astrophysical J.* 178, 57 (1972)
- (21) L.M. Ozernoy, G.V. Chibisov, *Soviet Ast. A.J.* 14, 915 (1970)
- (22) R. Peebles in *Comments Astrophys. Space Phys.* 1972  
F. Lucchin  
N. Dallaporta, ~~et al.~~, *Astronomy and Astrophysics* 19, 123 (1972)
- (23) G. Steigman, Preprint Cal Tech OAP 296, August 1972 (to be published in the Proceedings of the Cargèse Summer School, 1971)
- (24) F.W. Stecker, D.L. Morgan Jr., J. Bredekamp, *Phys. Rev. Letters* 27, 1469 (1971)
- (25) Ya. B. Zeldovitch and I.D. Novikov, Relativistic Astrophysics, University of Chicago Press, 1971.
- (26) G.R. Burbidge and E.M. Burbidge, Quasistellar objects, San Francisco, Freeman, 1967
- (27) M. Schmidt, *Annual Review of Astronomy and Astrophysics*, 527 (1969)
- (28) Quasistellar sources and gravitational collapse, I. Robinson, A. Schild and E.E. Schücking, editors, Univ. of Chicago Press, 1963

- (29) F. Hoyle and W.A. Fowler, *Nature* 197, 533 (1963, M.N.R.A.S. 125, 169 (1963)).
- (30) W.A. Fowler, *Rev. Mod. Phys.* 36, 545, 1104 (1964)
- (31) W.A. Fowler, *Astrophysical J.* 144, 180 (1966)
- (32) I.W. Rosburgh, *Nature* 207, 363 (1965)
- (33) G.S. Bisnovatyi-Kogan, Ya. B. Zel'dovitch, I.D. Novikov, *Astr. Zh.* 44, 525 (1967)
- (34) J.M. Bardeen, S.P.S. Anand, *Astrophysical J.* 144, 953 (1966)
- (35) R.V. Wagoner, *Ann. Rev. Astr. Astrophys.* 7, 553 (1969)
- (36) D. Layzer, *Astrophysical J.* 141, 837 (1965)
- (37) L.M. Ozernoy, *Astr. Zh.* 43, 300 (1966)
- (38) T. Gold, W.I. Axford, E.C. Ray, in reference (4)
- (39) S.M. Ulam, W.E. Walden, *Nature* 201, 1202 (1964)
- (40) L. Woltjer, *Nature* 201, 803 (1964)
- (41) R.H. Miller, E.N. Parker, *Astrophysical J.* 140, 150 (1964)
- (42) L.J. Spitzer, W.C. Saslaw, *Astrophysical J.* 143, 400 (1966)
- (43) E. Teller, Perspectives in Modern Physics (Essays in the honor of H.A. Bethe), R.E. Marshak, edit. (Interscience, New York 1966)
- (44) G.R. Burbidge, F. Hoyle, *Nuovo Cimento* 4, 558 (1956)
- (45) A.G. Ekspong, N.R. Yamdagni, B. Bonnevier, *Phys. Rev. Lett.* 16, 564 (1966)
- (46) S. Aldrovandi, T. Montmerle, D. Péquignot (unpublished)
- (47) E. Schatzman, Physics and Astrophysics (CERN, Geneva, 1970)
- (48) G.W. Clark, G.P. Garmire, W.L. Kraushaar, *Astrophysical J.* 153, 203 (1968)
- (49) G. Steigman, *Nature* 224, 477 (1969)
- (50) R.A. Sunyaev, Ya. B. Zel'dovitch, *Astronomy and Astrophysics* 20, 189 (1972)
- (51) L.J. Spitzer in Nuclei of galaxies, O'Connell Editor, North-Holland (1971)
- (52) J. Lequeux, private communication

- (53) G.W. Rougoor, J.H. Oort, Proc. Nat. Acad. Sc. U.S. 46, 1 (1960)
- (54) E. Schatzman, CERN lectures (1970)
- (55) N. Peyraud, Astronomy and Astrophysics, January 1971
- (56) J.J. Aly, to be published
- (57) T. Montmerle, Thesis, Paris (1971)
- (58) M. Schmidt, Astrophysical J. 162, 371 (1970)
- (59) K. Kellerman, Communication at the 6th Texas Symposium, New York (1972)
- (60) W. Dend, *ibid.*
- (61) J. Kristian, *ibid.*
- (62) D. Wampler, *ibid.*
- (63) F.J. Low, Astrophysical J. 159, L173 (1970).

The deuterium puzzle in the symmetric universe

by

B. LEROY, J.P. NICOLLE and E. SCHATZMAN

D.A.F. Observatoire de Meudon

92190 Meudon (France)

INVITED PAPER

INTERNATIONAL SYMPOSIUM AND WORKSHOP ON  $\gamma$ -RAY ASTROPHYSICS

Presented by E. Schatzman

Abstract.

The examination of the experimental data concerning the reaction  $\bar{p} + {}^4\text{He} \rightarrow \text{pions} + \text{nuclei}$  shows that the low abundance of  ${}^2\text{D}$  can be explained only by assuming a low He abundance at the beginning of the radiative era. This is a completely independent confirmation of the evasion of neutrons (and antineutrons) from the emulsion before the end of the epoch where nucleogenesis might have taken place, and leads to an estimate of the size of the emulsion when  $T = 1 \text{ MeV}$ ,  $L \approx 10^{4.6} \text{ cm}$ .

In our present understanding of the model of the symmetric universe, we are led to the following picture, proposed by Omnès (1972)<sup>x</sup> :

---

<sup>x</sup> further references can be found in the paper quoted

---

(1) Separation era, during which a partial separation between baryons and anti baryons takes place, at  $t < 10^{-5}$  sec or  $kT > 350$  MeV (critical temperature of the phase transition) ;

(2) annihilation era ( $t < 1600$  sec,  $350$  MeV  $> kT > 25$  keV). At the end of the annihilation era, the annihilation pressure becomes efficient to produce the coalescence ;

(3) coalescence era ( $1400$  sec  $< t < 10^6$  years ;  $25$  keV  $> kT > \frac{1}{3}$  eV).

At the end of the coalescence era, the mean free path of the products of the annihilation become comparable to the size of the emulsion.

During the annihilation era, the size of the emulsion is governed by the diffusion of nucleons. If we look more closely to the situation, we can see, as shown by Steigmann (1972) that the main process is the diffusion of neutrons (at least, as long as there are neutrons). The only way in which neutrons can be kept in the emulsion is by neutron electron scattering. However, this can last only as long as there are black body electrons. As soon as the temperature drops below  $(1/2)$  MeV, the number of free electrons, which goes like  $10^{32.3} T_{\text{MeV}}^{-3} 10^{-(0.25/T_{\text{MeV}})}$  decreases very quickly. If the size of the emulsion is large enough the neutrons are kept until nucleogenesis takes place around  $T \sim 0.1$  MeV. If the size of the emulsion is too

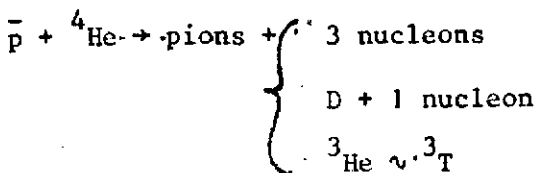
small, the neutrons are lost (they annihilate at the boundary of the emulsion), and no nucleosynthesis can take place. From the analysis of the diffusion process, this seems to be the case.

In the following, we shall consider how the present abundance of Deuterium can be used as an independent proof that no nucleosynthesis has taken place, and therefore that neutrons were lost before nucleosynthesis. The argument is the following :

- (1) we consider the nucleosynthesis during the radiative era ;
- (2) we estimate the relevant cross sections ;
- (3) we estimate the maximum abundance of  ${}^4\text{He}$  at the end of the nucleosynthesis era ;
- (4) we solve the diffusion problem in order to get an estimate of the rate of loss of the neutrons. This leads to a correction factor to the rate of formation of  ${}^4\text{He}$ . An estimate of this correction factor, to match the maximum abundance of  ${}^4\text{He}$  leads to an estimate of the maximum size of the emulsion.

### 1. Nucleosynthesis during the radiative era.

Let us consider the reactions taking place between nuclei and antinuclei at the boundaries of the emulsion. Let us assume that we have only protons and alpha particles. The reaction



leads mainly to the production of nucleons and the destruction of alpha particles. Half of the nucleons produced are destroyed in flight

in the regions of anti-matter, either in  $\bar{N}\bar{N}$  reactions or in  $N\bar{\alpha}$  reactions (fig. 1). Let us call  $R$  the probability of the reaction  $\bar{N}\bar{N}$  in flight and  $(1 - R)$  the probability of the reaction  $N\bar{\alpha}$  in flight. Neglecting provisionally the production of Deuterium and Tritium, we have the following expressions for the rate of reaction :

$$\frac{dp}{dt} = - \langle \sigma v \rangle_{pp} \bar{p}\bar{p} + \langle \sigma v \rangle_{p\alpha} \left[ -1 - \frac{3}{2}R + \frac{9}{2}(1-R) \right] p\bar{\alpha} \\ + \frac{3}{2} \langle \sigma v \rangle_{p\alpha} \bar{p}\bar{\alpha} + \langle \sigma v \rangle_{\alpha\alpha} \left[ \frac{3}{2} - \frac{3}{2}R + \frac{9}{2}(1-R) \right] \alpha\bar{\alpha}$$

$$\frac{d\alpha}{dt} = - \langle \sigma v \rangle_{p\alpha} \bar{p}\bar{\alpha} + \langle \sigma v \rangle_{p\alpha} \left[ -\frac{3}{2}(1-R) \right] p\bar{\alpha} \\ + \langle \sigma v \rangle_{\alpha\alpha} \left[ -1 - \frac{3}{2}(1-R) \right] \alpha\bar{\alpha}$$

By taking a proper average over space, and assuming  $\langle p \rangle = \langle \bar{p} \rangle$ ,  $\langle \alpha \rangle = \langle \bar{\alpha} \rangle$ , calling  $\lambda$  and  $\mu$  the ratios :

$$\lambda = \frac{\langle \sigma v \rangle_{p\alpha}}{\langle \sigma v \rangle_{pp}} ; \quad \mu = \frac{\langle \sigma v \rangle_{\alpha\alpha}}{\langle \sigma v \rangle_{pp}}$$

we obtain :

$$\frac{dp}{d\alpha} = \frac{p^3 + 2\lambda p^2\alpha + p\alpha^2(-5\lambda^2 + \frac{3}{4}\mu) - \frac{33}{4}\lambda\mu\alpha^3}{\lambda p^2\alpha + p\alpha^2(\mu + \lambda^2) + \frac{5}{2}\alpha^3\lambda\mu}$$

In a similar way, we can consider the rate of production of Deuterium. Estimating that the most important part in the balance equation for the deuterium arises from the deuterium production, we obtain,  $B$  being the branching ratio in the  $\bar{p}\alpha$  reaction :

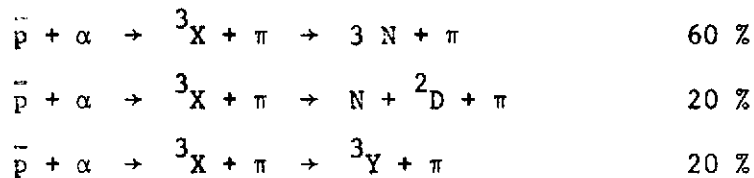
$$\frac{dD}{dt} \approx - \frac{\frac{\lambda p \alpha}{2} B (p + \frac{5}{2} \alpha \lambda)}{p^3 + 2\lambda p^2 \alpha + p \alpha^2 (-5\lambda^2 + \frac{3}{4} \mu) - \frac{33}{4} \lambda \mu \alpha^3}$$

It results from the experiments of Barkas et al. (1957), that in the reaction  $\bar{p}$  - nucleus, 1.3 pion on the average is absorbed in the nucleus, out of the average 5 pions produced in the annihilation.

After annihilation, we are left with an  ${}^3\text{He}$  or a  ${}^3\text{T}$  in excited states. We shall assume that the final nuclei left are in the same ratio as observed by Zaimidagora (1965, 1967) for the pion capture by  ${}^3\text{He}$ . According to the summary given by Koltun (1969), we have the following ratios :

$\pi^- + \text{He}^3 \rightarrow \text{H}^3 + \pi^0$	15.8 ± 0.8 %
$\pi^- + \text{He}^3 \rightarrow \text{H}^3 + \gamma$	6.9 ± 0.5 %
$\pi^- + \text{He}^3 \rightarrow p + 2n$	57.8 ± 5.4 %
$\pi^- + \text{He}^3 \rightarrow D + n$	15.9 ± 2.5 %
$\pi^- + \text{He}^3 \rightarrow D + n + \gamma$	3.6 ± 1.2 %
$\pi^- + \text{He}^3 \rightarrow p + 2n + \gamma$	?

To summarize briefly these datas, assuming that the  $\pi^-$  can do the same to  ${}^3\text{H}$  as to  ${}^3\text{He}$ , we shall accept the following branching ratios :



From these datas, we conclude immediately that very little  ${}^4\text{He}$  must have been left at the beginning of the radiative era, otherwise a too large abundance of  ${}^2\text{D}$  would have been produced.

## 2. Estimate of the cross section and rates of formation.

The  $\langle\sigma v\rangle$  includes both the nuclear part and the effect of the convergence of the wave function for caption at low energy. We have :

$$\sigma v = \sigma_{\text{nucl}} v \frac{2\pi n}{1 - e^{-2\pi n}}$$

with  $n = \frac{Z_1 Z_2 e^2}{\hbar v}$ . If we compare the two cross sections, and calculate the ratio :

$$\lambda = \frac{\langle\sigma v\rangle_{\bar{p}\alpha}}{\langle\sigma v\rangle_{\bar{p}\text{p}}}$$

we have to include the effect of the charge of the  $\alpha$ , the effect of the relative mass and of the relative velocity in the collision.

Assuming as already suggested by Schatzman (1970) :

$$\frac{\sigma_{\text{nucl}} \bar{p}\alpha}{\sigma_{\text{nucl}} \bar{p}\bar{p}} \approx 3.5$$

we obtain :

$$\lambda = \frac{\langle \sigma v \rangle_{\bar{p}\alpha}}{\langle \sigma v \rangle_{\bar{p}\bar{p}}} \approx 7$$

In the same way, we obtain, as an estimate :

$$\mu = \frac{\langle \sigma v \rangle_{\alpha\alpha}}{\langle \sigma v \rangle_{\bar{p}\bar{p}}} \approx 56$$

With these values, we get the main contribution to the rate of change of the abundances (for small values of  $\alpha$  and  $D$ ) ,

$$\frac{dp}{d\alpha} = \frac{1}{\lambda} \frac{p}{\alpha}$$

which gives .

$$\alpha = \alpha_0 (p/p_0)^\lambda$$

and .

$$\frac{dD}{dp} = - \frac{\lambda B}{2} \left( \frac{\alpha_0}{p_0} \right)^\lambda p^{\lambda-1}$$

which gives :

$$D = D_0 - \frac{B}{2} \alpha_0 \left( \frac{p}{p_0} \right)^\lambda$$

We see that we built the deuterium, whereas we destroy the  $\alpha$ 's.

Assuming that we start with zero deuterium, we have :

$$D_o = \frac{B}{2} \alpha_o$$

where the origin is taken at the end of the nucleosynthesis.

The final concentration (observed presently) gives :

$$\frac{D_o}{P} = \frac{D_o}{P_o} \frac{P_o}{P} \equiv \delta \quad \text{or} \quad \frac{D_o}{P_o} = \delta \frac{P}{P_o}$$

from which we derive :

$$\frac{\alpha_o}{P_o} = \frac{2}{B} \delta \frac{P}{P_o}$$

If we take the value of  $\delta$  at the surface of the Earth, as given by Urey et al., 1932, and Craig, 1961,  $\delta \approx 2.10^{-4}$  and with  $(2/B) \approx 10$ , we obtain :

$$\frac{\alpha_o}{P_o} \approx 2.10^{-3} \frac{P}{P_o}$$

If we take the protosolar gas value of Geiss and Reeves (1972),  $\delta = 3.10^{-5}$ , we obtain :

$$\frac{\alpha_o}{P_o} = 3.10^{-4} \frac{P}{P_o}$$

The ratio  $(p/p_o)$  is the annihilation ratio between 0.1 M.e.V, and 1/3 e.V. From the recent work of Aldrovandi, Caser, Omnès and Puget (1973), it is quite clear that most of the annihilation has

taken place already at 25 k.e.V., and we cannot expect  $(p/p_0)$  to be very small. For further calculations, we shall take  $(p/p_0) \approx 0.1$ , or  $(\alpha_0/p_0) \approx 2 \cdot 10^{-4}$  which represents a depletion factor  $\Delta$  at the end of the nucleosynthesis, compared to the results of Wagoner, Fowler and Hoyle (1967), of the order of  $10^{-3}$ .

This confirms entirely what has been announced earlier, that is to say that there is very little  ${}^4\text{He}$  left at the end of the epoch of nucleosynthesis.

### 3. Rate of loss of the neutrons and ${}^4\text{He}$ formation.

In order to get an idea of the rate of loss of the neutrons, we shall consider the diffusion with a time dependant diffusion coefficient to the surface of a sphere with a radius growing with time.

The equation of diffusion :

$$D \frac{1}{r^2} \frac{\partial}{\partial r} r^2 \frac{\partial \phi}{\partial r} = \frac{\partial \phi}{\partial t}$$

with  $\phi = 0$  at  $r = a(t)$ , can be solved in the following way :

Introducing  $r = x a(t)$ ,  $0 \leq x \leq 1$ ,  $d\tau = \frac{D dt}{a^2}$ , we have :

$$\frac{1}{x^2} \frac{\partial}{\partial x} x^2 \frac{\partial \phi}{\partial x} = \frac{\partial \phi}{\partial \tau}$$

A solution is  $\phi = \frac{\sin \pi x}{x} \exp(-\pi^2 \tau)$ , from which we derive the time scale of depletion by diffusion towards the boundary :

$$\left( \frac{dn}{dt} \right)_{\text{Diff}} = - \frac{\pi^2 D}{a^2} n$$

The equation of conservation of the neutrons becomes :

$$\frac{dn}{dt} = - n \frac{\pi^2 D}{a^2} - \frac{n}{\tau_n} + \frac{p}{\tau_p}$$

We are concerned by the last phase of nucleosynthesis, for  $kT < 1$  M.e.V., for which  $\tau_p$  increases very quickly to infinity. If we simplify the equation of formation of the  $\alpha$ 's to a pure neutron capture process, we obtain :

$$\frac{d\alpha}{dt} = \langle \sigma v \rangle_{pn} p n$$

and the number of  $\alpha$ 's at the end of the nucleogenetic period is :

$$\alpha = \int \langle \sigma v \rangle_{pn} p n_0 \exp \left( - \int \frac{1}{\tau_n} + \frac{\pi^2 D}{a^2} dt' \right) dt$$

We shall simplify the whole problem by assuming that the depletion factor  $\Delta$  can be estimated by the quantity :

$$\Delta = \left\langle \exp \left( - \int \frac{\pi^2 D}{a^2} dt' \right) \right\rangle$$

The average  $\Delta$  is obtained in the following way. We calculate the amount of Helium formed from the temperature  $T_1$  where the rate of destruction

${}^4\text{He}(\gamma, n){}^3\text{He}$  becomes negligible ( $T_1 \approx 0.8$  M.e.V.). The concentrations  $p$  and  $n_0$  are proportional to the expansion factor to the minus cube, and we can write :

$$\Delta \approx \frac{\int_0^{T_1} T^3 dT \exp \left[ - \int \frac{\pi^2 D}{a^2} dt' \right]}{\int_0^{T_1} T^3 dT}$$

From the estimate of the integral, and writing  $a = a_0 T_{\text{M.e.V.}}^{-n}$ , it is possible to get an estimate of  $a_0$ .

The result is not very sensitive to the value of  $n$ . With  $n = 17/6$  (corresponding to the rate of growth during the coalescence period), a diffusion coefficient :

$$D = 10^{8.15} T_{\text{M.e.V.}}^{-5/2} 10^{(0.25/T)_{\text{M.e.V.}}}$$

we obtain for  $\Delta = 10^{-3}$  a maximum value :

$$a_0 < 10^{4.69} \text{ for } \delta = 2 \cdot 10^{-4} \quad a_0 < 10^{4.64} \text{ for } \delta = 3 \cdot 10^{-5}$$

If we consider the formation of  ${}^3\text{He}$  and if we take the abundance ratio  ${}^3\text{He}/\text{H}$  as  $10^{-5}$ , we obtain  $a_0 < 10^{4.60}$ . This is quite compatible with the diffusion length. For a sphere :

$$L_D = \pi \left( \int D dt \right)^{1/2} \approx 10^{4.25} T_{\text{M.e.V.}}^{-9/4}$$

#### 4. Conclusion.

From this short discussion, we see that the low abundance of Deuterium is some sort of proof that the neutron loss has actually taken place before the beginning of the nucleogenesis.

We can then either assume that the diffusion length determines actually the size of the emulsion, and it seems quite possible that the abundance of the  $\alpha$ 's was vanishingly small at the end of the nucleogenesis. Or, we can assume that the abundance of Deuterium and other light elements results from the nucleogenesis. It then leads to a determination of the size of the emulsion during the nucleogenesis. In fact, a small amount of coalescence before the end of the annihilation period would be enough to increase the size of the emulsion beyond the diffusion length and put the two determinations in complete agreement.

A final comment is interesting to make. Since the beginning of the theory of the symmetric universe, a number of criticisms have been made, which have been met with success one after the other. Just like a puzzle, the pieces have been found to adjust to each other. In the present case, one has the feeling that the new piece has just matched a hole in between two pieces. This gives a great confidence for the future of the model.

Bibliography.

Aldrovandi, R., Caser, S., Omnès, R., Puget, J.L., 1973, A and A  
(to be published).

Barkas, W.H. et al , 1957, Phys. Rev., 105, 1037.

Craig, H., 1961, Science, 133, 1833.

Geiss, J., Reeves, H., 1972, A and A., 18, 126.

Koltun, D.S., 1969, Advances in Nuclear Physics, 3, 149.

Omnès, R., 1972, Phys. Reports, 3 C, 1.

Schatzman, E., 1970, Physics and Astrophysics, C.E.R.N. lectures.

Steigman, G., 1972, Caltech preprint O.A.P. - 280.

Urey, H.C. et al , 1932, Phys. Rev., 40, 1.

Wagoner, R.V., Fowler, W.A., Hoyle, F., 1967, Ap J 148, 3.

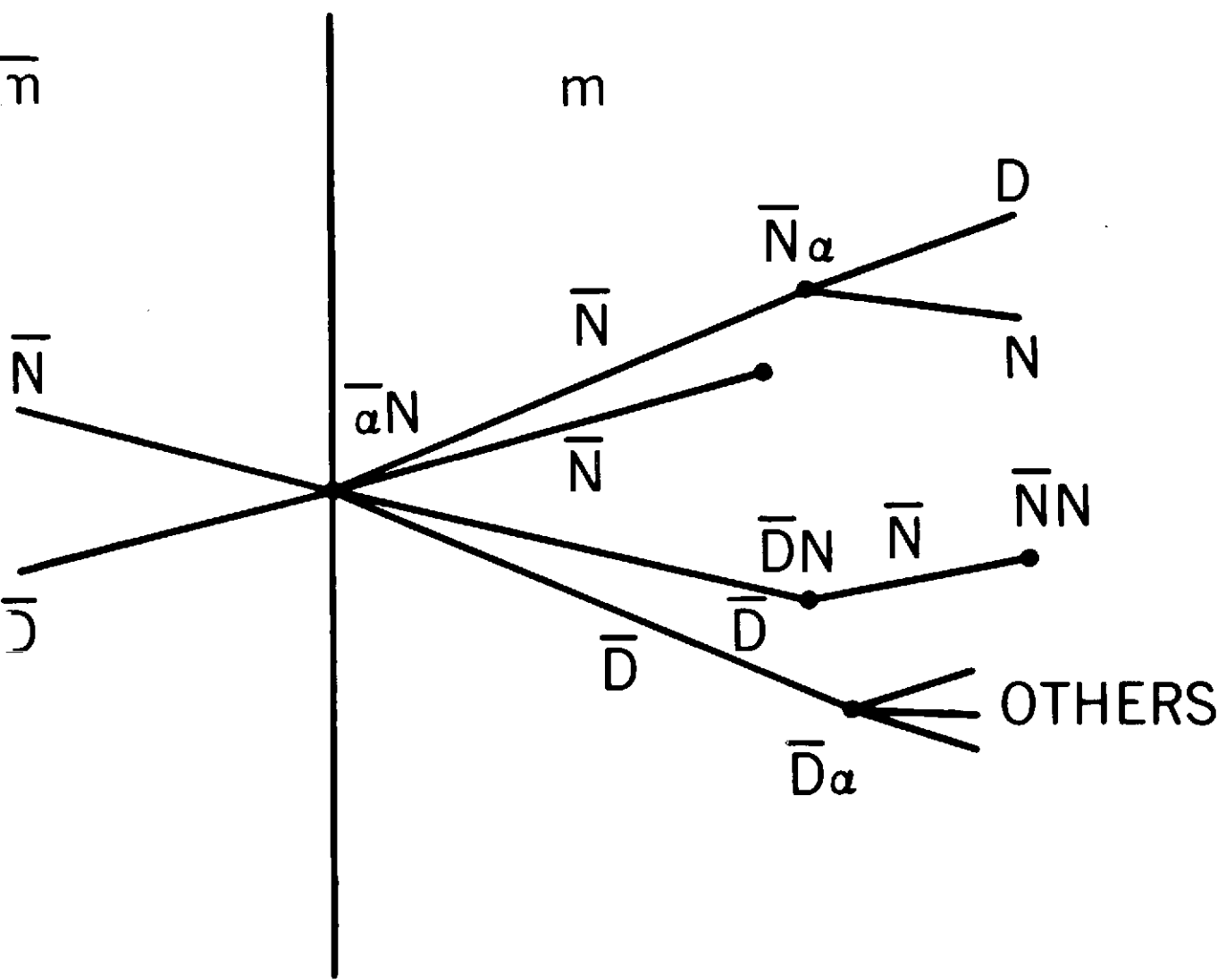
Zaimidoroga, O.A. et al , 1965, Sov. Phys. J.E.T.P., 21, 848.

Zaimidoroga, O.A. et al , 1967, Sov. Phys. J.E.T.P., 24, 1111.

Caption to the figures.

Figure 1 :

Schematic representation of the annihilation at the interface and the secondary reactions taking place in flight. Only the main reactions have been plotted following the  $\bar{\alpha} N$  reaction at the interface. A symmetric figure would have to be drawn, for the  $\alpha \bar{N}$  reaction.



Gamma-Ray Background Spectrum and Annihilation Rate  
in the Baryon-Symmetric Big-Bang Cosmology

J. L. Puget  
Department d'Astrophysique Fundamentale  
Observatoire de Meudon, France

The negative results of search for antimatter nuclei in cosmic rays, imply that if there is symmetry between matter and antimatter in the universe, each kind must be gathered in separated regions of galaxy or galaxy cluster size. In such a case, to try to get experimental information on the problem of baryon symmetry on a cosmological scale, we have to rely mostly on the observation of annihilation products. Among the annihilation products are gamma-rays and neutrinos which have very long mean free path. Neutrinos especially can reach us from dense regions; Steigman and Strittmatter (1971) used upper limits on the neutrino flux from space to put upper limits on the annihilation in Seyfert galaxies. Nevertheless for the diffuse background due to annihilation on a cosmological scale, gamma-rays are the best test available because they are easier to detect than neutrinos.

Two kinds of gamma-rays are produced in matter-antimatter annihilation; 0.511 MeV gamma-rays from positron annihilations (4.81 per annihilation); 70 MeV gamma-rays from  $\pi^0$  decay (3.4 per annihilation). The number of gamma-rays of each kind is roughly the same, and to compare them as a possible source of information on the annihilation rate we must look at their absorption cross-section and also at the background due to other sources.

The absorption cross sections are respectively  $10^{-25}$  and  $1.8 \cdot 10^{-28}$   $\text{cm}^2$  for 0.5 and 70 Mev gamma-rays; in a dense universe there is a "window" between 1 MeV and 10 GeV in which gamma-rays observed might come from a red-shift of about 100 (see Stecker, these proceedings). The X-ray background between 40 keV and 1 MeV can be represented by a power law with a spectral index 2.1, so it is more likely to detect the 70 MeV annihilation gamma-rays than the 0.5 MeV ones.

These considerations prove that the best direct experimental test for presence of antimatter on a cosmological scale lies in the gamma-ray background spectrum between 1 and 70 MeV.

#### I. Experimental data and red-shifted gamma-rays from annihilation

It has been shown by Stecker, Morgan and Bredekamp (1971) that the excess of gamma-rays observed above 1 MeV could be explained by annihilation of gamma-rays coming from high red-shift. They computed the spectrum (see Stecker, these proceedings) using a simple theoretical model for the annihilation rate dependence on the red-shift

$$\Psi_{\nu} = \Psi_{\nu,0} (1+z)^{6.36}$$

and they choose the constant  $\Psi_{\nu,0}$  to fit the data. That leads them to the conclusion, already found by Steigman (1969) that matter and antimatter cannot be mixed up in equal quantities in intergalactic space with a density larger than  $10^{-12}$   $\text{cm}^{-3}$ .

The most recent data show a very good agreement with the spectrum computed by Stecker et al. and leads us to a detailed discussion of the annihilation rate for red-shifts lower than 100. The theoretical spectrum below 70 MeV but above some MeV (when absorption is negligible) is a power law with an index (m = 3.5) (where the annihilation rate is written  $\Psi_v = \Psi_{v,0}(1+z)^m$ )

for  $-\Omega = \frac{n_0}{n_{crit}} = 1$  ( $n_{crit}$  is the so-called critical density of the Einstein-De Sitter model)

and (m = 3) for  $-\Omega = 0$

To get a good fit of the data one needs a spectral index of the order of 3 which means that m must be such that

$$6 \leq m \leq 6.5$$

so one can consider that the annihilation rate will fit the data if it falls in the range

$$\Psi_v = 10^{-34 \pm 0.5} (1+z)^{6.25 \pm 0.25} \text{ sec}^{-1} \text{ cm}^{-3} \quad (1)$$

## II. Matter-antimatter cosmology: theory

In the recent years, a baryon symmetric cosmology has been developed in the frame of the big-bang theory of the universe and is summarized in these proceedings by Omnes and Schatzman. In this model, matter and antimatter separate in an early stage and lead, at the end of the coalescence period, which coincides with the recombination time, to an emulsion of characteristic size given by

$$L = 5 \cdot 10^{29} (1+z)^{-\frac{17}{6}} \text{ cm} \quad (1+z > 600)$$

(fig 1)

and the fluid motions induced by the coalescence process on a scale of the order of  $L$  reach a velocity

$$V \sim \frac{L}{t} = 8.3 \cdot 10^{11} (1+z)^{-1.34} \text{ cm sec}^{-1} \quad (1+z < 600) \quad (\text{Fig. 2})$$

I want to discuss now what could happen in such a model after recombination (which takes place around  $1+z \sim 600$ ) to be able to discuss the problem of the annihilation rate. The following theory has been worked out by Stecker and Puget, 1972. On Fig. 1 is plotted the evolution of the characteristic dimension  $L$  of the emulsion as a function of red-shift. At the time of the original paper, the theory of coalescence in the radiative period has not been worked out completely yet and we developed a simple model in terms of cloud collisions to put upper and lower limits on  $L$ . Recent work (Aldrovandi et al. (1973)) allows us to plot the value of  $L$  up to the recombination red shift, and the corresponding fluid velocities induced by coalescence (Fig. 2). One can compute the Reynolds number corresponding to those coalescence motions and see that large scale turbulence is generated near recombination.

In a matter-antimatter symmetric big-bang, the annihilation electrons and positrons produce a large flux of X-rays by interaction with the cosmic black body photons, and these X-rays tend to keep the matter ionized longer than in a non-symmetric big-bang. Furthermore the recombination occurs very gradually and ionization remains high near the boundary regions, as shown on Fig. 3. The viscosity which was determined by the radiation field drops to the kinematic viscosity which

is 10 orders of magnitude lower when matter (or antimatter) becomes neutral and decouples from the radiation field. The large scale fluid motions become then supersonic. In order to compare the parameters of the annihilation generated turbulence with the parameters of primordial turbulence used by Ozernoi et al. (1970, 1971) in their theory of galaxy formation, we have neglected in a first step the remaining ionization after a red-shift of  $\sim 600$ . We find a good agreement taking account of the uncertainties in the theory of generation of turbulence.

I want to underline here the differences between the symmetric model and the non-symmetric one. Dallaporta and Lucchin (1972) have shown that it is likely that a primordial turbulence will be dissipated before recombination. In our model, turbulence is generated near or even during recombination, so this problem disappears. The question of dissipation during the phase of supersonic turbulence (before galaxy formation) and after galaxy formation might also be a very serious one as shown by Silk (1972). In the original model we just assumed for simplicity that no coalescence at all takes place after  $z \sim 600$ . In fact a source of motion exists. The ionization near the boundary shown on Fig. 3 which is due to photoionization collisions implies that the momentum carried away by these X-rays is transmitted to the matter with a mean free path which is of the order of the width of the ionized region. We are in a case where the annihilation pressure generates a surface tension of the type discussed by Omnes and co-workers (see Omnes in these proceedings). This surface tension which induces coalescence during the radiative period will take place also here and even if

the corresponding increase of size is negligible (which is certainly true for low  $z$  as we shall see later) the fluid motions induced will compensate at least partially the dissipation of kinetic energy.

The theory of this last period, which includes: galaxy formation from the density fluctuation induced by shocks in the supersonic turbulence generated at recombination time; formation of clusters by breaking of the emulsion in separate clouds; production of magnetic fields on the boundaries between matter and antimatter,.... is obviously a very complicated problem and it is not possible at this point to rely on a complete theory of this period to discuss the annihilation rate.

I shall now change my point of view and keeping in mind the general picture, make a detailed discussion of the annihilation rate relying on consistency of arguments and observations on one hand, and on the other hand on the elements of theory which have been worked out so far.

### III. Annihilation rate at $Z \ll 1$

As we have seen, the theory does not tell us if the regions of matter and antimatter are of a galaxy cell size or of a galaxy cluster cell size, so I shall consider the two hypotheses. If dense clusters contain as much matter as antimatter there will be several contributions to the annihilation. I shall consider these contributions without going into the details, considering only the conclusion we shall be lead to.

### 1. Intergalactic gas

Observation of diffuse sources of X-rays in 20 rich clusters shows that a hot intergalactic gas containing about as much mass as the galaxies themselves must exist in clusters. This inter-galactic medium must form an emulsion of matter and antimatter and considering the magnetic fields produced on the boundaries the diffusion can be slowed down to a level such that the annihilation rate does not exceed the value (1).

### 2. Galaxies - (Antigalaxies) and intergalactic-gas

The motion velocities of galaxies (antigalaxies) in a rich cluster are large (up to  $10^3$  km/s) and the cross time for a galaxy is smaller than the age of the universe, so a galaxy could be surrounded by matter or antimatter with equal probability. Accretion of intergalactic gas on large galaxies shall produce an annihilation rate

$$\Psi_{\nu, \text{gal}} \sim 1.2 \cdot 10^{-30} \left( \frac{M}{M_{\odot}} \right) \text{ sec}^{-1} \text{ cm}^{-3}$$

where  $M$  is the accreted mass by all the galaxies in one cluster per year and one sees that it must be smaller than  $10^{-4} M_{\odot}$  to bring the annihilation rate to the value (1) which seems too small.

### 3. Galaxy-Antigalaxy collisions

Detailed study of galaxy-antigalaxy collisions have shown that the annihilated mass is probably of the order of magnitude of  $M_A$  with

$$M_A = M_T \frac{V}{c}, \quad \left( \begin{array}{l} V \text{ is the relative velocity} \\ M_T \text{ the total interstellar gas} \\ \text{mass of the galaxy} \end{array} \right)$$
$$\Psi_{\nu, \text{gal}} = \frac{1.25 \cdot 10^{-16}}{T}$$

where  $\tau$  is the average collision time for one cluster; any evaluation of the collision time gives  $\tau \ll 10^{18}$  which means again that the annihilation rate from such a process would give more gamma-rays than observed.

If we consider cluster size regions, the annihilation takes place only on boundary regions and even with a dense intergalactic gas, magnetic fields slow down enough diffusion to bring the annihilation rate below the rate (1). (Puget, 1971)

In conclusion we shall make the hypothesis that clusters and groups of galaxies are of matter only or antimatter only; this gives us the present value of L:

$$L_0 = 2.5 \cdot 10^{25} \text{ cm}$$

and considering that for low  $z$ ,  $L$  is changing only with expansion because for coalescence to take place the fluid motions must be such that

$$V_f > V_{exp} = \frac{L}{t} = 4 \cdot 10^7 (1+z)^{1/2}$$

$V_{exp}$  is shown in Fig. 2 and it is clear that no/ significant coalescence can take place for  $Z < 200$  because the expansion velocity is then much larger than the maximum fluid velocity which we can expect.

We shall use  $L = L_0 (1 + Z)^{-1}$  up to  $1 + Z \sim 200$  and  $L = 5 \cdot 10^{29} (1 + Z)^{-17/6}$  for  $1 + Z > 200$  (we must nevertheless keep in mind that this last relation has not been fully justified for  $200 < 1 + Z < 600$  when the regions far from any boundary are neutral).

IV. Annihilation rate for  $1 + z < 100$

There is some observational evidence that cluster formation occurs at rather low  $z$ . In our picture the depression of density on boundary regions becomes deeper and larger and eventually gravity overcomes expansion and bound clusters are formed. We shall neglect here this process because other ones like ionizing radiation from quasars and/or young galaxies for  $z < 3$  also modifies the picture.

Let's study the motion of the plasma. For that purpose we need to find how the anisotropy and the temperature gradient affect the motion of the plasma. Physically, due to the importance of Thomson collisions of the electrons of the plasma with black body photons and with the X-rays and gamma-rays produced in annihilation, we are looking at the motion of the plasma on each side of the annihilation layer at distances much smaller than the mean free path of thermal photons. Technically, we write the Boltzman equation for the photons and integrate to get the equations of momentum conservation and energy conservation, to which we add the equations of motion of the plasma. These 3 equations have four unknown quantities: the temperature gradient, the anisotropy of the photon distribution, the velocity and the density of the plasma. We can eliminate the two first ones in order to get an equation of motion of the plasma which has to be combined with the continuity equation:

$$(2) \quad 0 = \frac{d}{dt} n v + N V (1 - \xi) \frac{c}{\lambda_0} e^{-u} - v_s^2 \frac{\partial n}{\partial x} - \frac{n v}{\tau_D} - \int_x^L \frac{N V}{L \tau_0} \frac{n - n_0}{n_0} dx$$

where  $v$  is the plasma velocity,  $n$  the plasma density,  $n_0 = \langle n \rangle$ ,  
 $N = n(x=0)$ ,  $V = v(x=0)$ ,  $u = \int_0^x \frac{n}{\lambda} dx$ ,  $\tau_D = \tau_0 k^{-1} = \frac{\lambda_0 k^{-1}}{c}$ ,

$\beta$  is the fraction of the momentum of the X-rays which is transmitted to the black body photons,  $v_s$  is the thermal velocity of the plasma,  
 $\beta = \frac{F_{\text{radiation}}}{F_{\text{matter}}}$ . During the radiative period, the second, third and fifth terms of this equation of motion of the plasma are negligible for distances smaller or of the order of  $L = \sqrt{2\tau_D v_s^2 t}$  which is the distance at which the density gradient extend. ( $\tau_D$  is the characteristic time for slowing down of charged particles by the radiation field.) The equation is then a simple equation of diffusion and the solution for  $n$  is:

$$n(x,t) = \frac{n_0}{\sqrt{4\pi\tau_D v_s^2 t}} \int_0^\infty e^{-\frac{(x-y)^2}{4\tau_D v_s^2 t}} dy$$

and

$$NV = (n v)_{x=0} = \frac{n_0 v_s}{2\sqrt{\pi}} \left(\frac{\tau_D}{t}\right)^{1/2}; \quad n(x) \text{ and } v(x) \text{ are plotted on fig 4.}$$

The annihilation rate is then given by

$$\Psi_v = \frac{3(n v)_{x=0}}{L} = 7.3 \cdot 10^{-29} (1+z)^{61/2}$$

The fifth term of equation (2) corresponds to the anisotropy of the photon field inducing a heat flow which dissipates the excess energy left by X-rays and gamma-rays in the regions where  $n$  is larger than the average  $n_0$ . For  $x \gg L$  it is the dominant term for the motion of the plasma, but it does not affect in a noticeable way the annihilation rate.

When  $(1+z)$  becomes lower than  $1.4 \cdot 10^3$ , the third term which is the flux of momentum from X-rays to the plasma, becomes as large as the fourth term which is the pressure gradient of the plasma, and must be included in the equation. The annihilation rate is given by

$$\Psi_v = \frac{3}{L} n_0 v_s \left( \frac{\tau_D}{t} \right)^{1/2} \frac{e^{-A^2}}{2\sqrt{\pi}} \left[ \frac{3}{8k} (1 - \text{Erf} A) + 1 \right]^{-1}$$

with

$$A = \left[ \int_0^t \tau_D \frac{NV}{m_0} \frac{1}{\lambda} (1-\xi) dt' \right] (4\tau_D v_s^2 t)^{-1/2}$$

$$\text{Erf}(x) = \frac{2}{\sqrt{\pi}} \int_0^x e^{-u^2} du \quad (\text{Aldrovandi et al 1973})$$

For  $\xi$  small enough to be negligible compared to 1, A is in fact almost a constant:  $A \sim 4.2$

$$\frac{NV}{n_0 v_s} = \frac{4k}{3\sqrt{\pi}} \left( \frac{\tau_D}{t} \right)^{1/2} e^{-A^2}$$

this leads to

$$\Psi_v = 1.7 \cdot 10^{-32} (1+z)^{73/12}$$

This solution is valid down to  $1+z \sim 600$ . Below that value it breaks down for two reasons having opposite effects

- L might increase slower than  $(1+z)^{-17/6}$  due to recombination

- The mean free path of the X-rays produced by the annihilation electrons and positrons which was equal to  $\lambda$ , becomes much shorter due to the large photo-ionization cross-section as shown on Fig. 1.

The equation of motion of the plasma in the vicinity of the boundary remains the same because of the ionization due to X-rays

(Fig. 3)\* but the momentum left in the plasma per unit time and unit volume is now proportional to  $\lambda_x^{-1}$  instead of  $\lambda_0^{-1}$ . ( $\lambda_x$  is taken equal to the distance from the boundary for which  $n_p/n_H = 1$ .) Figure 4 shows the density and velocity of the plasma as a function of distance from the boundary in units of  $v_c = v_s (\tau_D/\pi t)^{1/2}$ .

The equation giving the annihilation rate has to be solved numerically. The result is shown on Fig. 5\* which gives the annihilation rate as a function of red-shift and the range given by relation (1).

Considering the uncertainties of these calculations, the agreement is as good as can be expected. The major uncertainties affect the rate for  $1 + z \leq 5$  and must not affect very much the gamma-ray spectrum between 1 and 15 MeV. Furthermore, the gamma-ray flux must drop above 70 MeV and below 1 MeV so the theoretical spectrum is quite well defined. If the good agreement of this spectrum with the data is confirmed by future measurements, a way of checking this model will be to look at angular fluctuation of the background as a function of energy. The gamma-rays observed at the energy  $E_\nu$  come mostly from a red-shift  $1 + z \sim 70/E_{\nu(\text{MeV})}$  and the angular fluctuations will be related to  $L(1 + z)$ .

\*The results given on Fig. 3 and 5 are from preliminary numerical evaluations; exact numerical computations will be published later.

## References

- Aldrovandi R., Caser S., Omnes, R., Puget J. L., 1973, to be published.
- Dallaporta, N. and Lucchin, F., 1972, preprint GAT-IR 14.
- Ozernoi, L. M., Chibisov G. V., 1970, Astr. Zh. 47, 749, English translation in Soviet Astro. A.J. 14, 915.
- Ozernoi, L. M., 1971, Ap. Letters 7, 201.
- Puget, J. L., 1971, Nature 230, 173.
- Stecker, F. W., Morgan, D., Bredekamp, J., 1971, Phy. Rev. Letters 27, 1469.
- Stecker, F. W., Puget, J. L., 1972, Ap. J. 178, 57.
- Steigman, G., 1969, Nature 224, 477.
- Steigman, G., Stittmatter, 1971, Astron. and Astrophys. 11, 279.

## Figure Captions

- Fig. 1 The different lengths relevant to the problem are plotted as a function of red-shift.
- $\lambda_0$  is the mean free path of thermal photons
- $\lambda_x$  (10 percent) the mean free path of X-rays corresponding to 10 percent ionization rate.
- $\lambda_x$  (50 percent) the mean free path of X-rays corresponding to 50 percent ionization rate.
- Fig. 2 The velocities relevant to the problem are plotted as a function of red-shift.
- Fig. 3 The ratio of the proton density to the neutral hydrogen density is given for three values of the red-shift as a function of the distance from the annihilation layer.
- Fig. 4 The density and velocity of the plasma are given as a function of the distance from the boundary. The unit for the  $v$  scale is  $v_c = v_s (\tau_D / \pi t)^{1/2}$
- Fig. 5 The annihilation rate is given as function of red-shift.

FIG 1

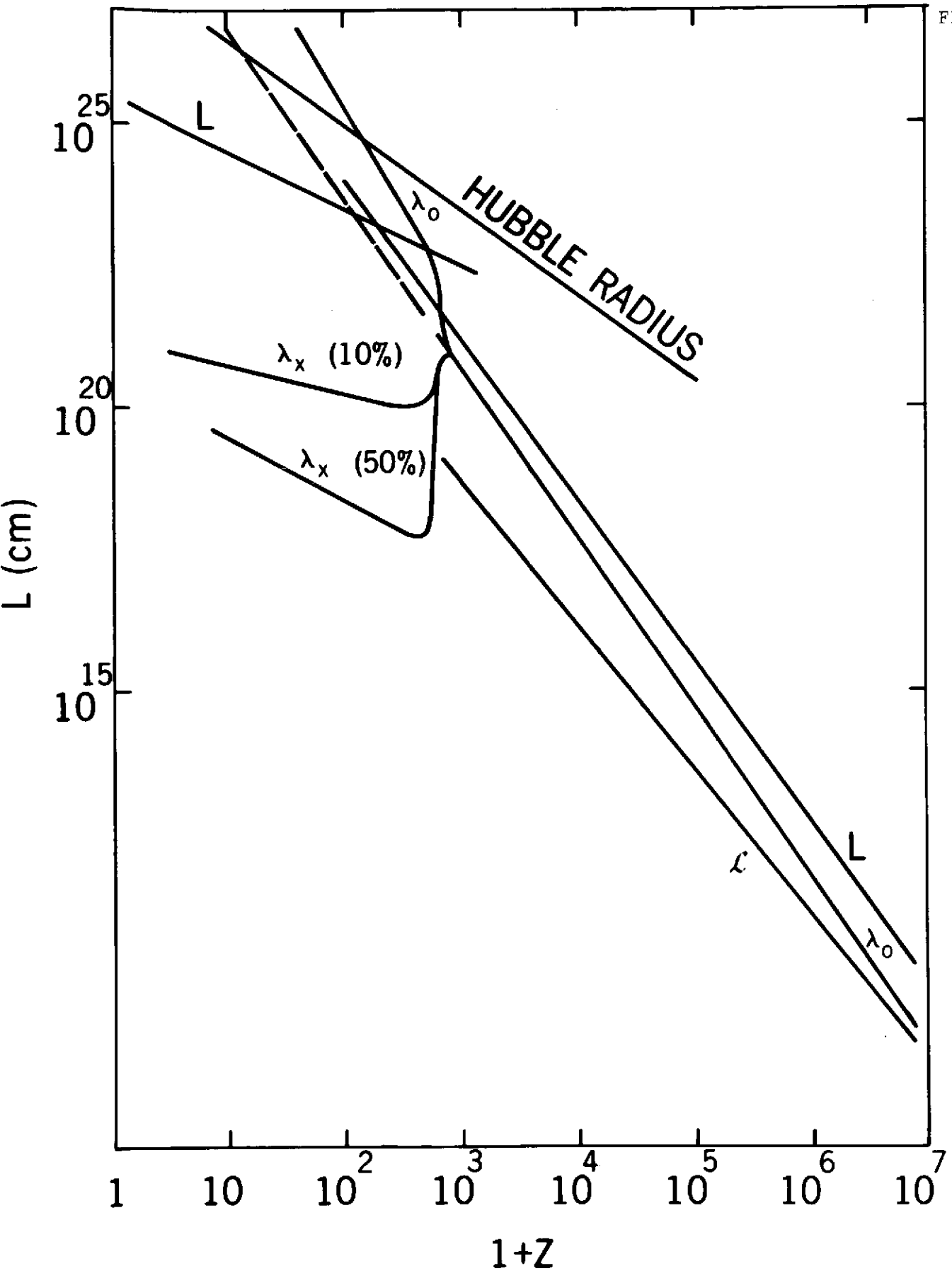


FIG 2

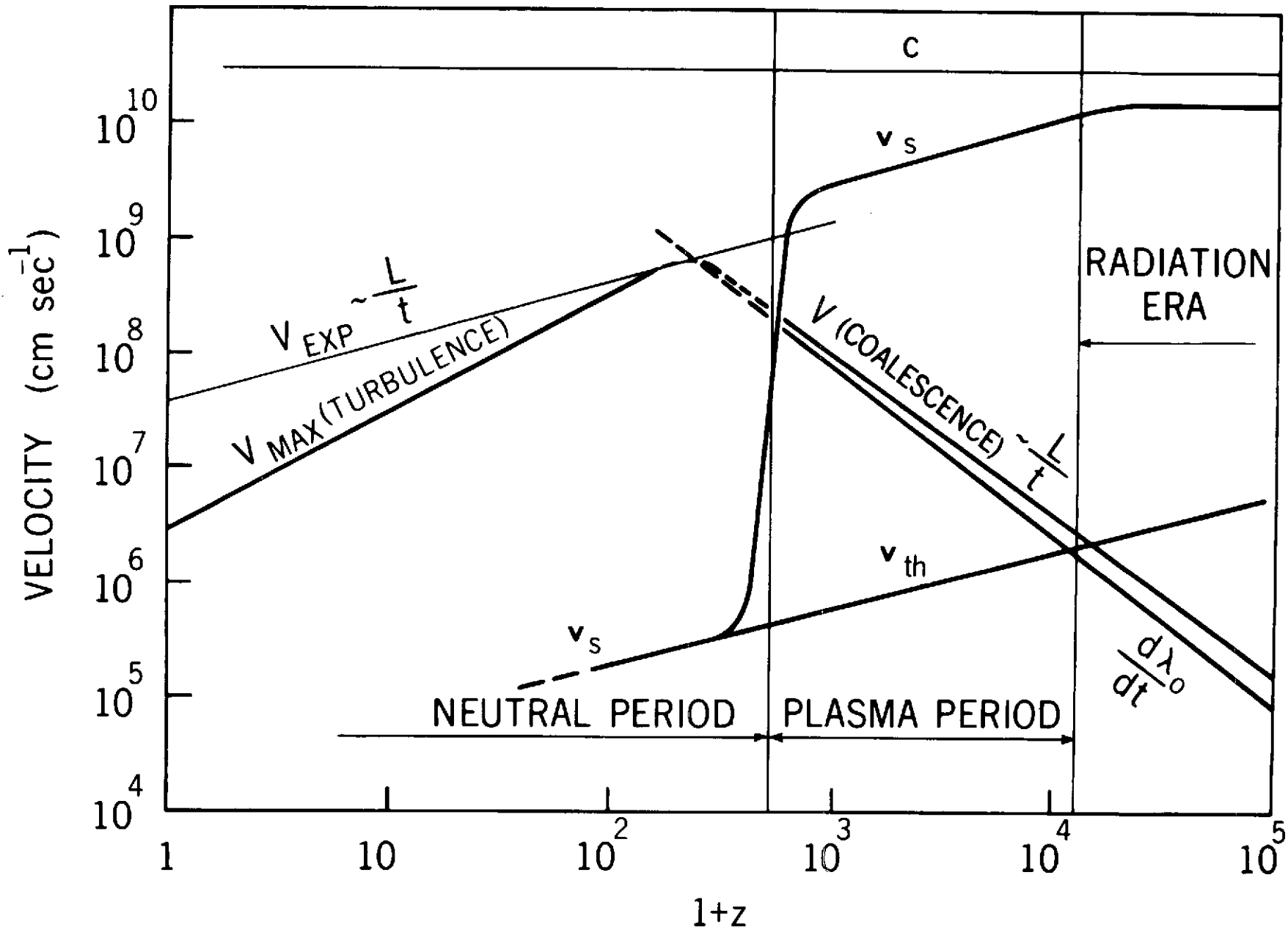
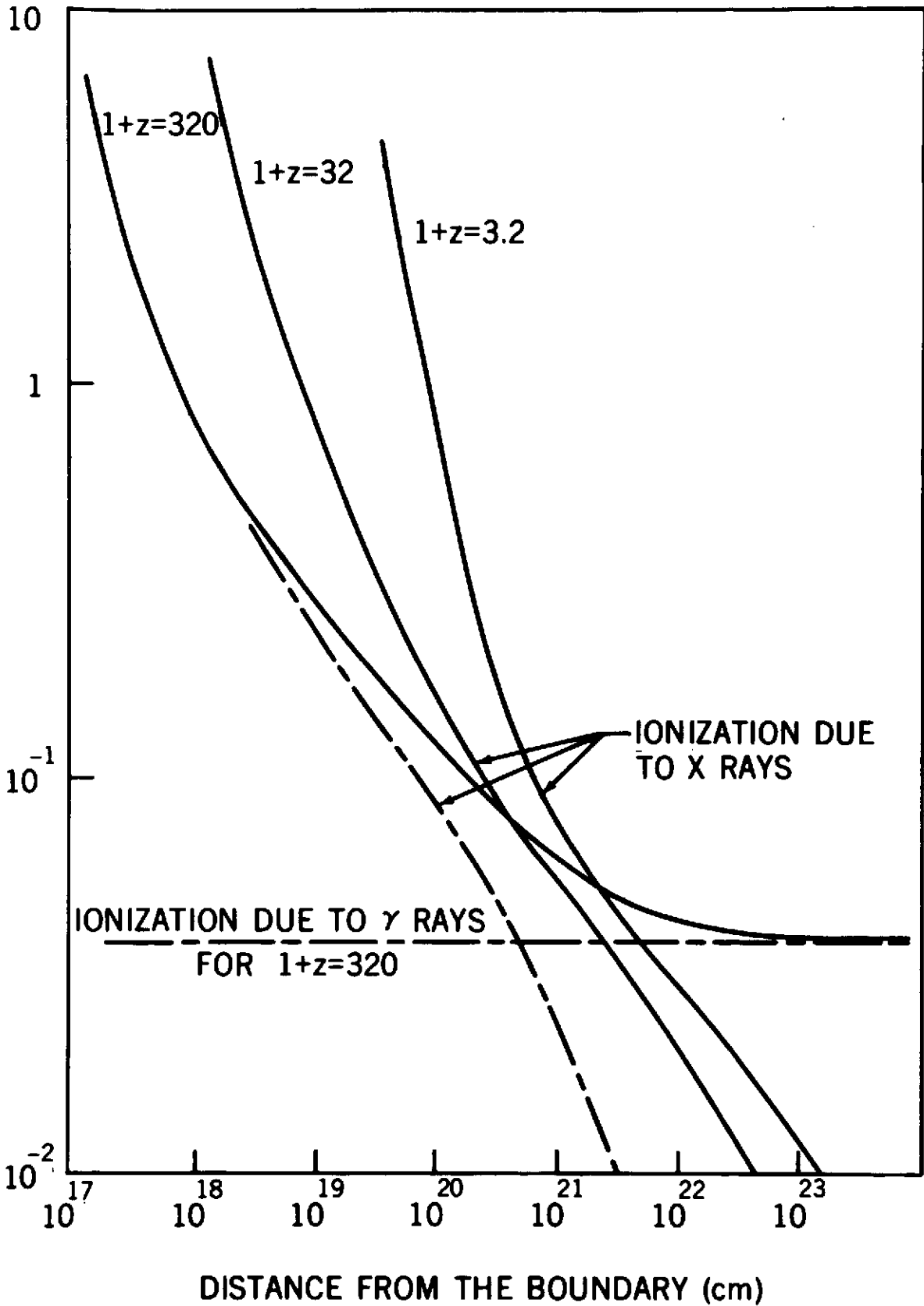


FIG 3



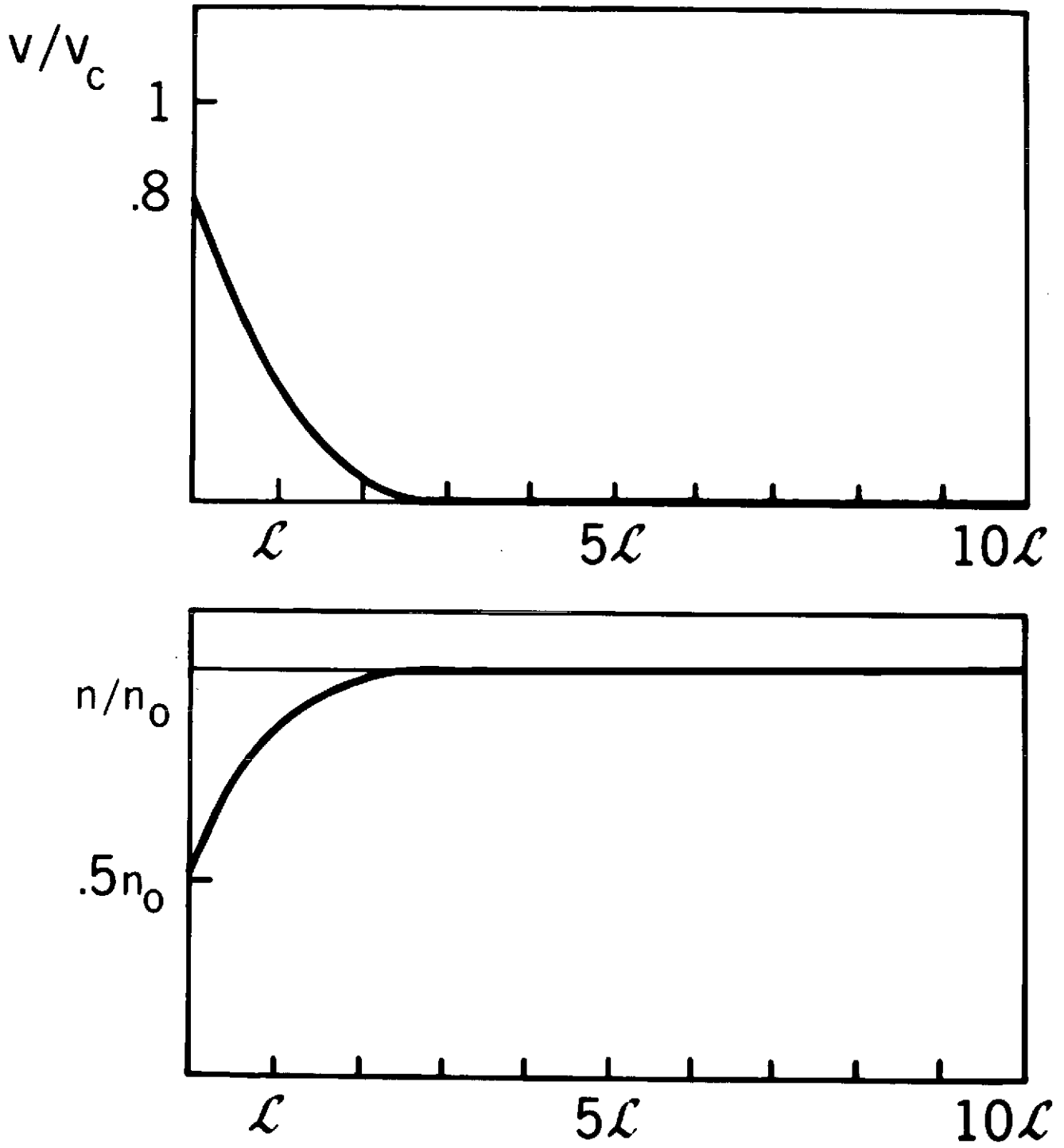
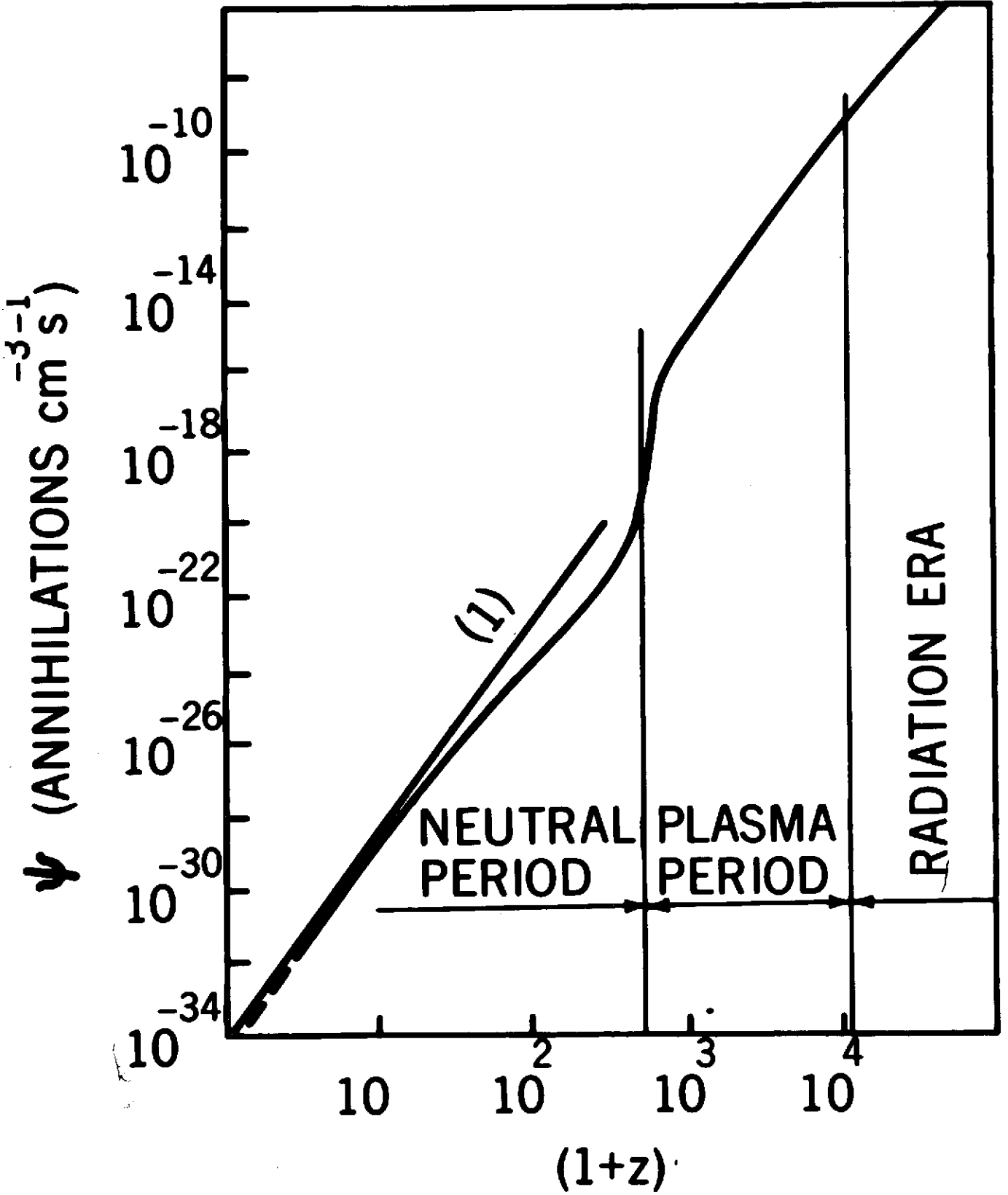


FIG 5



DISTORTION OF THE MICROWAVE BLACKBODY BACKGROUND  
RADIATION IMPLIED BY THE BARYON-SYMMETRIC  
COSMOLOGY OF OMNES AND THE GALAXY  
FORMATION THEORY OF STECKER AND PUGET

F.W. Stecker  
Theoretical Studies Branch  
NASA Goddard Space Flight Center  
Greenbelt, Maryland 20771

and

J.L. Puget  
Observatoire de Paris  
Meudon, France

One consequence of the baryon-symmetric cosmological model of Omnes is the continuing annihilation of matter and antimatter throughout all stages in the evolution of the universe which can cause a distortion in the microwave blackbody spectrum from a purely thermal spectrum because of deposition of annihilation energy at redshifts less than  $10^4$  and particularly at redshifts less than  $10^3$ . The theory of this distortion was first discussed by Zel'dovich and Sunyaev (1969; see also Sunyaev and Zel'dovich 1970a,b). They show that because of the varying evolution of the optical depth of the universe to radiation at various wavelengths, and because the Compton process conserves photon number and does not lead to pure thermalization, two different distortions arise in the blackbody spectrum. Distortions in the Rayleigh-Jeans ( $\propto \nu^2$ ) portion of the spectrum are due to

energy deposition at redshifts between  $10^4$  and  $10^3$  (Zel'dovich, Illarionov and Sunyaev, 1972). Distortions in the Wien portion of the spectrum ( $\propto e^{-\nu}$ ) are due to energy deposition at lower redshifts after the cosmic gas cools to its atomic state and thermalization does not take place as efficiently.

In order to quantitatively estimate the expected distortions, we define the parameter

$$q \equiv \int \frac{\Delta \epsilon(t)}{\epsilon(t)} dt \quad (1)$$

which is a measure of the maximum fraction of the energy density in the radiation which contributes to the nonthermal part of the microwave background.

In equation (1),  $\epsilon(t)$  is the energy density in the blackbody radiation as a function of time (or redshift  $z$ , where  $t = t(z)$ ).

It then follows that

$$q \approx \int dz \frac{\Psi_V(z) M_p c^2}{\epsilon(z)} \frac{dt}{dz} \quad (2)$$

where  $\Psi_V(z)$  is the annihilation rate function discussed in the main paper by Puget (these proceedings).

For the redshift range  $600 < z < 10^4$ , the annihilation rate is given by

$$\Psi_V(z) = 1.7 \times 10^{-32} (1+z)^{6+1/12} \text{ cm}^{-3} \text{ s}^{-1} \quad (3)$$

(see Puget, these proceedings). The resulting value of  $q_{R-J}$  affecting the Rayleigh-Jeans part of the spectrum is then

$$q_{R-J} \approx 1.2 \times 10^{-2} \quad (4)$$

which is, in fact, an upper limit because part of the energy goes into large-scale fluid motions. The corresponding distortion in the Rayleigh-Jeans part of the blackbody spectrum is of the order of 2 per-cent, well below the observational uncertainties of about 20 per-cent in the wavelength region greater than 1 cm.

For the redshift range  $z < 600$ , we will adopt the annihilation rate fitting the  $\gamma$ -ray observations (i.e. the largest value consistent with the present observations, see Puget paper).

$$\Psi_V(z) \approx 10^{-34} (1+z)^{6.25} \text{ cm}^{-3} \text{ s}^{-1} \quad (5)$$

The resulting value of  $q$  affecting the Wien part of the blackbody spectrum is

$$q_W \approx 6 \times 10^{-5} \quad (6)$$

This may be related to the parameter  $y$  used in the calculations of Zel'dovich and Sunyaev, since

$$y = q/4 \approx 1.5 \times 10^{-5} \quad (7)$$

This is well below the observational upper limit on  $y$  set by Zel'dovich of 0.15.

In fact, we expect more distortion than indicated by equation (7) because of dissipation of turbulence created at

higher redshifts which feeds energy into the microwave background below  $z = 600$ . To estimate this effect, we have made a more detailed numerical calculation of the mean gas temperature as a function of redshift (Stecker, Puget and Bredekamp, in preparation) and used the relation given by Zel'dovich and Sunyaev

$$y_T \approx n_0 \sigma_0 c H_0^{-1} \int dz \frac{kT_e}{m_e c^2} (1+z)^{1/2} \quad (8)$$

where  $n_0$  is the present mean gas density in the univers, taken to be  $x 10^{-6} \text{ cm}^{-3}$ ,  $\sigma_0$  is the Thomson cross section and  $H_0$  is the Hubble constant where  $H_0^{-1} \approx 6 \times 10^{17} \text{ s}$ . We then obtain from equation (8) a value of

$$y_T \approx 2 \times 10^{-4} \ll 0.15 \quad (9)$$

Sunyaev and Zel'dovich discussed the problem of black-body distortion due to antimatter annihilation, but they estimated the annihilation rate without taking account of limitations due to annihilation pressure on the boundary regions between matter and antimatter. They therefore, overestimated the annihilation rate by a large factor (see Stecker and Puget, 1972).

Our conclusion is that the annihilation rate for our model of galaxy formation (Stecker and Puget, 1972), while large enough to provide the turbulence needed to explain galaxy formation (Stecker and Puget, 1972, Aldrovandi, Caser,

Omnes and Puget, 1973), does not produce a distortion in conflict with present observations of the microwave blackbody radiation.

REFERENCES

- Aldrovandi, R., Caser, S., Omnes, R., and Puget, J.L. 1973.  
Preprint LPTHE 73/5, to be published.
- Stecker, F.W., and Puget, J.L. 1972. *Astrophys. J.* 178, 57.
- Sunyaev, R.A., and Zel'dovich, Ya.B. 1970a. *Astrophys. and  
Space Sci.* 7, 3.
- 
- 1970b. *Astrophys. and  
Space Sci.* 9, 368.
- Zel'dovich, Ya.B., Illarioniv, A.F., and Sunyaev, R.A. 1972.  
*Zh. Eksp. Teor. Fiz.* 62, 1217.
- Zel'dovich, Ya.B., and Sunyaev, R.A. 1969. *Astrophys. and  
Space Sci.* 4, 301.

ANTIMATTER IN THE UNIVERSE?\*

Gary Steigman  
Yale University

\* A talk presented at the, "International Symposium and Workshop on Gamma Ray Astrophysics" held at NASA/Goddard Space Flight Center, Greenbelt, Maryland from April 30 to May 2, 1973.

## INTRODUCTION

In several previous papers you have heard of the development of a cosmological model which is symmetric in the sense that exactly half the particles in the Universe are, in fact, anti-particles. You have also heard of some of the observational consequences of such a model, particularly as they relate to gamma-ray astronomy. The conclusions the previous speakers have reached is that it is possible to build such a model without violating the many constraints set by observation. I am much less convinced than they of this conclusion and have in the past addressed myself to some of the problems posed by a "symmetric" cosmology. Although, I think we are all agreed that this subject is in a rather early stage of development and that there are many, as yet unsolved, problems, the subject is sufficiently important to justify our continuing interest in it.

In these remarks, I wish to adopt an approach which is different from that of the previous speakers. Rather than asking if a symmetric cosmological model can be constructed which is consistent with observations, I wish to ask the question, "If the Universe does indeed contain equal amounts of matter and anti-matter, how would we know about it?" There are several straightforward ways in which antimatter could signal its presence to us and I shall discuss them shortly. As we shall see, there is no evidence whatever for large amounts of antimatter in the Universe. From that we may reach one of two conclusions. Either the Universe,

is not symmetric, or if it is, the ubiquitous antimatter prefers to remain clandestine. If, indeed, we adopt the latter conclusion, then the limits set by observations set severe restraints on the possible cosmological models. The conclusion that appears to emerge is that matter and antimatter must be separated on the scale of clusters of galaxies if the Universe really is symmetric. Much of what I am going to present has already appeared in print and so I shall limit myself to a general discussion, omitting the details which may be found in the original papers. (1-4)

#### DIRECT EVIDENCE

In principle it is easy to detect the presence of antimatter. You travel to where you suspect a concentration of antimatter, put your detector down (the most rudimentary device will do) and watch. If your detector disappears then you'd better get out of there fast; you've detected antimatter. Seriously though, just such experiments have in fact been performed within the solar system via the manned flights to the Moon and the unmanned probes to Venus. So, now we know, as we suspected with very good reason, that the Moon and Venus are made of ordinary matter. Even before the days of space flights we had pretty good reason to believe the solar system was all made of ordinary matter: The solar wind which sweeps out from the Sun past the planets acts as a probe just as our detector would.

Unfortunately, we are not likely to learn very much

about a sizable part of our Galaxy by this method. However, we are fortunate that, rather than having to travel around ourselves, there are particles which oblige by coming to us: the cosmic rays. Now, unfortunately, the cosmic rays give us no information of their sources since (except for the very highest energy cosmic rays) they are tied to the magnetic field and do not travel in straight lines. So, we cannot be sure of what region of space we are sampling when we examine the cosmic rays. However, we can be certain that, despite extensive searches, no antinucleus has ever been found in the cosmic rays. Now, at some level ( $\sim 1$  part in  $\gtrsim 10^4$ ) we would expect to detect secondary antiprotons in the cosmic rays. The secondary production of antihelium or heavier antinuclei in collisions between the cosmic rays and the interstellar gas will be down by many orders of magnitude. These antinuclei would provide, if detected, clear evidence that somewhere in the Galaxy (Universe?) there were large amounts of antimatter. Evenson<sup>(5)</sup> has set limits to the fraction of helium nuclei which are antihelium. No antihelium nucleus has been found and at the 95% confidence level he finds limits for the rigidity range 1-10 GV,  $< 1 \times 10^{-3}$  and for the range 10-25 GV,  $< 8 \times 10^{-2}$ . For heavier antinuclei, limits at the 95% confidence level have been set by Golden et. al.<sup>(6)</sup> for rigidities 4-125 GV,  $< 5 \times 10^{-3}$  and by Buffington et. al.<sup>(7)</sup> for rigidities  $< 33$ GV they set  $< 2 \times 10^{-4}$  and in the range 33-100 GV their limit is  $< 2 \times 10^{-2}$ .

As I emphasized, we can't be sure where the observed cosmic rays come from. From the ratio of light (Li, Be, B) nuclei to

medium (C, N, O) nuclei we know that the cosmic rays must be able to travel several hundred parsecs in a few million years. So the cosmic rays we sample probably come from a volume whose typical dimension is roughly a few hundred parsecs. They may in fact come from a much larger volume. The isotropy of the cosmic rays, the smoothness of the distribution of galactic, non-thermal, radio emission, the relative constancy of the cosmic ray flux at Earth over periods as long as 4.5 billion years all indicate the cosmic rays we observe fill a volume comparable in size to and perhaps even greater than our Galaxy. The lack of antimatter in the cosmic rays gives us good evidence that every second star in our Galaxy is not made of antimatter. Indeed, the limits on antinuclei in the cosmic rays are already so low that even if a small fraction (say, a percent or so) of them were extragalactic in origin, they would be telling us that very few, if any, extragalactic systems could be made of antimatter.

In summary then, the cosmic rays provide us with the only practical means of sampling the Universe outside our solar system. The evidence is straightforward: no antinuclei have ever been found in the cosmic rays. Therefore some region of space contains very little, if any, antimatter. Unfortunately we just can't be certain what region of space it is.

#### INDIRECT EVIDENCE

When matter and antimatter meet, they annihilate. The

annihilation products are typically pions; roughly 5-6 charged and neutral pions in a typical annihilation. The charged pions decay into muons with the emission of a muon neutrino; the neutral pions decay most often into two gamma-rays. The muons themselves decay into electrons (and positrons) with the emission of both an electron neutrino and a muon neutrino. The end products of a typical annihilation are high energy electron-positron pairs, gamma rays and two kinds of neutrinos. We may therefore hope to learn of the presence of antimatter indirectly by detecting the products of its annihilation with ordinary matter. Now the electron-positron pairs will probably not travel very far from where they are created either because they will be tied to magnetic fields or because they will scatter on any photons present (starlight, infra-red, black-body, etc.) and lose energy rapidly. Furthermore, we know there exist mechanisms for accelerating electrons and positrons to high energy in any case (pulsars). Hence the electron-positron component of annihilation is not likely to provide us with any unambiguous information about the presence of antimatter.

Neutrinos, of course are very difficult to detect. As a result, large fluxes are required and hence the limits one might set are not very interesting. A major fraction of the matter in the Universe would have to be annihilating before a detectable flux of neutrinos would be produced. If that were the case there would be other, more immediate, consequences. Of course, a strong, nearby source (e.g. the Galactic center) might produce a detectable flux of neutrinos,

but there too we'd expect other, more obvious effects (e.g. gamma ray emission). For a discussion of these questions see reference (3).

Finally, we come to the gamma rays produced in annihilation. It is of course most appropriate that they be discussed at this conference. A typical annihilation produces a spectrum of gamma rays extending from several tens of MeV to several hundred MeV. On average, 3-4 gammas are produced per annihilation. Observations of  $\sim 100$  MeV gamma rays then enable us to place limits on the amount of contemporaneous annihilation.

The OSO-3 observations<sup>(8)</sup> of  $\sim 100$  MeV gamma rays indicates a Galactic component superimposed upon an isotropic, presumably, extragalactic component. From their results we may draw the following conclusions (see references (1), (2) and (4) for details). If there is a cool, neutral intergalactic gas which is symmetric its density could be no larger than  $n \sim 10^{-11} \text{ cm}^{-3}$ . I remind you that the average density of matter in galaxies is  $\gtrsim 10^{-7} \text{ cm}^{-3}$ ; hence such a cool, intergalactic gas would constitute a minor component of our Universe. For a hot, ionized intergalactic gas we find that if it is symmetric, then its density must be low ( $\lesssim 10^{-9} \text{ cm}^{-3}$ ). If, in fact, there is a hot, intergalactic gas whose density is close to the critical density, then the fraction of it which could be mixed matter and antimatter would be less than one part in  $10^8$ . Thus, either such a gas is not symmetric, or it maintains very well separated regions of matter and antimatter. While on the subject of intergalactic gas, it is worth pointing

out that the Coma cluster of galaxies has been detected as an x-ray source<sup>(9)</sup> whose spectrum is interpreted as thermal bremsstrahlung radiation from a hot intracluster gas. If this interpretation is correct, then from the lack of gamma rays from Coma, we can say that less than one part in  $10^4$  of that gas is antimatter.

The observations of the Galactic, gamma ray component indicates an annihilation rate per interstellar hydrogen atom of less than  $10^{-25}$  sec<sup>-1</sup>. If, in fact, these gamma rays are interpreted as annihilation products, then we can set the following limits on the antimatter component in the Galaxy: If the annihilation occurs in interstellar clouds then less than one particle in  $10^{16}$  is an antiparticle; If the annihilation occurs in the intercloud medium the limits are less than one in  $10^{12}$ . Indeed, it is worth pointing out that an antiparticle will only survive  $\sim 30$  years in an interstellar cloud and  $\sim 300,000$  years in the intercloud medium; both times are very short compared to the age of the Galaxy ( $\sim 10^{10}$  years). Hence, it is clear that any model which requires the Galaxy to be symmetric must find an extremely efficient mechanism which keeps large amounts of matter and antimatter very well separated over long periods of time. The most straightforward interpretation of course is that the Galaxy probably contains no macroscopic amounts of antimatter.

Finally a word about gamma ray sources. There have been no detections of extragalactic gamma ray sources at about the level of  $\sim 10^{-5}$  photons/cm<sup>2</sup>/sec. If we wish to use annihilation as an

energy source for some of the more spectacular extragalactic objects (e.g. QSO's, Seyfert galaxies, radio galaxies, etc.) then we predict that they would be gamma ray sources. The lack of detections of any of them as sources sets severe restraints on such models. Either annihilation has nothing to do with these sources or, somehow, the gamma rays are absorbed at the source. This latter suggestion is not unreasonable. However, it should be remembered that twice as much energy is released in gamma rays as in electron-positron pairs in a typical annihilation. Then we must inquire into the effect on the source if these gamma rays are to be absorbed. Will the absorption result in re-radiation in another part of the spectrum? Can such a model be made consistent with all observations?

### CONCLUSIONS

We have been discussing the means of detecting the presence of antimatter in the Universe. We have seen there are several, straightforward observational tests and all have, thus far, proved negative. The most straightforward interpretation of these results is that the Universe is, in fact, not symmetric. Of course, it is possible the Universe is symmetric but the matter and antimatter are well separated from each other. Choosing between these two possibilities of course must be a personal decision. Perhaps, in making this decision, we should all bear in mind a quotation which sits, framed, on the desk of William A. Fowler at Caltech.

He attributes it to, "Proverbs for Graduate Students, c.1933". It reminds us that, "The terrible tragedies of science are the horrible murders of beautiful theories by ugly facts".

Note: In the discussion following my talk, D. Clayton of Rice suggested that we search for the evidence of annihilation by looking for the 1 BeV gamma ray line formed when nucleon-anti-nucleon annihilate directly into two gammas. This purely electromagnetic channel should occur but only very infrequently compared to the strong interaction channels via mesons. A rough estimate indicates only one in  $\sim 10^4 - 10^6$  annihilations will be of the two gamma type. The two gamma annihilation has been searched for, unsuccessfully in several experiments<sup>(9)</sup> (P. Nemethy, 1973 Private Communication). As a result I don't expect a detectable  $\sim 1$  BeV annihilation line even if all the observed  $\sim 100$  MeV gammas are from annihilation.

REFERENCES

- (1) Steigman, G. Nature, 224, 477 (1969).
- (2) Steigman, G. Proc. Int. Sch. Phys. Enrico Fermi (ed. R. K. Sachs, Academic Press) Course XLVII, 373 (1971).
- (3) Steigman, G. and Strittmatter, P. A. Astron. and Astrophys. 11, 279 (1971).
- (4) Steigman, G. Cargese Lectures in Physics, 6 (ed. E. Schatzman, Gordon and Breach) (1972).
- (5) Evenson, P. Ap.J. 176, 797 (1972).
- (6) Golden, R. L., Adams, J. H., Boykin, W. R., Deney, C. L., Marar, T. M. K., Heckman, H. H. and Lindstrom, P. L. (Private Communication) (1973).
- (7) Buffington, A., Smith, L. H., Smoot, G. F., Alvarez, L. W. and Wahlig, M. A. Nature 236, 335 (1972).
- (8) Kraushaar, W. L., Clark, G. W., Garmire, G. P., Boriken, R., Higbie, P., Leong, V. and Thorsos, T. Ap.J. 177, 341 (1972).
- (9) Gursky, H., Kellogg, E., Murray, S., Leong, C., Tananbaum, H. and Giacconi, R. Ap. J. (Lett.) 167, L81 (1971).